

NASA CR-151923

(NASA-CR-151923) WIND TUNNEL AND GROUND  
STATIC TESTS OF A .094 SCALE POWERED MODEL  
OF A MODIFIED T-39 LIFT/CRUISE FAN V/STOL  
RESEARCH AIRPLANE (Boeing Aerospace Co.,  
Seattle, Wash.) 35 & NC A14/MF A01

N77-17036

Unclassified  
GS/CB 14985

WIND TUNNEL AND GROUND STATIC TESTS  
OF A .094 SCALE POWERED MODEL  
OF A MODIFIED T-39 LIFT/CRUISE FAN V/STOL RESEARCH AIRPLANE

By D. Hunt, J. Clingan, V. Salemann and E. Omar

D180-20338-1

January 1977

Prepared under contract NAS2-9178 by

THE BOEING AEROSPACE COMPANY

BOEING MILITARY AIRPLANE DEVELOPMENT

P.O. BOX 3999

SEATTLE, WASHINGTON 98124

for

AMES RESEARCH CENTER

NATIONAL AERONAUTICS AND SPACE ADMINISTRATION



1 Report No <b>NASA CR-151923</b>	2 Government Accession No	3 Recipient's Catalog No	
4 Title and Subtitle <b>Wind Tunnel and Ground Static Tests of a .094 Scale Powered Model of a Modified T-39 Lift/Cruise Fan V/STOL Research Airplane</b>		5 Report Date <b>January 1977</b>	6 Performing Organization Code
7 Author(s) <b>D. Hunt, J. Clingan, V. Salemann, and E. Omar</b>		8 Performing Organization Report No <b>D180-20338-1</b>	10 Work Unit No
9 Performing Organization Name and Address <b>Boeing Aerospace Company Boeing Military Airplane Development Organization P. O. Box 3999 Seattle, WA 98124</b>		11 Contract or Grant No <b>NAS2-9178</b>	13 Type of Report and Period Covered <b>Final Report</b>
12 Sponsoring Agency Name and Address <b>National Aeronautics and Space Administration Washington, D.C. 20546</b>		14 Sponsoring Agency Code	
15 Supplementary Notes <b>Technical Monitor, Bedford A. Lampkin Ames Research Center, Moffett Field, CA 94035</b>			
16 Abstract <b>This report presents the results of ground static tests and wind tunnel tests of a .094 scale model of a V/STOL research airplane. The configuration represents a modification to a T-39 airplane involving addition of a lift fan in the nose and replacement of the existing nacelles with tilting lift/cruise fans. The model was powered with three 14 cm diameter tip driven turbo-powered simulators. Forces and moments were measured by an internal strain gauge balance. Engine simulator thrust and mass flow were measured by calibrated pressure and temperature instrumentation mounted downstream of the fans. The tests were conducted to define the low speed handling qualities and general aerodynamic characteristics of the modified T-39. Test variables included: thrust level and thrust balance, forward speed, model pitch and sideslip angle at forward speeds, model pitch, roll, and ground height during static tests, lift/cruise fan tilt angle, flap and aileron deflection angle, and horizontal stabilizer angle. Tests were also conducted to determine the effects of removing the landing gear, the lift/cruise fans, and the tail surfaces.</b>			
17 Key Words (Suggested by Author(s)) <b>V/STOL Lift Fan Vectorized Thrust Wind Tunnel Test Powered Lift</b>		18 Distribution Statement	
19 Security Classif. (of this report) <b>Unclassified</b>	20 Security Classif. (of this page) <b>Unclassified</b>	21 No. of Pages	22 Price*

\*For sale by the National Technical Information Service, Springfield, Virginia 22151

NASA CR-151923

WIND TUNNEL AND GROUND STATIC TESTS  
OF A .094 SCALE POWERED MODEL  
OF A MODIFIED T-39 LIFT/CRUISE FAN V/STOL RESEARCH AIRPLANE

By D. Hunt, J. Clingan, V. Salemann and E. Omar

D180-20338-1

January 1977

Prepared under contract NAS2-9178 by  
THE BOEING AEROSPACE COMPANY  
BOEING MILITARY AIRPLANE DEVELOPMENT  
P.O. BOX 3999  
SEATTLE, WASHINGTON 98124

for

AMES RESEARCH CENTER  
NATIONAL AERONAUTICS AND SPACE ADMINISTRATION



## FOREWORD

This report was prepared in fulfillment of National Aeronautics and Space Administration contract NAS2-9178. The contract was awarded March 30, 1976, to the Boeing Military Airplane Development Group of the Boeing Aerospace Company as part of a program to develop a Lift/Cruise Fan V/STOL Research Airplane.

The contract effort involved the design, fabrication, static ground testing, and wind tunnel testing of a .094 scale powered model of a modified T-39 Lift/Cruise Fan Airplane. Modifications to the T-39 included: expanding the forebody to house a lift fan, replacing the T-39 engines with tilting lift/cruise fans, raising the horizontal stabilizer to a T-tail position, and replacing the T-39 gear with A-4 gear. The model was powered by three 13.97 cm (5.5 inch) diameter turbo-powered simulators. Tests were conducted in the Boeing Static Test Facilities and in the Boeing 9-foot Low Speed Wind Tunnel. Forces and moments were measured by an internal strain-gauge balance. Engine simulator thrust and mass flow were measured by calibrated pressure and temperature instrumentation mounted downstream of the fan.

The tests were conducted to define the low speed handling qualities and general aerodynamic characteristics of the modified T-39. Test variables included: thrust level and thrust balance, forward speed, model pitch and sideslip angle at forward speeds, model pitch, roll, and ground height during static tests, lift/cruise fan tilt angle, flap and aileron deflection angle, and horizontal stabilizer angle. Tests were also conducted to determine the effects of removing the landing gear, the lift/cruise fans, and the tail surfaces.



## CONTENTS

	<u>PAGE</u>
1.0 SUMMARY	1
2.0 INTRODUCTION	4
3.0 NOMENCLATURE	6
4.0 TEST PROGRAM	10
4.1 Model Description	10
4.2 Test Facilities	14
4.3 Test Conditions and Procedures	16
4.4 Thrust Bookkeeping	22
4.5 Data Acquisition	23
5.0 TEST RESULTS	24
5.1 General Remarks	24
5.2 Static Hover Characteristics	26
5.3 Jet-Induced Aerodynamic Forces and Moments at Forward Speeds	31
5.4 Cross-Wind and Differential Thrust Effects	39
5.5 Configuration Component Effects	41
6.0 CONCLUSIONS	43
7.0 REFERENCES	45
FIGURES	47
APPENDICES	93
A - Wind Tunnel Test Data	94
B - Thrust Calibration	251
C - Data Reduction	290



WIND TUNNEL AND GROUND STATIC TESTS  
OF A .094 SCALE POWERED MODEL OF  
A MODIFIED T-39 LIFT/CRUISE FAN V/STOL RESEARCH AIRPLANE

by

D. Hunt, J. Clingan, V. Salemann, and E. Omar

#### 1.0 SUMMARY

A .094 scale powered model of a modified T-39 Lift/Cruise Fan V/STOL airplane was designed, fabricated and tested statically and in a low speed wind tunnel. The test program was conducted in fulfillment of NASA contract NAS2-9178, "Design and Fabrication of a Lift/Cruise Fan V/STOL Model for Wind Tunnel Tests", and was directed towards verifying the basic concept of a shaft-connected tilting lift/cruise fan V/STOL configuration and defining its general aerodynamic characteristics.

Modifications to the basic T-39 included extending the forebody to house the forward lift fan, replacing the T-39 engine pods with tilting lift/cruise fans, replacing the T-39 gear with A-4 gear, raising the horizontal stabilizer to a T-tail position, and providing a flap cutout door to provide clearance for the lift/cruise fan exhaust at high tilt angles. The model was powered by three tip-driven turbo-powered simulators. High pressure air to drive the simulators was supplied to the model through the sting support system and on through the internal "flow-thru" strain gauge balance.

The model was tested in four configurations. Namely:

- A VTOL configuration with flaps deployed, gear down, and engines tilted to 80°, 90° and 95°.
- A STOL configuration with flaps and gear down and engines tilted to 50°.



- A CTOL configuration with flaps and gear down and engines not tilted.
- A loiter configuration with flaps and gear retracted and engines not tilted.

In addition, tests were conducted to assess the effects of removing the gear, nacelles, and tail surfaces and drooping the ailerons. Static tests of the hover configuration were conducted in the Boeing Static Test Facilities and test variables included model pitch, roll and ground height. All four configurations were tested at forward speeds in the Boeing 9' Low Speed Wind Tunnel at speeds ranging from 65 knots to 120 knots. Other test variables included model pitch, sideslip and thrust coefficient.

The static tests were directed towards defining the impact of ground effects upon hover lift and stability. The hover test results show an induced lift loss of 2% of gross thrust for heights far above the ground. With the model in a level attitude there was no additional lift loss due to ground effect at any height. The largest induced lift loss due to ground effect occurred at a combination of 10° of pitch and 10° of roll where a loss equal to 5% of gross thrust was measured. Instabilities in pitch and roll are present, however, the destabilizing moments are small relative to the control power available through differential thrust variation. The largest pitching moments and rolling moments found did not exceed 15% and 10% respectively of the control power available.

The emphasis during wind tunnel tests was on propulsion induced lift for STOL operation and the impact of the tilting lift/cruise fans upon longitudinal and directional stability. The useable propulsion induced lift of the STOL configuration was found to be 19% of the lift produced by the basic model with the lift/cruise fan nacelles removed. The induced lift from the T-39 model has been compared with that of a

**THE BOEING COMPANY**

0.7 scale model of a lift/cruise fan configuration (Reference 1) which is based on thrust vectoring nozzles as opposed to tilting nacelles. The induced lift effects for the two configurations are quite comparable with the present configuration having somewhat greater induced lift for typical STO lift-off conditions.

The present combination of T-tail height and lift/cruise fan inlet length has a varying effect upon the longitudinal stability of the modified T-39 configuration. The configuration stability is very dependent on nacelle tilt angle, angle of attack, and thrust level. The longitudinal stability is adequate for the cruise configuration and degrades at some combinations of high nacelle tilt angle and high angle of attack. The control available using thrust transfer is more than adequate to handle the longitudinal moments. Horizontal tail control effectiveness is near the theoretical value for the cruise and CTOL configurations where the tail is required for control.

Directional stability is good in the VTOL mode at high angles of attack and degrades at lower pitch angles.



## 2.0 INTRODUCTION

NASA has undertaken the development of a Lift/Cruise Fan Research Airplane to provide a technical data base from which a Navy type "A" V/STOL aircraft and possible civil aircraft can be designed with confidence. The Navy requires a type "A" multi-mission V/STOL aircraft in the late 1980's which is capable of sea control operations from many small ships as well as ship-to-shore and shore-to-ship functions. The Lift/Cruise Fan concept exhibits an excellent potential for a type "A" aircraft because of its high speed, high altitude and range capabilities coupled with its ability to operate from small ships.

As a part of the NASA program, a contract was awarded to the Boeing Company to design, fabricate, and wind tunnel test a powered model of a modified T-39 Lift/Cruise Fan Airplane based on a tilt nacelle concept. The objective of the test program was to define the handling qualities of the T-39 configuration during hover in ground effects and at forward speeds out of ground effects. Static ground tests were conducted in the Boeing Static Test Facilities. Wind tunnel tests were conducted in the Boeing 9' Low Speed Wind Tunnel. Four configurations were tested. These include:

- A VTOL configuration with flaps deployed, gear down, and engines tilted to 80°, 90°, and 95°.
- An STOL configuration with flap and gear down and engines tilted to 50°.
- A CTOL configuration with flaps and gear down and engines not tilted.
- A loiter configuration with flaps and gear up and engines not tilted.



In accordance with the terms of NASA contract NAS2-9178, this document is submitted as the final technical report. Presented herein is a description of the contract test program and of the analysis of the test results. The data acquired during the contract test program are included in Appendix "A". Details of the thrust calibration of the turbo-powered simulators are included in Appendix "B". Data reduction details are included in Appendix "C".

THE **BOEING** COMPANY

### 3.0 NOMENCLATURE

The ensuing list of definitions in most instances include two symbols. The first is the conventional symbol while the second represents a computer name appearing on the machine plotted data of Appendix "A". Units are presented in the SI system followed in parenthesis by the British Gravitational units.

- $b, B$  - wing span, centimeters (inches) = 127.3 (50.11)
- $\bar{c}, C, MAC$  - mean aerodynamic chord, centimeters (inches) = 24.02 (9.46)
- $C_J, CJT$  - thrust coefficient =  $F_G/qS$ . CJA, CJB, and CJC are the thrust coefficients of each individual propulsion unit Fan A, Fan B, and Fan C (see Figure 2) "C<sub>J</sub> = RAM" is defined in Section 5.3
- CFR - ram force coefficient = ram force/qS. CFRA, CFRB, and CFRC are the ram force coefficients of each individual propulsion unit

The following group of stability axis coefficients includes all forces and moments on the model (i.e., aerodynamic, thrust, and ram).

- $C_L$  - lift coefficient =  $L/qS$
- $C_D$  - drag coefficient =  $D/qS$
- $C_{PM}$  - pitching moment coefficient =  $PM/qS\bar{c}$
- $C_{SF}$  - side force coefficient =  $SF/qS$
- $C_{YM}$  - yawing moment coefficient =  $YM/qSb$
- $C_{RM}$  - rolling moment coefficient =  $RM/qSb$

**THE BOEING COMPANY**

This next group of stability axis coefficients and ratios ending in "A" denotes aerodynamic forces and moments. That is, the direct thrust and ram forces and moments have been removed (see Figure C.1).

$C_{LA}$ , CLA	- aerodynamic lift coefficients = $L_A/qS$
$C_{DA}$ , CDA	- aerodynamic drag coefficient = $D_A/qS$
$C_{PMA}$ , CPMA	- aerodynamic pitching moment coefficient = $PM_A/qSc$
$C_{SFA}$ , CSFA	- aerodynamic side force coefficient = $SF_A/qS$
$C_{YMA}$ , CYMA	- aerodynamic yawing moment coefficient = $YM_A/qSb$
$C_{RMA}$ , CRMA	- aerodynamic rolling moment coefficient = $RM_A/qSb$
$L_A/F_G$ , LA/FGT	- aerodynamic lift ratio
$D_A/F_G$ , DA/FGT	- aerodynamic drag ratio
$PM_A/F_G \bar{c}$ , PMA/FGT*C	- aerodynamic pitching moment ratio
$SF_A/F_G$ , SFA/FGT	- aerodynamic side force ratio
$YM_A/F_G b$ , YMA/FGT*B	- aerodynamic yawing moment ratio
$RM_A/F_G b$ , RMA/FGT*B	- aerodynamic rolling moment ratio
D	- drag, newtons (pounds)
$D_{HI}$	- highlight diameter, centimeters (inches) = 15.66 (6.164)
$F_G$ , FGT	- total gross thrust of all three propulsion units = $FGA + FGB + FGC$ , FGA, FGB and FGC represent the gross thrust of each individual propulsion unit, newtons (pounds)
FPR	- fan pressure ratio = $P_{T_3}/P_0$
h, HGT	- height of model reference point above ground plane (see Figure 2), centimeters (inches)

**THE BOEING COMPANY**

$h/c$ , HGT/C	- ratio of model ground height to mean aerodynamic chord
L	- lift, newtons (pounds)
$P_{T_3}$	- total pressure downstream of fan, newtons/meter <sup>2</sup> (psf)
$P_0$	- wind tunnel test section static pressure, newtons/meter <sup>2</sup> (psf)
PM	- pitching moments, newton meters (ft-lbs)
q, Q	- wind tunnel test section dynamic pressure, newtons/meters <sup>2</sup> (psf)
RM	- rolling moments, newton meters (ft-lbs)
S	- wing reference area, centimeters <sup>2</sup> (in <sup>2</sup> ), = 2808 (435.17)
$\alpha$	- incidence of horizontal tail - degrees
SF	- side force, newtons (pounds)
$V/V_J$	- ratio of freestream velocity to fan efflux velocity
YM	- yawing moments, newton meters (ft-lbs)
$\alpha$ , ALPHA	- angle of attack of body axis, degrees
$\beta$ , BETA	- angle of sideslip of body axis, degrees (positive nose left)
$\lambda$ , LAMBDA	- lift/cruise fan tilt angle relative to body axis degrees
$\epsilon_a$	- downwash gradient at horizontal tail, $d\epsilon/d\alpha$ ( $\epsilon$ positive for downflow at tail)
$\phi$	- angle of roll relative to ground plane (positive right wing down), degrees

THE **BOEING** COMPANY

- Notes:
- (1) The moment reference center is at the station of  $.3\bar{c}$ , F.S.  
60.95 cm (23.994) and at water line 22.68 cm (8.93 in).
  - (2) The sign convention for forces and angles is given in  
Figure C.5 of Appendix C.

## 4.0 TEST PROGRAM

### 4.1 Model Description

The .094 scale model represented a V/STOL technology demonstrator airplane based on a modified T-39 (Model 1041-135-2R of Reference 2). The modifications include:

- Expanding the forebody to house a lift fan
- Replacing the T-39 engine pods with tilting lift/cruise fan pods
- Raising the stabilizer to a T-tail position
- Replacing the gear with A-4 gear
- Adding a flap door to provide clearance for the lift/cruise fan efflux when the nacelles are tilted to the hover position.

The model was sting-mounted, which necessitated some distortion of the aft fuselage to allow sting clearance (see Figure 1), and was supported on a six-component strain-gauged, "flow-thru" balance (illustrated in Figure 3 and discussed in Reference 3).

Figure 2 shows the model in its various configurations and gives the principal dimensions. The top view depicts the CTOL configuration, with the nacelles at  $\lambda = 0^{\circ}$  and the front fan doors open; the side view depicts a VTOL configuration, showing the nacelles at  $\lambda = 90^{\circ}$ . The flaps and flap doors are shown extended in the VTOL configuration.

Three Technology Development Inc. 14 cm (5.5 inch) diameter tip driven fans were used to simulate the propulsion system. One of these units is shown, disassembled, in Figure 4 and a description is found in Reference 4. The units were furnished by NASA for this test program.

Each fan was rated at 35000 RPM with a design fan pressure ratio of 1.25. At this rating each had a fan airflow of 2.5 kg/sec (5.55 lbs/sec) and used .5 kg/sec (1.1 lbs/sec) of drive air. For the purpose of this test, they were operated up to a maximum of 30000 RPM. The drive air was supplied to the model at 41.4 bars (600 psig) and heated to 71°C (160°F) to prevent icing at the turbine exit. Remotely controlled valves and critical-flow venturi meters located within the model were used to control and monitor the airflow to each individual fan (Figure 5).

The high pressure air supplied to the L/C nacelles was divided into two portions, one part for driving the fan and the other for simulating the primary exhaust efflux. Since both portions were always choked the simulated primary weight flow varied in direct proportion to the fan supply weight flow. The primary air was passed through a choke plate and screens to obtain a uniform total pressure distribution and representative pressure ratio before exhausting from the primary nozzles. Figure 6 shows details of the lift/cruise nacelle assembly. Each nacelle can be pre-set to various tilt positions, representing various flight configurations. A serrated interconnection allowed angular settings in increments of 5°. The limits of angular rotation were determined by instrumentation cables and tubes which were routed out of the nacelle around the periphery of this connection. This allowed rotation from  $\lambda = 0^\circ$  (aligned with the model axis) to  $\lambda = 105^\circ$ , with the pivot point located at fuselage station 82.93 cm (32.65 inches) and water line 30.53 cm (12.02 inches).

The external lines of the nacelle were generated to represent those of the technology demonstrator having Allison PD 370-16 engines installed. The model scale was selected such that the fan exit area was scaled exactly. A more complete description of the design process is included in Appendix "B" which describes how the inlet contours were chosen and gives details of the nacelle ordinates. Appendix "B" also describes the instrumentation in the nacelle. The external cross-section of the core engine cowl was elliptical as indicated by the shading in Figure 6.

THE **BOEING** COMPANY

This was done on the assumption that the engine accessories could be distributed between the top and bottom of the core engine.

Fairings were used to cover the Lift/Cruise Fan nacelle pivots, instrumentation connections and air supply lines. These fairings are not completely representative of the full scale airplane. Part of each fairing was attached to, and rotated with, the nacelle and part was attached to the fuselage. These fairings are shown detailed in Figure 7. In order to determine the aerodynamic effect of the fairing attached to the nacelle, it was removed for one test and the leading edges of the nacelle fittings were faired with modelling clay as shown in Figure 7.

Yaw vanes were located at the fan nozzle exit for thrust deflection and are shown in their undeflected position in Figure 6. The vane chord was 35.56 cm (14 in) full scale and its section was that of a NACA 0012 airfoil. The pivot point was at 10% of vane chord with the vane leading edge located at the fan exhaust plane. Deflection angles of  $0^{\circ}$ ,  $\pm 10^{\circ}$ , and  $\pm 20^{\circ}$  were provided.

Details of the nose fan installation are given in Figure 8. The nose fan was located as low in the fuselage as possible in order to allow length for development of the inlet contours. The fuselage forebody was hand-worked to provide the desired inlet shape. Sections of the inlet are presented in Appendix "B".

The nose fan inlet doors, which when closed form the upper surface of the airplane nose, are shown diagrammatically on Figure 8 in the open and closed positions. When the doors were in the open position, they were stowed at the sides of the fuselage as shown. Parts were provided to test both open and closed configurations.

The nose fan exit doors which, when open, can be deflected to provide thrust vectoring for yaw control are shown in the open position in Figure 8. The outboard doors opened towards the airplane plane of symmetry and the inboard doors opened from that plane outwards to form

THE **BOEING** COMPANY

the projections shown. A disc was provided to fair and seal the exit when a "door-closed" configuration was tested.

The basic T-39 model airframe was defined in accordance with the Saberliner Specifications Document (Reference 5) with additional consideration of measurements taken from a full scale T-39. Wing and tail planforms and section definitions are presented in Figures 9 and 10. The model wing was positioned .38 cm (.15 inches) lower relative to the fuselage than full scale airplane definitions indicated. This had the effect of increasing the body depth in the vicinity of the wing and was done to provide more space within the model for structure and instrumentation. The wing dihedral was  $3.15^{\circ}$ . The wing was twisted linearly from zero incidence at the root to  $-2.9^{\circ}$  at the construction tip. The tip of the vertical fin was modified to support the horizontal stabilizer. A NACA-0010 airfoil section was used for the vertical fin. The airfoil section of the all new horizontal stabilizer varied linearly from a NACA-0010 airfoil at the tip to a NACA-0015 airfoil at the root. The stabilizer had an anhedral of  $9^{\circ}$ .

The basic high lift system (i.e., slats and flaps) were positioned in accordance with measurements of a full scale airplane in their fully deployed position. The slats and flaps were unchanged throughout the test with the exception of tests of the loiter configuration at which time the slats and flaps were nested. The flap doors, designed to provide clearance for the lift/cruise fan efflux, were deflected for tests of the hover configuration when  $\lambda$  was  $90^{\circ}$  or greater and retracted for all other tests.

No transition grit was used on the model for any of the tests reported herein..

## 4.2 Test Facilities

All tests were conducted in Boeing facilities located in Seattle, Washington. The facilities involved are described briefly below.

### 4.2.1 Flight Simulation Chamber (FSC)

Preliminary calibrations of the model fans were conducted in the Boeing Wind Tunnel Flight Simulation Chamber. This facility was developed over a period of years specifically for the purpose of calibrating wind tunnel model propulsion simulators. The facility includes thrust and mass flow measuring systems and allows for variation of back pressure by means of evacuating the chamber into which the thrust simulator discharges. A schematic of the chamber is shown in Figure 11. A detailed description of the facility is presented in Reference 6.

### 4.2.2 Boeing Static Checkout Area

All of the static hover tests were conducted in this facility. The primary use of this area is for checkout of models being prepared for tests in the Boeing Transonic Wind Tunnel. This facility is essentially a 8.5m x 12.2m by 4.0m high room (28 ft x 40 ft x 13 ft) as shown in Figure 12, equipped with a model support system providing for pitch and vertical translation of sting mounted models. The model is controlled from an adjacent control room with visibility provided by both a window and closed circuit television. Instrumentation outputs are carried to the Boeing Supersonic Wind Tunnel Data System by means of a permanent hardwired interconnect. Both on-line and final data reduction are accomplished by the wind tunnel central computing system. The model was installed in approximately the center of the room with the model axis aligned with the longer (12.2m) room dimension. The room floor served as the ground plane.

### 4.2.3 Boeing 9'-B Low Speed Wind Tunnel

The wind tunnel testing was conducted in the 9' -B Low Speed Wind

THE BOEING COMPANY

Tunnel located at the Propulsion Laboratories' North Boeing Field Test Complex. The 9'-B LSWT is an open circuit wind tunnel which draws air directly from the atmosphere through a test section 2.59 meters (102 inches) high by 2.67 meters (105 inches) wide. A schematic of the tunnel is shown on Figure 13 and a view of the model installed in the tunnel is shown in Figure 14. The tunnel is powered by an Allison model 501-D13 gas turbine engine using a variable pitch propellor. Flow straighteners and screens are located in the tunnel inlet to minimize the effect that atmospheric wind conditions have on the tunnel flow profile. Tunnel velocities can be varied from 0 to approximately 180 knots. The tunnel is equipped with a sting support system mounted in the aft portion of the constant area section of tunnel. The motion of the support system is in the horizontal plane such that the model wings are in the vertical plane as shown in Figure 14.

The 9'-B LSWT Data System was used for recording the data on magnetic disc. The Acquisition System is a software controlled, Boeing designed Standard Digital Data System (SDDS). A PDP-8 computer is used for system control and on line "quick-look" data calculation with CRT output. A PDP-8/I is used for on/off-line final data calculation.

THE **BOEING** COMPANY

### 4.3 Test Conditions and Procedures

#### 4.3.1 Test Conditions

The model was tested in four basic configurations. These are defined as follows:

- A VTOL configuration with flaps deployed, gear down, and engines tilted to  $80^{\circ}$ ,  $90^{\circ}$  and  $95^{\circ}$ .
- A STOL configuration with flaps and gear down and engines tilted to  $50^{\circ}$ .
- A CTOL configuration with flaps and gear down and engines not tilted.
- A loiter configuration with flaps and gear retracted and engines not tilted.

The conditions under which each was tested are summarized in Figure 15. Included are lift/cruise fan tilt angle, forward speed, thrust, pitch and sideslip angle, stabilator angle as well as component effects. In addition, the VTOL configuration was tested with differential thrust, side-to-side and fore and aft, representative of thrust control variations. Only the VTOL configuration was tested statically. Test conditions for the static test included: engine tilt angles of  $80^{\circ}$ ,  $90^{\circ}$ , and  $95^{\circ}$ ; pitch angles of  $-5^{\circ}$ ,  $0^{\circ}$ ,  $5^{\circ}$ ,  $10^{\circ}$ , and  $15^{\circ}$ ; roll angles of  $-5^{\circ}$  and  $-10^{\circ}$ ; ground height variation from .12 meters (4.7 inches) to 1.83 meters (72 inches).

#### 4.3.2 General Procedures

The model fans were supplied with high pressure air from a plenum inside the model. This plenum is essentially part of the internal balance and the pressure level in the plenum has some effect on the balance outputs. The balance plenum pressure was always set and maintained at

THE **BOEING** COMPANY

a level of 41.4 bars (600 psig) for all tests, fan calibrations, and balance calibrations. This procedure is standard with this type of balances and insures that the measured force levels are not influenced by balance pressure tares. Since the individual fan control valves are downstream of this plenum there is still complete control of fan thrust without varying the balance plenum pressure.

The high pressure air used to drive the fans was pre-heated to eliminate icing problems. During the initial calibration it was determined by observation of the fans that the minimum supply air temperatures at which visible ice would not form was about  $71^{\circ}\text{C}$  ( $160^{\circ}\text{F}$ ) as measured in the balance plenum. This temperature was used for all further testing. In the colder environment of the open circuit wind tunnel, it was infrequently observed that under some conditions ice could be seen on the fan shroud between stator blades. This condition would only last for a few minutes when the ice would fall off.

Since warmed air was being carried across the internal balance it was necessary to establish procedures to minimize balance zero drift. During the static test, it was found that by pre-warming the balance to about  $54^{\circ}\text{C}$  ( $130^{\circ}\text{F}$ ) prior to recording zeros, the problem of balance output drift was minimized. However, during the wind tunnel test it was not possible to maintain the balance at this temperature during a run because the heat input from the warmed air was not adequate in the presence of the large heat transfer from the model to the tunnel stream. This resulted in greater thermal gradients and consequently greater balance output drifts than those occurring during the static tests.

A serious problem in measuring fan exit total and static pressures occurred during the static test. Erratic readings were observed and were eventually traced to an accumulation of fan lubricating oil in the pressure measuring lines. This problem is apparently related to the large quantity of oil-mist which must be supplied to the fan bearings. The oil-mist is blown into the bearing cavity and subsequently flows out

into the fan air stream ahead of the pressure instrumentation. Because of this problem, RPM rather than pressures was used to reduce the static data. For the wind tunnel data it was not considered adequate to rely on RPM in the presence of the substantial levels of fan flow distortion and back pressure variations expected during forward speed operation at large nacelle tilt angles. The pressure measuring problem was eliminated for the wind tunnel tests by replumbing the model to utilize external rather than internal pressure scanning valves. This allowed the use of an existing system which is designed to blow dry nitrogen from the pressure scanner back through the pressure lines to remove any foreign matter. This is accomplished by an automated system during the off-shift and on this test every pressure measuring line was blown out after each day's testing. This procedure was sufficient to solve the problem since some time was required to accumulate sufficient oil to cause a problem.

#### 4.3.3 In-Place Fan Calibrations

During both the static and wind tunnel tests, the fans were calibrated in place.

In the static test facility this calibration consisted of positioning the complete model at about 1.8 meters (72 inches) above the floor and at an angle of attack of  $15^{\circ}$  to minimize the ground effects within the constraints of the support system. Each fan was then run separately (lift cruise fans tilted to their  $90^{\circ}$  position) to determine the relationships between RPM and thrust as measured by the internal force balance. (Thrust was also computed from fan pressure instrumentation but due to instrumentation difficulties this data was not utilized for the static test data reduction.) The fans were run at thrust levels up to about 400 newtons (90 lbs).

In the wind tunnel, similar calibrations were run with the exception that the fan efflux was directed into a scavenging pipe which directed it outside the test section. This prevented re-circulation of the fan flow around the model and also prevented the inducement of a flow

**BOEING** COMPANY

velocity through the wind tunnel by the ejector action of the fans. The pressure instrumentation difficulties of the static test had been solved and the calibrations were used to relate the forces measured by the internal balance to those computed from the fan exit pressure instrumentation.

The above calibrations established the basis for determining thrust during actual tests. In addition, a variation of thrust coefficient with back pressure was included in the data reduction. This relationship had been established during the initial calibration of each fan in the Flight Simulation Chamber.

The calibrations are described in greater detail in Appendix "B".

#### 4.3.4 Static Test Procedure

For the static testing the model was initially positioned with the landing gear clear of the ground plane by about .25 cm (.1 inch). Each fan was set at a specified RPM value selected to give the desired thrust level. The lift/cruise fans were generally set to give about 350 newtons (79 lb) thrust each. This amount of thrust corresponds to a fan pressure ratio of 1.14 which matches the full scale airplane value. The nose fan was set to give an approximate pitching moment trim about the moment reference center. This value was computed from geometric considerations and varies with nacelle tilt angle as shown in Figure 16. Certain runs were also made with the thrust intentionally unbalanced, either side to side or fore and aft.

The model was then traversed away from the floor with periodic stops for pressure stabilization and data recording. Constant angle of attack was held throughout a height traverse. Due to ground effects, the thrust levels (especially of the nose fan) tended to change somewhat with height above the floor. No attempt was made to maintain the original thrust levels. The control parameter was tip turbine supply pressure which was maintained constant during height traverses.

#### 4.3.5 Wind Tunnel Test Procedures

In general the desired variations in thrust coefficient ( $C_J$ ) were obtained by changing the tunnel speed at a constant fan thrust setting. The predominant thrust setting used corresponded to a fan pressure ratio of about 1.14. The tunnel speeds run were in the range 33 to 62 m/sec (65-120 kts) giving a  $C_J$  range of about 1.8 to 5.5 and corresponding to a Reynolds number range from .6 million to 1.2 million based on the model reference chord. However, partway through the test a model structural problem was discovered which required limiting the tunnel speed to about 36 m/sec (90 kts) compared to the previously selected maximum of 62 m/sec (120 kts). Thereafter the lowest  $C_J$  value ( $C_J = 1.8$ ) was run at a fan pressure ratio of about 1.10 while for all higher  $C_J$  values the FPR = 1.14 setting was maintained.

The upper  $C_J$  limit of 5.5 was selected based on considerations of tunnel flow breakdown. While time did not permit a detailed study of that limitation, observations were made of tufts on the tunnel walls at several fixed angles of attack as  $C_J$  was gradually increased. These runs were made with the nacelle tilt angle set at  $90^\circ$ . It was observed that the flow on the tunnel wall beneath and behind the model became increasingly rough as  $C_J$  increased. At  $V = 33$  m/sec (65 kts,  $C_J = 5.5$ ) the region of rough flow had moved forward to a position under the model tail but there were no significant areas of reversed flow. However, when the speed was lowered to about 31 m/sec there were large areas under the model where the flow was actually reversed. This was interpreted as a "flow breakdown" situation representing a region where valid free air testing was not possible. In no case was the tunnel flow observed to "climb the sidewalls" as has been observed by others for flow breakdown situations. It is worth noting that the test limit determined by this method is in good agreement with a detailed flow breakdown study presented in Reference 7.

The thrust balance among the three fans was generally set to provide approximate moment trim about the moment reference center for the

THE BOEING COMPANY

static case. No attempt was made to readjust the initial static supply pressure values to allow for thrust changes or aerodynamic moments resulting from forward speed.

In general, angle of attack series were taken with angle increasing from  $-8^{\circ}$  to  $+30^{\circ}$ . It was noted that some hysteresis existed and that for certain configurations this effect was appreciable. This phenomenon was not explored in any detail and in general the data presented are all on the same side of the hysteresis loop.

THE BOEING COMPANY

#### 4.4 Thrust Bookkeeping

The thrust subtracted from the measured forces was calculated differently in the resolution of wind tunnel data compared to static test data. In the static test, nozzle total pressure data were not reliable, and thrust was obtained from a calibration against fan corrected speed. In the wind tunnel, pressure data were reliable and thrust was calculated from nozzle total and static pressure measurements. As a result, full scale engine thrust calculations must be performed differently when they are to be combined with model wind tunnel aerodynamic data as compared to static ground effects data.

When applied to wind tunnel data, full scale thrust must reflect the effect of nozzle back pressure on engine performance. This requires knowledge of back pressure vs. nacelle attitude and airspeed, and the response of the engine to back pressure changes.

During static testing, corrected speed did not vary with height, therefore calculated thrust did not vary either. However, there was some evidence, particularly on the nose fan, that nozzle back pressure varied in ground effect. Any effect on actual fan thrust would therefore show up as an aerodynamic ground effect on the airframe. Therefore, where static model data is used for full scale predictions, it should be combined with full scale thrust out of ground effect. The result is valid if the model and full scale fans react similarly to increasing nozzle back pressure.

#### 4.5 Data Acquisition

The data acquired during the wind tunnel test program included:

- Model force and moment measurements (axial force, normal force, side force, and moments about the pitch, yaw and roll axis) from an internal, flow-thru, strain gauge balance.
- Balance temperature as well as the temperature and pressure within the balance plenum.
- Jet efflux total pressure, static pressure and total temperature.
- Pressure and temperature of the individual air supplies to power the three turbo-powered simulators.
- Simulator inlet total pressures at the forward (or lower in the case of the lift/cruise fans when not tilted) azimuth as well as inlet static pressure.
- Simulator RPM and bearing temperature. The bearing temperature was monitored but not recorded.
- Test section conditions including static and total pressure and total temperature.
- Model pitch and side slip angles during wind tunnel tests and ground height, pitch and roll angle during static ground tests.

## 5.0 TEST RESULTS

### 5.1 General Remarks

The results of the static hover and wind tunnel tests are presented in the following sections. In general the results are presented in terms of forces and moments which have had the direct thrust and ram forces removed. The resulting forces are given the subscript "A" (e.g.,  $C_{LA}$ ) for "aerodynamic". There are several reasons for presenting the data in this form as summarized below.

- 1.0 It is not always possible to exactly balance the two lift cruise fans. This can introduce rolling and yawing moments which must be removed in order to reveal the aerodynamic contributions.
- 2.0 The nose fan thrust was not exactly constant with angle of attack. This introduces a variation of pitching moment with angle of attack which is best removed to reveal the aerodynamic forces.
- 3.0 The ram force at a given  $C_j$  is not exactly representative of the airplane value. This occurs basically because of the mass flow added to drive the tip turbine and because of exhaust temperature differences between the model primary and the actual engine exhaust. Removing ram forces from the wind tunnel data facilitates correction to actual airplane ram force levels.

The relationship of the aerodynamic forces to the total model forces is illustrated in Figure 17 for a forward speed case representing a typical STOL liftoff condition. It is seen that the aerodynamic forces are small relative to the overall model forces. The aerodynamic data therefore represent the difference between two large numbers (total forces minus thrust and ram forces). This of course has an effect on the relative accuracy which can be achieved in the aerodynamic data.

In using the data to predict airplane performance the "thrust-drag"

THE BOEING COMPANY

bookkeeping system must be taken into account and it should be noted that there is a difference between the systems used for static data compared to that used for wind tunnel data. In using the static data the full scale thrust "out of ground effect" should be applied since the backpressure effect on thrust is already included in the data. However, in using the wind tunnel data any effects of backpressure on the full scale fan performance must be taken into account in the propulsion data used since the thrust removed from the wind tunnel data was based on actual measured backpressure. This subject is discussed in more detail in Section 4.4.

When using the "aerodynamic data" ( $C_{L_A}$ ,  $C_{D_A}$ , etc.) contained herein to determine total forces on the configuration, the reverse of the wind tunnel data reduction procedure is applied. Unless identified otherwise, the aerodynamic data presented were determined with the distribution of thrust indicated in Figure 16. If this is the condition of interest the coefficients plotted can be used directly. If a different thrust distribution is being considered, the data concerning thrust distribution effects (e.g., Figure 31) can be used to determine an adjustment to the basic (e.g., Figure 30) data. The components of direct thrust and ram force for each of the three fans can then be added to the aerodynamic data to give total forces. In adding ram moments equations, C.11 through C.13 can be used. Typical measured ram forces from the wind tunnel data are summarized in Figure C.3. However, in predicting airplane forces it is recommended that ram forces more representative of the flight propulsion system be used.

## 5.2 Static Hover Characteristics

### 5.2.1 Effect of Ground Height for Level Model Attitude

The effect of the ground on the induced forces for the basic VTOL configuration ( $\lambda = 90^\circ$ ) is shown in Figure 18 for zero pitch and roll angles. It should be noted that all of the data plotted represent repeat runs of the same configuration. This was treated as a control configuration to establish repeatability. It is seen that all four runs have the same shape while one of the four is displaced by about 2% from the others. This shift was apparently associated with measuring accuracy and probably is not unique to this run. In interpreting the subsequent plots, where multiple runs are not available, this accuracy limitation on level must be considered. Since curve shapes are apparently not much affected, the magnitude of the ground effect can be determined as an increment from the free air level measured on the particular run involved.

It is seen in Figure 18 that the induced forces on this configuration are small. Based on the three consistent runs the lift force is within about  $\pm 2\%$  of the direct thrust component depending on ground height. The regions of positive lift are associated with the "fountain" which forms under the model as the three jets impinge on each other as they spread out on the ground plane.

It is seen that at the largest ground height tested ( $h/c = 5$ ) the induced lift is negative and equal to about 2% of total gross thrust. Subsequent tests run with the model inverted to give a more certain "free air" condition have confirmed this 2% negative induced lift. Since the fans were installed on the model during calibration and were run individually, this indicates that when all three fans are run simultaneously, the lift realized is 2% less than the sum of the individual fan contributions to lift.

THE BOEING COMPANY

The free air region extends down to about  $h/c = 3.3$  ( $h = 8.4$  meters for the full scale T-39 demonstration) below which the ground effect begins to produce a lift increase. The beneficial ground effect peaks out at about  $h/c = 2.3$  and then decreases gradually until at  $h/c = .8$ , the lift is back to the free air value.

The induced "drag" (longitudinal force) and pitching moments are small. The negative slope of pitching moment vs. height is apparently associated with a rearward displacement of the point of impingement of the fountain on the model. This would be expected from geometric considerations since the nose fan is pointed  $14^{\circ}$  rearward. The induced pitching moments of Figure 18 could be trimmed by changes in nose fan thrust of  $\pm 4\%$  (from the free air setting) combined with  $\pm 2\%$  changes in L/C fan thrust to hold total thrust constant.

### 5.2.2 Effect of Angle of Attack

The effect of angle of attack on the induced forces is shown in Figure 19 for the case of  $\lambda = 90^{\circ}$ . For positive angles of  $5^{\circ}$  to  $15^{\circ}$  the favorable fountain effect found at  $0^{\circ}$  does not occur while at  $\alpha = -5^{\circ}$  the magnitude of the favorable fountain effect has increased considerably. This effect is related to the location of the fountain as seen in the photos of oil flow on the ground shown in Figure 20. The projection of the model was drawn on the floor to help visualize the fountain location relative to the model. The dark line is an accumulation of oil at the stagnation point where the three jets meet. Figure 21 presents a tracing from oil flow photos at various angles of attack. It is seen that the fountain moves forward with angle of attack and at  $\alpha = 5^{\circ}$  it passes ahead of the wing and therefore produces little upward force on the model. Oil on the lower model surface indicated that the ground oil pattern was in fact, indicative of the location of the fountain impingement on the model. However, these model oil patterns were very faint and distinct photographs were not obtained.

For the pitch range tested the greatest lift loss due to ground effect is about 3% of gross thrust relative to the free air lift level.

At  $\alpha = 10^\circ$ , and  $\alpha = 15^\circ$  the induced drag changes noticeably with height. This implies that horizontal force trim will occur at combinations of  $\alpha$  and  $\lambda$  somewhat different than those calculated from direct thrust considerations alone.

The effect of angle of attack at  $\lambda = 80^\circ$  is shown in Figure 22. The effect is similar to that found at  $\lambda = 90^\circ$ . As the model is pitched up the fountain moves forward of the wing and its effect is largely lost. There is, of course, a shift in the angle of attack at which the fountain is directly under the wing compared to the  $\lambda = 90^\circ$  case.

### 5.2.3 Effects of Lift/Cruise Fan Tilt Angle

The effects of tilting the lift/cruise fans upon the hover characteristics is presented in Figure 23. This effect is similar to that of changing pitch angle. Reducing the tilt angle to  $30^\circ$ , thereby causing the fountain to move aft, produced a lift increase similar to that occurring at a pitch angle of  $-5^\circ$ . Increasing the nacelle tilt angle to  $95^\circ$  moves the fountain forward and thereby reduces lift as did an increase in pitch angle. Increasing the nacelle tilt angle to  $95^\circ$  also altered the pitching moment characteristics as did positive pitch angles. Namely, producing more negative pitching moments upon approaching the ground.

### 5.2.4 Effect of Roll Angle

Data for combinations of angle of attack and roll are presented in Figure 24 and 25. The effect of roll angles of  $10^\circ$  and greater is seen to be unfavorable on lift, especially for angles of attack greater than zero. At  $\alpha = 10^\circ$  and  $\phi = -10^\circ$  the lift reduction is about 4% of gross thrust relative to the free air lift for the same run. This is the most adverse model orientation found on this test.

The induced side force tends to resist airplane motion that would be caused by a bank angle, thus providing a stabilizing influence. The magnitude of this influence, however, is quite small. For example, at  $\phi = -15^\circ$ , the induced side force is about 2% of thrust. For combined pitch and roll, side force, which is most affected by pitch changes,

THE BOEING COMPANY

only varies 2% for a  $10^{\circ}$  change in pitch. Induced rolling and yawing moment ratios change .01 or less for a  $10^{\circ}$  pitch variation.

#### 5.2.5 Pitch and Roll Control Capability in Hover

The maximum pitch and roll control power in hover are shown in Figure 26. This control capability is compared to the thrust induced aerodynamic pitching moments and rolling moments produced with  $\alpha = 10^{\circ}$  and  $\phi = -10^{\circ}$ . In both cases, the available control power is substantially greater than the induced aerodynamic moments for that airplane attitude. The control power shown is that available when the total airplane thrust is held constant. The maximum nose up pitching moment is generated by increasing the full scale airplane nose fan thrust to maximum (2495 newtons, 11,150 lbs) while reducing the thrust of each L/C fan by half the nose fan increment. For each of the three fans, maximum thrust is determined by the fan blade pitch limit. For the Boeing 1041-135-2R configuration of a lift cruise fan V/STOL airplane (Reference 2), the nominal thrust of the three fans is:

$$L/C = 2018 \text{ newtons (8975 lbs)}$$

$$\text{Nose} = 1877 \text{ newtons (8350 lbs)}$$

Therefore, the L/C fans are reduced to 1709 newtons (7680 lbs) thrust each when the nose fan is increased to maximum thrust. For maximum nose down pitching moment, each L/C fan is increased to maximum thrust (2495 newtons) while reducing the nose fan thrust by an amount equal to the total increase in L/C fan thrust. The nose fan thrust is therefore reduced to 922 newtons (4100 lbs). For roll control, one L/C fan is increased in thrust (up to the maximum) while the other L/C fan is decreased by an equal amount

#### 5.2.6 Static Test Result Summary

In summary, the propulsion induced aerodynamic effects upon the hover configuration of the T-39 lift/cruise fan airplane are small and show no sudden changes with ground height, pitch, or roll. In free air,

THE **BOEING** COMPANY

there is a 2% loss of lift due to running all three fans simultaneously. The largest lift loss due to ground effect occurs at a combination of  $10^0$  of pitch and  $10^0$  of roll where lift is 4% of gross thrust below the free air value. From the induced aerodynamic moments observed during the static ground tests, the greatest variation in thrust of any one fan required for trim is 7%. This variation is required of the front fan for pitch trim and assumes that the thrust of the two lift/cruise fans is altered by 3.5% to maintain a constant level of total thrust. The variation is from a setting for trim in the static free air hover condition.

### 5.3 Jet Induced Aerodynamic Forces and Moments at Forward Speeds

The presence of the nacelle and the fan efflux produce large interference forces on the model. These forces are a strong function of the thrust coefficient and the angle and location of the jet relative to the wing. This is essentially a jet-flap type of effect with the added complication that the nacelle, at high  $\lambda$ 's represents a large bluff body. The data of the following sections are presented as a function of  $C_J$ , the total thrust coefficient of all three fans. Unless otherwise noted, the distribution of thrust among the three fans is as indicated by Figure 16. Some of the plots contain the notation " $C_J = \text{RAM}$ ". This indicates that the gross thrust was set to a value approximately equal to the ram drag by adjusting the RPM until fan exit total pressure was approximately equal to free stream total pressure.

#### 5.3.1 Effect of Thrust on Aerodynamic Lift

The induced effect of the propulsion system on lift is illustrated in Figure 27 for a value of thrust coefficient representative of STO lift-off. The direct thrust component has been subtracted from the data and the baseline run shown is the nacelles-off case. It is seen that the propulsion system induces an increase in the lift coefficient at all angles of attack. The maximum aerodynamic lift coefficient and the angle at which it occurs are both increased by the propulsion system. For both nacelle tilt angles shown ( $\lambda = 50^\circ$  and  $\lambda = 90^\circ$ ) the increase in maximum aerodynamic lift coefficient is about .28 which is a 19% increase from the nacelles-off value.

The propulsion induced lift effects as a function of thrust coefficient are summarized in the following paragraphs.

#### 5.3.2 Effect of Thrust on Aerodynamic Lift at Constant Angle of Attack

The effect of thrust coefficient on model aerodynamic lift at various  $\lambda$ 's is summarized in Figure 28. For  $\lambda = 0^\circ$  the effect of  $C_J$  is seen to be small. It is slightly favorable when only the L/C fans are

operating and slightly adverse when, in addition to the L/C fans, the nose fan is operated at about 30% thrust (the nose fan doors were open in both cases).

When  $\lambda$  is increased to  $50^{\circ}$  the lift at  $C_J = 0$  is unaffected (although this may result from a trade of lift gain on the nacelles for lift loss on the wing). As  $C_J$  is increased a positive lift increment of about .4 is realized followed by a declining lift above  $C_J = 3.0$ . The decrease at higher  $C_J$ 's is apparently associated with the adverse effect of the nose fan thrust as will be discussed below.

At  $\lambda = 90^{\circ}$  and  $C_J = 0$  the nacelle causes a  $C_{LA}$  loss of about .4 relative to the level at  $\lambda = 0^{\circ}$ ,  $C_J = 0$ . The nacelle is very close to the wing trailing edge and its pressure field apparently prevents development of the normal flow over the inboard wing. As  $C_J$  is increased the  $C_{LA}$  increases and at  $C_J = 5.5$  it reaches a level about .6 above the  $\lambda = 0^{\circ}$  level. At this point, the curve has become very flat and possibly would turn down at higher  $C_J$  due to the adverse nose fan effect. The beneficial effect of  $C_J$  extends to higher values at  $\lambda = 90^{\circ}$  (compared to  $\lambda = 50^{\circ}$ ) apparently because of the relatively greater influence of the L/C jets at the higher angle.

The adverse nose fan effect mentioned above is demonstrated in Figure 29. In this case, the incremental induced lift due to nose fan thrust is plotted with the base level being the value of induced lift when the nose fan is set for static moment trim. The nose fan thrust values which result in static moment trim at each  $\lambda$  are indicated on the plot. For the STOL case ( $\lambda = 50^{\circ}$ ) it is seen that reducing the nose fan thrust to zero produces a  $C_{LA}$  gain of .3. The effect is similar at  $\lambda = 0^{\circ}$  (note that the nose fan thrust used as reference level was lower at  $\lambda = 0^{\circ}$ ). At  $\lambda = 90^{\circ}$  the range of nose fan thrusts tested was too small for good definition but a similar trend is indicated within the data accuracy.

It is of interest to compare the present lift results with those of

Reference 1 which represent a large scale model of a somewhat similar configuration. Both configurations have a nose fan and two lift/cruise fans, however, the present configuration obtains thrust vectoring by tilting the L/C nacelles while the Reference 1 configuration utilizes a thrust vectoring exhaust nozzle. In order to make the comparison the data of the present test were converted to the form found in Reference 1. This involves taking the difference in aerodynamic lift between a powered lift case and a reference case and dividing by the total gross thrust of the former. The reference case used, as in Reference 1, is with nose fan covered and L/C thrust undeflected at a large  $V/V_J$  value. The results are shown in Figure 30. It is seen that the propulsion induced lift of the two configurations is similar. The present configuration has somewhat higher propulsion induced lift at typical STO jet deflection angles.

### 5.3.3 Effect of Thrust on Maximum Aerodynamic Lift

The effect of thrust on maximum aerodynamic lift coefficient is shown in Figure 31. At  $\lambda = 0^\circ$  the effect of thrust is slightly beneficial when the nose fan is at zero thrust but is detrimental when the nose fan is set at a value which trims the static thrust moments. Increasing  $\lambda$  progressively lowers  $(C_{LA})_{max}$  when the thrust is zero. As the thrust is increased at  $\lambda = 50^\circ$  or  $\lambda = 90^\circ$  a further decrease in  $(C_{LA})_{max}$  occurs up to about  $C_J = 1.5$  followed by a recovery of maximum lift at higher  $C_J$  values. At the highest  $C_J$  values tested the maximum aerodynamic lift is increased by about .2 compared to the  $\lambda = 0^\circ$ ,  $C_J = 0$  case.

The effect of thrust balance between the L/C fans and the nose fan on the maximum aerodynamic lift is shown in Figure 32. At  $\lambda = 0^\circ$  and  $\lambda = 50^\circ$  the nose fan thrust is clearly detrimental to  $(C_{LA})_{max}$  while at  $\lambda = 90^\circ$  the range of nose fan thrust values tested was too small to reveal any effect on  $(C_{LA})_{max}$ .

THE BOEING COMPANY

#### 5.3.4 Effect of Thrust on Aerodynamic Drag

The effect of thrust on the aerodynamic drag is illustrated in Figure 33. In this case, the data have been plotted in terms of drag increment from the zero thrust case. This presentation is used because it is felt that the actual drag levels of the model must be adjusted for the nonrepresentative strut fairing as discussed later on (see configuration component effects).

Figure 33 shows that the effect of power is to increase the aerodynamic drag at a given value of aerodynamic lift. As  $C_J$  is increased, a limiting value of this adverse drag increment is reached with both the limiting drag increment and the  $C_J$  at which it is reached being dependent on  $\lambda$ .

The effect of thrust balance between the nose fans and the L/C fans is shown in Figure 34. Compared to the very large effect of thrust level, it is seen that the thrust distribution has a relatively small effect on drag. For the CTOL case ( $\lambda = 0^\circ$ ) increasing the nose fan thrust ratio from 0 to .3 has a beneficial effect while the STOL case ( $\lambda = 50^\circ$ ) shows an adverse effect of increasing nose fan thrust. The range of data at  $\lambda = 90^\circ$  is too small to reveal any trends.

#### 5.3.5 Effect of Thrust on Pitching Moment

The induced effect of thrust on the aerodynamic component of pitching moment is shown in Figures 35 thru 37 for tail-on and tail-off cases at various engine tilt angles. Some general observations will be made from these curves before summarizing the effects of power upon trim requirements and stability parameters in the succeeding paragraphs.

When the nacelles are tilted (Figures 35 and 36) the pitching moment curves are seen to display a double break characteristic with a first nose-up break occurring at a lift coefficient between about .6 and 1.2, depending on nacelle tilt angle and thrust level, and a second break occurring at higher lift coefficient when the wing stalls. With the

THE BOEING COMPANY

nacelles not tilted (Figure 37), the break is not so prominent. In the following discussion reference to low  $C_L$  and high  $C_L$  will be used to indicate the regions which are, respectively, below and above the first pitching moment break.

At  $\lambda = 90^\circ$  (Figure 35) it is seen that the tail provides a large increase in stability at low  $C_L$  values but not at high  $C_L$ 's. The tail contribution to stability at low  $C_L$ 's is seen to increase with increasing thrust coefficient.

At  $\lambda = 50^\circ$  (Figure 36) the tail-off configuration is seen to be stable at low  $C_L$  values. However, the tail contribution to stability in this case is much less than at  $\lambda = 90^\circ$ . Also the sensitivity of tail-on stability to power at low  $C_L$ 's is greatly reduced at  $\lambda = 50^\circ$  compared to  $\lambda = 90^\circ$ . At higher  $C_L$ 's the tail is seen to provide a stability increase at the high  $C_J$  values.

In the loiter configuration, flaps up with  $\lambda = 0^\circ$ , an increase in thrust coefficient produces a small increase in tail-off stability as seen in Figure 37. It is also seen that when the tail is on, an increase in  $C_J$  appears to have little effect on stability, as far as can be determined with the relatively small number of data points for the power-off case. This data represents the high speed end of the V/STOL flight envelope. For this case, it is important that the tail provide all of the stability and control functions. It is clear that the tail is providing effective alpha stability. Trim requirements appear to be within airplane capability with the nose fan disengaged.

### 5.3.6 Effect of Thrust on Trim Requirements

Because of the high degree of non-linearity in the data (Figures 35 and 36) any summary of trim requirements becomes dependent on the conditions chosen to perform the analysis. To illustrate the effect of power and nacelle tilt angle on trim requirements, pitching moment will be summarized for a constant value of aerodynamic lift coefficient,  $C_{LA} = 1.0$ .

THE BOEING COMPANY

The effect of thrust on pitching moment for the tail off configuration is summarized in Figure 38. The result obtained for aerodynamic pitching moment is strongly dependent on the manner in which ram moments are accounted for. The method of removing ram moments has been described in detail in Appendix C. The effect of ram drag is to produce a large positive pitching moment proportional to  $C_j$ . It is seen in Figure 38, that for all values of  $\lambda$  this moment is at least partially compensated by the negative value of aerodynamic pitching moment induced by thrust effects. For  $C_j$  below 3.0 at  $\lambda = 50^\circ$  the negative induced moment is even greater than the positive ram moments with the result that the total moment is negative. For  $\lambda = 0^\circ$  and nose fan inoperative, the total moments are nose down. By first removing the direct thrust moments, then removing the ram moments, it can be seen as stated above, that for this case also, the ram moments are positive and are partially offset by the negative aerodynamic moments. As discussed in Appendix C, the model ram force is less than that which will occur full scale at the same thrust coefficient. The required correction to full scale has been made for the cases shown in Figure 38, as shown by the curves thus labeled in that figure.

The moments resulting from ram forces and aerodynamic forces can be trimmed by varying the thrust distribution, by changing horizontal tail incidence, or by some combination of these two methods. Figure 39 illustrates the change in thrust distribution required if the moments are trimmed entirely by means of thrust forces (the data shown are tail-off). An iteration was performed to allow for the fact that ram moment changes as the thrust distribution is changed. The ram moments used were those which had been corrected to full scale and it was assumed that the nose fan and L/C fan thrusts were collectively changed so as to hold total thrust constant. It is seen that the nose fan thrust ratio reduction required for trim is about .10 at  $\lambda = 50^\circ$  and .20 at  $\lambda = 90^\circ$  relative to the static hover case.

### 5.3.7 Effect of Thrust Upon Longitudinal Stability and Control Parameters

Several longitudinal stability and control parameters have been evaluated

for the tested configurations and are summarized in Figures 40 thru 44. These include lift curve slope, neutral point location, horizontal tail effectiveness and downwash at the horizontal tail. It should be remembered that only the aerodynamic characteristics are being analyzed in that the effects of thrust and ram forces have been excluded.

The aerodynamic lift curve slopes are presented in Figure 40. The nacelles are shown to produce an increase in lift curve slope while in their untilted position. Tilting the nacelles degrades the lift curve slope. The effect of thrust is to increase lift curve slopes for the CTOL and STOL configurations, while it was found that thrust increases reduce the lift curve slopes of the cruise and VTOL configuration.

As discussed in the previous section, the pitching moment curves exhibit a double break characteristic. Hence, evaluation of the aerodynamic neutral point location (i.e., the center of gravity position at which the aerodynamic contribution to static stability is zero) was conducted separately for low lift values (Figure 41) occurring below the first break in the pitching moment curve and for higher lift values (Figure 42) occurring between the first break and wing stall. The analysis was conducted only at low lift values for the VTOL configuration since the first break occurs at fairly high lift levels. Neutral point locations are presented with the horizontal tail set at zero incidence and with tail-off. For comparison, the neutral point location with nacelles and horizontal tail removed is also presented. At the lower lift levels (Figure 41) it is seen that for all tilt angles the complete configuration is more stable than the nacelles-off tail-off configuration. In all cases presented, the horizontal tail contributes to the stability. The smallest contribution made by the tail is at  $\lambda = 50^\circ$ . The stability of the cruise and STOL configurations is relatively insensitive to thrust increases, whereas the stability of the VTOL configuration is significantly increased at high thrust values. For high lift levels (Figure 42) the general trend with thrust for the cruise configuration remains the same. For  $\lambda = 50^\circ$  the complete configuration is slightly less stable than the nacelles-off tail-off configuration at low  $C_L$ .

THE **BOEING** COMPANY

values and shows a further decrease in stability at thrust coefficients above 3.5. Comparison of tail-on versus tail-off for both the cruise and STOL configurations indicates that the tail still contributes to the longitudinal stability.

Figure 43 presents the horizontal tail control effectiveness. The control effectiveness is the change in pitching moment due to changes in horizontal tail incidence ( $\partial C_{PM_A} / \partial \alpha$ ). The figure compares the tail control effectiveness measured in the test with a pre-test theoretical estimate. For the cruise and STOL configurations, the tail effectiveness is near the theoretical value and is not appreciably affected by thrust variation. The tail effectiveness of the VTOL configuration is far below the theoretical level when power is off, but is shown to approach the theoretical level with increasing thrust.

The downwash gradient at the horizontal tail is shown in Figure 44. This parameter was computed from the intercepts of the lower part of the plots of aerodynamic pitching moment as a function of angle of attack for horizontal tail-off and for horizontal tail-on at two different incidence angles. The intercepts of the tail-off and tail-on curves provide the angle of attack at which downwash is equal to the horizontal tail incidence. For the cruise and STOL configurations, an increase in thrust coefficient increases the downwash gradient while it decreases with thrust for the VTOL configuration. This relates to the previous discussion of neutral point location which showed that the contribution of the horizontal tends to diminish with thrust for the STOL configuration and tends to increase with thrust for the VTOL configuration.

#### 5.4 Cross-Wind and Differential Thrust Effects

The effects of differential thrust and sideslip upon the model in its VTOL configuration ( $\lambda = 90^\circ$ ) were investigated at sideslip angles of  $0^\circ$ ,  $5^\circ$  and  $10^\circ$  (Figures A.7, A.8, and A.9 in Appendix A). Yawing moments are somewhat difficult to interpret due to large zero shifts in that balance component. This problem is illustrated in Figure 45 which shows yawing moments as a function of angle of attack for several configurations and sideslip angles with  $\lambda = 90^\circ$  and  $C_J = 3.7$ . It is seen that the data at zero sideslip indicates a yawing moment coefficient of about +.03. However, the zero shifts encountered for the group of runs shown in the figure ranged from 0 to +.02 with a shift of +.015 being typical. This amount of uncertainty could well affect the interpretation of the data. Because of this problem, it is felt that the cross-wind characteristics are not definitive. Assuming, however, that the model had no residual yawing moments at  $\beta = 0^\circ$ , the data at both sideslip angles would indicate the configuration was stable in that mode over most of the angle of attack range with neutral stability at low angles of attack. The contribution of the vertical tail surface is marginally stabilizing at  $\beta = 5^\circ$  and destabilizing at  $\beta = 10^\circ$ .

The lateral-directional static derivatives for the VTOL configuration at angles of attack near zero are shown on Figure 46. This analysis indicates that for the most part, the configuration is statically stable except for the directional stability. The directional stability is degraded by increased thrust but improves dramatically with angle of attack as shown on Figure 46 by the data at  $\alpha = 8^\circ$ . As mentioned above, if the model is assumed to have no residual yawing moments at  $\beta = 0^\circ$ , the directional stability would be neutral to positive for all thrust values. This analysis is based on the data shown on Figure A.10 thru A.17 of Appendix A. The increments shown are the difference between the  $\beta = 0^\circ$  and  $\beta = 5^\circ$  data.

The effect of differential thrust upon the model in its VTOL configuration was found to be negligible (Figures A.7, A.8 and A.9 in Appendix A). The

THE **BOEING** COMPANY

thrust differential amounted to as much as a 20% increase in the nose fan thrust from its nominal setting for the fore-and-aft differential, and a 20% reduction in one of the lift/cruise fans for the side-to-side differential. In some cases, the differential was produced by increasing the thrust of one lift/cruise fan while reducing the thrust of the other. The differential thrust effects did not change with side-slip angle. Note that in Figures A.8 and A.9, the differential thrust effects were only explored near zero pitch angle.

## 5.5 Configuration Component Effects

A limited amount of configuration buildup testing was performed as summarized in this section. The discussion will generally be limited to the lift and pitching moment effects because the drag data are generally not sufficiently accurate to allow comparisons of relatively small differences between configurations. Some of the drag data are discussed in a separate paragraph at the end of the section.

### 5.5.1 Effect of Nacelles

The effect of nacelles on the tail-off lift and pitching moment data is shown in Figure 47 and Figure 48 for the CTOL and loiter configurations, respectively. It is seen that the nacelles produce a negative change in lift at low angles of attack but increase the lift curve slope and result in an increase of about .13 in maximum lift coefficient. For both flaps-up and flaps-down cases, the nacelles produce an increase in tail-off stability.

### 5.5.2 Effect of Flaps

The effect of extending the trailing edge flaps and leading edge slats is shown in Figure A.33 (Appendix A) for the CTOL configuration and Figure A.37 (Appendix A) for the nacelles-off case. For both the nacelles-off case and the CTOL at ram thrust case, the increment in maximum lift coefficient due to flaps is about .50. The somewhat larger increment of .65 for the power-on case is due to a premature stall for the power-on flaps-up case. For the CTOL power-off and the nacelles-off cases, there is no change in stability due to flaps while the flaps are slightly stabilizing for the CTOL power-on case. It is noted that the negative shift in pitching moment due to flaps is much less with the nacelles on than for the nacelles-off case.

### 5.5.3 Effect of Aileron Droop

The effect of drooping both ailerons  $15^{\circ}$  on the STOL configuration is shown in Figure A.28 (Appendix A). It is seen that a gain in maximum

lift coefficient of about .2 was realized.

#### 5.5.4 Effect of Nacelles on Drag Level

The effect of the nacelles upon drag for the ram thrust case is summarized in Figure 49 in terms of  $C_{DA}$  as a function of nacelle tilt angle. Two curves are shown, one for the basic nacelle strut and one for a modified nacelle strut. Out of necessity, a portion of the lift/cruise fan nacelle strut was rotated with the nacelles during the wind tunnel test program to cover plumbing to the turbopowered simulators and the "blown" primary. That fairing, which would not be present on the full scale airplane, had a large effect upon the drags of the STOL and VTOL test configurations. To assess the drag difference due to the fairing, a test run was made with the fairing removed and tape and wax applied to cover and fair over the exposed plumbing and instrumentation. The basic fairing and an indication of the wax fairing are shown in Figure 7. The reduction in drag coefficient due to removing the basic fairing amounted to about .15. A further reduction is anticipated if the plumbing and instrumentation and their fairing could have been eliminated. Also presented in Figure 49 is an estimate of the STOL configuration drag from Reference 9. It is seen that the estimated level is very close to the level measured on the model. This indicates that the estimate is probably conservative for the power-off case since the model drag level is believed to be subject to further reduction with a more representative nacelle strut fairing.

## 6.0 CONCLUSIONS

1. Propulsion induced forces and moments measured during static ground tests were found to be small and showed no sudden changes with variation of ground height, pitch and roll.
2. A hover lift loss of 2% of gross thrust was found for heights far from the ground. With the model in a level attitude, there was no additional lift loss due to ground effect at any ground height. The largest induced lift loss due to ground effect occurred at a combination of  $10^0$  of pitch and  $10^0$  of roll where a loss equal to 5% of gross thrust was measured.
3. Observed induced moments for static hover in ground effect can be trimmed with less than 7% variation of nose fan thrust from the value for free air static trim.
4. Usable propulsion induced lift for the STOL configuration was found to be 19% of the nacelles-off lift level. The increment is based on maximum lift.
5. Drag levels measured with lift/cruise fans tilted are not representative of the drag of the full scale airplane due to non-representative nacelle struts which rotated with the lift/cruise fans out of necessity to cover plumbing to the turbo-powered simulators. The aerodynamic drag tended to increase with thrust.
6. Propulsion induced aerodynamic (wing) pitching moments were large nose-down moments with the lift/cruise fans tilted. The ram moments are counteracting, thereby reducing trim requirements.
7. The effect of the nacelles on longitudinal stability is very dependent on nacelle tilt angle, angle of attack, and thrust coefficient. In general, the nacelles tend to be stabilizing at low nacelle angles and destabilizing at the highest nacelle angles.

THE **BOEING** COMPANY

8. The effect of increasing thrust coefficient is generally to increase the longitudinal stability, especially at high nacelle tilt angles.
9. The VTOL configuration has good directional stability at high angles of attack which degrades as angle of attack is reduced.

## 7.0 REFERENCES

1. "Wind Tunnel and Ground Static Investigation of a Large Scale Model of a Lift/Cruise Fan V/STOL Aircraft", NASA CR-137916, August 1976.
2. "Follow-On Studies for Design Definition of a Lift/Cruise Fan Technology V/STOL Airplane", Boeing Military V/STOL Group, NASA CR-137976, January 1976.
3. Curry, T. M., "Multi-Component Force Data Reduction Equations", Third SESA International Congress on Experimental Mechanics, Los Angeles, CA, May 1973.
4. Lowe, W. H., and Sanger, R. W., "Static Performance of a 13.97 cm (5.5 inch) Diameter Model VTOL Lift Fan", NASA CR-2051, May 1972.
5. "Saberliner Twin-Jet Executive Aircraft Specifications - Airplane Serial No. 292-91 and Subsequent", North American Aviation, Inc., Los Angeles, CA, June 1966.
6. Fromm, E. H., "The Boeing Flight Simulation Chamber for Static Calibrations of Engine Simulators", 45th Meeting of the Supersonic Tunnel Association, April, 1976.
7. Cull, M. J., "V/STOL Wind Tunnel Model Test and Experimental Assessment of Flow Breakdown Using Multiple Fan Model", AGARD-CPP-174.
8. "Allison PD 370-16 Compound Turbofan/Shuttle Engine, A T701 Derivative", EDR 8489, August 1975.
9. Zabinsky, J. M. and Higgins, H. C., "Design Definition Study of a Lift/Cruise Fan Technology V/STOL Airplane", NASA CR-137750, August, 1975.

10. Syberg, J., and Koncsek, J. L., "Low Speed Tests of a Fixed Geometry Inlet for a Tilt Nacelle V/STOL Airplane", NASA CR-151922, January 1977.
11. Heyson, H. H., "Linearized Theory of Wind - Tunnel Jet Boundary Corrections and Ground Effects", NASA TR R-124, 1962.
12. Trussell, D. R., "Report on WT1533, A Wind Tunnel Data Reduction Program Used to Compute Wall Corrections Based on Heyson's Interference Theory", Boeing Document D6-40794TN, 1973.
13. Heyson, H. H., "The Effect of Wind Tunnel Wall Interference on the Performance of a Fan-In-Wing, VTOL Model", NASA TN D-7518, 1974.

**FIGURE 1 - VIEW OF MODEL MOUNTED IN STATIC TEST AREA**

**ORIGINAL PAGE IS  
OF POOR QUALITY**

REF. M. 23.80 IS T-39 REFERENCE WATER LINE (FULL SCALE M. 100)

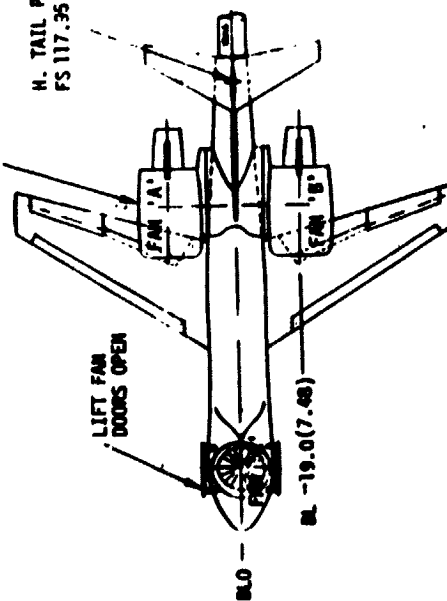
M. = MATT LINE

FS = FUSELAGE STATION

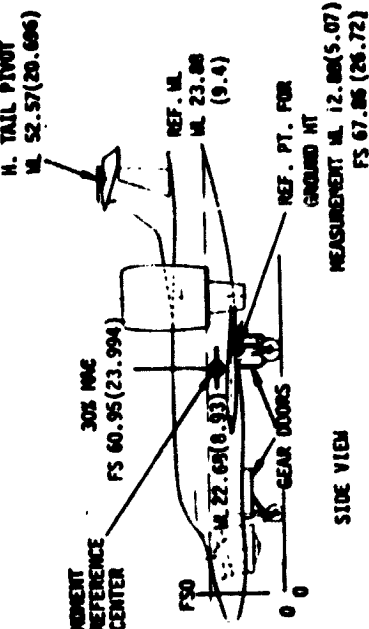
WL = WATER LINE

REFERENCE AREA OF<sup>2</sup>(in<sup>2</sup>) 2200(45.17) 523 (61.07) 341(52.85)  
 FS (IN) 127.350, 115.51.26(20.16) 22.32(9.16)  
 WL (IN) 26.25(9.46) 10.24(4.03) 14.62(5.76)

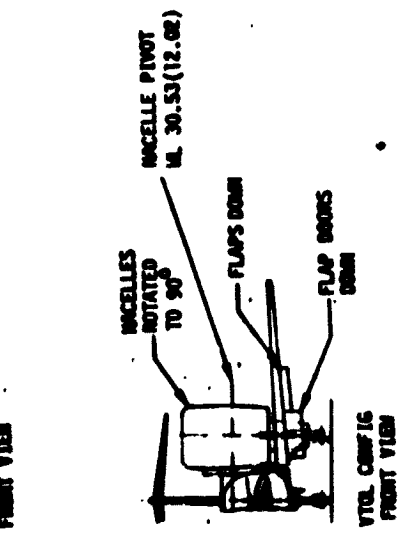
	WL	WL. TAIL	Y. TAIL
REFERENCE AREA OF <sup>2</sup> (in <sup>2</sup> )	2200(45.17)	523 (61.07)	341(52.85)
FS (IN)	127.350, 115.51.26(20.16)	22.32(9.16)	
WL (IN)	26.25(9.46)	10.24(4.03)	14.62(5.76)
ASPECT RATIO	5.77	4.95	1.59
DOVER RATIO	.325	.35	.367
WEP. 25% LINE	207.552	20.55°	30°



TOP VIEW



FRONT VIEW  
DIMENSIONS: IN (MM)      MODEL SCALE = .004  
MEASUREMENT M. 12.80(5.07)  
FS 67.86 (25.72)



SIDE VIEW

FIGURE 2 MODIFIED T-39 LIFT/CRUISE FAN AIRPLANE MODEL

ORIGINAL PAGE IS  
OF POOR QUALITY

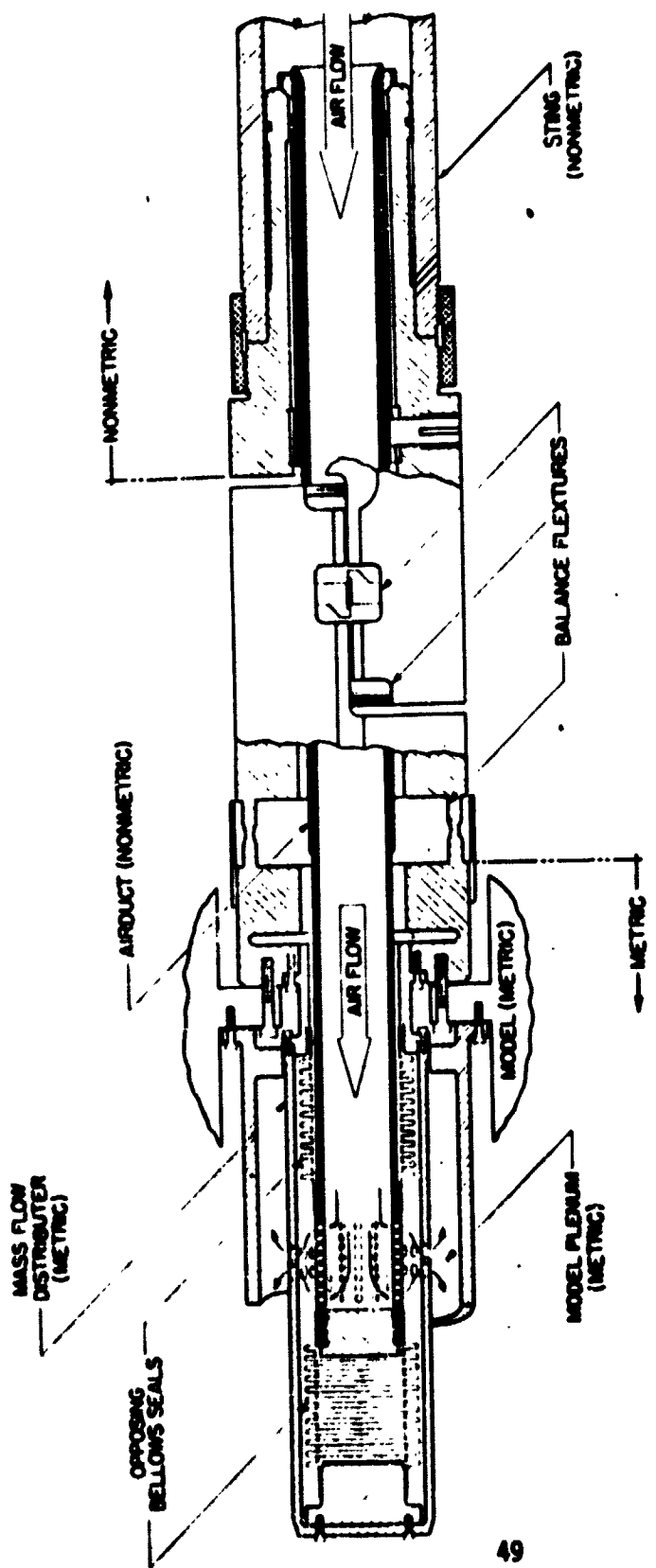


FIGURE 3 SCHEMATIC OF "FLOW-THRU" INTERNAL BALANCE

FIGURE 4 MODEL 1D-457 TIP DRIVEN FAN AND DRIVE PLENUM



ORIGINAL PAGE IS  
OF POOR QUALITY

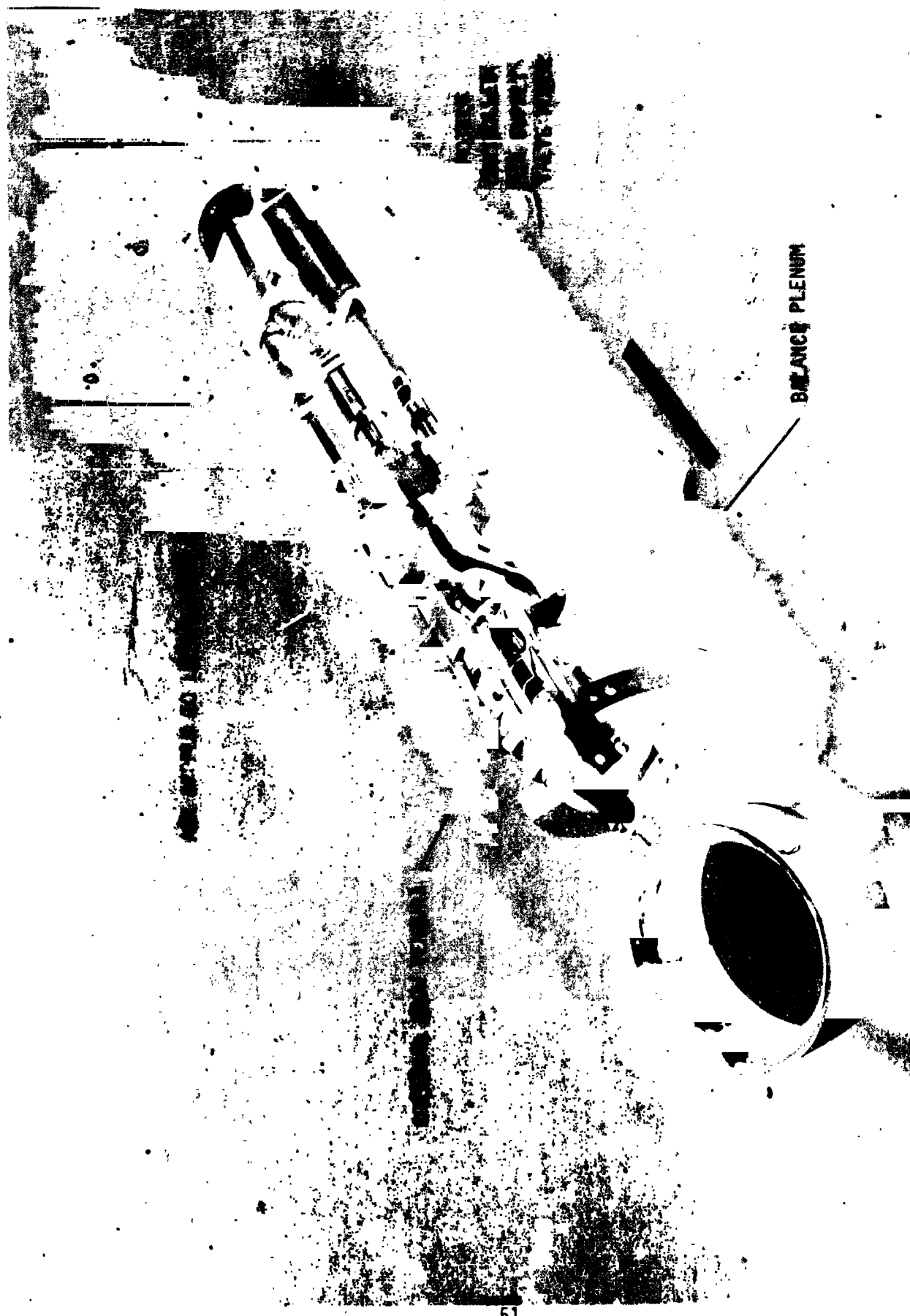


FIGURE 5 MODEL BASIC STRUCTURE

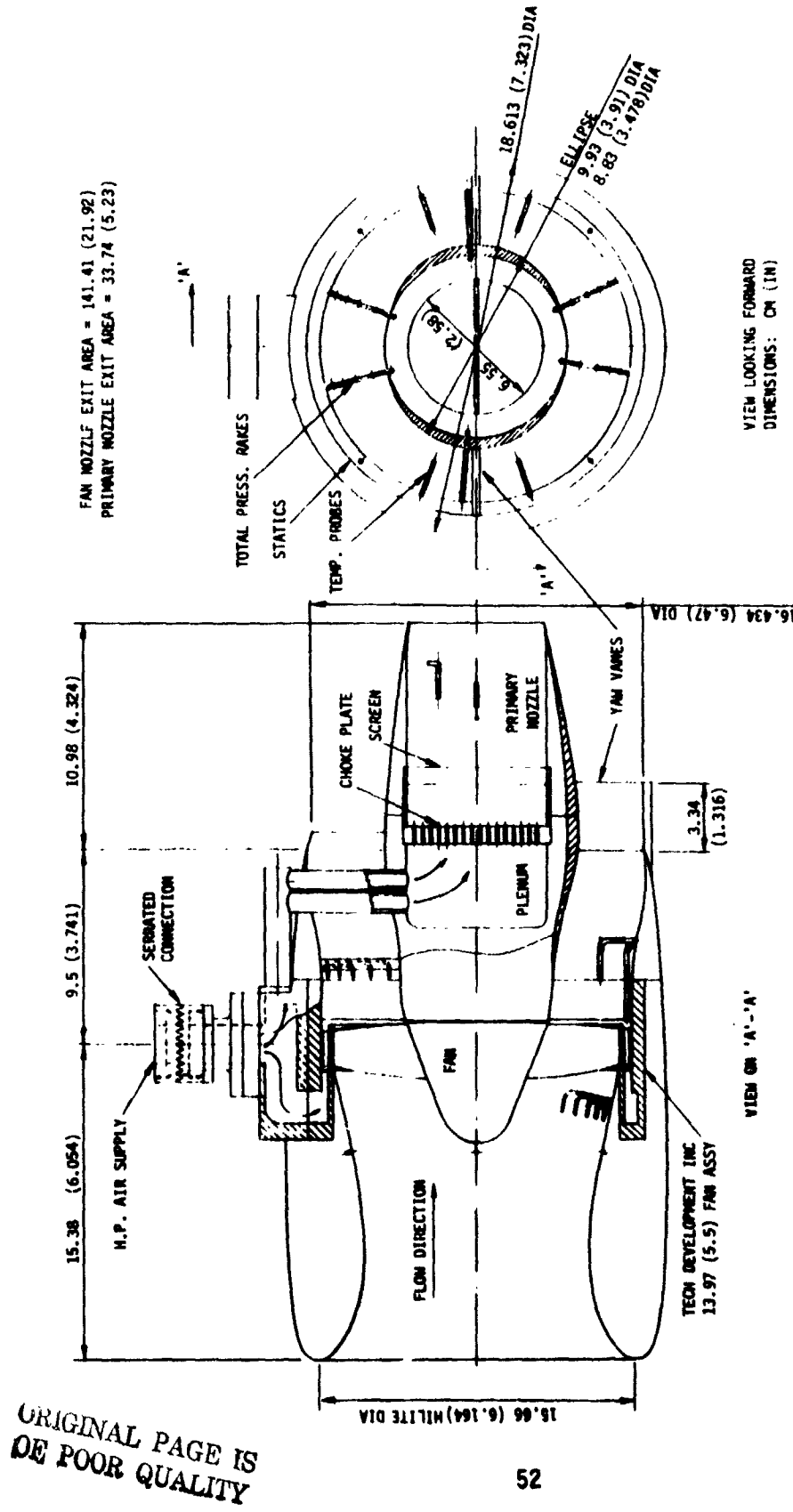


FIGURE 6 ASSEMBLY OF L/C FAN NACELLE

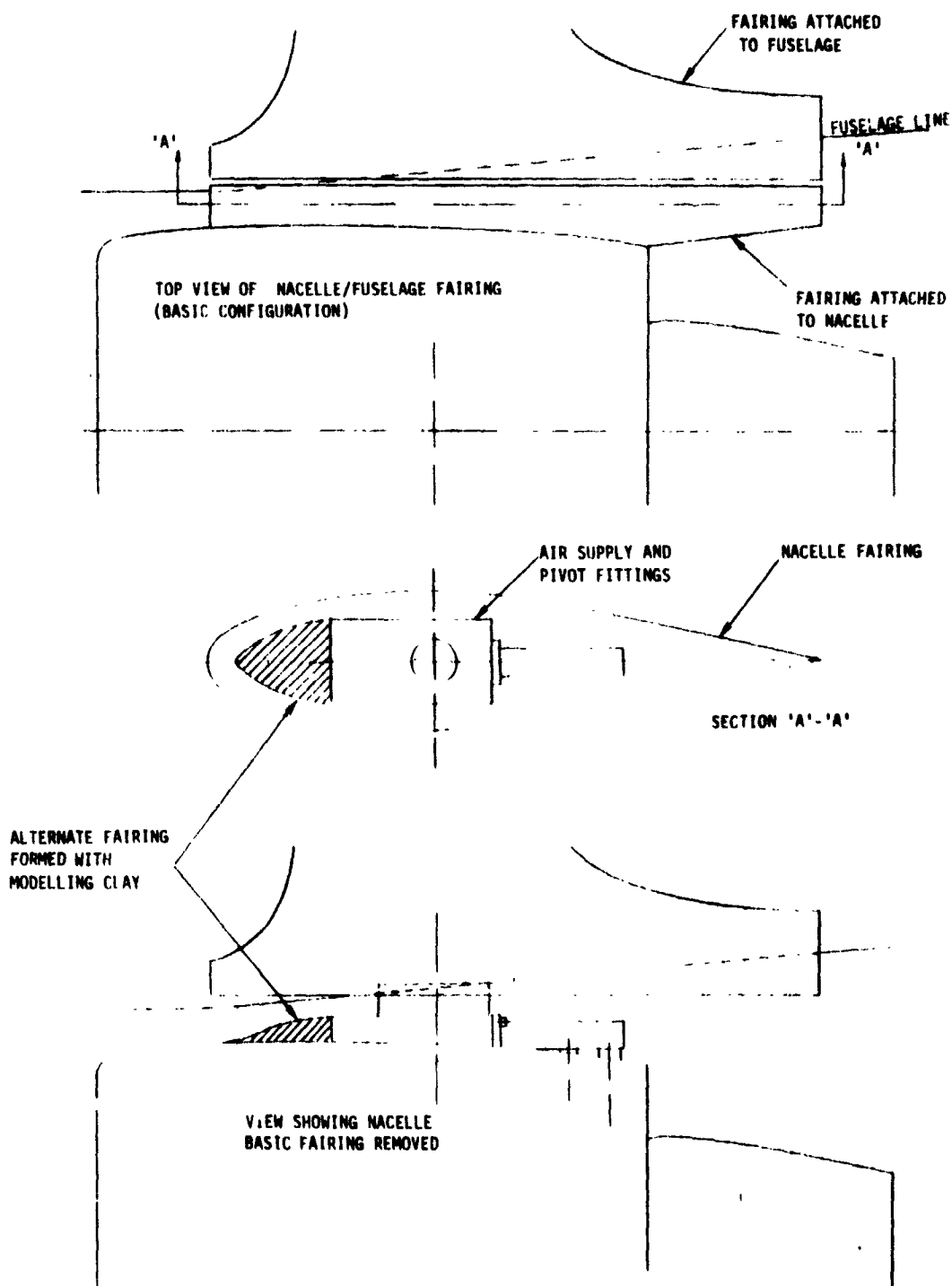


FIGURE 7 DETAILS OF NACELLE/FUSELAGE FAIRING

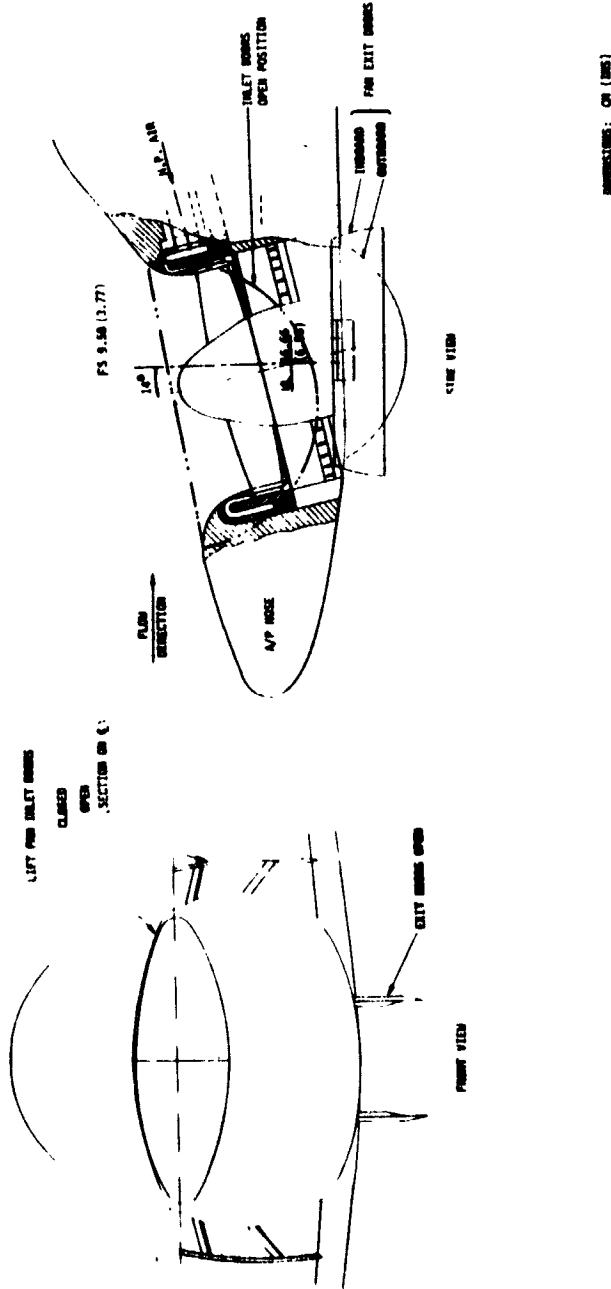


FIGURE 8 ASSEMBLY OF LIFT FAN

ORIGINAL PAGE IS  
OF POOR QUALITY

DIMENSIONS: CM (INS)

WING

- DIMS IN WING REF SYSTEM
- 0.25 MAC AT FS 59.752 (23.524)
- REF PLANE INTERSECTS PLANE OF SYMMETRY  
@ WL 15.635 (6.155)
- REF PLAN = WING CHORD PLANE @ BL = 0
- DIHEDRAL:  $3.15^{\circ}$
- SECTION: NACA 64, A212 (MOD) AT WBL = 15.021 (5.91)  
NACA 64, A012 (MOD) AT WBL = 60.87 (23.96)

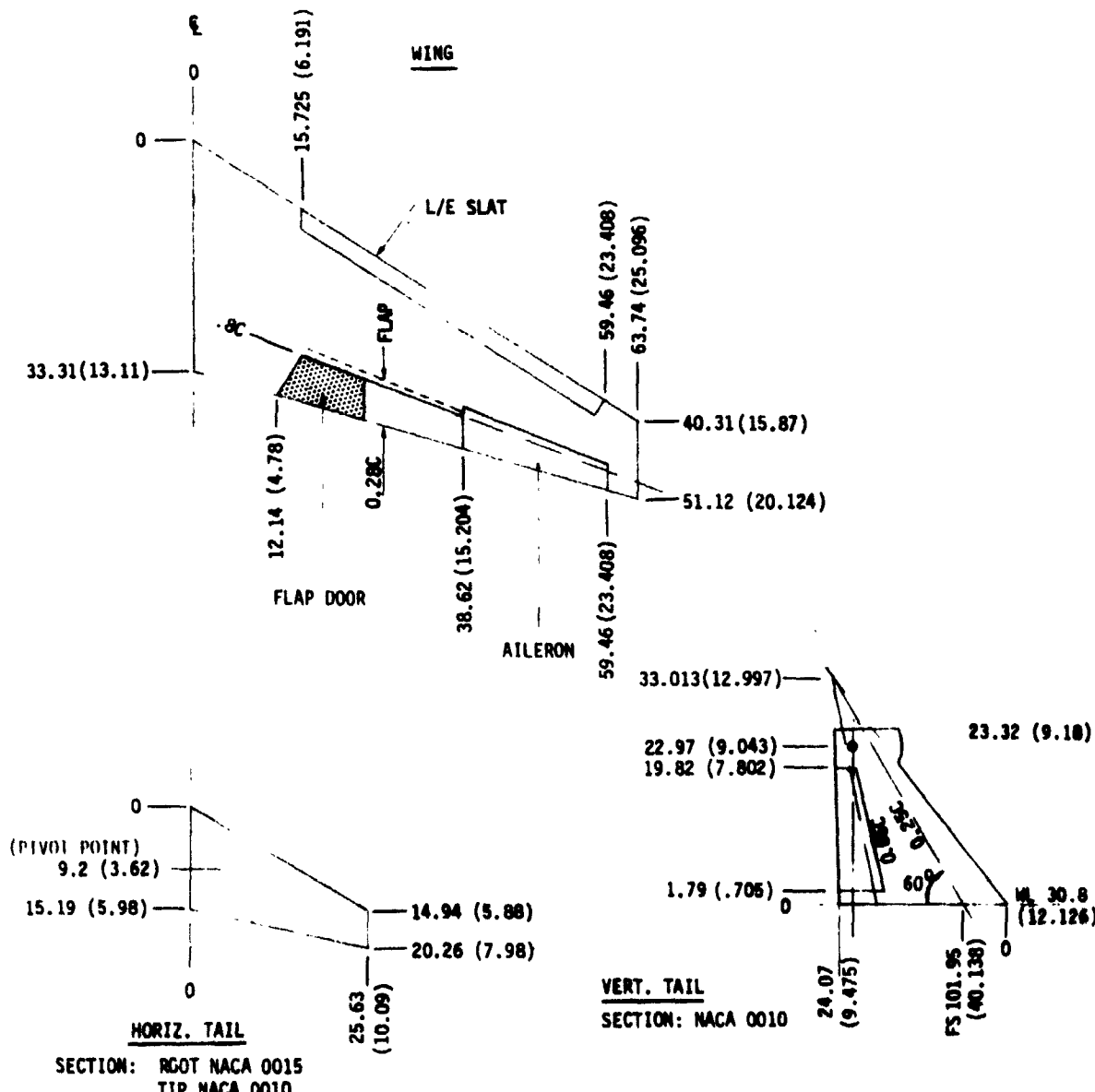
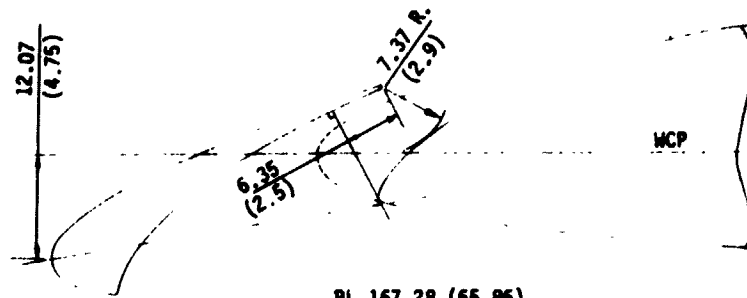


FIGURE 9 MODEL PLANFORM DETAILS



BL 167.28 (65.86)  
INBOARD EDGE OF L.E. SLAT

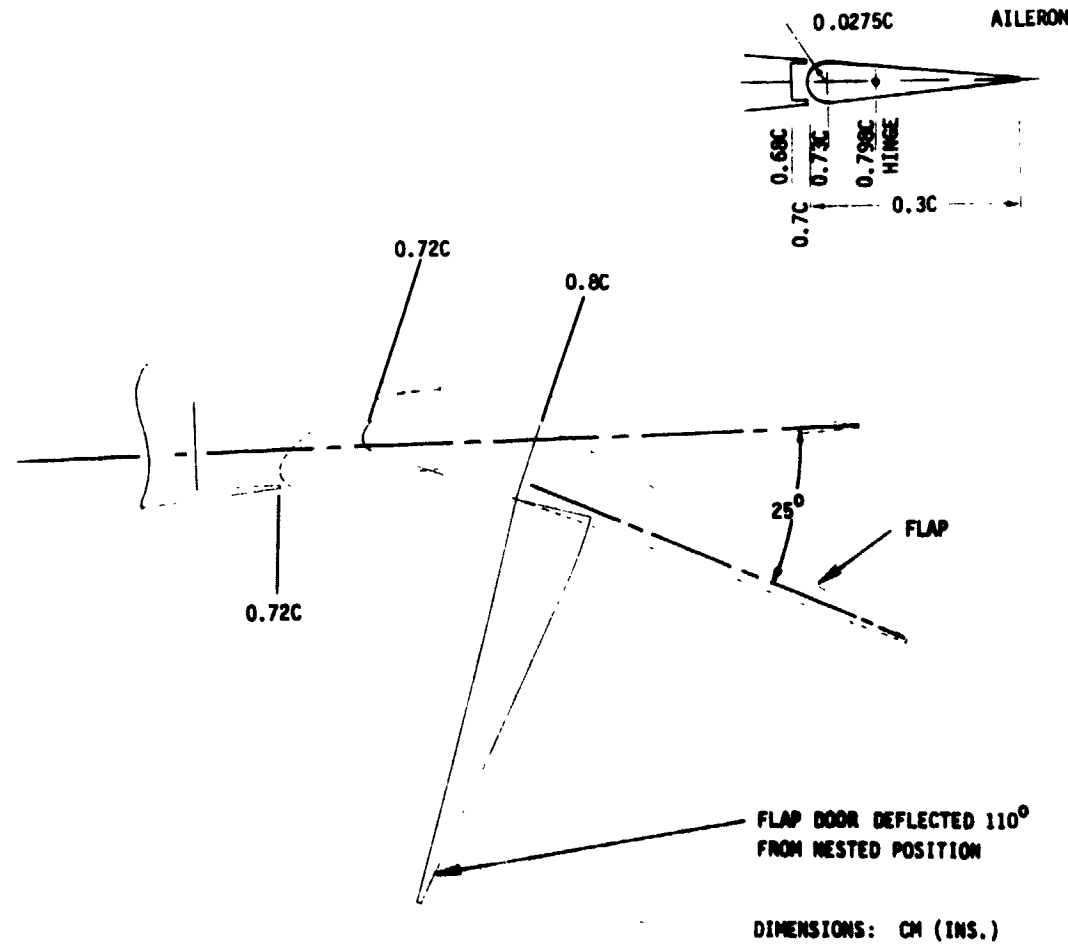


FIGURE 10 MODEL SECTION DETAILS

5E

ORIGINAL PAGE IS  
OF POOR QUALITY

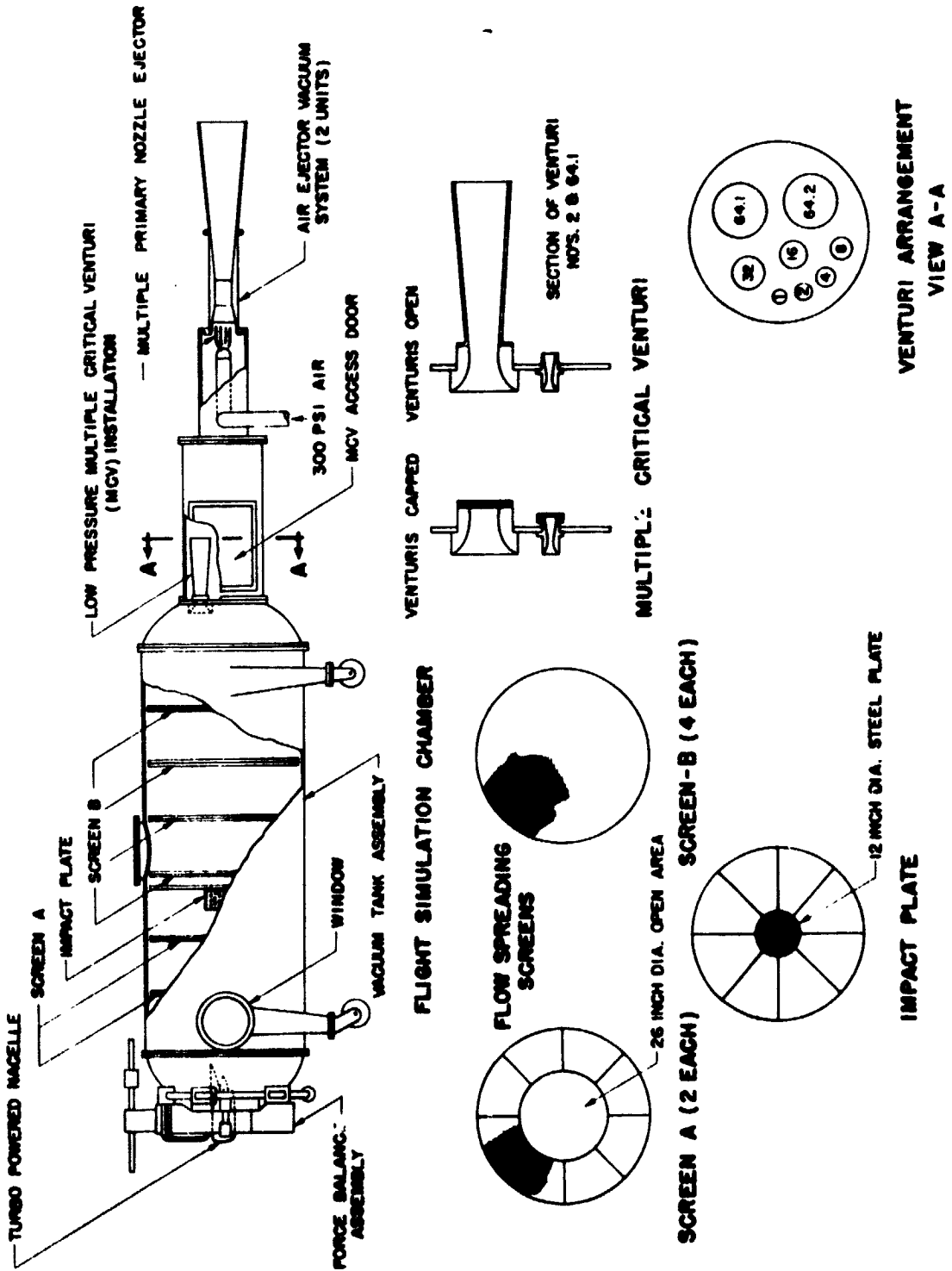


FIGURE 11 FLIGHT SIMULATION CHAMBER

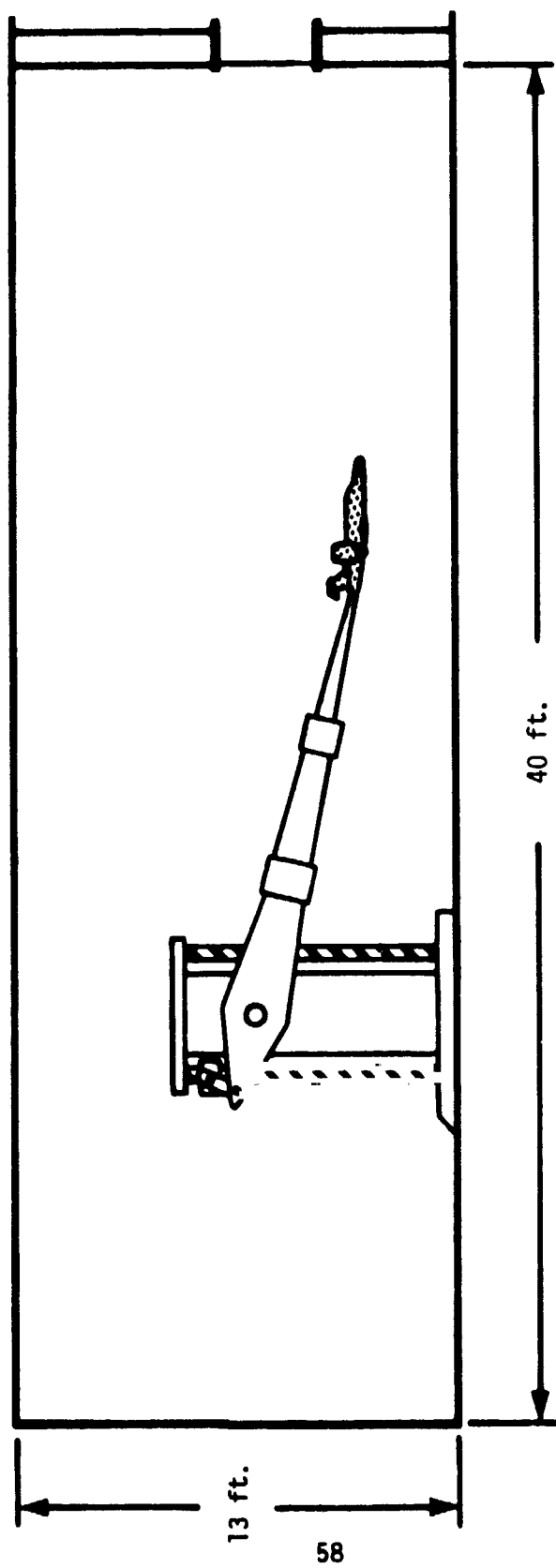


FIGURE 12 BOEING STATIC CHECKOUT FACILITIES

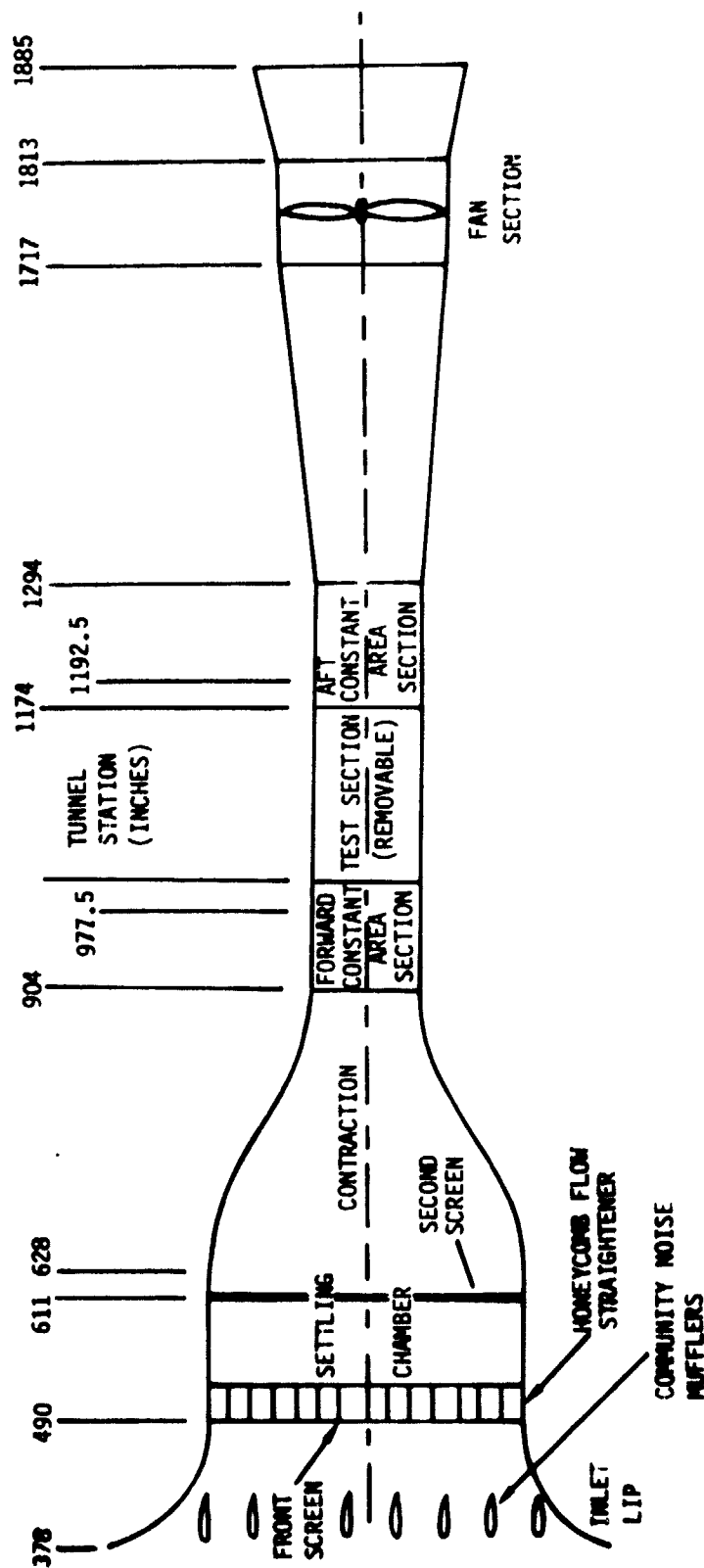


FIGURE 23 GENERAL ARRANGEMENT OF BOEING 9' X 9' WIND TUNNEL

AD 1546 D

REV SYM

ORIGINAL PAGE IS  
OF POOR QUALITY

60

BOEING NO.  
PAGE

TURBULENT CHILLING



FIGURE 14 MODEL INSTALLED IN THE BOEING 9' LOW SPEED WIND TUNNEL

CONFIGURATION	VARIABLES EXPLORED					COMPONENT EFFECT
	L/C FAN TILT ANGLE	PITCH ANGLE	YAW ANGLE	TUNNEL SPEEDS	THRUST COEF.	
VTOL	80°, 90°, 95°	-8° TO +30°	5°, 10°	65 KTS TO 120 KTS	0.0 TO 5.5	0°, 20° STABILATOR, FIN, NACELLES, GEAR
ST0	50°	-8° TO +30°	—	65 KTS TO 120 KTS	0.0 TO 5.5	0°, 10° STABILATOR, GEAR, AILERON DROOP (15°), NACELLES
CT0L	0°	-8° TO +30°	—	120 KNOTS	0.0 TO 1.2	— GEAR, NACELLES
LOITER	0°	-8° TO +30°	—	120 KNOTS	0.0 TO 1.2	0°, 10° STABILATOR, NACELLES

FIGURE 15 WING TUNNEL TEST CONDITIONS

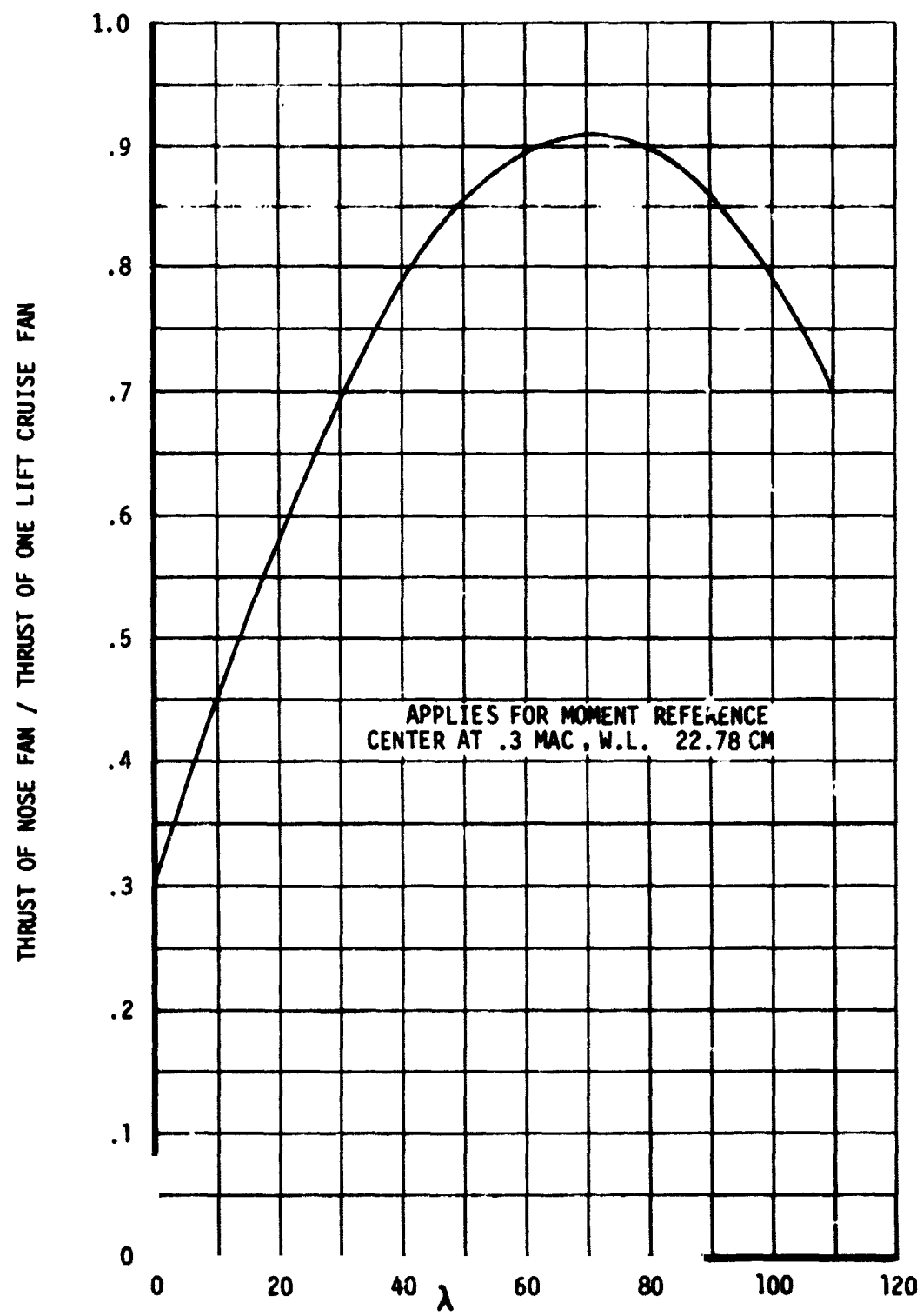
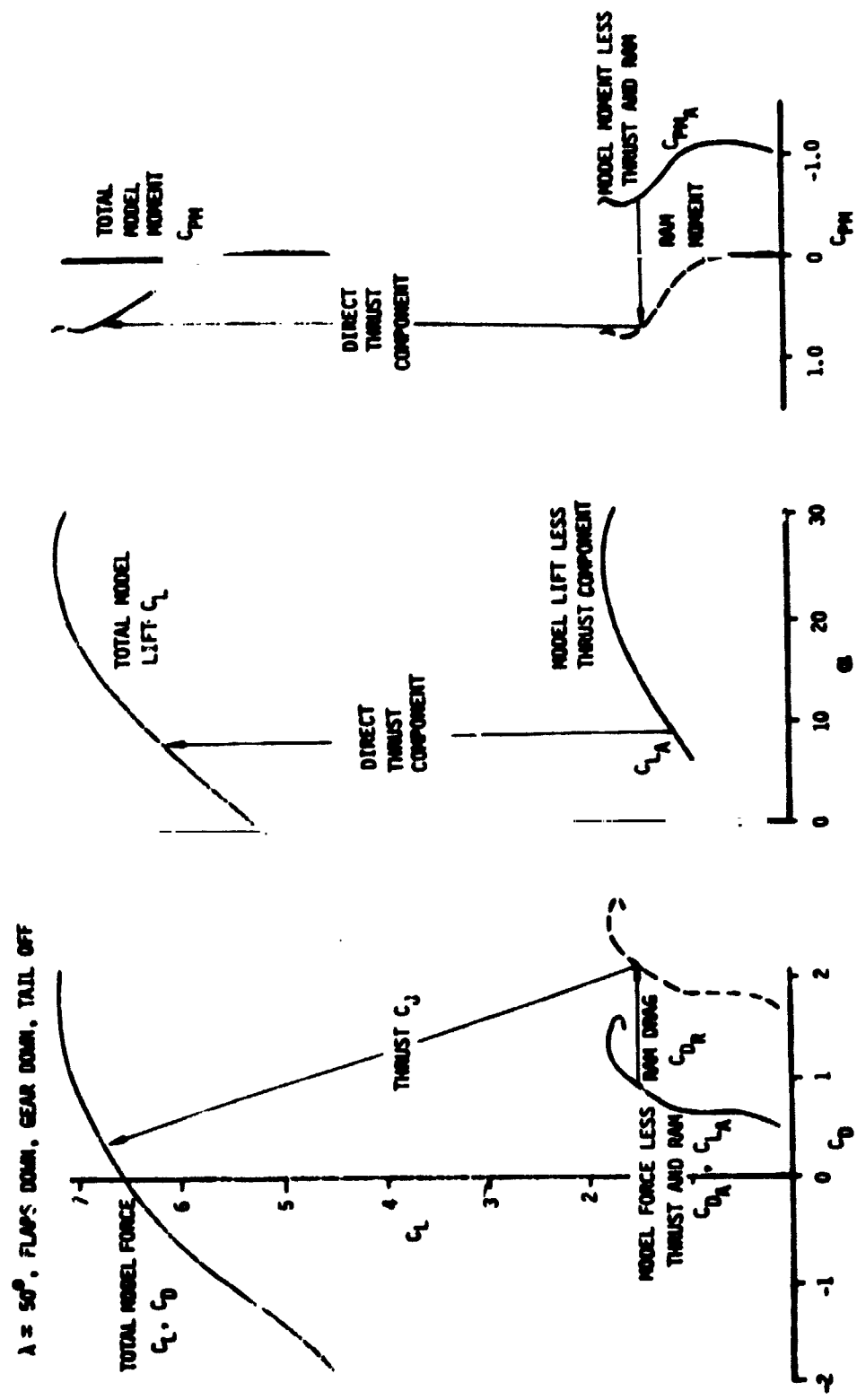


FIGURE 16 NOSE FAN THRUST REQUIRED FOR PITCHING MOMENT TRIM  
IN STATIC FREE AIR HOVER



**FIGURE 17** RELATIONSHIP OF AERODYNAMIC FORCES TO TOTAL FORCES

P.RUN	SYM	$\alpha$
127	○	0°
132	□	0°
114	◇	0°
76	△	0°

$\lambda = 90^\circ$   
 HOVER THRUST  
 $V/V_f = 0$   
 FLAPS DOWN  
 GEAR DOWN  
 $\delta = 0^\circ$

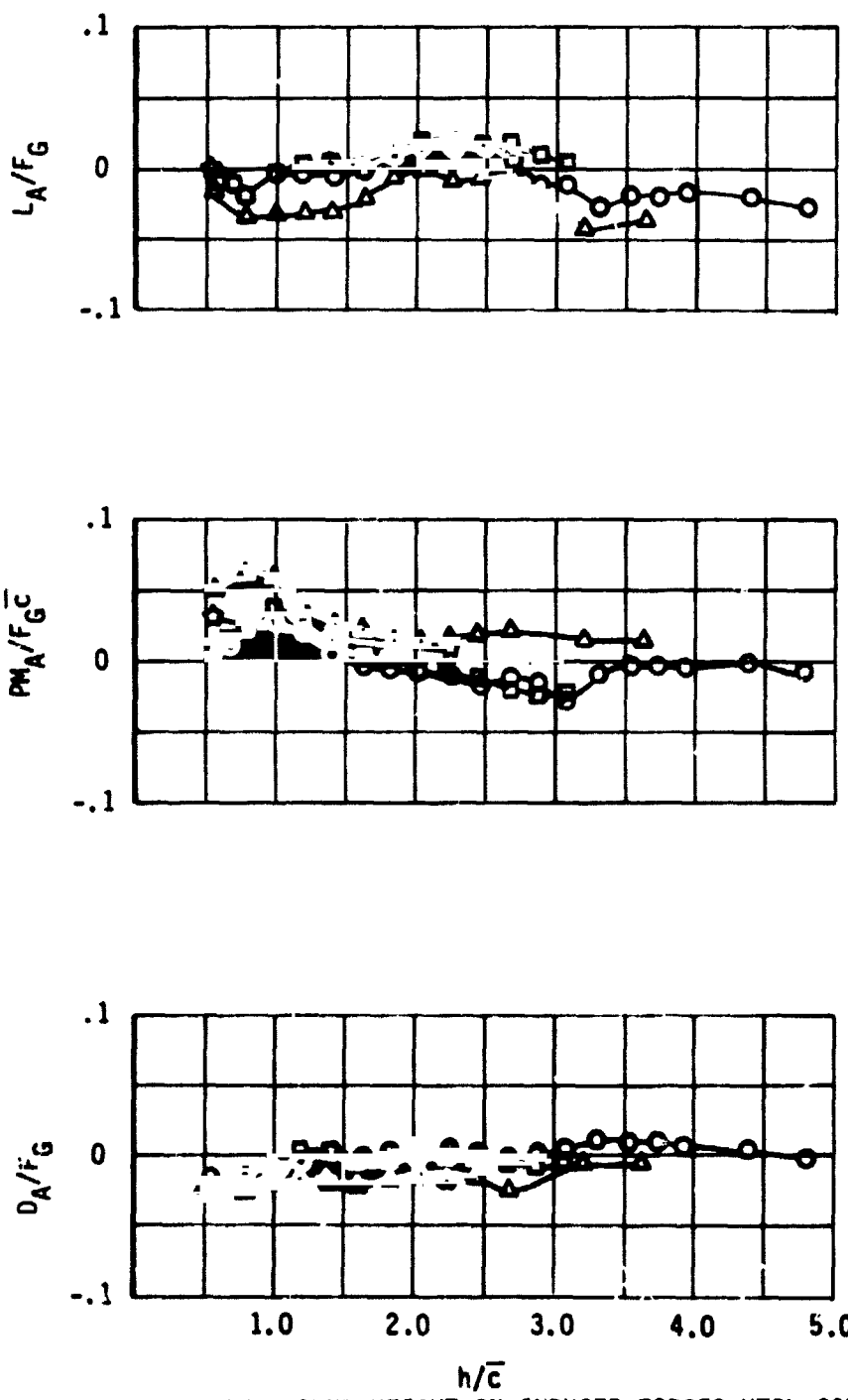


FIGURE 18 EFFECT OF GROUND HEIGHT ON INDUCED FORCES VTOL CONFIGURATION

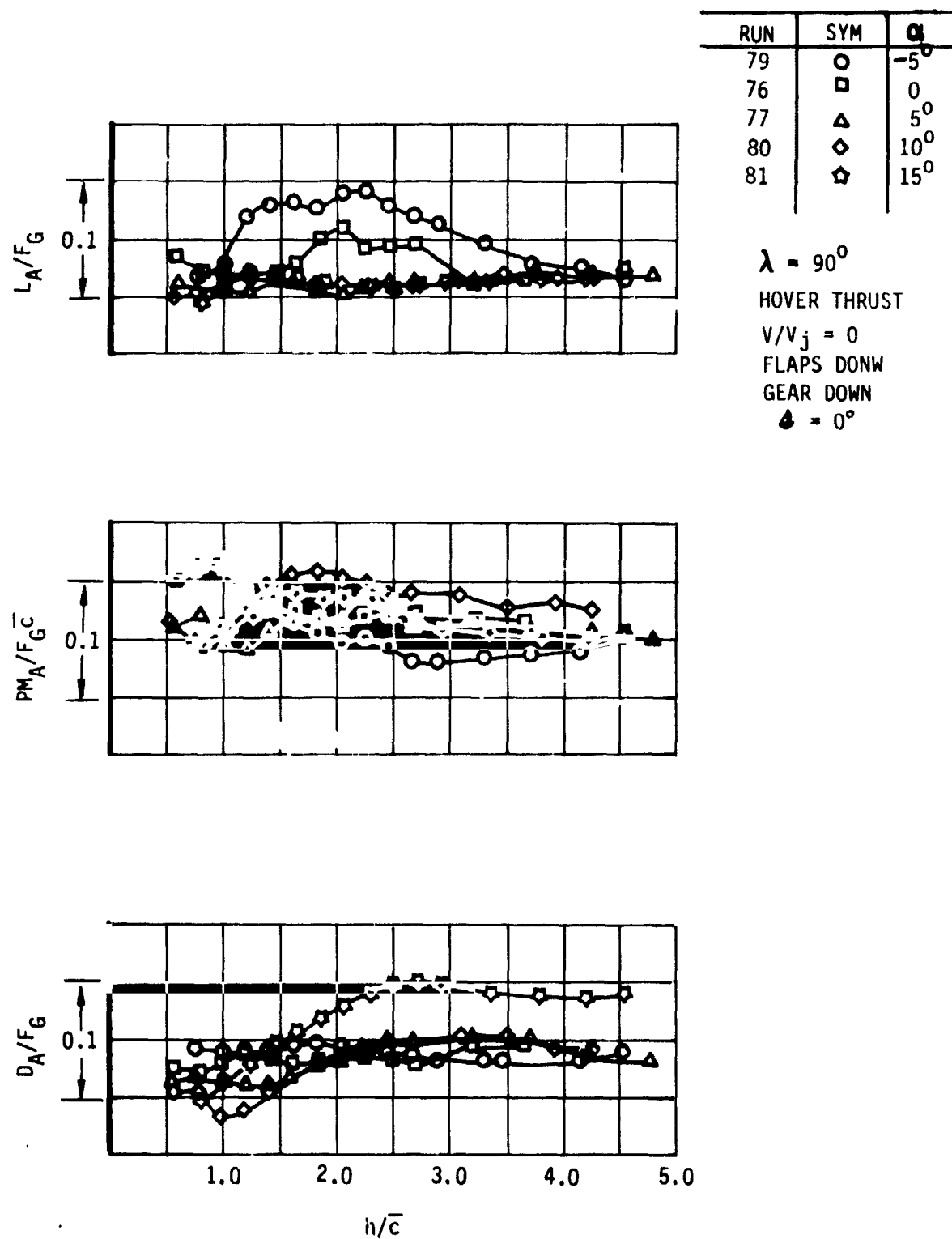
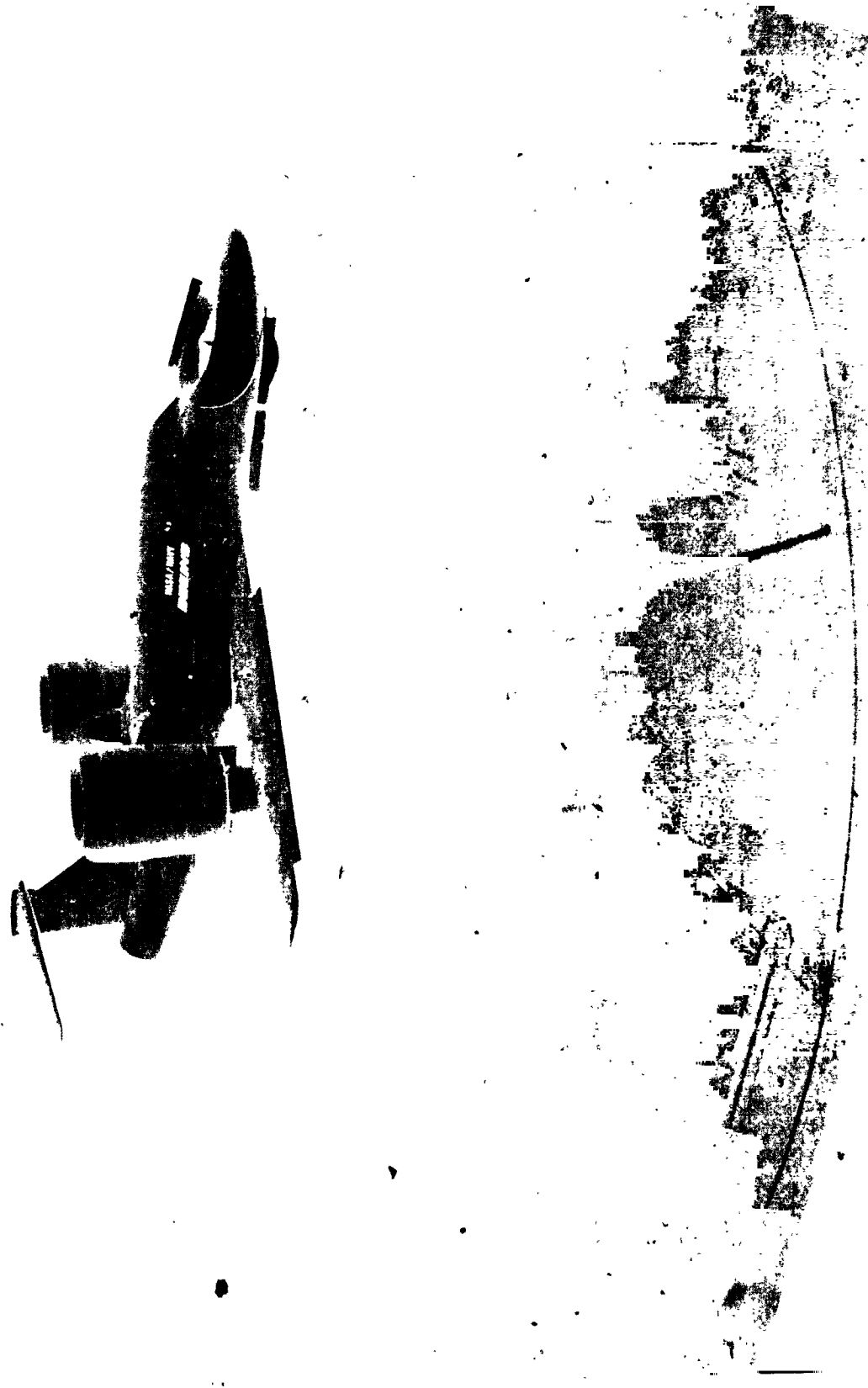


FIGURE 19 EFFECT OF ANGLE OF ATTACK ON INDUCED FORCES  
VTOL CONFIGURATION,  $\lambda = 90^\circ$

ORIGINAL PAGE IS  
OF POOR QUALITY



CALC			REVISED	DATE
CHECK				
APPD				
APPD				

TYPICAL OIL FLOW PATTERN ON GROUND PLANE

STATIC HOVER AT ALPHA = 5°

FIGURE 20

THE BOEING COMPANY

PAGE  
66

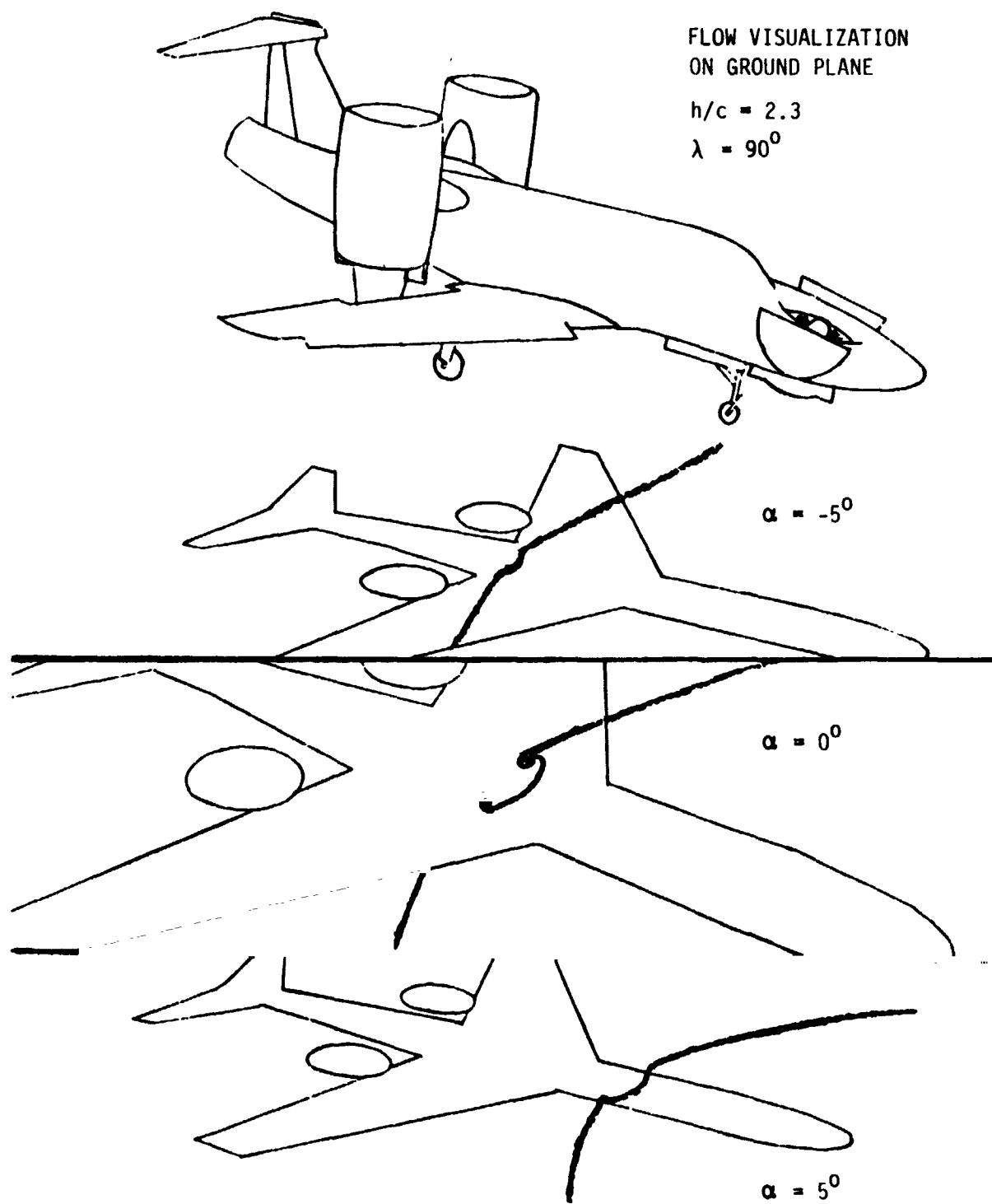


FIGURE 21 EFFECT OF ANGLE OF ATTACK ON  
STATIC GROUND PLANE FLOW PATTERNS

RUN	SYM	$\alpha$
125	○	0°
126	□	10°

$\lambda = 80^\circ$   
 HOVER THRUST  
 $V/V_j = 0$   
 FLAPS DOWN  
 GEAR DOWN  
 $\delta = 0^\circ$

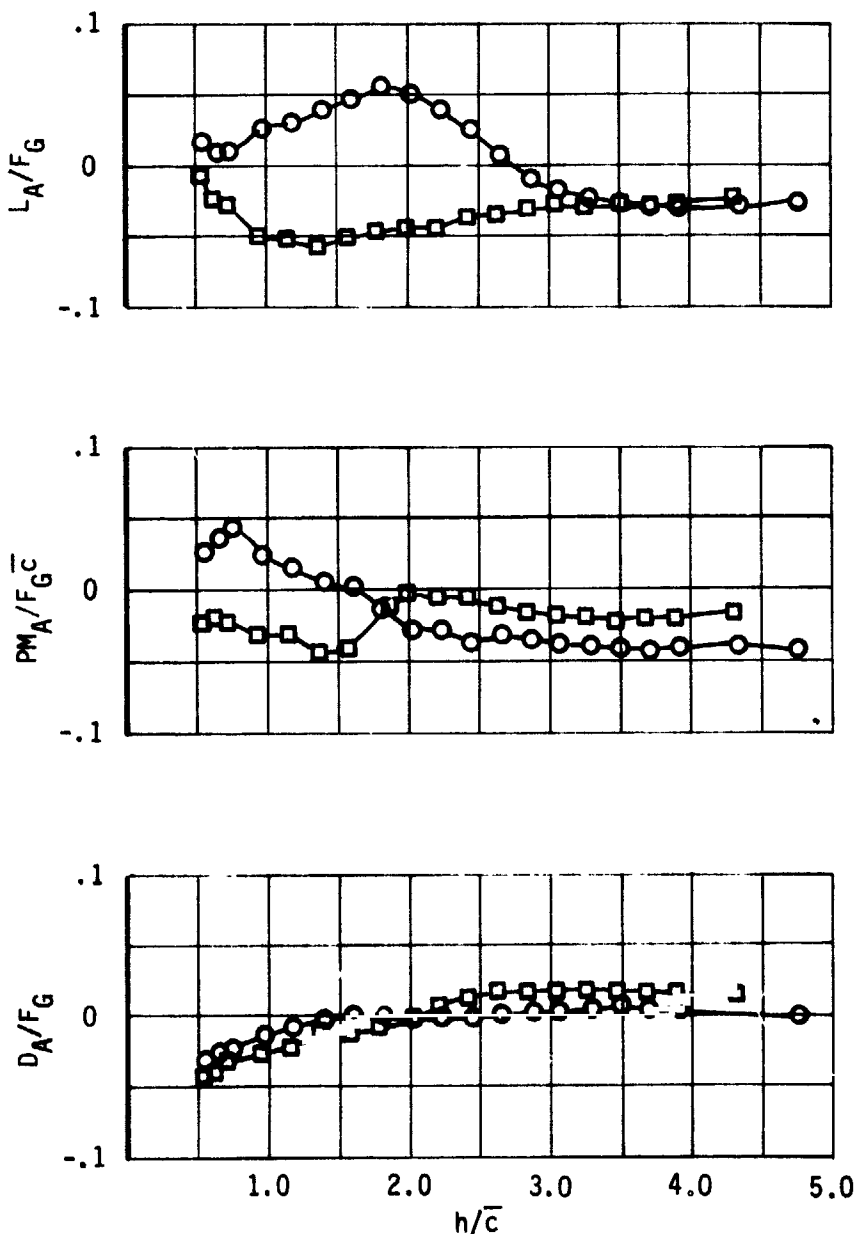


FIGURE 22 EFFECT OF ANGLE OF ATTACK  
VTOL CONFIGURATION,  $\lambda = 80^\circ$

RUN	SYM	$\lambda$
125	○	80°
127	□	90°
123	△	95

$\alpha = 0^\circ$   
 HOVER THRUST  
 $V/V_j = 0$   
 FLAPS DOWN  
 GEAR DOWN  
 $\Delta = 0^\circ$

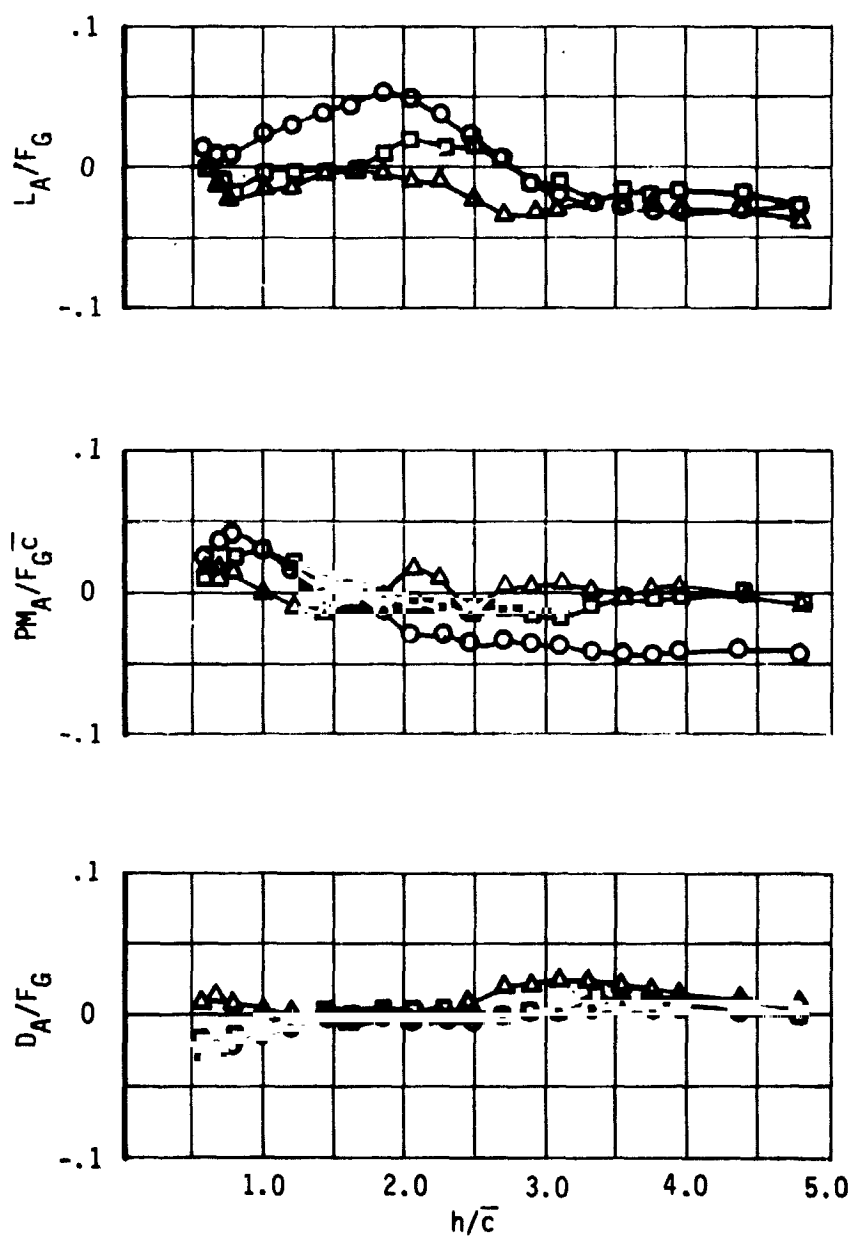


FIGURE 23 EFFECT OF NACELLE TILT ANGLE VTOL CONFIGURATION

RUN	SYM	$\alpha$
76	○	0°
84	△	-5°
83	□	-10°
85	◊	-15°

$\alpha = 0^\circ$   
 $\lambda = 90^\circ$   
 HOVER THRUST  
 $V/V_j = 0$   
 FLAPS DOWN  
 GEAR DOWN  
 $\beta = 0^\circ$

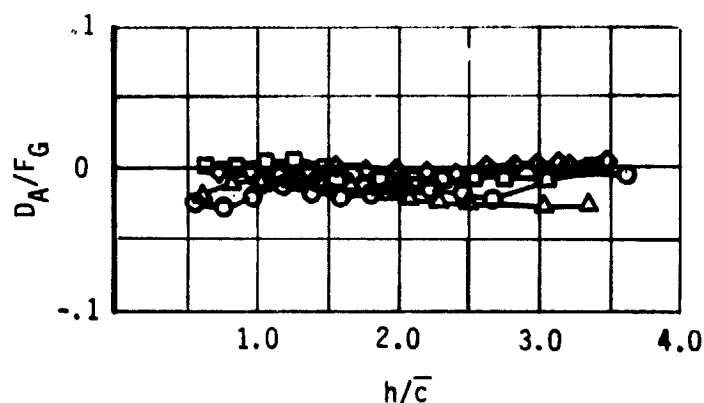
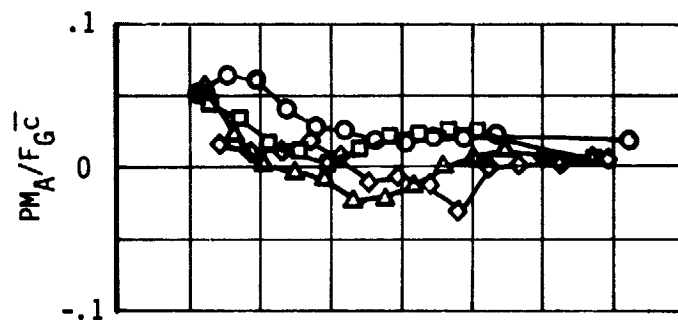
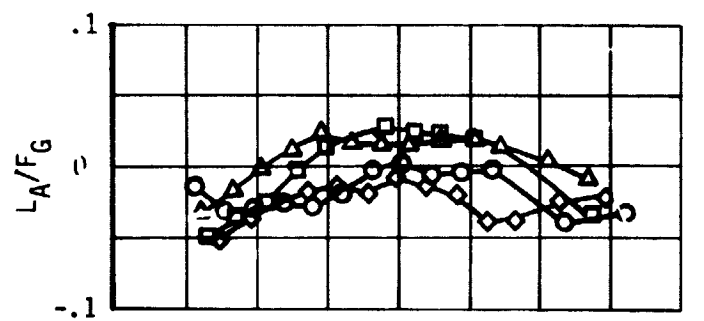


FIGURE 24a EFFECT OF ROLL ANGLE  
VTOL CONFIGURATION

RUN	SYM	$\alpha$
76	○	0°
84	△	-5°
83	□	-10°
85	◊	-15°

$\alpha = 0^\circ$   
 $\lambda = 90$   
 HOVER THRUST  
 $V/V_j = 0$   
 FLAPS DOWN  
 GEAR DOWN  
 $\Delta = 0^\circ$

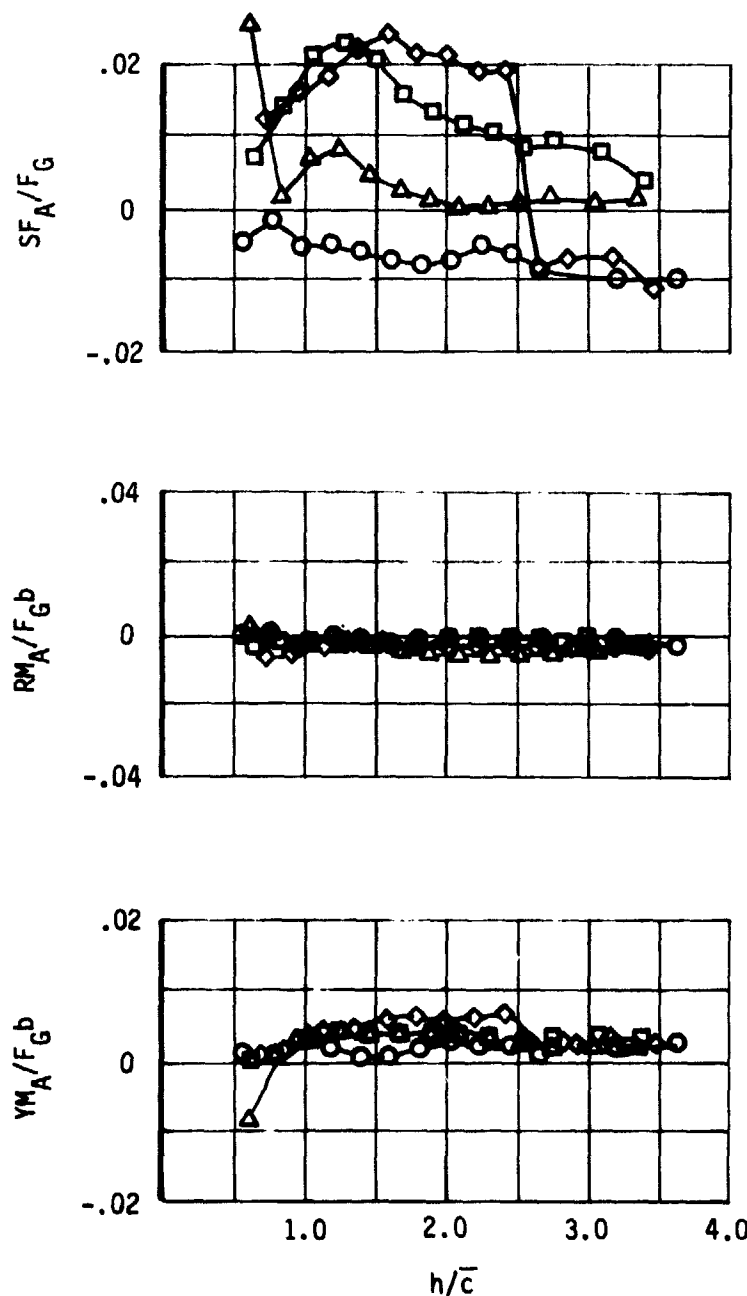


FIGURE 24b EFFECT OF ROLL ANGLE  
VTOL CONFIGURATION

RUN	SYM	$\alpha$
83	○	0°
88	□	5°
90	◊	10°

$\bullet = -10^{\circ}$   
 $\lambda = 90^{\circ}$   
 HOVER THRUST  
 $V/V_j = 0$   
 FLAPS DOWN  
 GEAR DOWN  
 $\delta = 0^{\circ}$

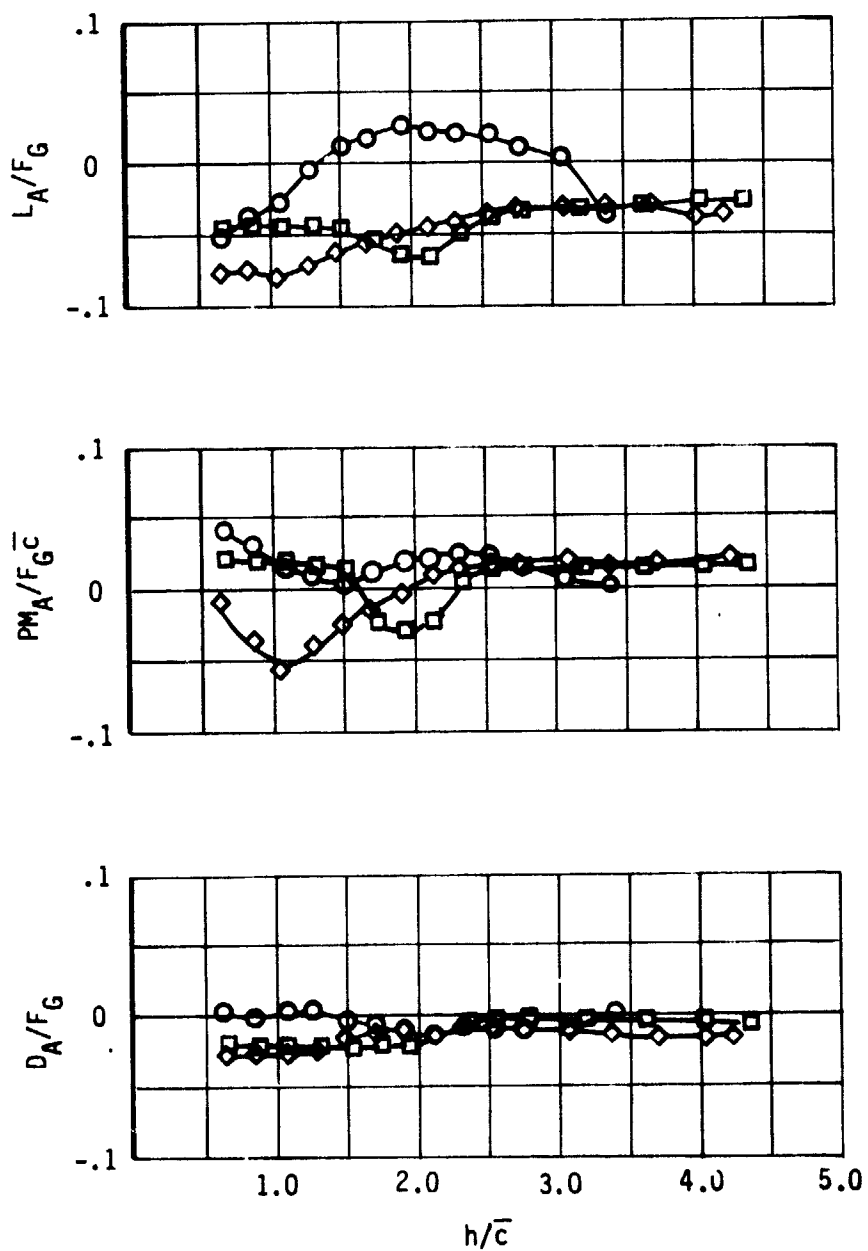


FIGURE 25a EFFECT OF ANGLE OF ATTACK WITH ROLL  
VTOL CONFIGURATION

RUN	SYM	$\alpha$
83	○	0°
88	□	5°
90	◊	10°

$\phi = -10^\circ$   
 $\lambda = 90^\circ$   
 HOVER THRUST  
 $V/V_j = 0$   
 FLAPS DOWN  
 GEAR DOWN  
 $\Delta = 0^\circ$

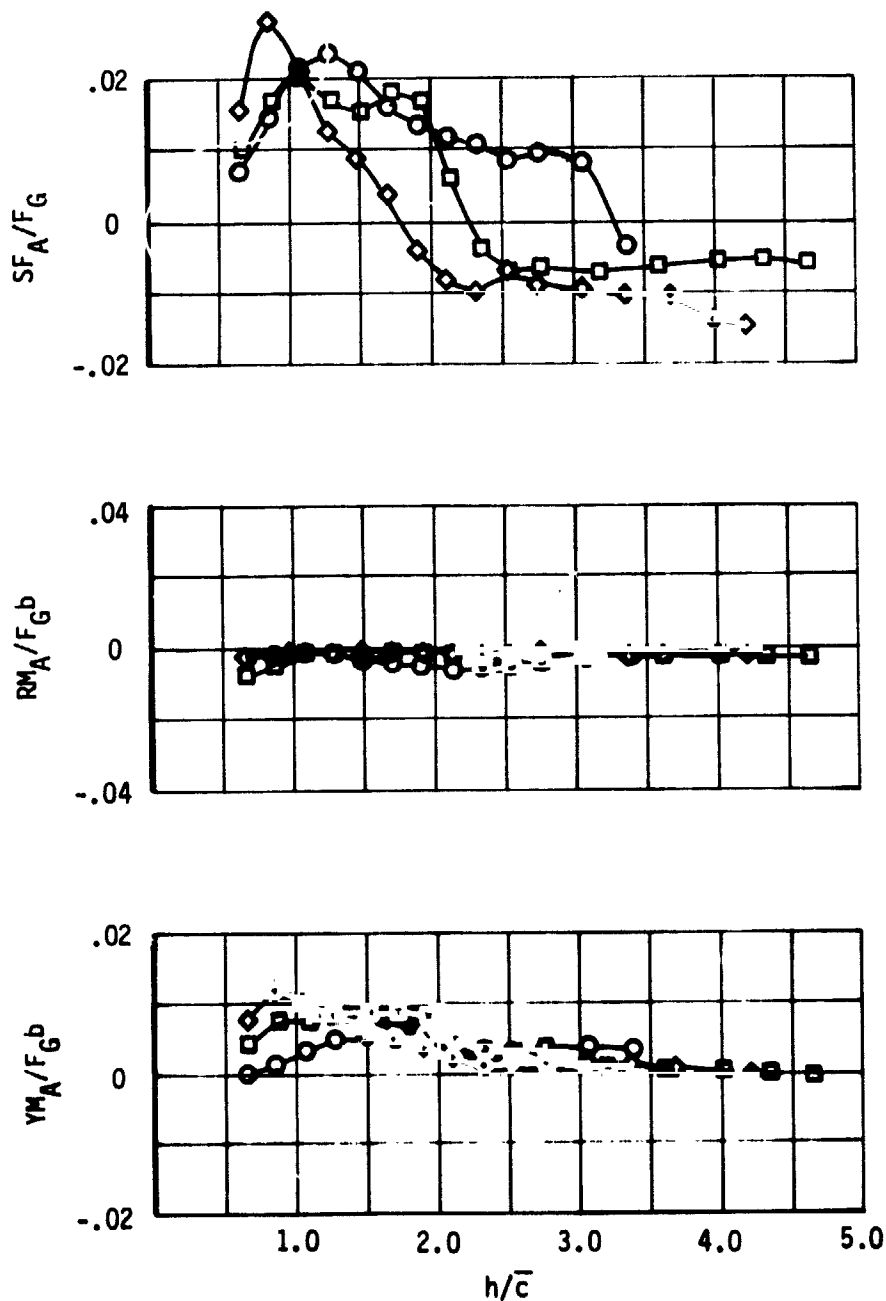


FIGURE 25b EFFECT OF ANGLE OF ATTACK WITH ROLL  
VTOL CONFIGURATION

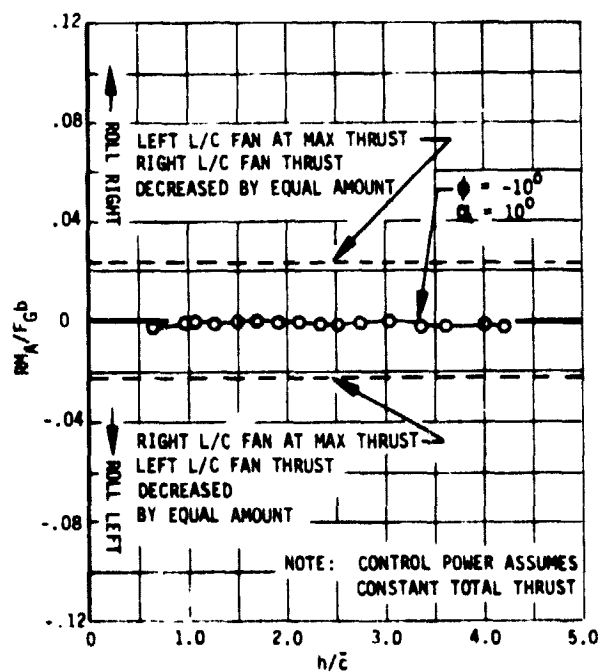
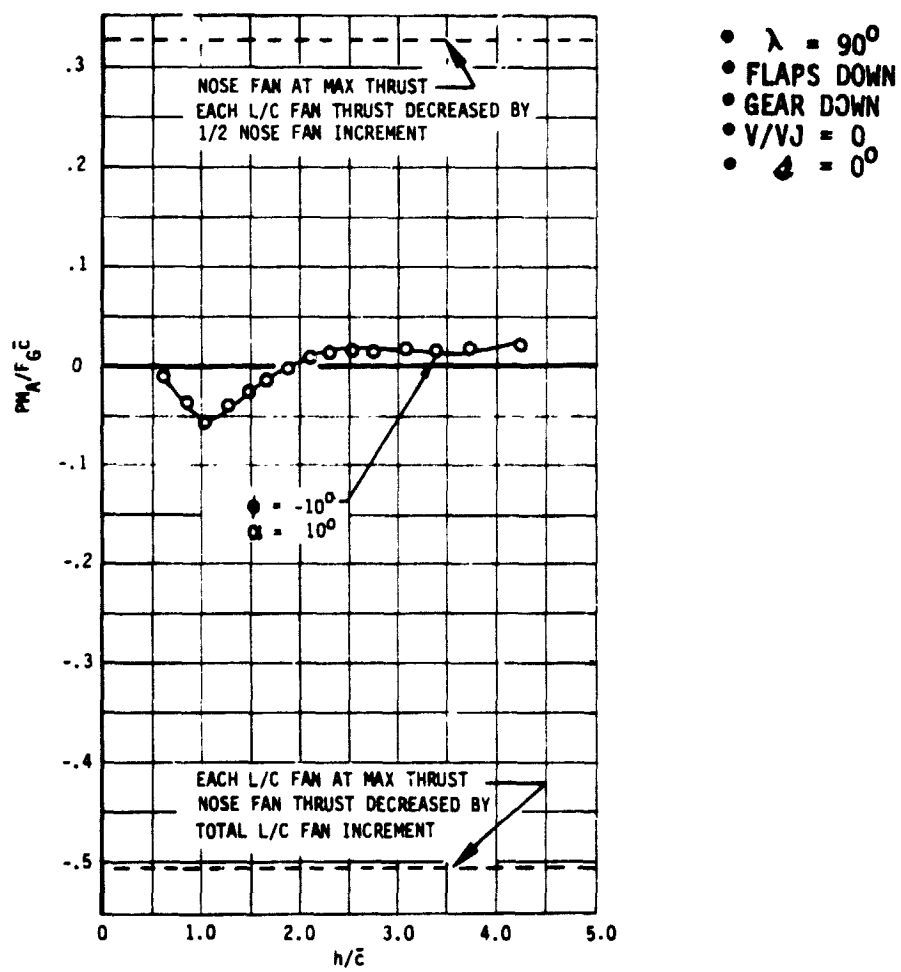


FIGURE 26 COMPARISON OF TYPICAL INDUCED PITCH AND ROLL MOMENTS  
IN STATIC HOVER WITH AVAILABLE PITCH AND ROLL CONTROL POWER

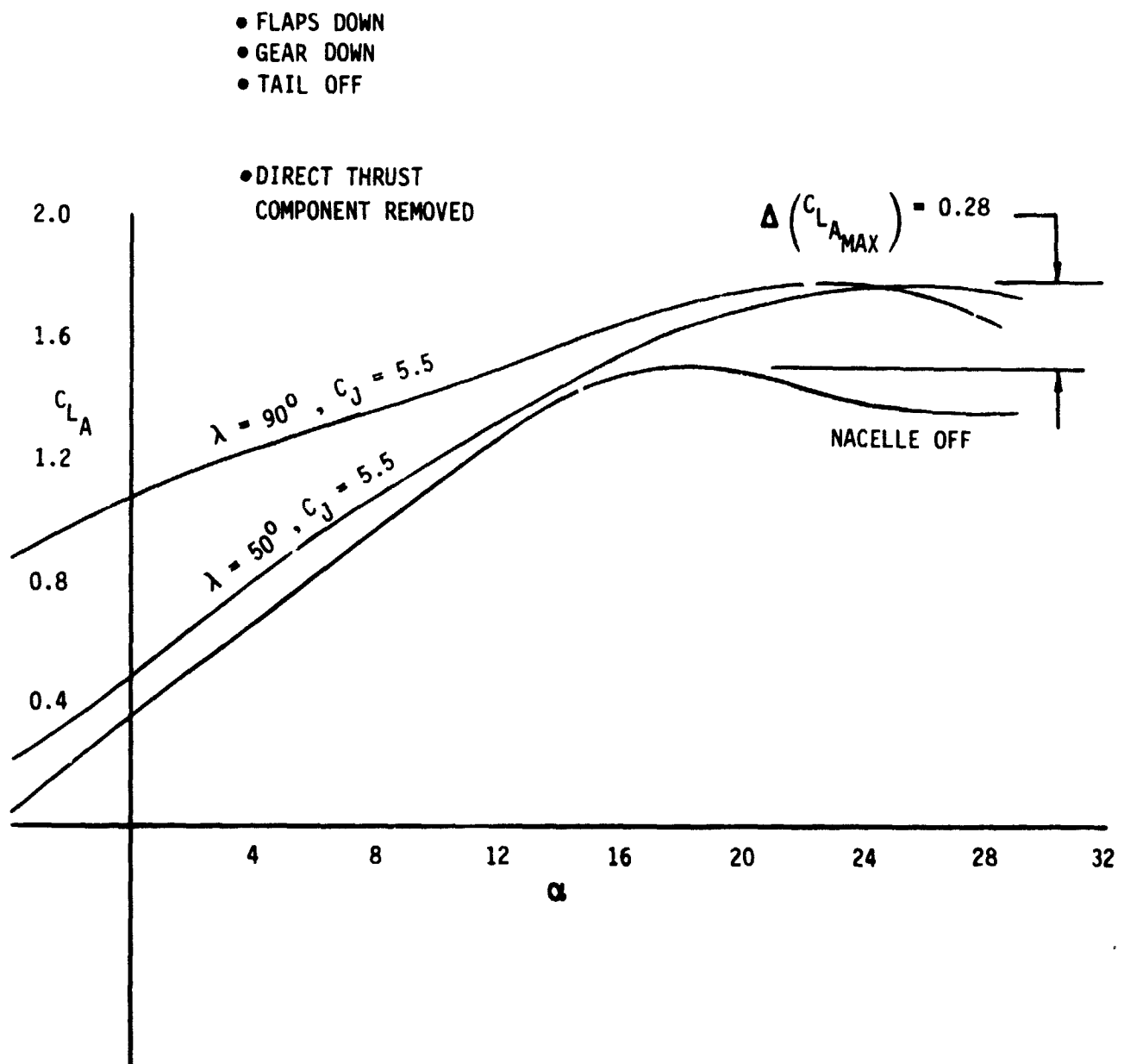


FIGURE 27 INDUCED EFFECT OF PROPULSION SYSTEM  
ON LIFT AT  $C_J = 5.5$

- FLAPS DOWN
- GEAR DOWN
- TAIL OFF
- DIRECT THRUST COMPONENT REMOVED
- $\alpha = 8^\circ$

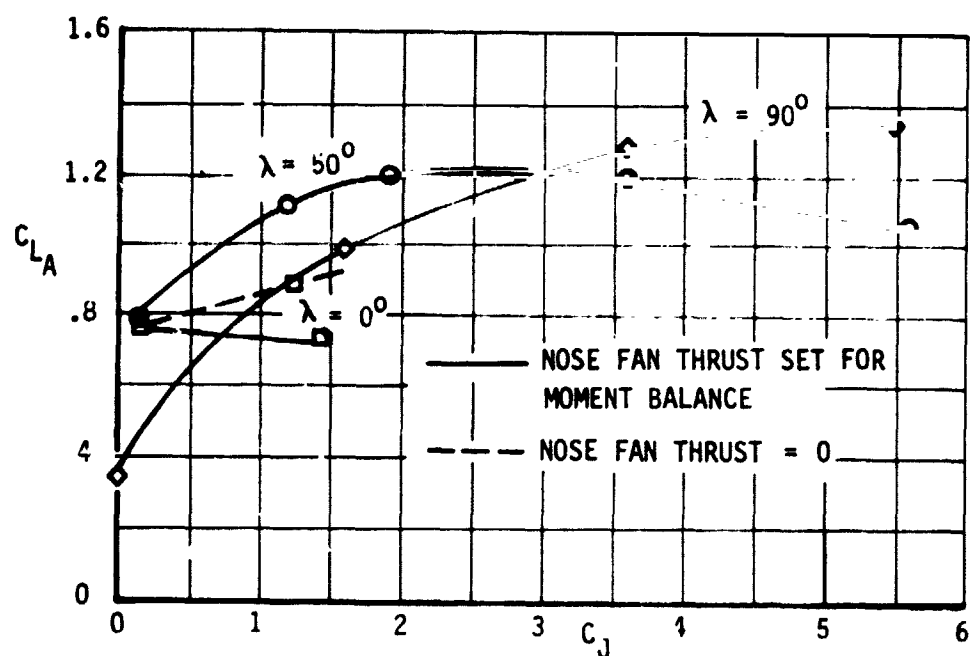


FIGURE 28 EFFECT OF THRUST COEFFICIENT ON LIFT

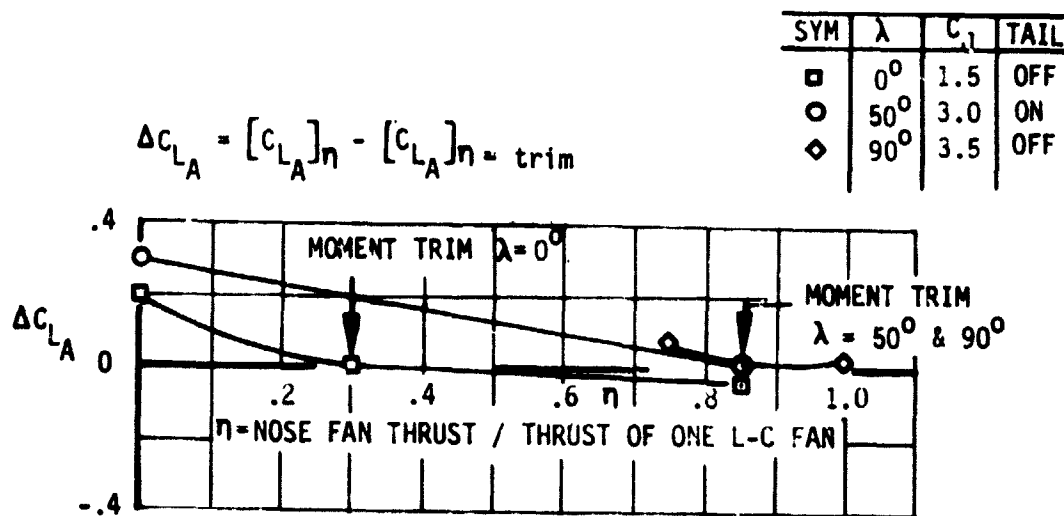
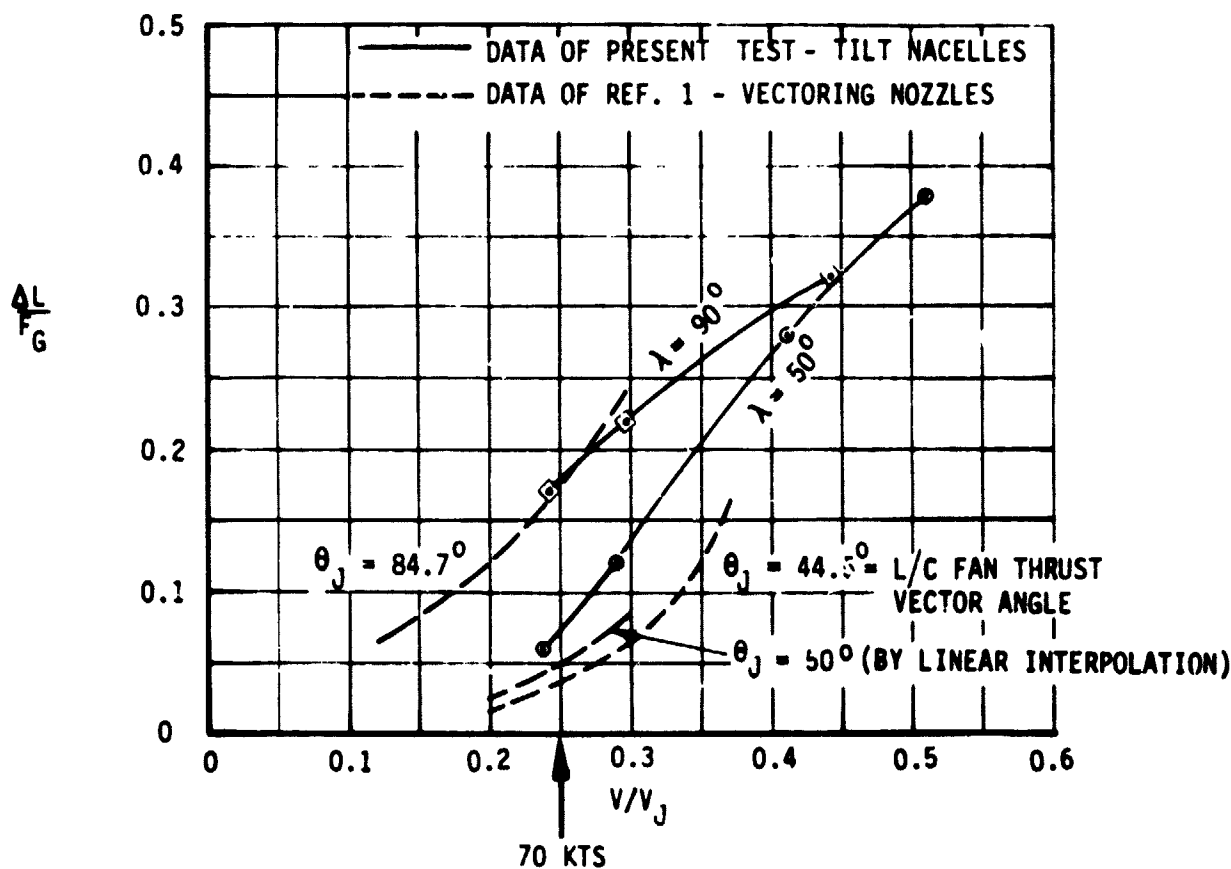


FIGURE 29 EFFECT OF THRUST BALANCE ON LIFT

- $\alpha = 0^\circ$
- FLAPS DOWN
- GEAR DOWN
- TAIL OFF



NOTES

- (1)  $\Delta L = (L_A) - (L_A)_{\text{REFERENCE}}$
- (2)  $L_A$  = LIFT WITH DIRECT THRUST REMOVED
- (3)  $(L_A)_{\text{REFERENCE}}$  IS BASED ON:  
 $\lambda = 0^\circ$ ,  $C_J = \text{RAM}$ , NOSE FAN COVERED,  
 FLAPS DOWN, GEAR DOWN, TAIL OFF

FIGURE 30 A SUMMARY OF INDUCED EFFECT OF PROPULSION SYSTEM ON LIFT

- FLAPS DOWN
- GEAR DOWN
- TAIL OFF
- DIRECT THRUST COMPONENT REMOVED

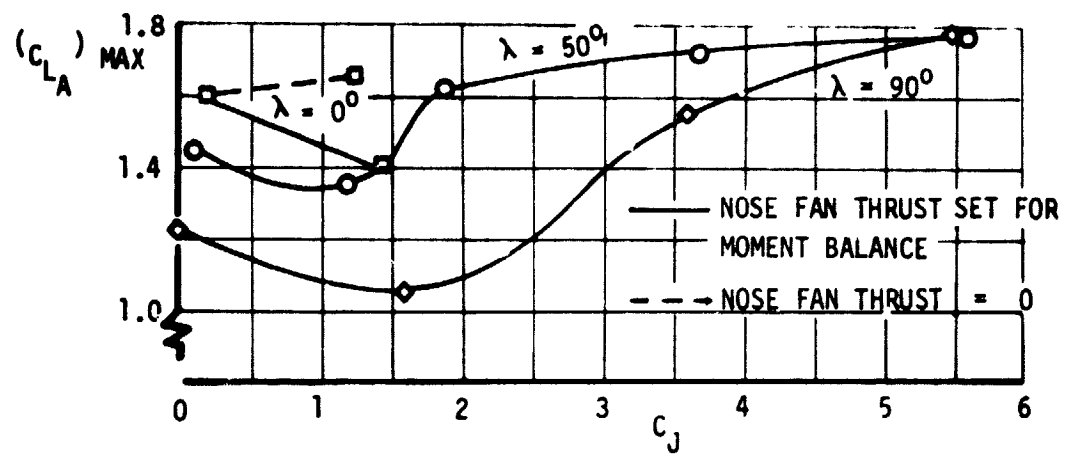


FIGURE 31 EFFECT OF THRUST COEFFICIENT ON MAXIMUM LIFT

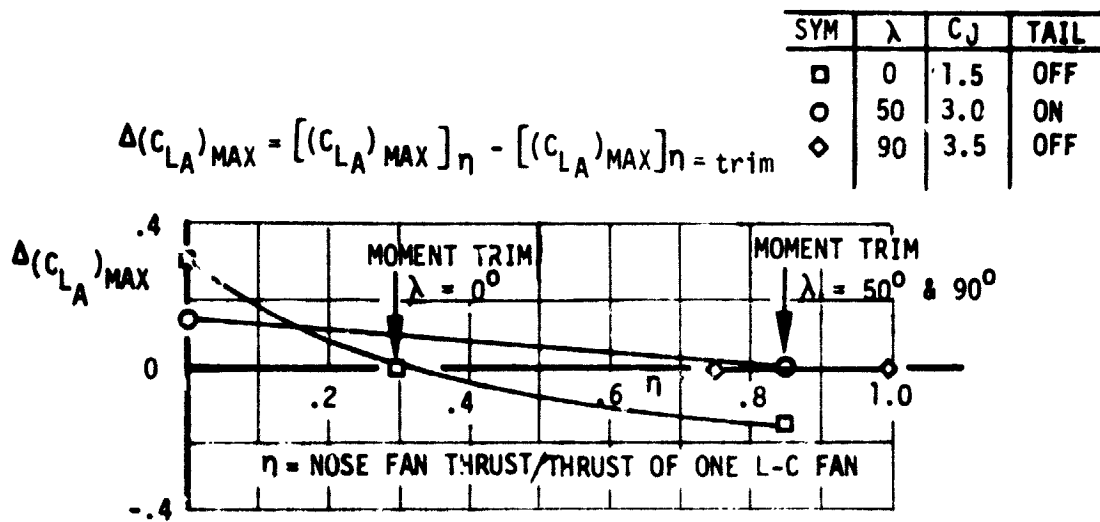


FIGURE 32 EFFECT OF THRUST BALANCE ON MAXIMUM LIFT

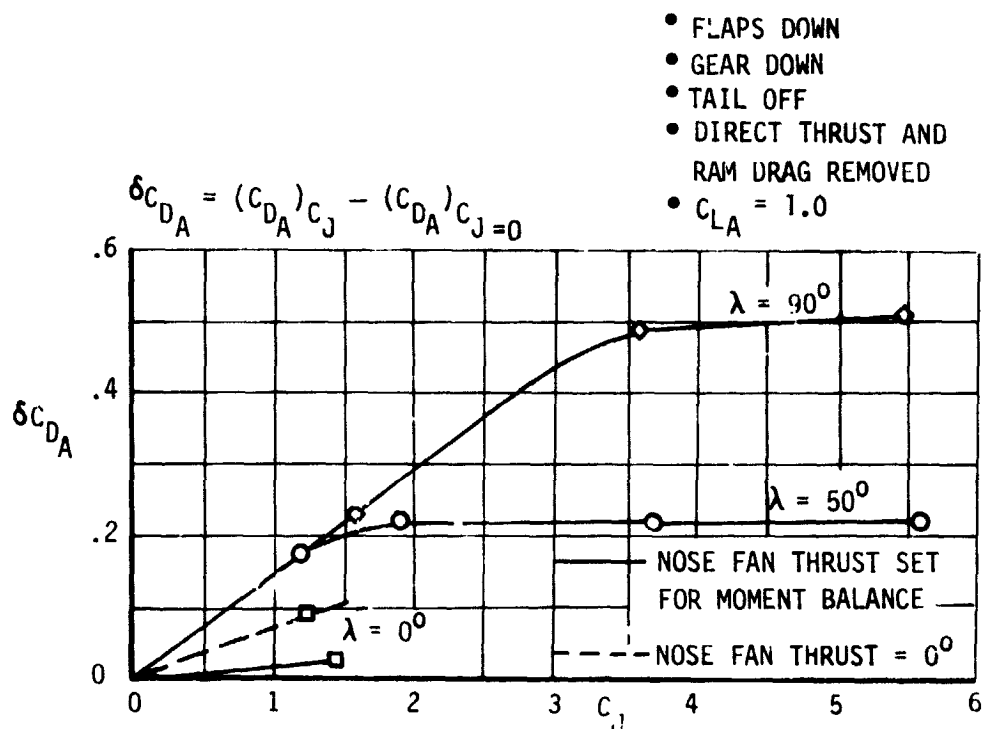


FIGURE 33 EFFECT OF THRUST COEFFICIENT ON DRAG

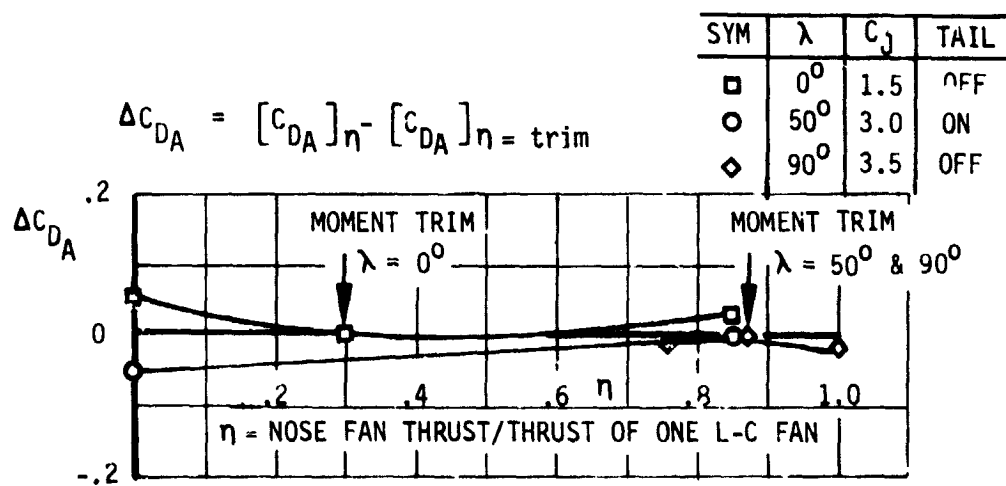


FIGURE 34 EFFECT OF THRUST BALANCE ON DRAG

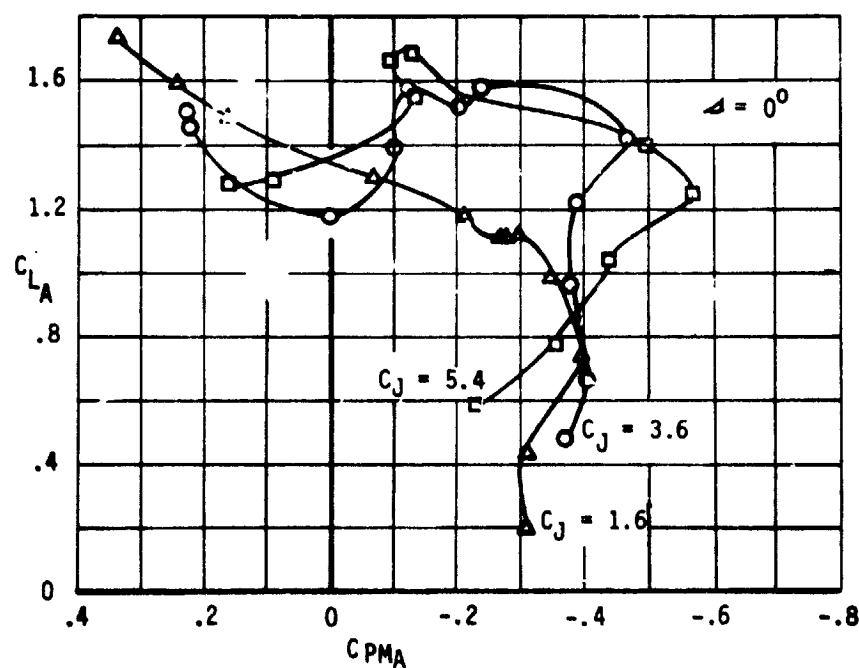
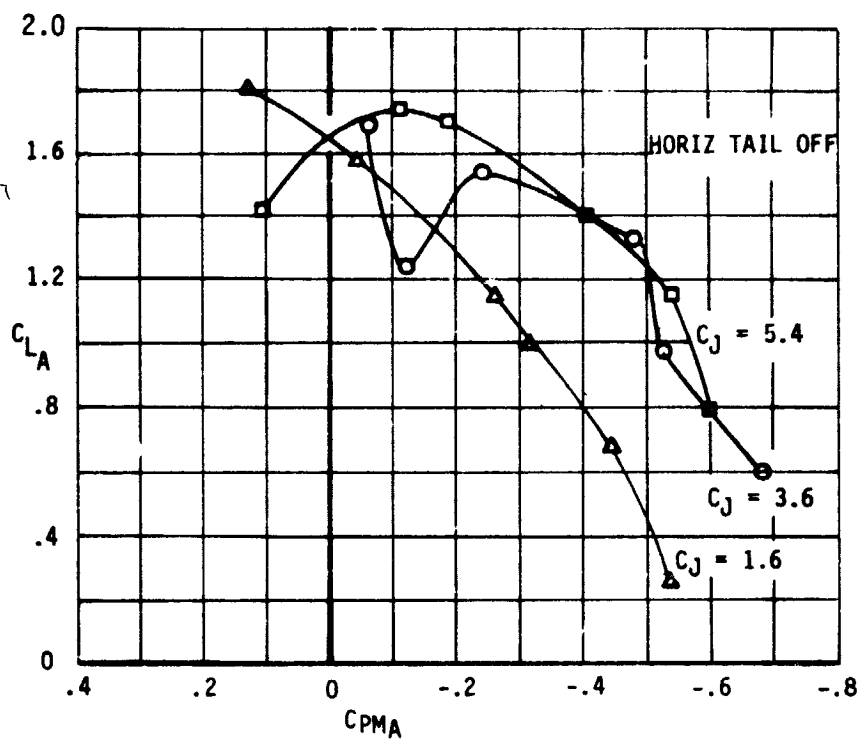


FIGURE 35 EFFECT OF THRUST COEFFICIENT AND HORIZONTAL TAIL ON LONGITUDINAL STABILITY -  $\gamma = 90^\circ$

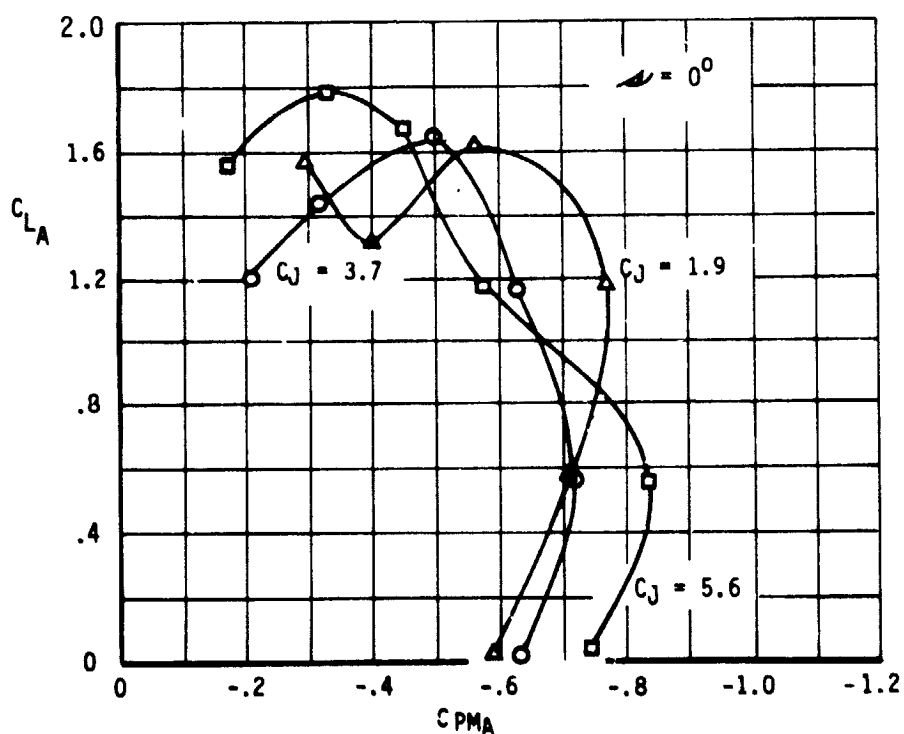
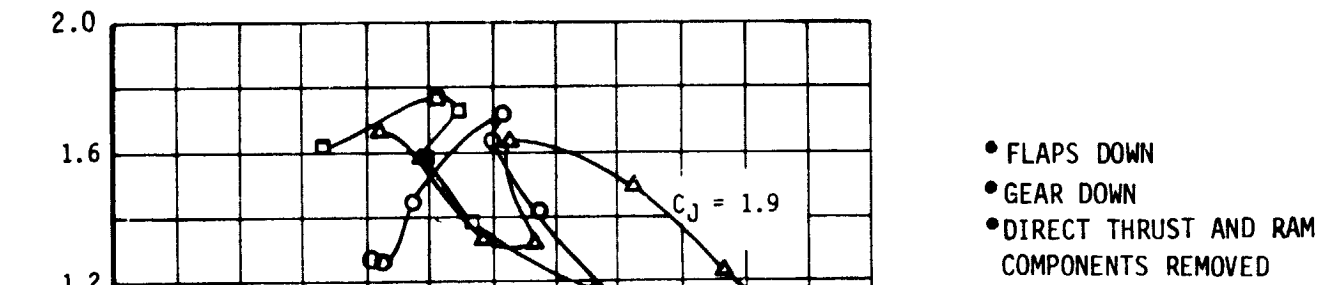


FIGURE 36 EFFECT OF THRUST COEFFICIENT AND HORIZONTAL TAIL ON LONGITUDINAL STABILITY -  $\lambda = 50^\circ$

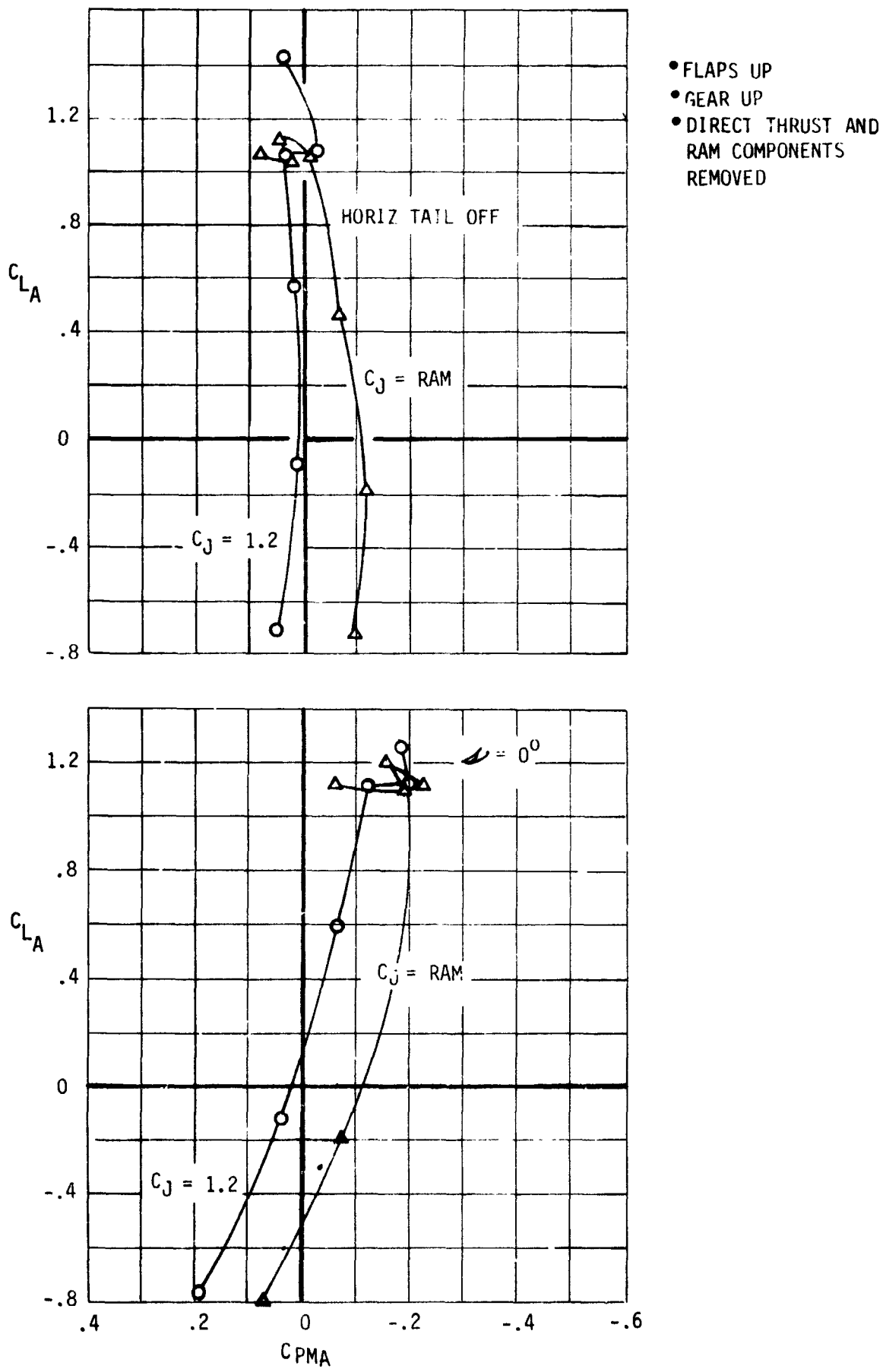
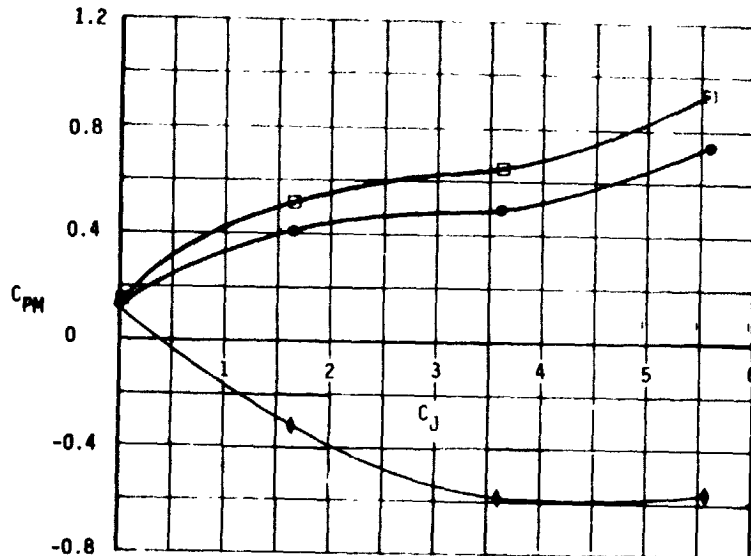


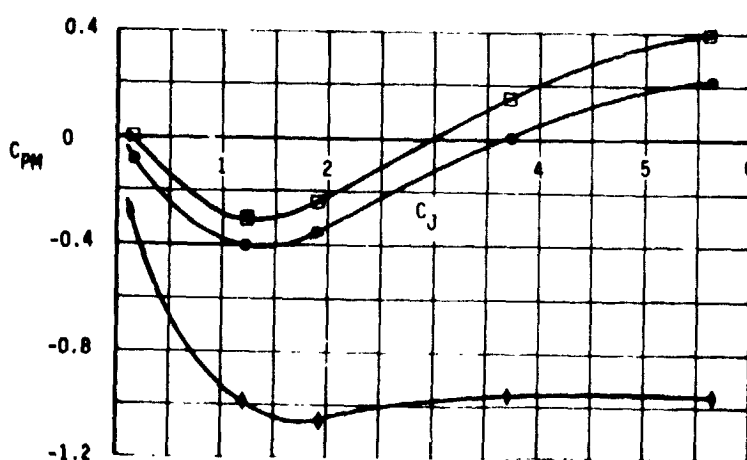
FIGURE 37 EFFECT OF THRUST COEFFICIENT AND HORIZONTAL TAIL ON LONGITUDINAL STABILITY -  $\lambda = 0^\circ$

● FLAPS DOWN  
 ● GEAR DOWN  
 ● TAIL OFF  
 ●  $C_{LA} = 1.0$   
 ○  $C_{PM}$  (TOTAL MEASURED MODEL MOMENTS)  
 □  $C_{PM}$  (TOTAL MOMENTS WITH RAM MOMENTS CORRECTED)  
 TO FULL SCALE  
 ♦  $C_{PM_A} = C_{PM}$  LESS CALCULATED RAM MOMENT AND  
 DIRECT THRUST MOMENTS  
 (MODEL DATA)



$$\lambda = 90^\circ$$

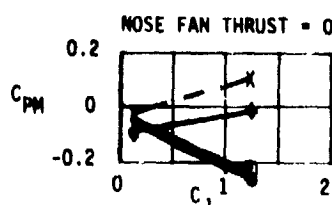
NOSE FAN THRUST SET  
FOR STATIC MOMENT TRIM  
(SEE FIGURE 16)



$$\lambda = 50^\circ$$

NOSE FAN THRUST SET  
FOR STATIC MOMENT TRIM  
(SEE FIGURE 16)

--X--  $C_{PM_A}$  PLUS MODEL RAM MOMENTS



NOSE FAN THRUST SET  
FOR STATIC MOMENT TRIM  
(SEE FIGURE 16)

$$\lambda = 0^\circ$$

FIGURE 38 EFFECT OF THRUST COEFFICIENT ON PITCHING MOMENT

THRUST OF NOSE FAN / THRUST OF ONE LIFT CRUISE FAN

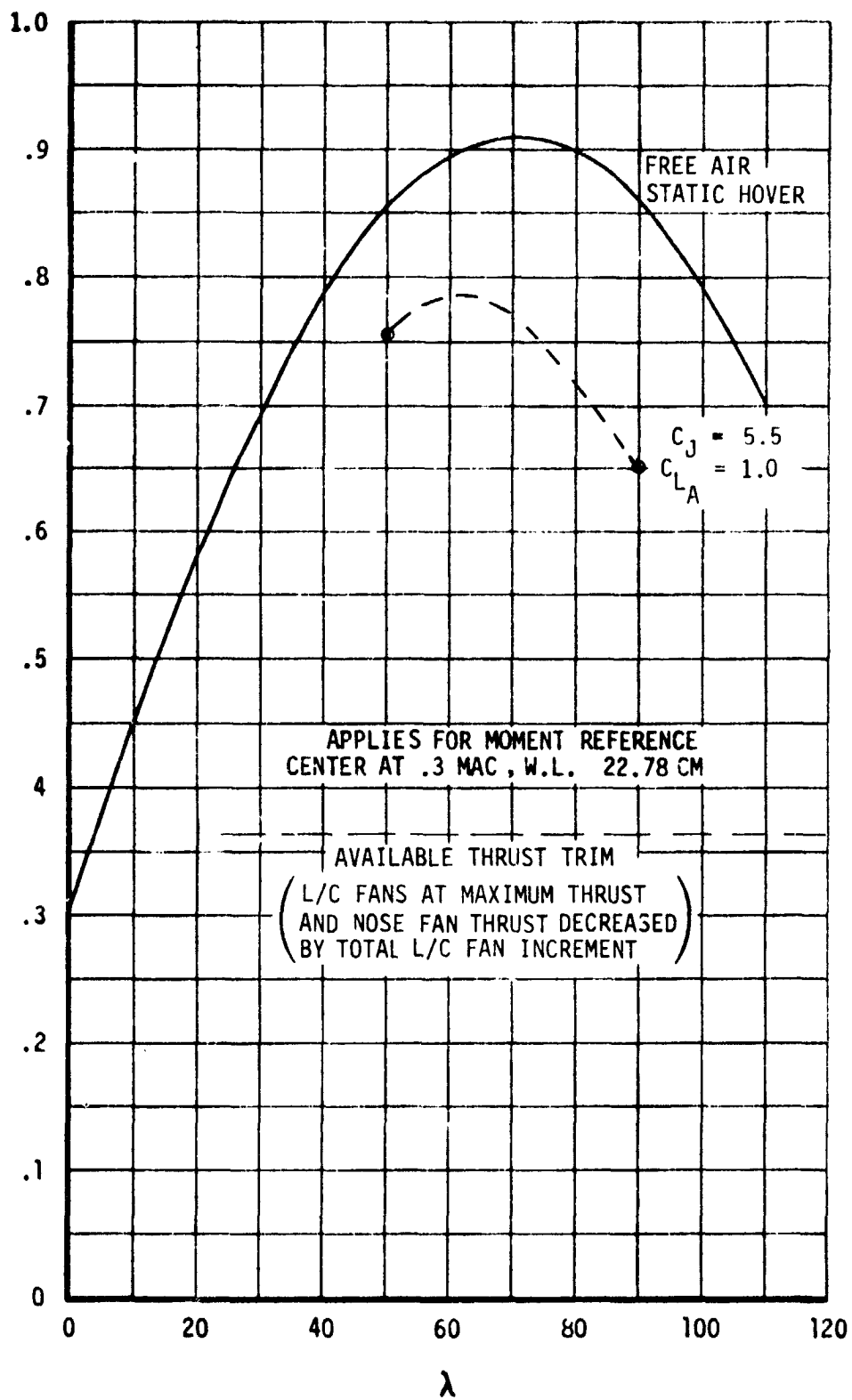


FIGURE 39 NOSE FAN THRUST REQUIRED FOR PITCHING MOMENT TRIM, TAIL OFF, FLAPS DOWN

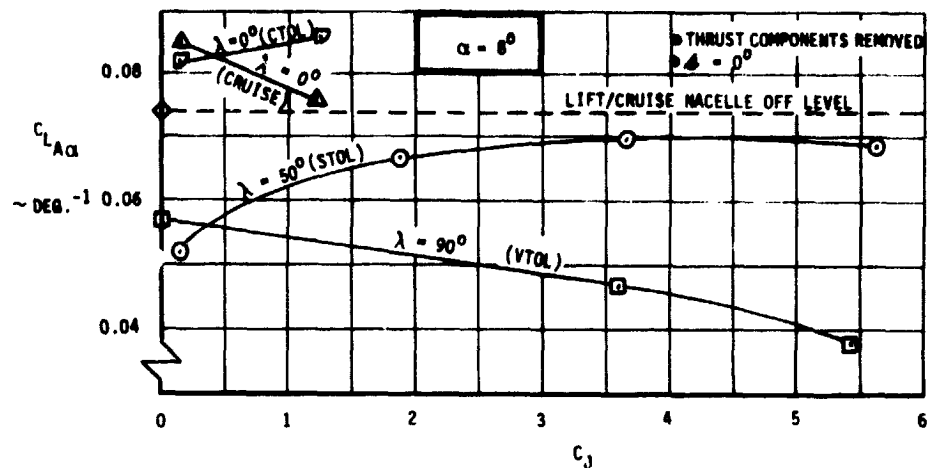


FIGURE 40 EFFECT OF THRUST ON LIFT CURVE SLOPE

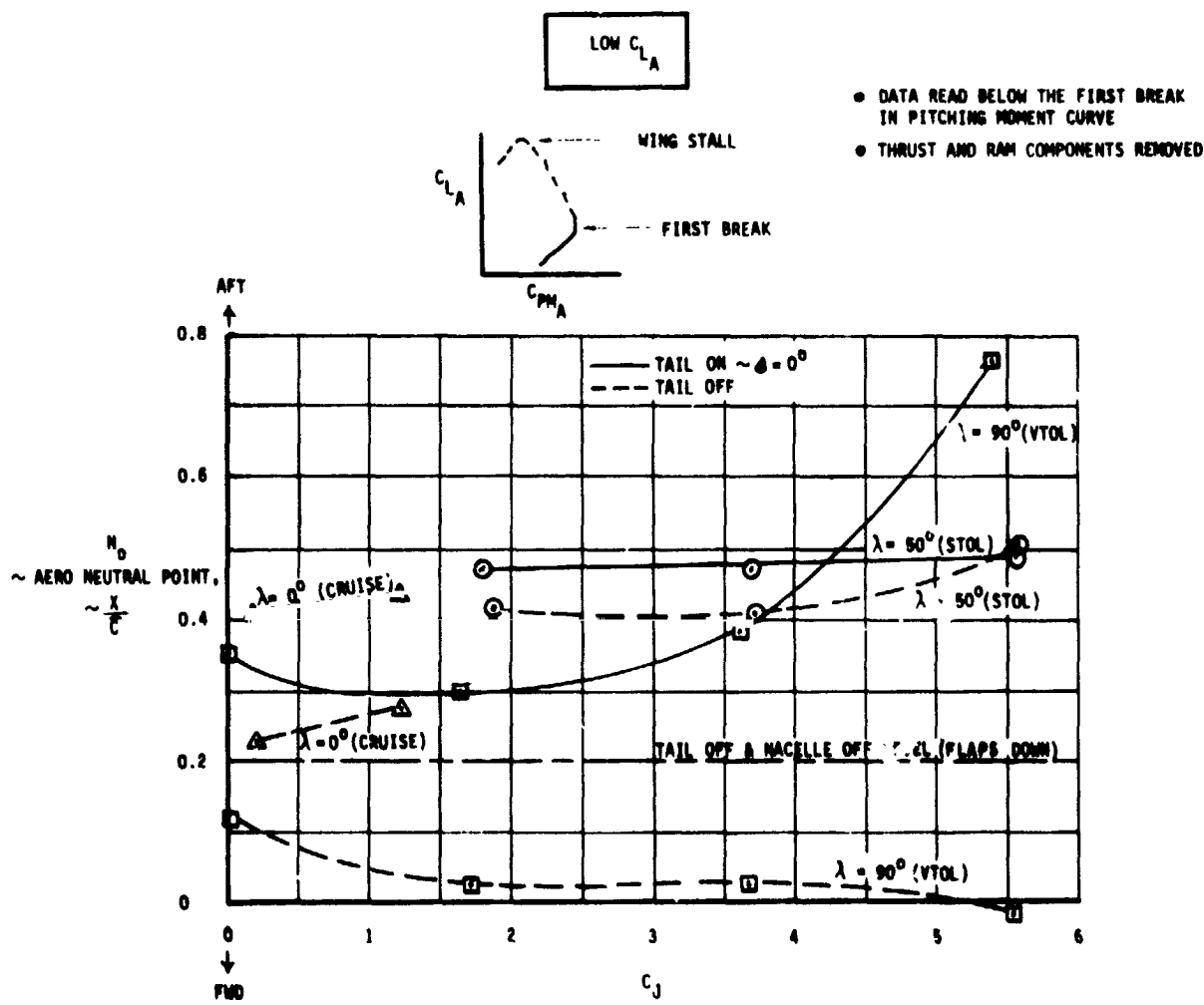


FIGURE 41 EFFECT OF THRUST ON NEUTRAL POINT LOCATION (LOW  $C_{L_A}$ )

HIGH  $C_{L_A}$

- DATA READ ABOVE FIRST BREAK IN PITCHING MOMENT CURVE BUT BELOW THE BREAK FOR WING STALL
- THRUST AND RAM FORCES REMOVED

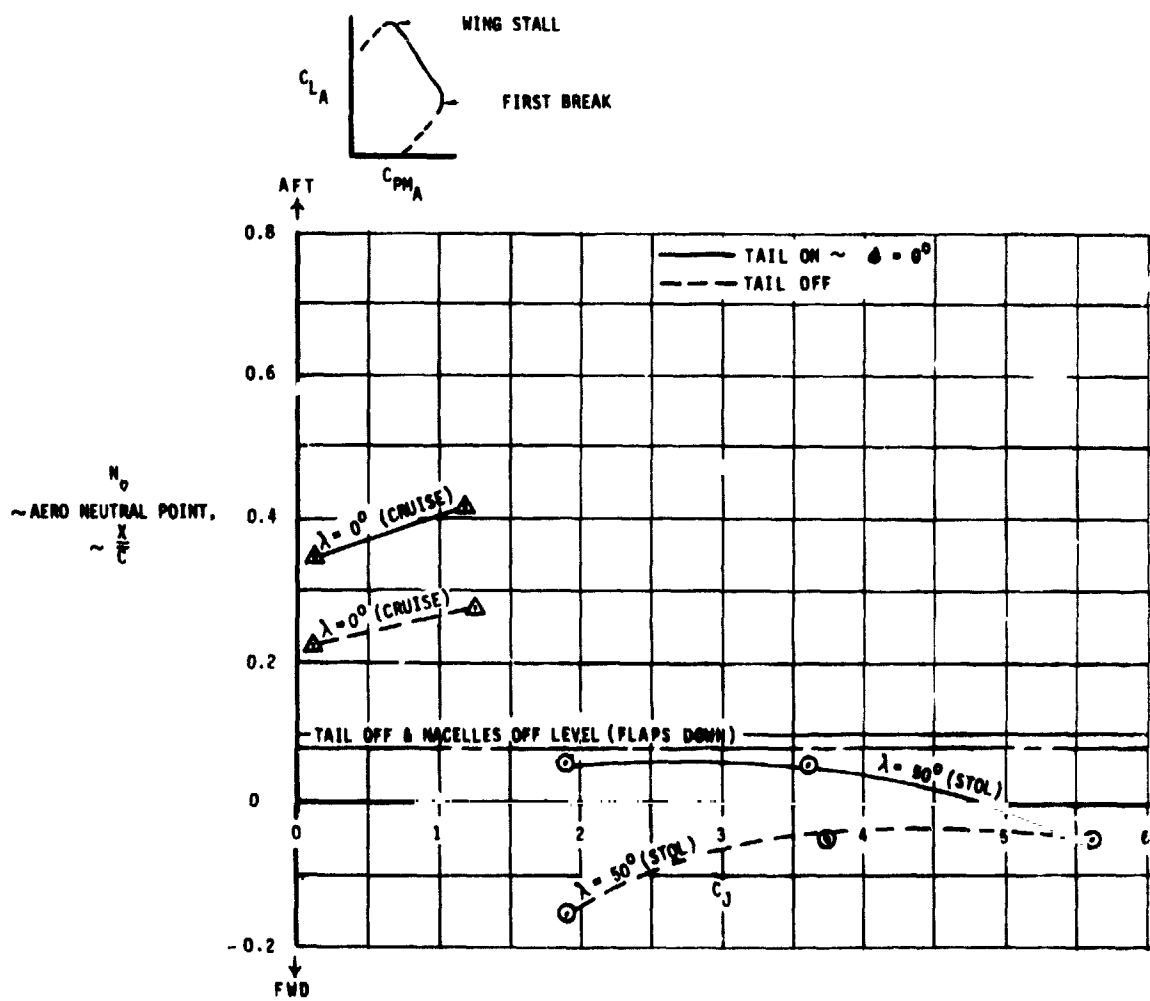


FIGURE 4.2 EFFECT OF THRUST ON NEUTRAL POINT LOCATION (HIGH  $C_{L_A}$ )

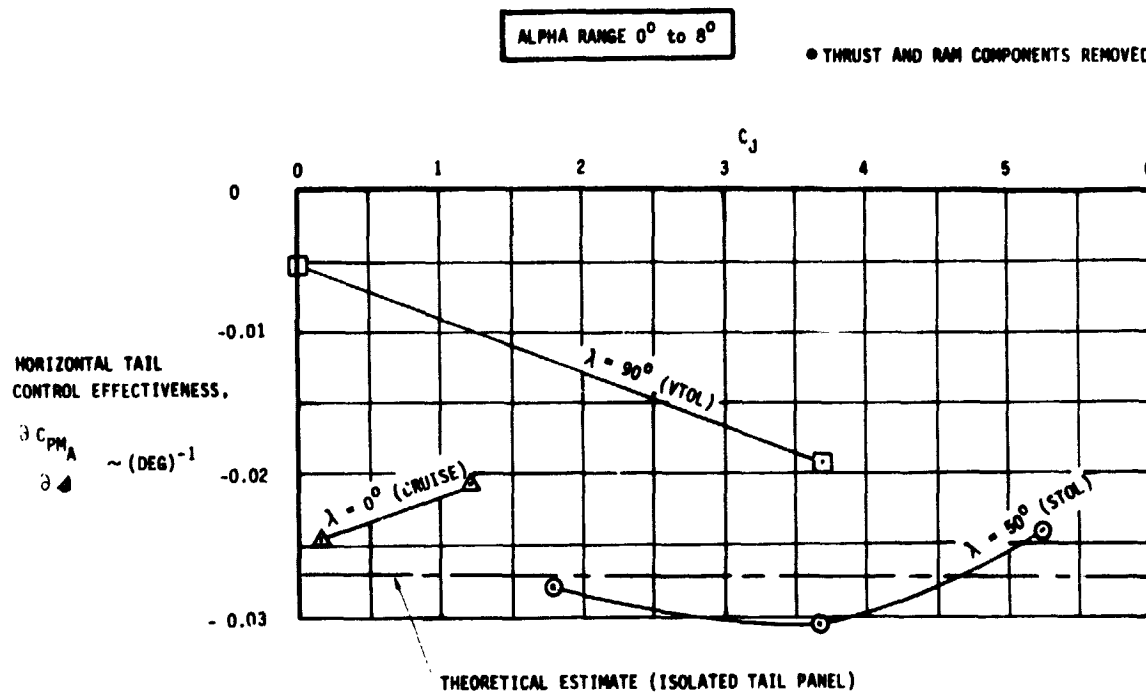


FIGURE 43 EFFECT OF THRUST ON HORIZONTAL TAIL CONTROL EFFECTIVENESS

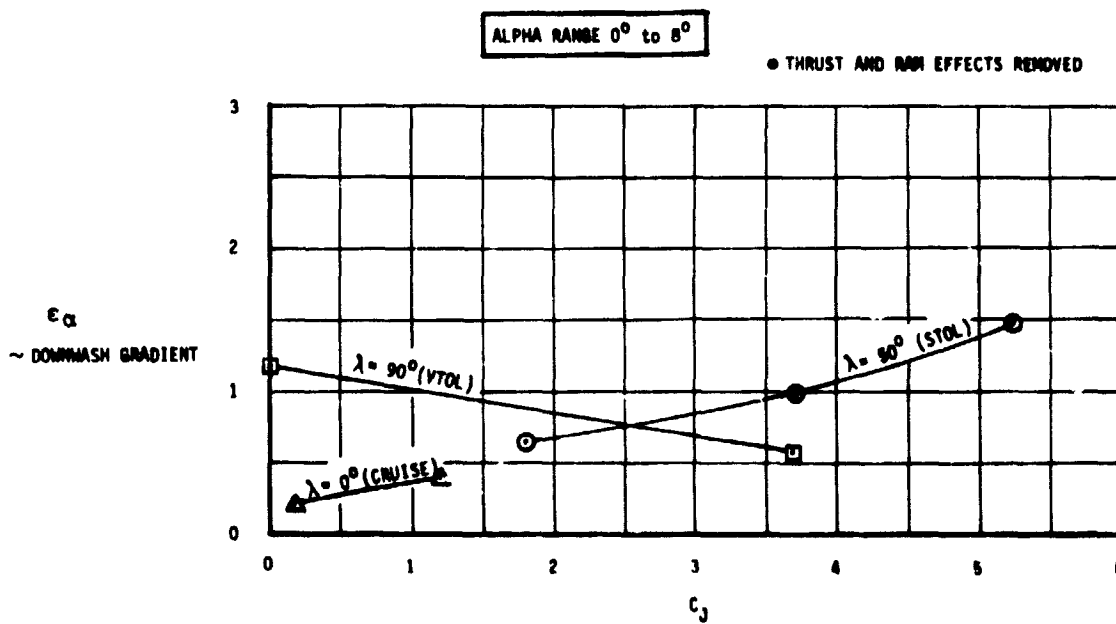


FIGURE 44 EFFECT OF THRUST ON DOWNWASH GRADIENT

- $\lambda = 90^\circ$
  - FLAPS DOWN
  - GEAR DOWN
  - THRUST AND RAM  
COMPONENTS REMOVED
  - $C_J = 3.6$
  - $V/V_J = 0.29$
- V.H OFF DENOTES VERTICAL AND HORIZONTAL TAILS OFF

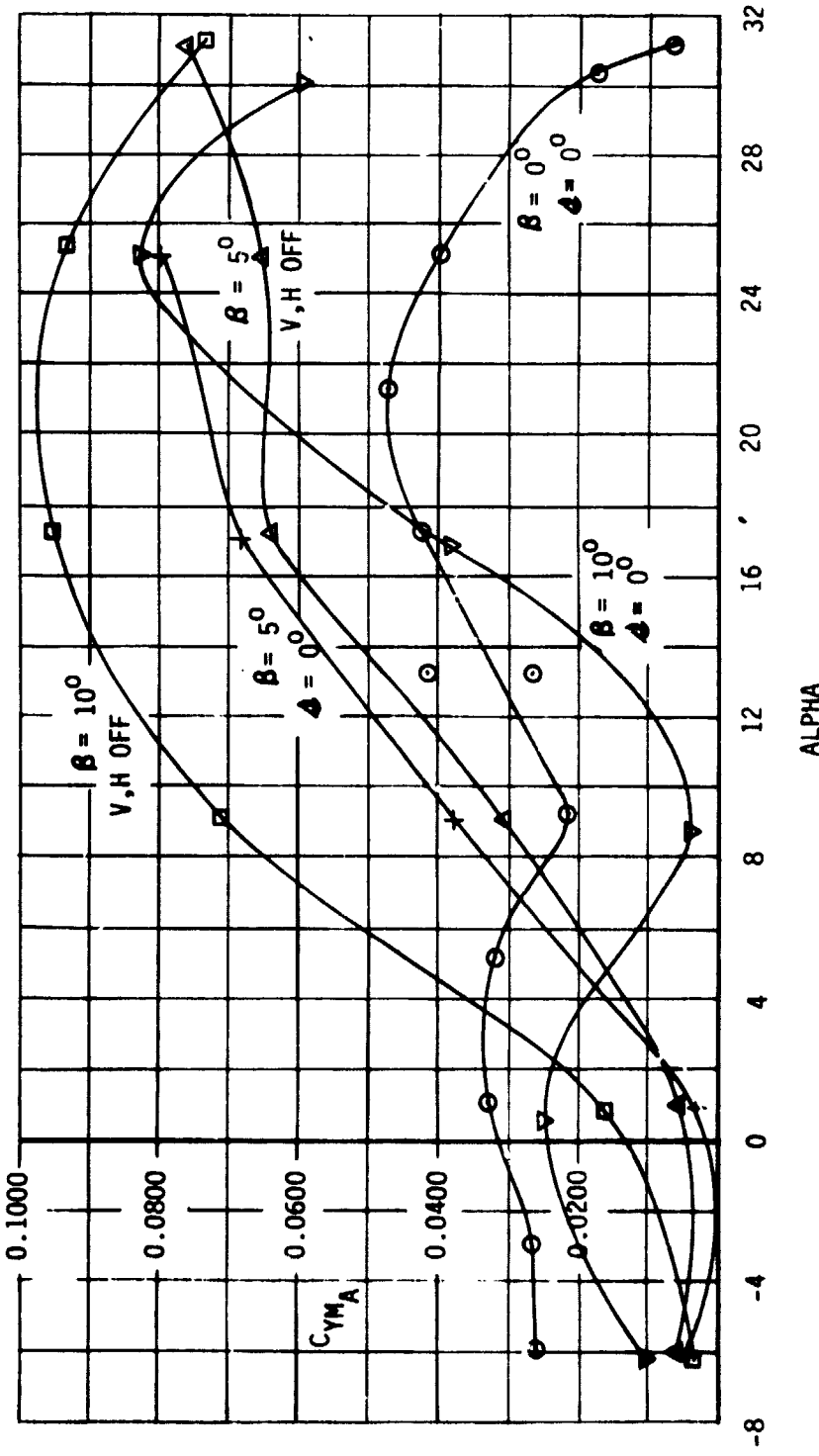


FIGURE 45 VERTICAL TAIL EFFECTIVENESS  $\lambda = 90^\circ, C_J = 3.7$

$\alpha \approx 0^\circ$   
 FLAPS DOWN  
 GEAR DOWN  
 THRUST & RAM COMPONENTS REMOVED  
 $C_J = 3.6$   
 $V/V_J = 0.29$

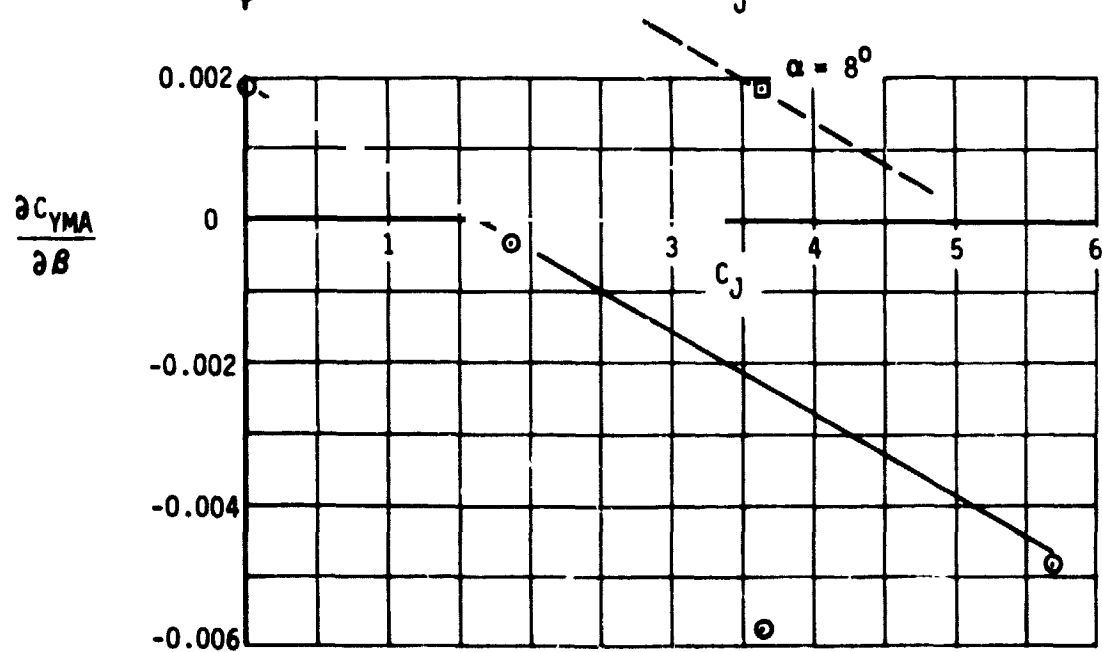
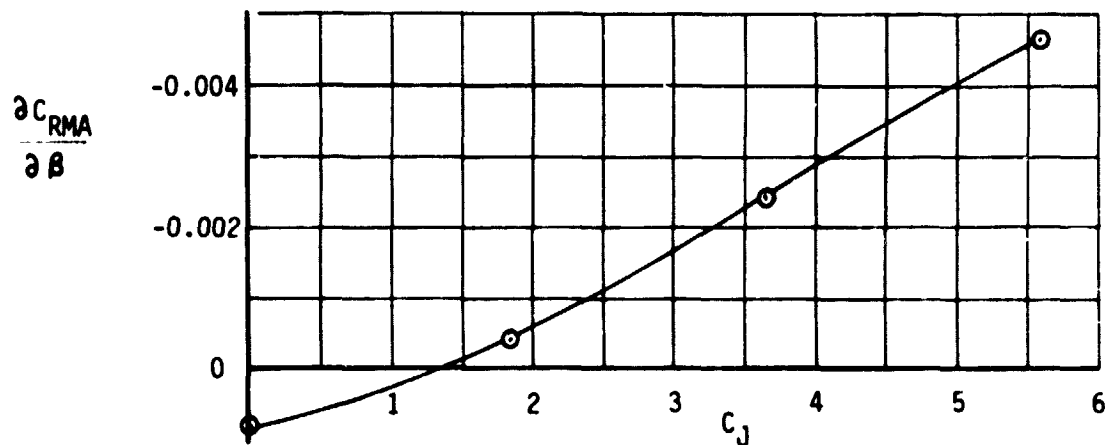
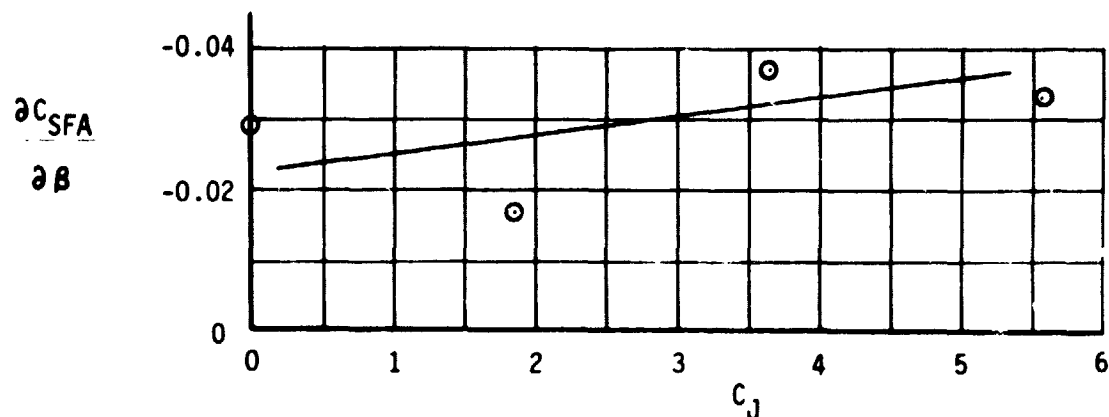


FIGURE 46 LATERAL - DIRECTIONAL DERIVATIVES  $\lambda = 90^\circ$  LOW ANGLE OF ATTACK  
89

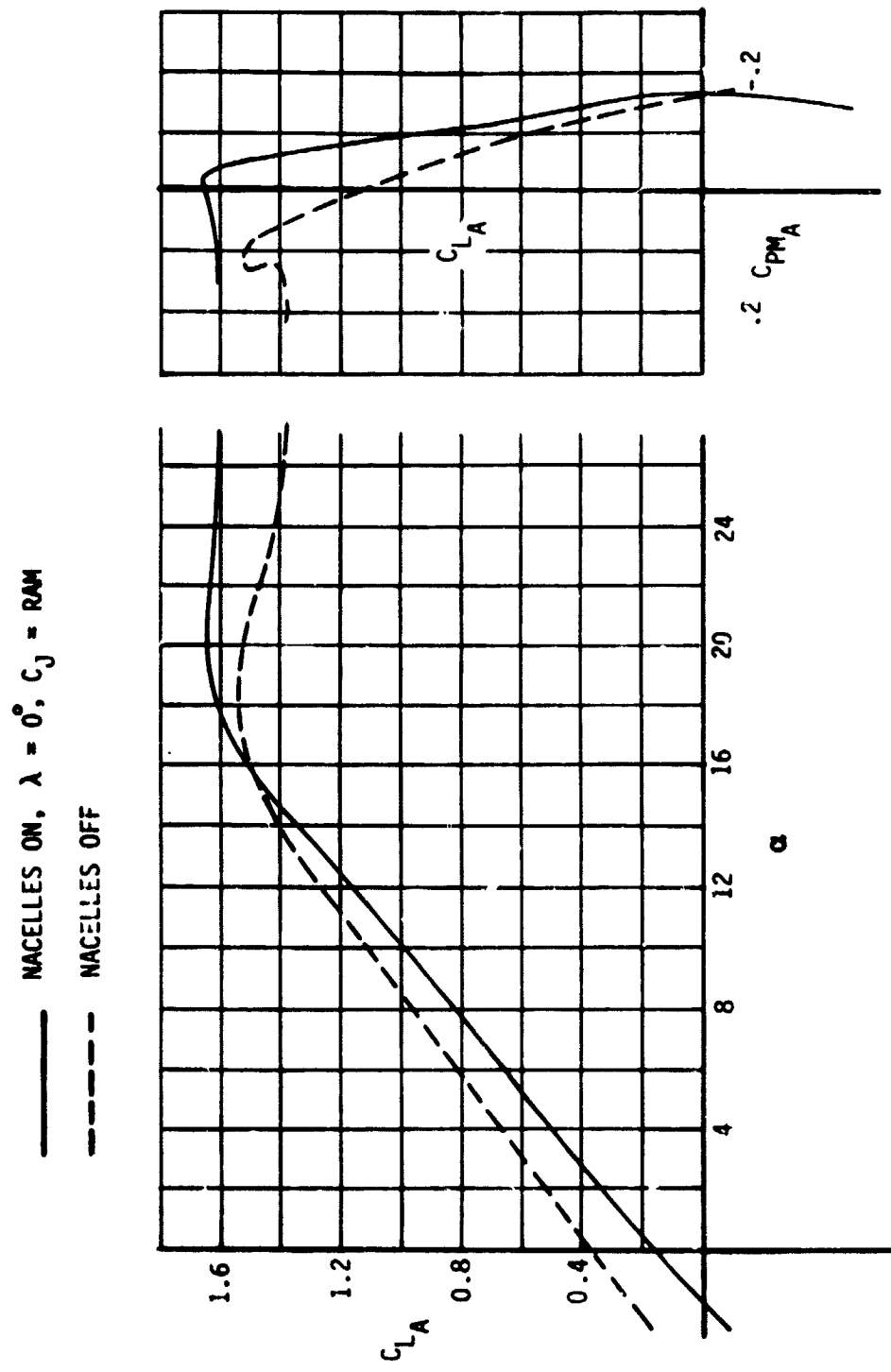


FIGURE 4 - EFFECT OF NACELLES FLAPS DOWN

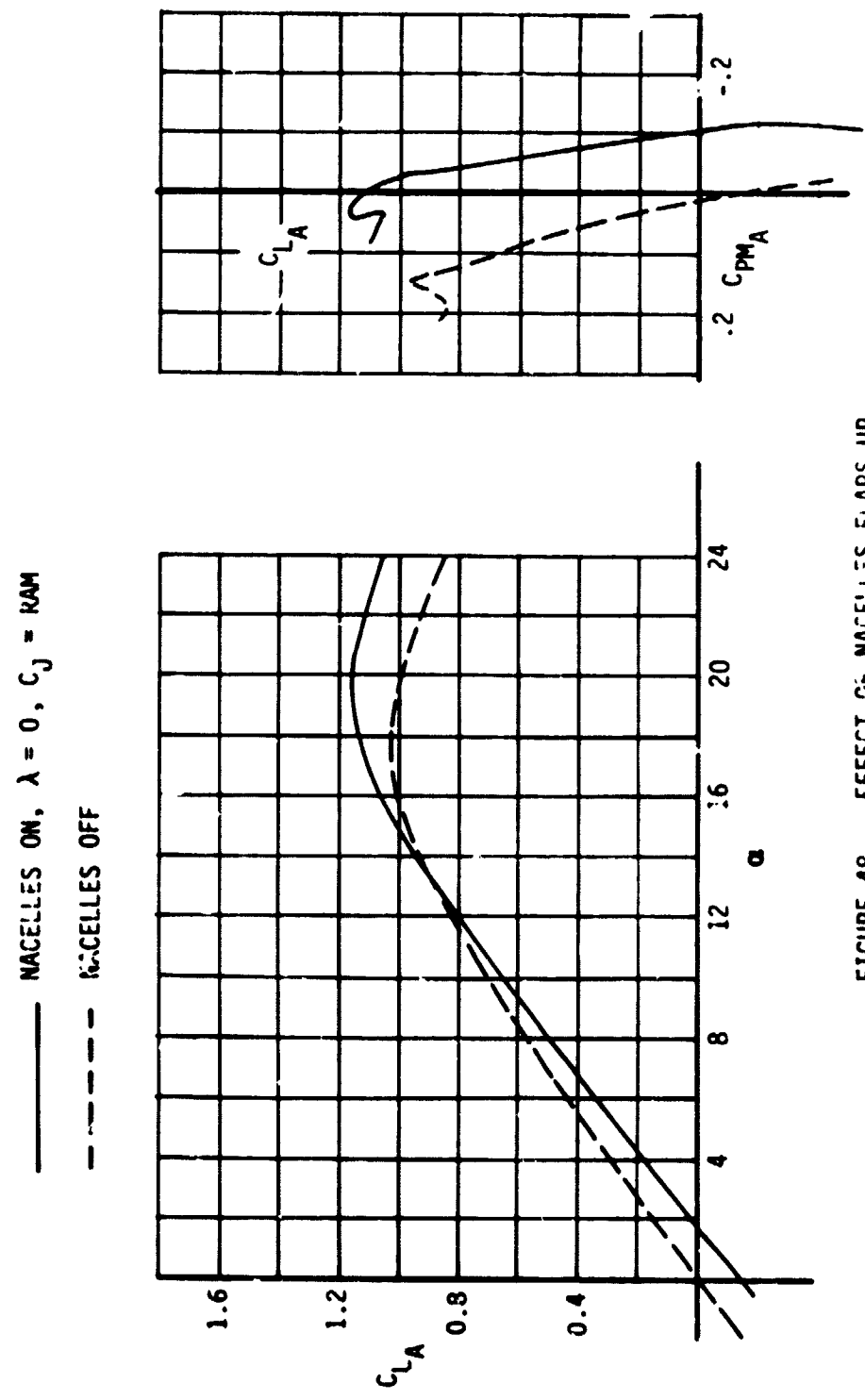


FIGURE 48 EFFECT OF NACELLES, FLAPS UP

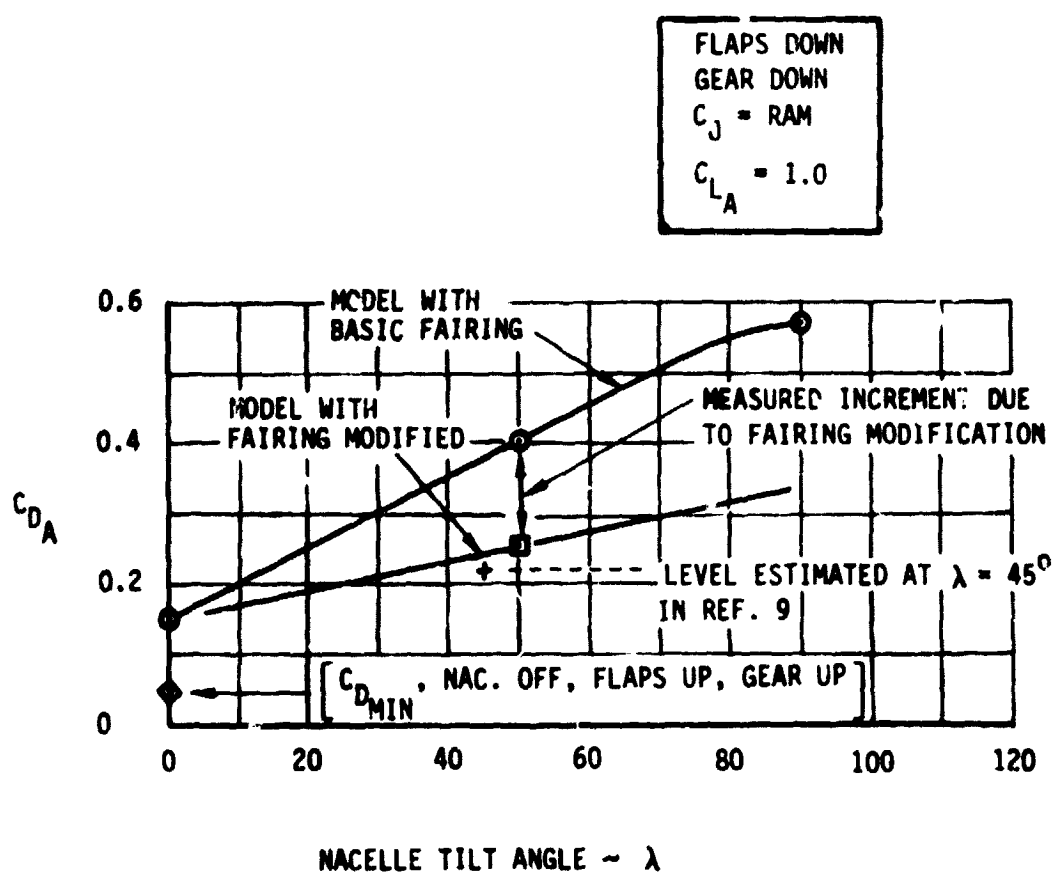


FIGURE 49 EFFECT OF NACELLES ON DRAG LEVEL,  $C_J = \text{RAM}$

THE **BOEING** COMPANY

APPENDIX A

WIND TUNNEL TEST DATA

## INDEX OF FIGURES IN APPENDIX A

FIGURE	TITLE
A.1	VTOL configuration characteristics LAMBDA = 90 <sup>0</sup> Tail Angle = 0 <sup>0</sup>
A.2	VTOL configuration characteristics LAMBDA = 90 <sup>0</sup> H. Tail off
A.3	Effect of horizontal tail LAMBDA = 90 <sup>0</sup> , C <sub>J</sub> = 0
A.4	Effect of horizontal tail LAMBDA = 90 <sup>0</sup> , C <sub>J</sub> = 3.7
A.5	Effect of landing gear LAMBDA = 90 <sup>0</sup> , C <sub>J</sub> = 3.7
A.6	Effect of thrust level at C <sub>J</sub> ≈ CONST.
A.7	Effect of differential thrust LAMBDA = 90 <sup>0</sup> , H. Tail off, $\beta$ = 0 <sup>0</sup>
A.8	Effect of differential thrust LAMBDA = 90 <sup>0</sup> , C <sub>J</sub> = 3.7, $\beta$ = 5 <sup>0</sup>
A.9	Effect of differential thrust LAMBDA = 90 <sup>0</sup> , C <sub>J</sub> = 3.7, $\beta$ = 10 <sup>0</sup>
A.10	Vertical tail effectiveness LAMBDA = 90 <sup>0</sup> , C <sub>J</sub> = 0
A.11	Vertical tail effectiveness LAMBDA = 90 <sup>0</sup> , C <sub>J</sub> = 0
A.12	Vertical tail effectiveness LAMBDA = 90 <sup>0</sup> , C <sub>J</sub> = 1.8
A.13	Vertical tail effectiveness LAMBDA = 90 <sup>0</sup> , C <sub>J</sub> = 1.8
A.14	Vertical tail effectiveness LAMBDA = 90 <sup>0</sup> , C <sub>J</sub> = 3.7
A.15	Vertical tail effectiveness LAMBDA = 90 <sup>0</sup> , C <sub>J</sub> = 3.7
A.15	Vertical tail effectiveness LAMBDA = 90 <sup>0</sup> , C <sub>J</sub> = 5.5

THE **BOEING** COMPANY

FIGURE	TITLE
A.17	Vertical tail effectiveness LAMBDA = 90°, C <sub>J</sub> = 5.5
A.18	Effect of engine tilt angle C <sub>J</sub> = 3.7 ground plane installed
A.19	Effect of engine tilt angle C <sub>J</sub> = 5.5, ground plane installed
A.20	Effect of ground plane LAMBDA = 90°, C <sub>J</sub> = 3.7
A.21	Effect of ground plane LAMBDA = 50°, C <sub>J</sub> = 1.8
A.22	STOL configuration characteristics LAMBDA = 50°, H. Tail off
A.23	STOL configuration characteristics LAMBDA = 50°, tail angle = 10°
A.24	Effect of horizontal tail LAMBDA = 50°, C <sub>J</sub> = 1.8
A.25	Effect of horizontal tail LAMBDA = 50°, C <sub>J</sub> = 3.7
A.26	Effect of nose-fan thrust variation LAMBDA = 50°, tail angle = 0°
A.27	Effect of nose fan thrust variation LAMBDA = 50°, H. Tail off
A.28	Effect of Aileron Droop LAMBDA = 50°
A.29	Effect of landing gear LAMBDA = 50°
A.30	CTOL configuration characteristics LAMBDA = 0°, H. Tail off
A.31	Effect of landing gear LAMBDA = 0°, flaps down, power off
A.32	Effect of landing gear LAMBDA = 0°, flaps down, power on
A.33	Effect of flap and slat LAMBDA = 0°

THE **BOEING** COMPANY

FIGURE	TITLE
A.34	Effect of horizontal tail $\text{LAMBDA} = 0^\circ$ , flaps up, $C_J = 1.2$
A.35	Effect of horizontal tail $\text{LAMBDA} = 0^\circ$ , flaps up, $C_J = 1.8$
A.36	Effect of flap door Nacelles off
A.37	Effect of flap and slat Nacelles off
A.38	Configuration buildup Power off
A.39	Effect of nose fan thrust variation $\text{LAMBDA} = 0^\circ$ , H. Tail off

## APPENDIX A

## WIND TUNNEL TEST DATA

Appendix A contains plots of all valid data runs obtained from the wind tunnel tests conducted under this contract. Each figure consists of three pages for symmetrical data, or six pages for assymmetrical data. Parameters plotted are:

Symmetrical Data       $\left\{ \begin{array}{l} CLA \text{ vs } \text{ALPHA} \\ CDA \text{ vs } CLA \\ CPMA \text{ vs } CLA \end{array} \right.$

Asymmetrical Data       $\left\{ \begin{array}{l} \text{The above parameters plus} \\ CRMA \text{ vs } \text{ALPHA} \\ CYMA \text{ vs } \text{ALPHA} \\ CSFA \text{ vs } \text{ALPHA} \end{array} \right.$

The data represent "aerodynamic data" in that direct thrust and ram forces have been removed. The aerodynamic data does contain propulsion induced effects. The determination of direct thrust and ram forces is discussed in Appendix B and the removal of direct thrust and ram forces is discussed in Appendix C. Also presented in Appendix C (Figure C.1) is a tracking of data through the reduction process and a description of the wind tunnel wall constraint corrections which were applied to the data.

Out of necessity, a portion of the lift/cruise fan nacelle strut was rotated with the nacelles during the wind tunnel test program to cover plumbing to the turbopowered simulators and the "blown" primary. That fairing had a large effect upon the drags of the STOL and VTOL test configurations which would not be present on the full scale airplane. To assess the drag difference due to the fairing, a test run was made with the fairing removed and tape and wax applied to cover and fair

THE **BOEING** COMPANY

over the exposed plumbing and instrumentation. As discussed in the body of the report, the reduction in drag coefficient due to removing the fairing amounted to 0.15 but further reductions are probably possible. The drag data in this appendix are not representative of airplane drag levels to the extent that they are affected by this fairing.

Figures A.18 thru A.21 contain data which were taken with a ground plane installed in the tunnel. While these data do not represent ground height series, there was some variation of ground height as the model was pitched. Since these data were corrected for wall effects of three walls only, the ground effect is a part of the data. The ground height to model mean aerodynamic chord ratios can be represented by straight lines between the following three points:  $\alpha = -5^0$ ,  $h/\bar{c} = 2.45$ ;  $\alpha = 12^0$ ,  $h/\bar{c} = 3.40$ ;  $\alpha = 31^0$ ,  $h/\bar{c} = 4.90$ . It should also be noted that the ground plane reduced the tunnel width (which is "height" relative to the model since it is installed with wings vertical) from 105 inches to 77 inches.

Model Nomenclature

The plots in this appendix contain a shorthand notation to designate the specific model configuration. This notation is defined as follows:

- C1      Trailing edge flaps deflected  
          Trailing edge flap door down  
          Leading edge slat extended  
          Nose fan doors in open position (both upper & lower)  
          Basic nacelles and nacelle - fuselage fairings installed
- C2      Same as C1 except trailing edge flap door is up  
(i.e., it is aligned with the basic trailing  
edge flap)
- C3      Trailing edge flaps deflected  
          Trailing edge flap door up  
          Leading edge slat extended  
          Nose fan doors in closed position (both upper & lower)  
          Basic nacelles and nacelle - fuselage fairings installed
- C4      Trailing edge flaps & flap door nested  
          Leading edge slat nested  
          Nose fan doors in closed position (both upper & lower)  
          Basic nacelles and nacelle - fuselage fairings installed
- C5      The lift/cruise nacelles and the portion of the nacelle -  
          fuselage fairing attached to the nacelles are removed from  
          the model. The resulting cavities on the body sides are  
          taped over for a smooth fairing.  
          Nose fan doors in closed position  
          Leading edge slat nested  
          Trailing edge flap position as noted by "F" designation
- G        Main and nose landing gear and landing gear doors installed

THE **BOEING** COMPANY

V Vertical tail installed

H Horizontal tail installed

F25/25 Trailing edge flap deflected

Trailing edge flap door aligned with flap

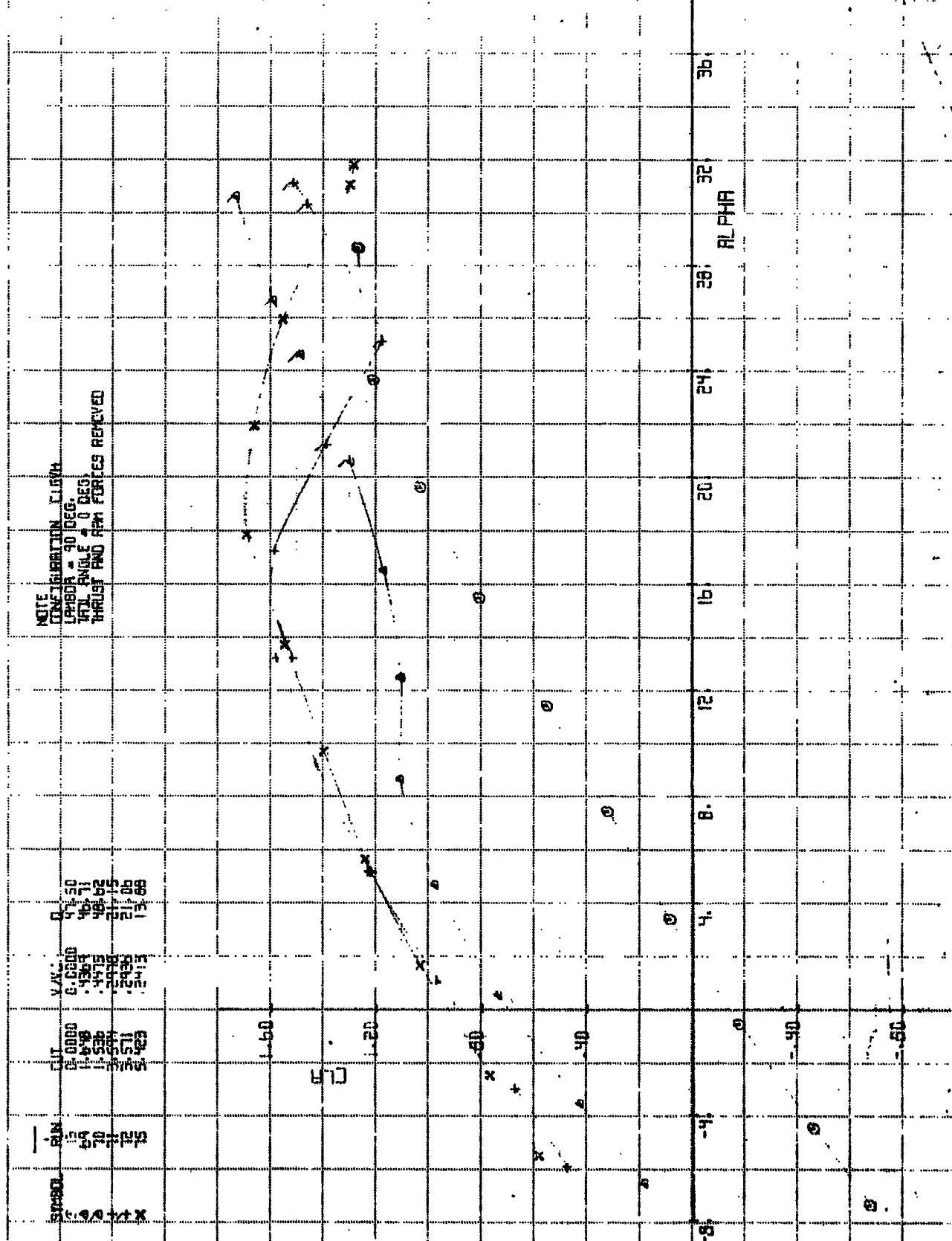
F25/110 Trailing edge flap deflected

Trailing edge flap door down

Note: C1 thru C5 do not have tail surfaces and gear installed unless followed by the appropriate symbols,

Example: C1GVH is C1 with gear, vertical tail and horizontal tail installed.

ORIGINAL PAGE IS  
OF POOR QUALITY



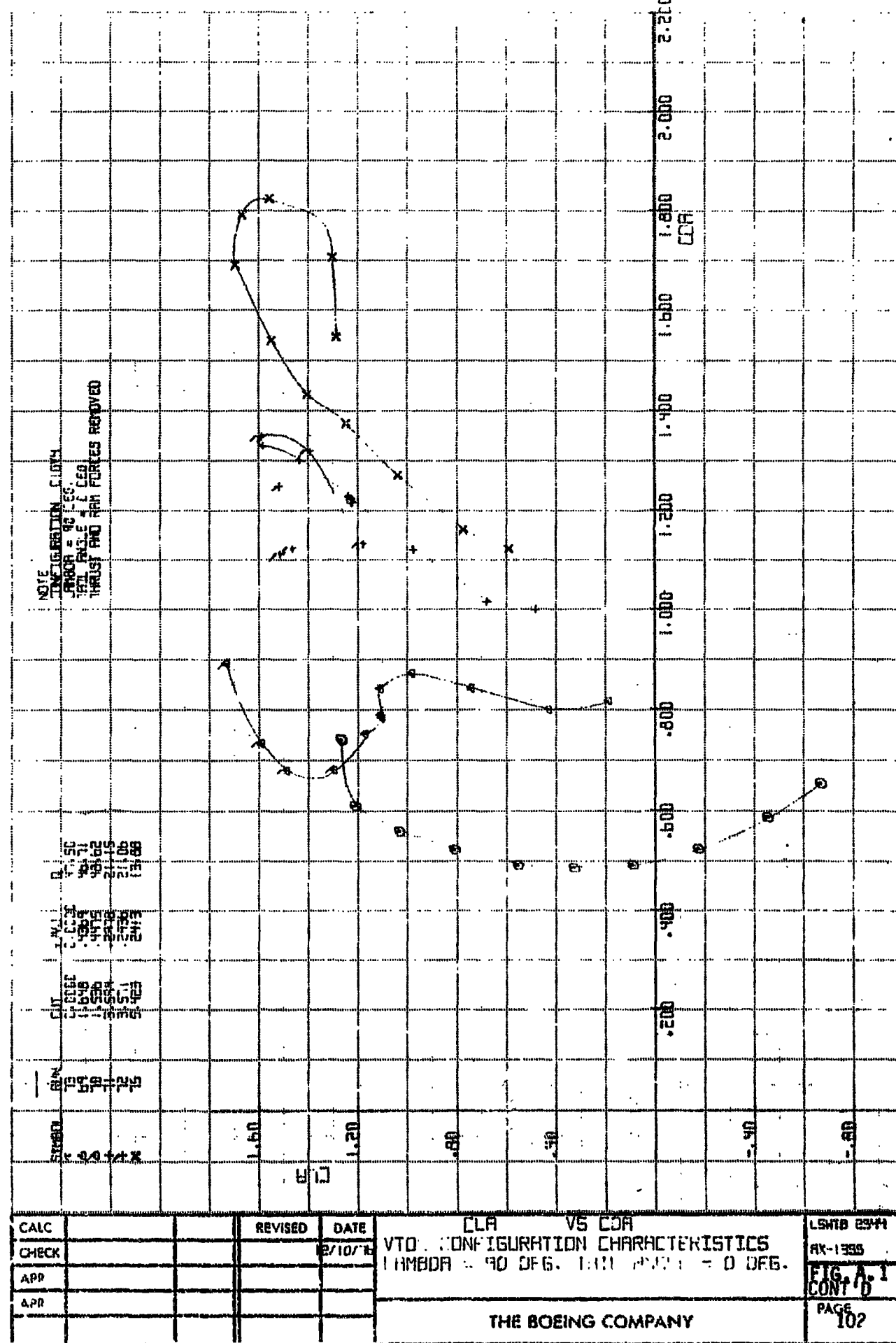
CALC			REVISED	DATE
CHECK				8/10/11
APR				
APR				

C.I.A VS ALPHA  
VITAL CONFIGURATION CHARACTERISTICS  
LAMBDA = 90 DEG. TAIL. ANGLE = 0 DEG.

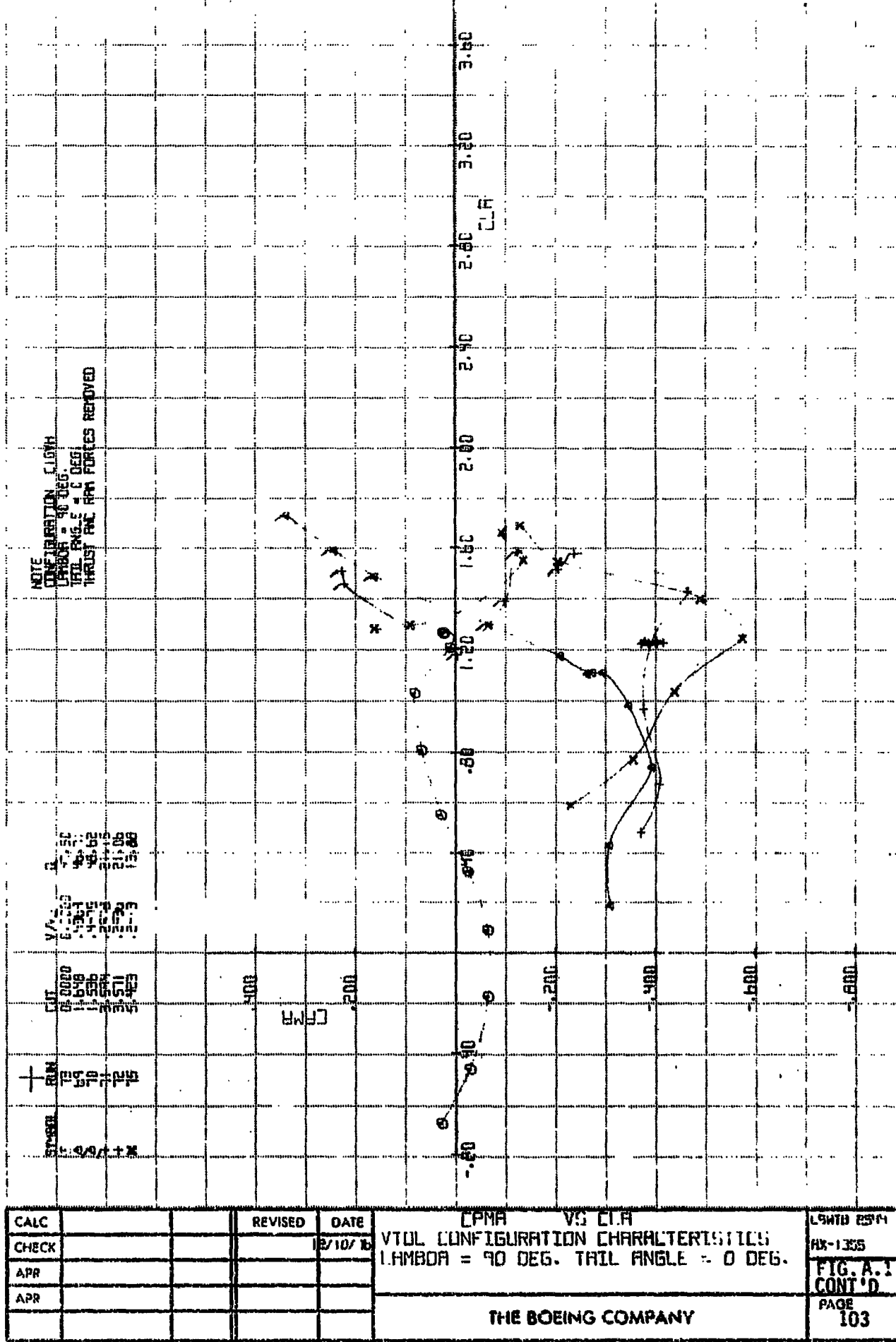
THE BOEING COMPANY

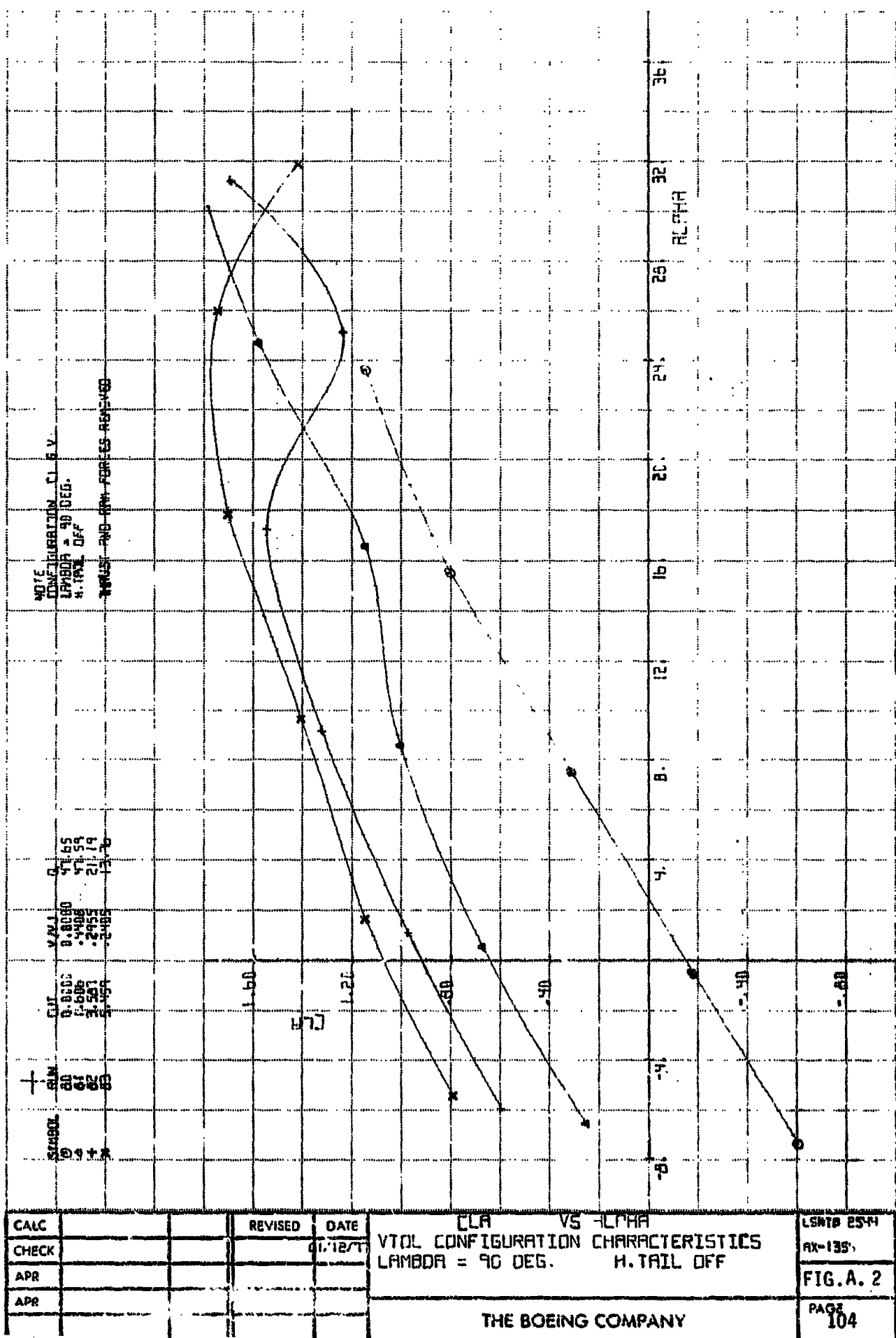
LSW1B 2544  
RIV-1353  
**FIG.A.1**  
PAGE  
**101**

କବିତା ପରିଚୟ

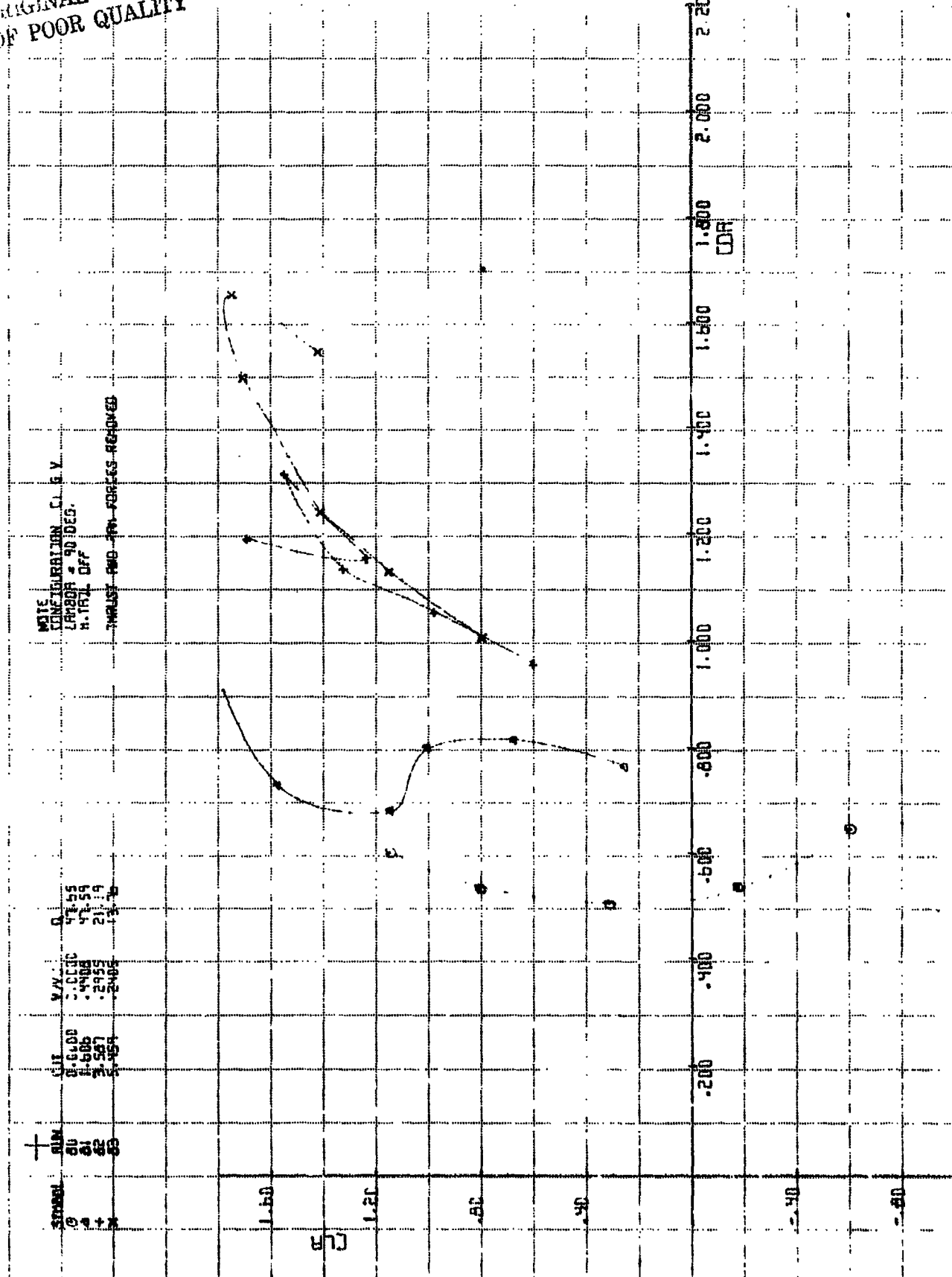


ORIGINAL PAGE IS  
OF POOR QUALITY

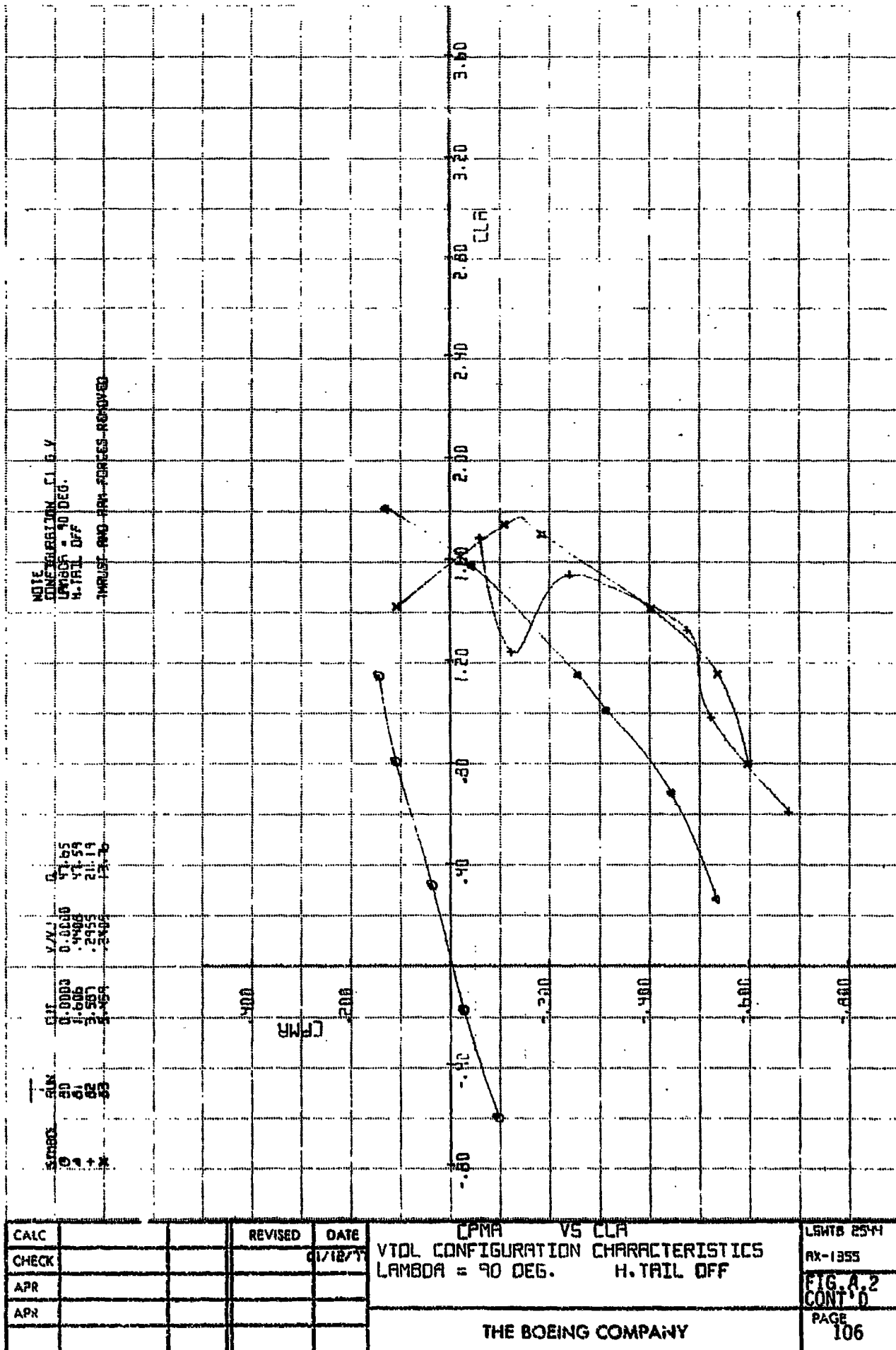




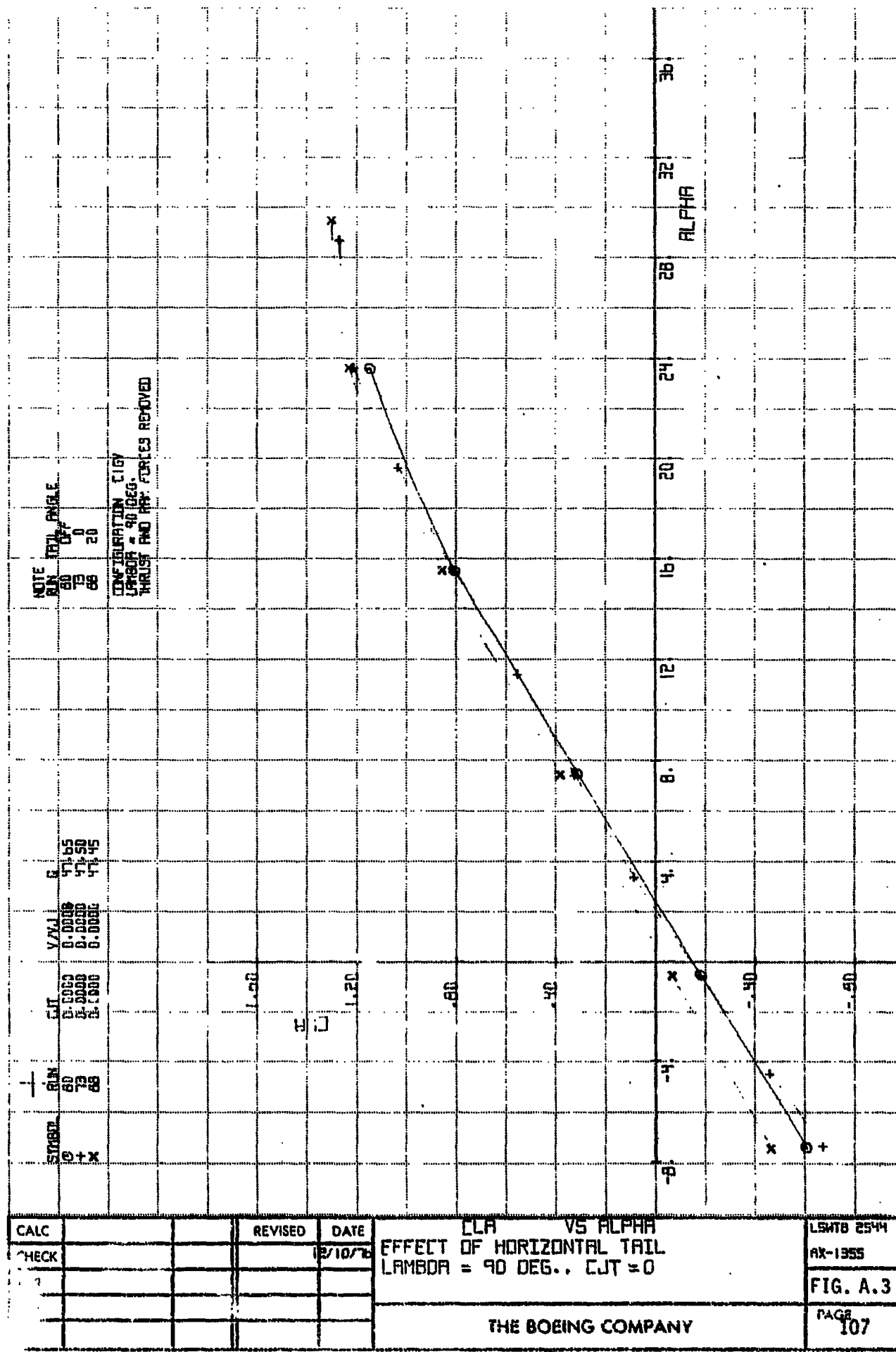
MARGINAL PAGE IS  
OF POOR QUALITY

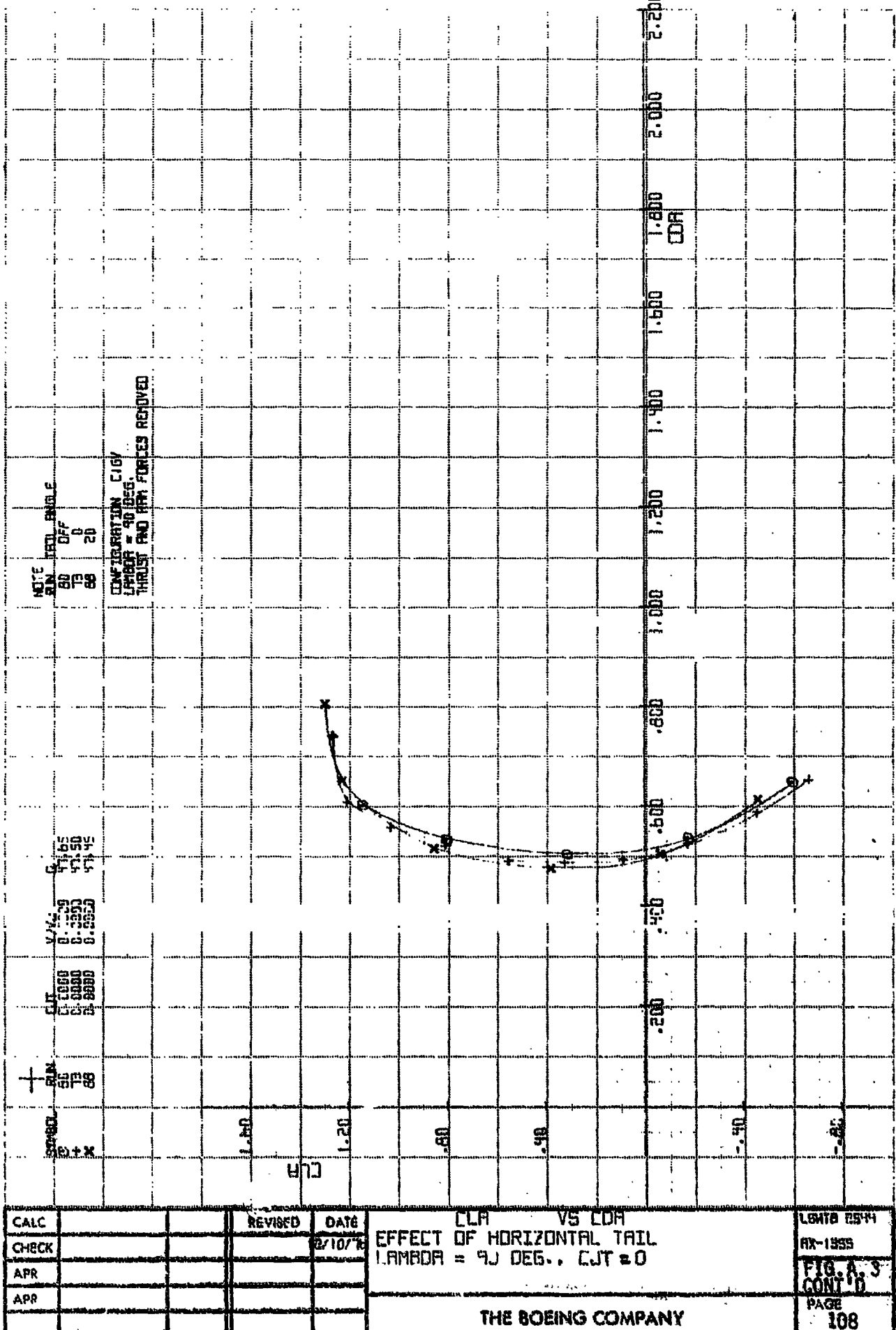


CALC		REVISED	DATE 01/12/11	LTH V.T CDR VTOL CONFIGURATION CHARACTERISTICS LAMBDA = 90 DEG. H.TAIL OFF	LSH10 2511 HX-135
CHECK					FIG. A.2 CONT'D
APR					PAGE 105
APR					
				THE BOEING COMPANY	

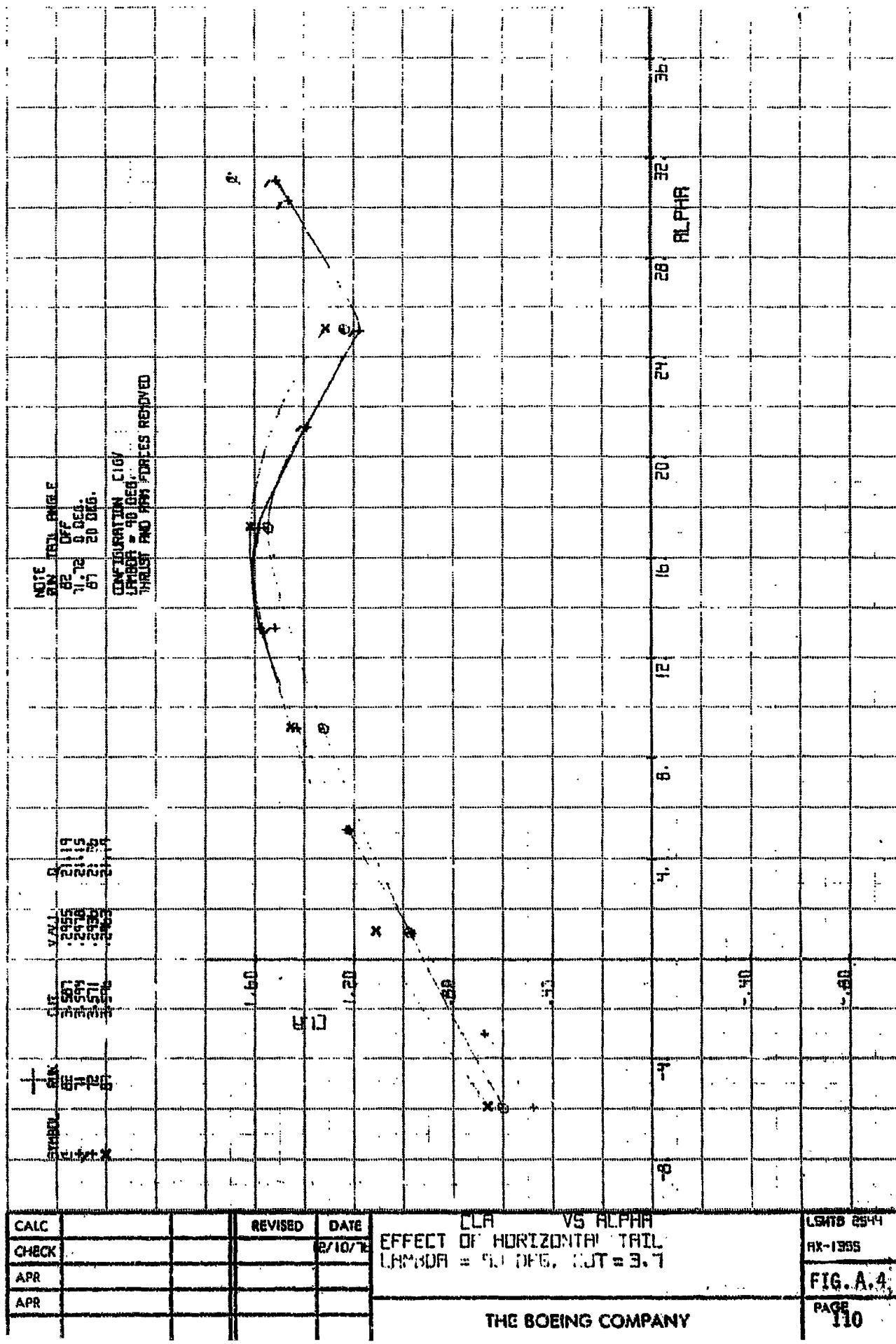


CREATED PAGE IS  
OF POOR QUALITY

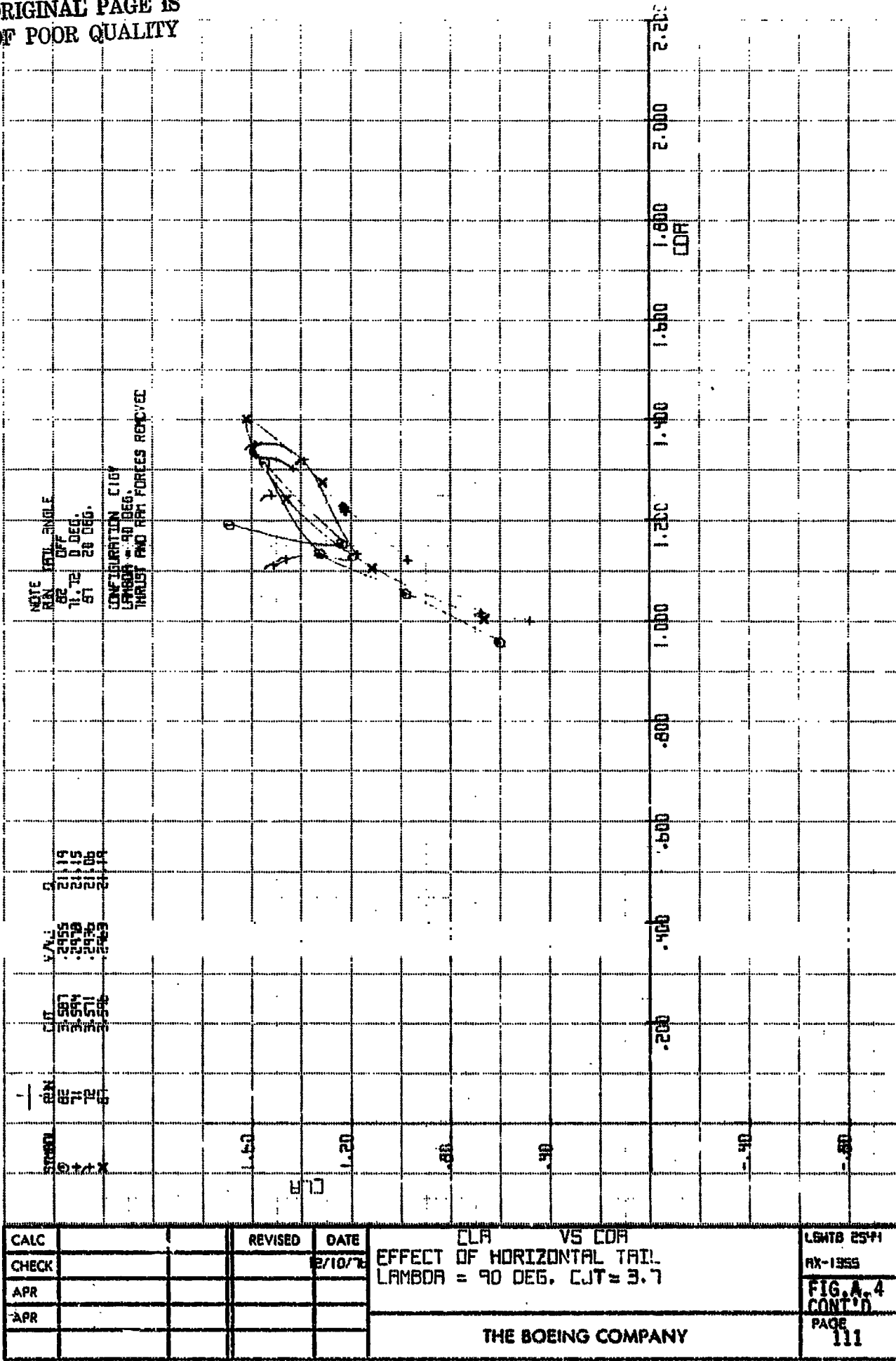


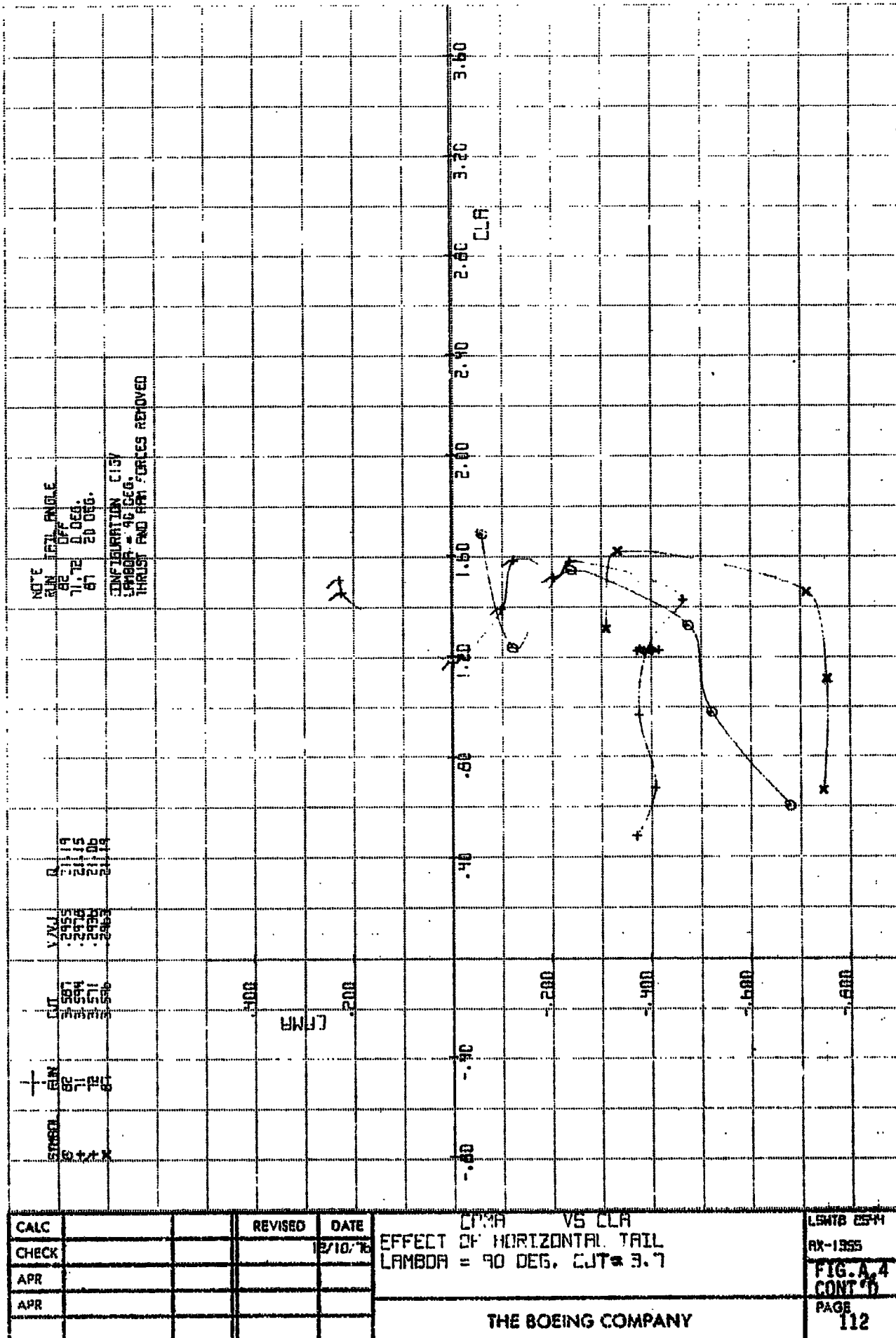


NOTE BIN		1511-BN-1-E		OFF		00		13		0		21	
BIN		88											
CONFIRMATION C16/				LHMMA = 90 DEG.		TRAIL AND FORCES REVERSED							
CALC		85		85		0.0000		0.0000		0.0000		0.0000	
CHECK		85		85		0.0000		0.0000		0.0000		0.0000	
APR		85		85		0.0000		0.0000		0.0000		0.0000	
APR		85		85		0.0000		0.0000		0.0000		0.0000	
REVISED		DATE		CPMA VS CLR		EFFECT OF HORIZONTAL TAIL		LHMMA = 90 DEG., C1T=0		LSM101594		RX-1989	
FIG 5		11		5/10/86								FIG A-3	
THE BOEING COMPANY										PAGE		109	



ORIGINAL PAGE IS  
OF POOR QUALITY





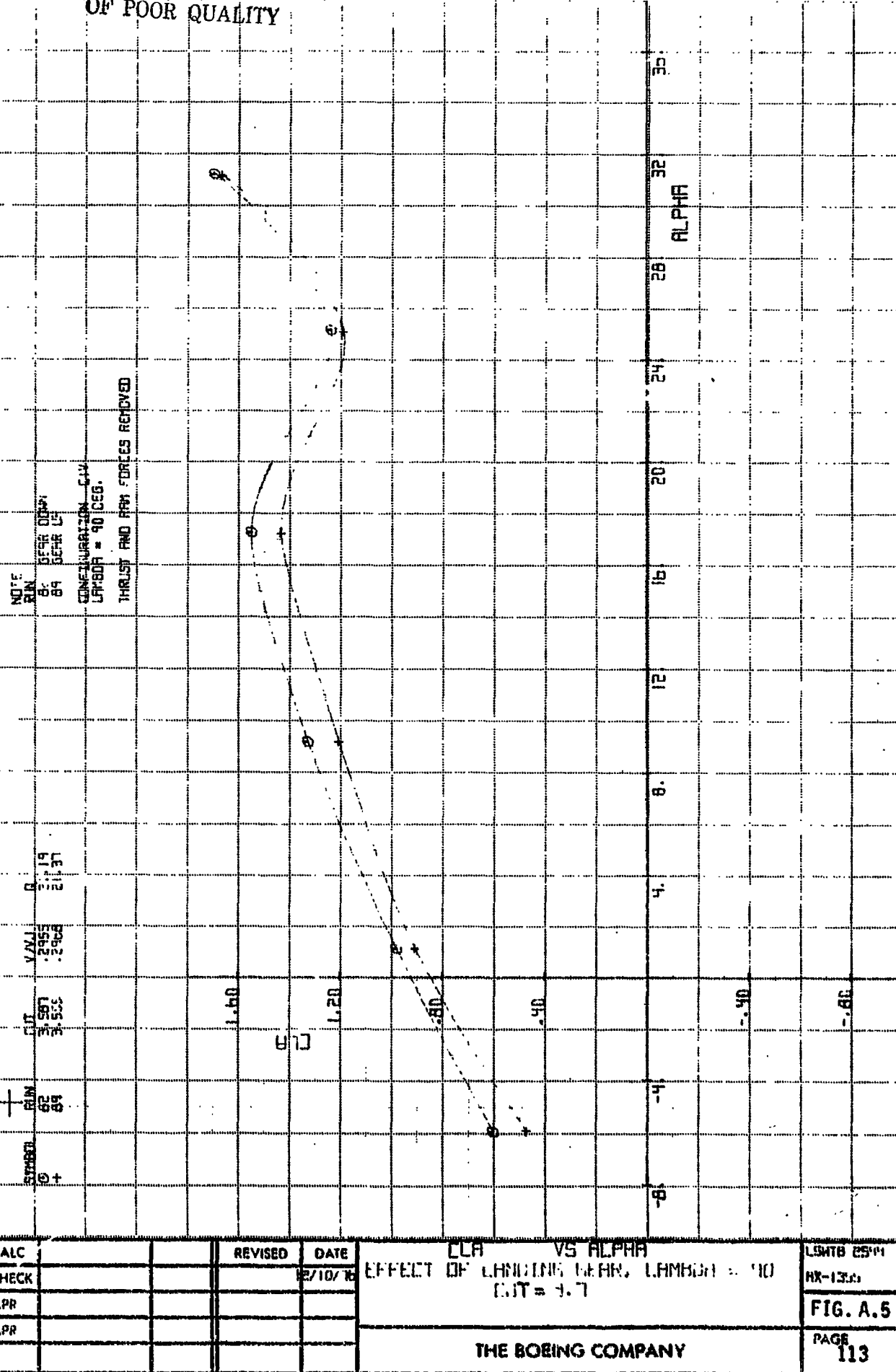
ORIGINAL PAGE IS  
OF POOR QUALITY

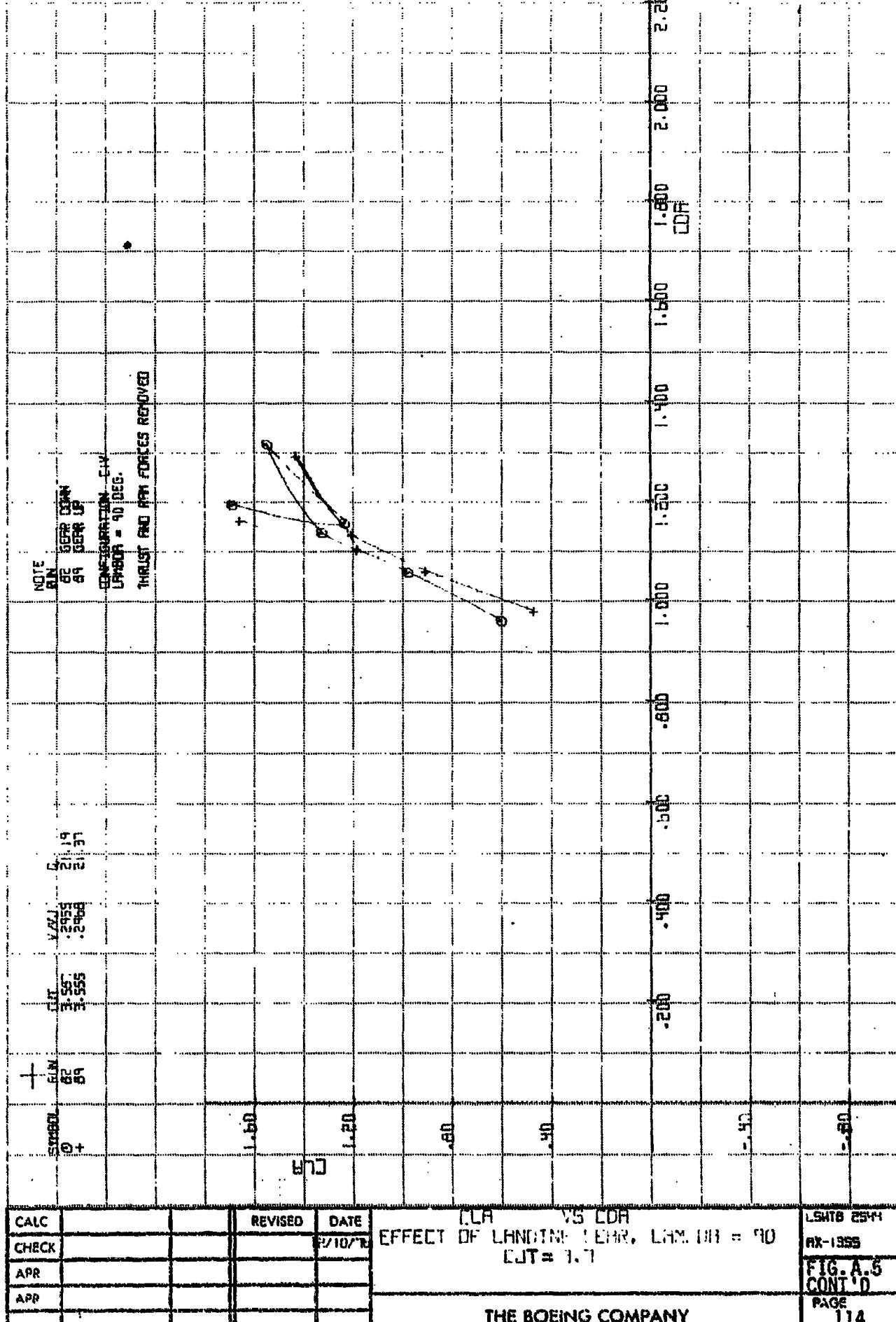
STABIL	FUN	FIT	Y/N	8	19	21	31	33
G	62	3.597	.295					
G +	65	3.555	.295					

CONFIGURATION CYL

LFBDA = 90 CEG.

THRUST AND RAM FORCES REMOVED





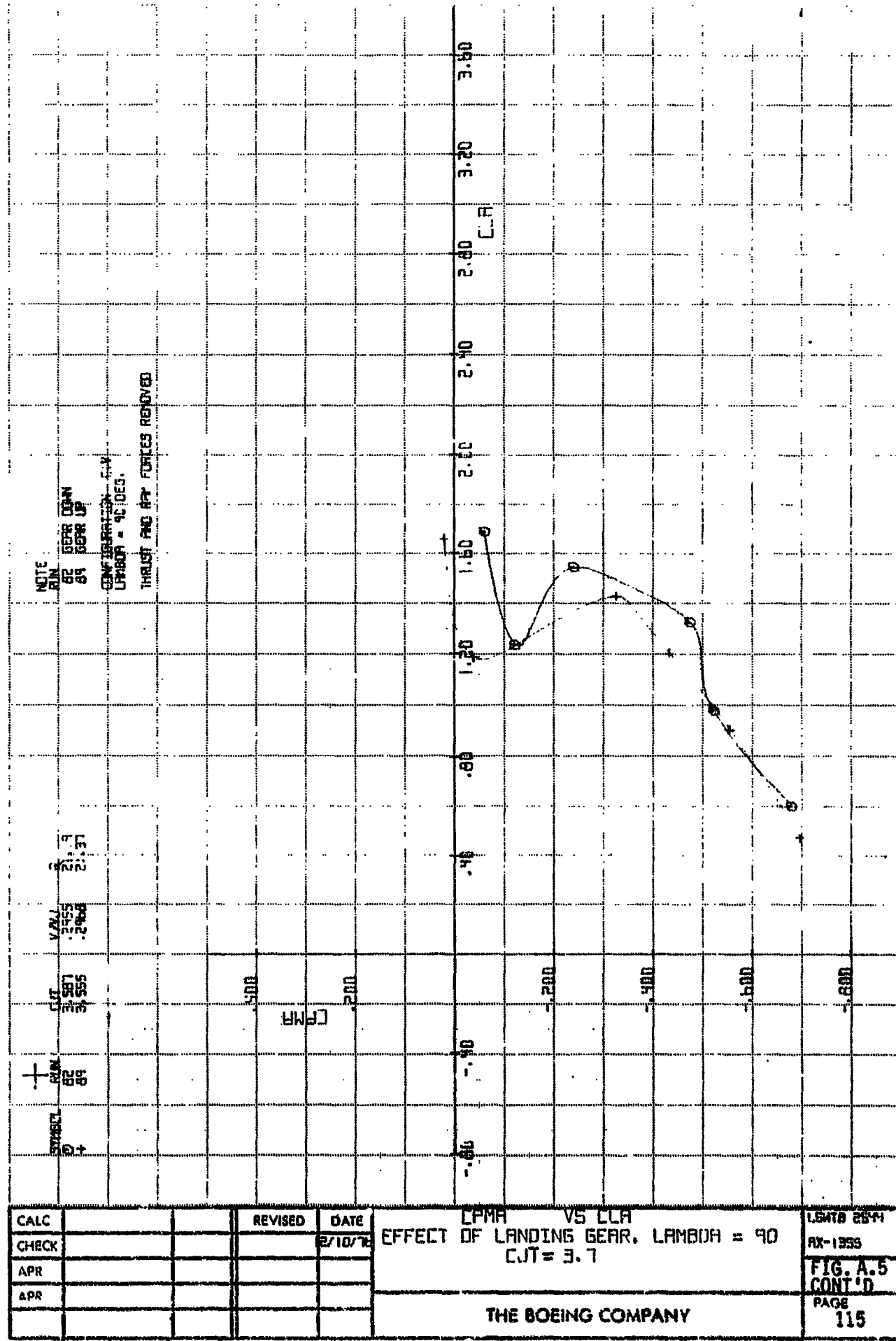
EFFECT OF LANDING GEAR, LAM.DR = 90  
CJT = 1.1

L5HTB ८५४

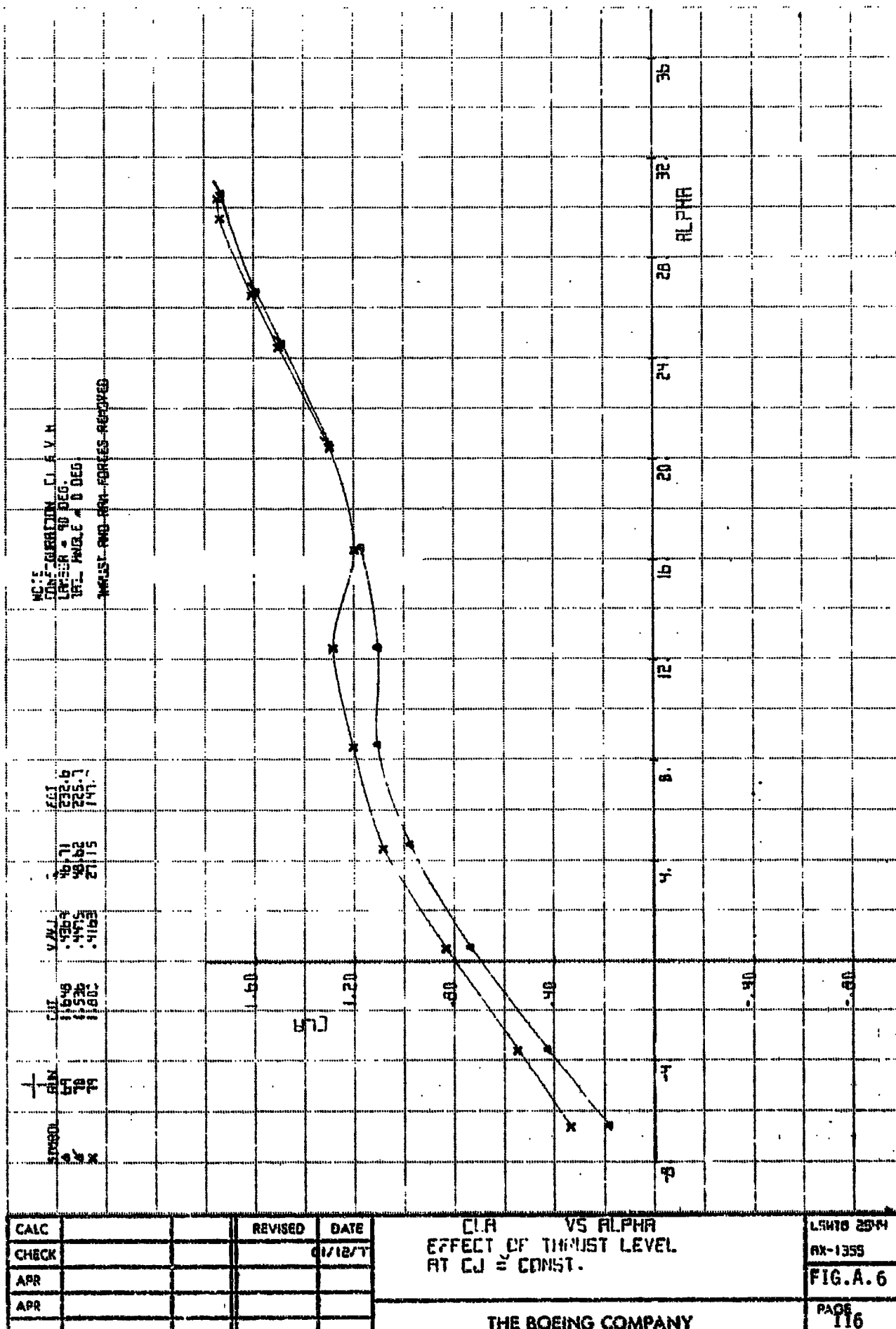
AX-1955

**FIG. A.5**  
**CONT'D**

PAGE  
173



F15 7

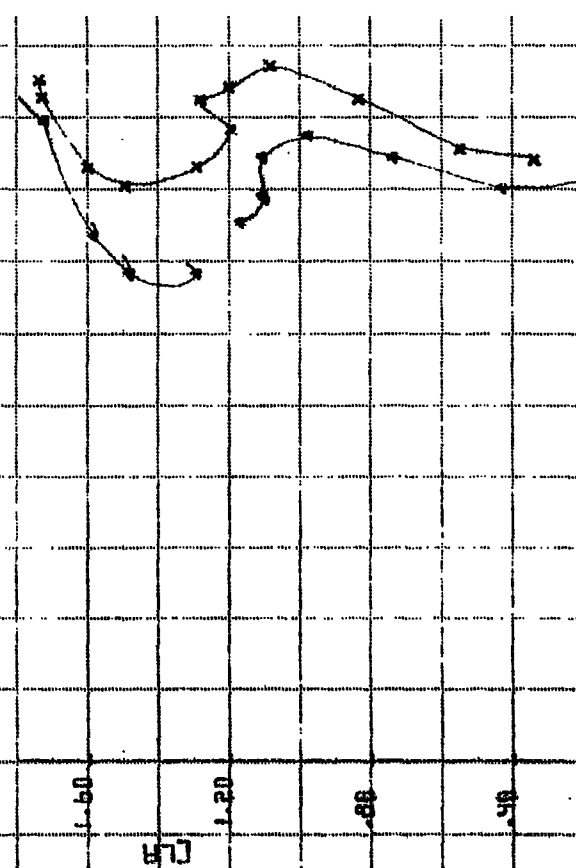


ORIGINAL PAGE IS  
OF POOR QUALITY

NOTE:  
CLB INJECTION C. J. G. V.  
US = 1.0 • 90 DEG.  
US = 1.0 • 0 DEG.  
THERM. ANGLE = 0 DEG.  
PARTS NUMBER

CLB  
0.71  
0.72  
0.73  
0.74  
0.75  
0.76  
0.77  
0.78  
0.79  
0.80

CLB  
0.71  
0.72  
0.73  
0.74  
0.75  
0.76  
0.77  
0.78  
0.79  
0.80



1.000 1.200 1.400 1.600 1.800 2.000 2.200

-0.40

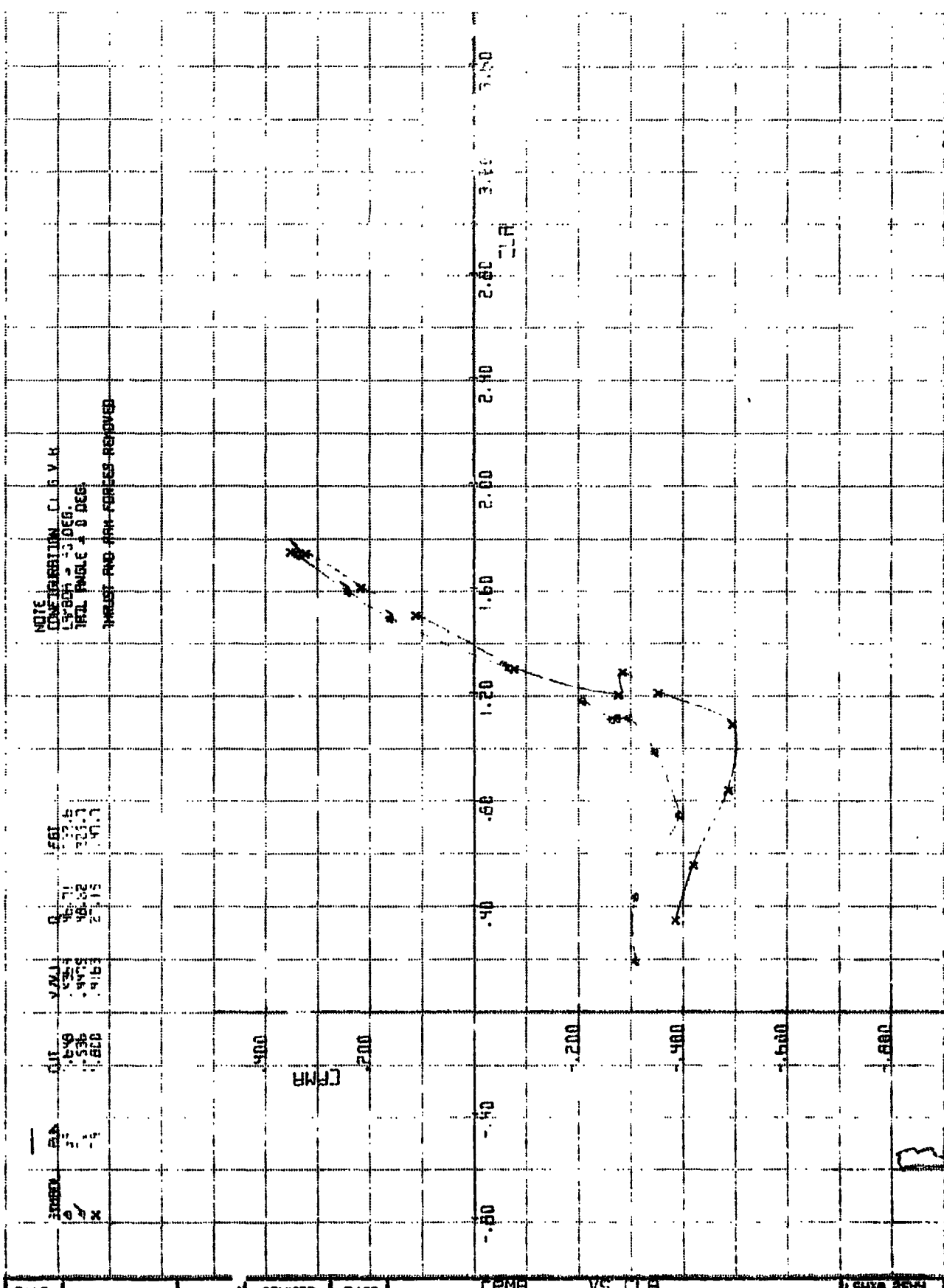
-0.40

CALC		REVISED	DATE
CHECK			6/12/71
APP			
APP			

CLA VS CDH  
EFFECT OF THRUST LEVEL  
AT CJ = CONST.

THE BOEING COMPANY

L5HTD 2544
FIG. A.5
CONT'D
PAGE 117

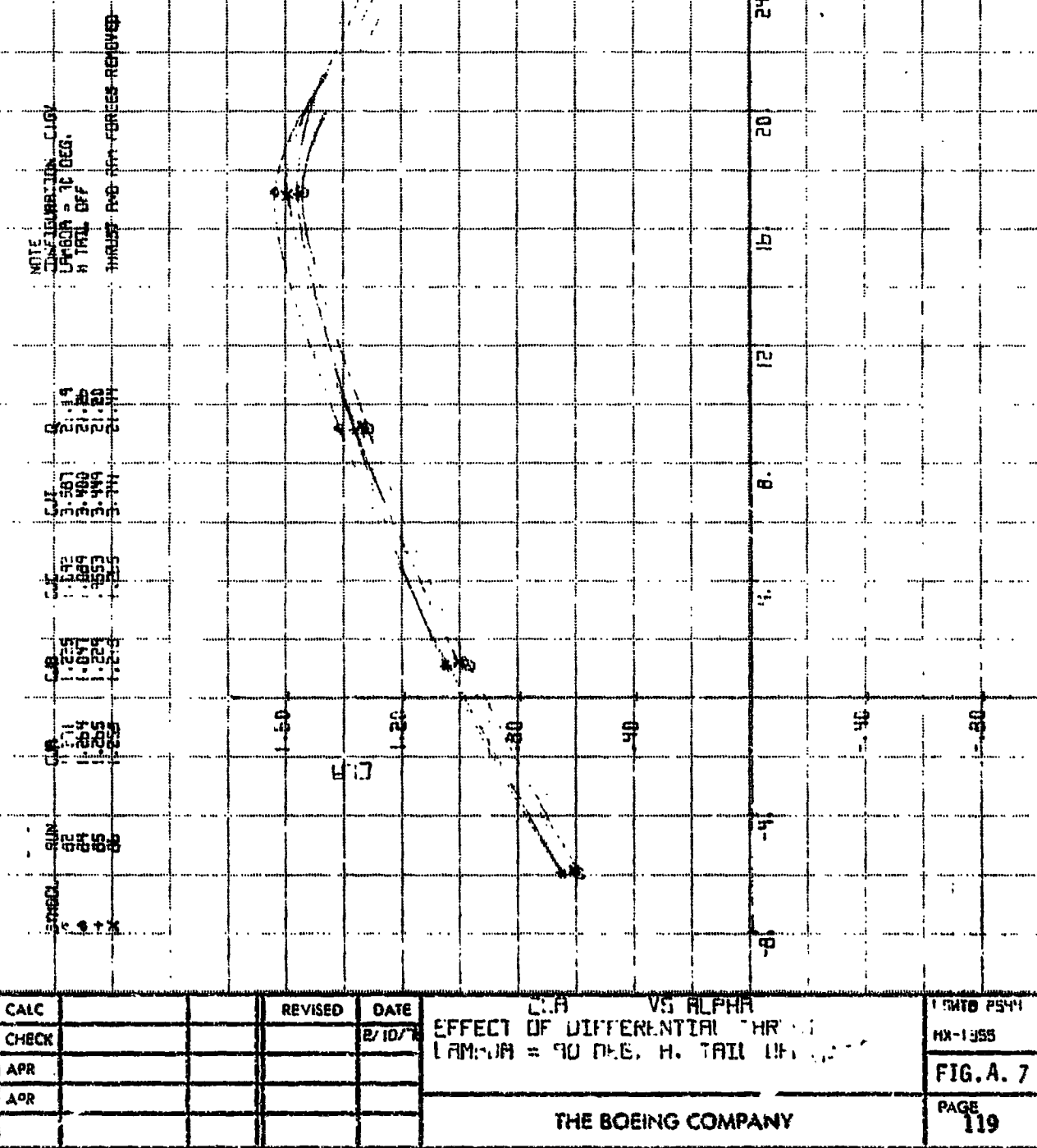


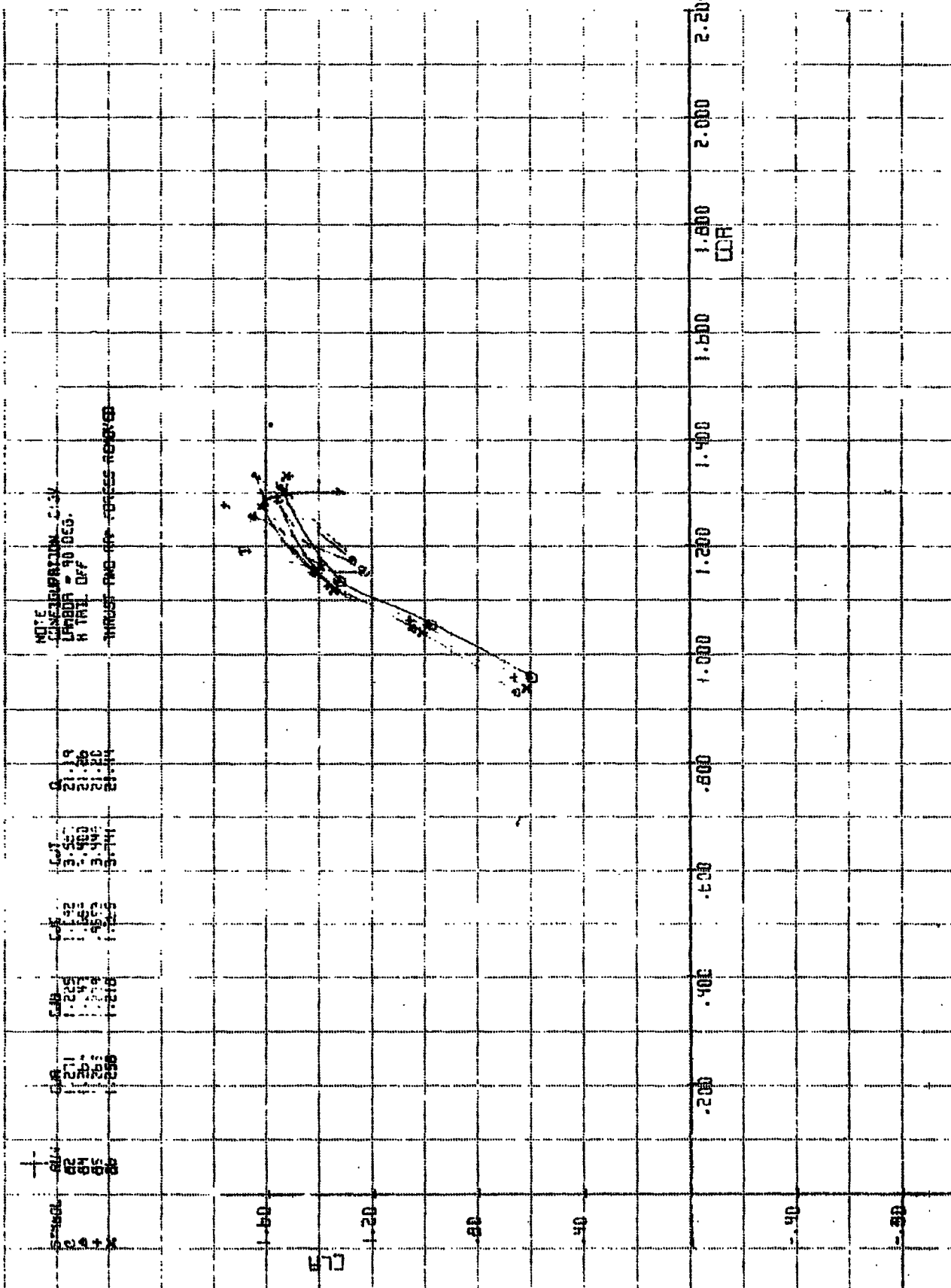
THE BOEING COMPANY

LSHYD 2544  
RX-1950  
FIG.A.6  
CONT'D  
PAGE  
118

( )  
FD  
5.

ORIGINAL PAGE IS  
OF POOR QUALITY





CALC	REVISED	DATE
CHECK		3/10/78
APR		
APR		

CL<sub>A</sub> VS CDR  
EFFECT OF DIL. AERONAUTIC THRUST  
HMMDDH - 90 DEG. H. TAIL OFF,

LW102544  
MX-1359  
FIG. A.7  
CONT'D  
PAGE  
120

ORIGINAL PAGE IS  
OF POOR QUALITY

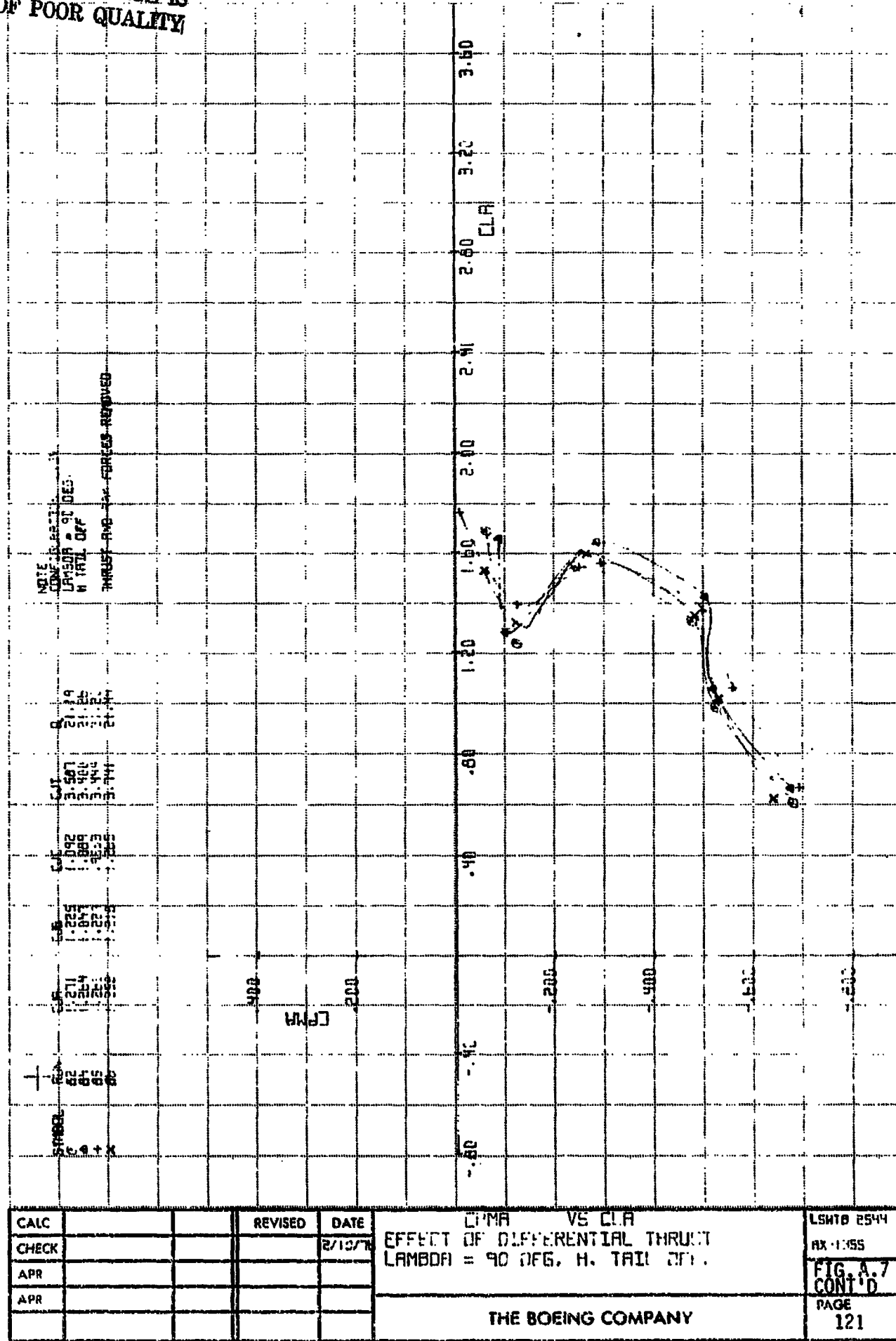
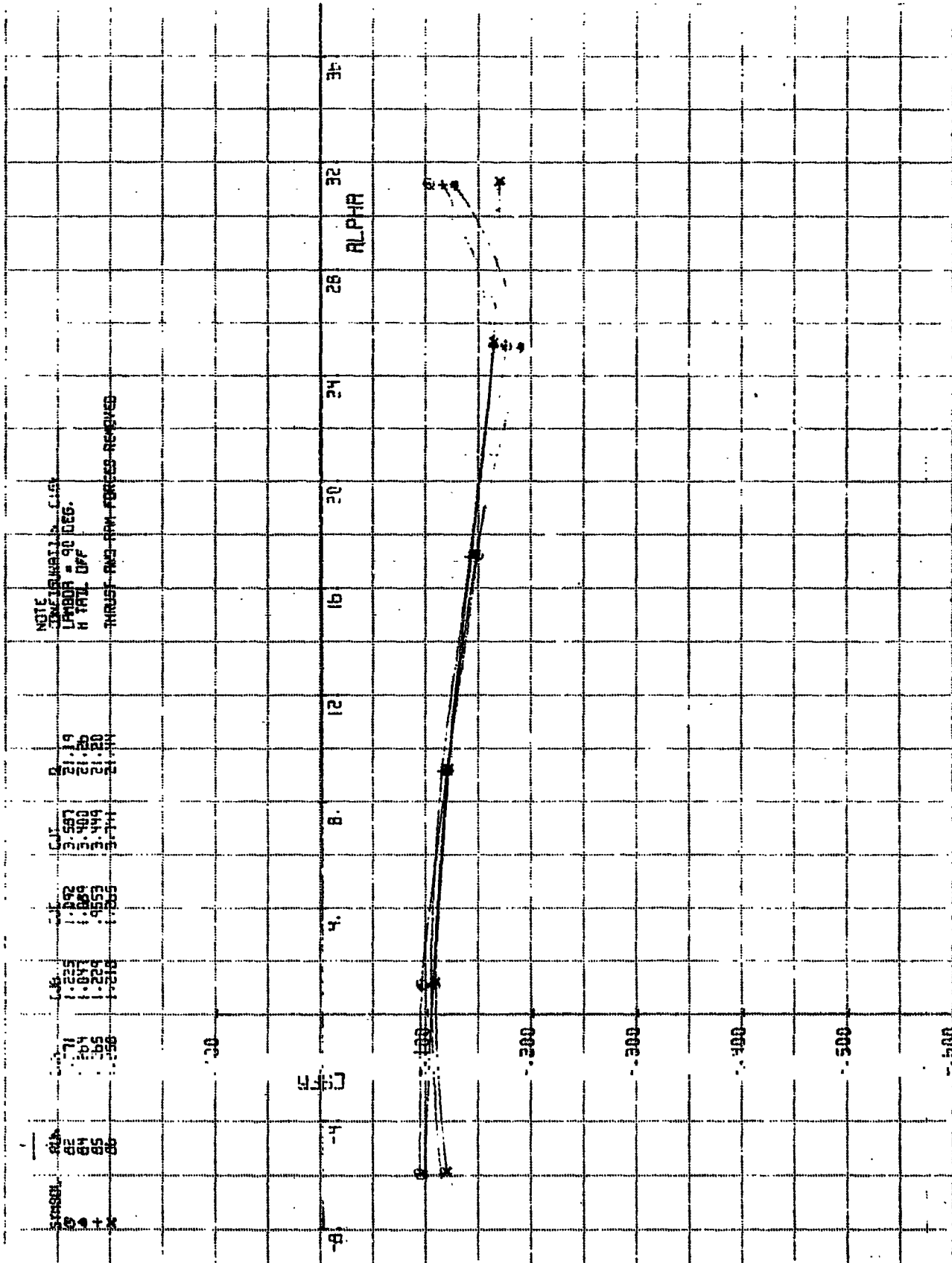
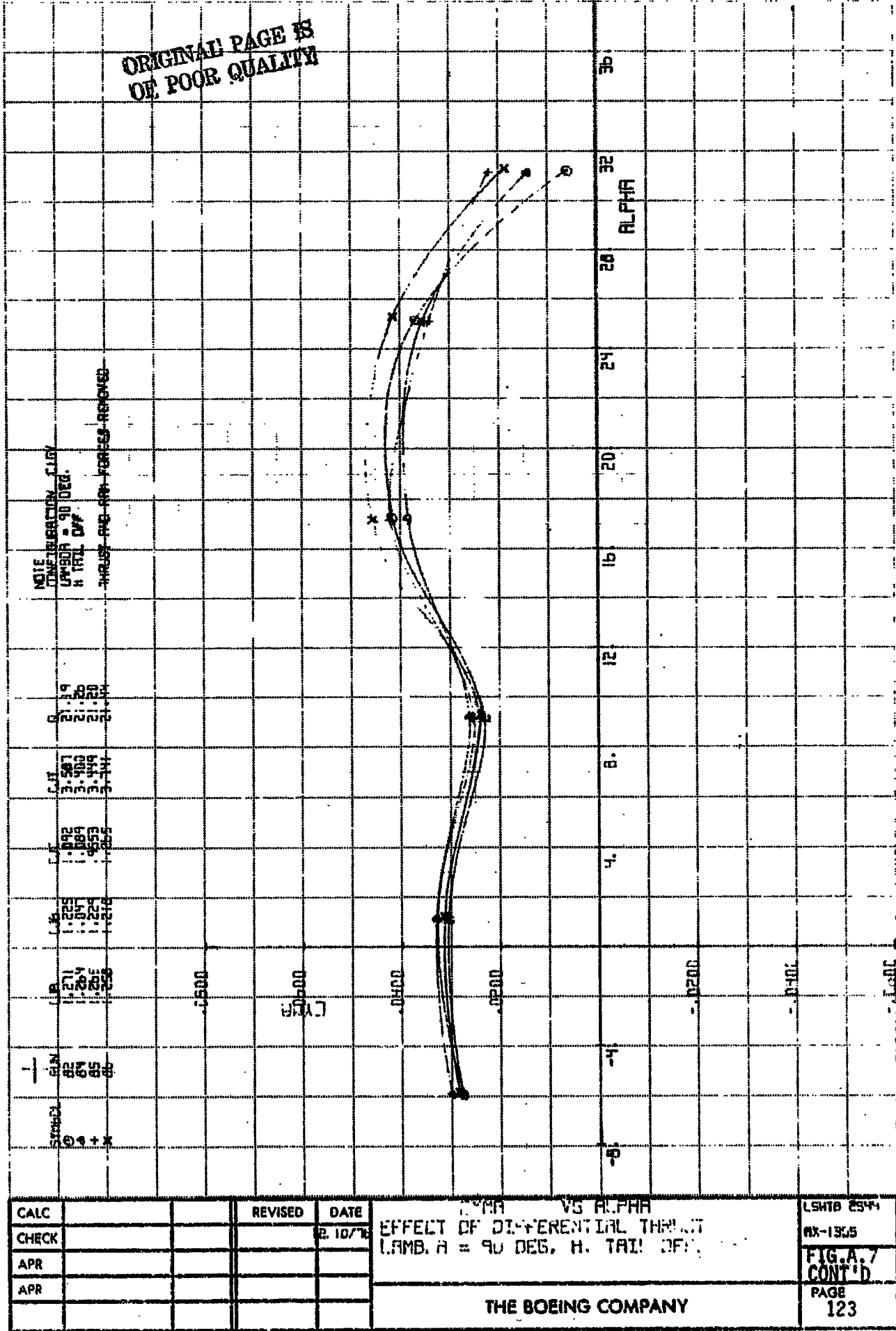
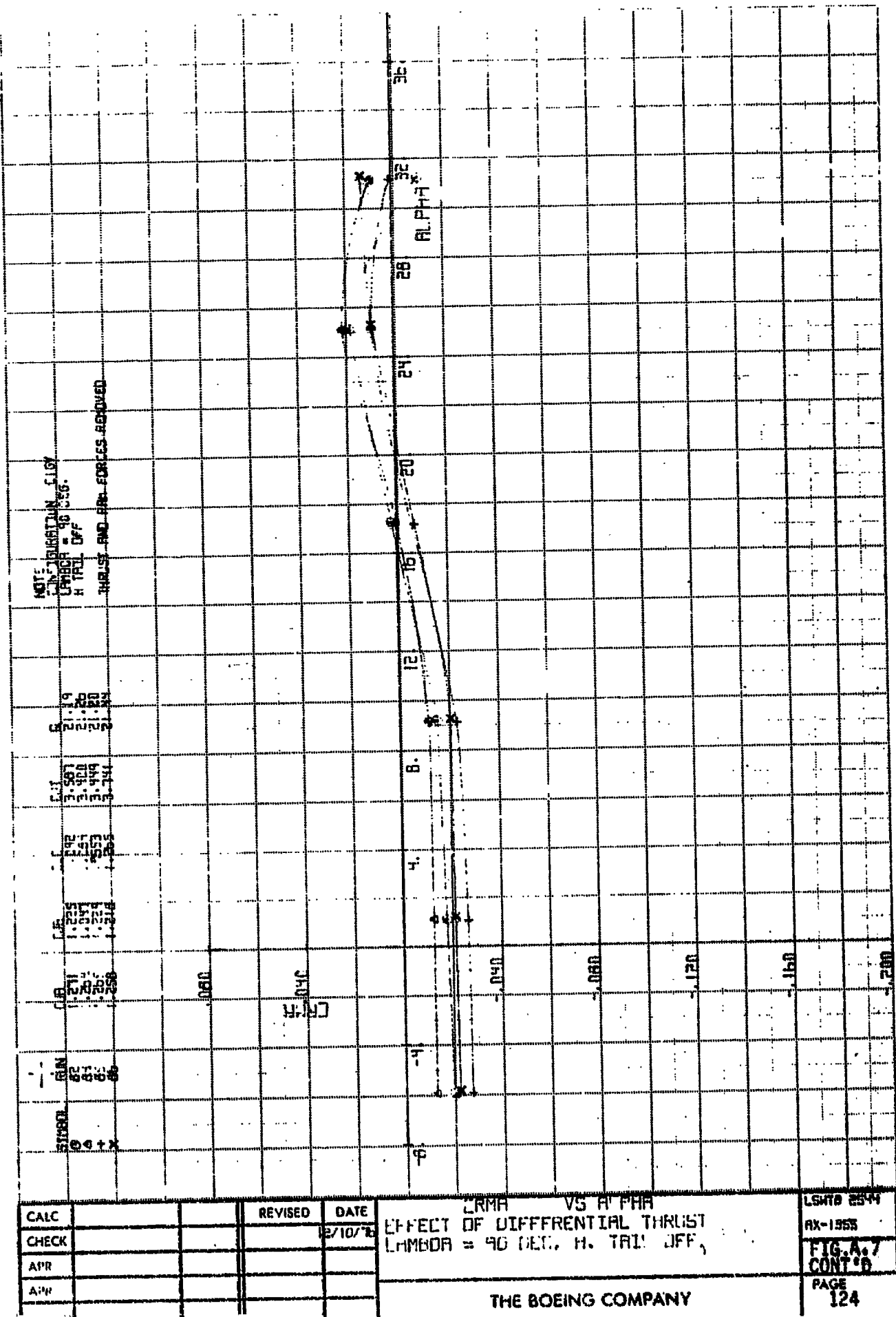


FIG 4  
4.



CALC	REvised	DATE	LIFT COEFFICIENT	ANGLE OF ATTACK (DEG.)	REF ID
CHECK		8/10/71	EFFECT OF VARIOUS ANGLES OF ATTITUDE	LAMBDA = 40 DEG. H. TAT. 10°	FIG. A-7 CONT'D
APP					FIG. A-7 CONT'D
APP					FIG. A-7 CONT'D



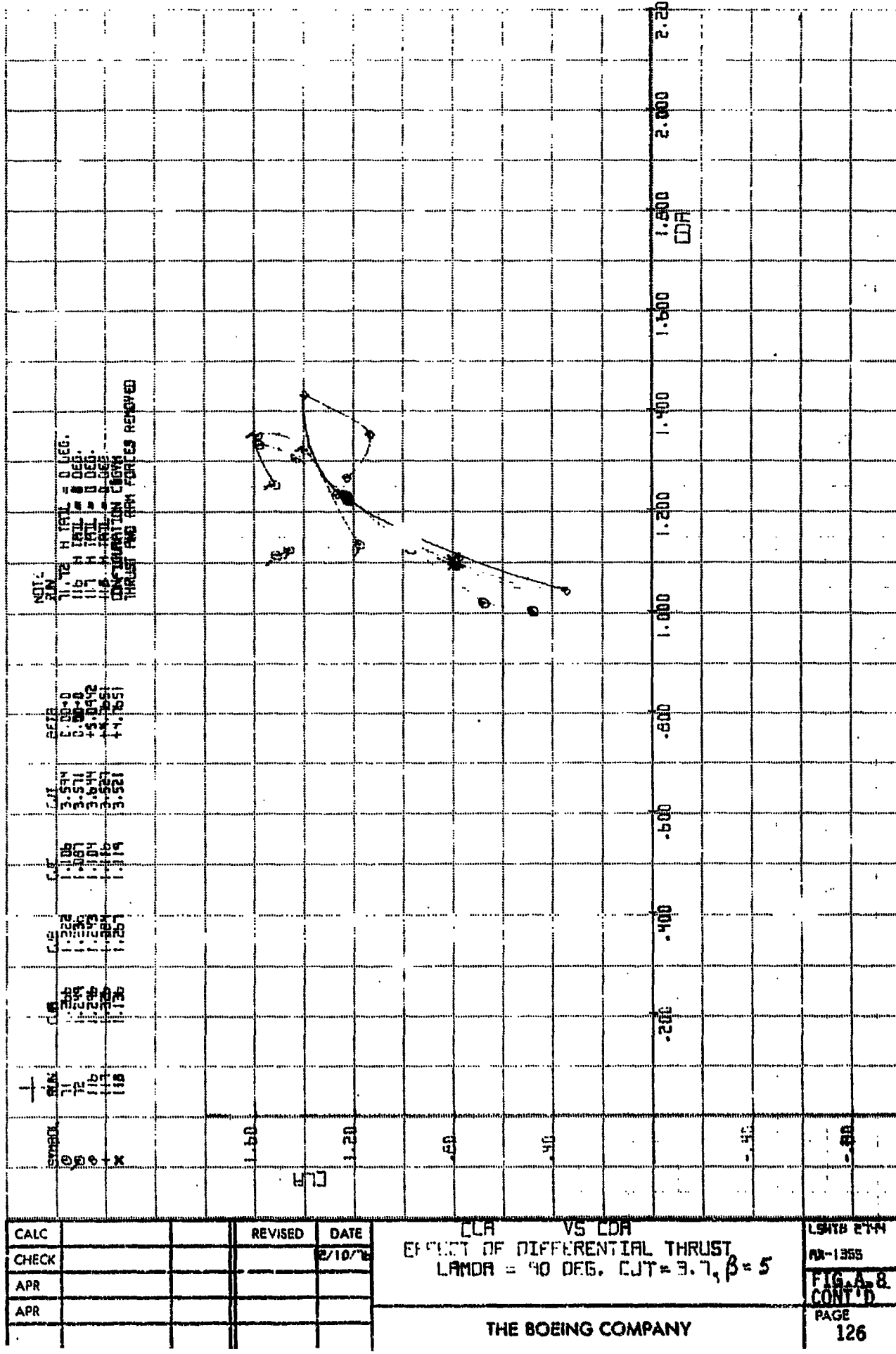


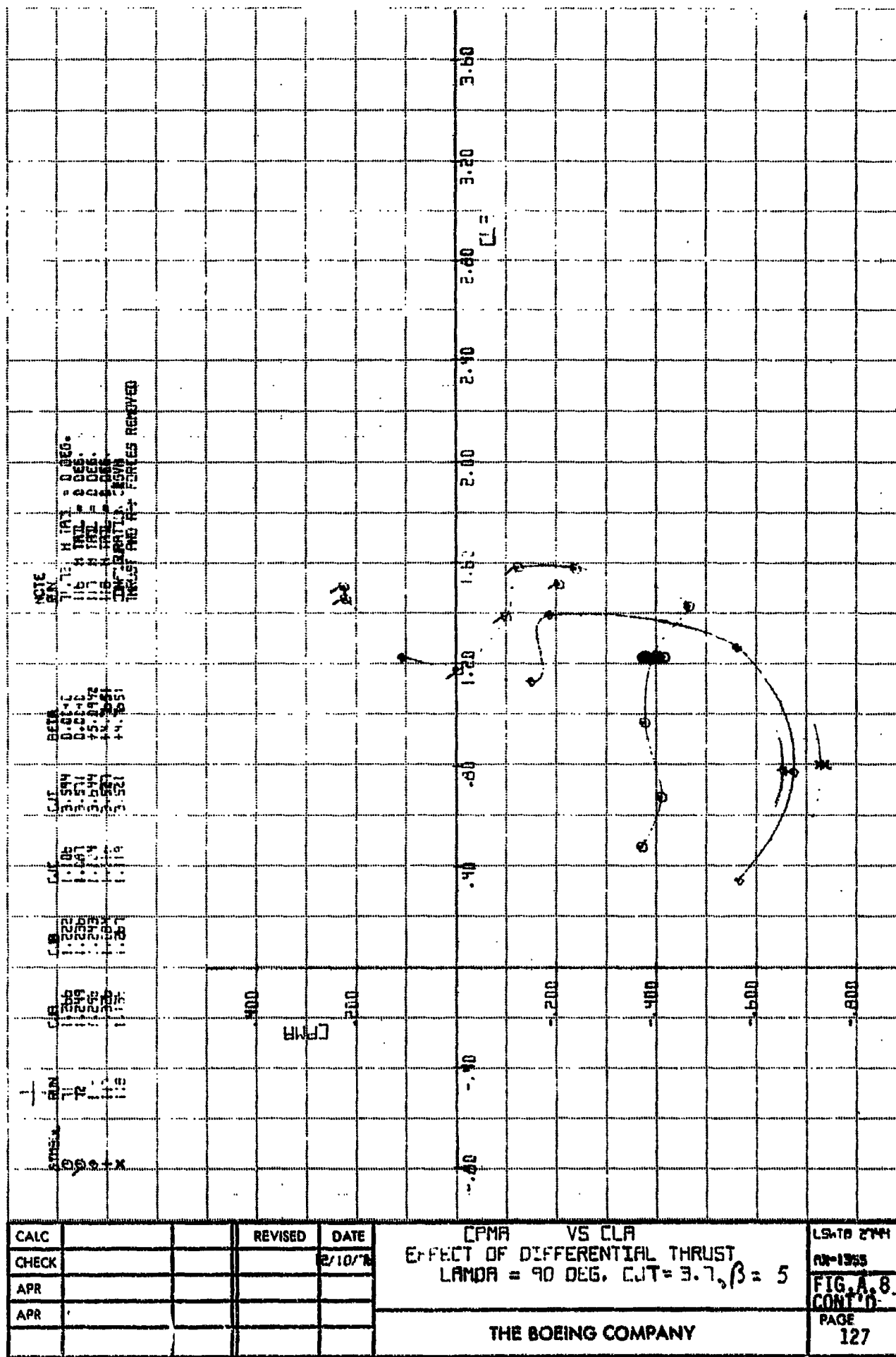
CALC			REVISED	DATE
CHECK				2/10/16
APR				
APR				

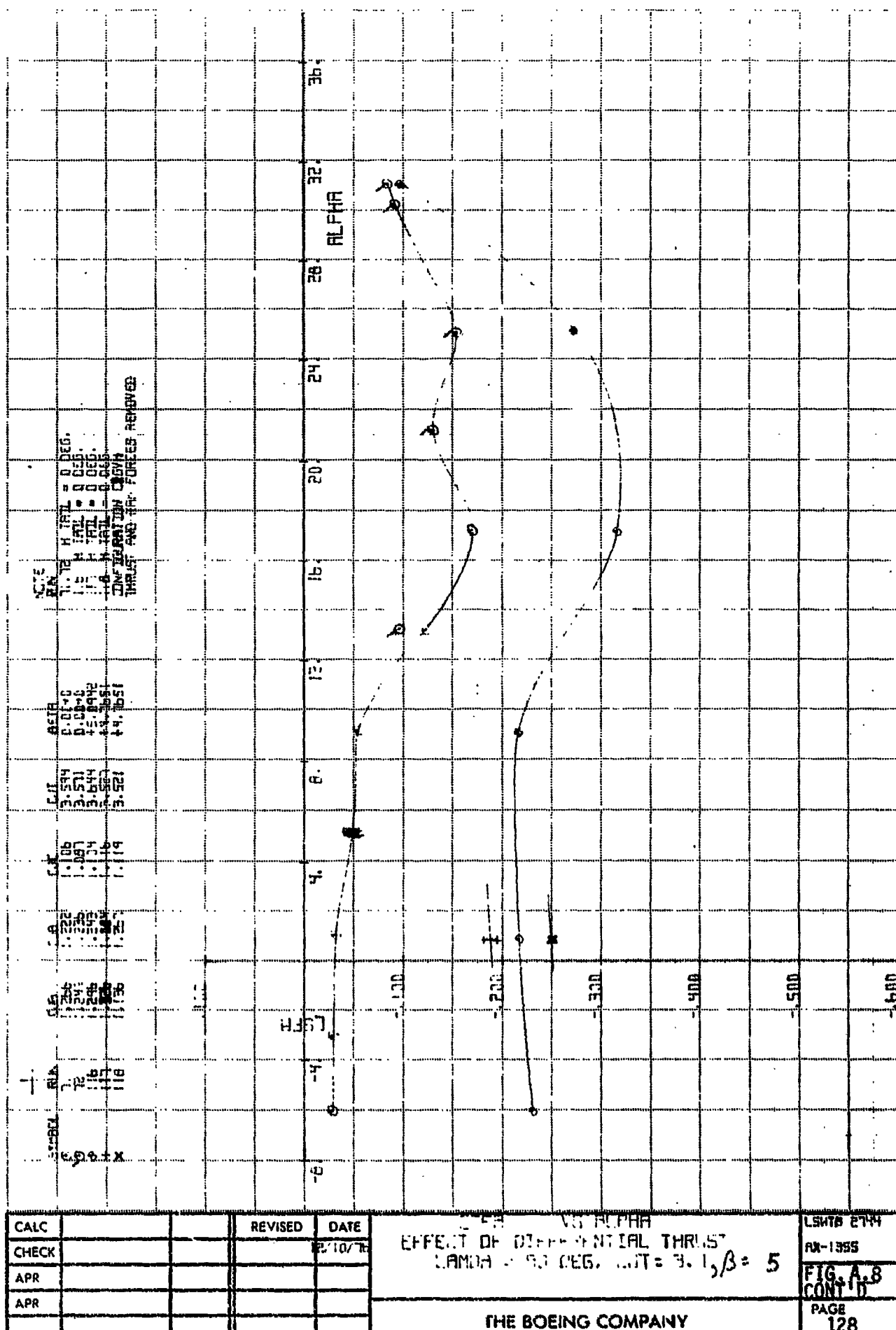
CLA VS ALPHA  
EFF. TIT = 1.15 VENTILATION THROAT  
LAMINA = 10 MM. G.I.T = 4.1,  $\beta = 5$

THE BOEING COMPANY

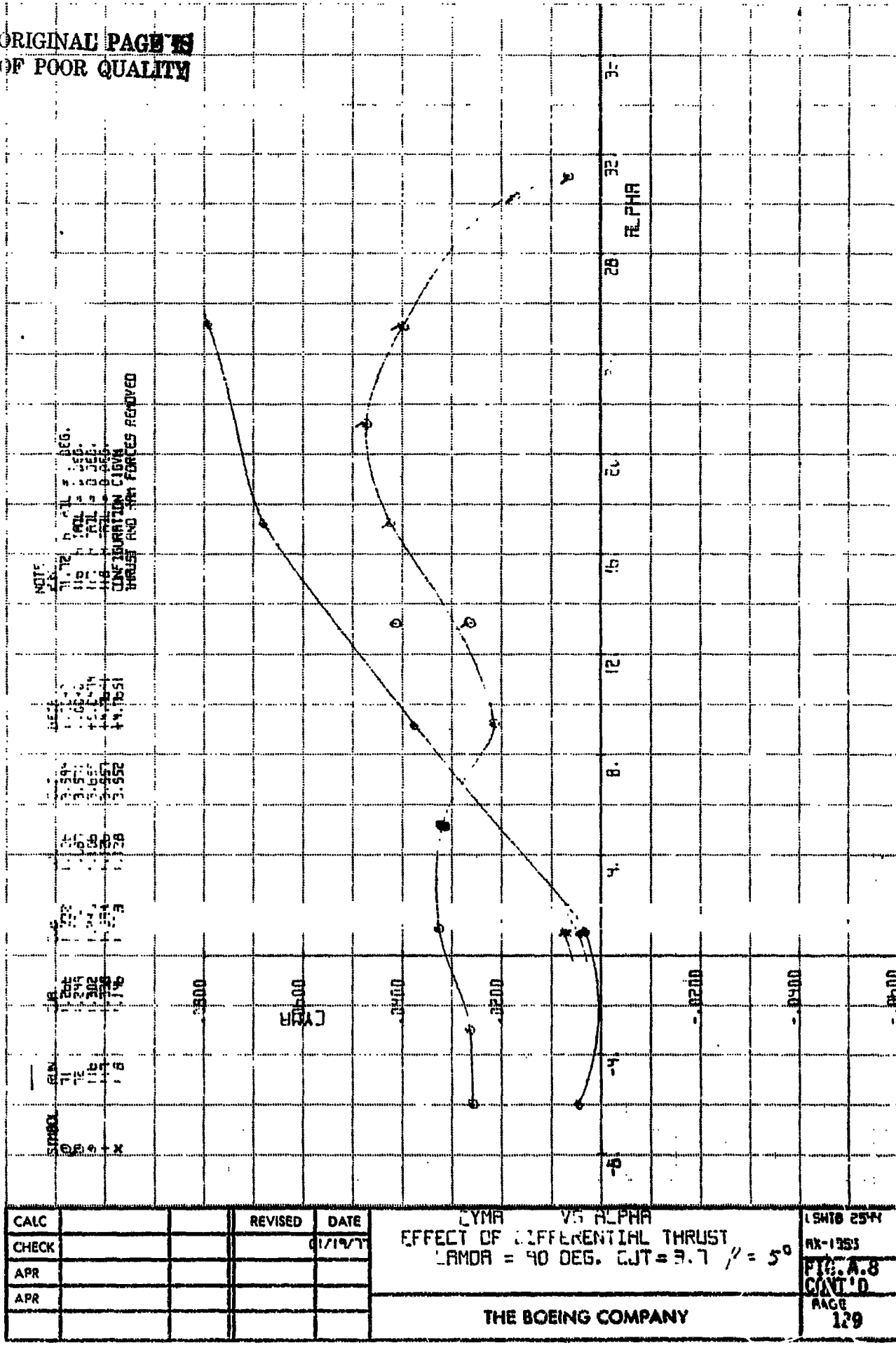
L.SHTD 2744  
PX-1356  
**FIG.A.8**  
PAGE  
125

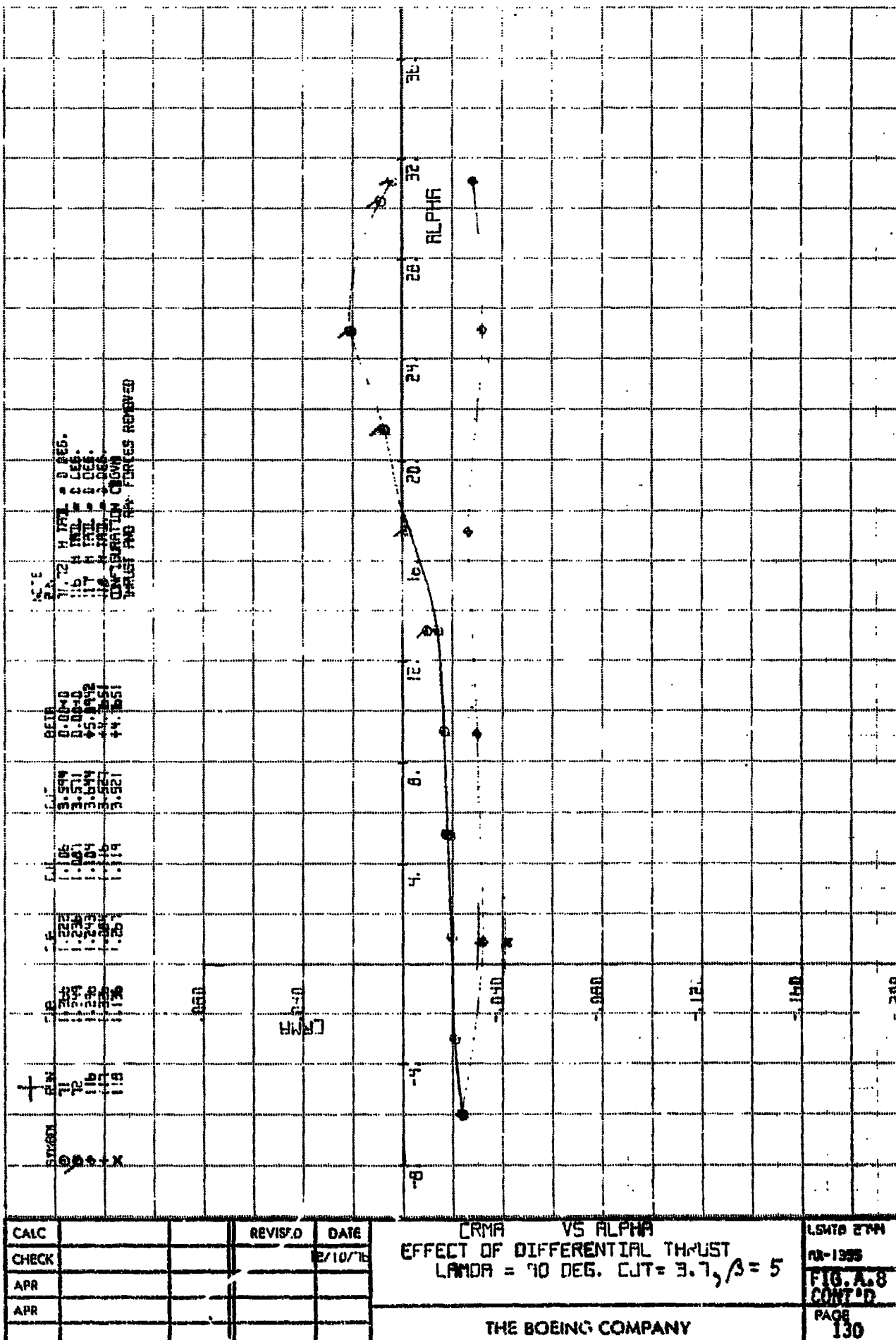






ORIGINAL PAGE IS  
OF POOR QUALITY





ORIGINAL PAGE IS  
OF POOR QUALITY

DIFFERENTIAL CROWN  
THESE TWO FORCES REMOVED

CALC		REVISED	DATE
CHECK			10/10/72
APR			
APR			

CLA VS ALPHA  
EFFECT OF DIFFERENTIAL THRUST  
LAMDA = 90 DEG, CJT = 3,  $\beta = 10$

THE BOEING COMPANY

LMTB 2744  
AX-1352  
FIG.A.9  
PAGE  
131

C.L. VS C.R.  
EFFECT OF DIFF. RENTIAL THRUST  
LANTH = 70 DEG. CJT = 3.7.3 = 10

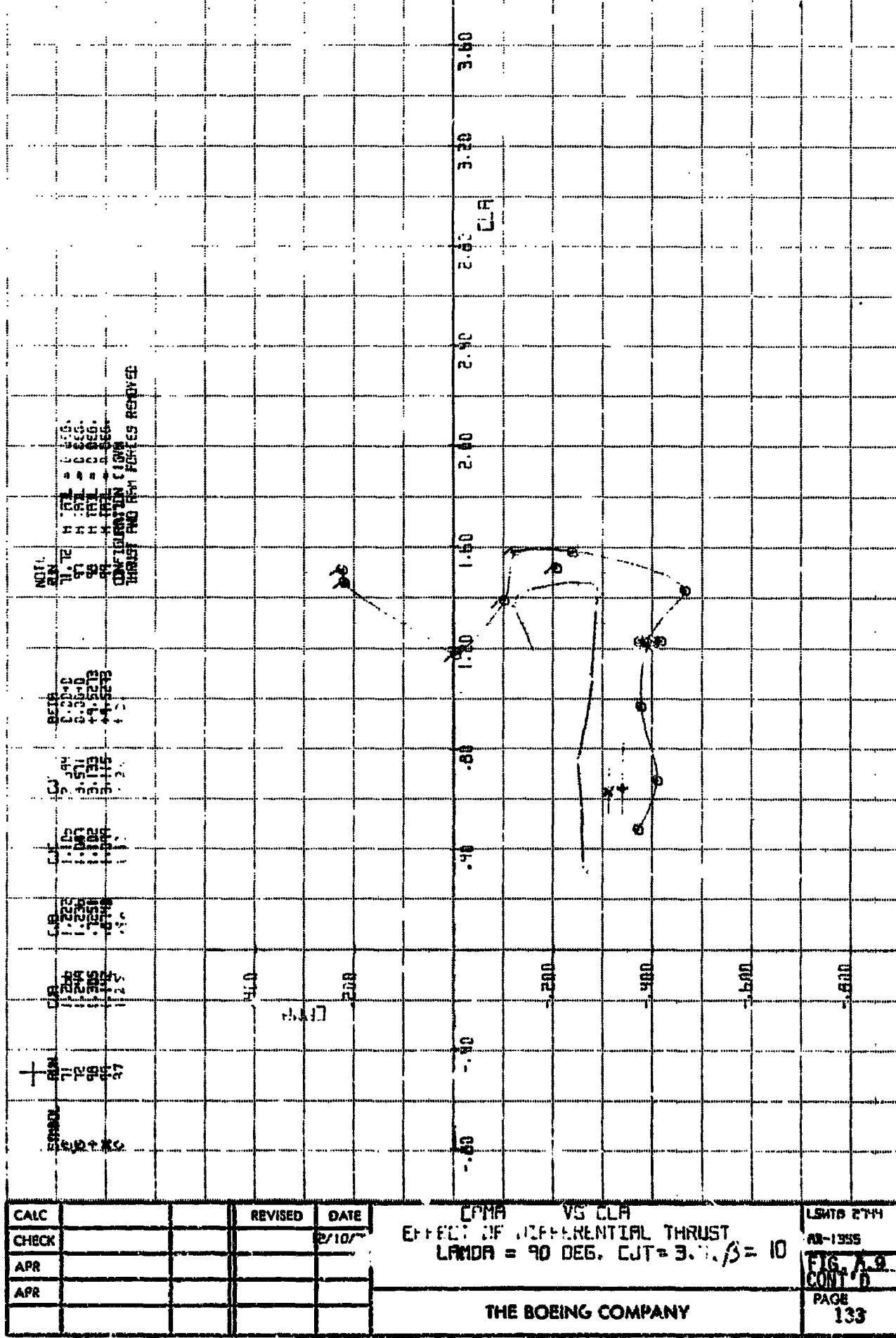
**THE BOEING COMPANY**

ਪੰਜਾਬ ਸਾਹਮਣਾ

CH. 13336

**FIG. A. 9**  
**CONT'D.**

PAGE



ORIGINAL PAGE IS  
OF POOR QUALITY

CALC			REVISED	DATE
CHECK				3/10/76
APR				
APR				
-				

EFFECT OF DIFFERENT THRUST ANGLE - 90 DEG. C.R.T = 3.7.  $\beta$  = 10

L.SHTB २७५५

۱۳۵۰

FIG. A.9

卷之三

PAGE 32

THE BOEING COMPANY

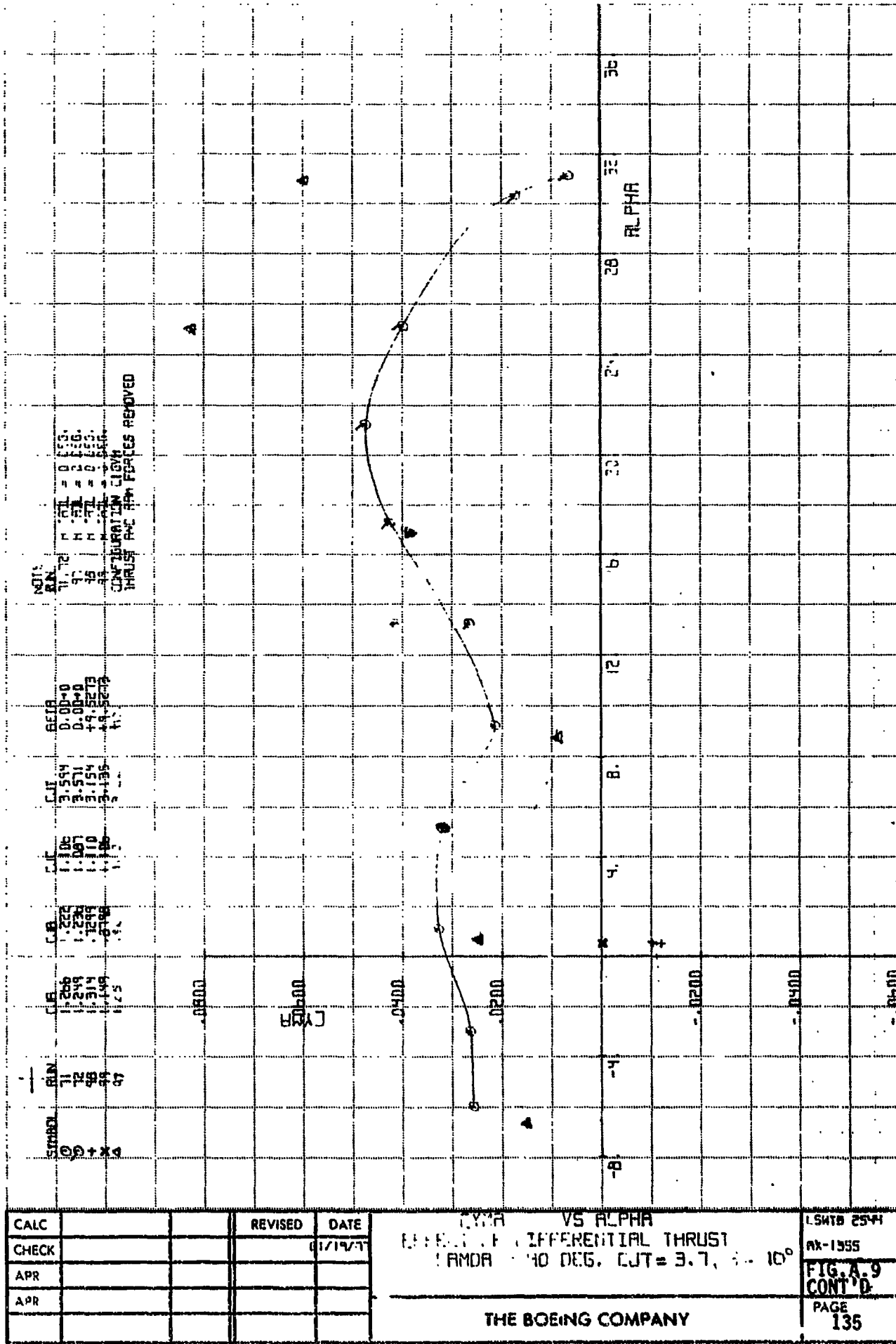


FIG. 55

ZYMA VS ALPHA  
E/F/H/L/F : DIFFERENTIAL THRUST  
AMDA : 40 DEG. CJT = 3.7,

L5H19 2544

87-1986

11A 1355

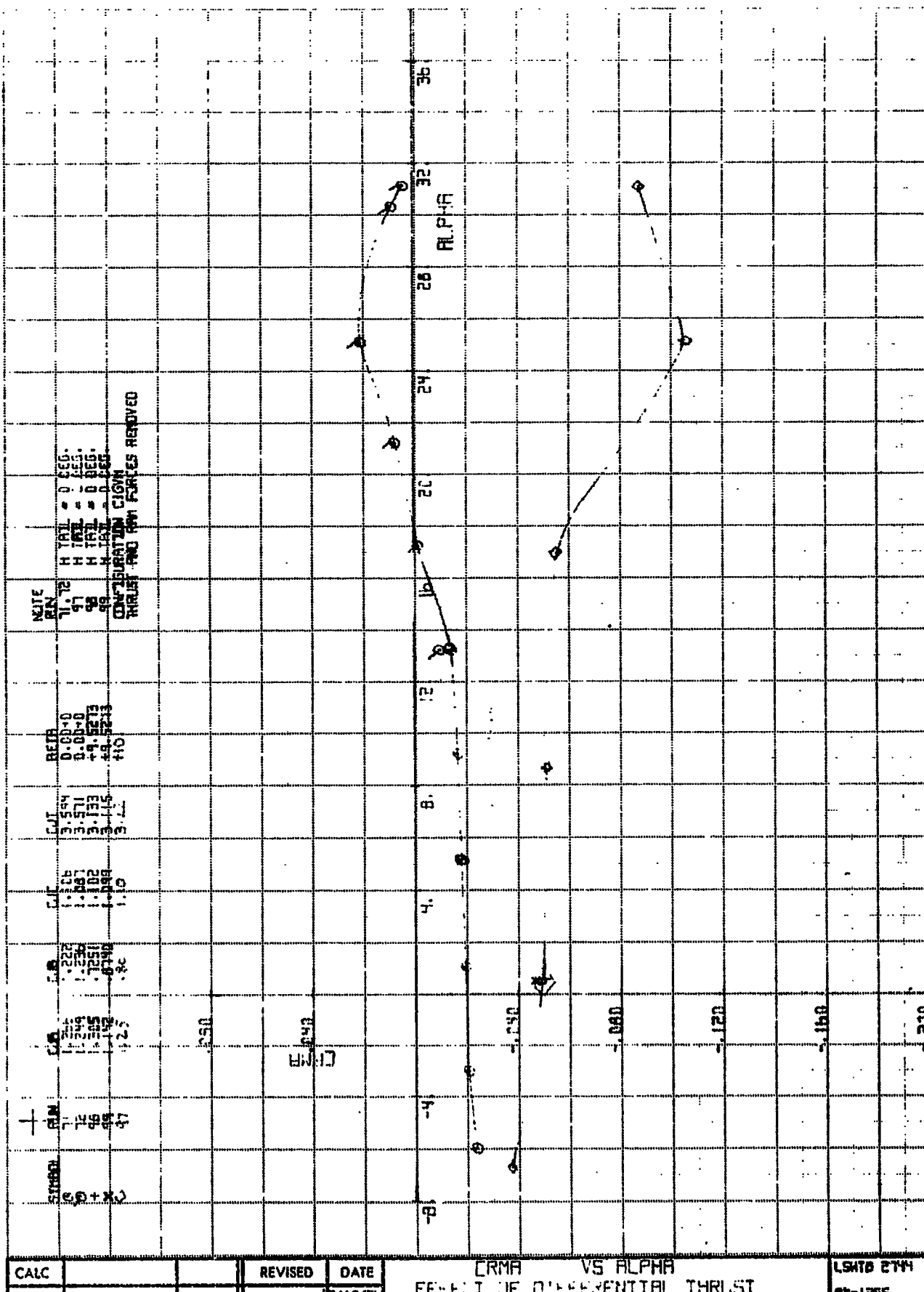
FIG. A.9  
CONT'D.

PAGE

135

THE BOEING COMPANY

PAGE  
136



CRMA VS ALPHA  
EF-E T OF DIFFERENTIAL THRUST  
LAMBDA = 90 DEG. CJT = 3.1,  $\beta$  = 10

CALC			REVISED	DATE
CHECK				12/10/16
APP				
APP				

THE BOEING COMPANY

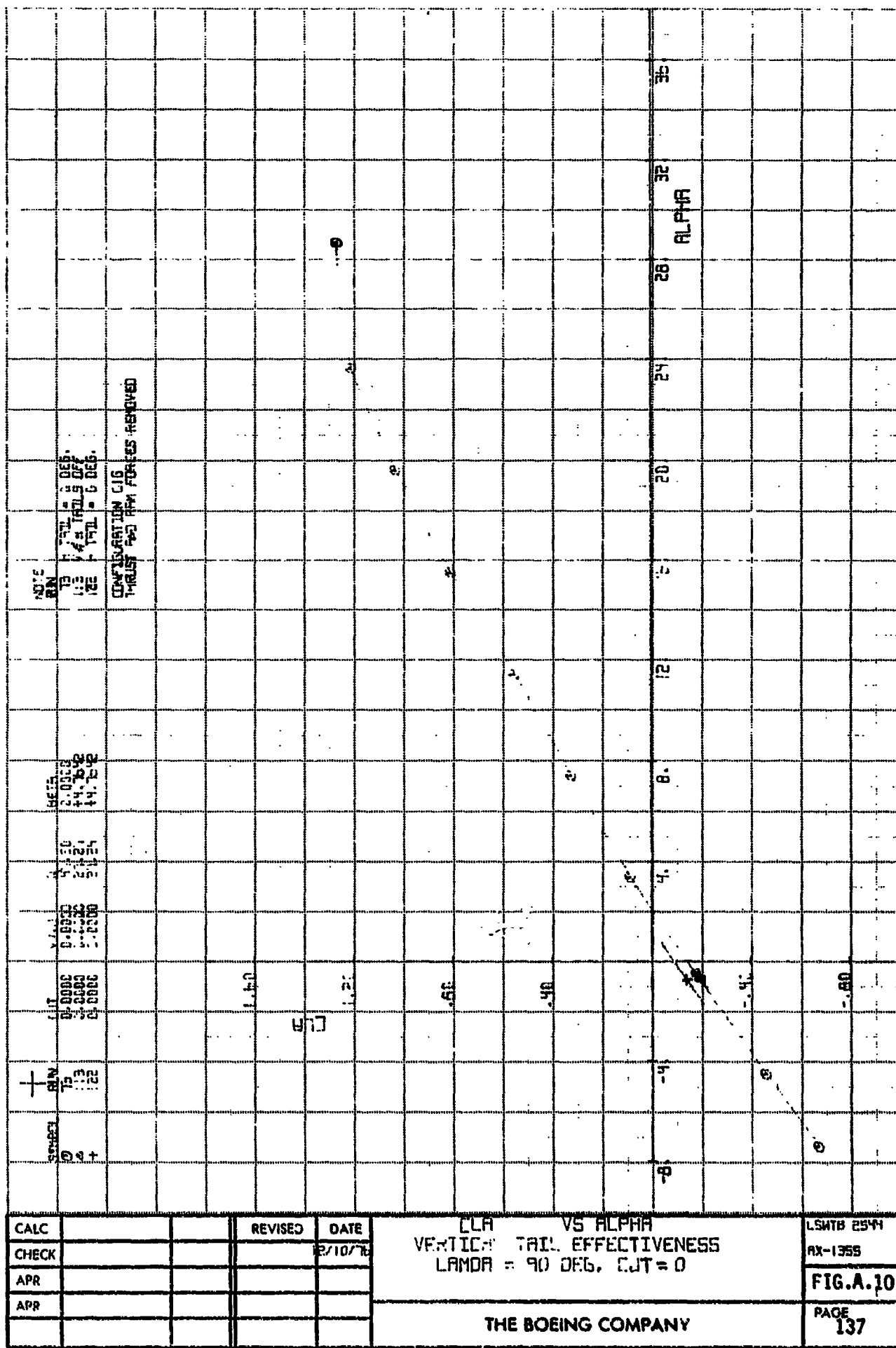
LSHTB CT44

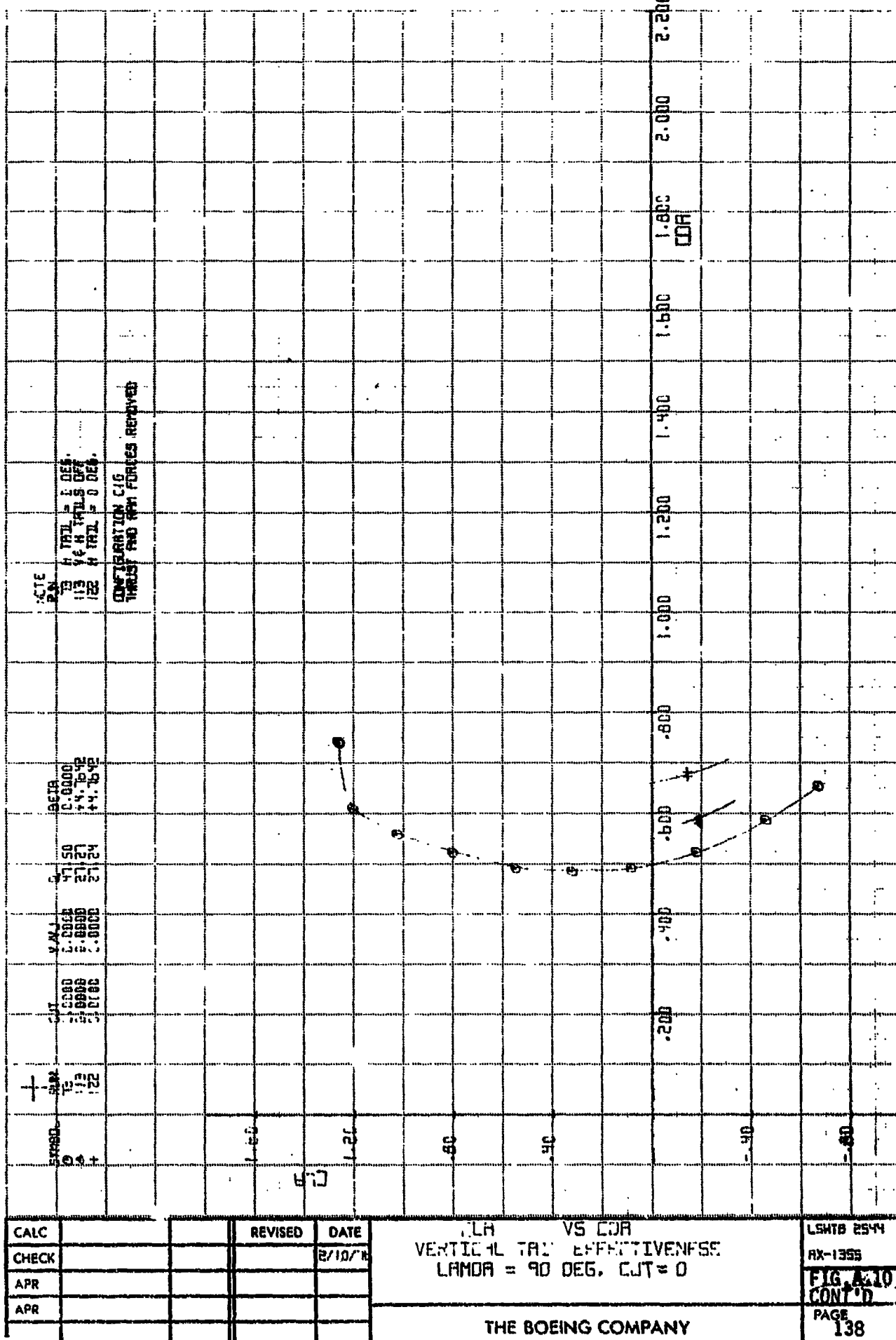
88-1335

卷之三

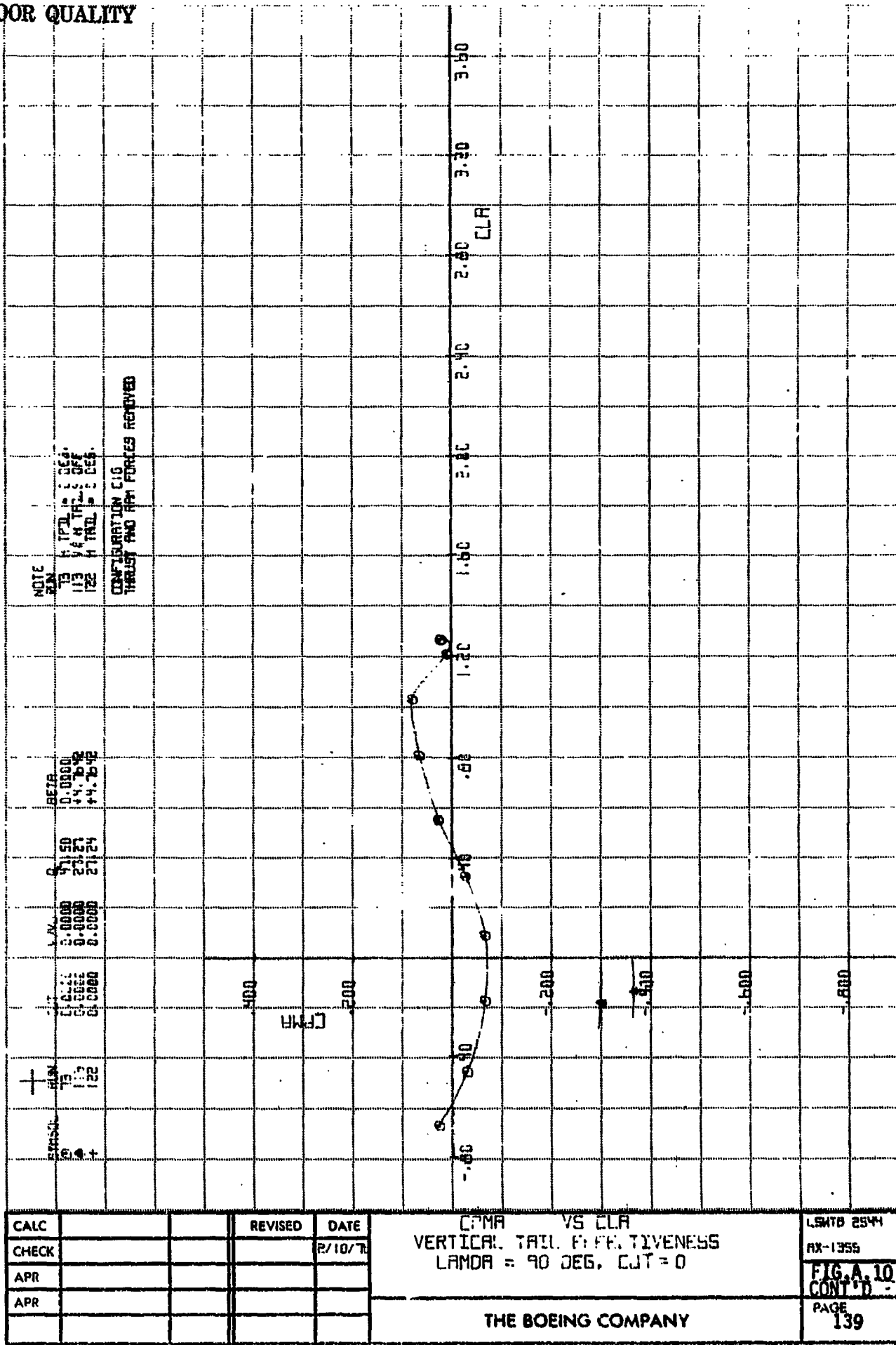
100

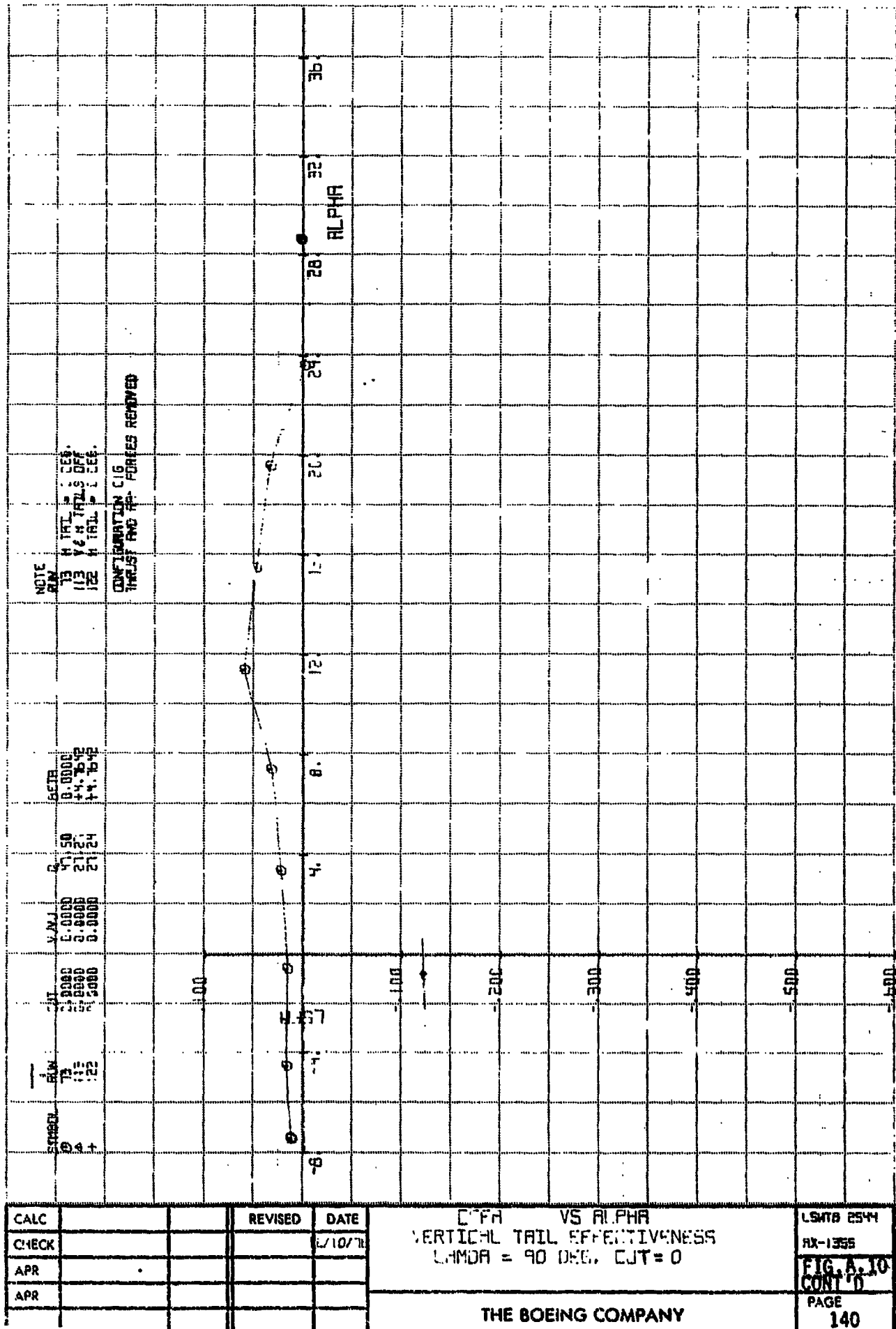
PAGE  
101

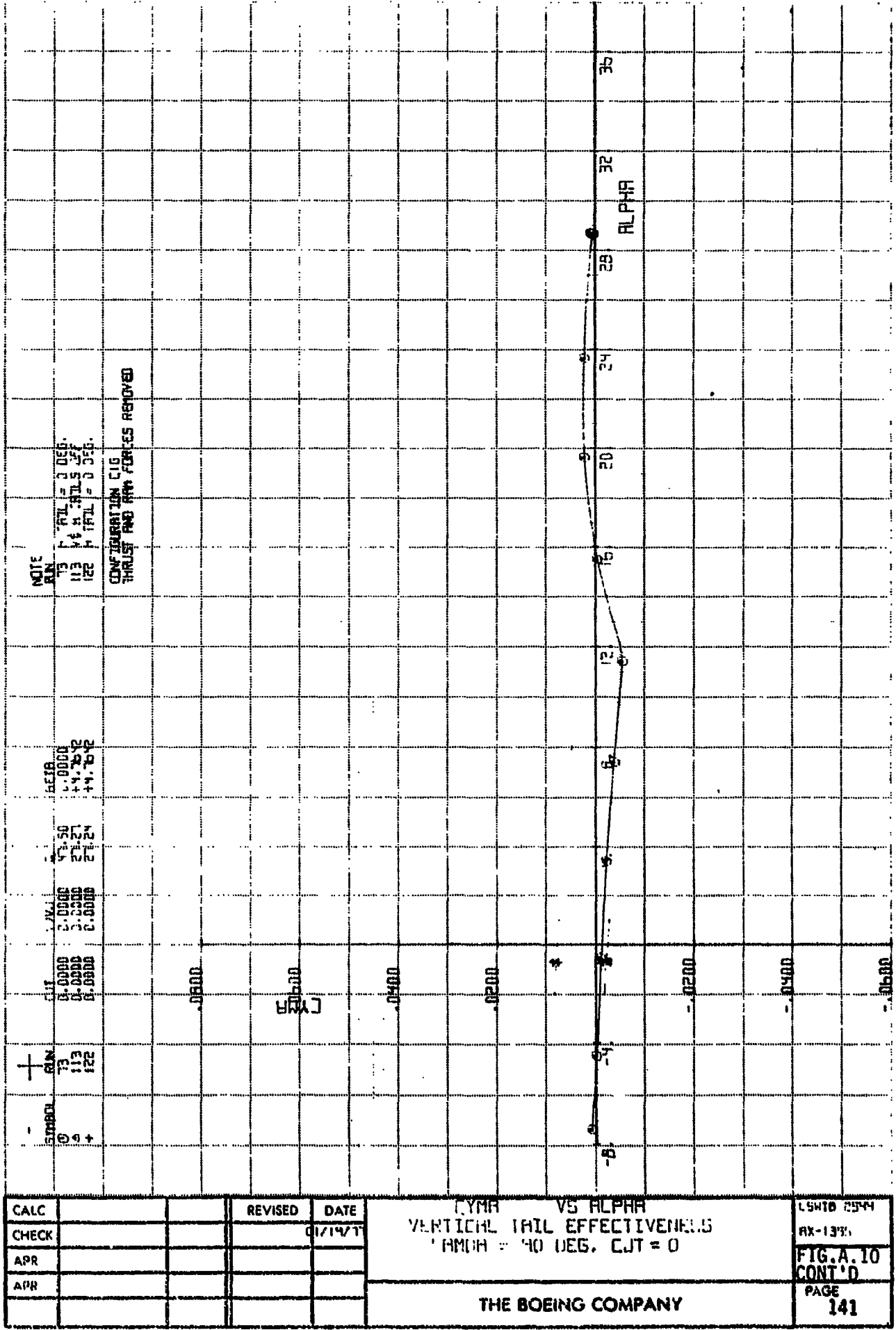




ORIGINAL PAGE IS  
OF POOR QUALITY







CRM V. HI.PHR  
VERTICAL TAIL EFFECTIVENESS  
 $L_{MMU} = 70$  DEG. CJT = 0

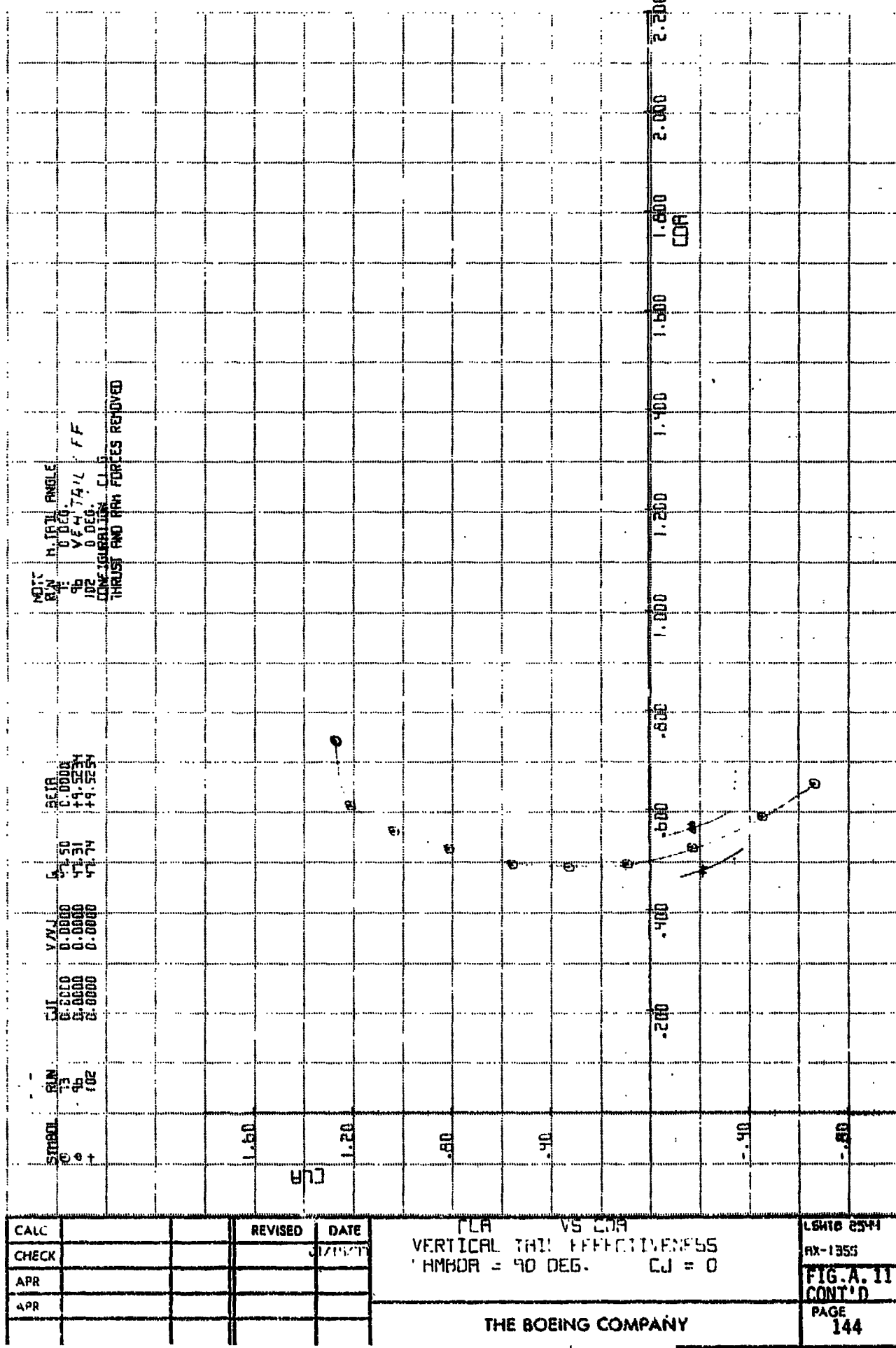
THE BOEING COMPANY

NAME	AGE	SEX	RELATION	ADDRESS	STATE	POSTAL DIST.	TELEGRAM	TELEPHONE	TELEGRAPH	TELETYPE	TELEFAX	TELEMAIL
HANNAH	32	F	MOTHER	1234 BOSTON AVENUE	MASSACHUSETTS	02134	123456789	(617) 555-1234	123456789	123456789	123456789	123456789
JOHN	35	M	FATHER	1234 BOSTON AVENUE	MASSACHUSETTS	02134	123456789	(617) 555-1234	123456789	123456789	123456789	123456789
JANE	18	F	SISTER	1234 BOSTON AVENUE	MASSACHUSETTS	02134	123456789	(617) 555-1234	123456789	123456789	123456789	123456789
MARK	22	M	BROTHER	1234 BOSTON AVENUE	MASSACHUSETTS	02134	123456789	(617) 555-1234	123456789	123456789	123456789	123456789
ROBERT	25	M	SON	1234 BOSTON AVENUE	MASSACHUSETTS	02134	123456789	(617) 555-1234	123456789	123456789	123456789	123456789
ROSE	28	F	DAUGHTER	1234 BOSTON AVENUE	MASSACHUSETTS	02134	123456789	(617) 555-1234	123456789	123456789	123456789	123456789
RONALD	30	M	SON	1234 BOSTON AVENUE	MASSACHUSETTS	02134	123456789	(617) 555-1234	123456789	123456789	123456789	123456789
SUSAN	26	F	DAUGHTER	1234 BOSTON AVENUE	MASSACHUSETTS	02134	123456789	(617) 555-1234	123456789	123456789	123456789	123456789
THOMAS	33	M	SON	1234 BOSTON AVENUE	MASSACHUSETTS	02134	123456789	(617) 555-1234	123456789	123456789	123456789	123456789
WILLIAM	37	M	SON	1234 BOSTON AVENUE	MASSACHUSETTS	02134	123456789	(617) 555-1234	123456789	123456789	123456789	123456789

CALC			REVISED	DATE
CHECK				01/15/77
APR				
APR				

FLR VS ALPHA  
VERTICAL TRAIL EFFECTIVENESS  
1 HMBDR = 40 DEG. C.J. = 0

L5HTB 2544  
HX-1335  
FIG.A. 11  
PAGE  
143



VERTICAL THI FFFFDDDEE55  
' HMBDR = 40 DEG. CJ = 0

THE BOEING COMPANY

લાલ કાળી

- RX-1355

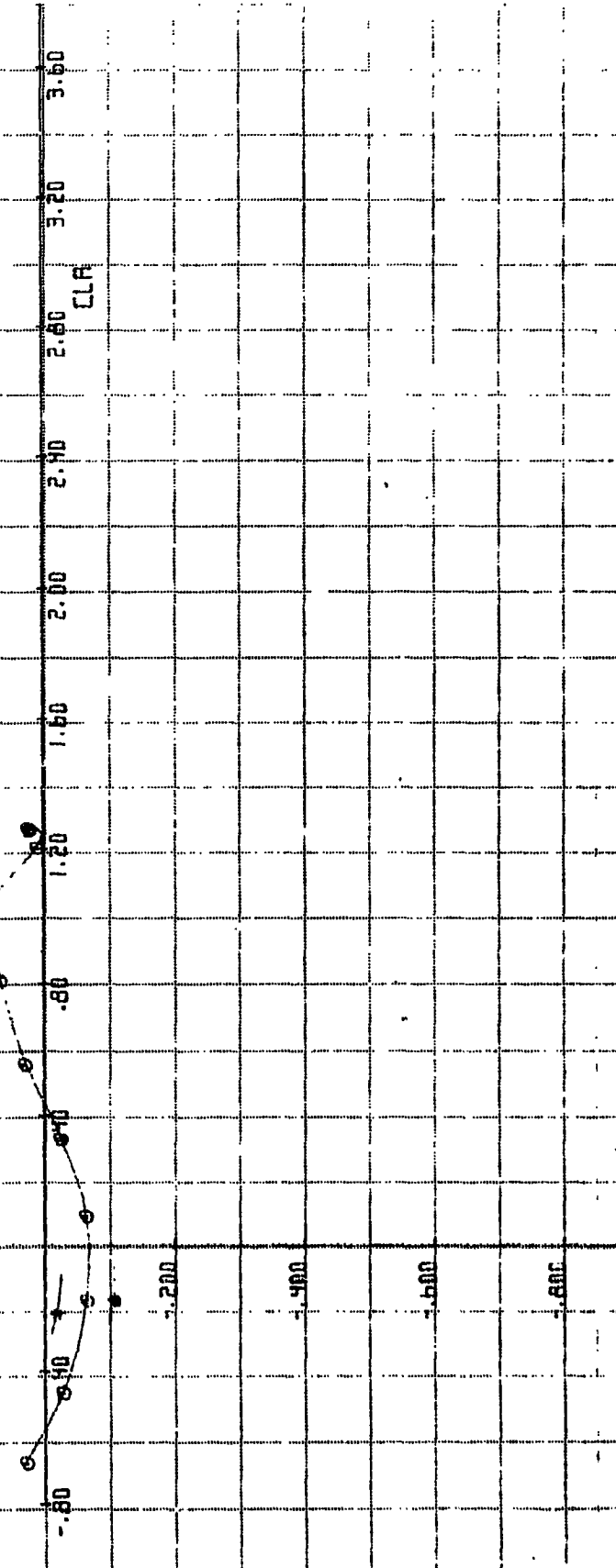
**FIG. A. II**  
**CONT'D**

PAGE  
144

ORIGINAL PAGE IS  
OF POOR QUALITY

STAB	RIN	SUS	SEIR		NO. OF TAIL ANGLE
			13	15	
1.00	1.00	1.00	1.00	1.00	0 DEG.
1.02	1.02	1.02	1.02	1.02	10 DEG.
1.04	1.04	1.04	1.04	1.04	20 DEG.
1.06	1.06	1.06	1.06	1.06	30 DEG.
1.08	1.08	1.08	1.08	1.08	40 DEG.
1.10	1.10	1.10	1.10	1.10	50 DEG.
1.12	1.12	1.12	1.12	1.12	60 DEG.
1.14	1.14	1.14	1.14	1.14	70 DEG.
1.16	1.16	1.16	1.16	1.16	80 DEG.
1.18	1.18	1.18	1.18	1.18	90 DEG.
1.20	1.20	1.20	1.20	1.20	100 DEG.
1.22	1.22	1.22	1.22	1.22	110 DEG.
1.24	1.24	1.24	1.24	1.24	120 DEG.
1.26	1.26	1.26	1.26	1.26	130 DEG.
1.28	1.28	1.28	1.28	1.28	140 DEG.
1.30	1.30	1.30	1.30	1.30	150 DEG.
1.32	1.32	1.32	1.32	1.32	160 DEG.
1.34	1.34	1.34	1.34	1.34	170 DEG.
1.36	1.36	1.36	1.36	1.36	180 DEG.
1.38	1.38	1.38	1.38	1.38	190 DEG.
1.40	1.40	1.40	1.40	1.40	200 DEG.
1.42	1.42	1.42	1.42	1.42	210 DEG.
1.44	1.44	1.44	1.44	1.44	220 DEG.
1.46	1.46	1.46	1.46	1.46	230 DEG.
1.48	1.48	1.48	1.48	1.48	240 DEG.
1.50	1.50	1.50	1.50	1.50	250 DEG.
1.52	1.52	1.52	1.52	1.52	260 DEG.
1.54	1.54	1.54	1.54	1.54	270 DEG.
1.56	1.56	1.56	1.56	1.56	280 DEG.
1.58	1.58	1.58	1.58	1.58	290 DEG.
1.60	1.60	1.60	1.60	1.60	300 DEG.
1.62	1.62	1.62	1.62	1.62	310 DEG.
1.64	1.64	1.64	1.64	1.64	320 DEG.
1.66	1.66	1.66	1.66	1.66	330 DEG.
1.68	1.68	1.68	1.68	1.68	340 DEG.
1.70	1.70	1.70	1.70	1.70	350 DEG.
1.72	1.72	1.72	1.72	1.72	360 DEG.

CLM  
CLR



CPMA VS CLR  
VERTICAL TAIL EFFECTIVENESS  
LAMBDA = 90 DEG. CJ = 0

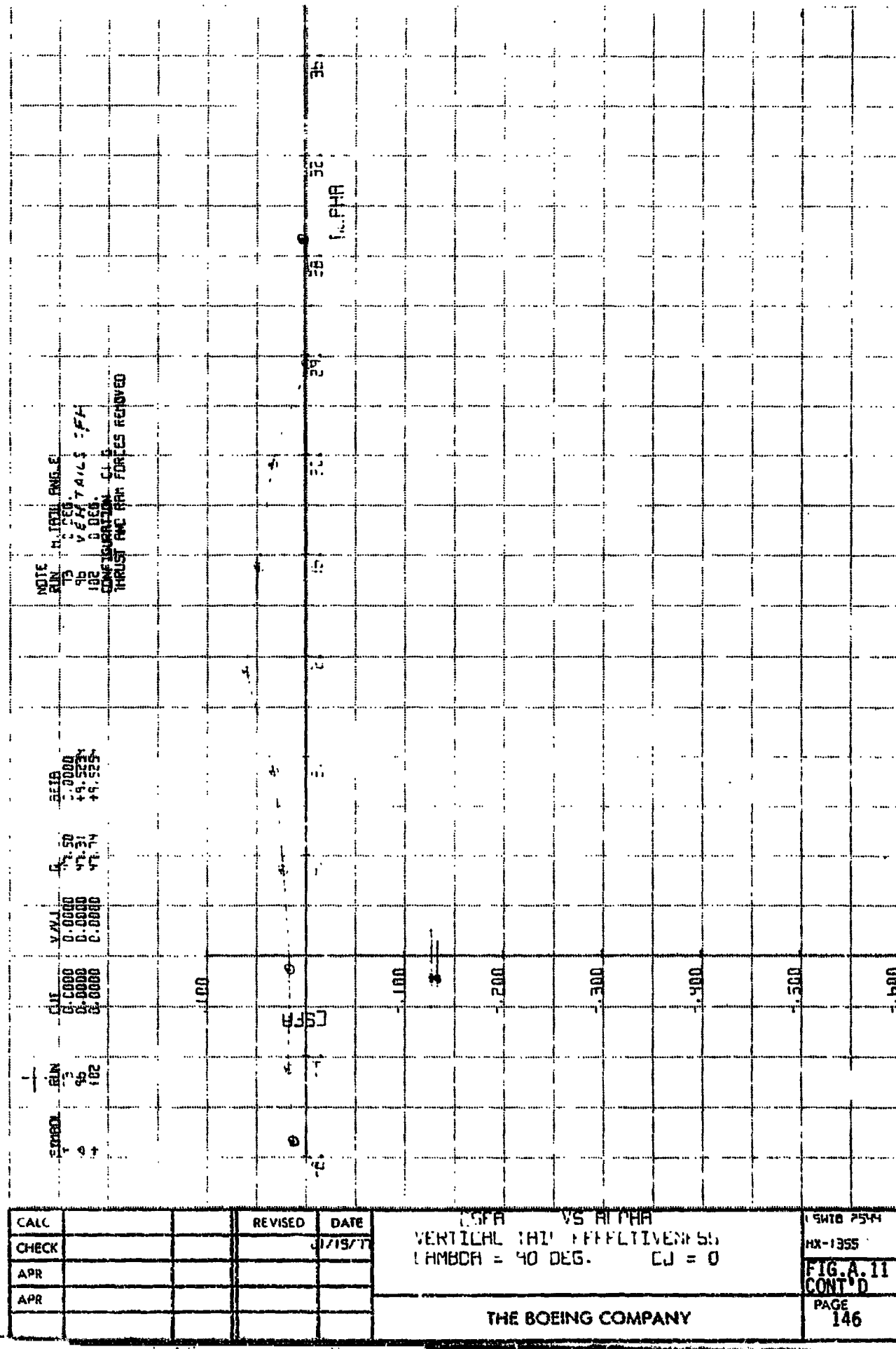
CALC	REVISED	DATE
CHECK		0/15/71
APR		
APR		

THE BOEING COMPANY

L5H10 2544  
NX-1355

FIG. A.11  
CONT'D

PAGE  
145



CSFA VS ALPHA  
VERTICAL HI: FFLTIVENE50  
LHMBDA = 40 DEG. CJ = 0

THE BOEING COMPANY

॥ ५४० २५४

HX-1355

**FIG. A.11**  
**CONT'D**

PAGE  
146

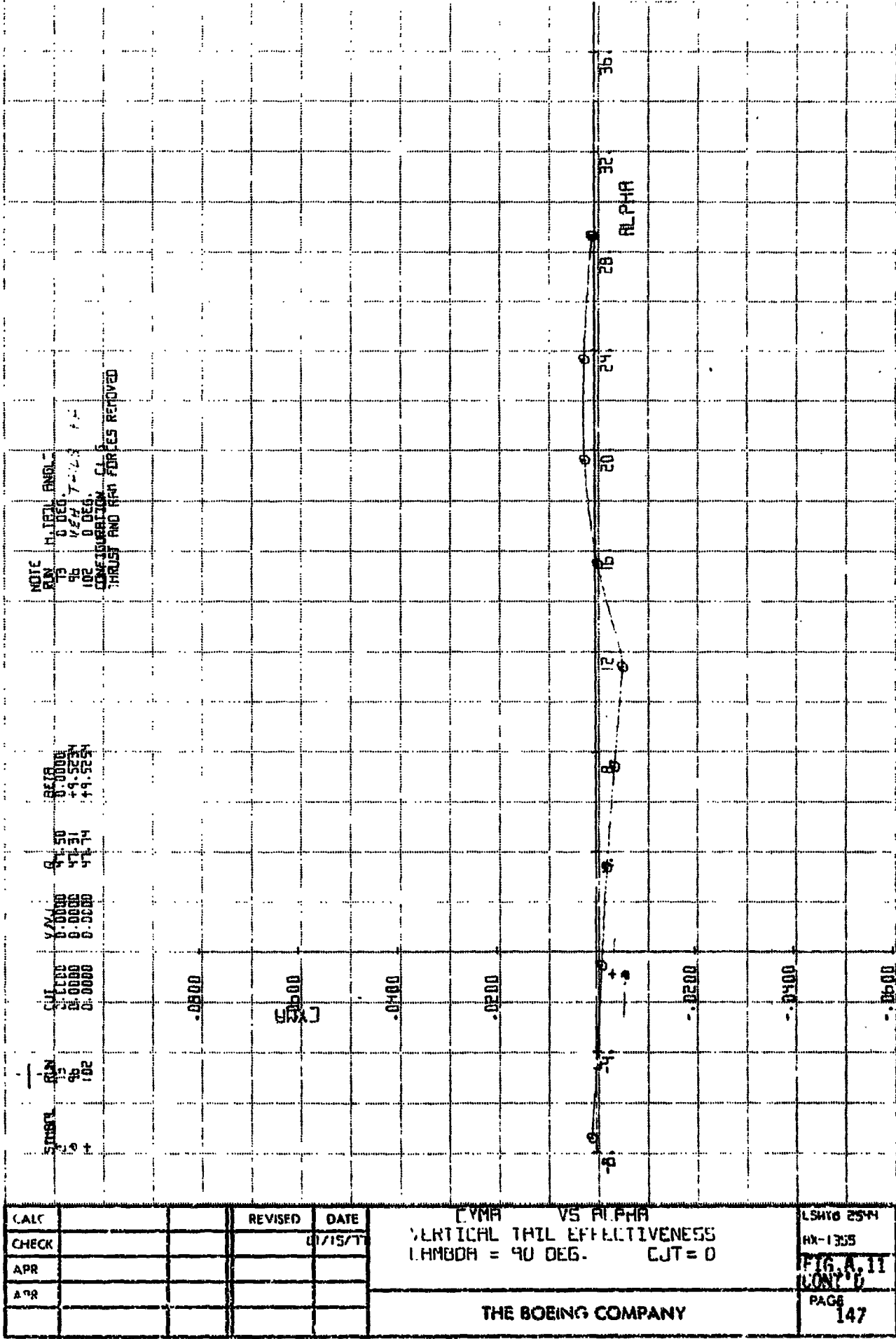


FIG 3B  
b.

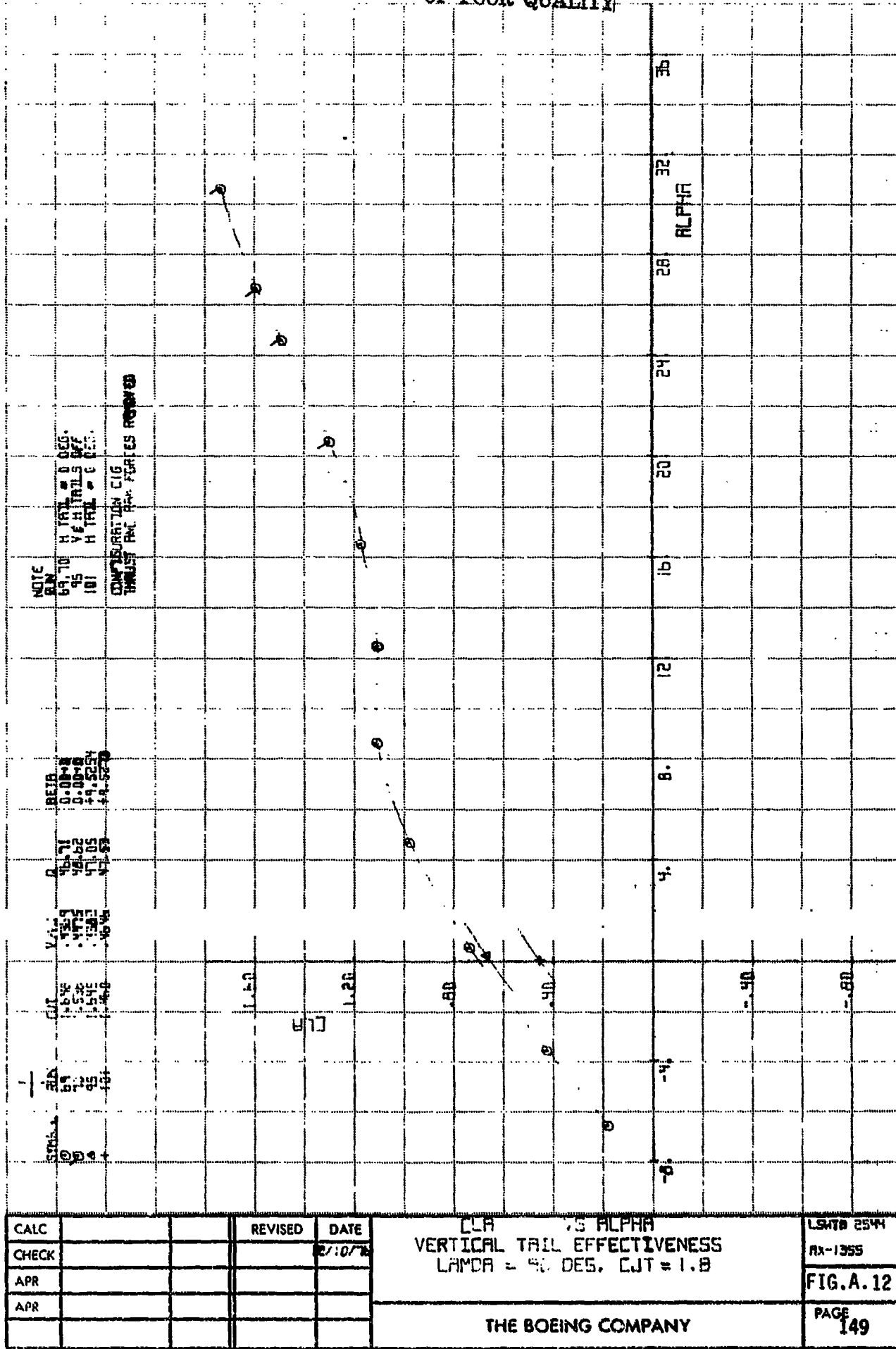
LC			REVISED	DATE
ECK				01/15/17
R				
R				

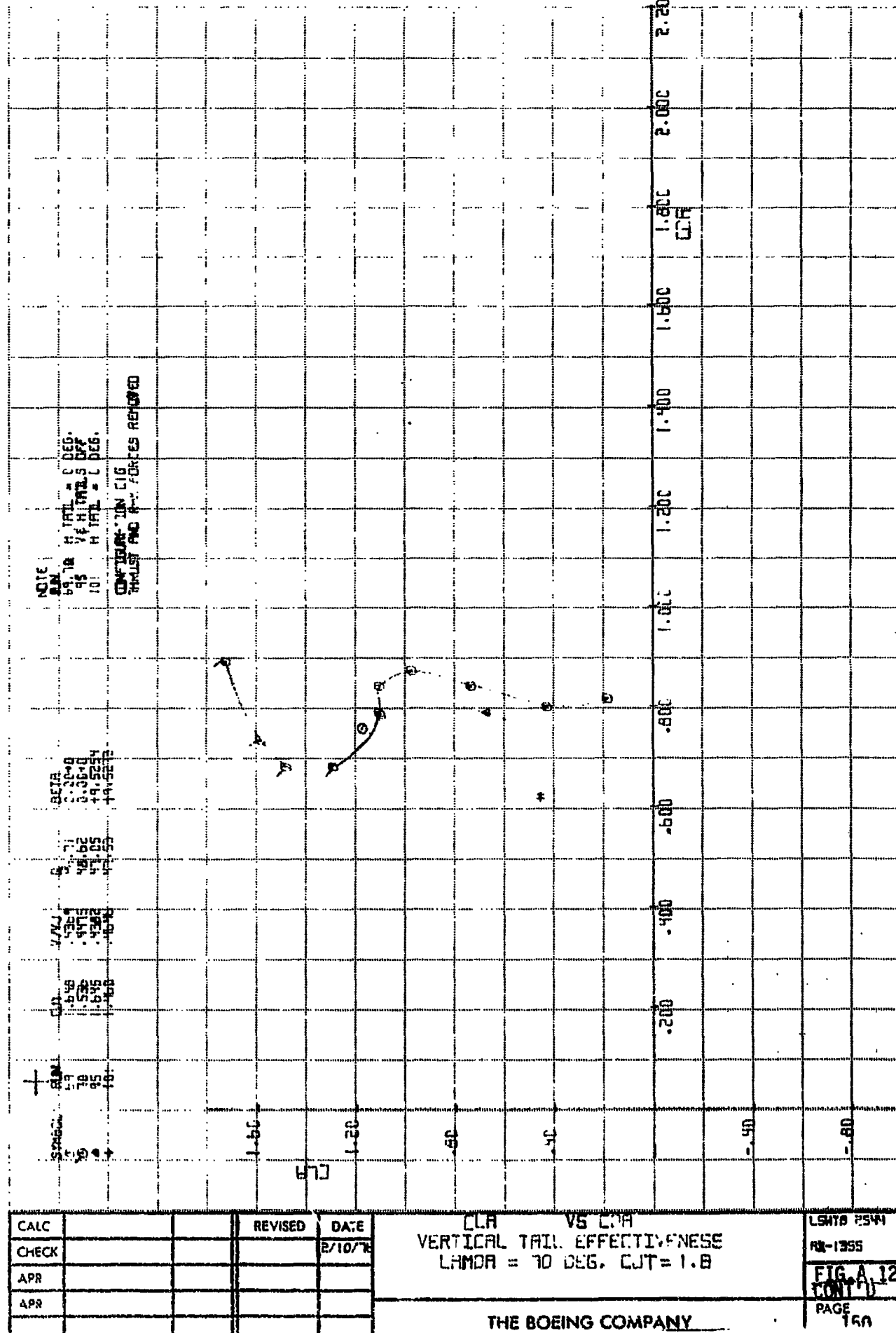
CRM VS ALPHA  
VERTICAL TAIL EFFECTIVENESS  
LAMBDA = 90 DEG. CJ = 0

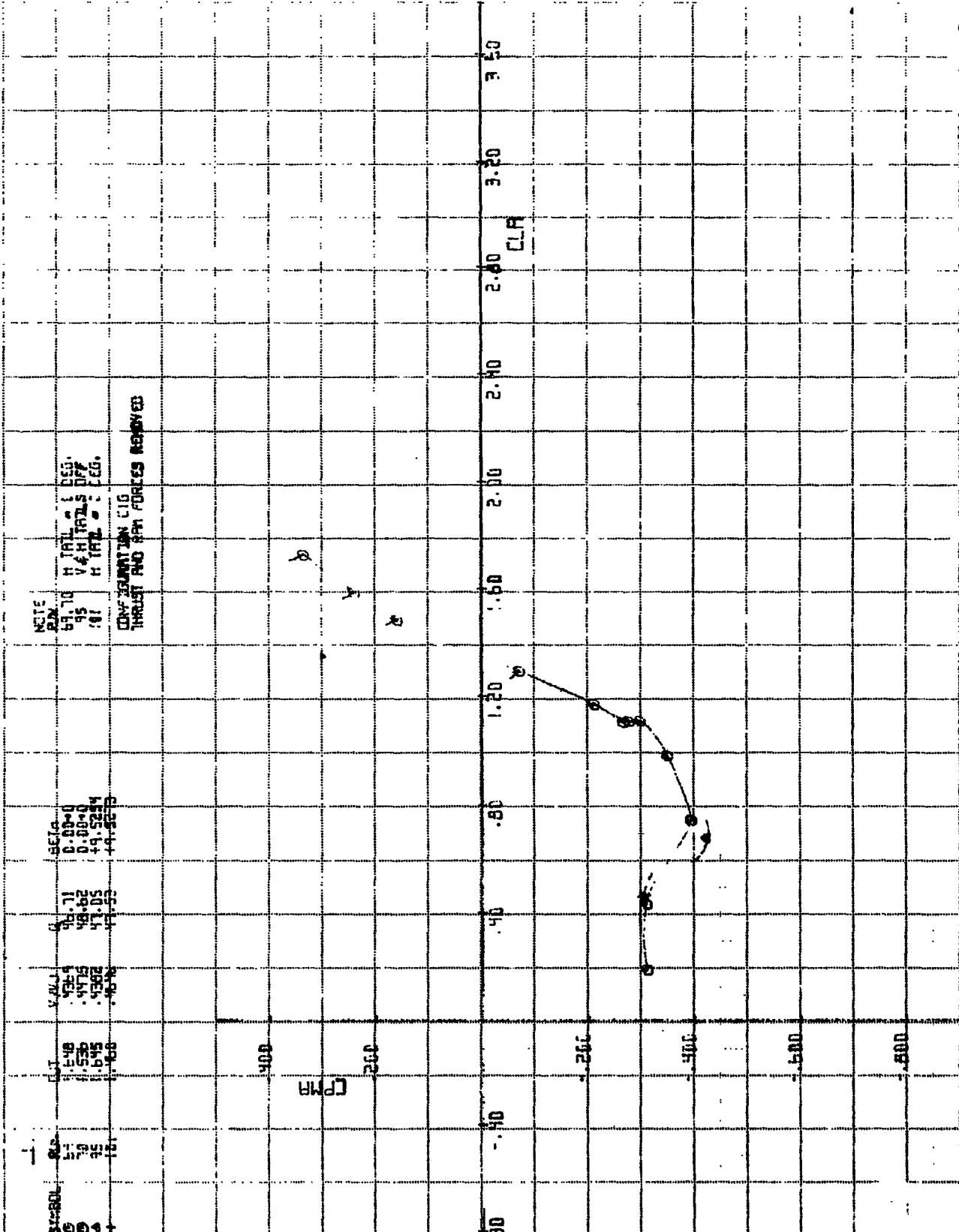
THE BOEING COMPANY

SHTB 2544  
AK-1355  
FIG.A.11  
CONT'D  
PAGE  
148

ORIGINAL PAGE IS  
OF POOR QUALITY





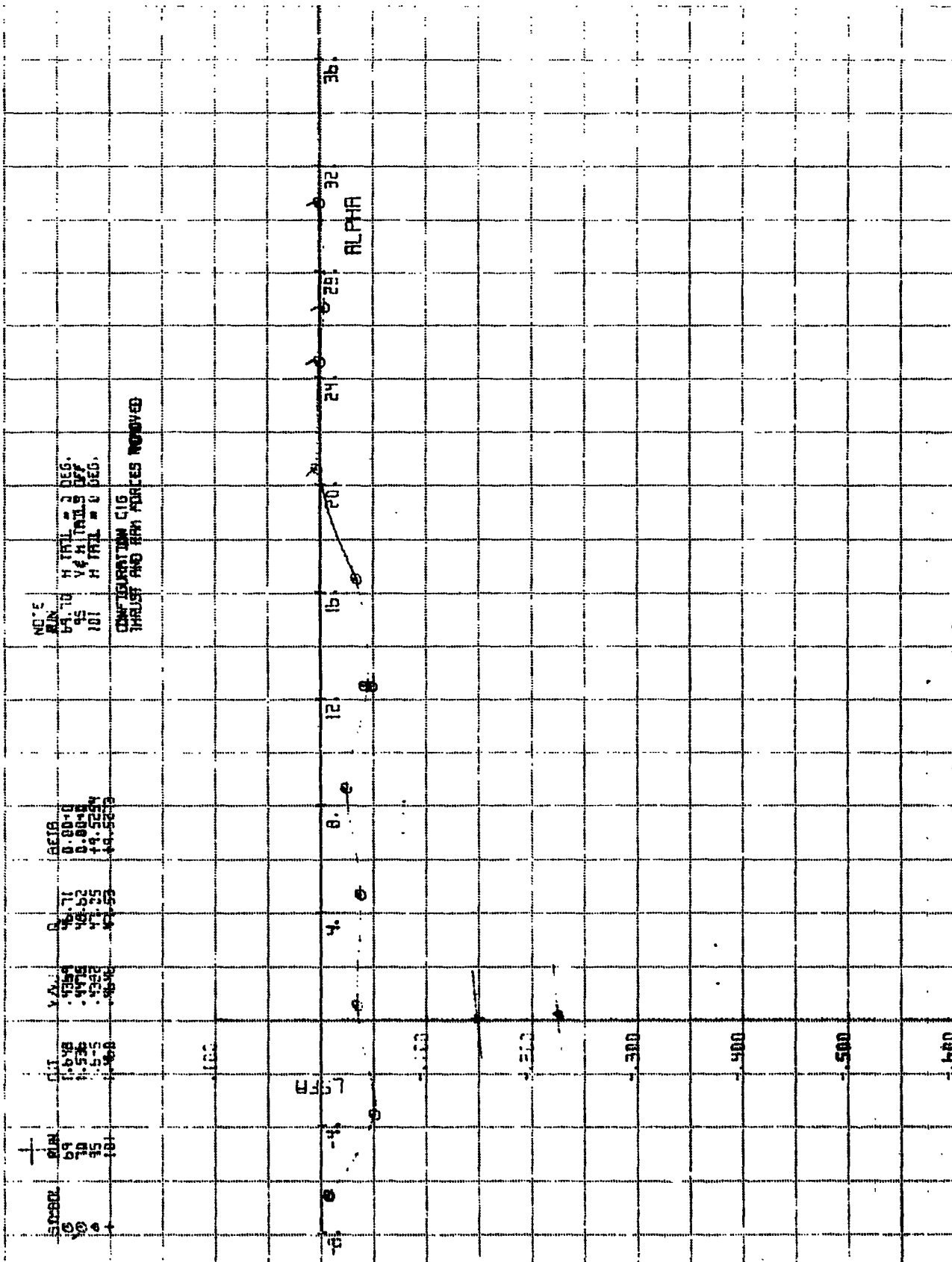


CALC		REVISED	DATE
CHECK			2/10/78
APR			
APR			

LPMR VS CLH  
VERTICAL TAIL EFFECTIVENESS  
LHMRA = 90 DEG, CLJ = 1.8

LMTB 2544  
MA-1355  
FIG.A.12  
CONT'D  
PAGE  
151

THE BOEING COMPANY



CALC	REvised	DATE
CHECK		8/10/10
APR		
APR		

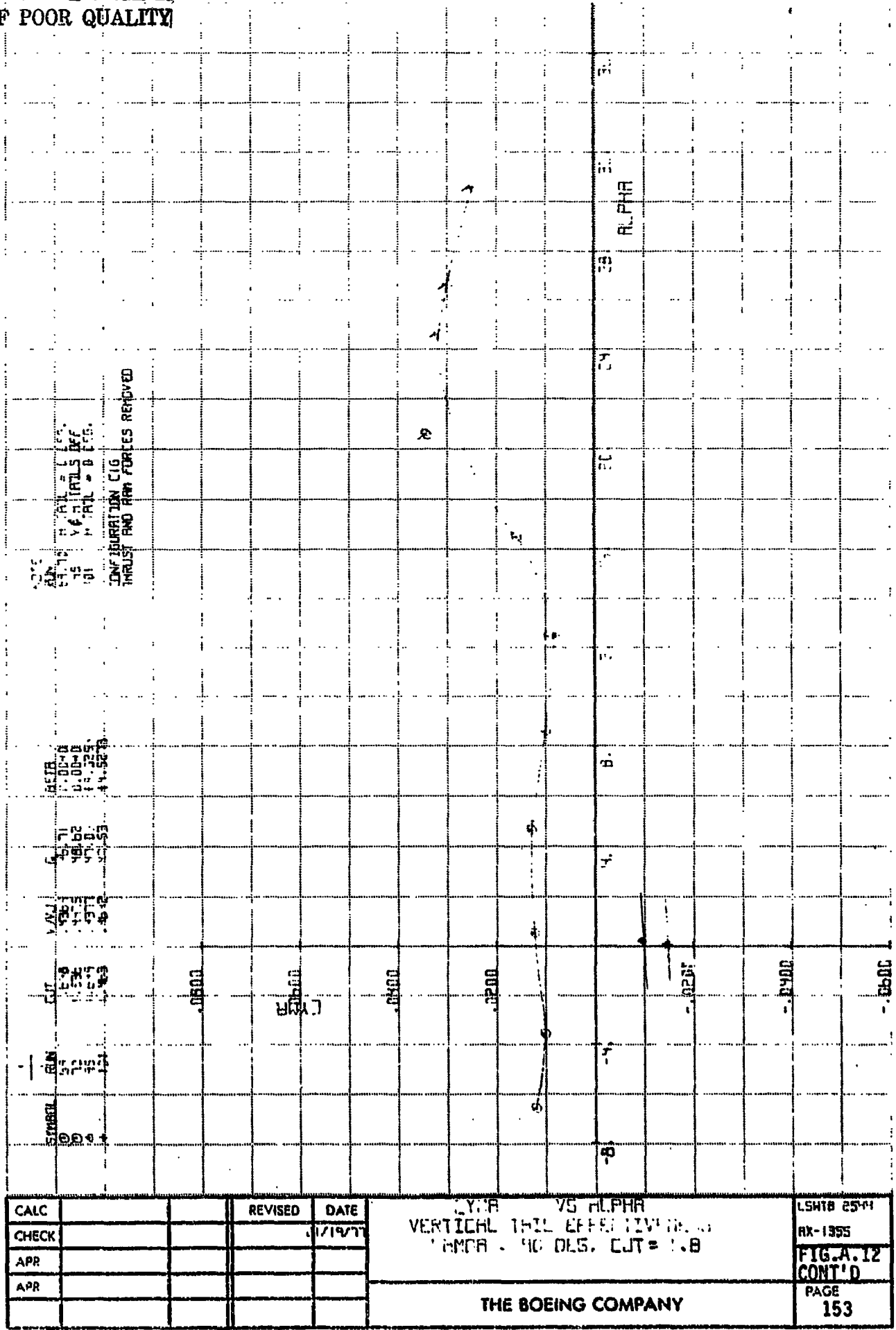
LSPH VS ALPHA  
VERTICAL THRILL EFFECTIVENESS  
L.M.M.H = 90 DEG. CUT = 1.0

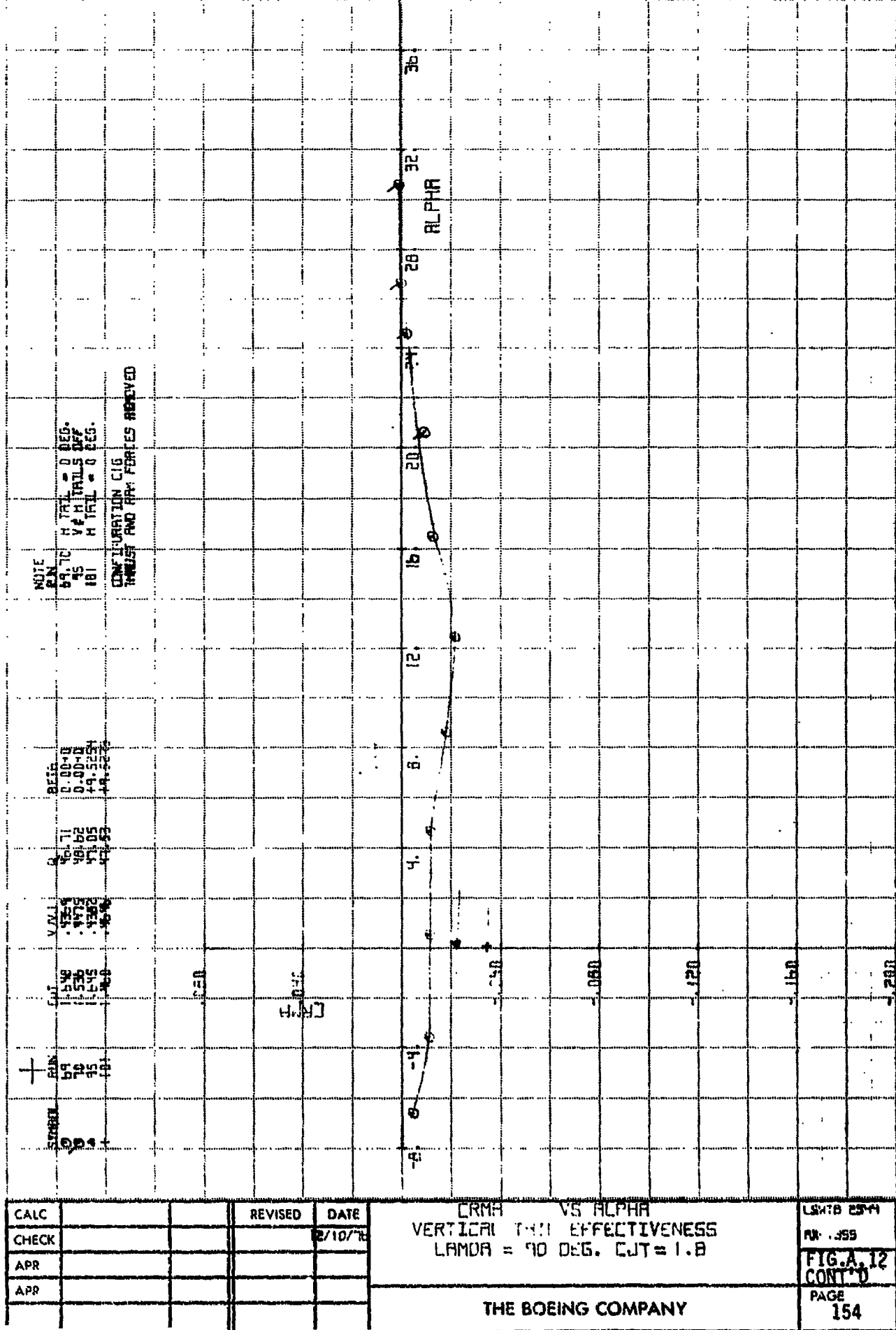
THE BOEING COMPANY

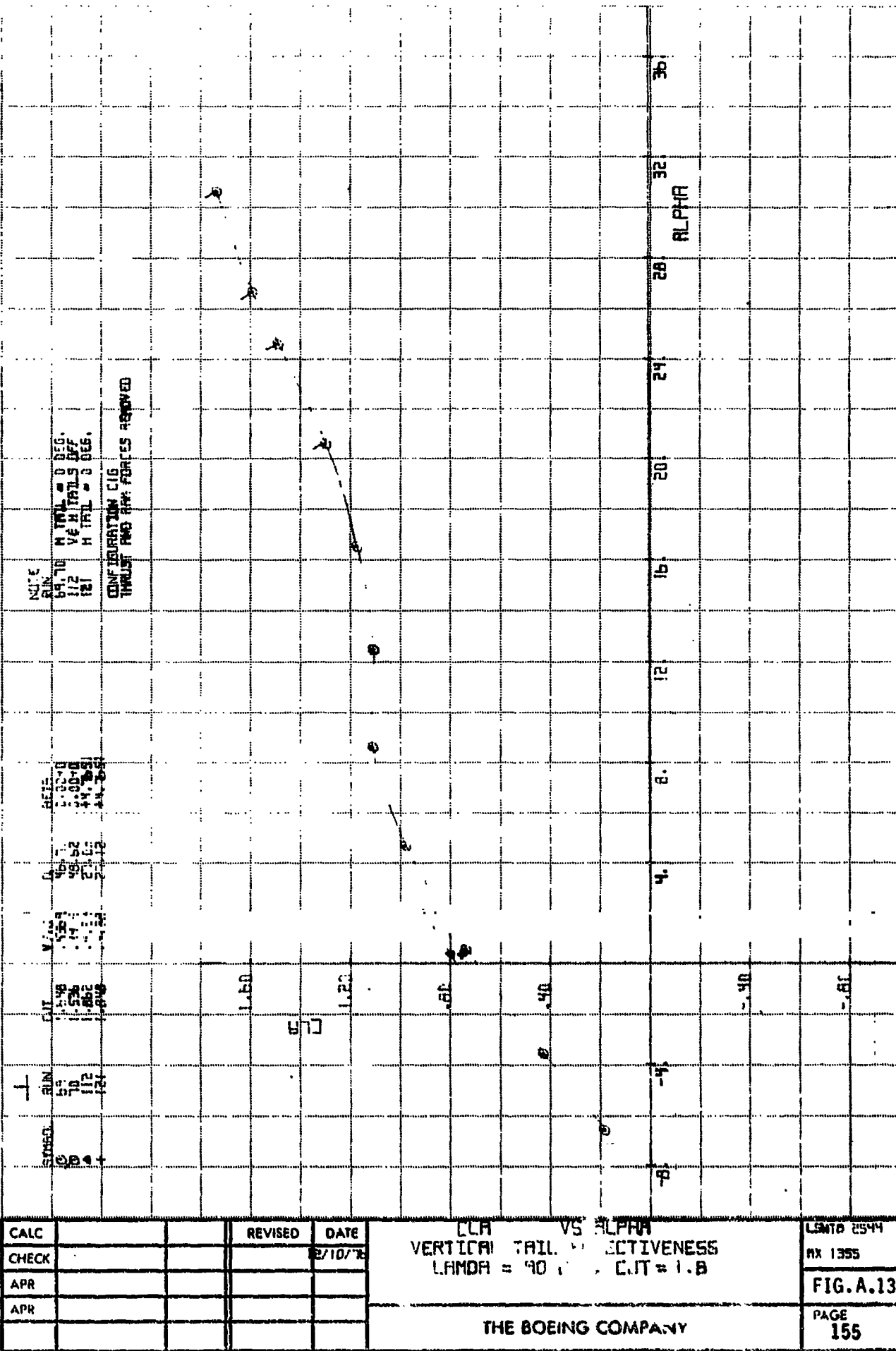
FIG. A.12  
CONT'D

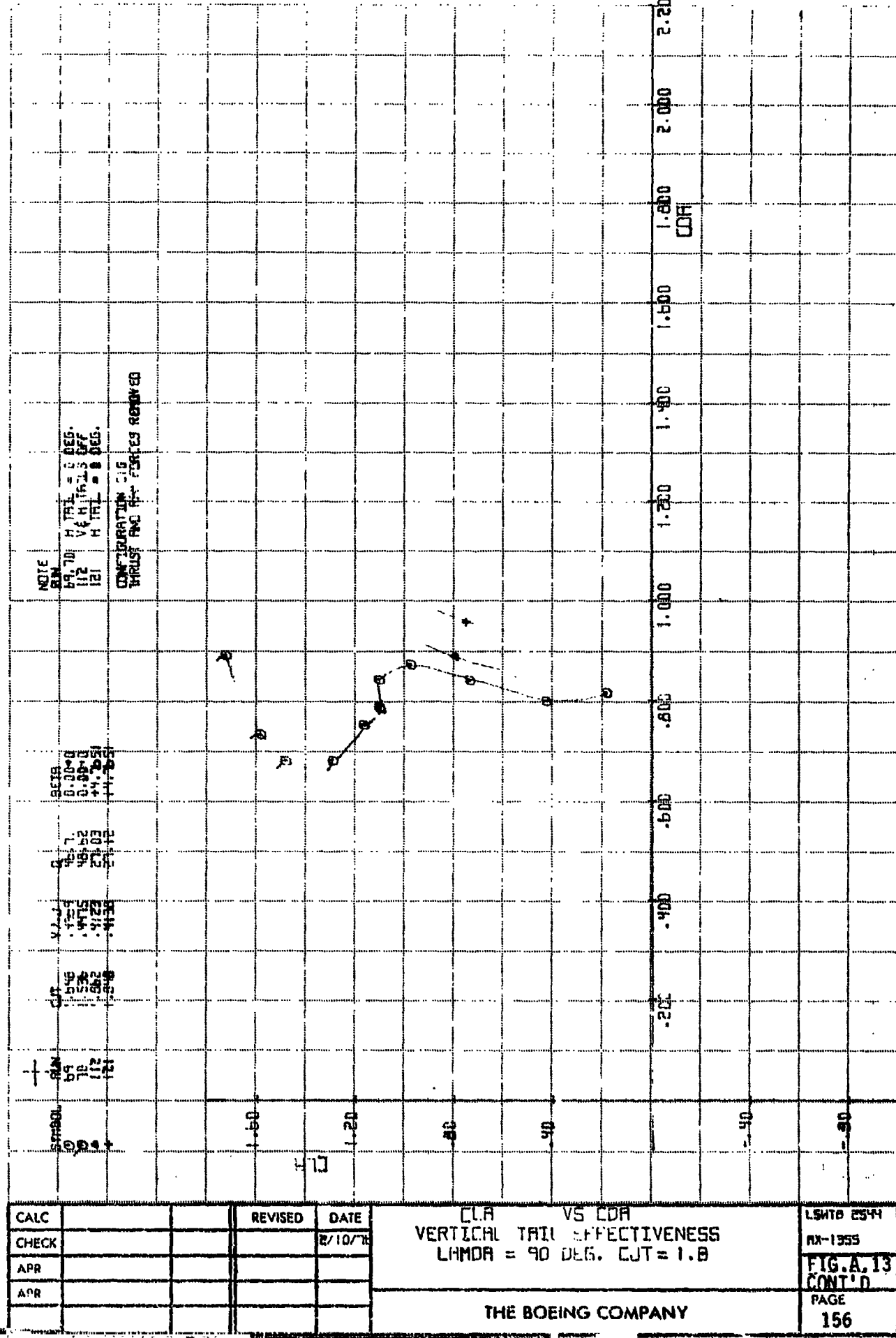
PAGE  
152

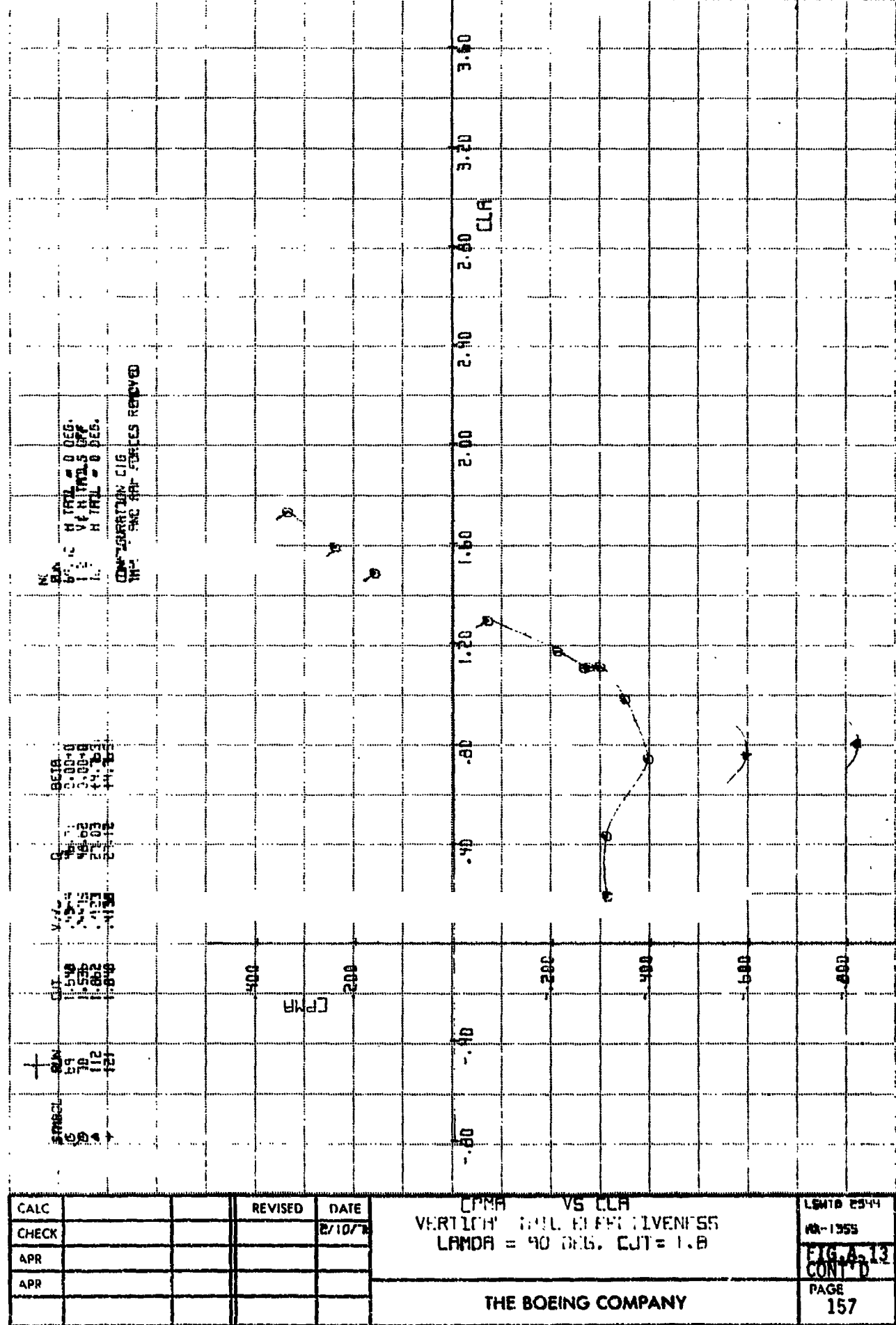
ORIGINAL PAGE IS  
OF POOR QUALITY

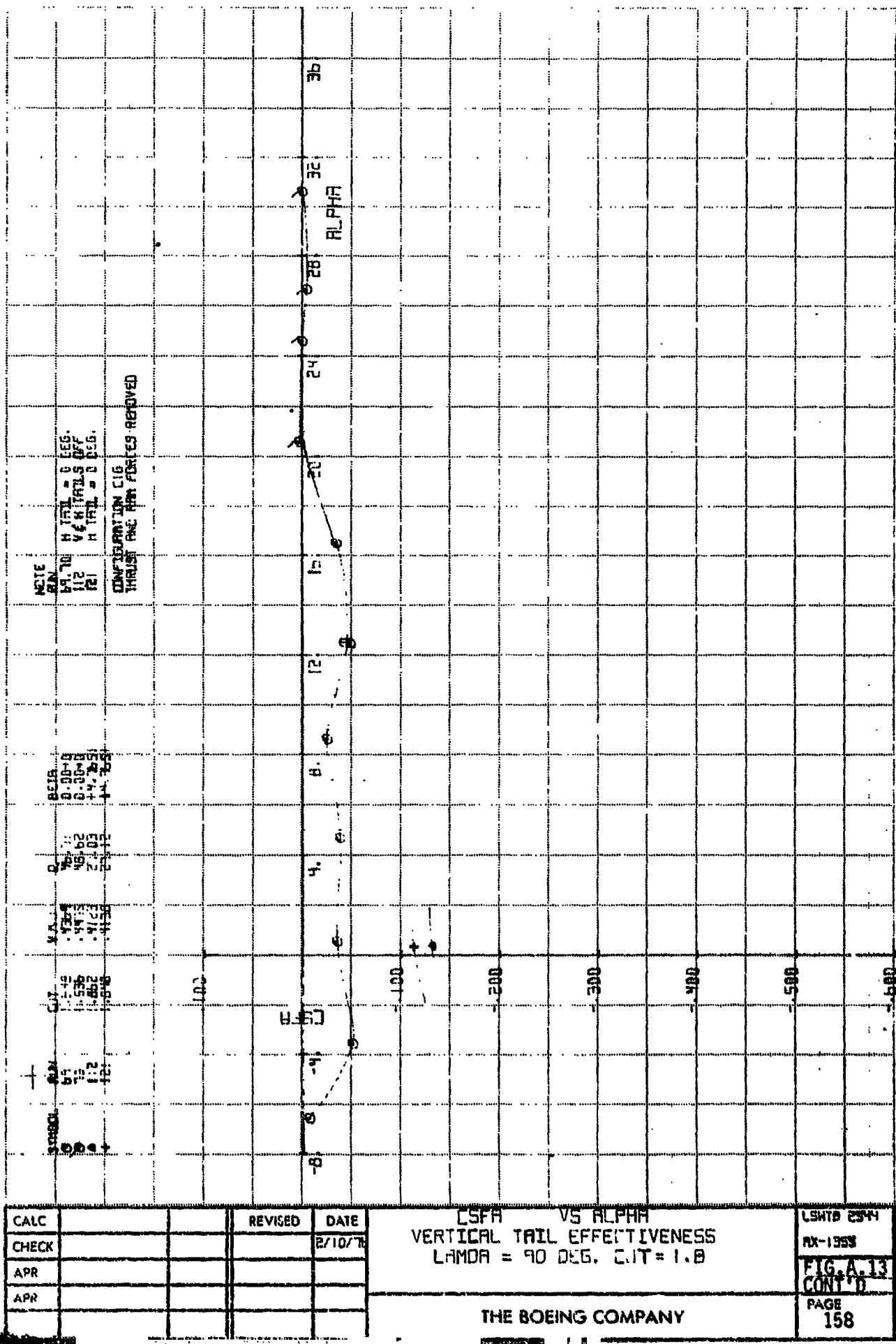












CSFA VS ALPHA  
VERTICAL TAIL EFFECTIVENESS  
LAMDA = 90 DEG. C.I.T = 1.0

LSHTB ESTD

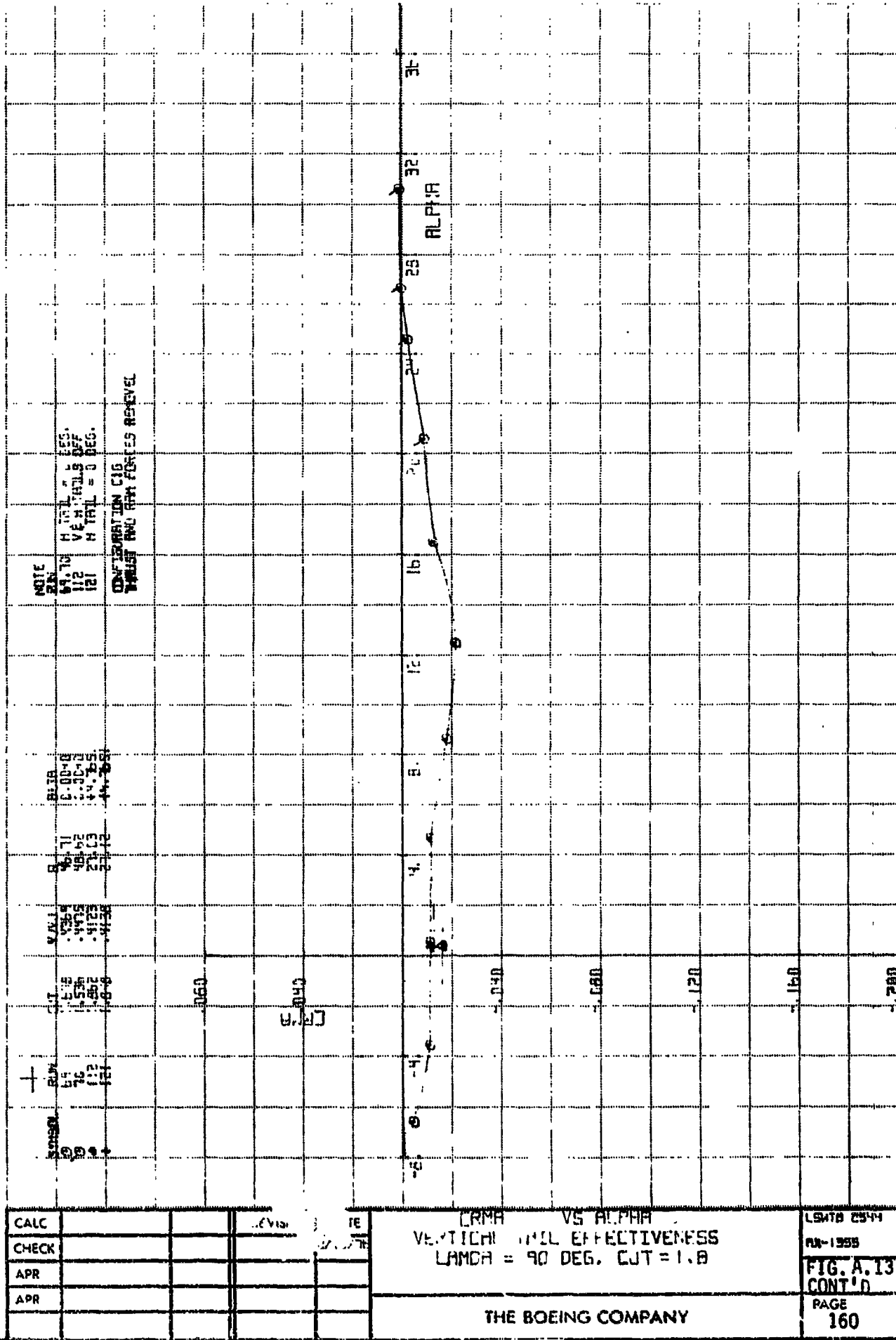
八-1353

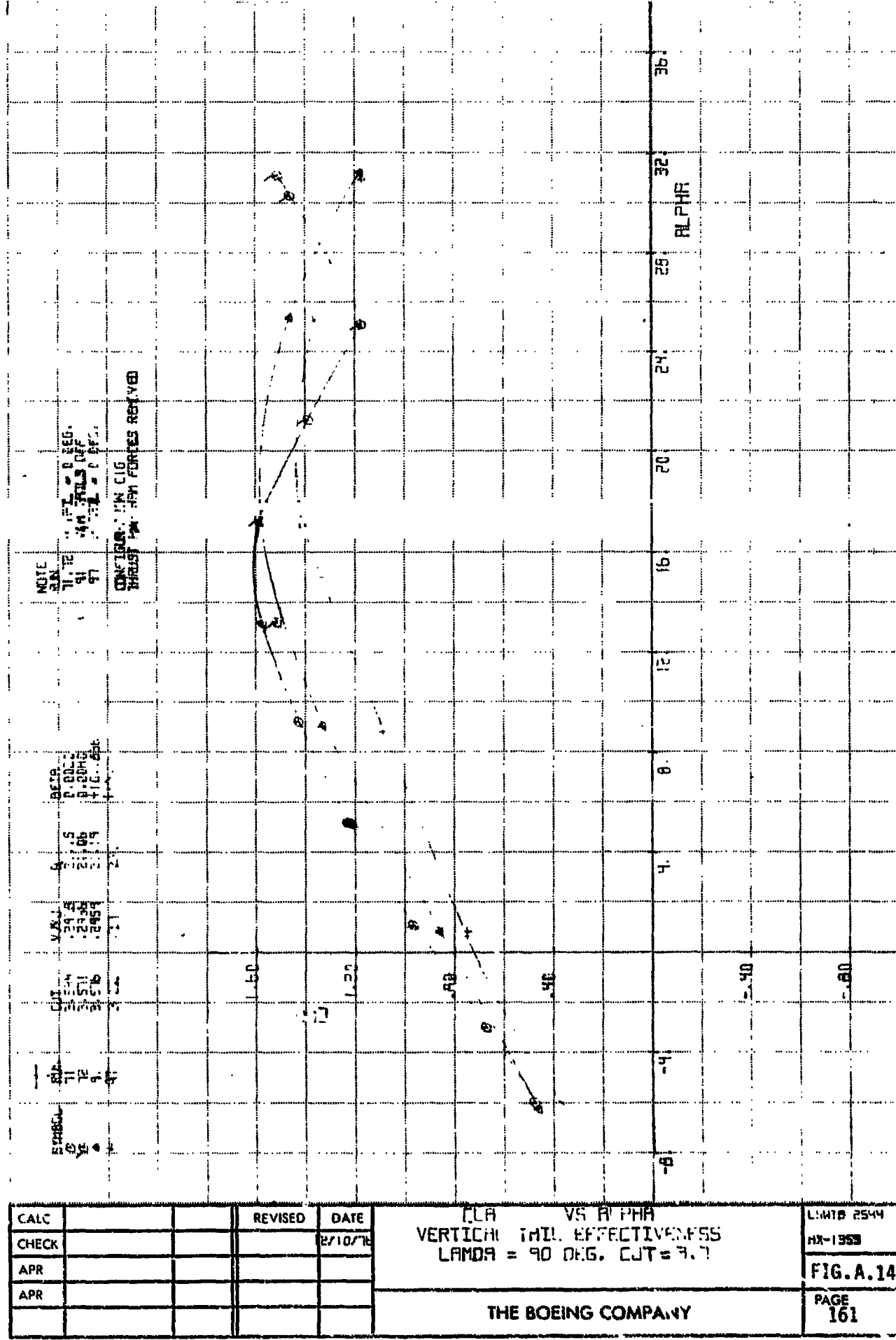
**FIG. A.13**  
**CONT'D.**

PAGE  
158

**THE BOEING COMPANY**

ORIGINAL PAGE IS  
OF POOR QUALITY





CALC			REVISED	DATE
CHECK				2/10/78
APR				
APR				

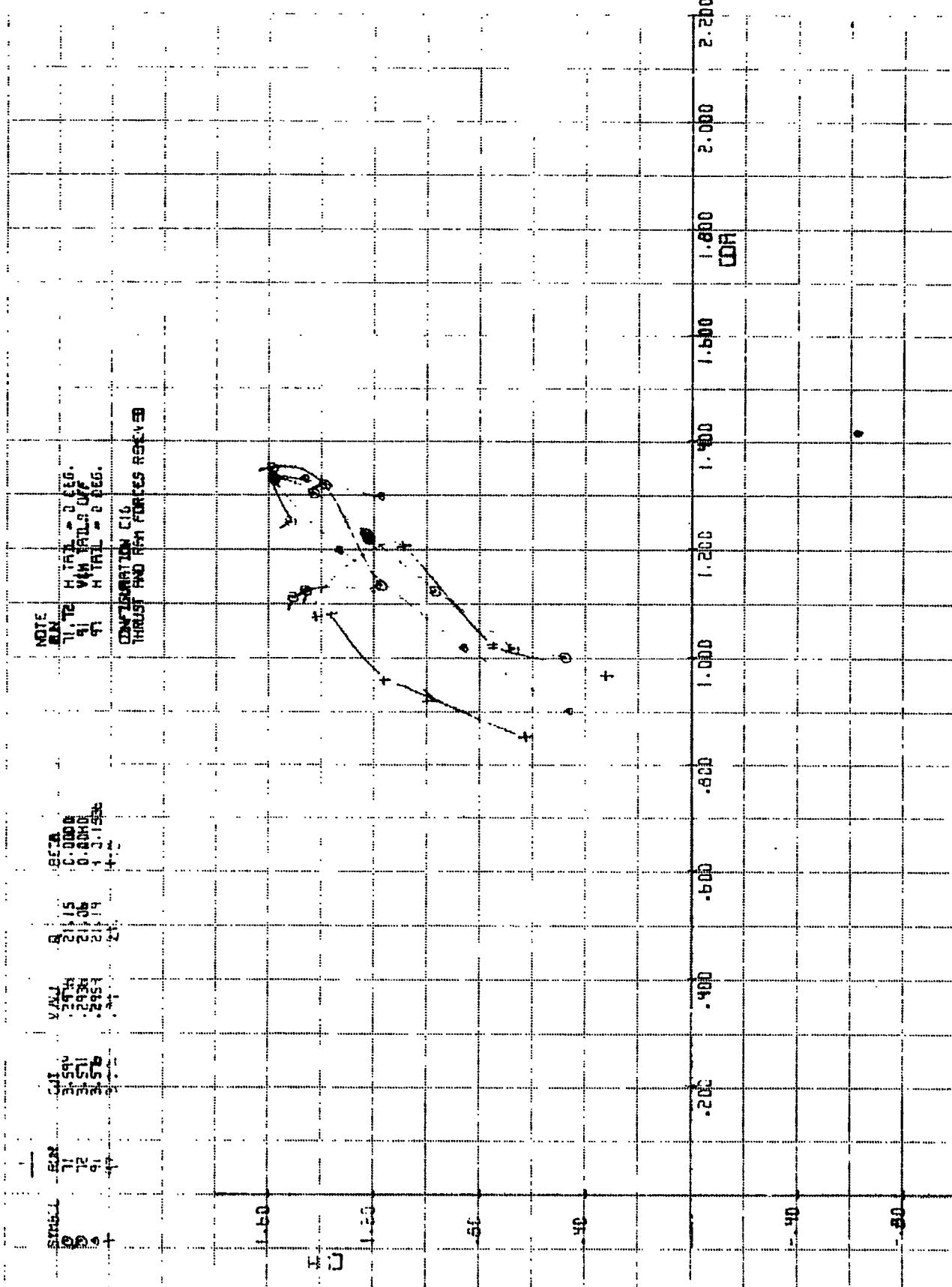
CLA VS ALPHABT  
VERTICAL TAIL EFFECTIVENESS  
 $\lambda_{M0} = 90 \text{ DEG}$ ,  $CJT = 3.7$

THE BOEING COMPANY

LIMITS 2544  
HX-1953

FIG. A.14

PAGE  
161



CALC			REVISED	DATE
CHECK				PWJ 1
APP				
APR				

DIR VS C.R.  
VERTICAL TILT = 11.5 DEGREES  
LAMDA = 70 DEG. LUT = 3.1

1970 2544

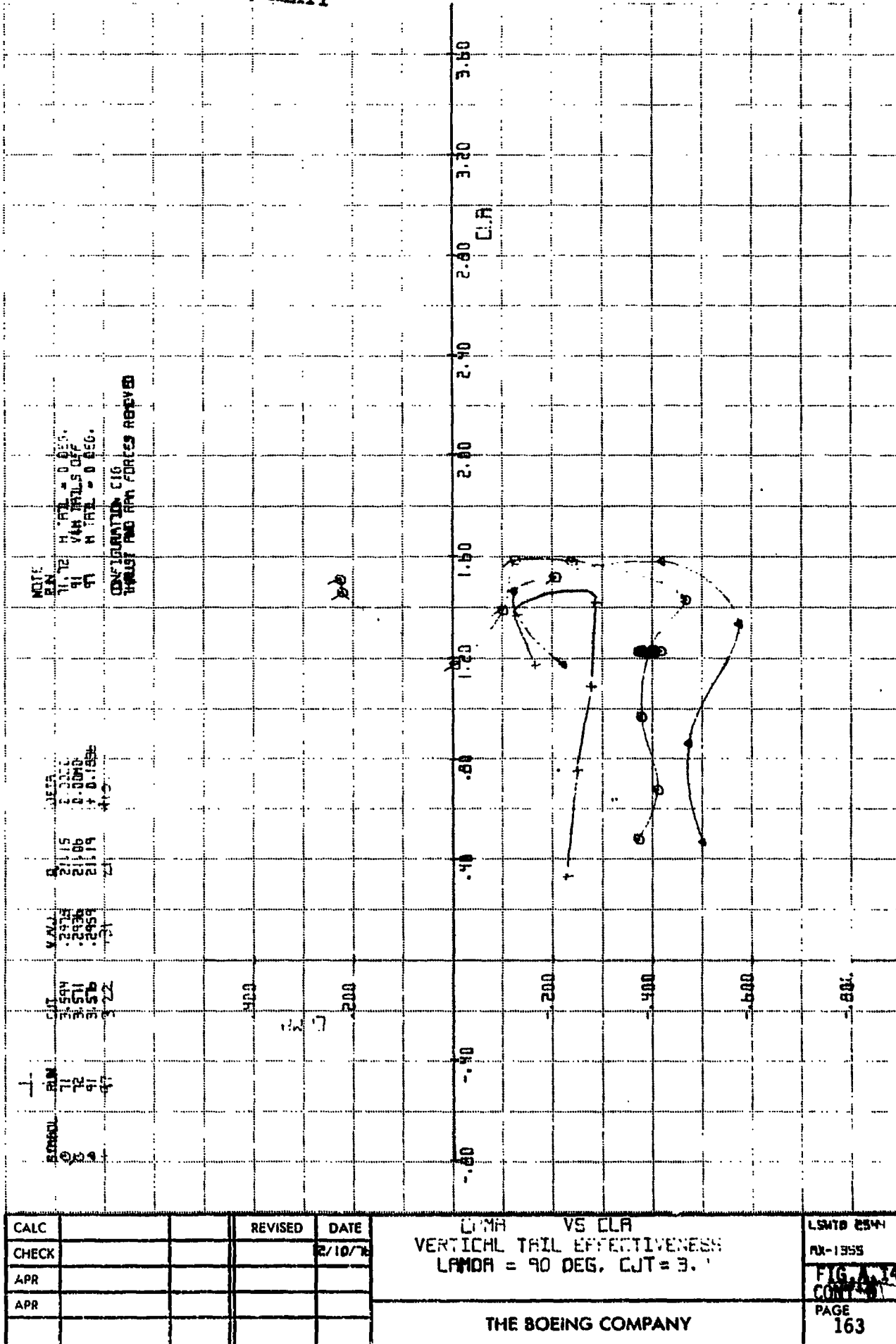
18-1355

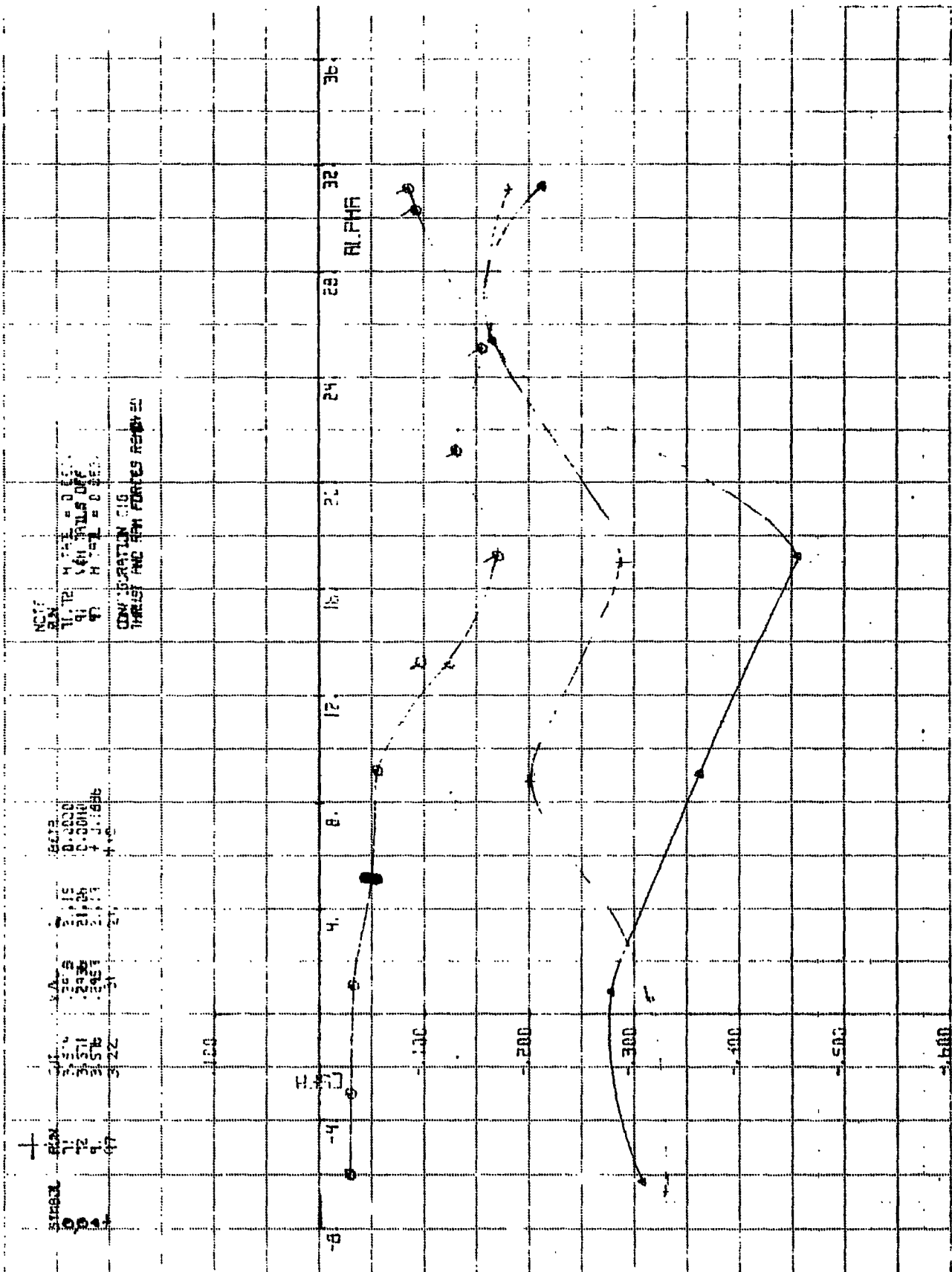
FIG. A.14  
CONT'D

PAGE  
162

THE BOEING COMPANY

ORIGINAL PAGE IS  
OF POOR QUALITY





CAIC			REVISED	DATE
CHECK				2/10/78
APR				
APR				

FSFH VS ALPHA  
VERTICAL TAIL EFFECTIVENESS  
LAMON = 70.046, CDT = 3.1

1578 3550

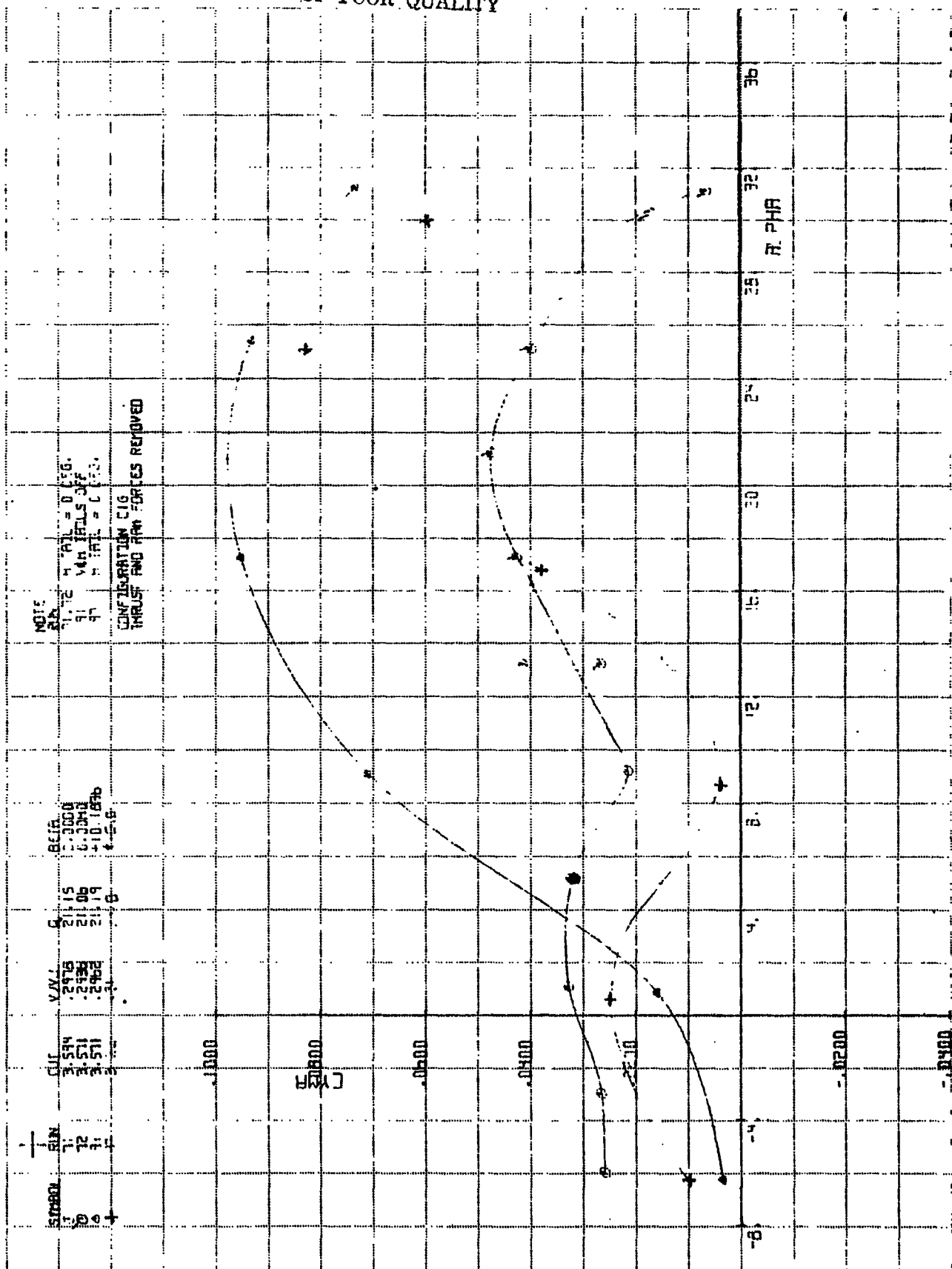
Ex-1355

FIG. A.14  
CONT'D

PAGE  
164

**THE BOEING COMPANY**

ORIGINAL PAGE IS  
OF POOR QUALITY

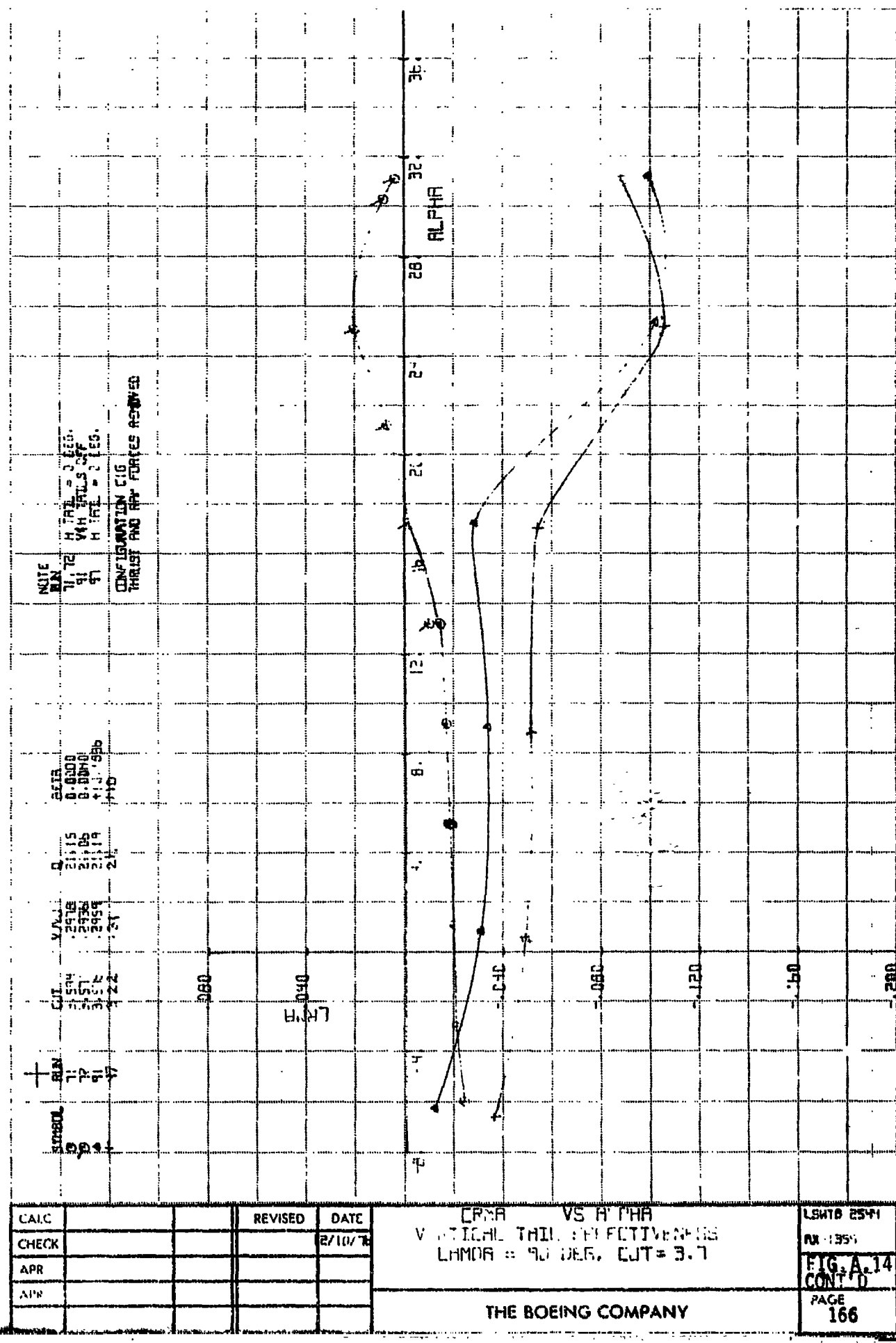


CALC			REVISED	DATE
CHECK				11/19/77
APR				
APR				

ZYMA VS ALPHA  
VERTICAL THIN EFFECTIVENESS  
LAMDA = 40 DEG. CJT = 3.7

THE BOEING COMPANY

LSM18 2544  
MX-1955  
FIG.A.14  
CONT'D  
PAGE  
165



CRM VS HTPA  
VERTICAL THIN EFFECTIVENESS  
LHMOR = 90 DEG. CUT = 3.7

THE BOEING COMPANY

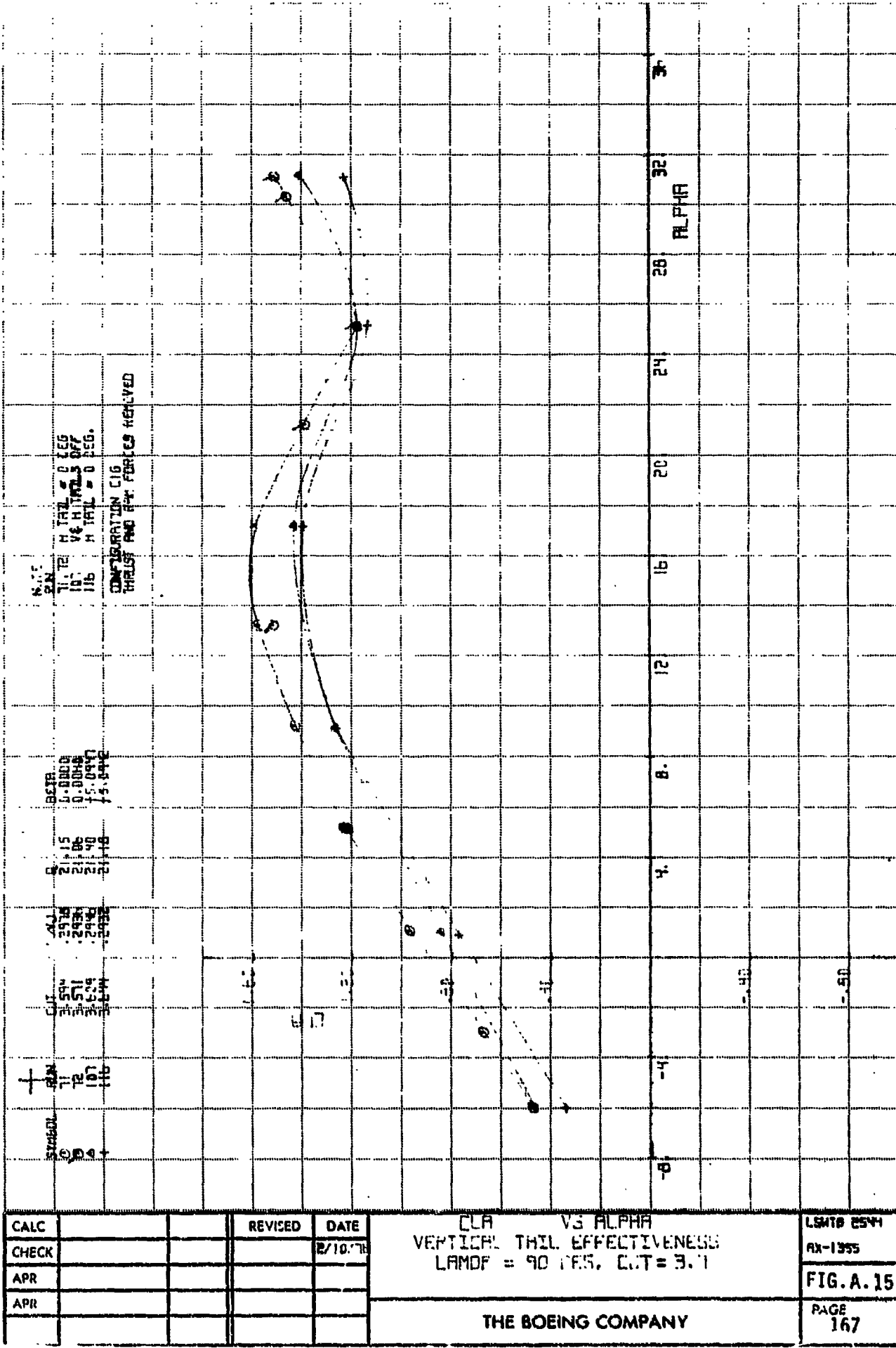
LSHTB 2541

• 135 •

**FIG. A.14**  
**CONT'D.**

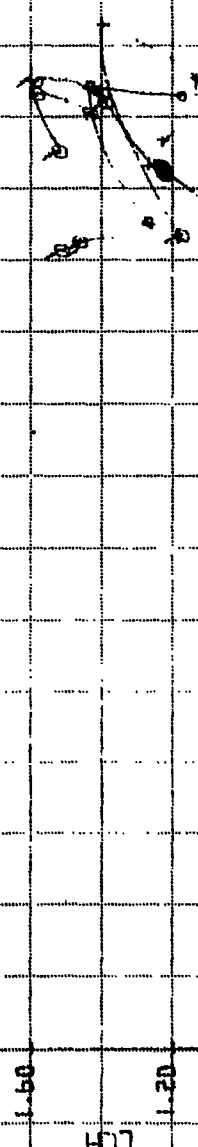
PAGE  
121

PAGE  
166



REF.	CL	CL	Y	Y	NOTE
71	1.594	1.575	5	5	0.000
72	1.511	1.530	21.45	21.45	0.000
73	1.504	1.504	21.45	21.45	45.000
74	1.504	1.504	21.45	21.45	

CONFIDENTIAL C16  
GRUSS AND PARTNERS REVIEWED



1 APR	2 APR	3 APR	4 APR	5 APR	REVISED	DATE
✓						17/07/64

C.L.A. VS C.D.R.  
VERTICAL TILT, ELEV. TILTNESS  
LHMRA = 10 DEG. EJT = 1.7

THE BOEING COMPANY

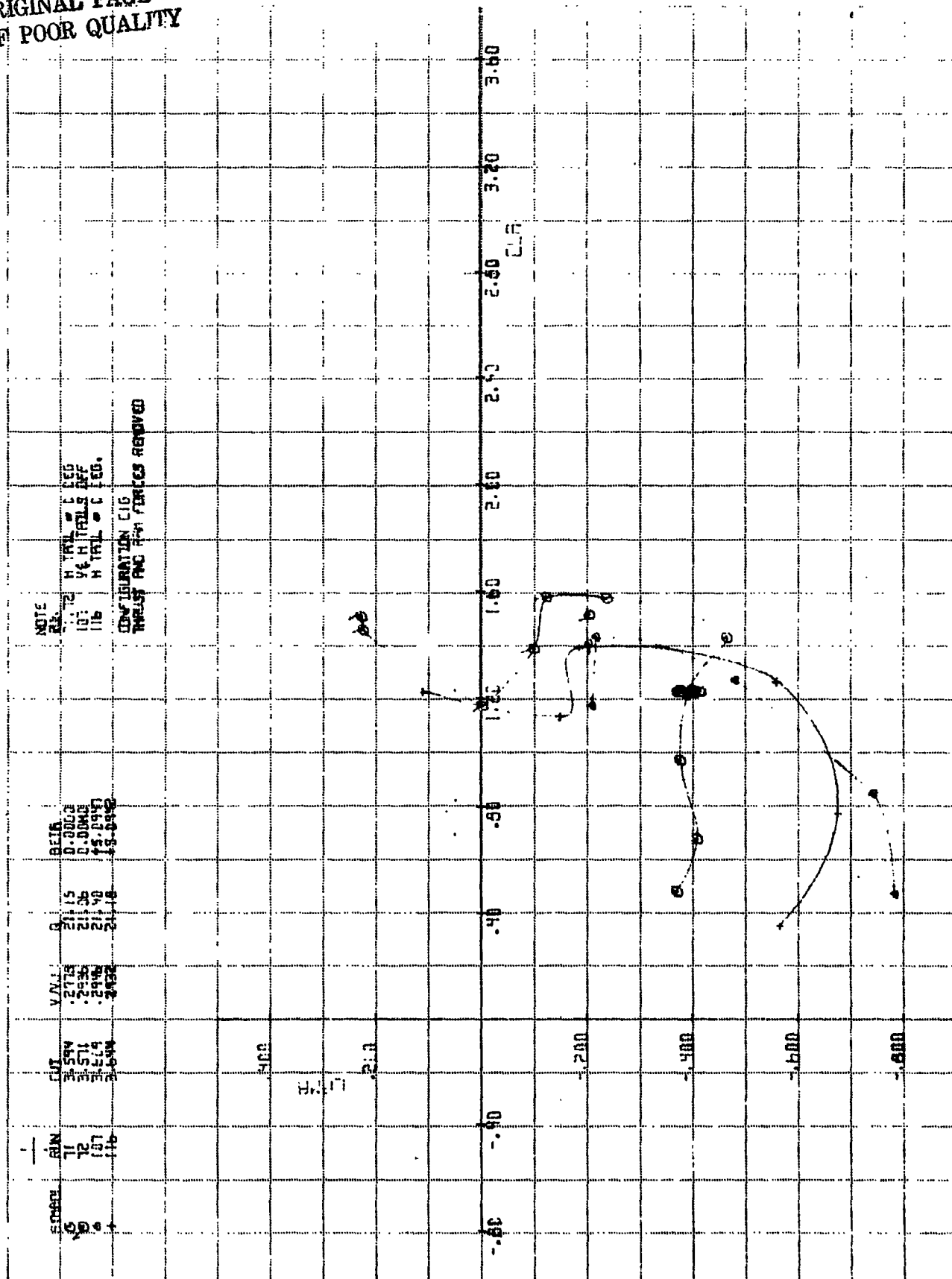
LHMB P-44

MX-1555

FIG. A.15  
CONT'D

PAGE  
168

ORIGINAL PAGE IS  
OF POOR QUALITY



CALC			REVISED	DATE
CHECK				2/10/16
APR				
APR				

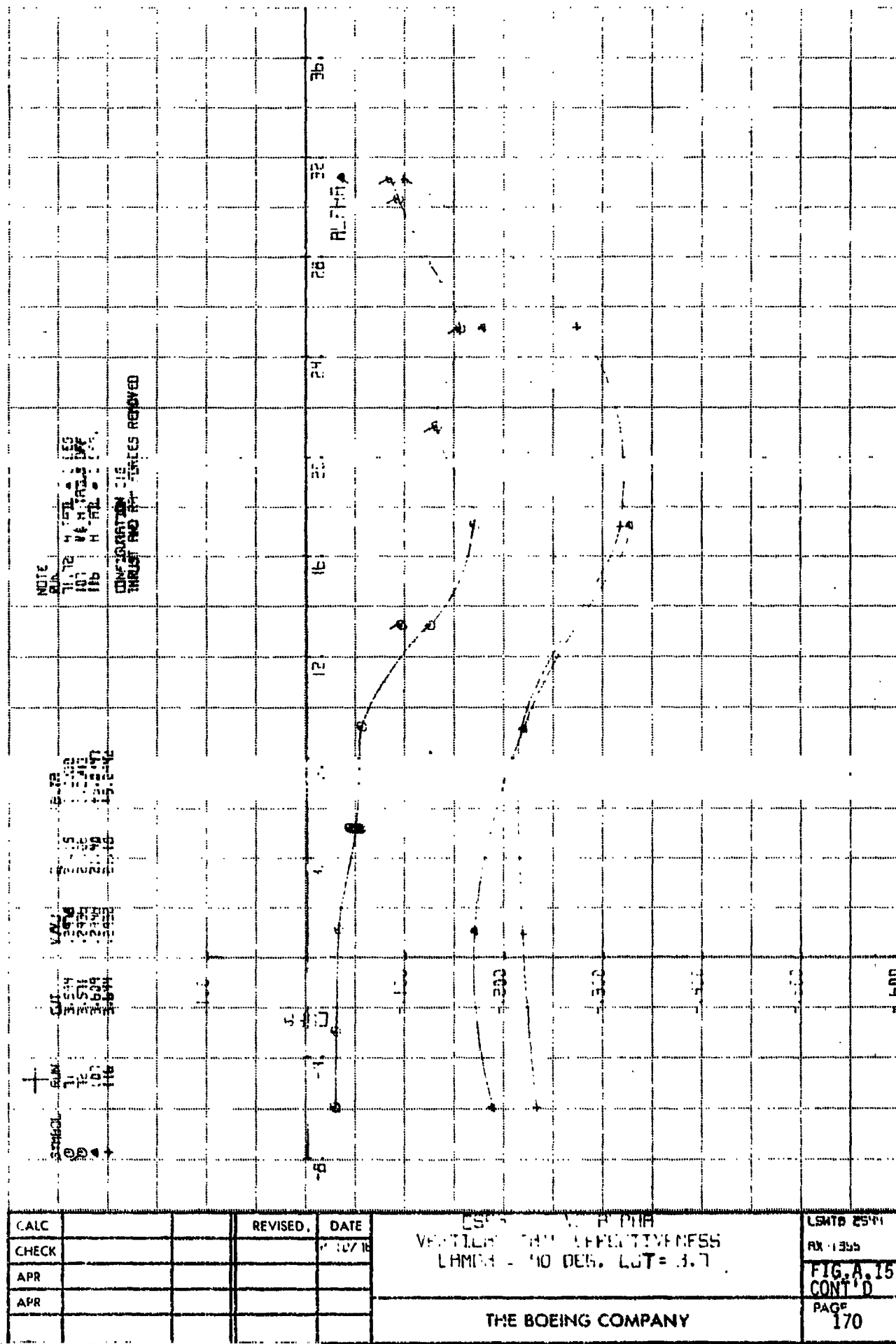
[CMA] VS CLA  
VERTICAL TAT + EFFECTIVENESS  
LAMDA = 90 DEG. C.I.T = 3.7

**THE BOEING COMPANY**

LSMTB 2544  
01-1955

**FIG. A-25**  
**CONT'D.**

PAGE  
169



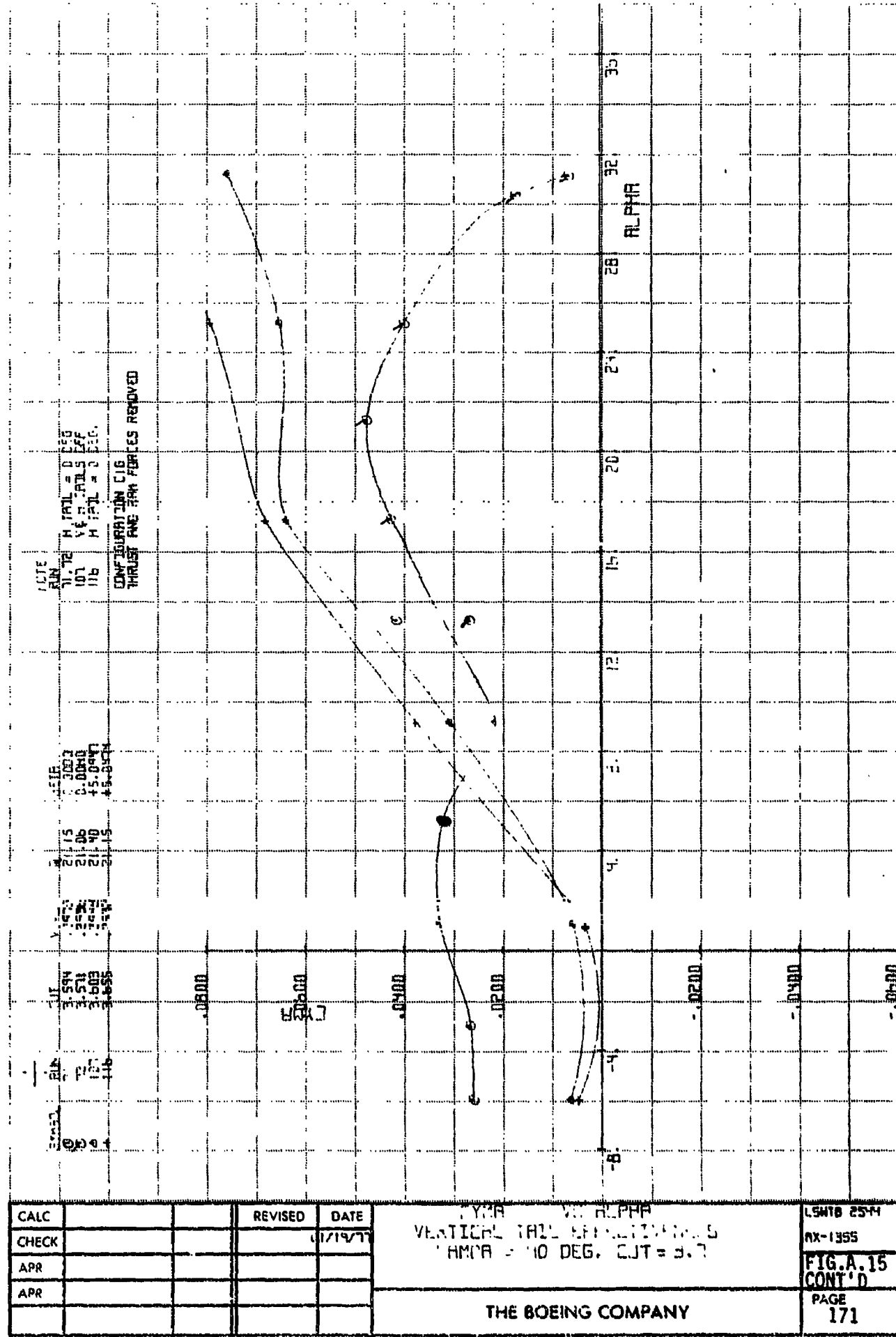
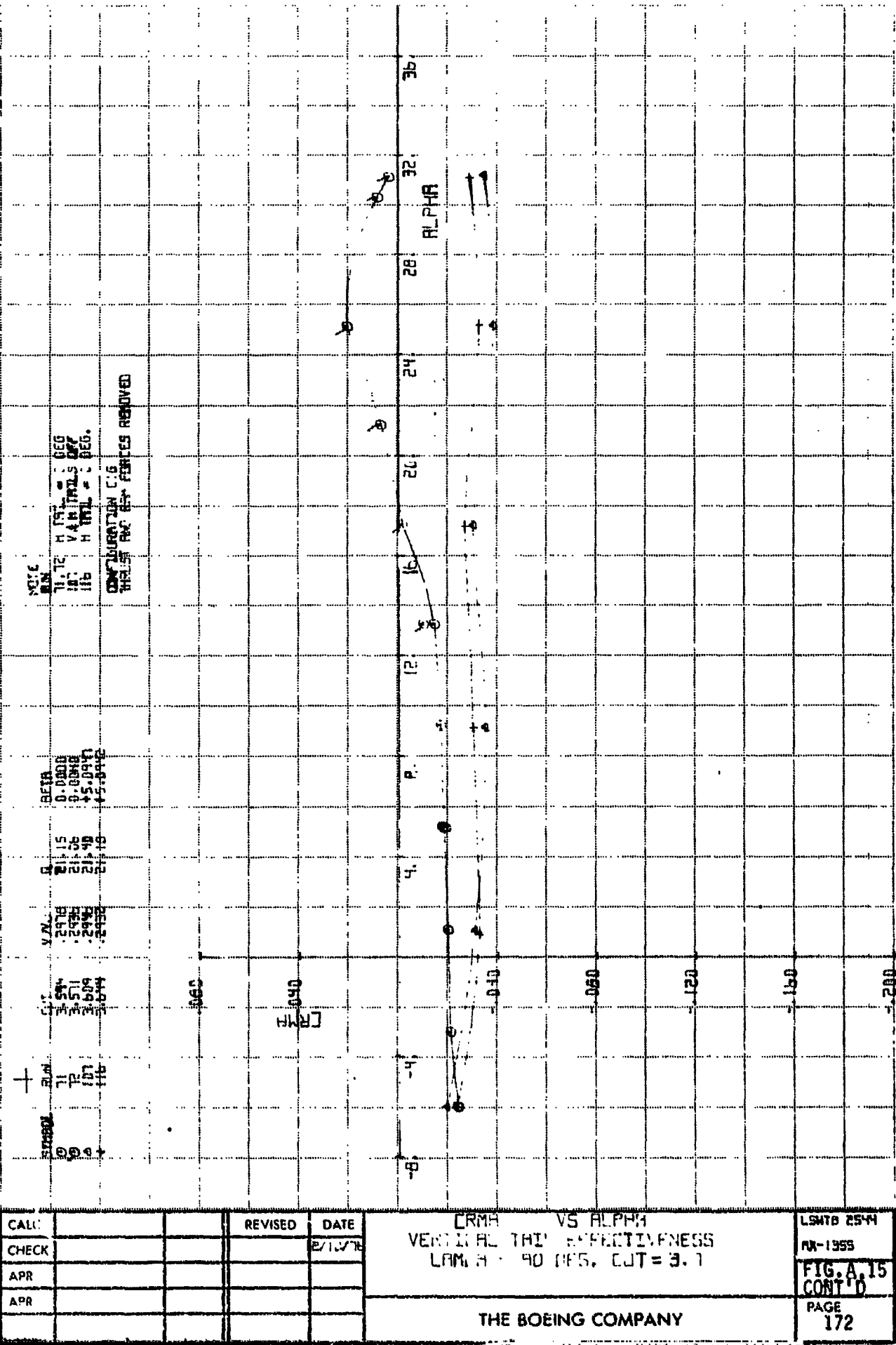
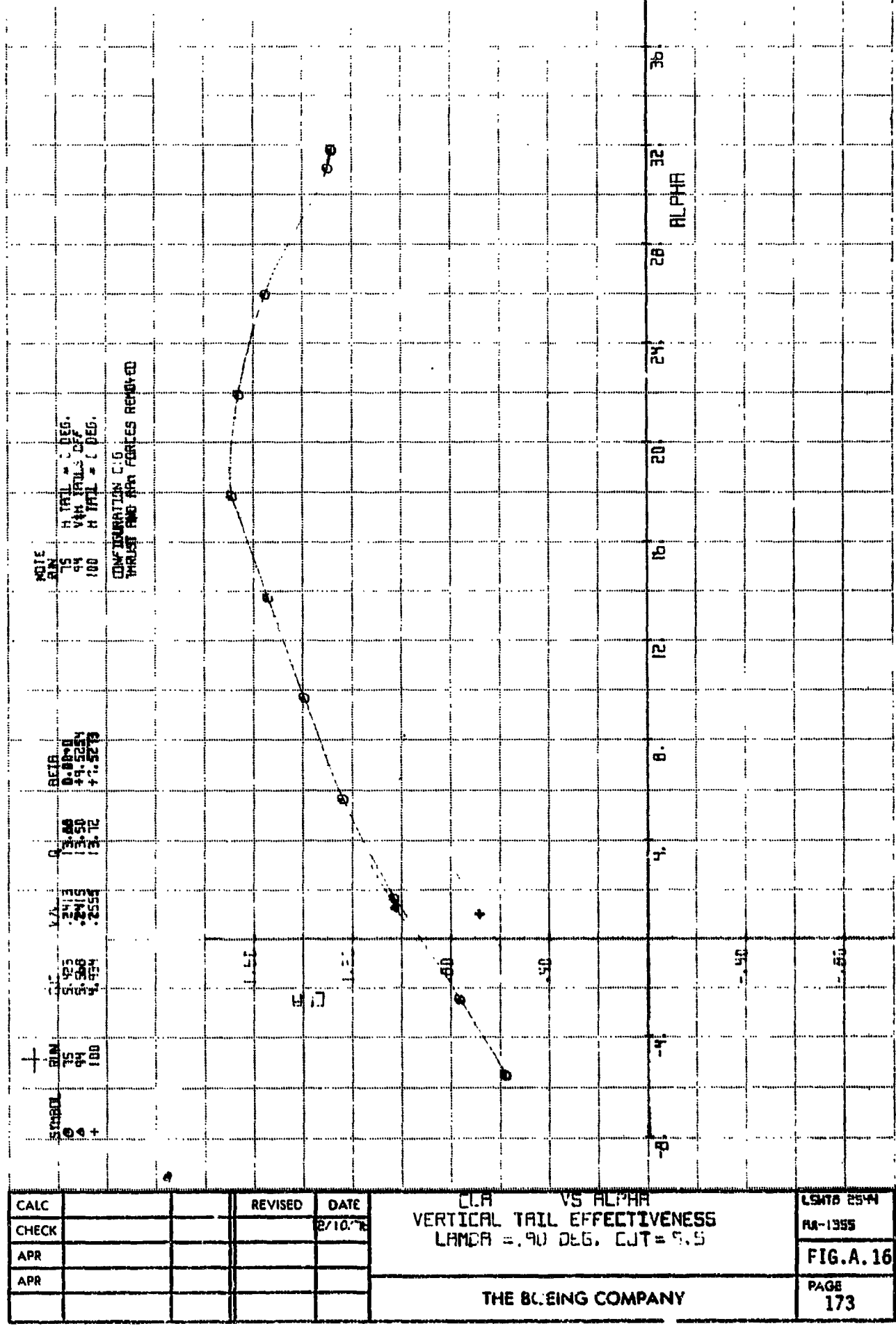
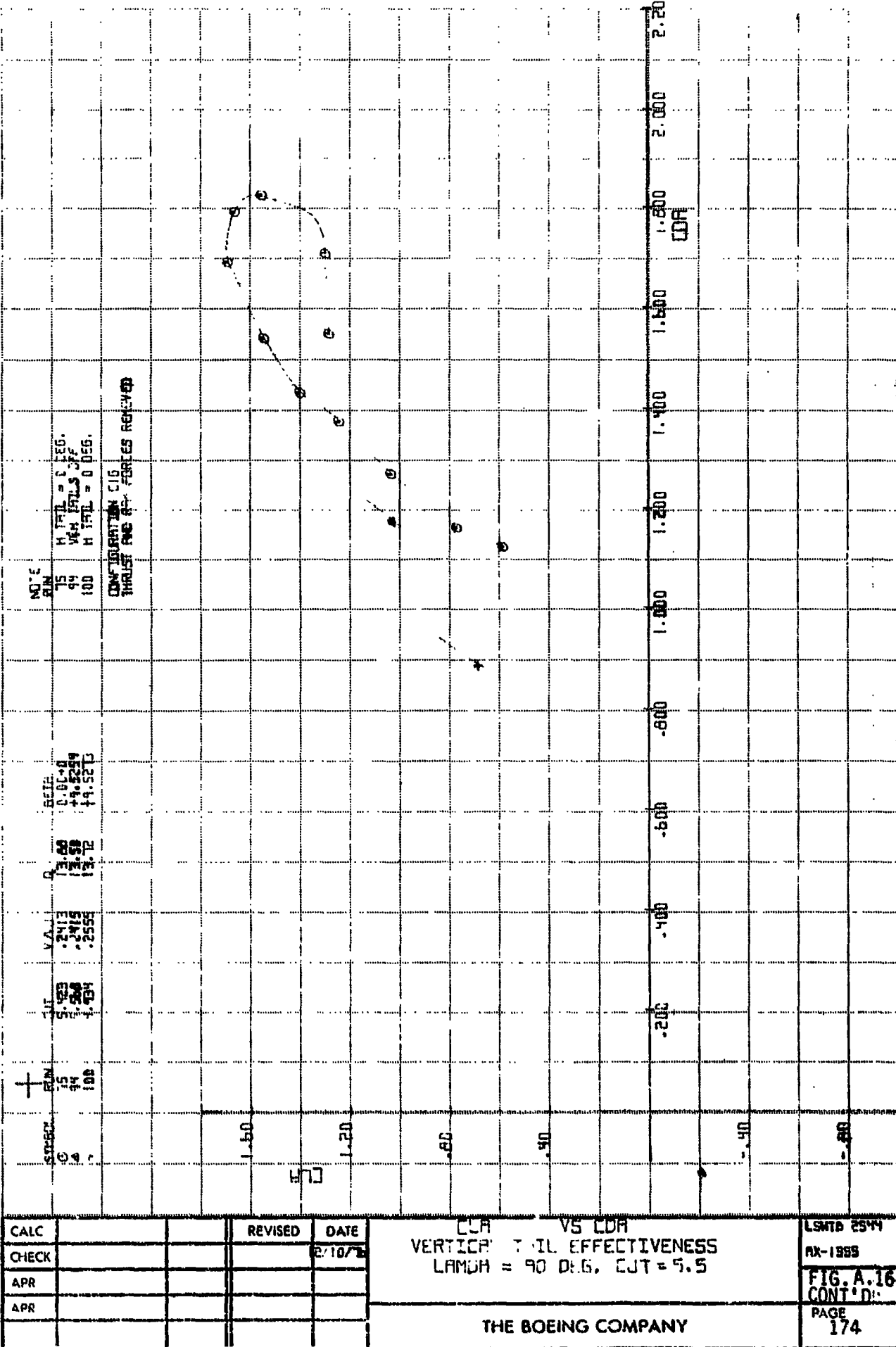


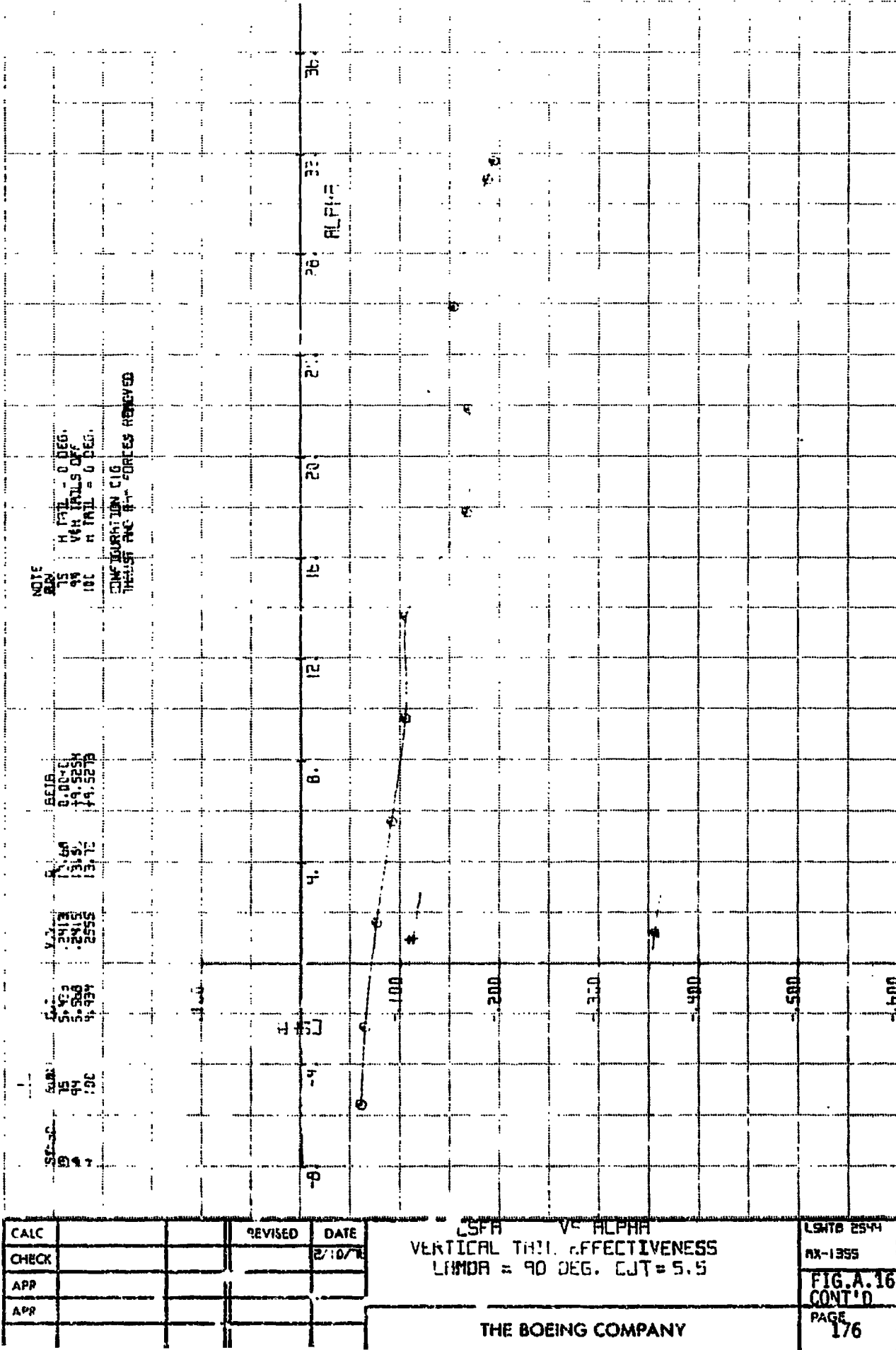
FIG. 3C



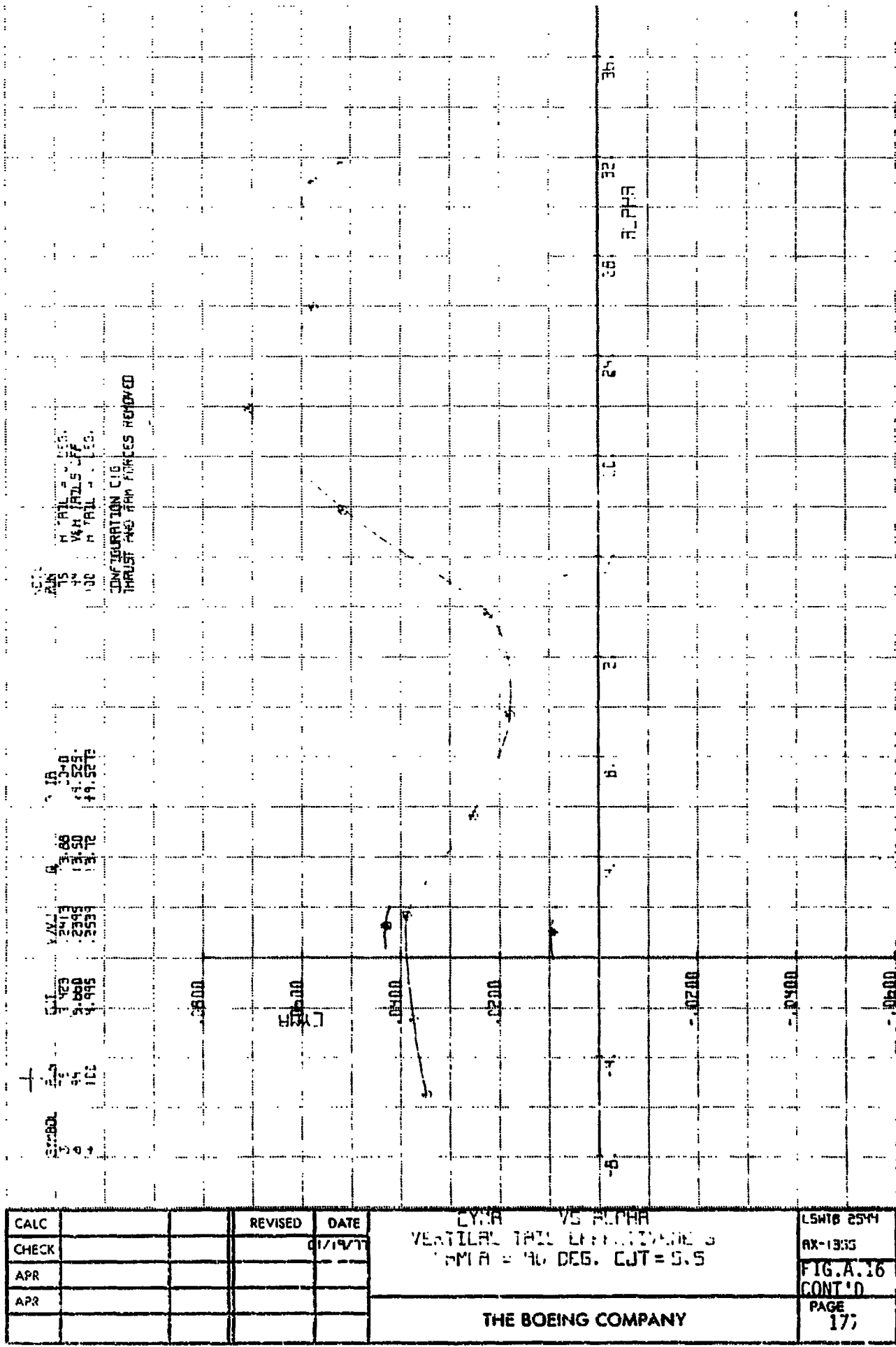


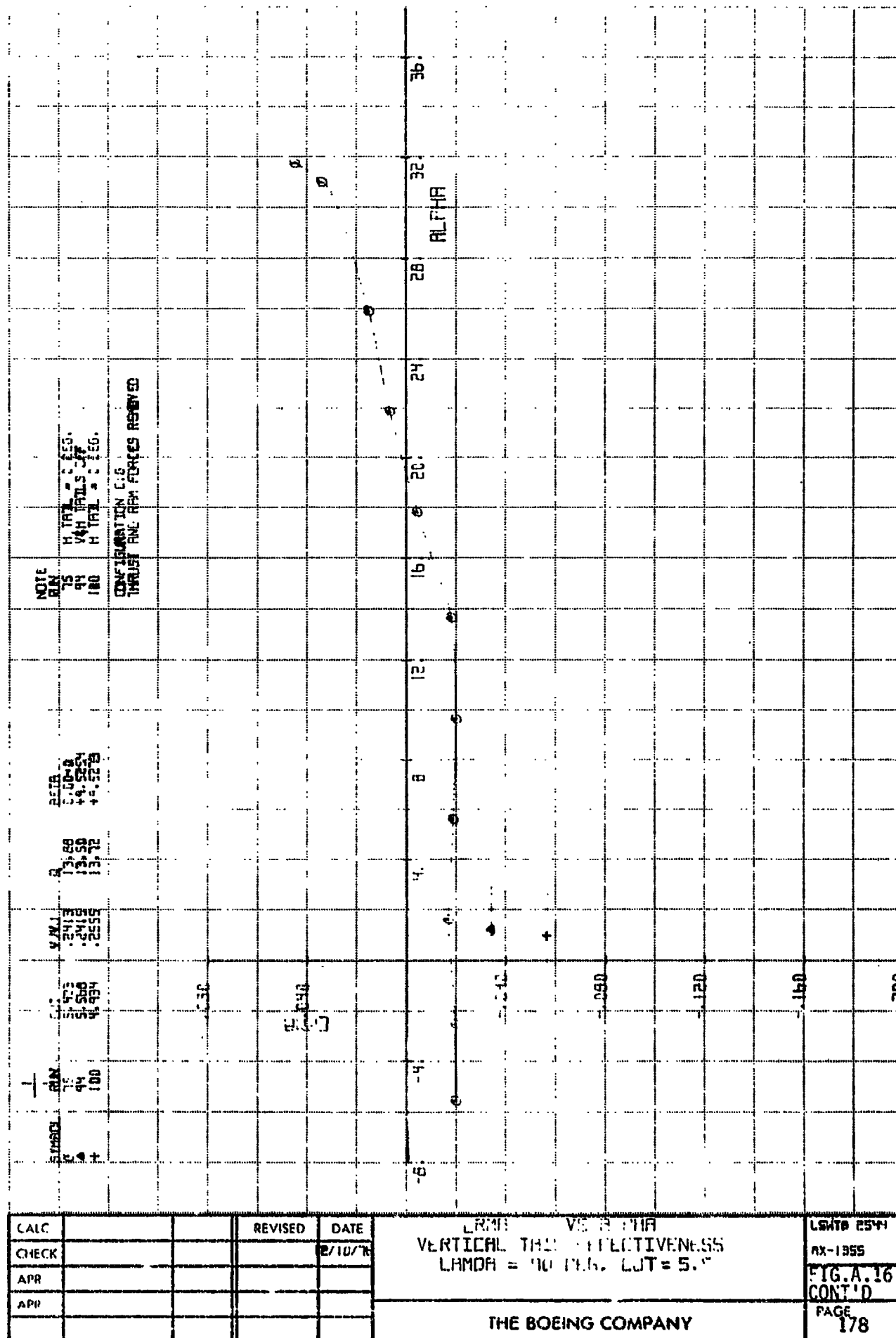


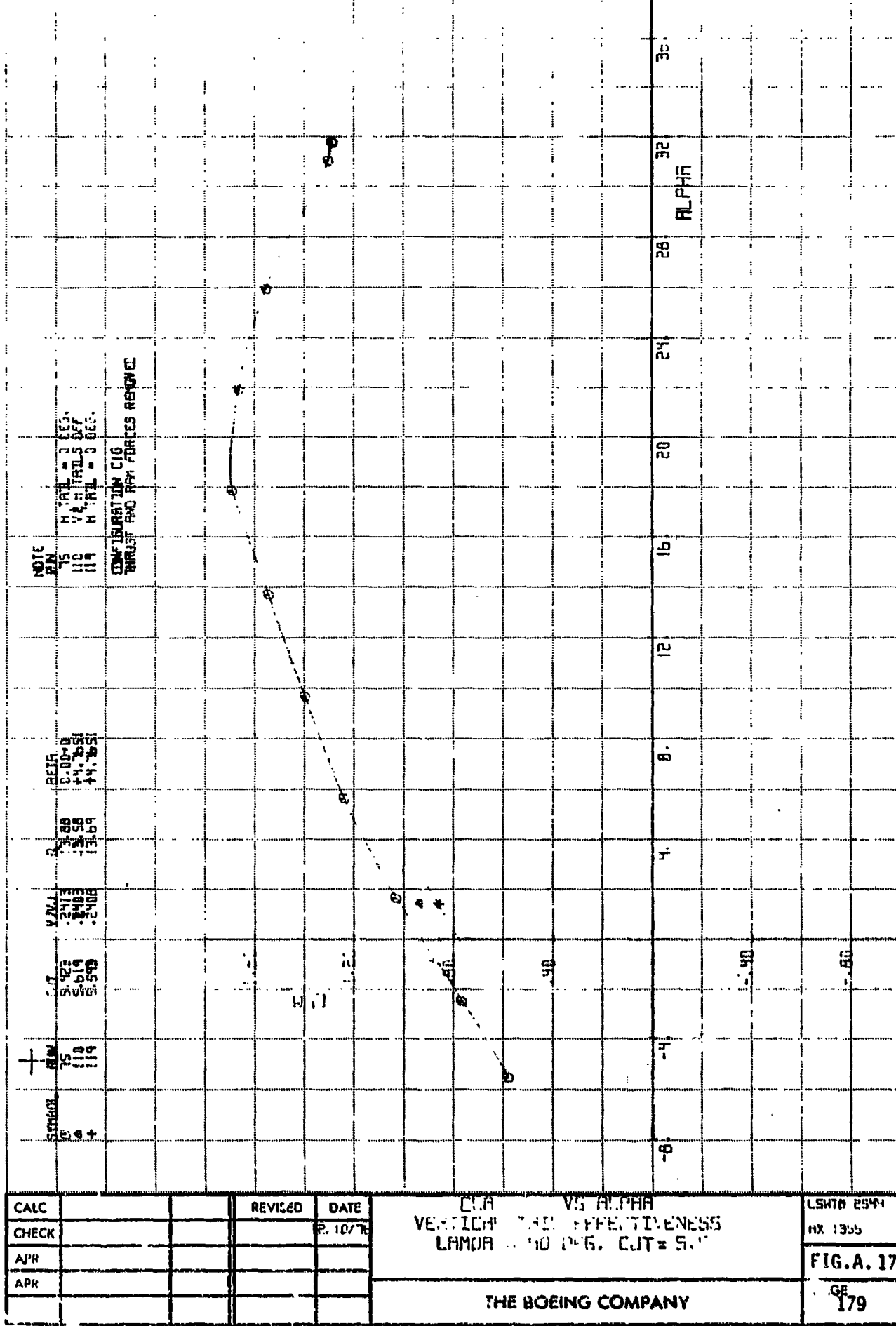


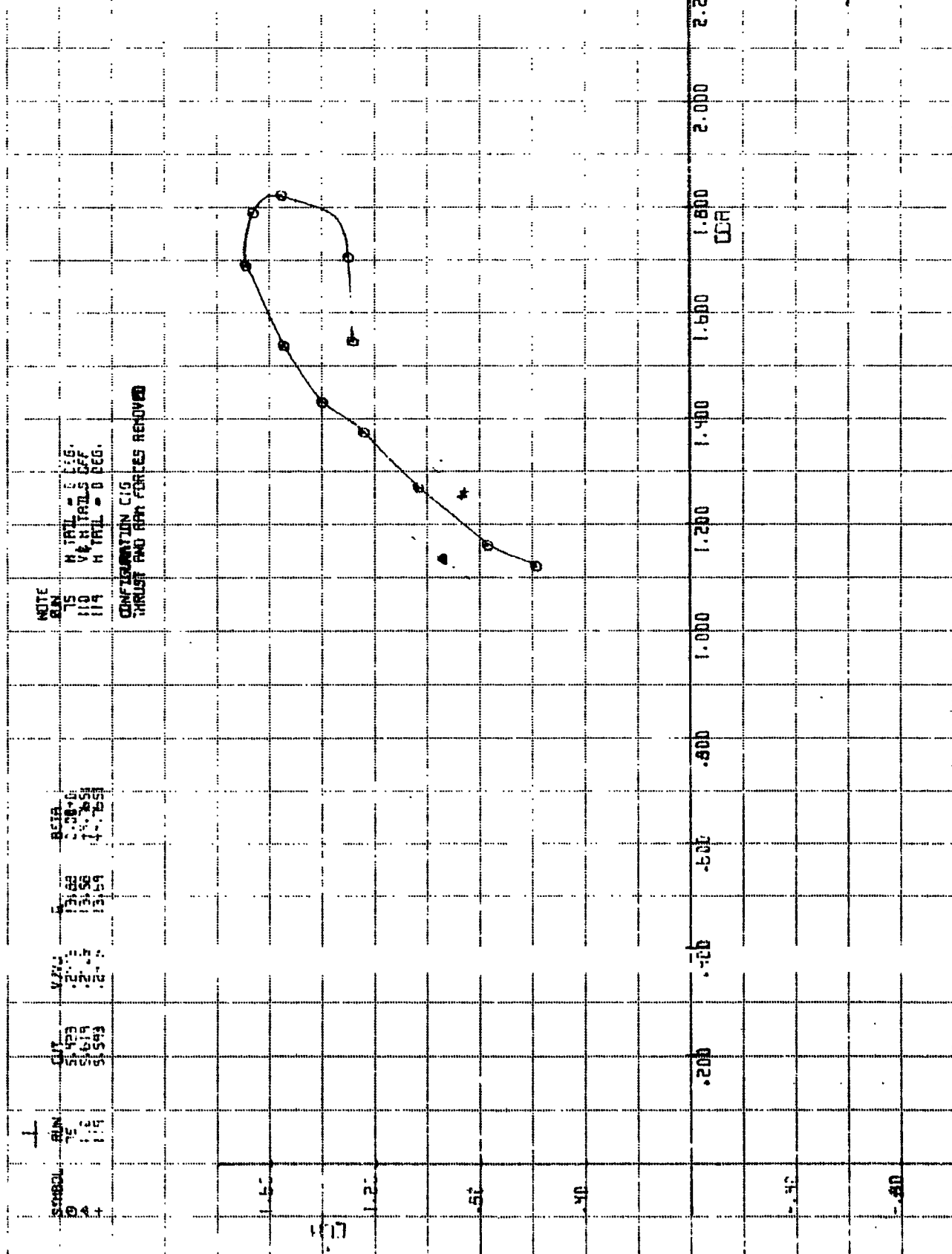


ORIGINAL PAGE IS  
OF POOR QUALITY









CALC			REVISED	DATE
CHECK				2/10/78
APR				
APR				

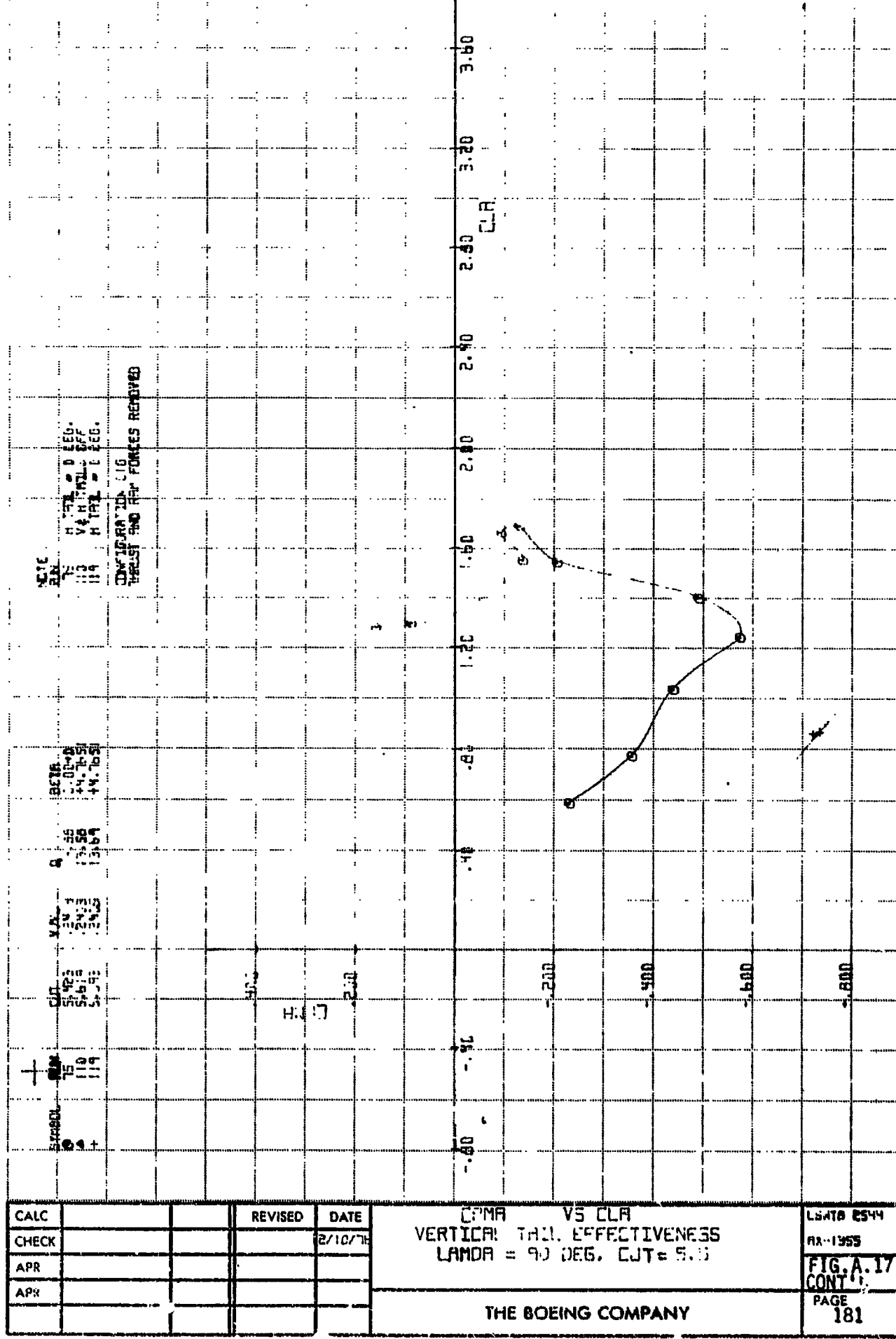
CL A VS CDA  
VERTICAL TILT EFFECTIVENESS  
LHMDDA = 9.1 DEG. CUT = 5.5

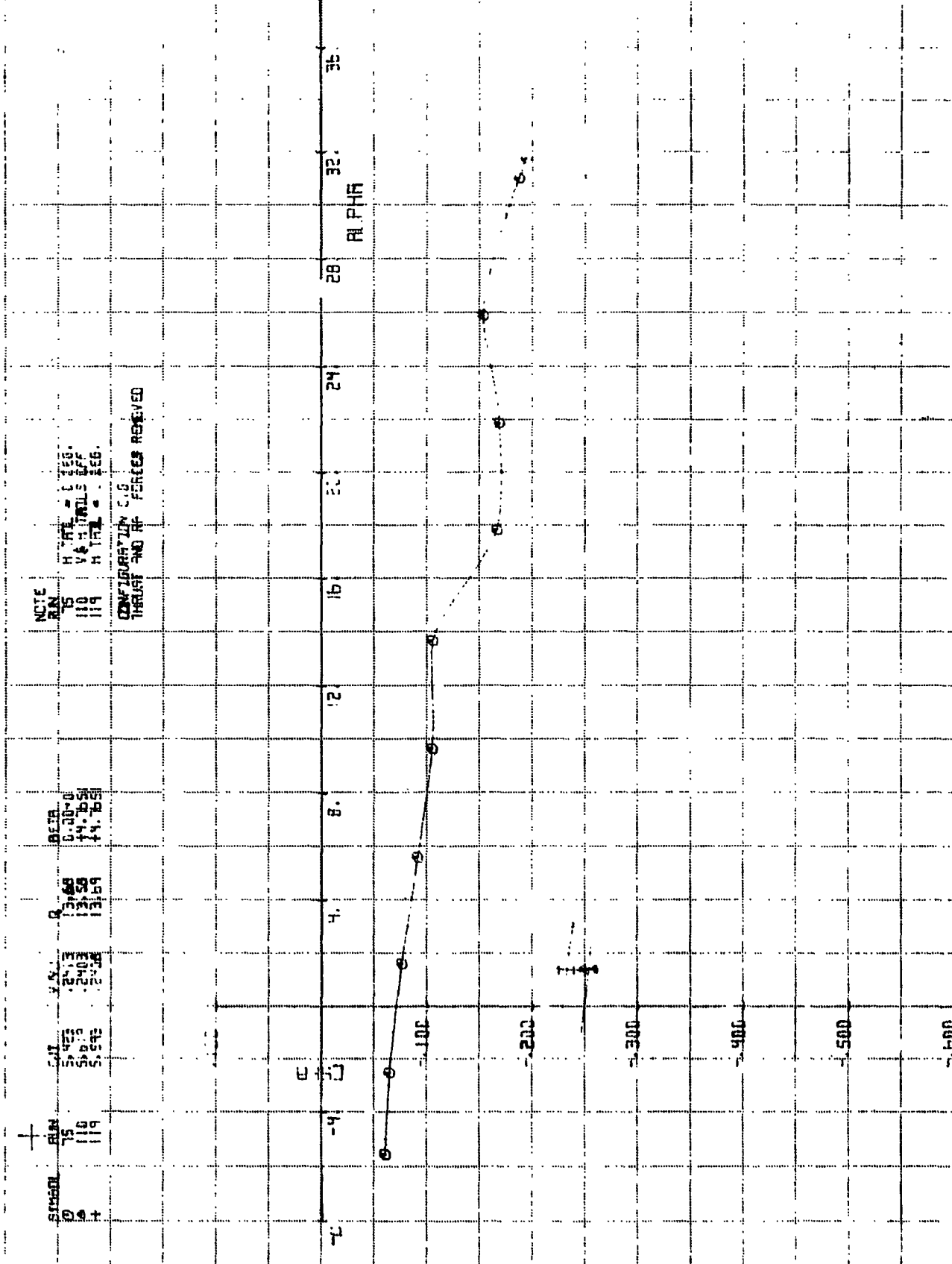
LSHTD ES44

八九-1365

**FIG. A. 17  
CONT'D**

PAGE  
100

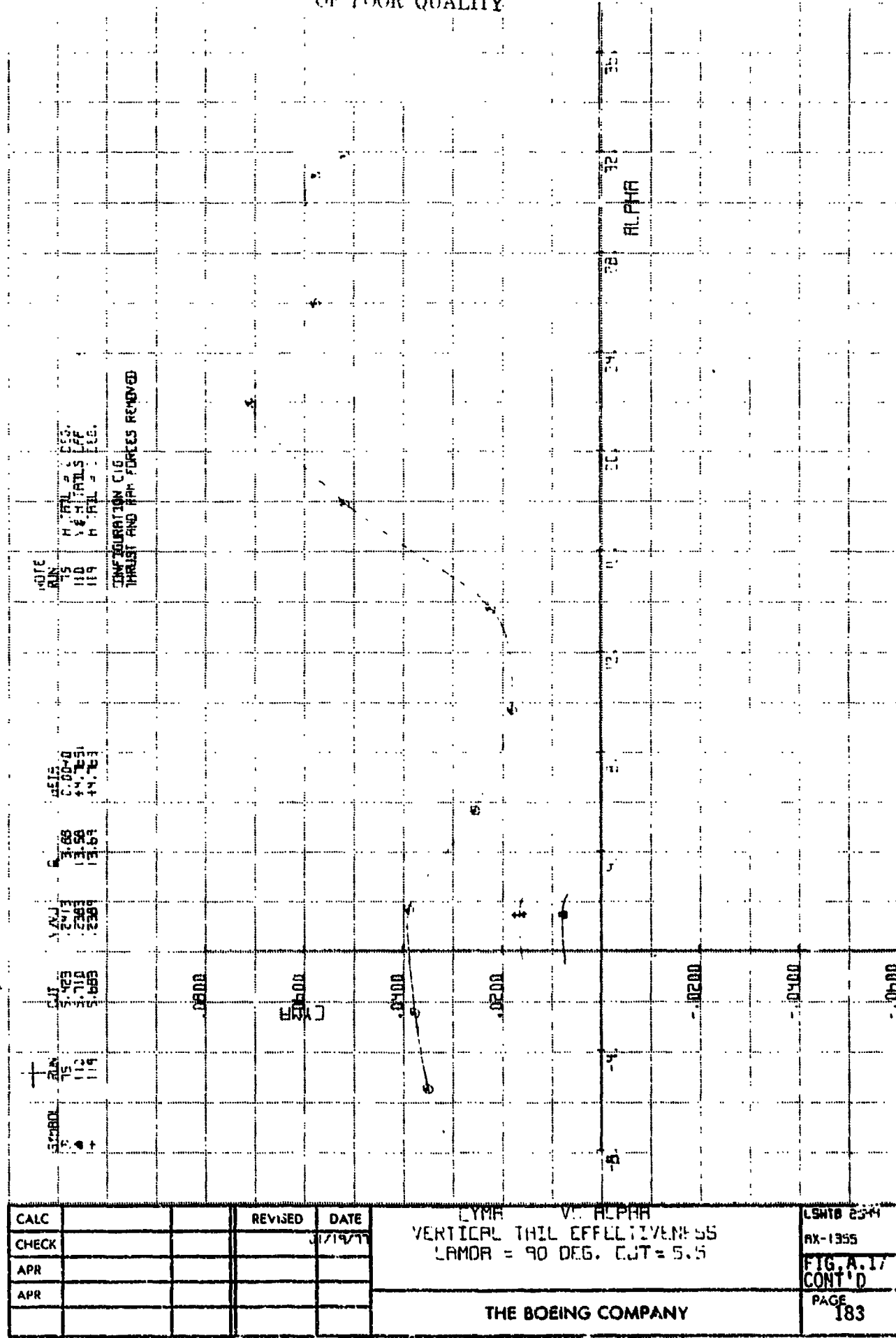




CALC		REVISED	DATE	VTE PHM	LSPH 2544
CHECK			P/10/78	VERTICAL TAIL EFFECTIVENESS	FIG.A.17
APP				LAMDA = 90 DEG. FJT = 5.5	CONT'D
APP					PAGE 182

THE BOEING COMPANY

ORIGINAL PAGE IS  
OF POOR QUALITY



ERMA VS ALPHA  
VERTICAL TAIL. EFFL. TIVENESS  
LHM. A = 90 DEG. CJT = 5.5

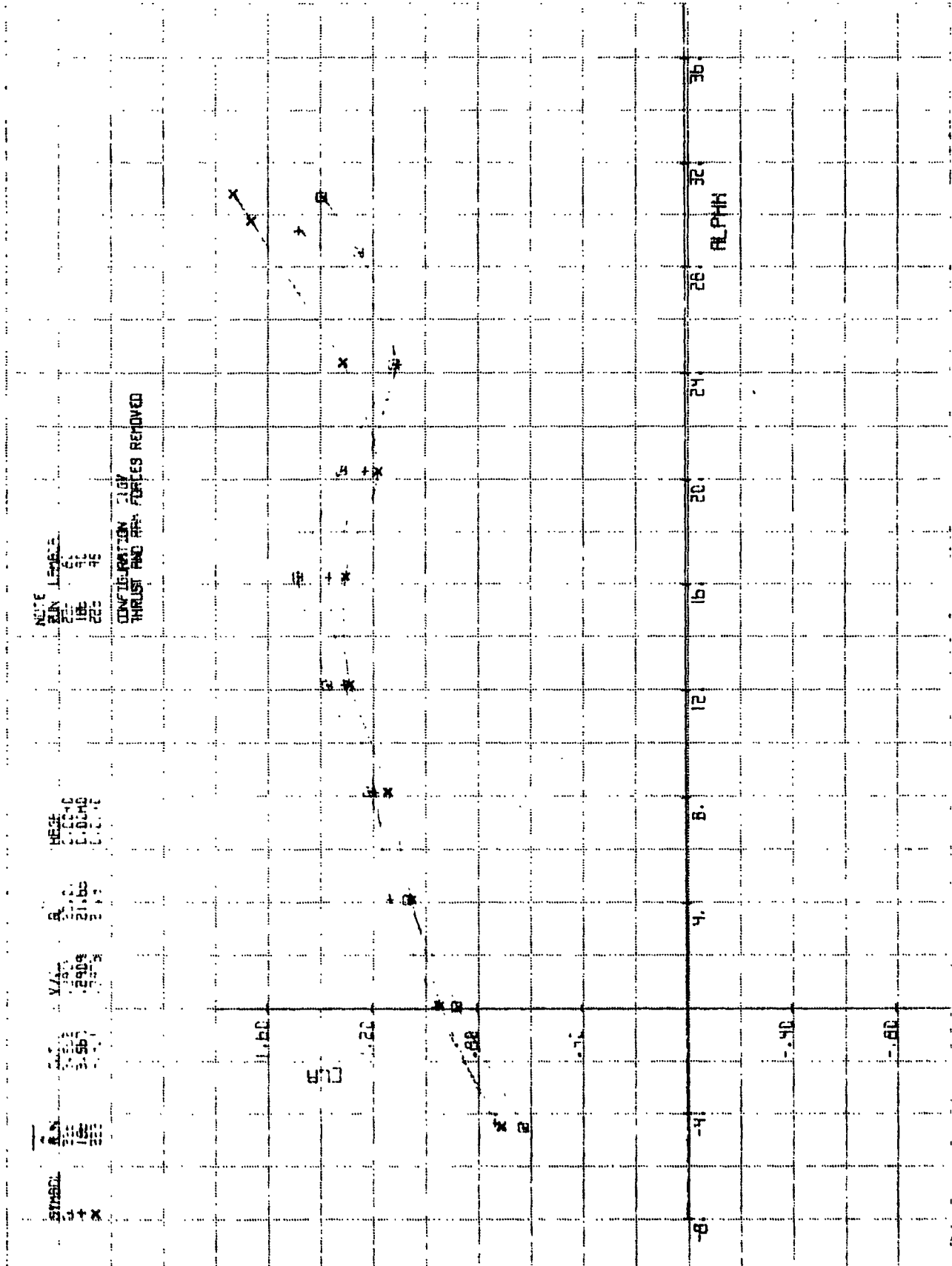
THE BOEING COMPANY

ਪੰਨਾ ੬੫੪

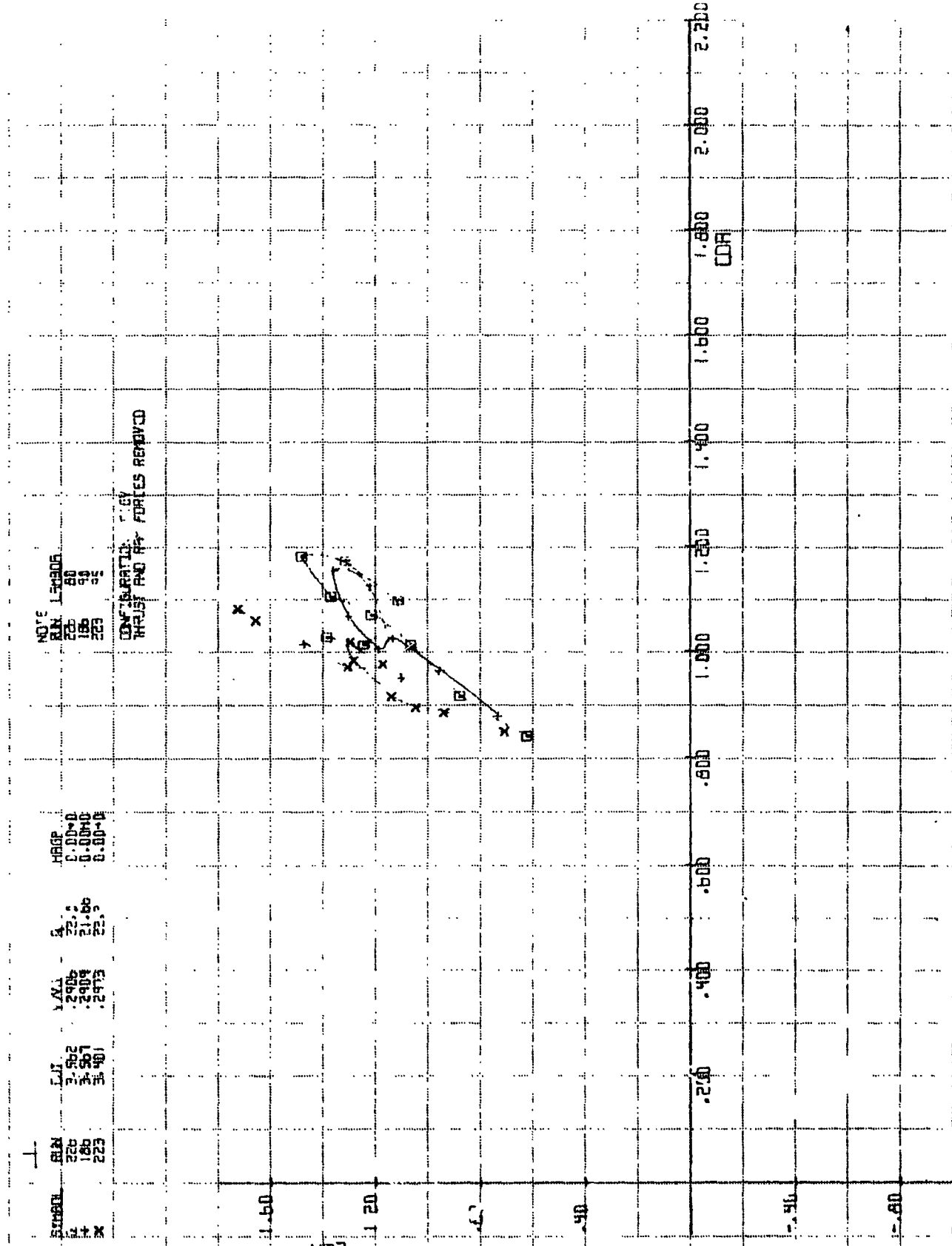
IX-1355

FIG. A.17  
CONT'D

PAGE  
184



CALC			REVISED	DATE	CLR VS ALPHA	LSMTB 2544
CHECK				12/10/76	EFFECT OF ENGINE TILT ANGLE	RX-1355
APR					E.I.T. = 7.7. GROUND PLANE INSTALLED	
APP						
					THE BOEING COMPANY	PAGE 185



CALC		REVISED	DATE
CHECK			2/10/12
APR			
APR			

C H VS CDA  
SIGHT OF ENGINE INT ANGLE  
INT= 9.7. GROUND PLATE INSTALLED

L5HTB 2944

AX-1353

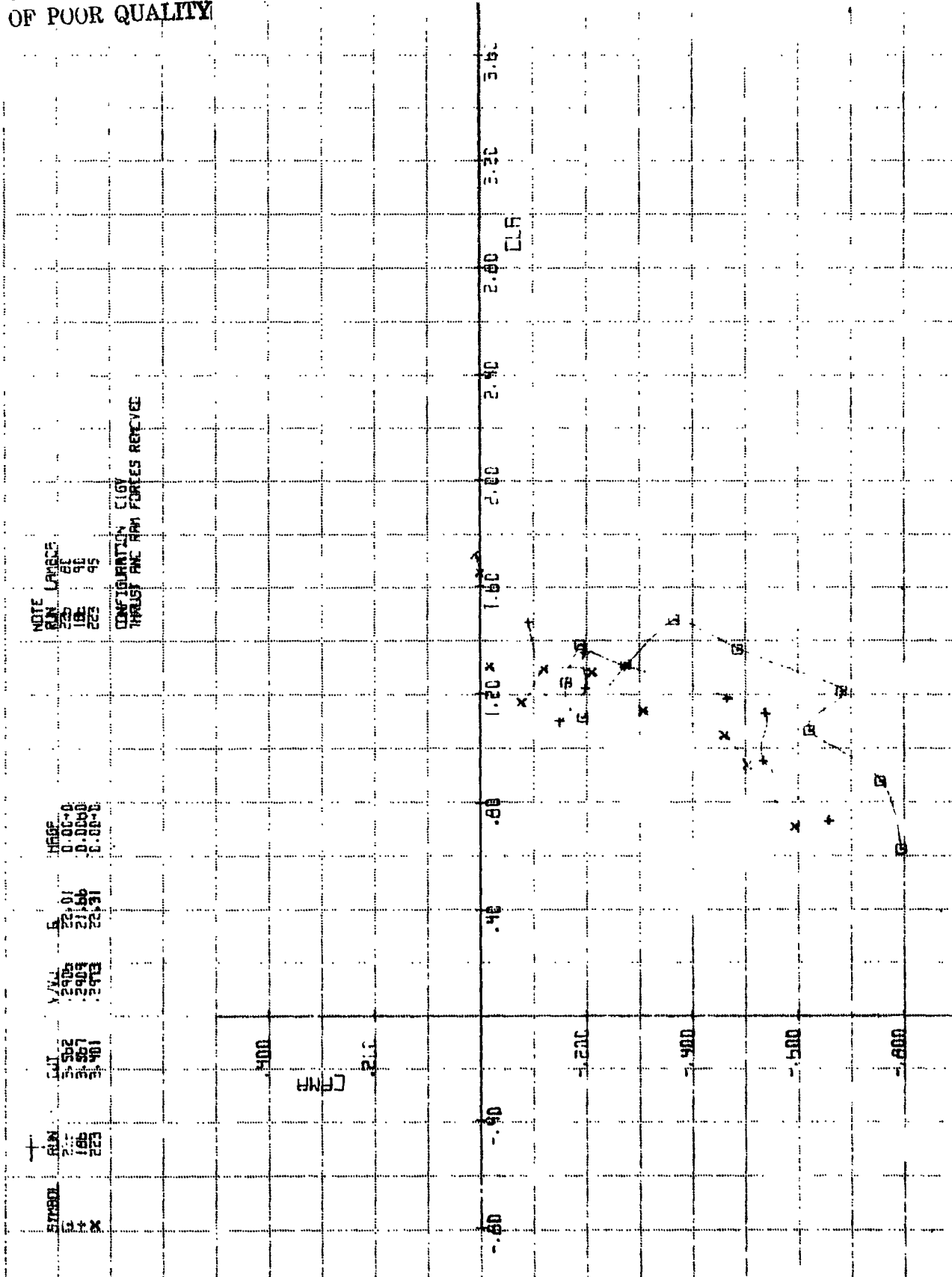
FIG. A. 18  
CONT'D

PAGE

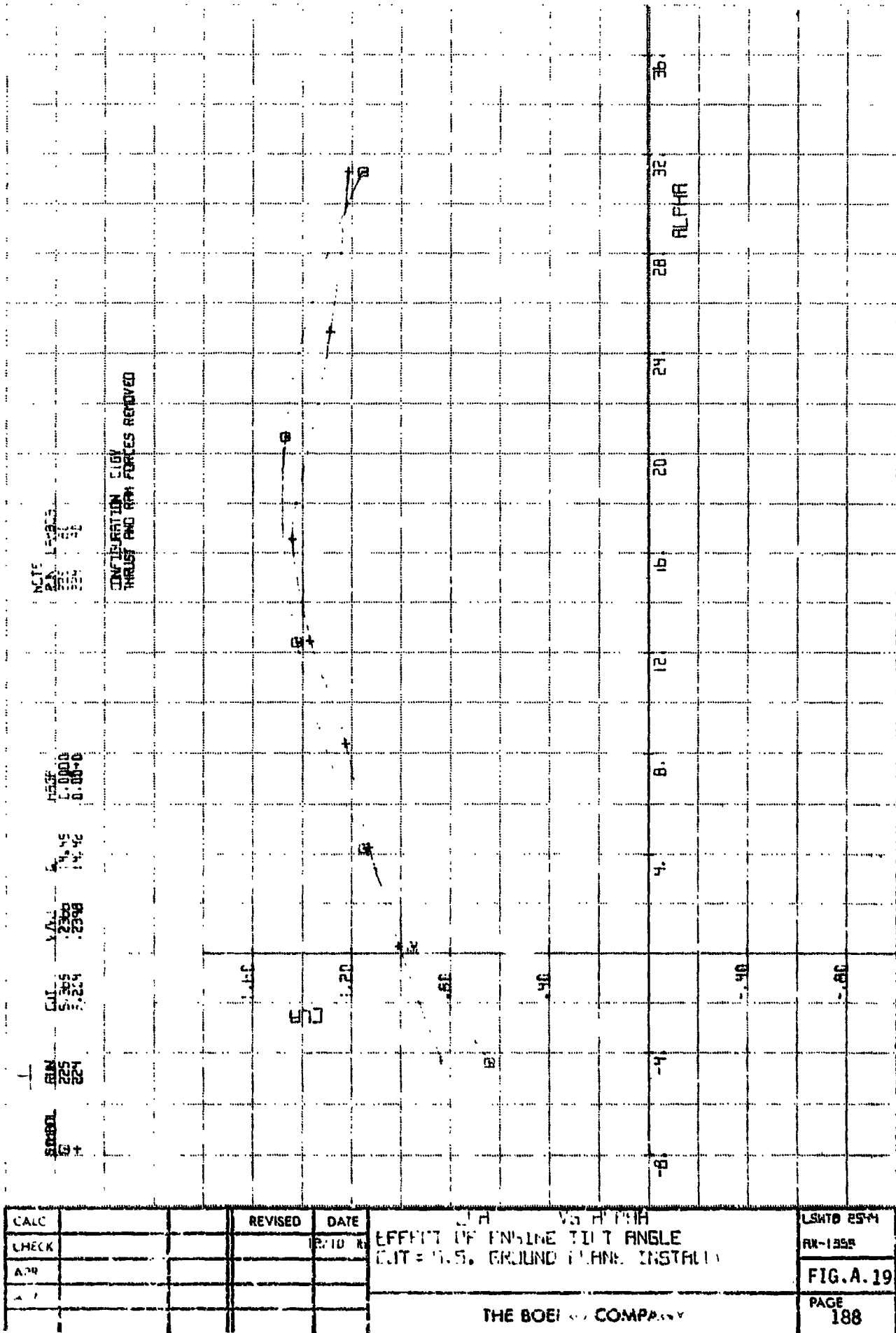
186

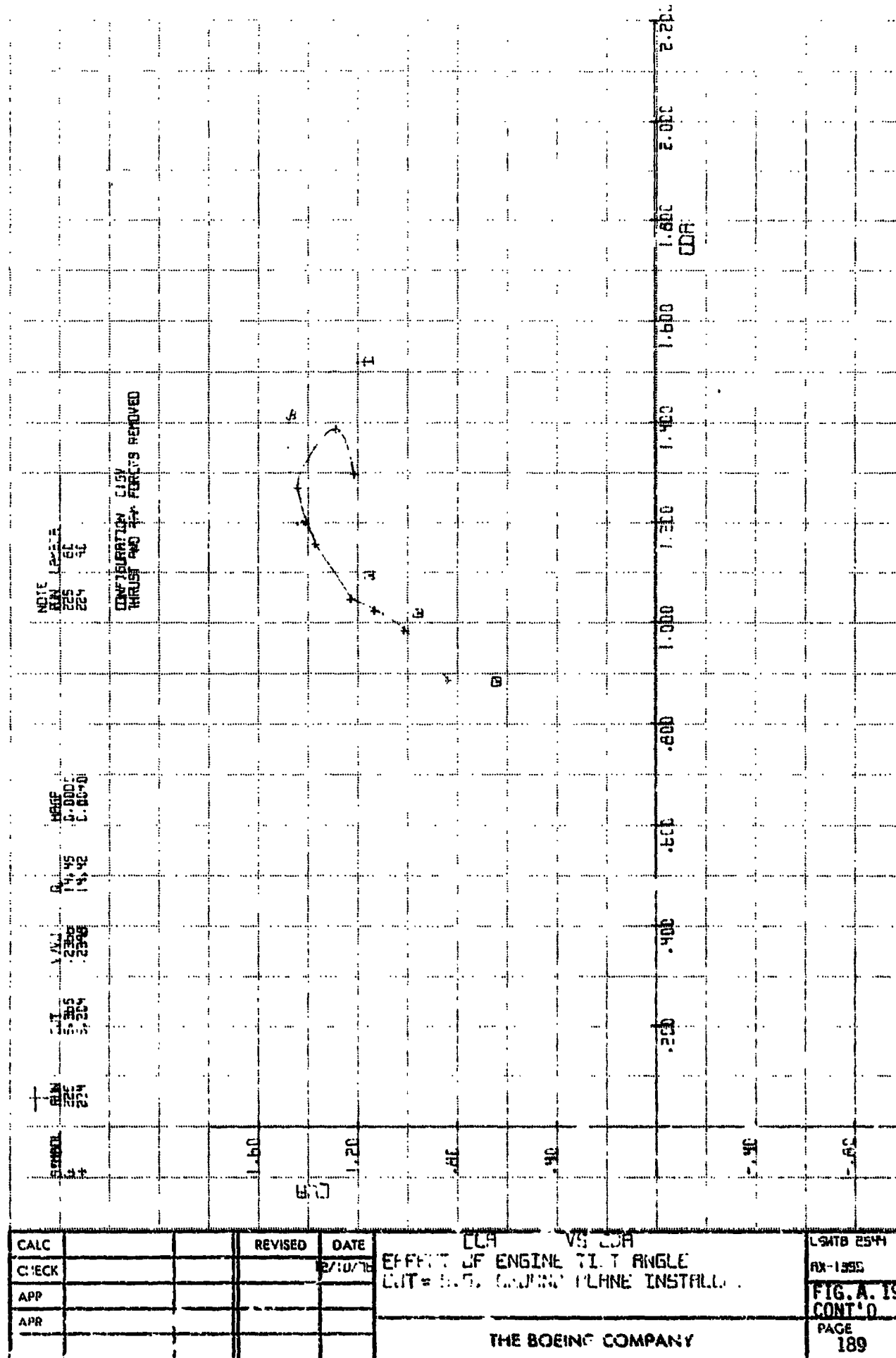
THE BOEING COMPANY

ORIGINAL PAGE IS  
OF POOR QUALITY



CALC	REvised	DATE	EFFECT OF ENGINE TILT ANGLE GUT = 3.1, GROUND PLANE INSTALLED	LSNTO 2544 RX-1355 FIG. A.18 CONT'D PAGE 187
CHECK		12-11-76		
APR				
AIR				
			THE BOEING COMPANY	





11.

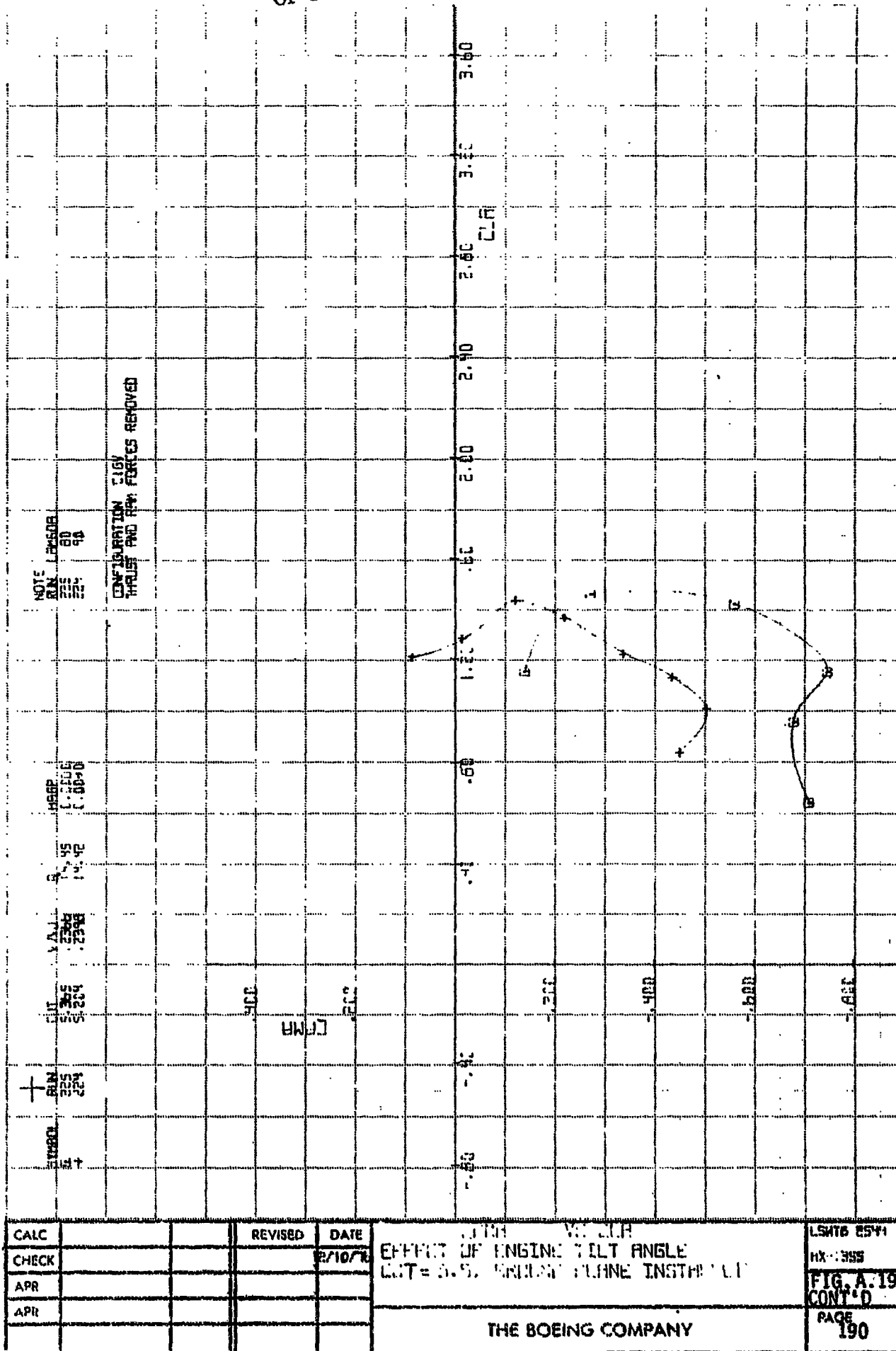
CALC			REVISED	DATE
CHECK				7/10/11
APP				
APR				

ELA VS CSA  
EFFECT OF ENGINE TILT ANGLE  
LUT = 5.5. (WING PLANE INSTALLED)

THE BOEING COMPANY

94TB 2544  
X-1955  
FIG. A. 19  
CONT'D.  
PAGE  
189

ORIGINAL PAGE IS  
OF POOR QUALITY



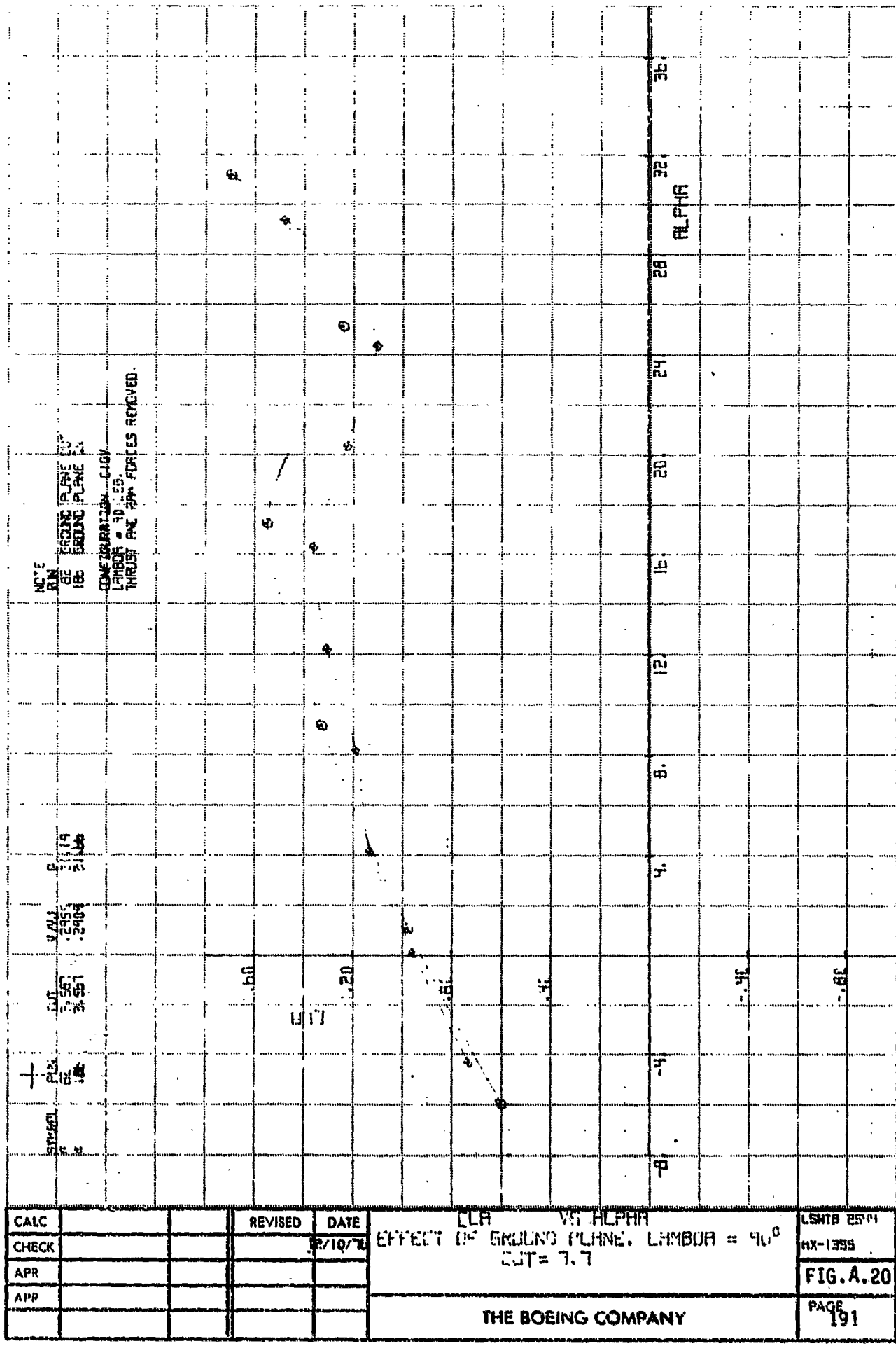


FIG. 11  
21.

LLA = 90 ALPHABET  
EFFECT OF GRADING PLAN. LHMBOA = 90  
CUT = 7.7

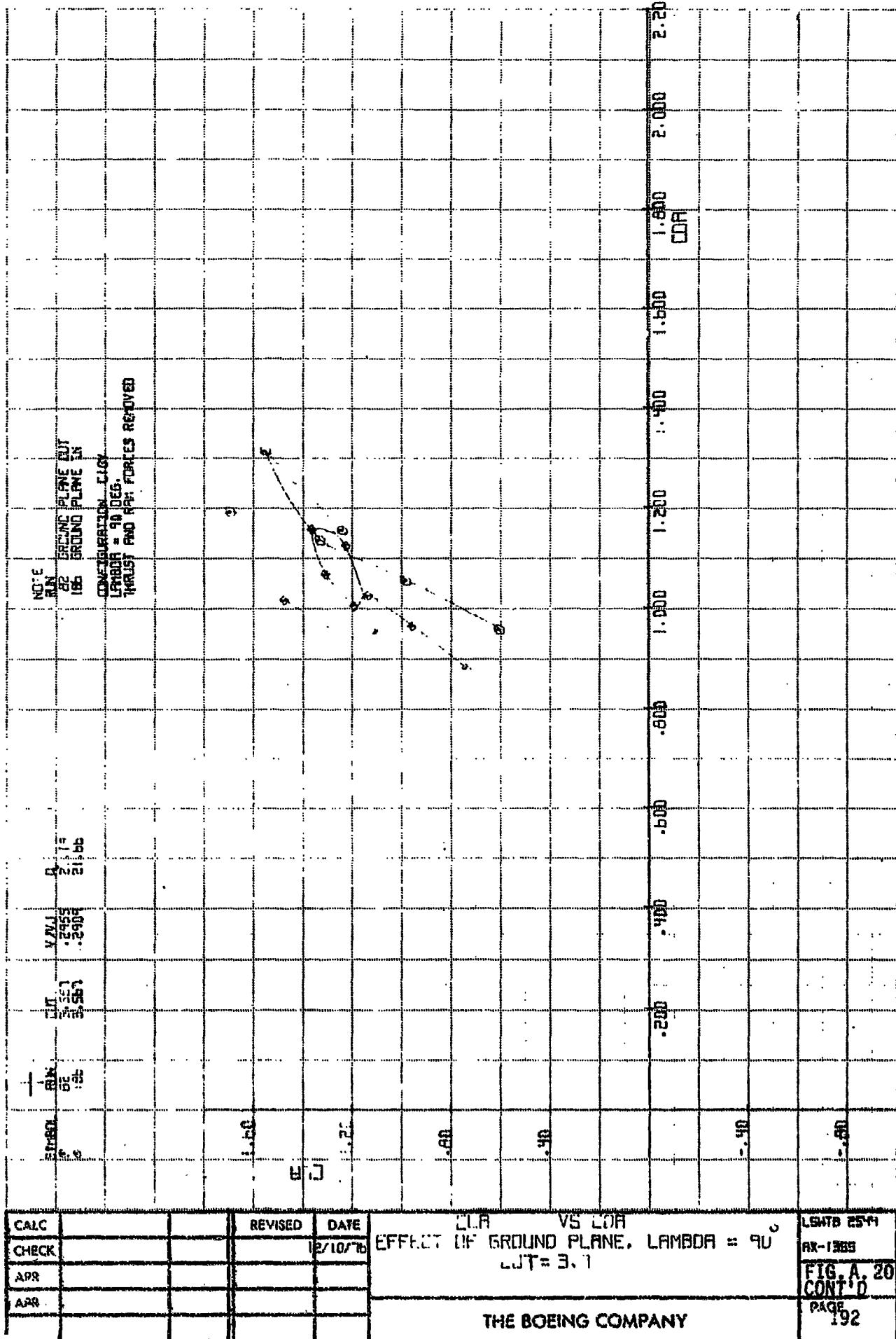
LSHTB 254

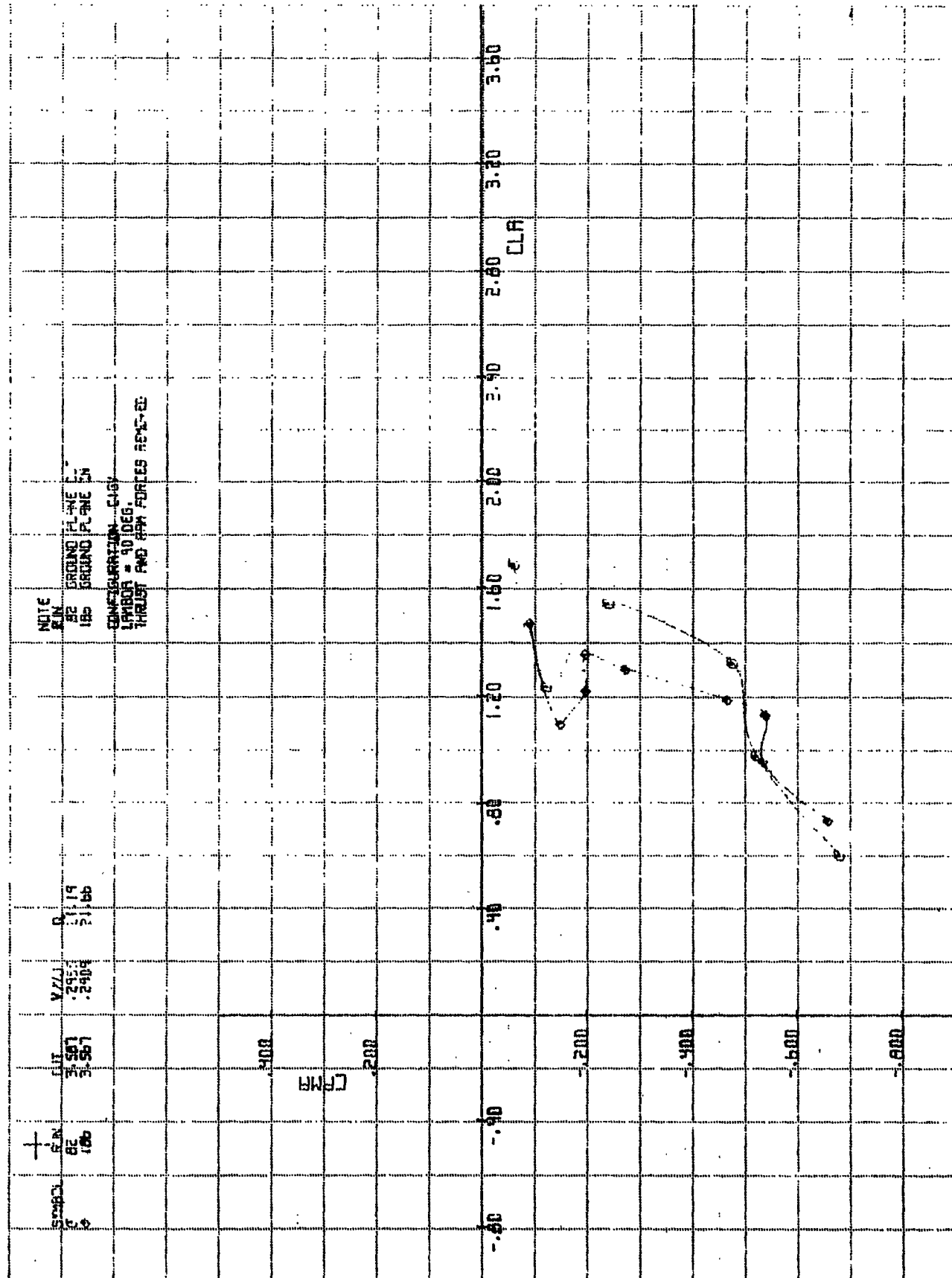
EX-1339

**FIG.A.20**

THE BOEING COMPANY

PAGE  
191



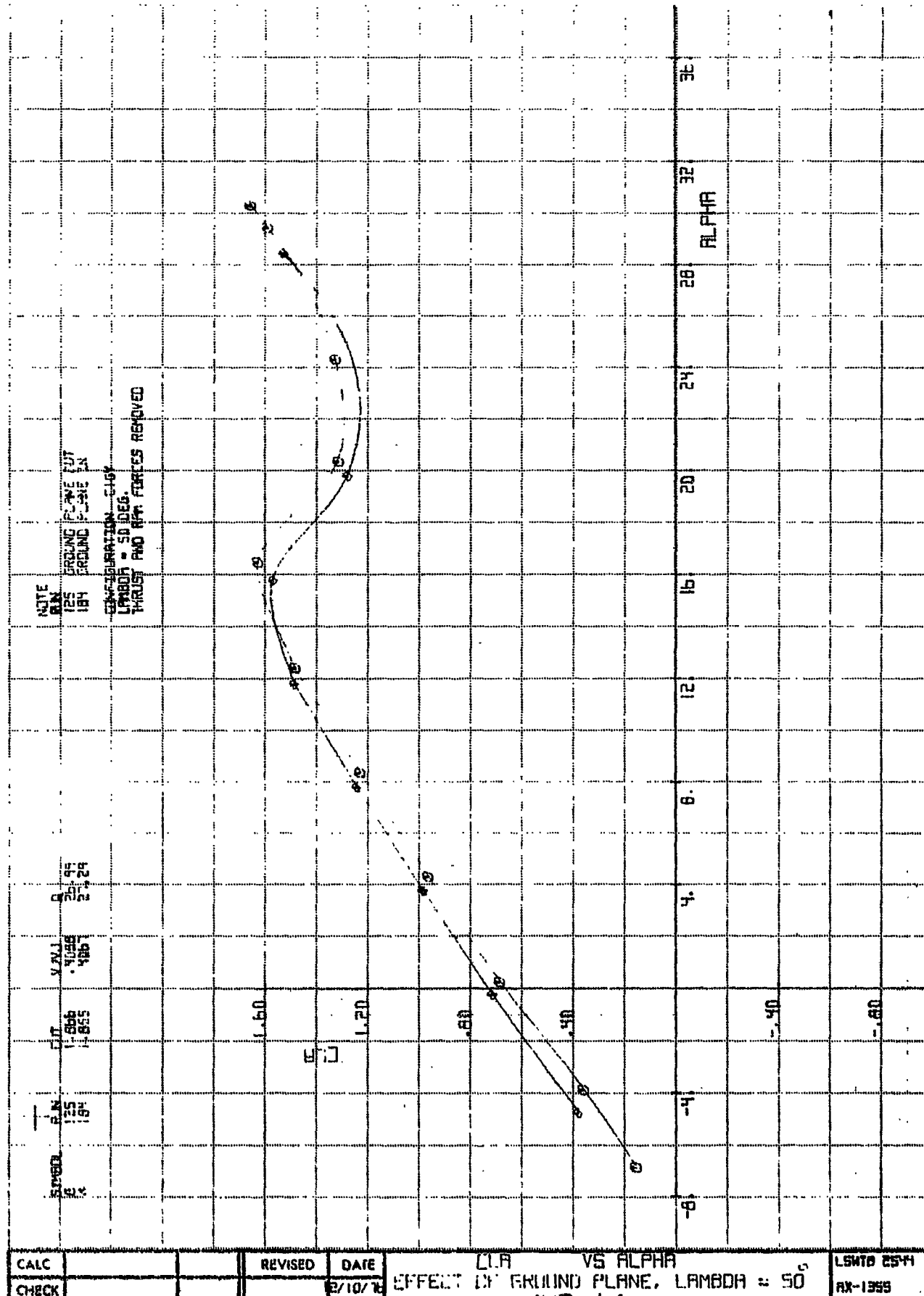


CALC			REVISED	DATE
CHECK				10/10/11
APR				
APP				

CPMA VS CLA  
EFFECT OF GROUND PLANE. LAMBDA = 40'  
CJT = 3.7

THE BOEING COMPANY

L5H-3 E544  
HX-1355  
FIG. A.20  
CONT'D.  
PAGE  
193



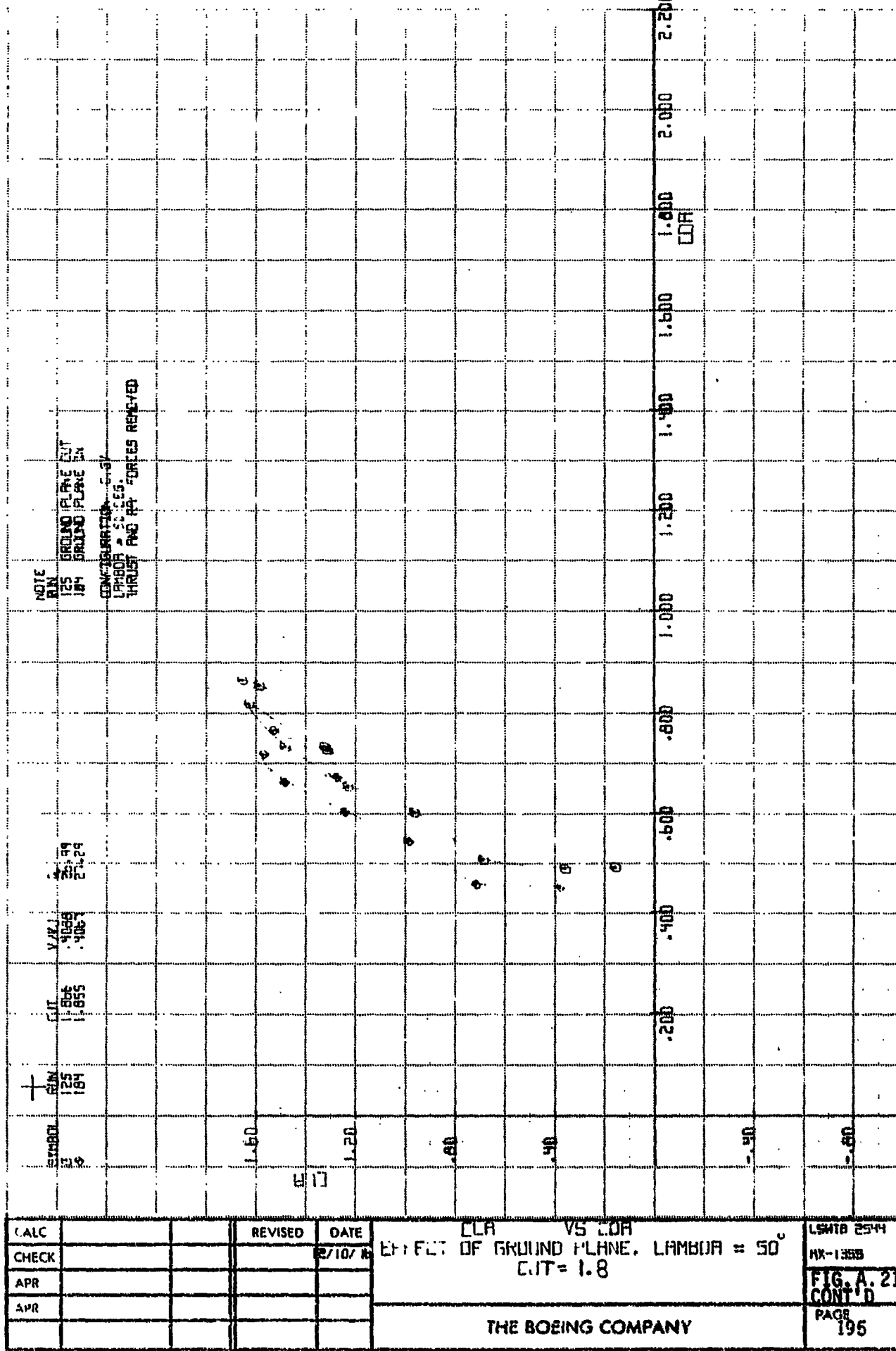
CALC			REVISED	DATE
CHECK				3/10/16
APR				
APP				

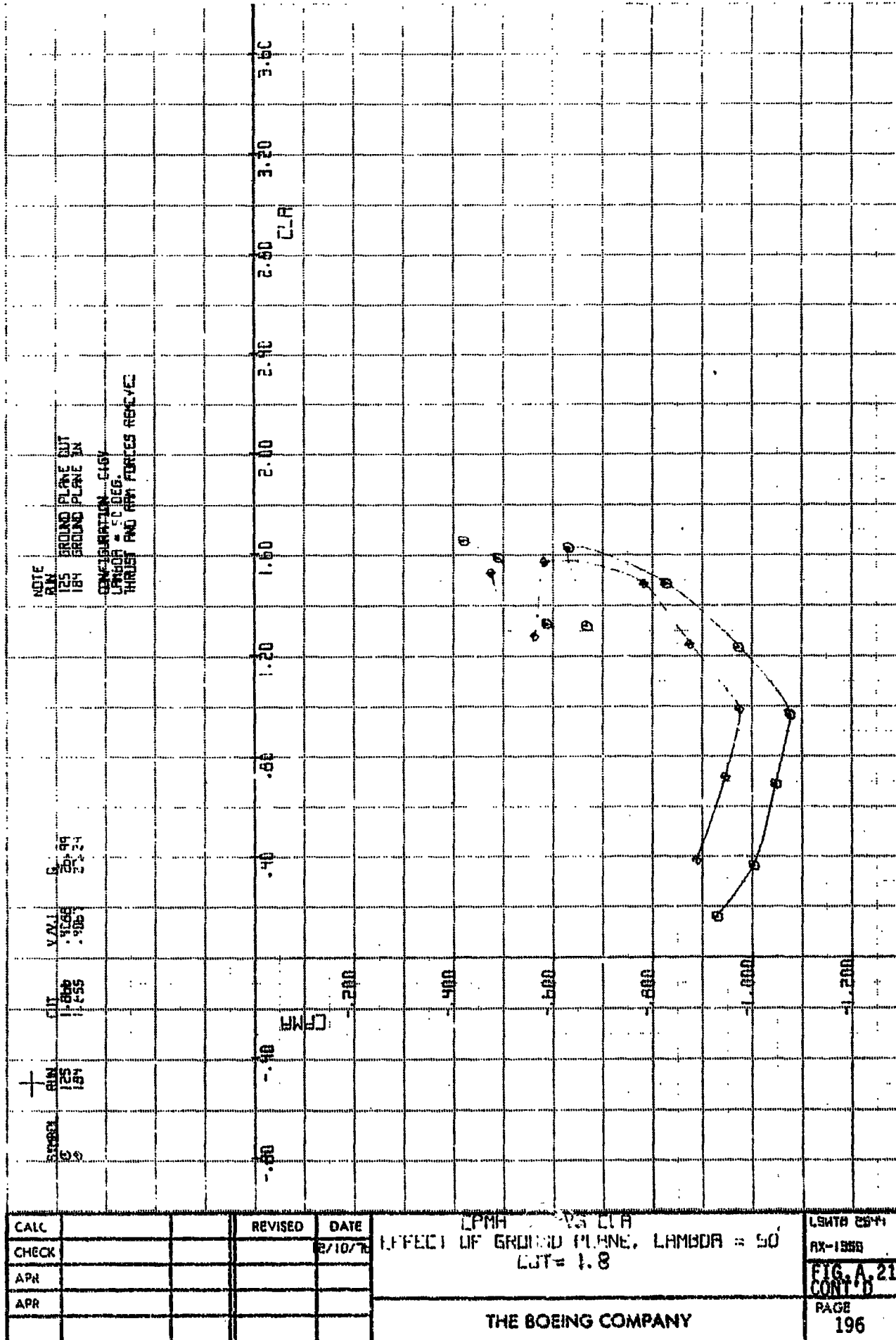
CIA VS ALPHA  
EFFECT OF GROUND PLANE, LAMBDA = 50  
CJT = 1.8

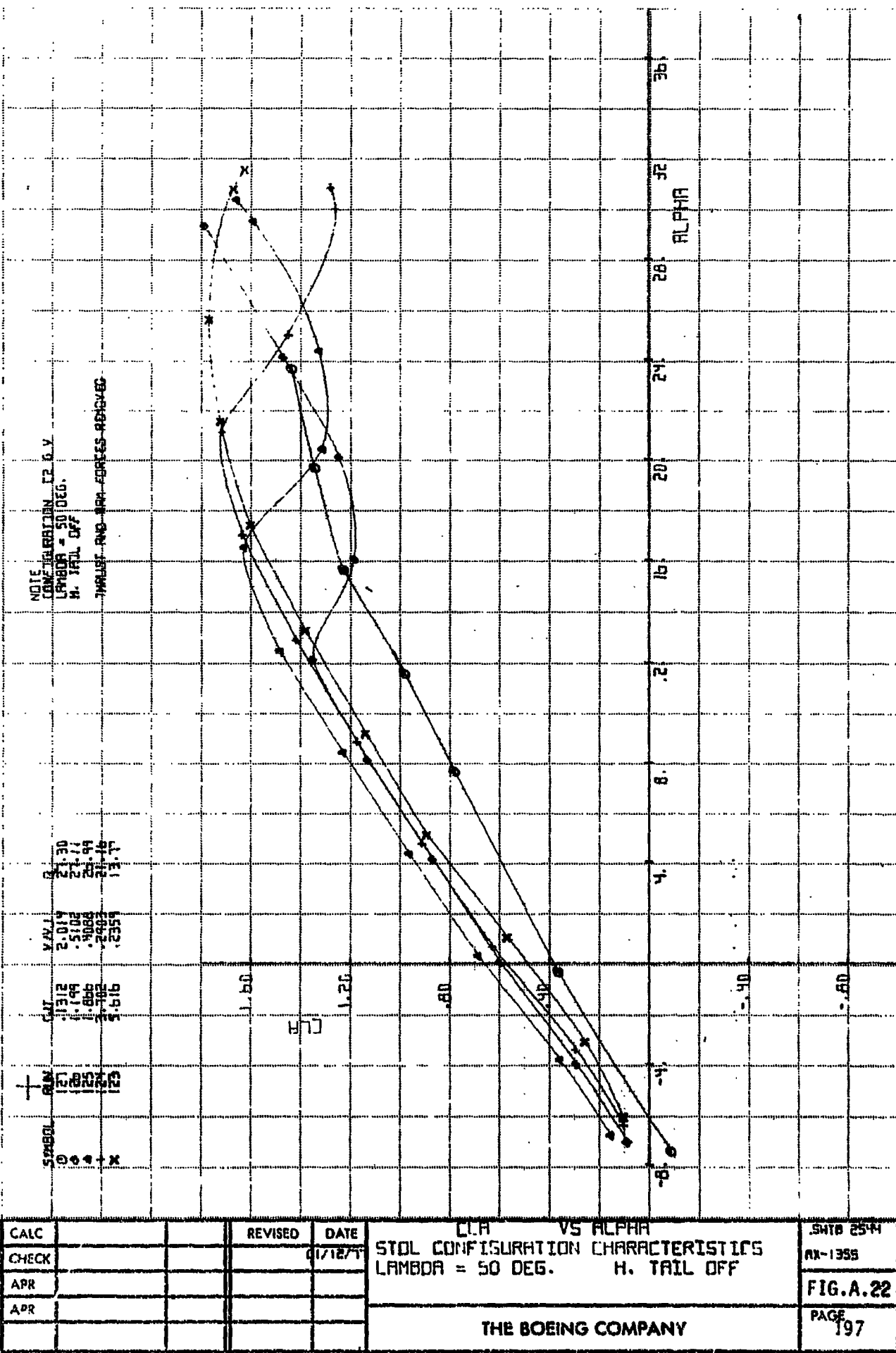
18 MARCH 1954

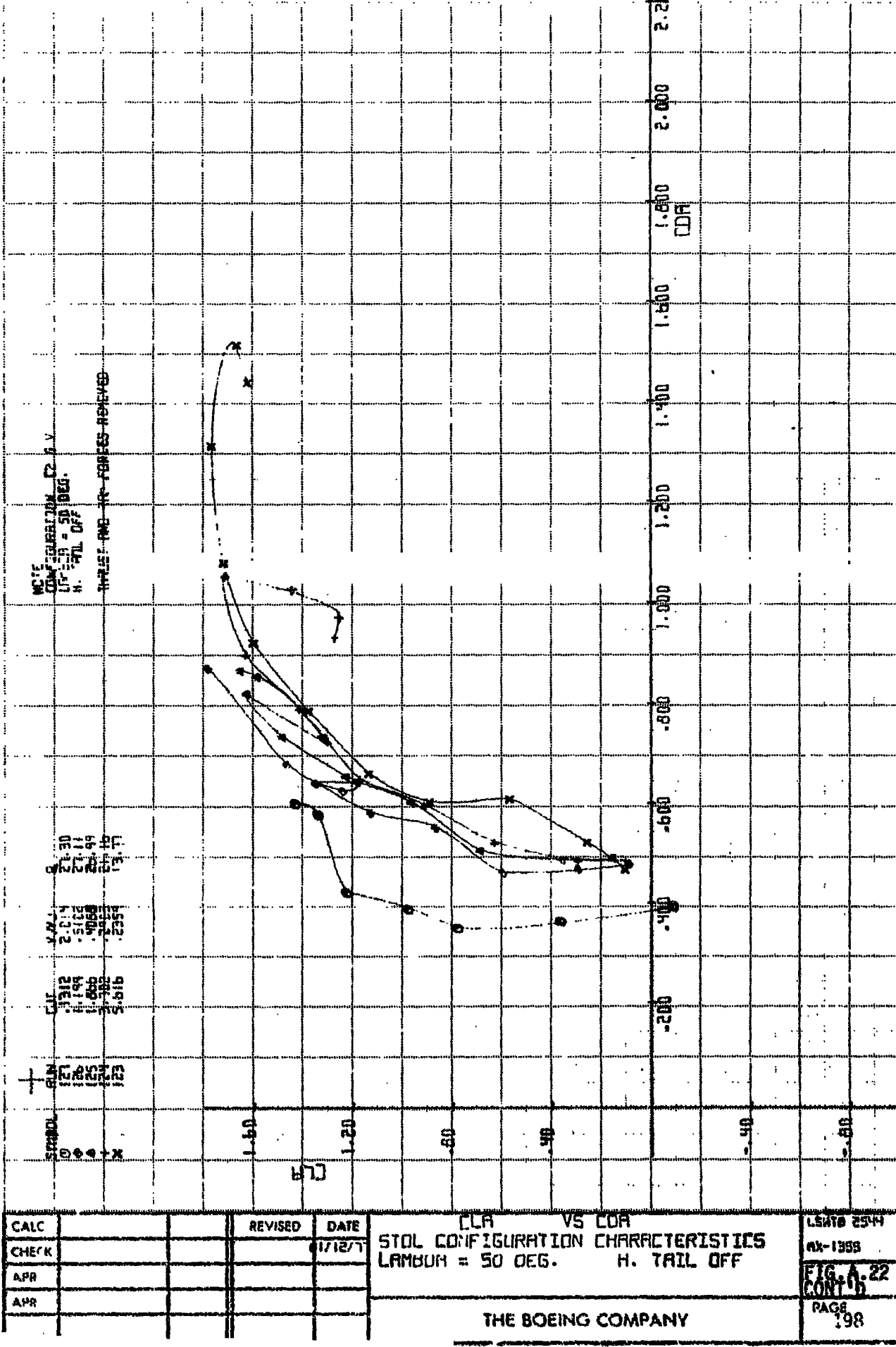
五~1559

FIG. A.21

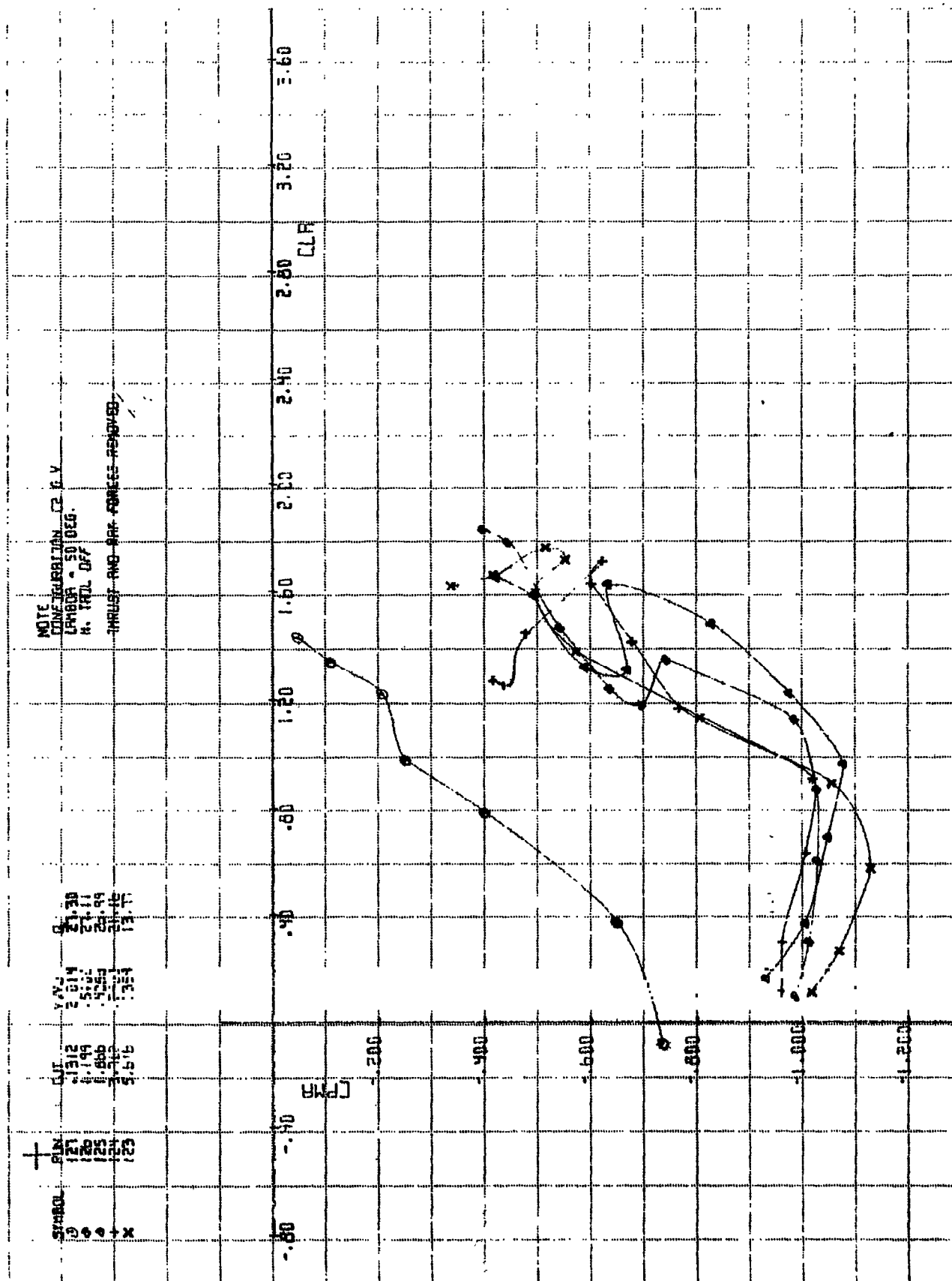




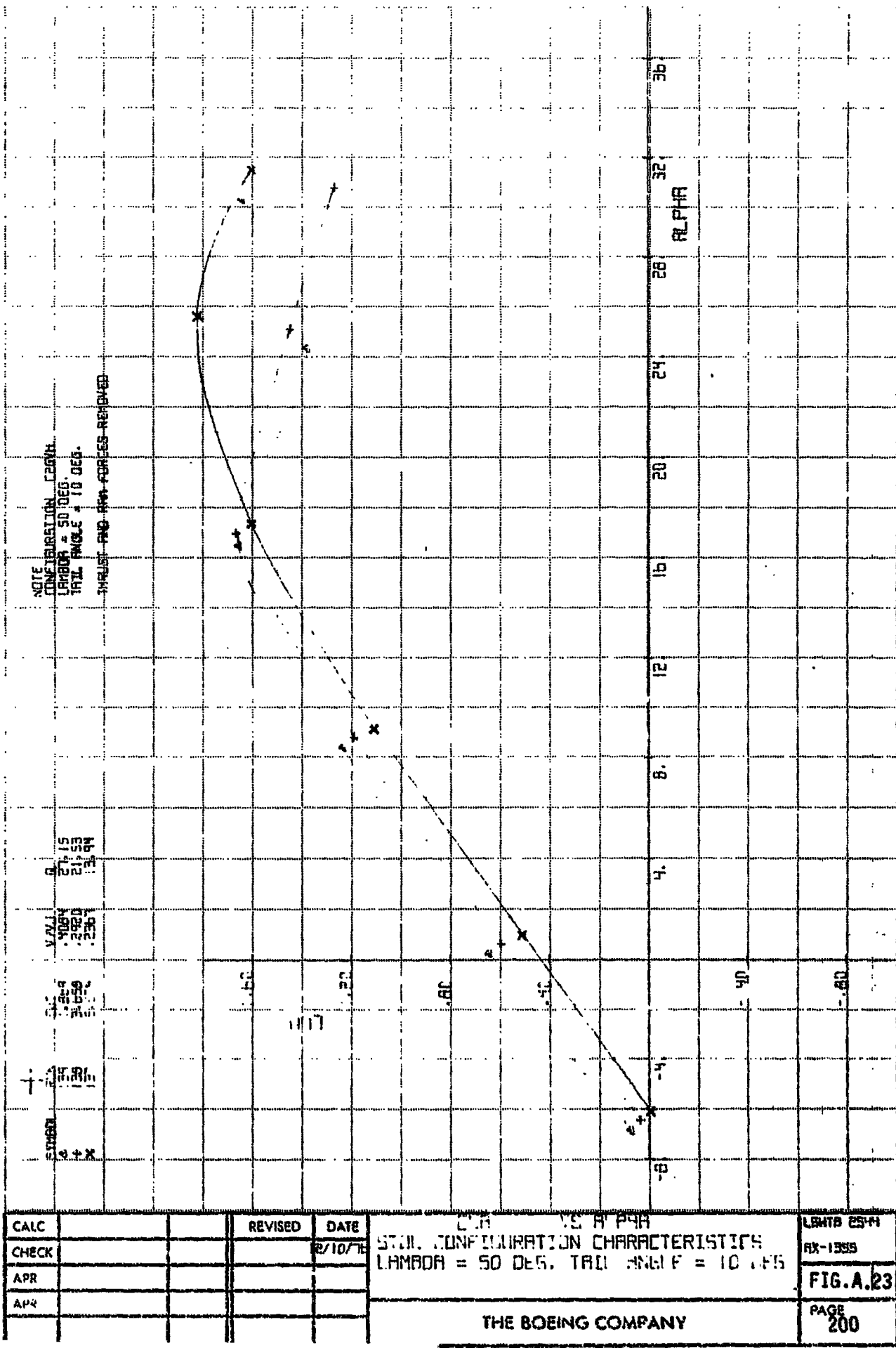




ORIGINAL PAGE IS  
DE POOR QUALITY



CALC		REVISED	DATE	L9HTB 25TH CPMA VS CLA STOL CONFIGURATION CHARACTERISTICS LAMBDA = 50 DEG. H. TRAIL OFF FIG. A-22 CONT'D	07/27/71	AR-1355	PAGE 199
CHECK							
APR							
APR							
				THE BOEING COMPANY			



NOTE  
TIME TABULATION  
PROBES = 1000  
TET. ANGLE = 0  
TABLES AND SPEC. = 1000

L.A.C.		REVISED	DATE	L.I.M. V.V. LDA STILL LOW FLOW RATE IN THE HETEROGENEITY HAMBURG = 50 DEG., THIS ANGLE = 10 DEG.	LSHTB 2544 HR 1358 FIG. A.23 CONT'D
CHECK			2/10/76		
APR					
Q.R.					
THE BOEING COMPANY					PAGE 201

CALL		REVISED	DATE	TYPE	VS CLR	LIGHTED DRAWING
1000			5/10/74	1000	1000	HR-1945
APR				1000	1000	FIG. A.23
APR				1000	1000	CONT'D

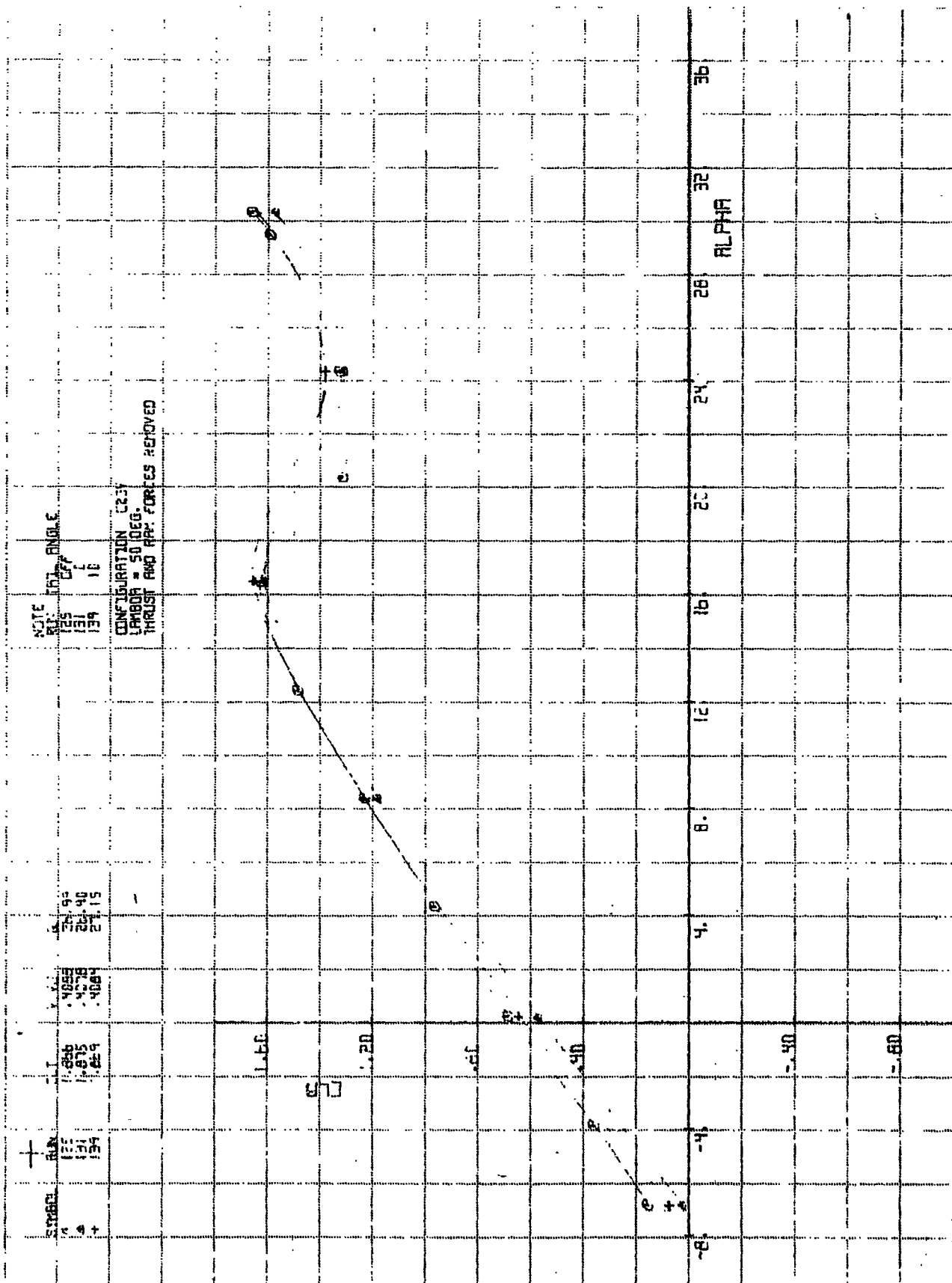
THE BOEING COMPANY

PAGE  
202

NAME: SPENCER, ED. 2204  
PAGES: 11, LEP.  
PAGE: 11, LEP.

PRINTED AND RECORDED: 5/10/74

ORIGINAL PAGE IS  
OF POOR QUALITY



CALC		REVISED	DATE	C'A VS ALPHA EFFECT OF HORIZONTAL TAIL LIFT = 50 DEG, CDT = 1.8	L5H1B 1574 RX-1955
CHECK			2/10/74		
APR					FIG. A.24
APR					PAGE 203
				THE BOEING COMPANY	

LIP VS LDR  
EFFECT OF HORIZONTAL TAIL  
LAMBDA = 50 DEG., C/D = 1.8

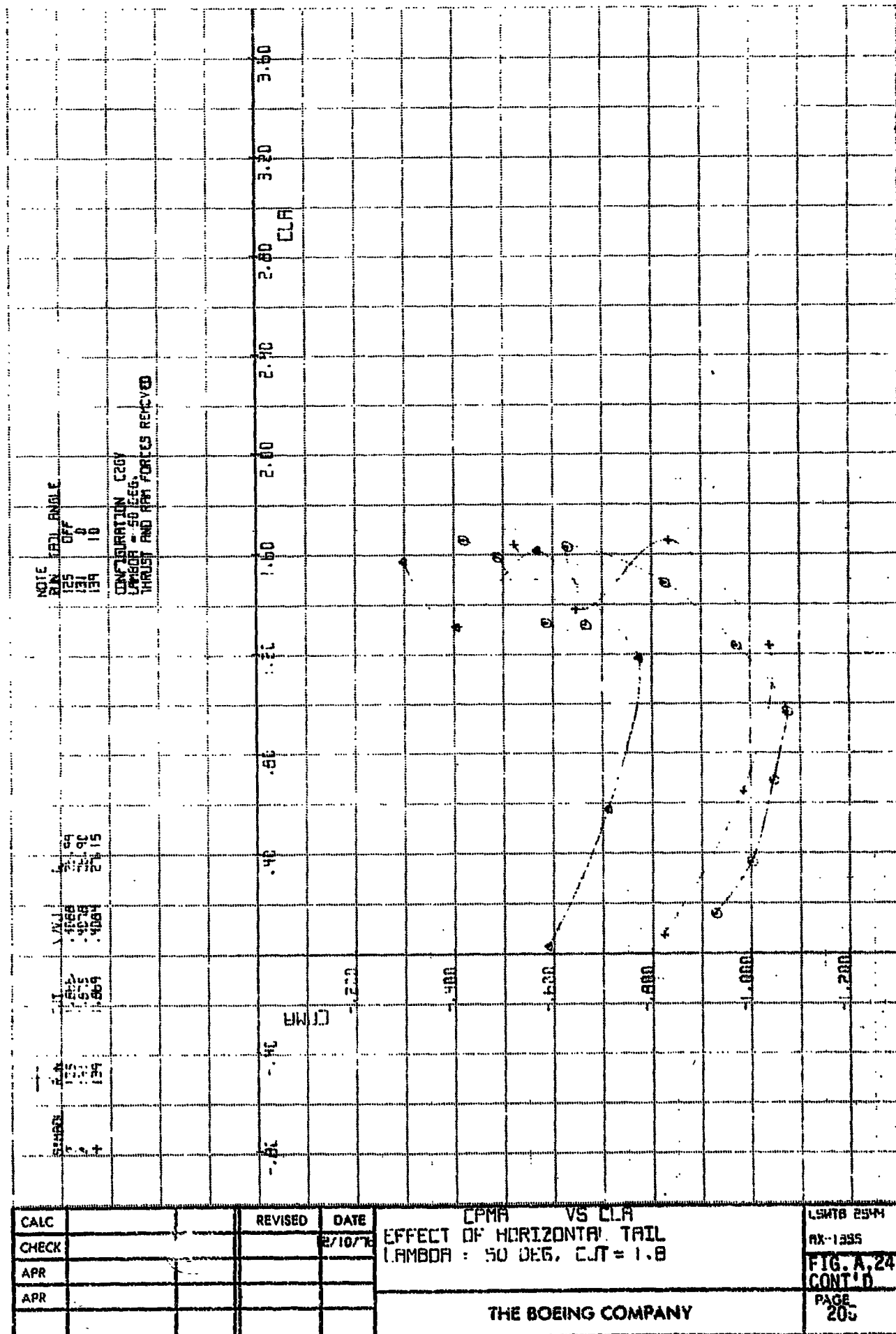
**THE BOEING COMPANY**

LSHTB 254H

RX-1355

**FIG. A-24  
CONT'D.**

PAGE  
204



F15 14  
114.

CALC		REVISED	DATE
CHECK			2/10/7
APR			
APR			

CPMA VS CLR  
EFFECT OF HORIZONTAL TAIL  
LAMBDA : 50 DEG, CJT = 1.8

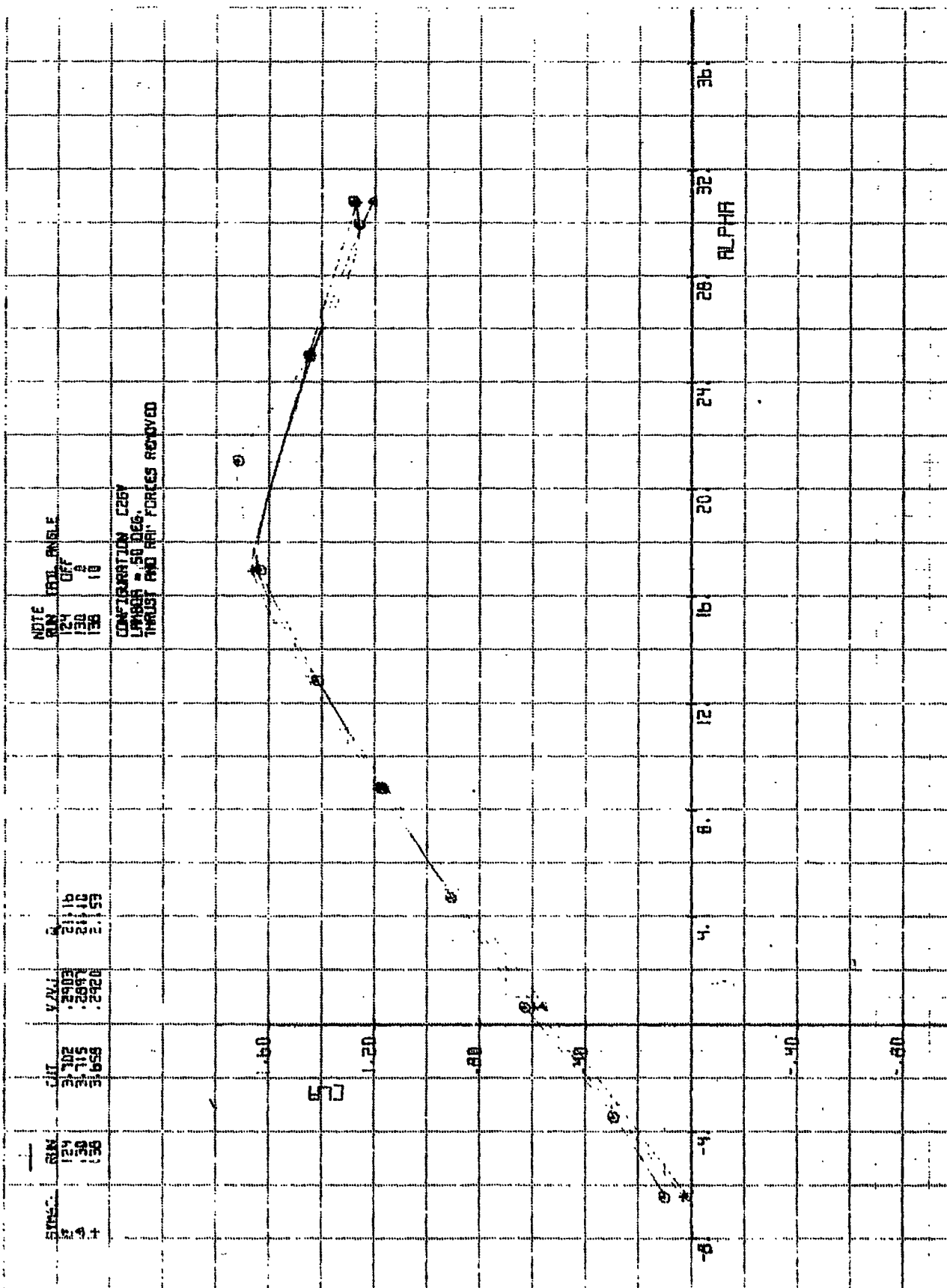
THE BOEING COMPANY

L54TB 2544

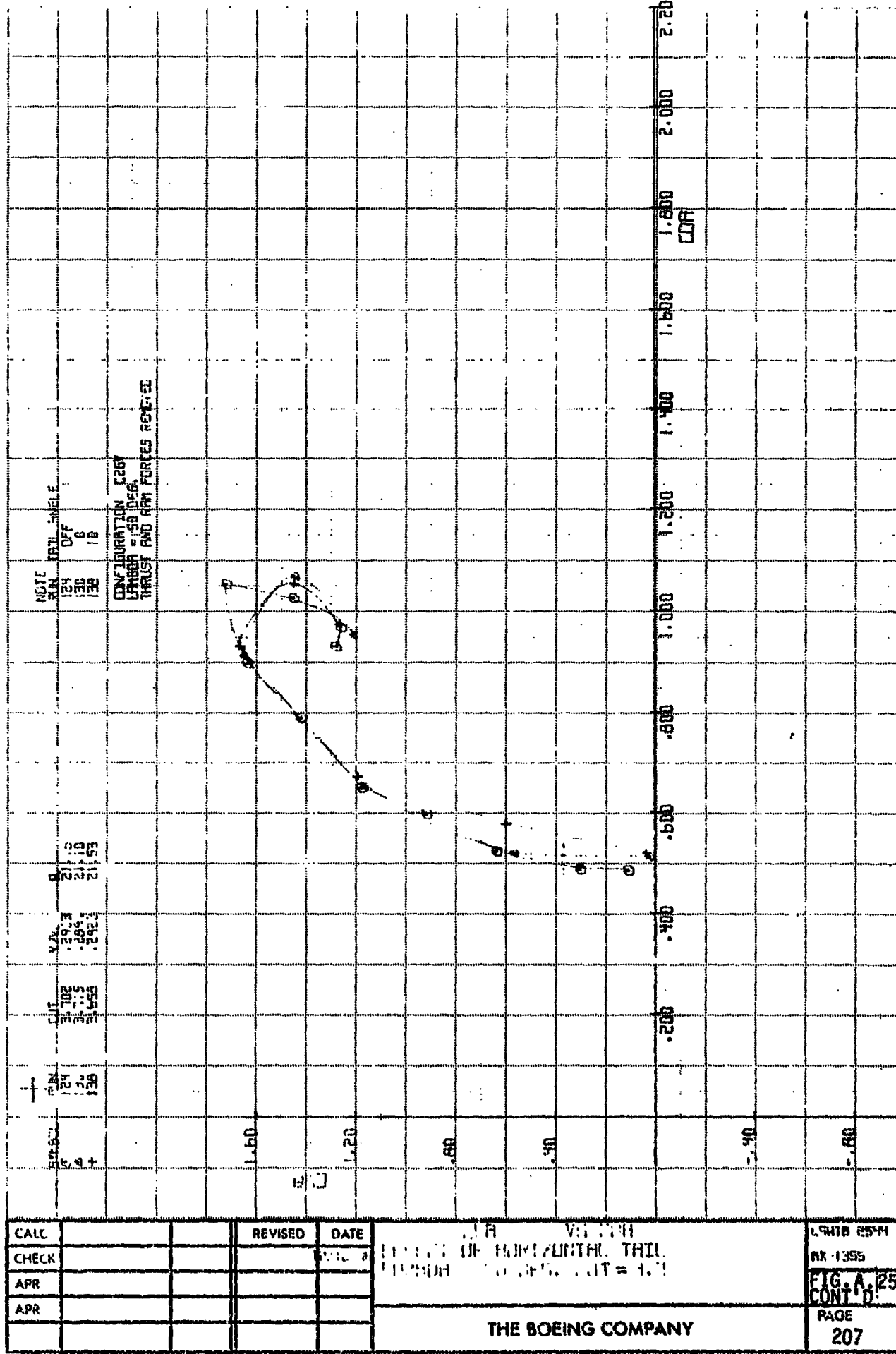
AX-1255

**FIG. A.24**  
**CONT'D**

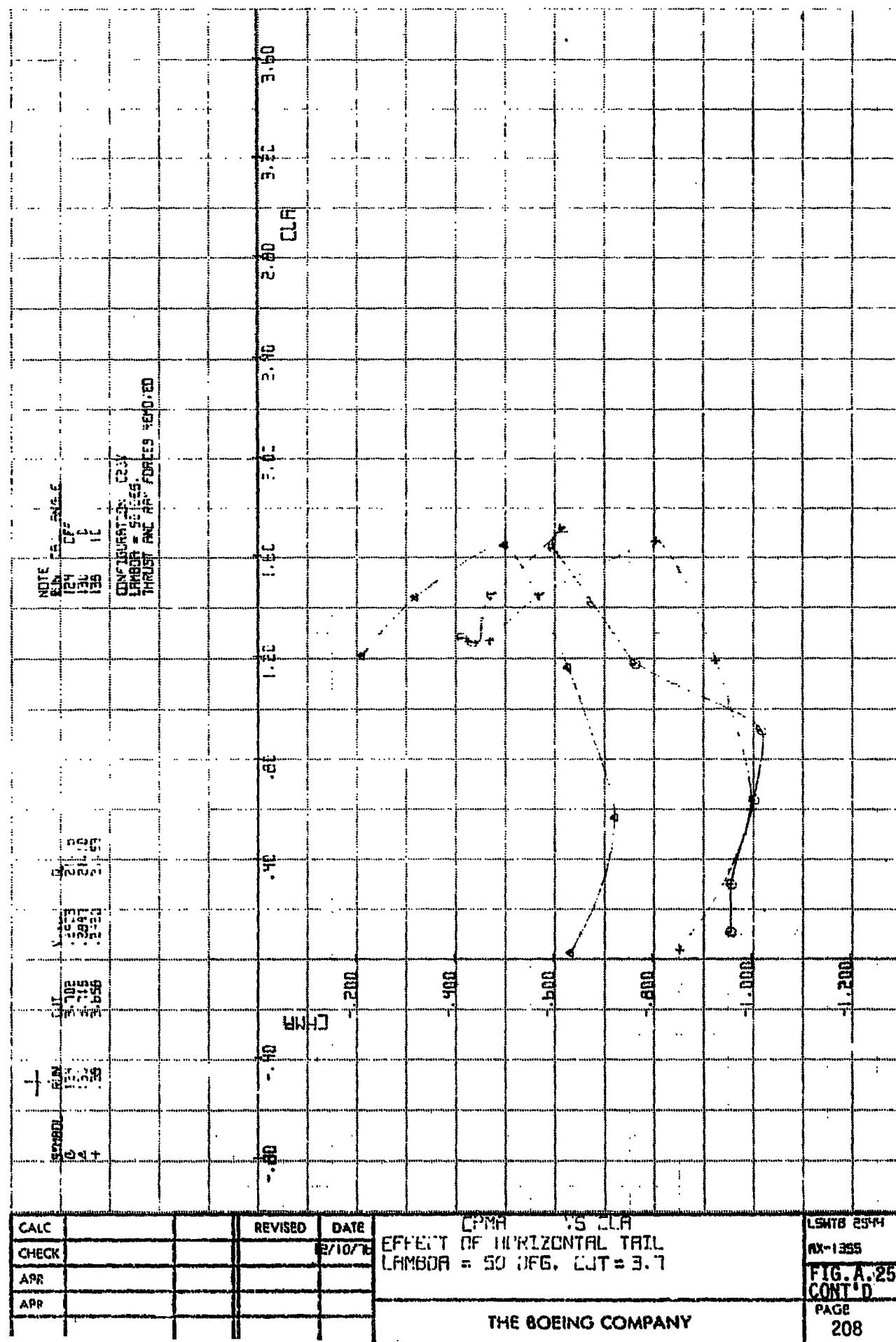
PAGE  
203



CALC		REVISED	DATE	EFFECT OF HORIZONTL TILT LPHM = 50 DEG THRU HAT = 1.1	LSHTB 2544 RX-1255
CHECK					FIG.A.25
APR					
APR					
					PAGE 206



THE BOEING COMPANY



CPMA VS CLA  
EFFECT OF HORIZONTAL TRAIL  
LAMBDA = 50 DEG, CJT = 3.7

LSHTB 2544

Box-1355

FIG. A.25  
CONT'D

PAGE

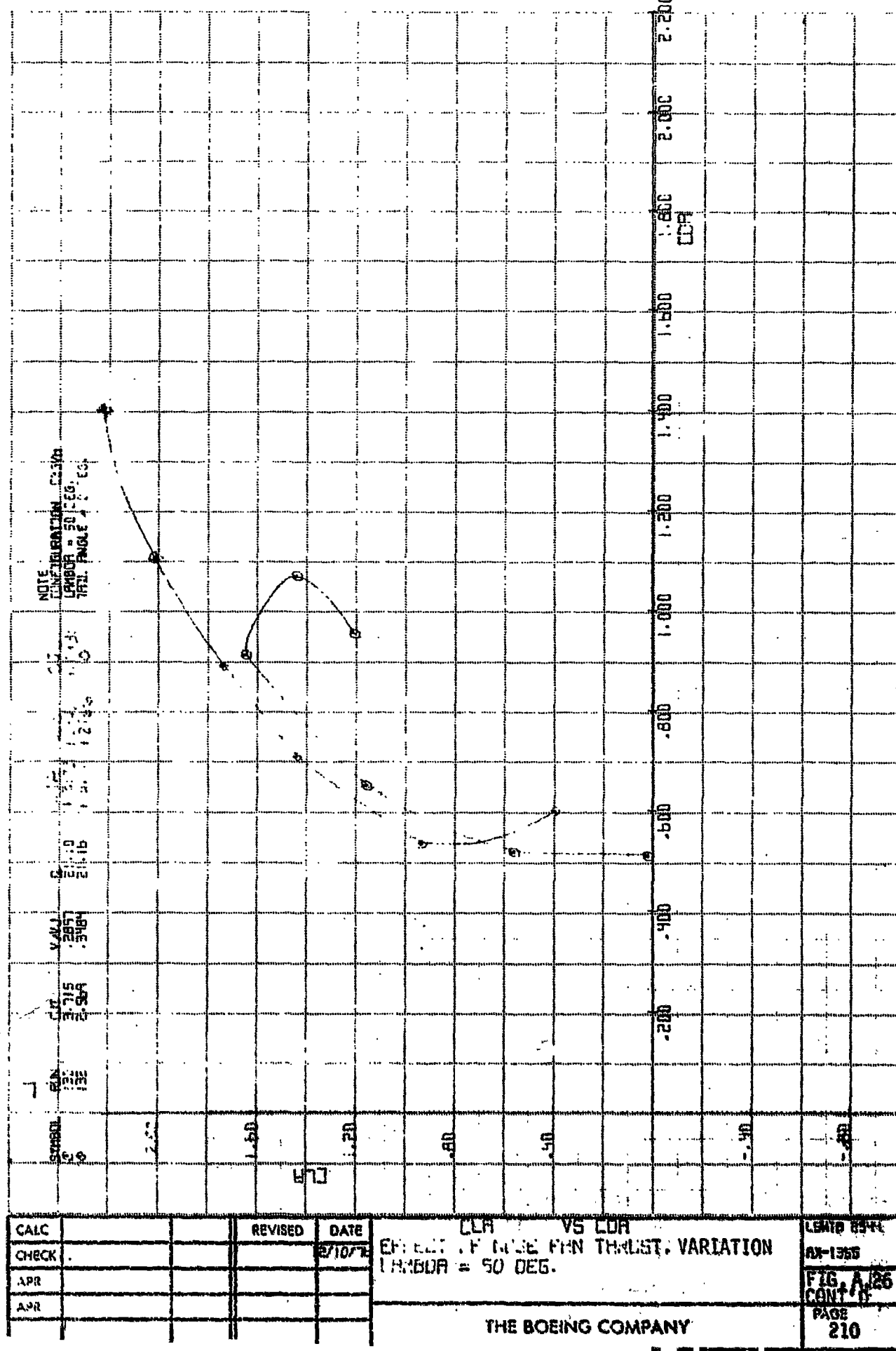
208

CALC			REVISED	DATE
CHECK				12/10/18
APP				
APR				

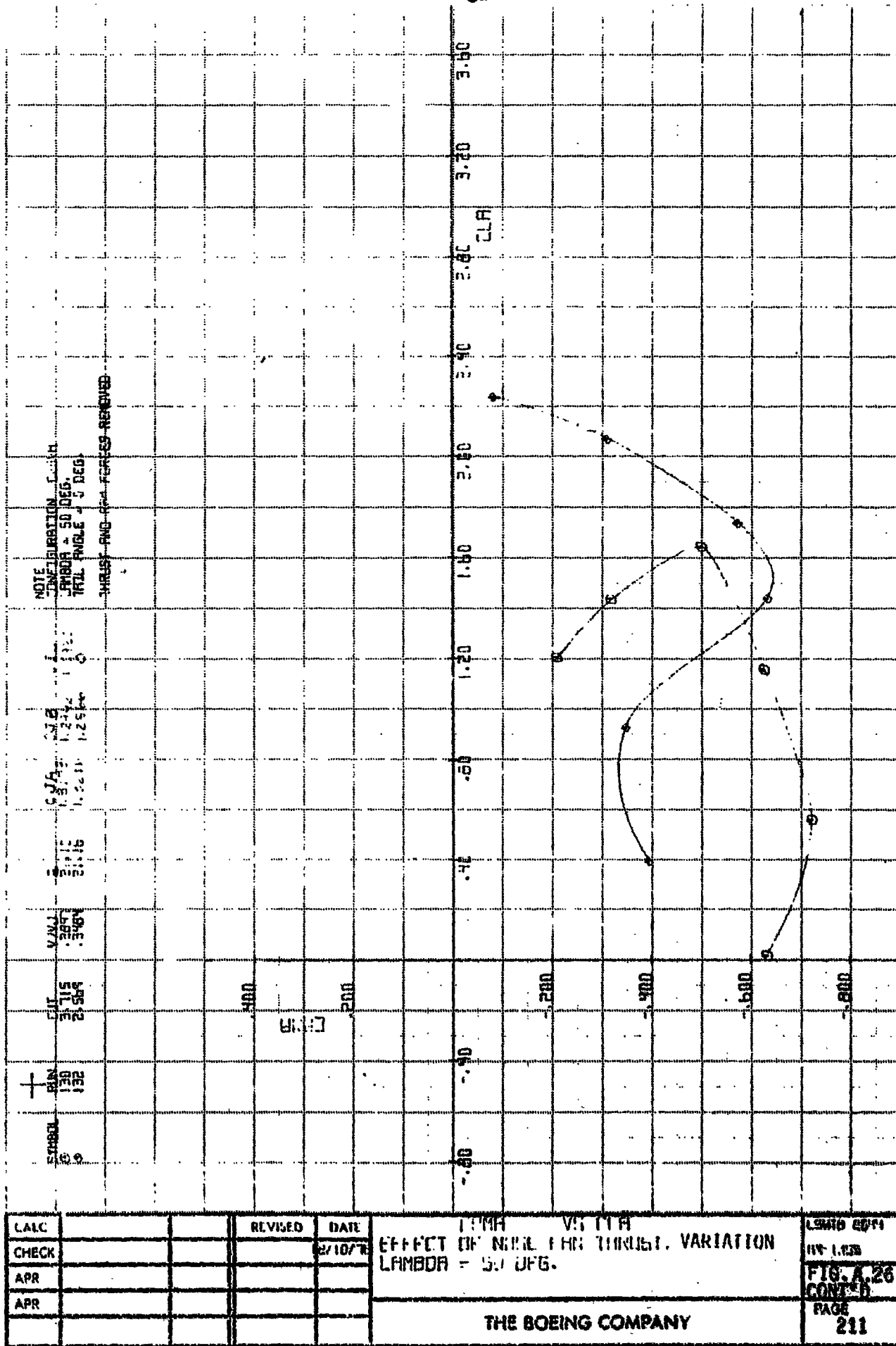
EFFECT OF ANGLED FAN THRUST, VARIATION  
THICKNESS & TILT.

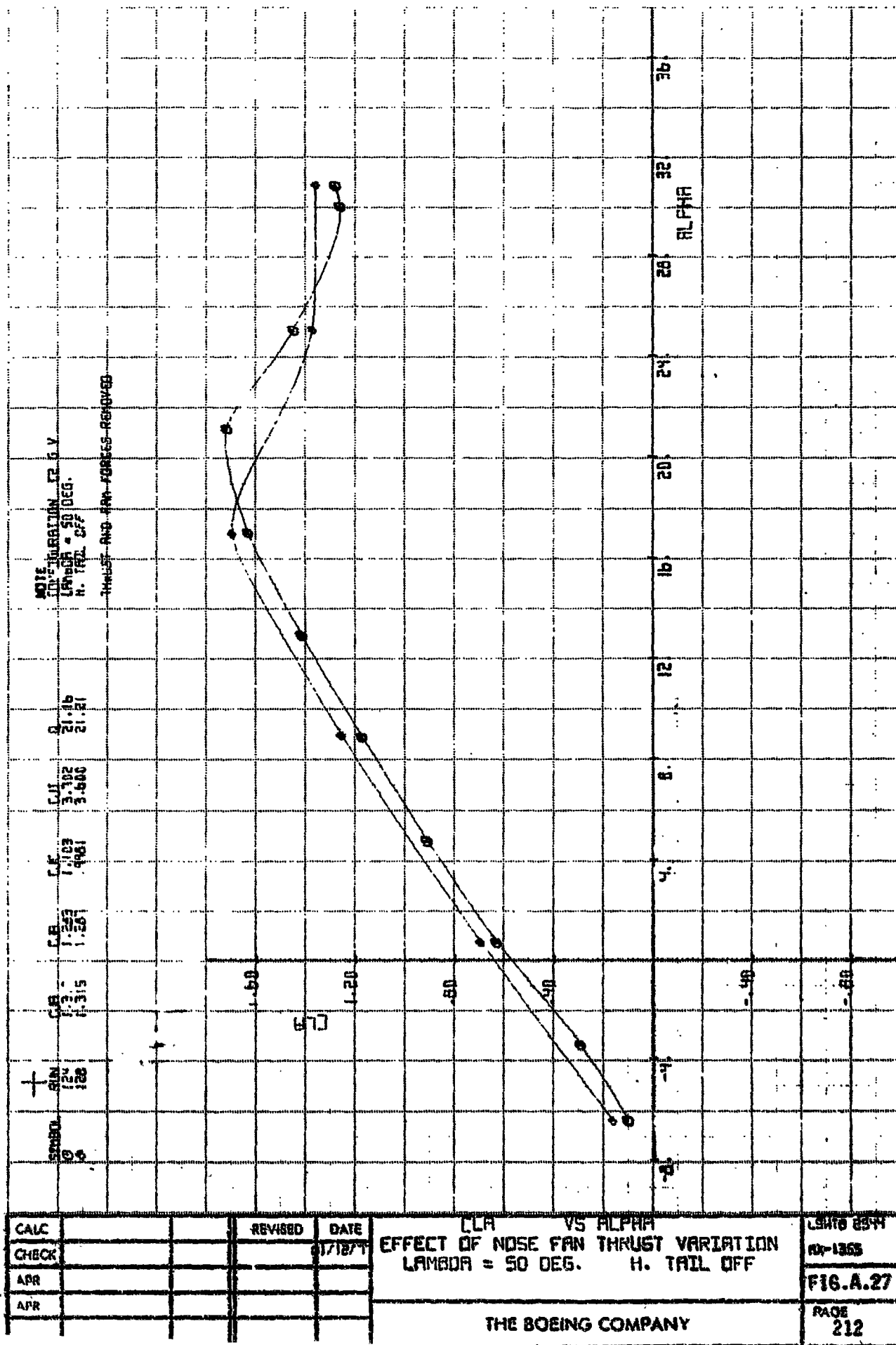
THE BOEING COMPANY

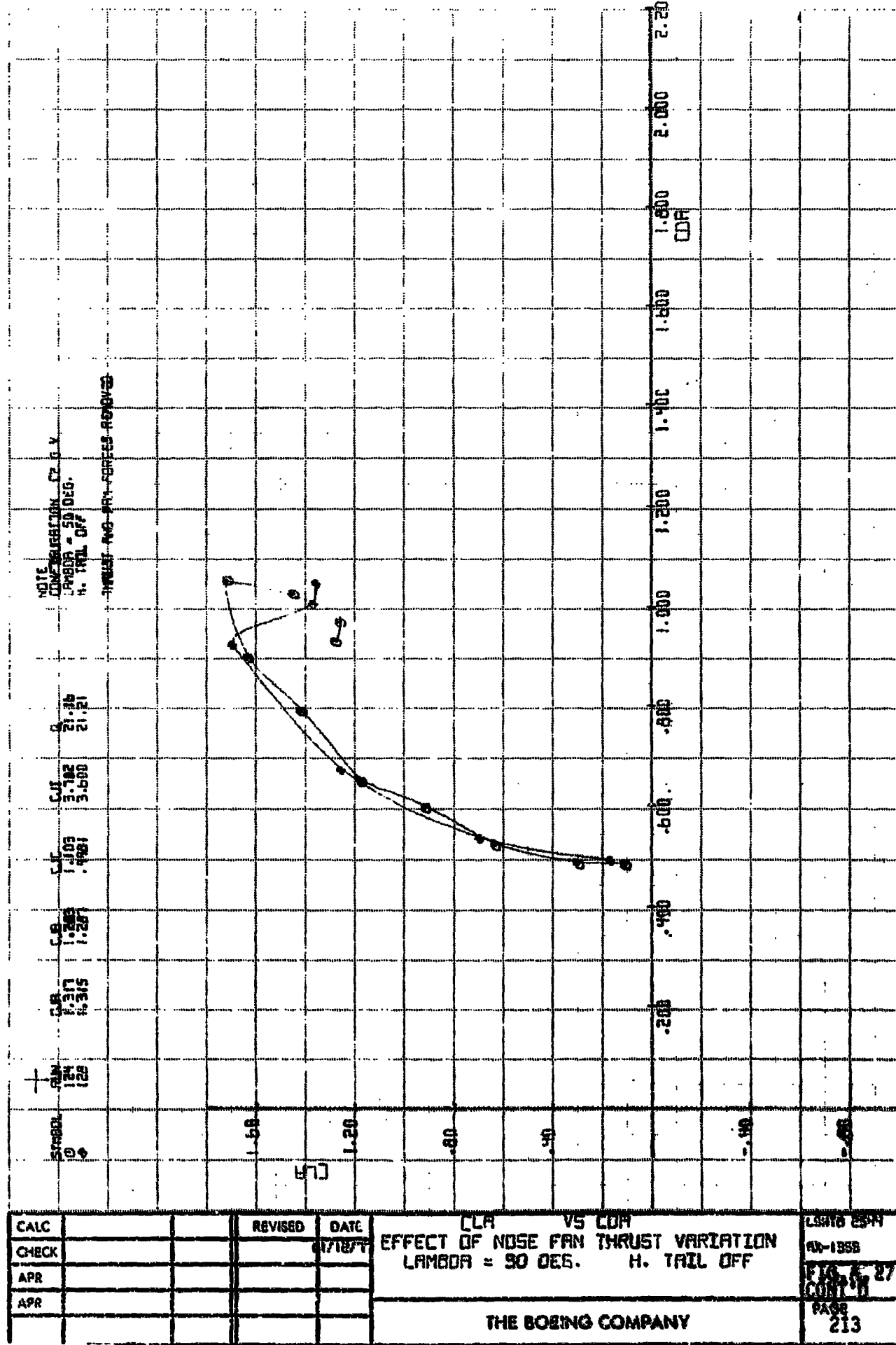
LSNTB 2544  
RJ-1353  
**FIG. A.26**  
PAGE  
**209**

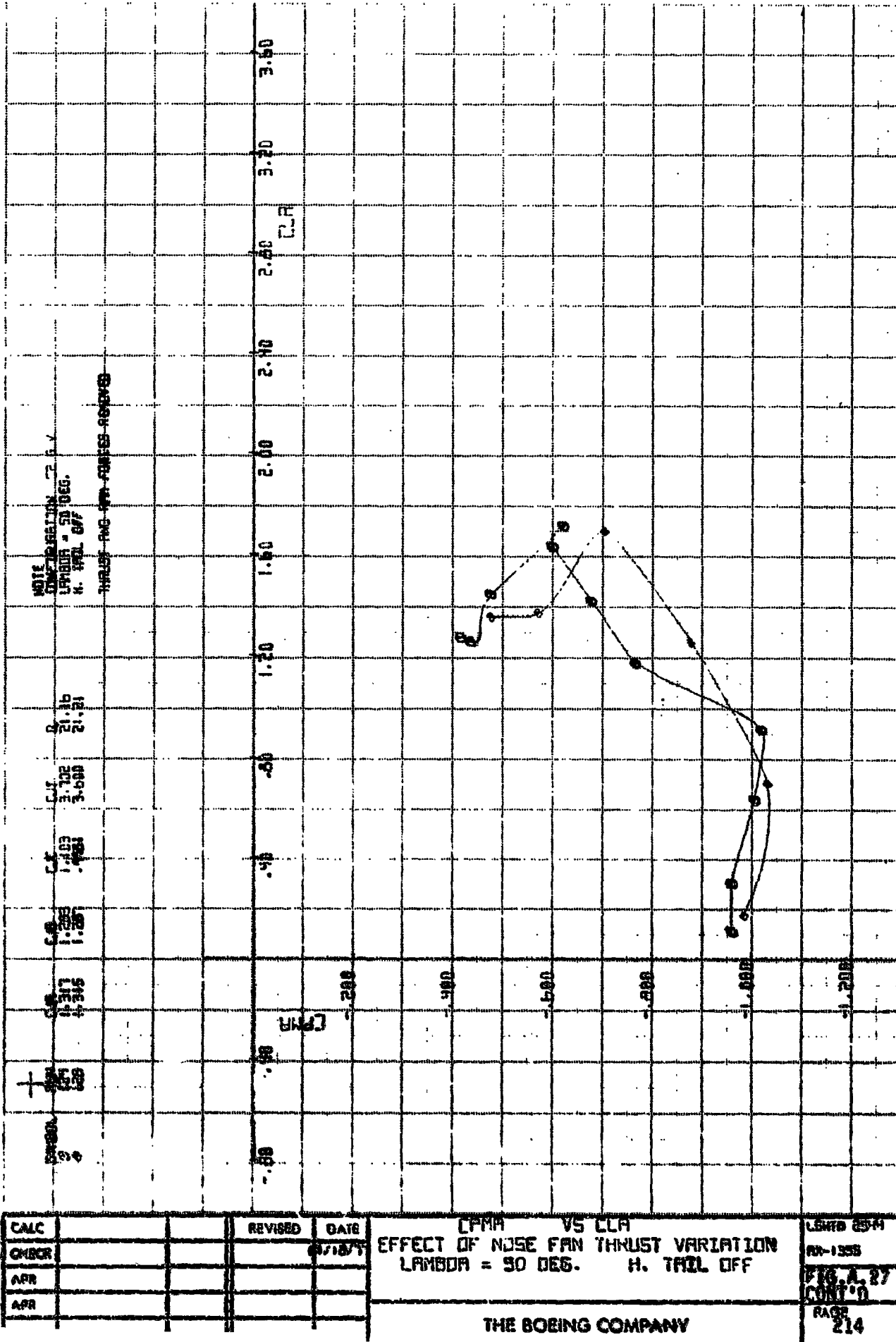


ORIGINAL PAGE IS  
OF POOR QUALITY









16 17 18 19 20 21 22 23 24 25 26 27 28 29 30 31 32 33 34 35 36 37 38 39 40 41 42 43 44 45 46 47 48 49 50 51 52 53 54 55 56 57 58 59 50 51 52 53 54 55 56 57 58 59 60 61 62 63 64 65 66 67 68 69 60 61 62 63 64 65 66 67 68 69 70 71 72 73 74 75 76 77 78 79 70 71 72 73 74 75 76 77 78 79 80 81 82 83 84 85 86 87 88 89 80 81 82 83 84 85 86 87 88 89 90 91 92 93 94 95 96 97 98 99 90 91 92 93 94 95 96 97 98 99 100

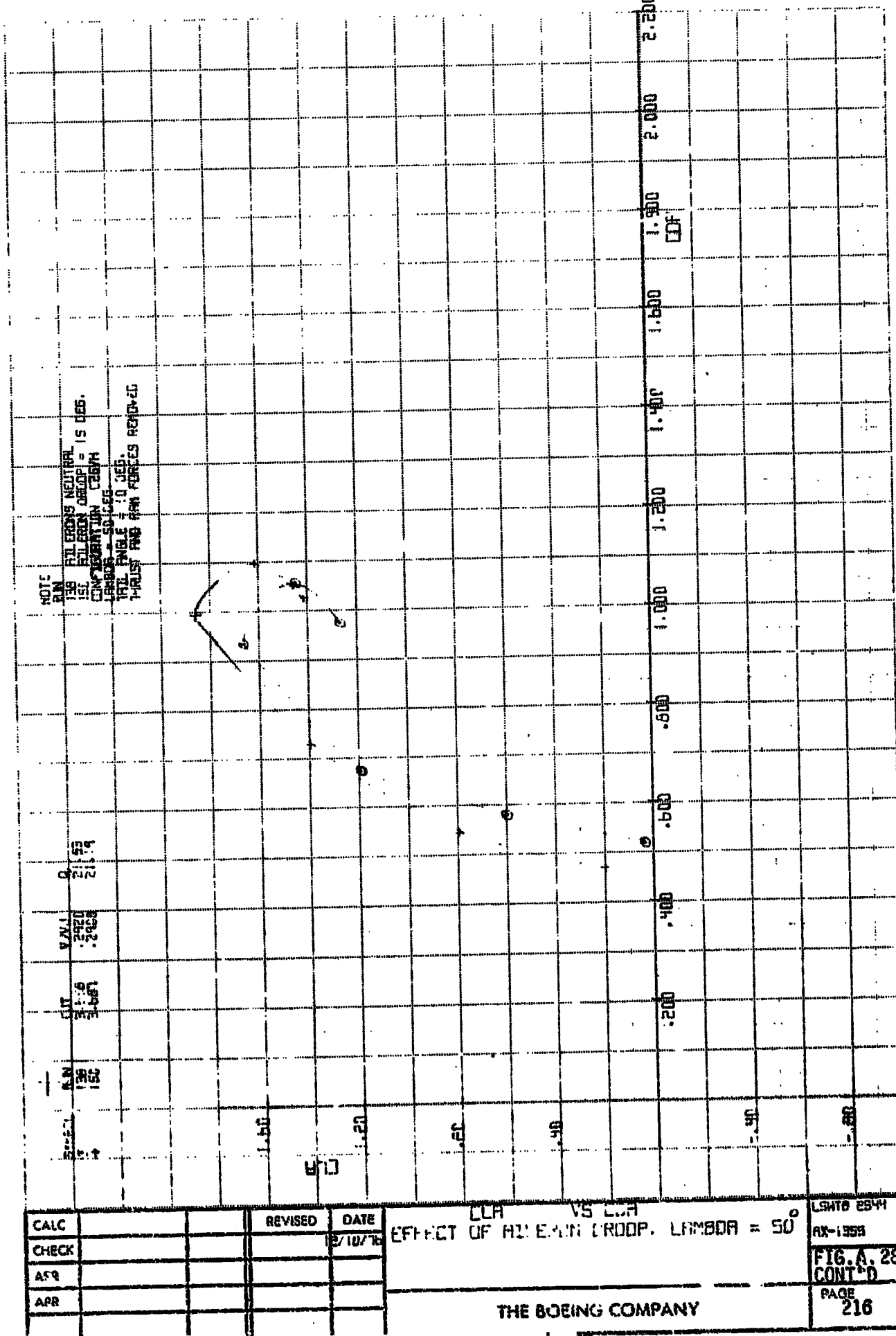
CALC			REVISED	DATE
CHECK				10/7
APR				
AMT				

CL<sub>A</sub> = 0.144  
LT OF AILERON DROOP, LAMBDA = 50°

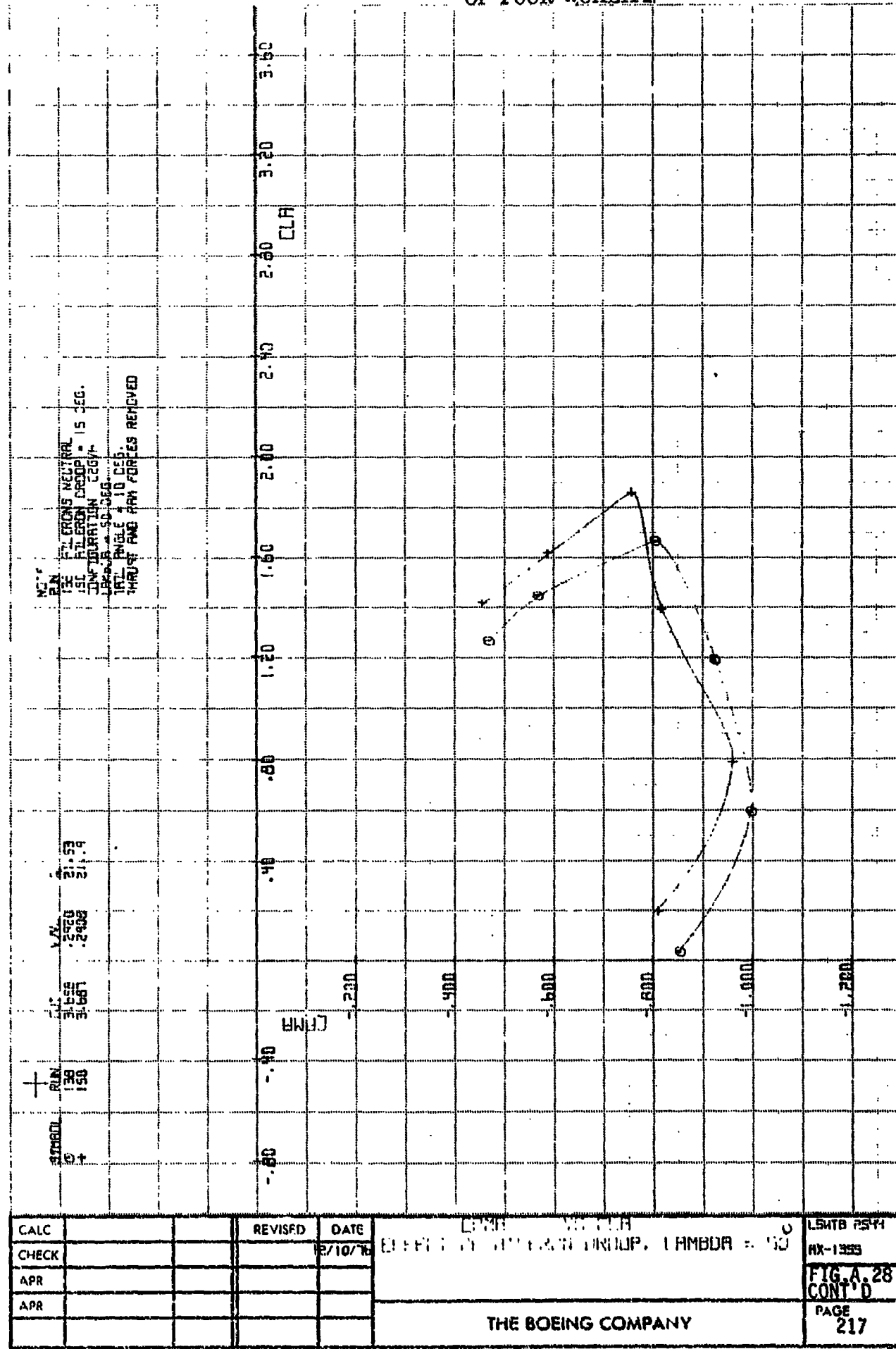
LSD 254

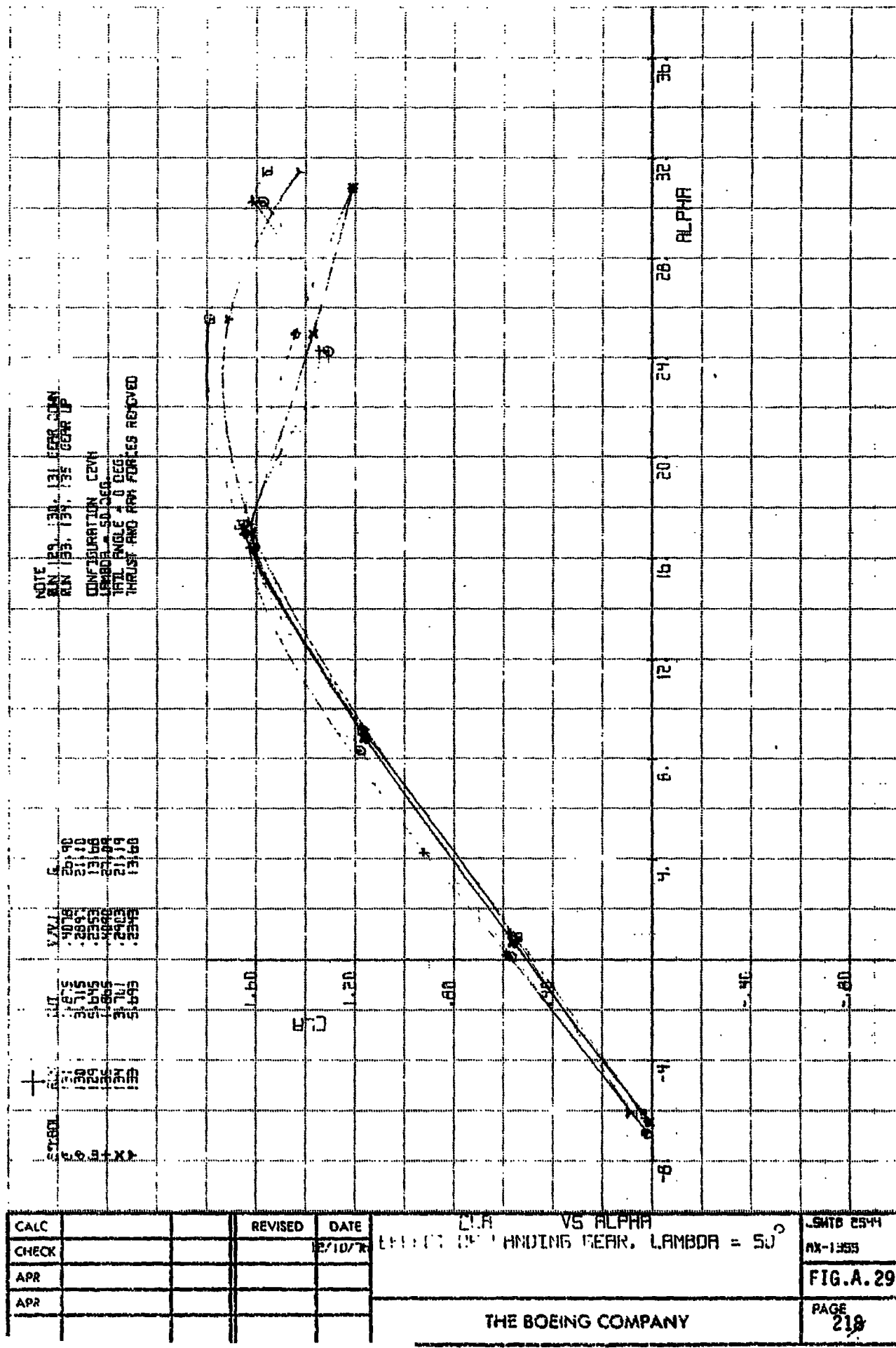
**FIG.A.28**

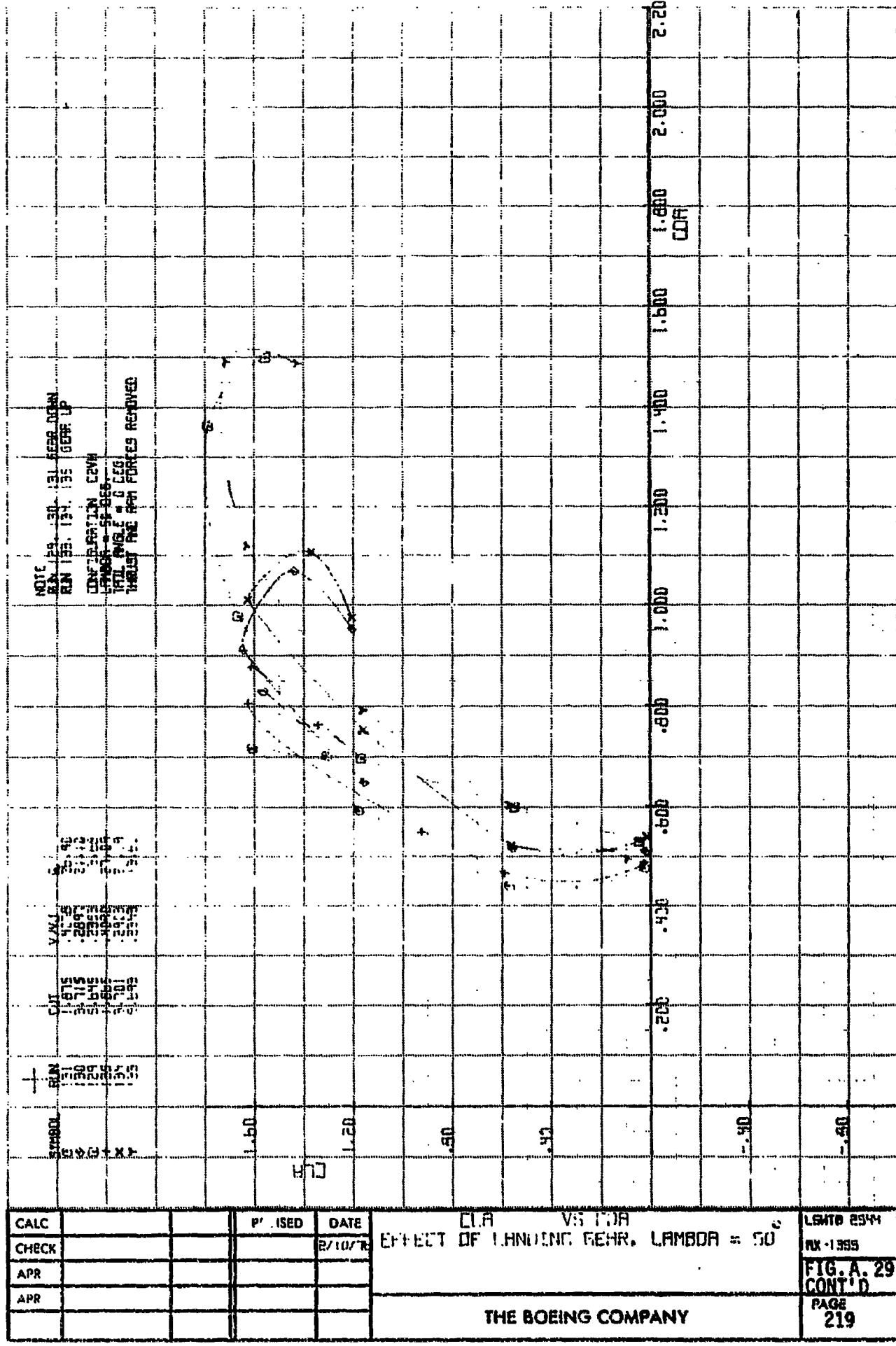
**THE BOEING COMPANY**

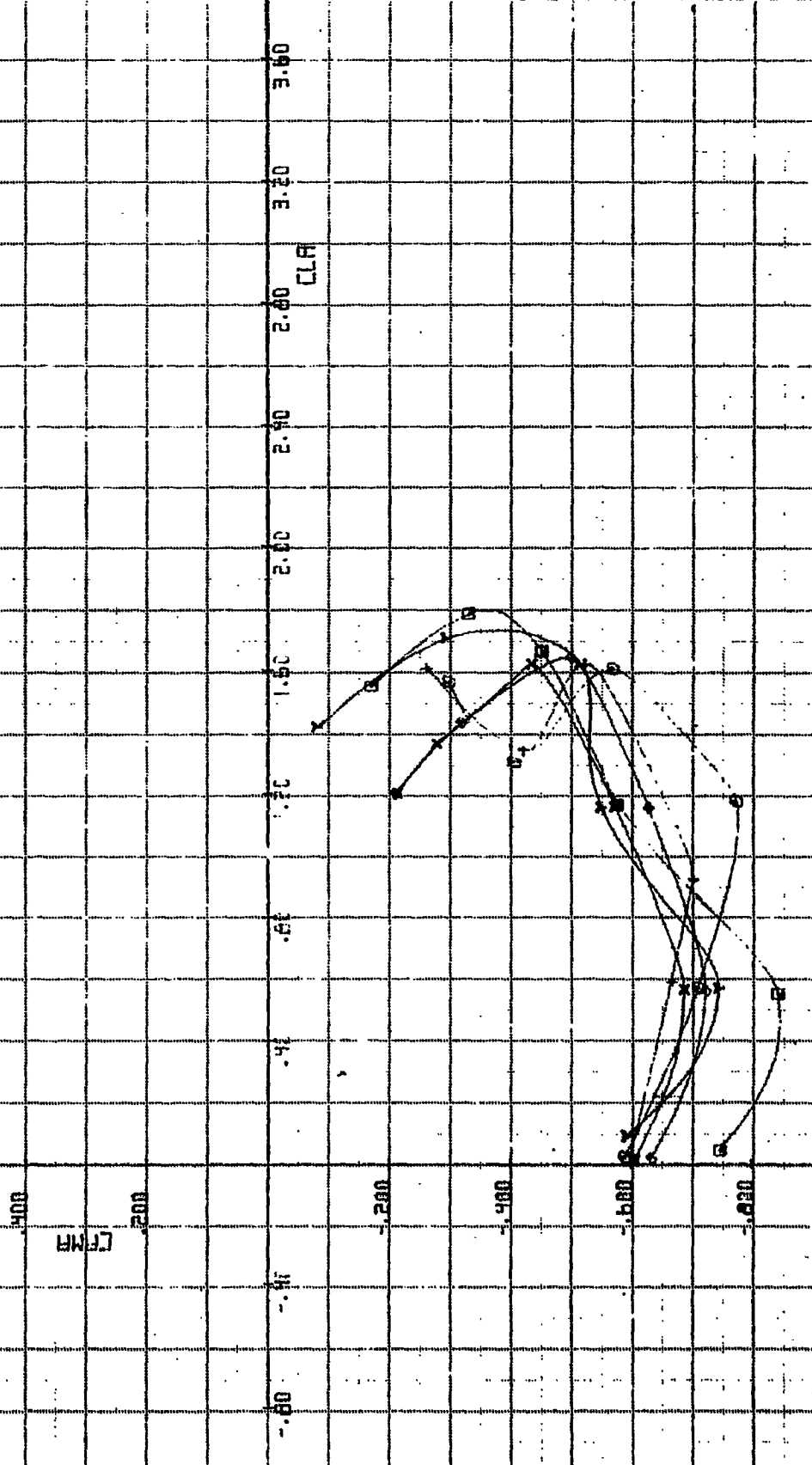


ORIGINAL PAGE IS  
OF POOR QUALITY









CALC			REVISED	DATE
CHECK				8/10/16
APR				
APR				

CPMA VS CLA  
EFFECT OF LANDING GEAR. LAMBDA = 50°

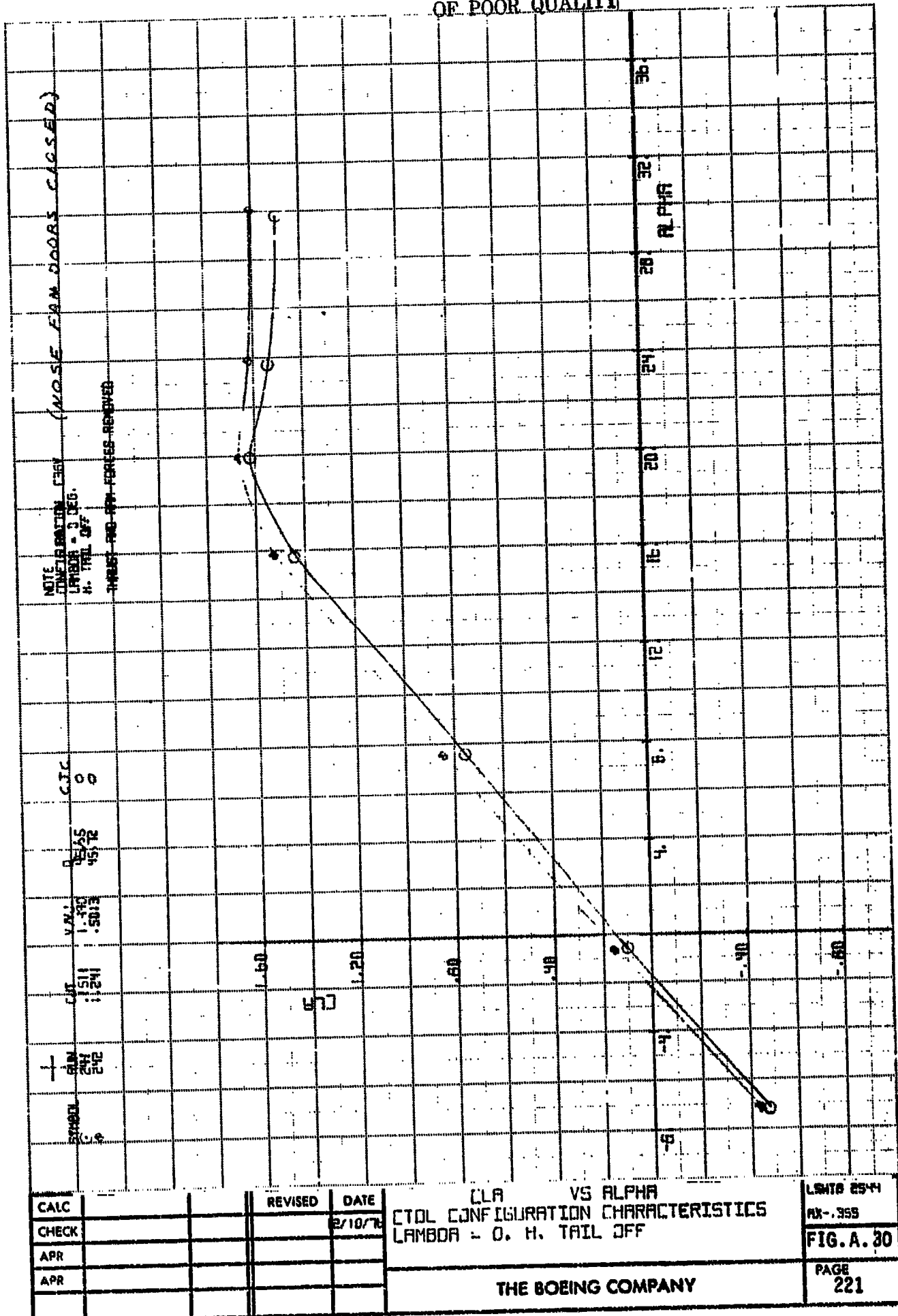
LSHTD 2344

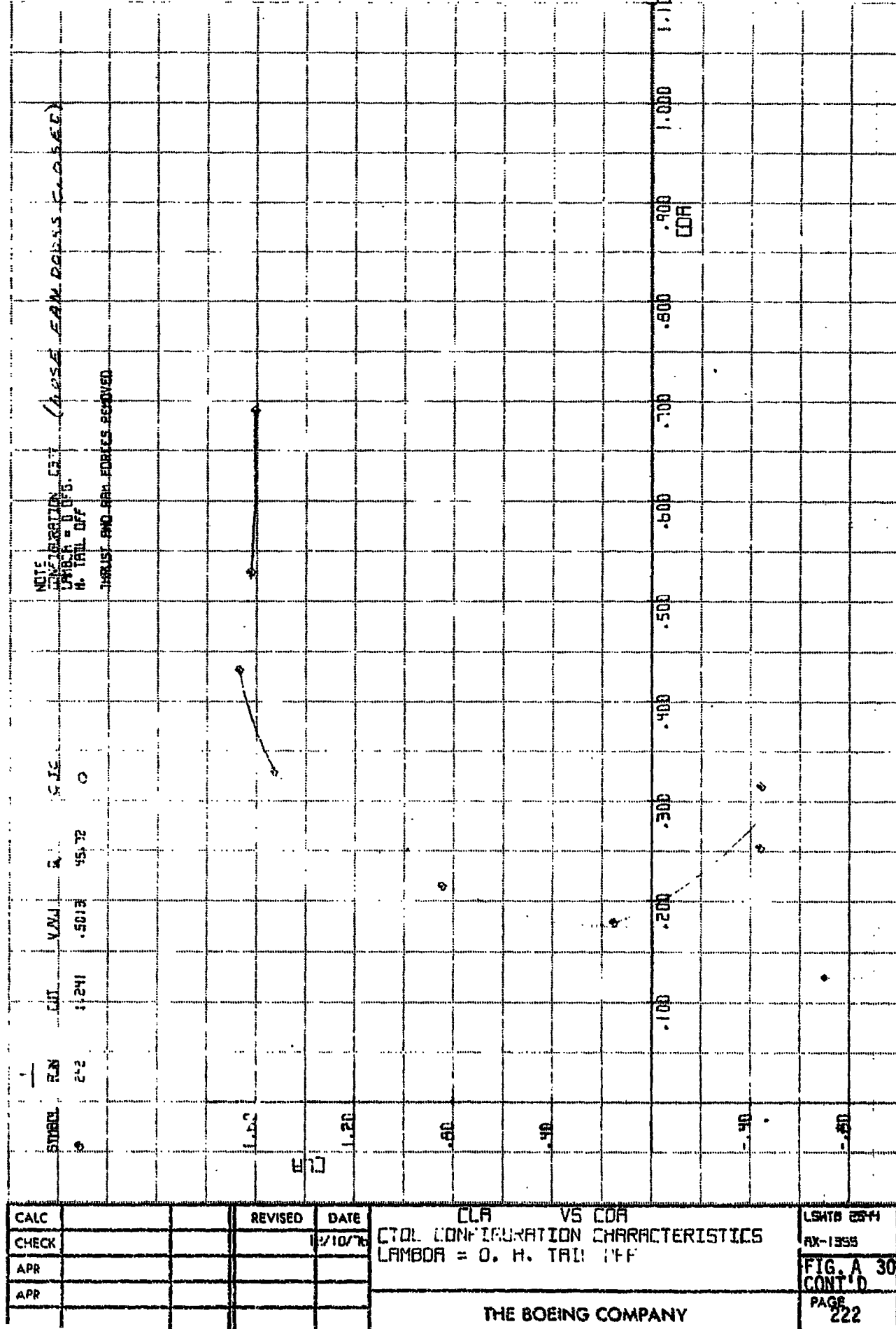
版 1355

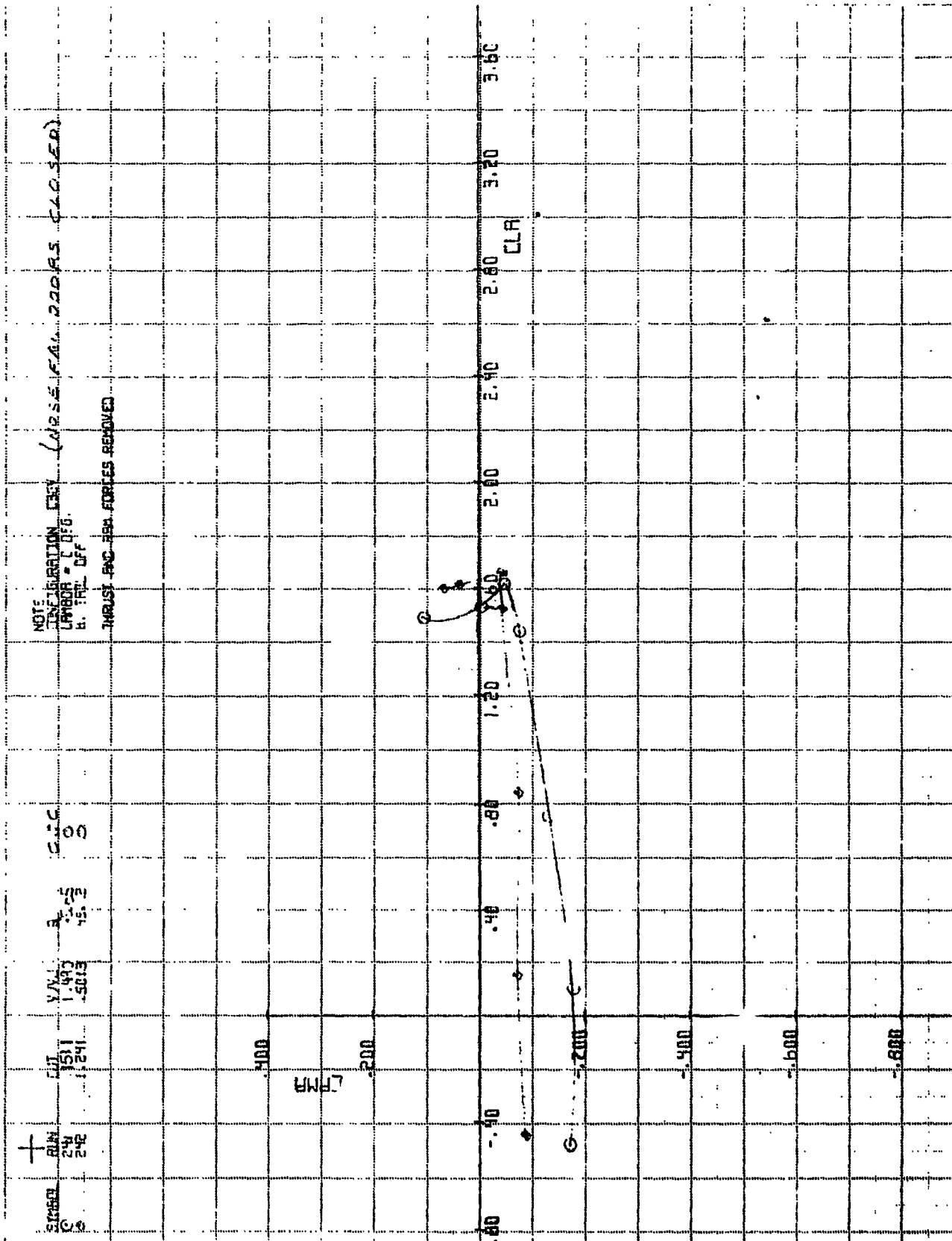
**FIG. A. 29**  
**CONT'D**

PAGE  
220

ORIGINAL PAGE IS  
OF POOR QUALITY







CALL			REVISED	DATE
CHECK				12/10/16
APR				
APP				

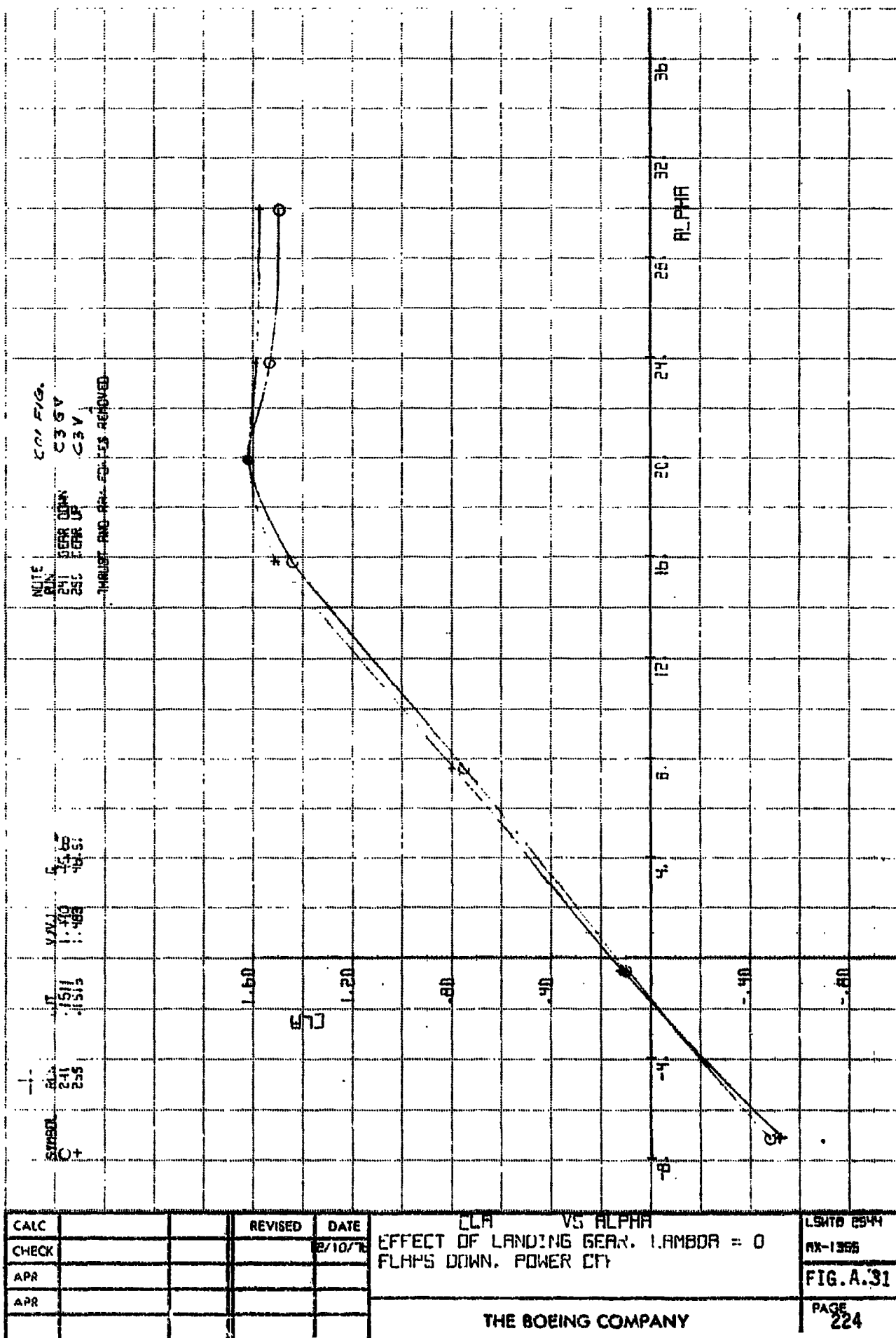
CPMA VS CLA  
LTL CONFIGURATION CHARACTERISTICS  
LAMBDA = 0. M. THI. OF

THE BOEING COMPANY

L941D 8544

**FIG. A.30**  
**CONT'D.**

PAGE  
223



REV.	REF.	REVISED	DATE
1	1	120174	12/17/73

FIG. A.31  
CONT'D

12/17/73  
EFFECT OF LANDING GEAR. LAMBDA = 0  
FLAPS DOWN, TAIL UP

THE BOEING COMPANY

FIG. A.31  
CONT'D

12/17/73  
EFFECT OF LANDING GEAR. LAMBDA = 0  
FLAPS DOWN, TAIL UP

225

CONFUS.  
NOTE  
GEAR DOWN C3 GV  
GEAR UP C3 V  
THRUST AND AIR FORCES ARE ZERO

CDA DATA FOR RUNS 241 and 256  
ARE NOT PRESENTED DUE TO DATA ERRORS.

STABIL. RUN 1.151 1.153 1.155  
+ 251 253 255

1.153  
1.155  
1.151

1.25

1.25

1.25

1.25

1.25

1.25

1.25

1.25

1.25

1.25

1.25

1.25

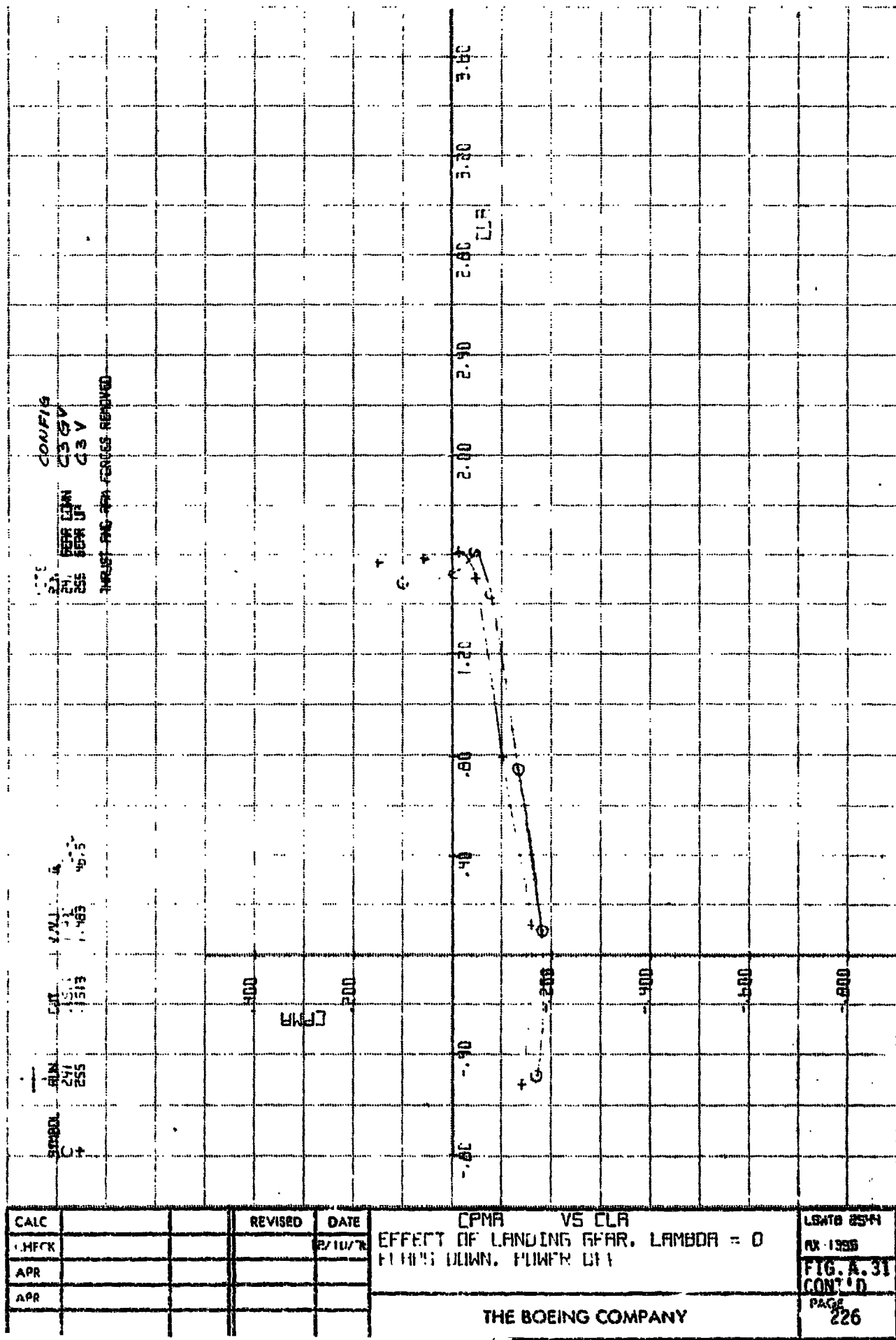
1.25

1.25

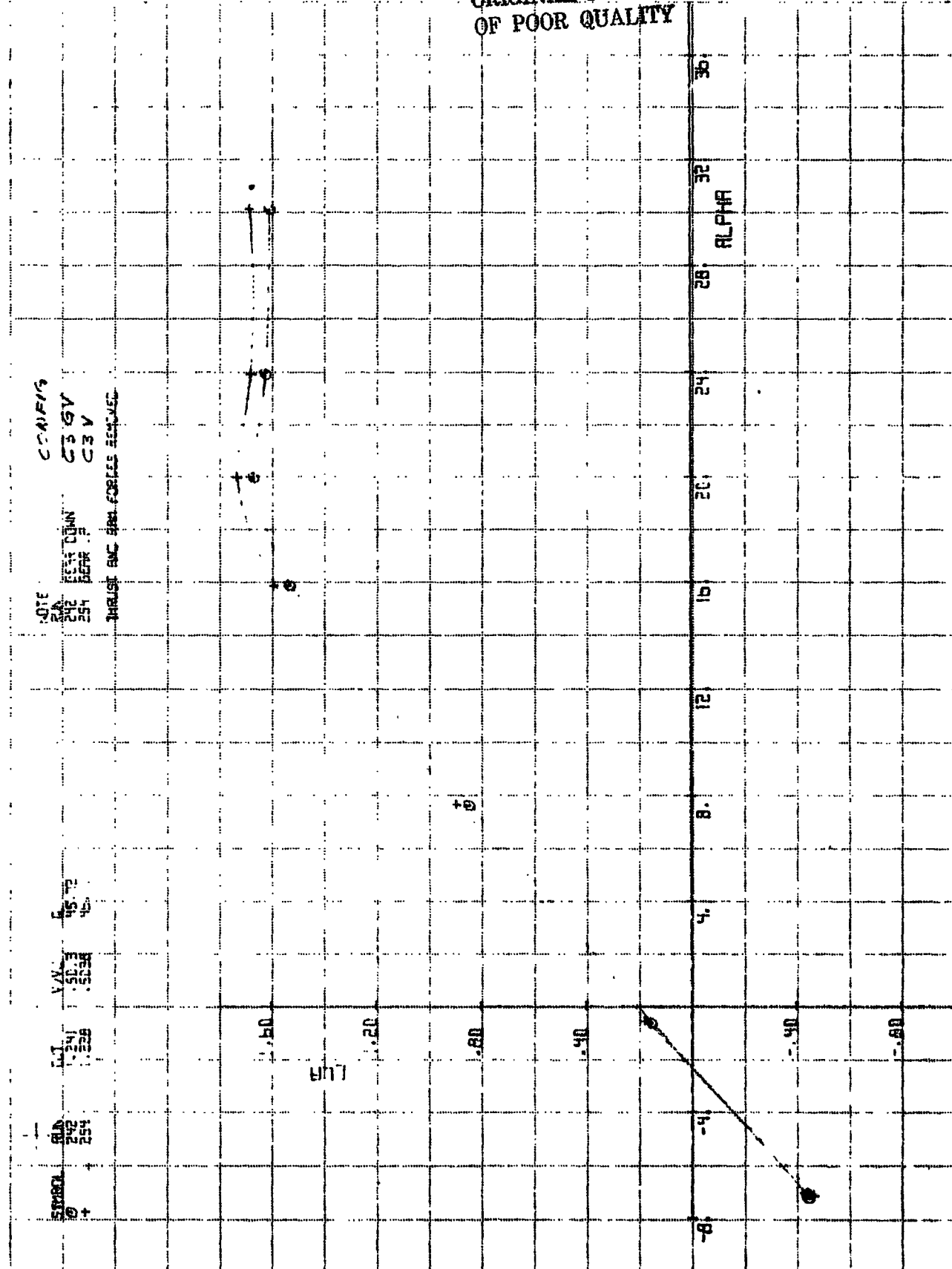
1.25

1.25

FIG. A.31



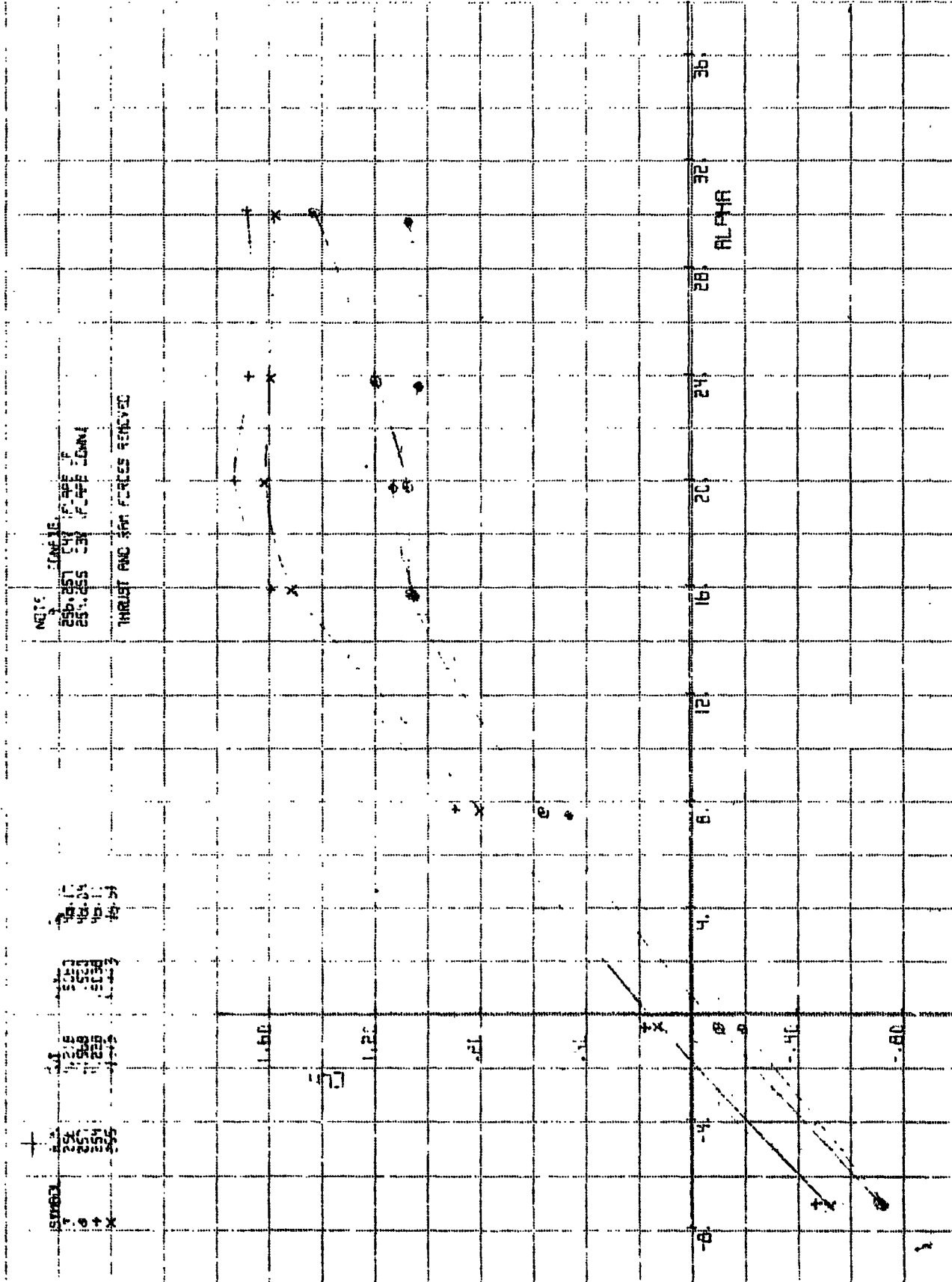
ORIGINAL PAGE IS  
OF POOR QUALITY





CALC		REVISED	DATE	11PM 7/11/68 LIFT OFF FROM LAFHR. LAMMOR - C FLAPS DOWN, FLUTTER ON	L5WTB 2544 MX-1355 FIG.A.32 CONT'D PAGE 229
CHECK			8/10/68		
APR					
APR					

THE BOEING COMPANY



SAC		REVISED	DATE
CHEK			11/7
APP			
ADM			

CL vs ALPHA  
EFFECT OF FLAP AN. SLAT  
LHMHR = 0

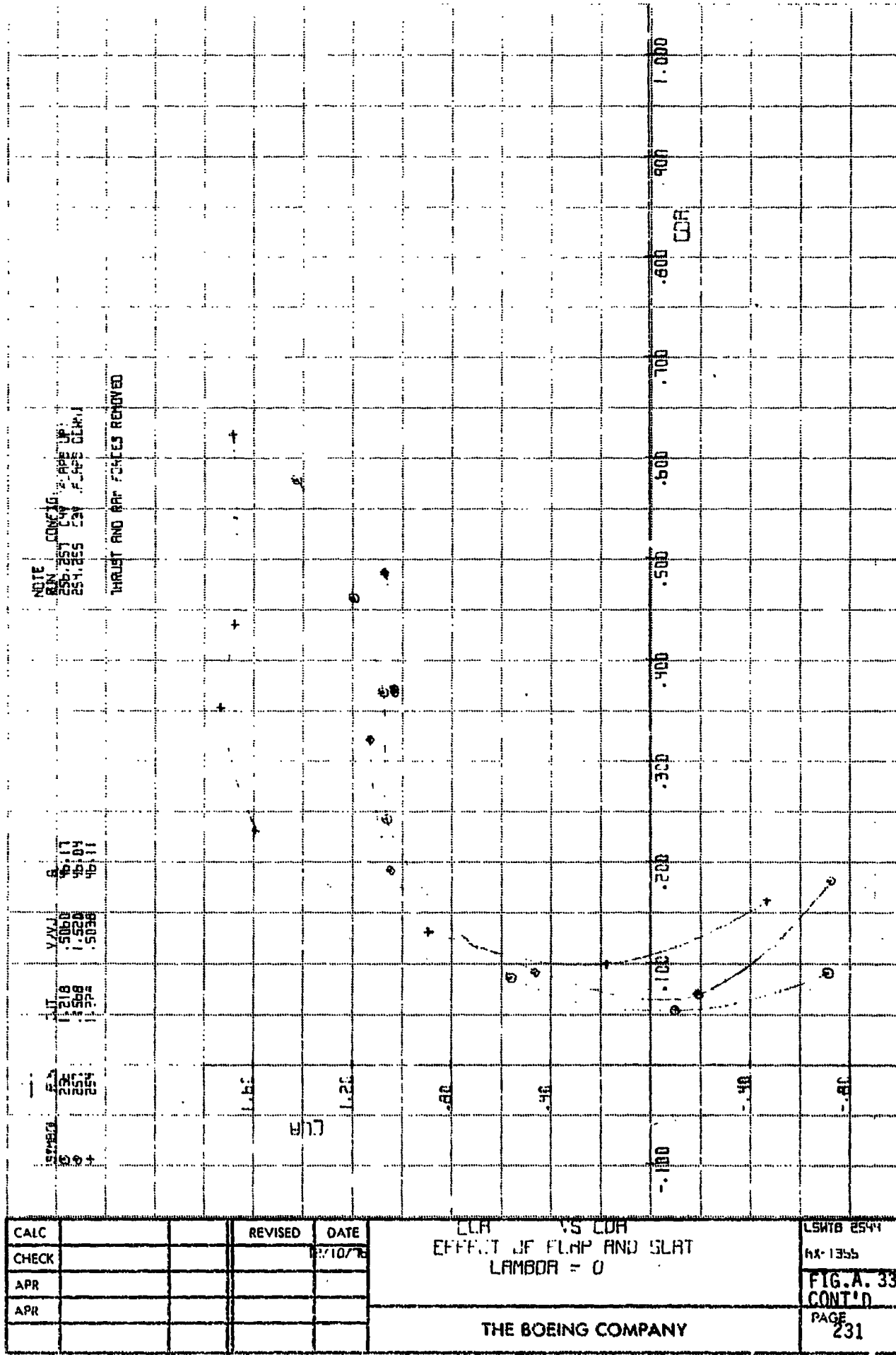
THE BOEING COMPANY

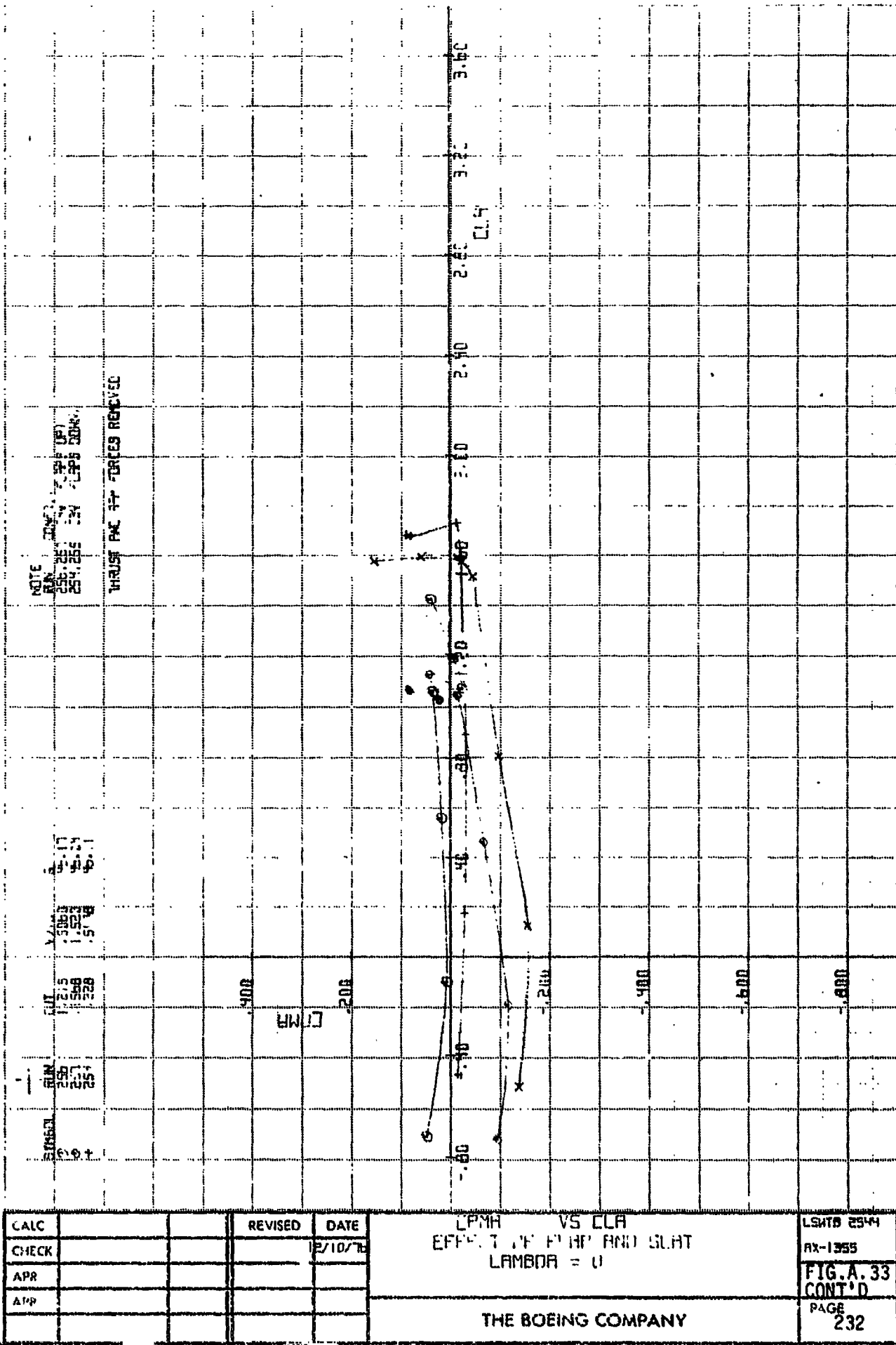
LSWTB 2544

RX 1369

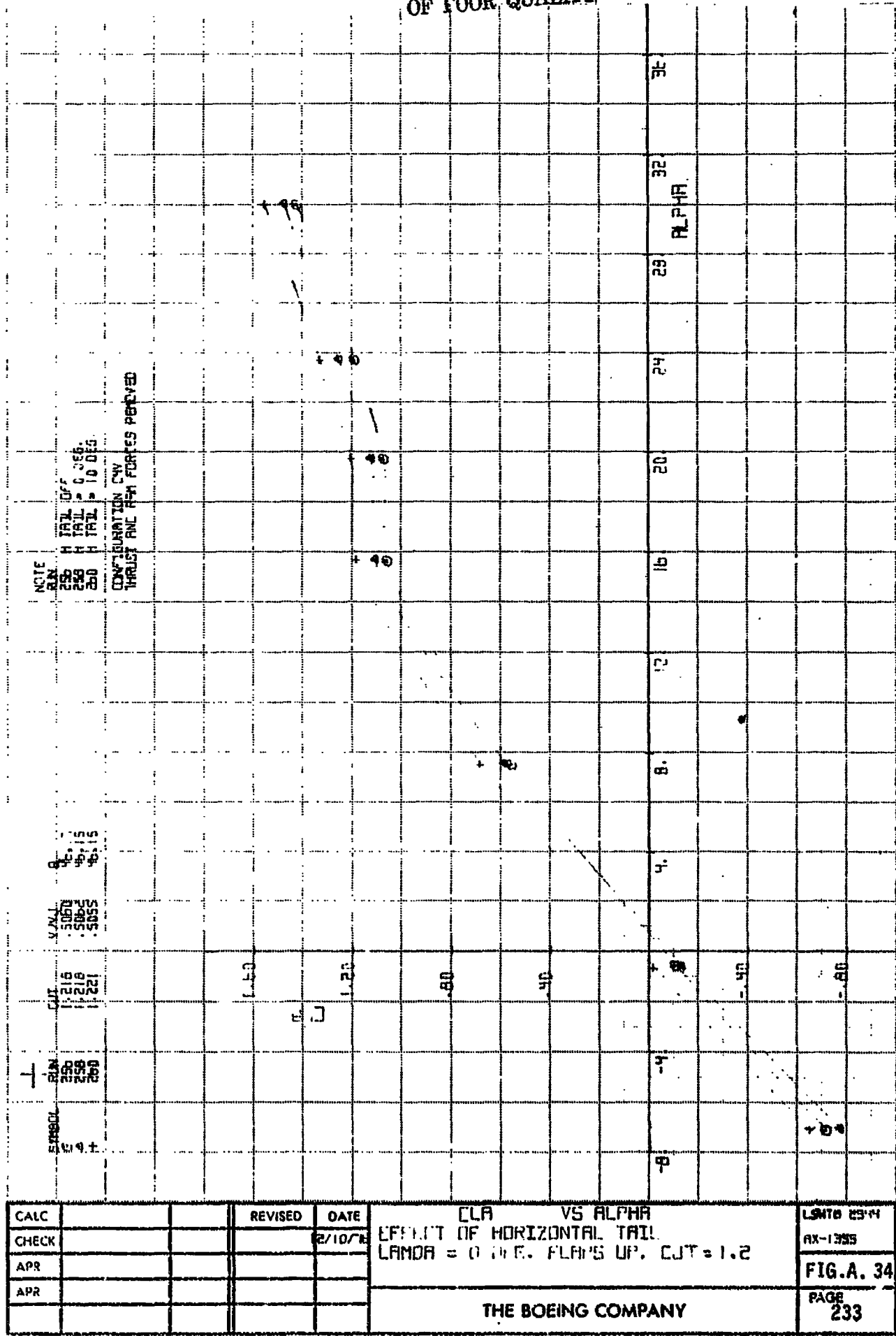
FIG.A. 33

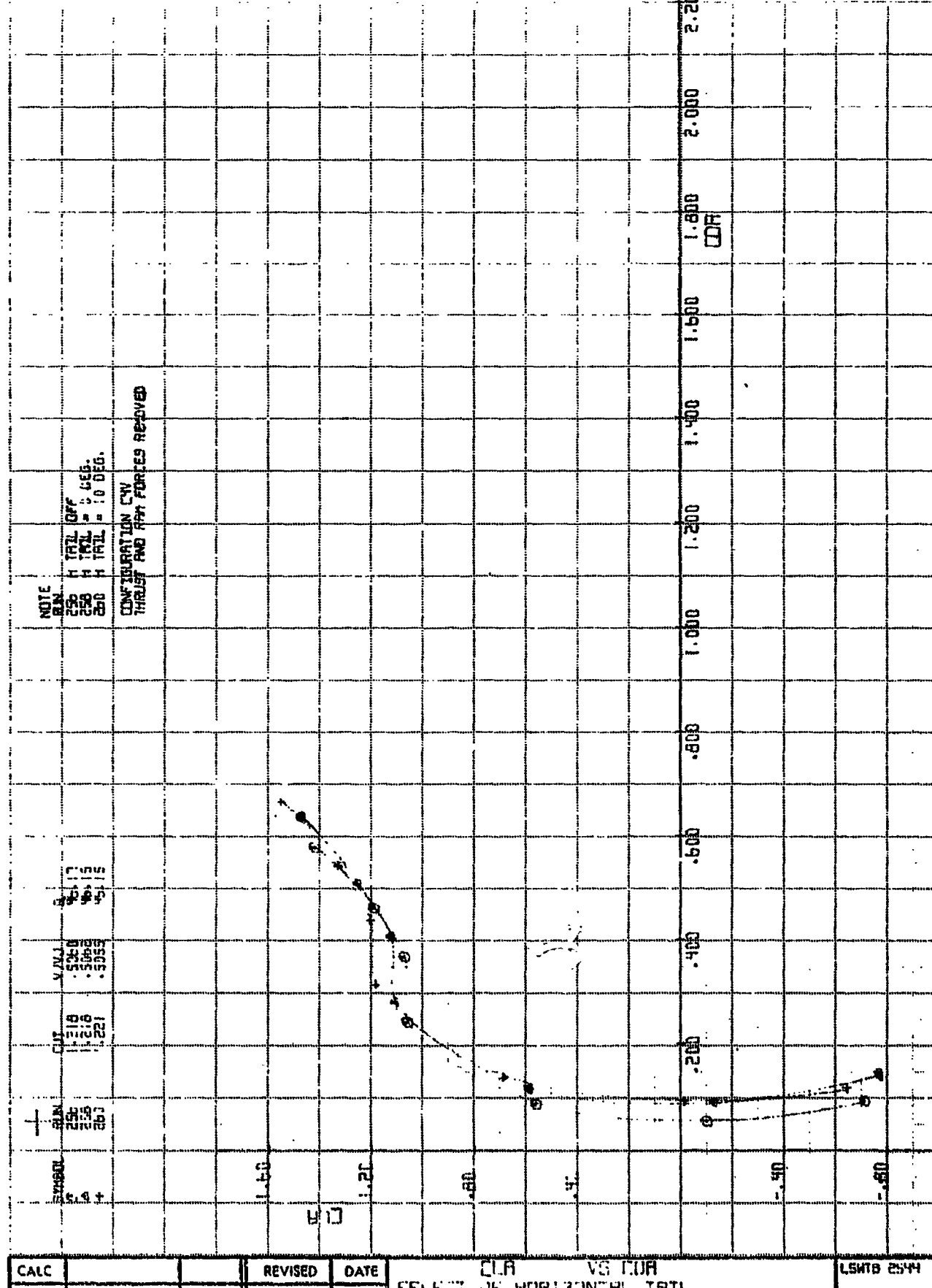
PAGE 200





ORIGINAL PAGE IS  
OF POOR QUALITY



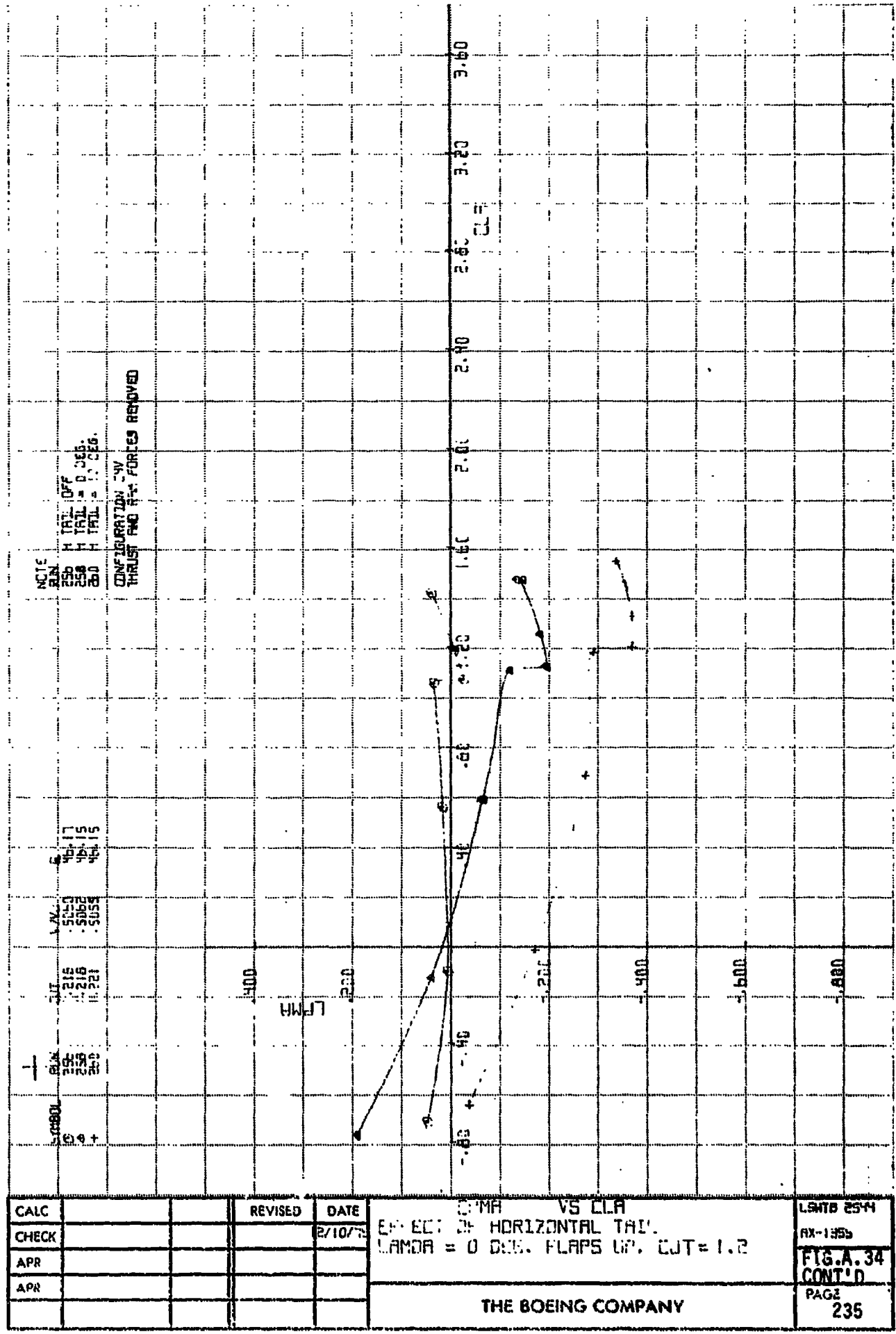


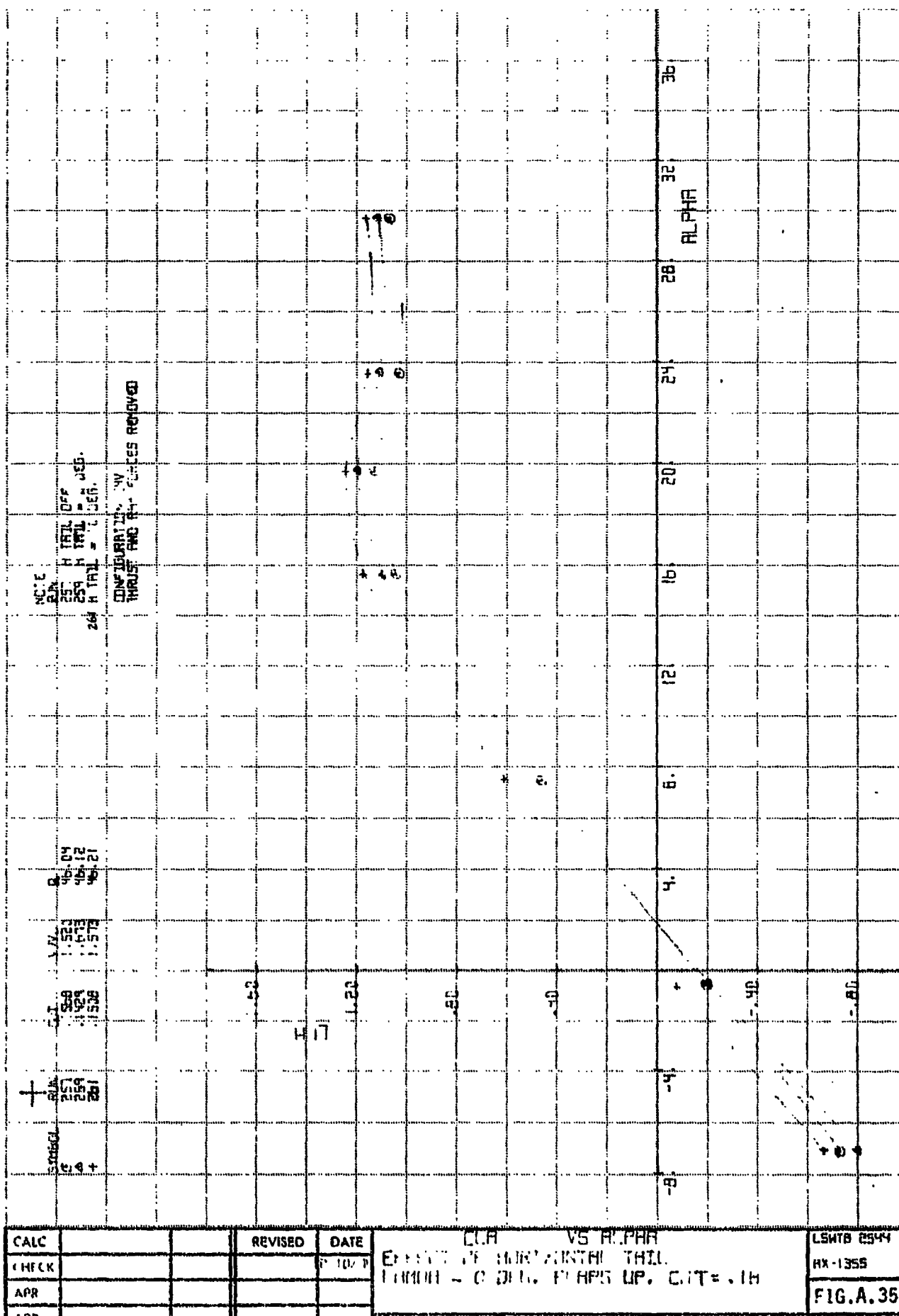
CLA VS COR  
EFFECT OF HORIZONTAL TAIL  
LMDR = 0 DEG. FLAPS UP. C/LT = 1.2

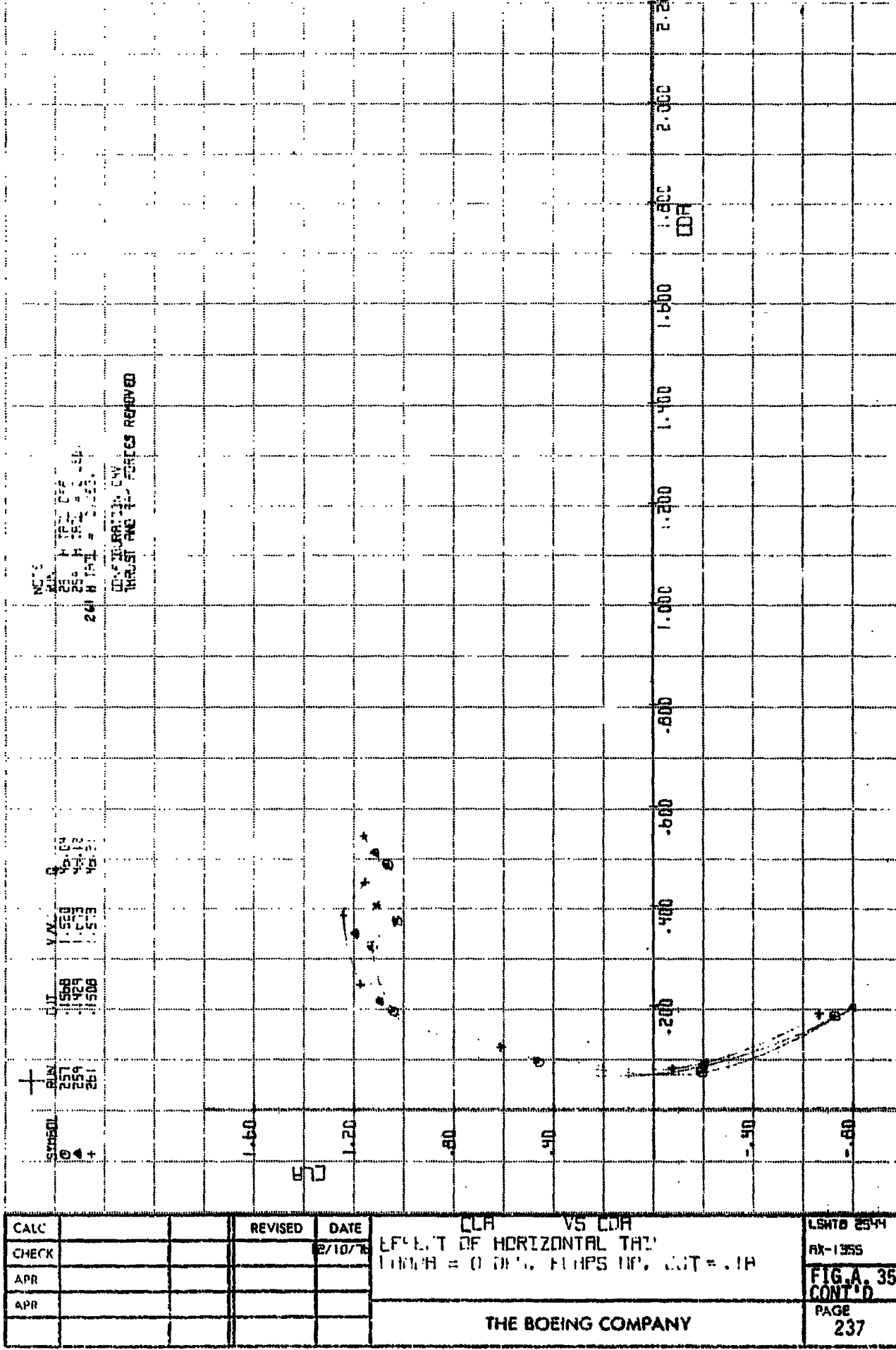
LSWTB 2544

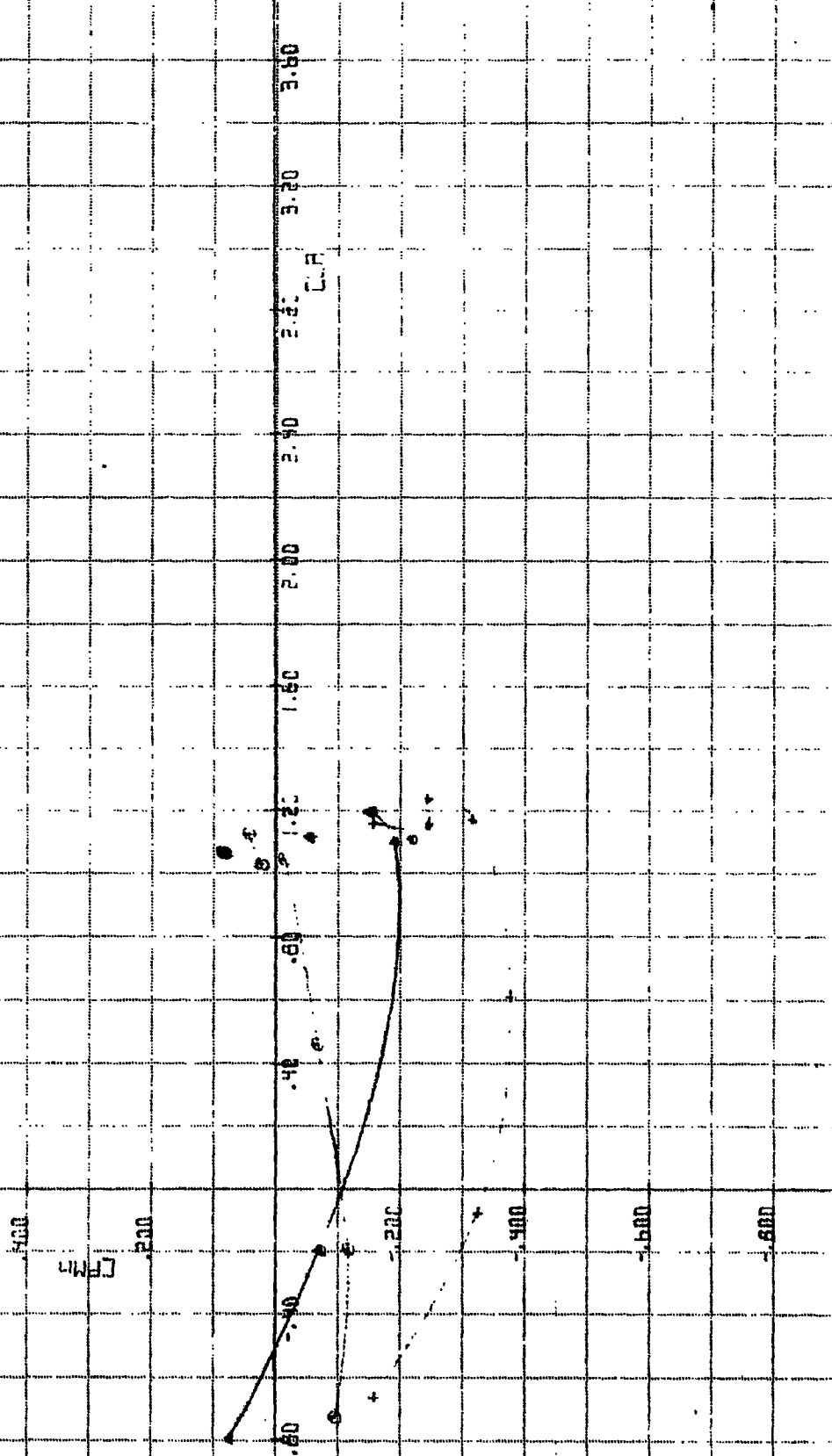
EX-1335

FIG. A. 34  
CONT'D

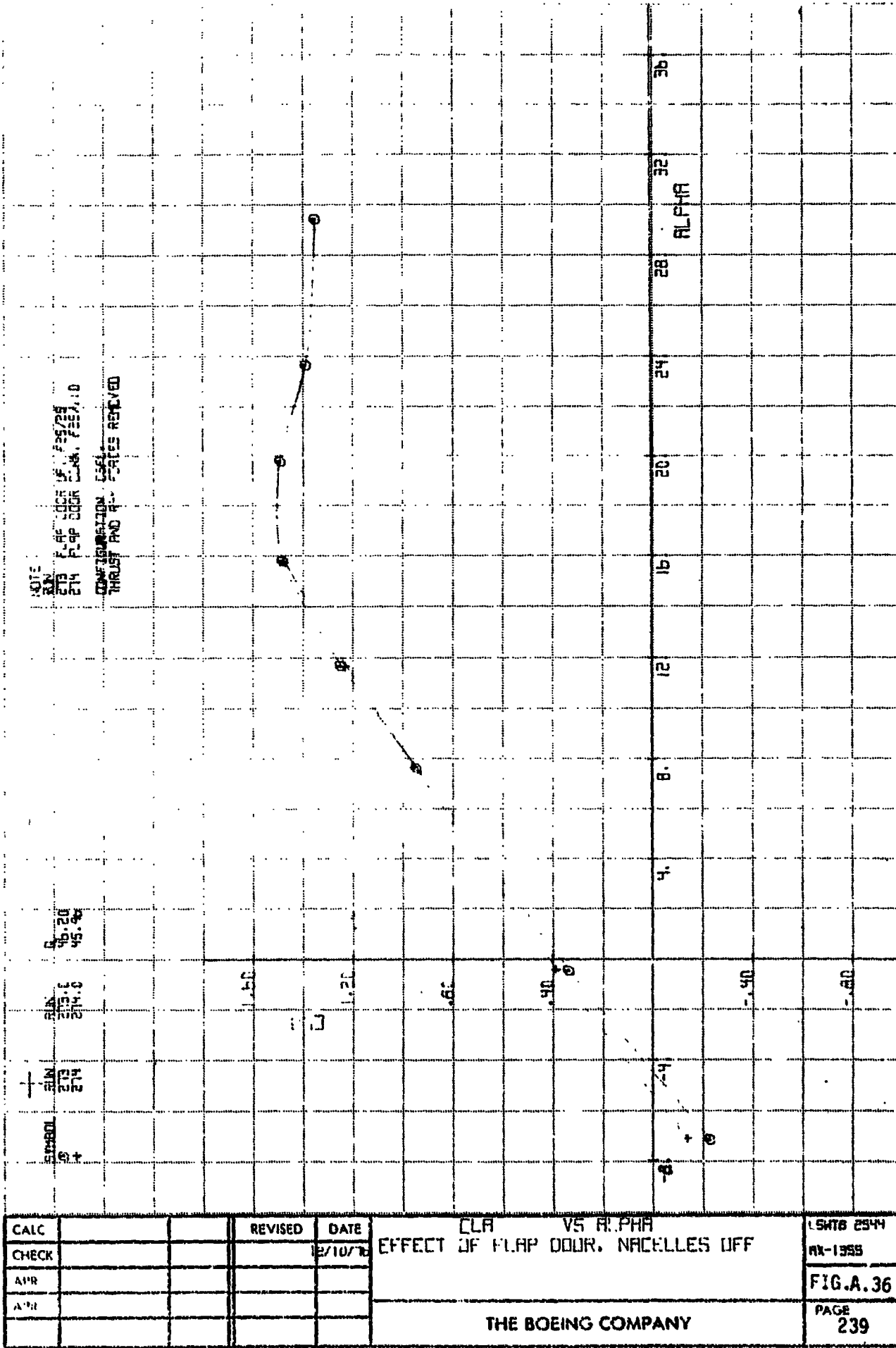








CALC			REVISED	DATE	CPMA VS CLA EFFECT OF HORIZONTAL TAIL LAMDA = 0 DEG. FLAPS UP. CJT = .18	LIGHT ESMH RX-1355 FIG.A.35 CONT'D
CHECK				12/10/76		
APR						
APR						
					THE BOEING COMPANY	PAGE 238



DATE 5/25/75  
 PAGE 1 OF 2  
 F-4E FLAP DOOR FORCES  
 COMPENSATION SECTION - CSEV  
 THRU RX-1355 FORCES RECEIVED

SUBMITTAL NO. 1  
 APPROVED BY  
 APPROVED BY  
 APPROVED BY  
 APPROVED BY

CALC			REVISED	DATE
CHECK				5/10/75
APR				
APR				

CLA VS TDA  
 EFFECT OF FLAP DOOR, NACELLES OFF

LSMTB 2E-1  
 RX-1355  
 FIG.A.36  
 CONT'D  
 PAGE 240

THE BOEING COMPANY

ORIGINAL PAGE IS  
OF POOR QUALITY



NOTE  
SIN CSV PROG FLEPS OF  
273 CSVL FAS/2E FLEPS QM.

THRUST AND THR FORCE REC, ET

SIN 273 273 273.0 273.0 273.0

1.61

LRB

12.1

5

5

5

5

5

5

5

5

1.000	.900	.800	.700	.600	.500	.400	.300	.200	.100	.000
1.000	.900	.800	.700	.600	.500	.400	.300	.200	.100	.000
1.000	.900	.800	.700	.600	.500	.400	.300	.200	.100	.000
1.000	.900	.800	.700	.600	.500	.400	.300	.200	.100	.000
1.000	.900	.800	.700	.600	.500	.400	.300	.200	.100	.000

CALC			REVISED	DATE
CHECK				12/10/78
APP				
App				

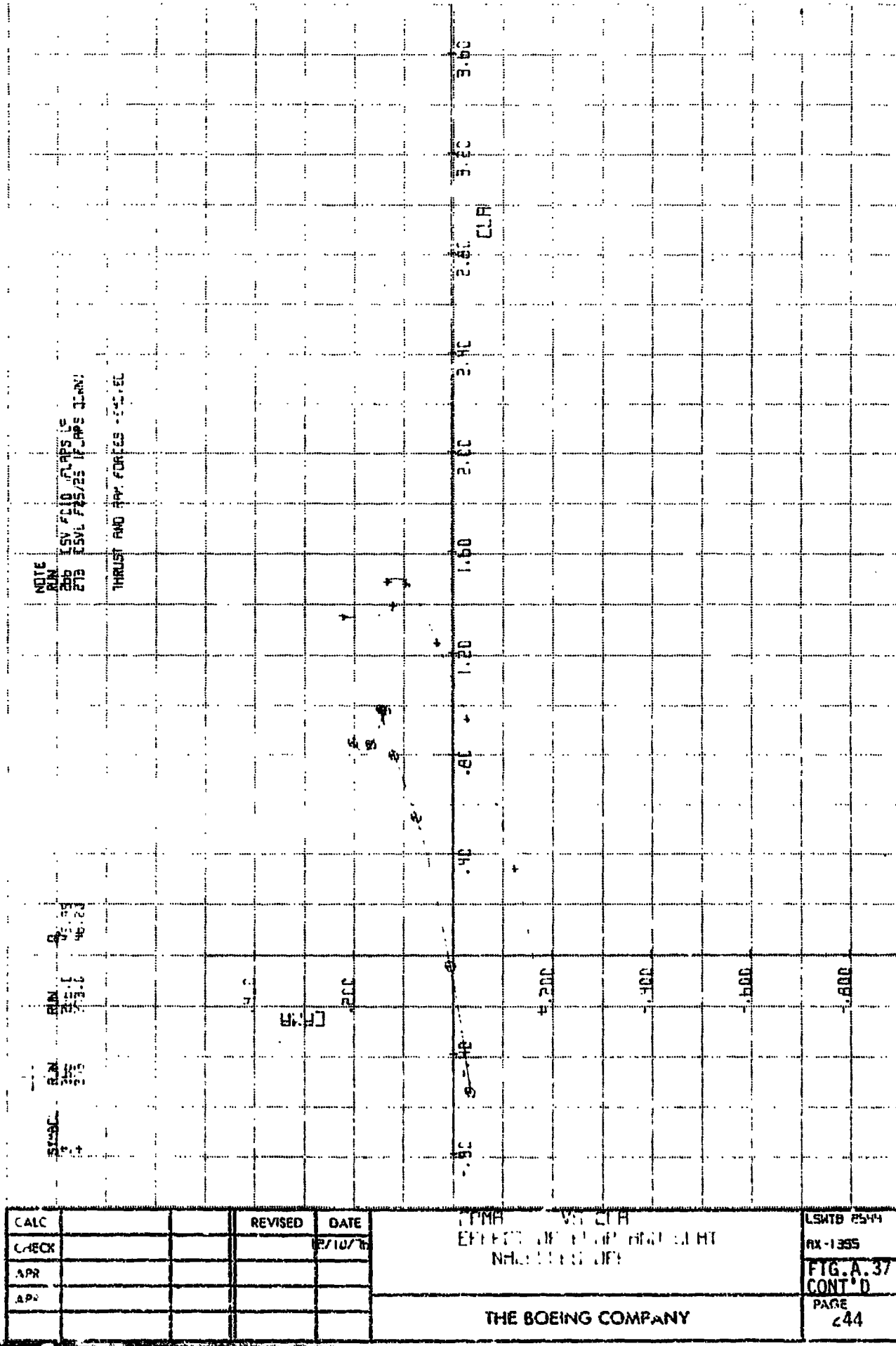
CH V3 LCR  
THT OF HLRP HNL WHT  
NHL LLL OFF

THE BOEING COMPANY

L5WTB 2544  
RX-1935  
FIG.A.37  
CONT'D  
PAGE  
243

NOTE  
B2N LSV F100 FLAPS LS  
273 TSVL F45/25 IF CAPS JAW

THRUST AND THR. FORCES - 70-111

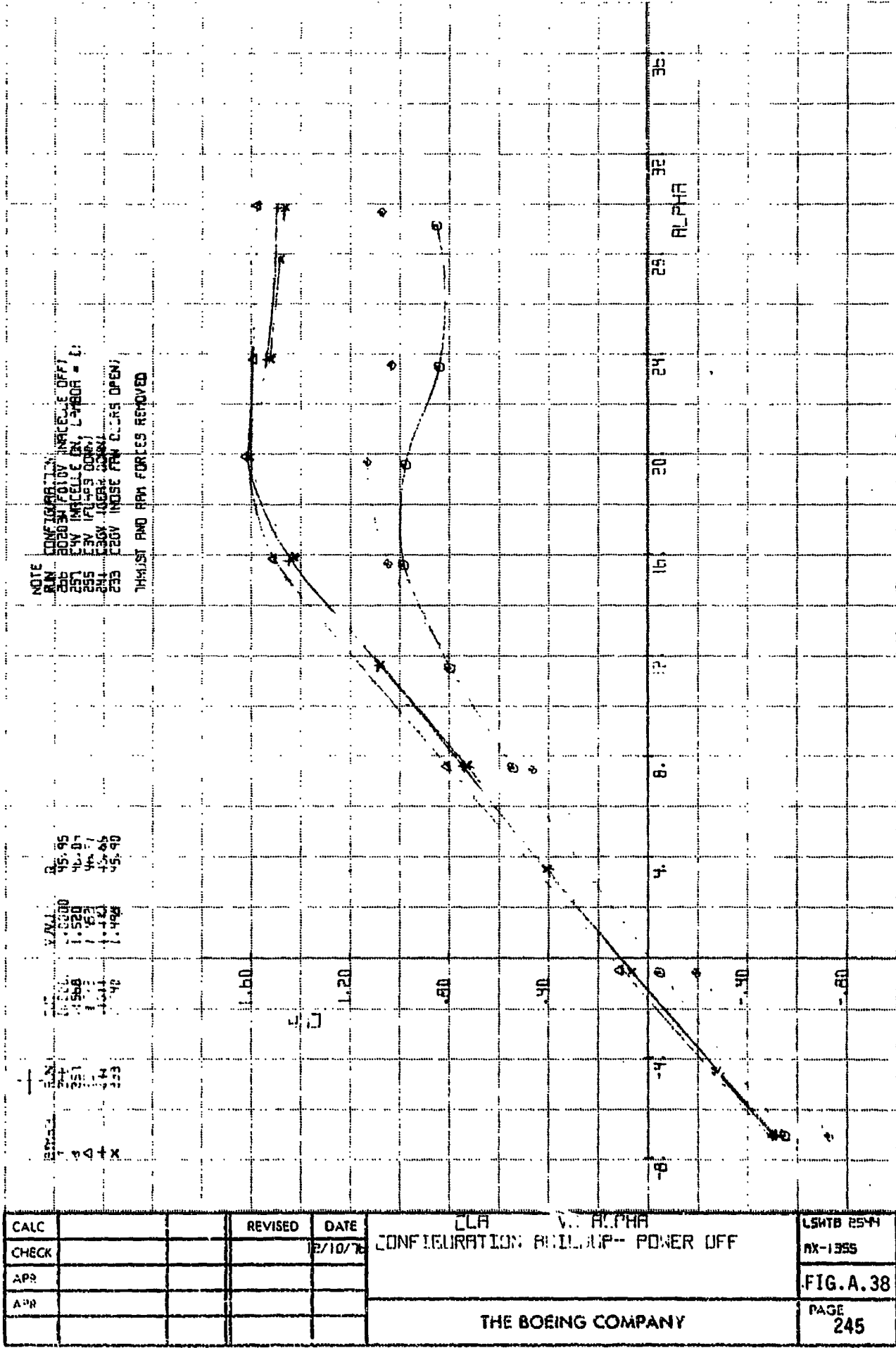


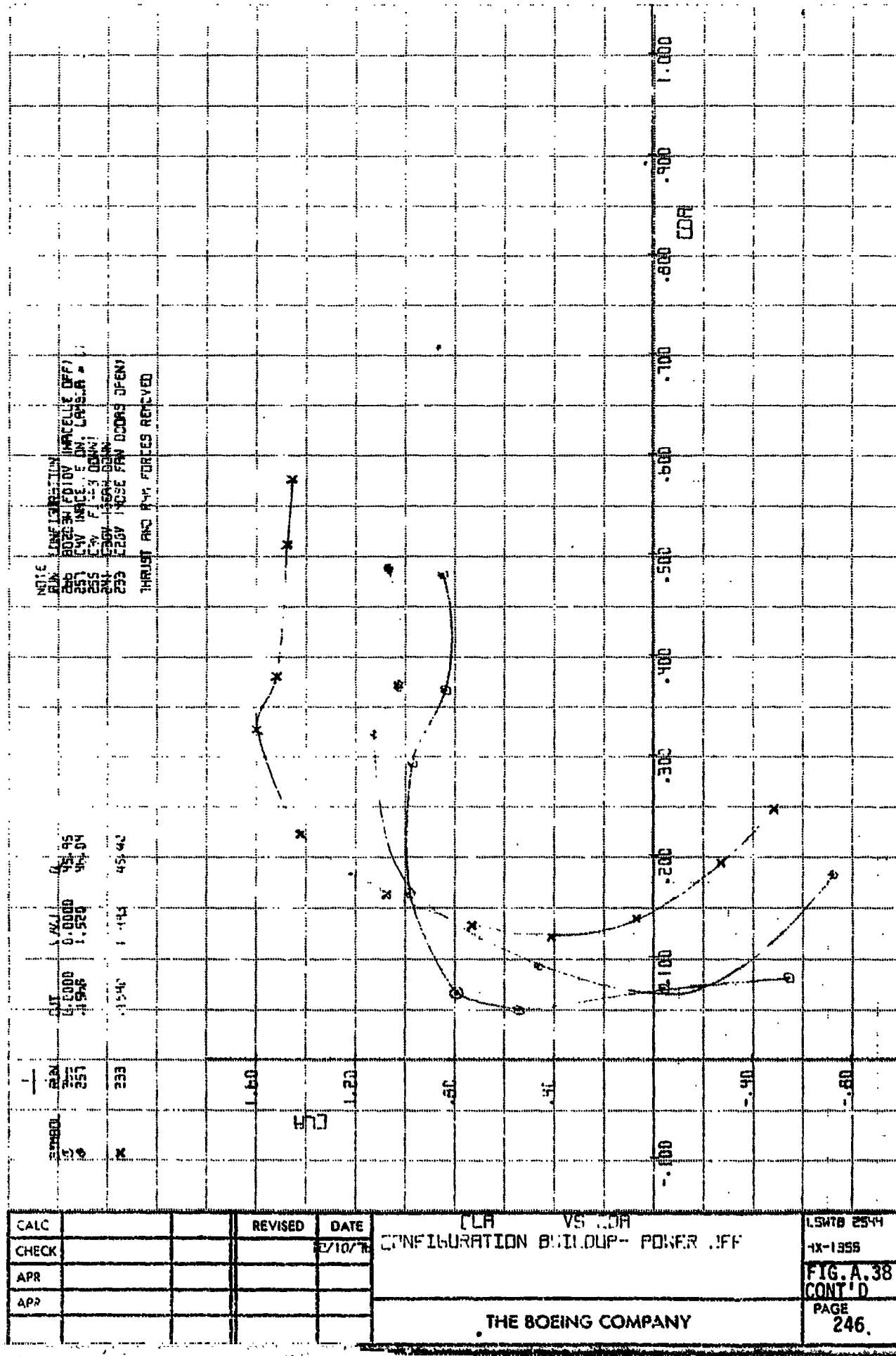
CALC			REVISED	DATE
CHECK				12/10/76
APR				
APR				

1FMH	VI 2TH	LSMTB 2544
EFFECTIVE WEIGHT OF AIRCRAFT		AX-1355
NMOL 1100000		FIG. A.37
		CONT'D

THE BOEING COMPANY

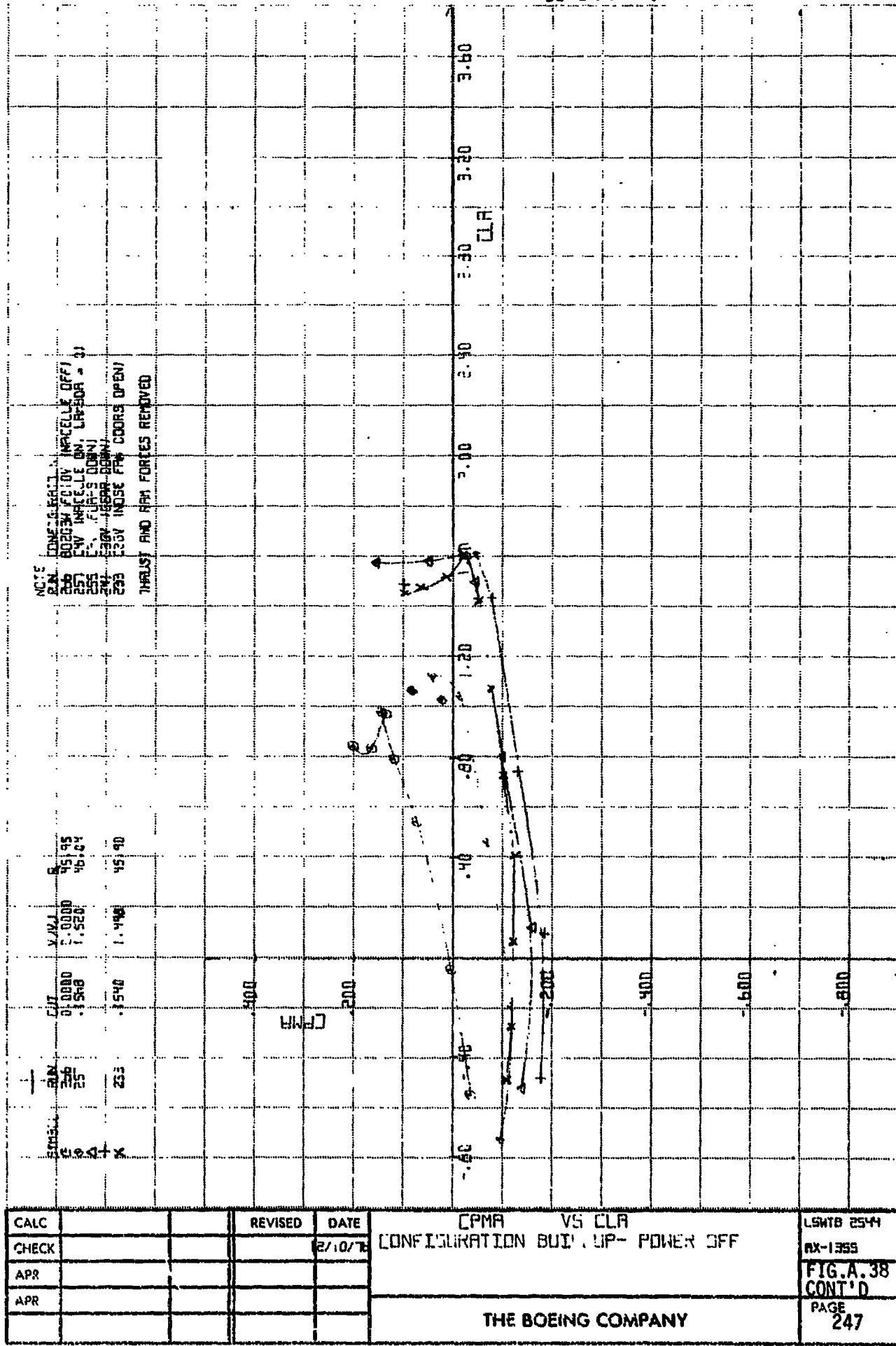
PAGE  
44





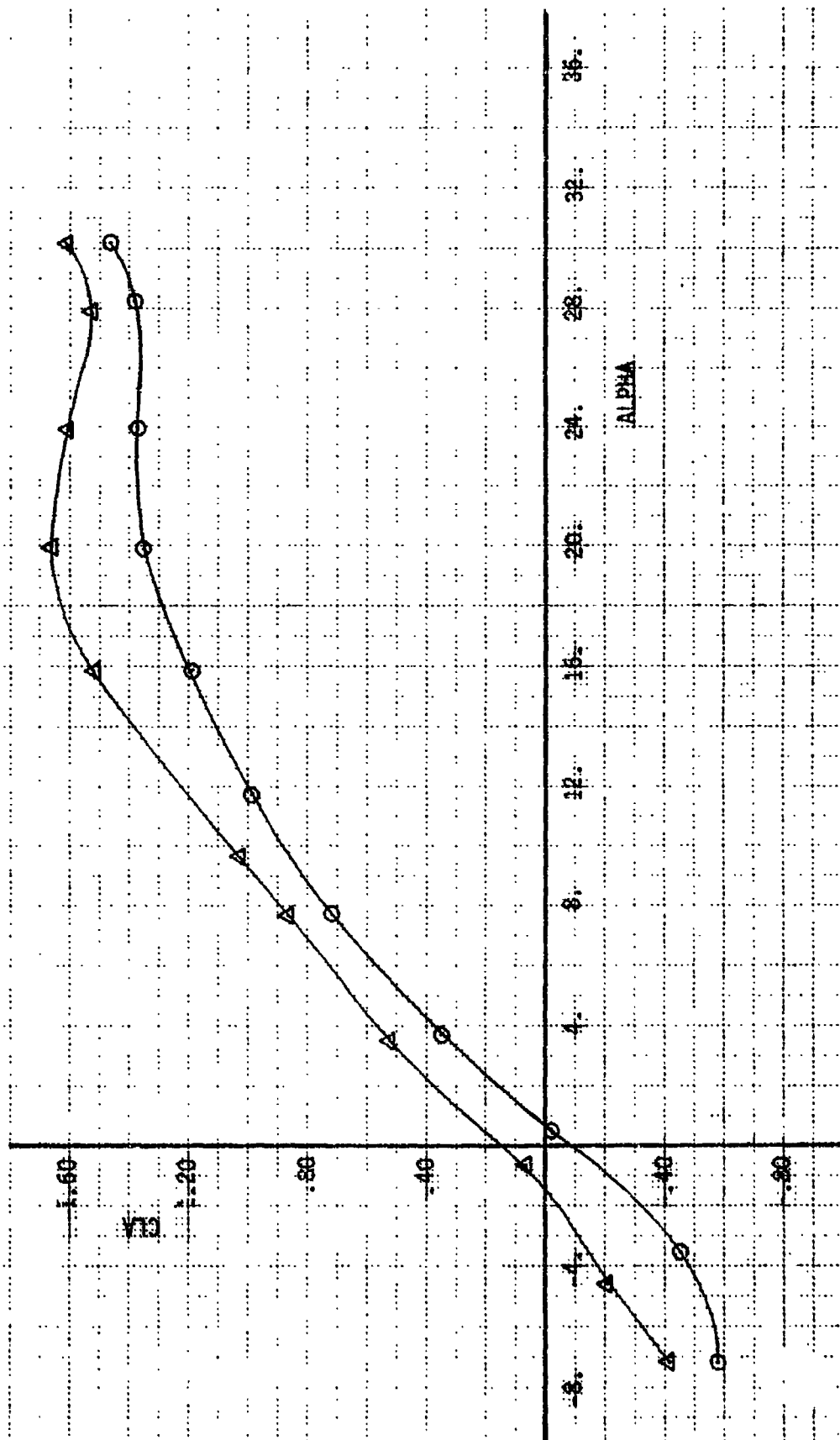
**THE BOEING COMPANY**

ORIGINAL PAGE IS  
OF POOR QUALITY



NOTE  
CONFIGURATION C2GV  
THRUST AND RAM FORCES REMOVED

SYMBOL	RUN	CIA	CJB	CJC	CJT	Q
O	229	.62	.61	.22	1.45	46.7
A	230	.64	.64	.06	1.28	45.6



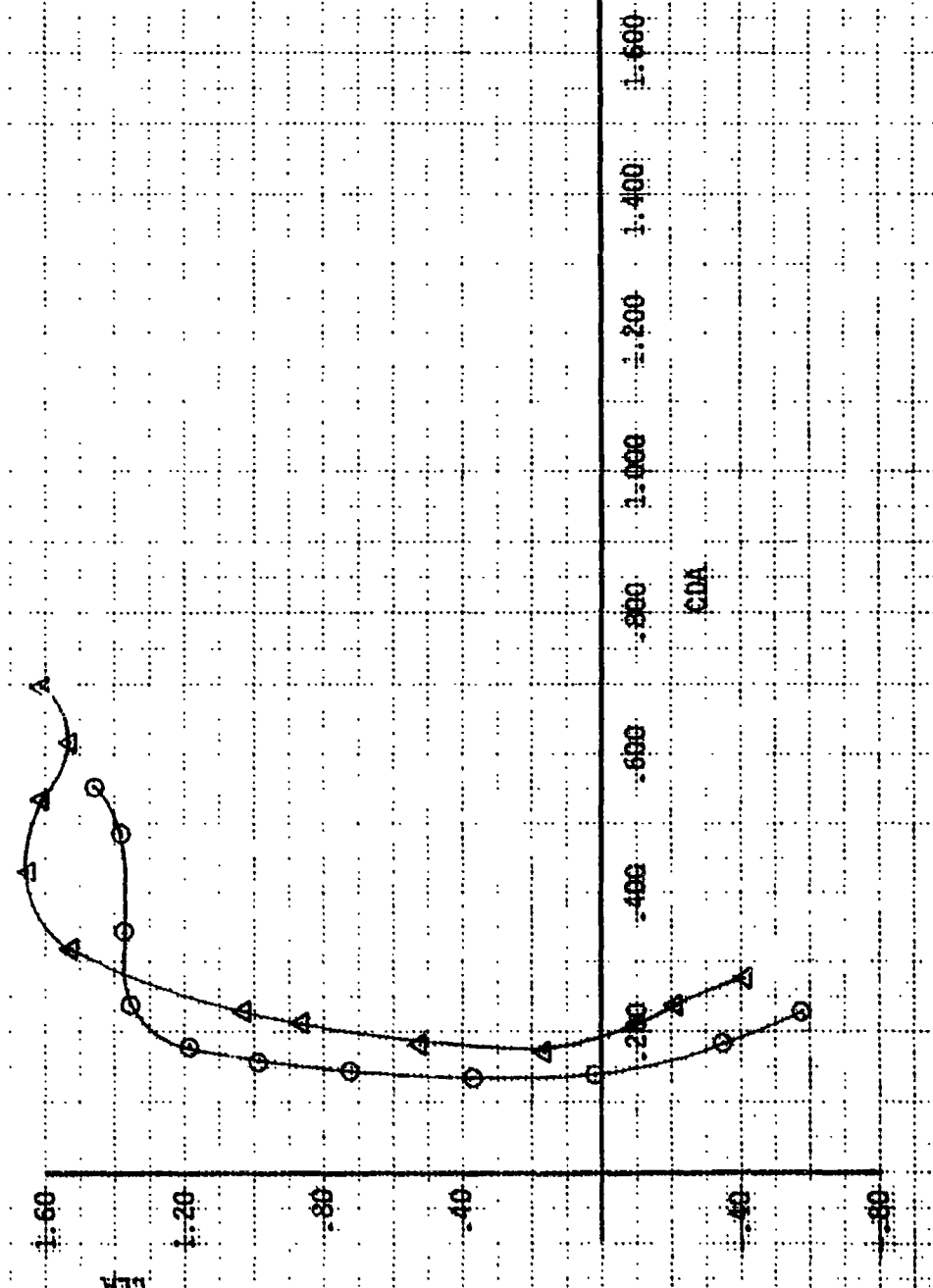
CALL	CHECK	REVISED	DATE	EFFECT OF NOSE FAN THRUST VARIATION LAMBDA = 0°, H. TAIL OFF	FIG. A.39
APR					
APR					

THE BOEING COMPANY

PAGE  
248

NOTE  
CONFIGURATION C2GY  
THRUST AND RAM FORCES REMOVED

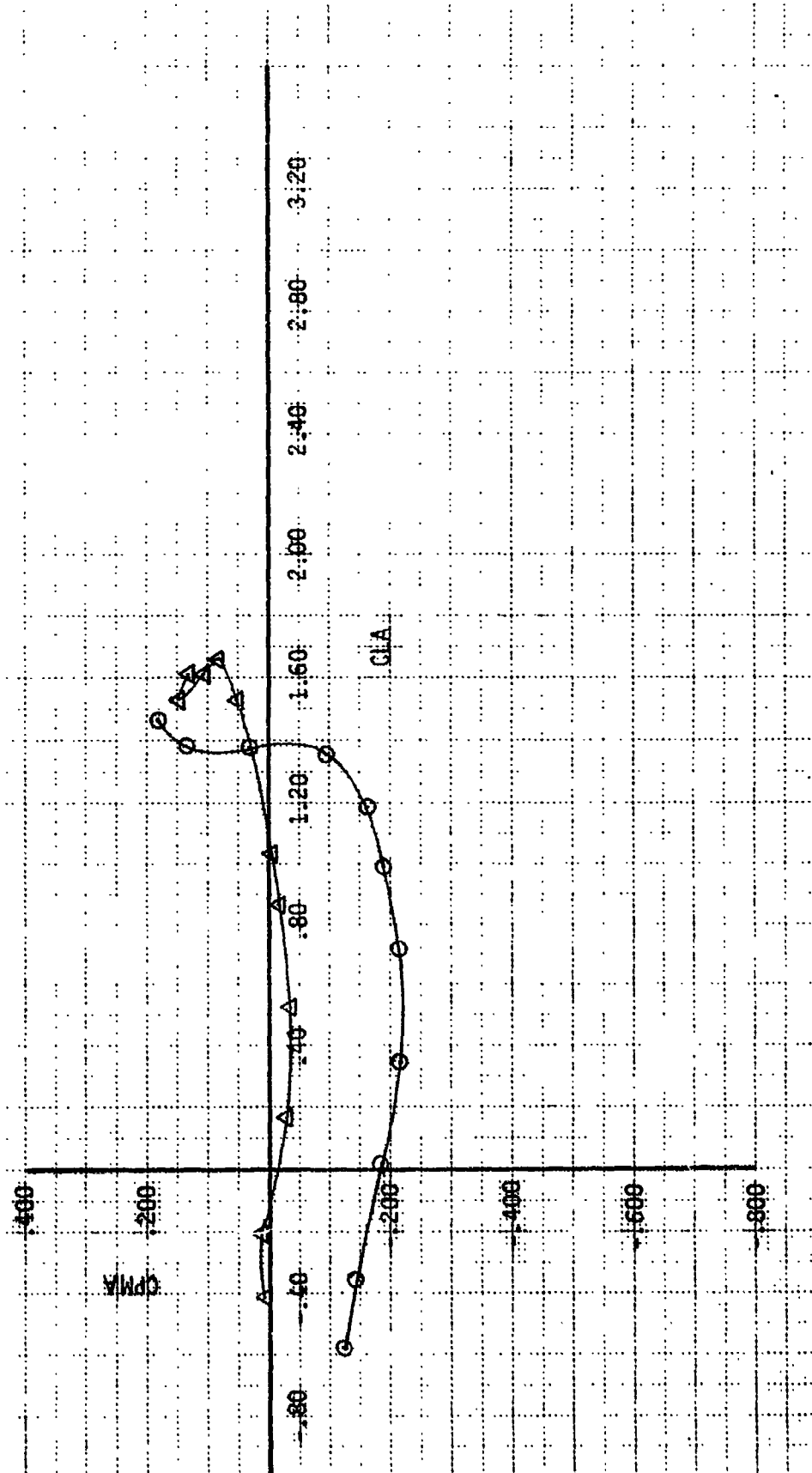
SYMBOL	RUN	CIA	CAB	LIC	CAT
O	229	.62	.61	.22	1.45 46.7
△	230	.64	.64	.00	1.28 45.6



CALL	REvised	DATE	EFFECT OF NOSE FAN THRUST VARIATION LAMBDA = 0°, H. TAIL OFF	FIG. A.39 CON'T
CHECK				
APP				
APP				PAGE 249

THE BOEING COMPANY

NOTE  
 CONFIGURATION 226Y  
 THRUST AND RAM FORCES REMOVED  
 SWING ROLL C/A CJB C/JT Q.  
 O 229 .62 .61 22 1.45 46.7  
 A 230 .64 .60 1.28 45.6



CALC		REVISED	DATE
CHECK			
APR			
APR			

THE BOEING COMPANY

FIG. A.39  
CON'T  
PAGE  
260

THE **BOEING** COMPANY

Appendix B  
THRUST CALIBRATION

THE BOEING COMPANY

Nomenclature for Appendix B

$A_{HI}$	Inlet Highlight Area
$A_{TH}$	Inlet Throat Area
$C_{VF}$	Fan Nozzle Velocity Coefficient
$C_{DF}$	Fan Nozzle Flow Coefficient
$C_{D2}$	Inlet Flow Coefficient
$T_G$ $\delta_{AMB}$	Corrected Gross Thrust
$M_{PR}$	Primary Mass Flow
$P_{\infty}, P_0$	FSC Chamber (Free Stream) Static Pressure
$P_{T2}$	Inlet Total Pressure
$P_{S2}$	Inlet Static Pressure
$P_{T3}$	Fan Nozzle Total Pressure
$P_{S3}$	Fan Nozzle Static Pressure
$P_{T4}, P_{TPR}$	Primary (Core) Nozzle Total Pressure
$P_{T5}$	Tip Turbine Discharge Total Pressure
$T_{TPR}$	Primary (Core) Nozzle Total Temperature
$\frac{RPM}{\theta_{AMB}}$	Corrected Speed
$V_{FS}$	Free Stream Velocity
$X_B$	Height of Distortion-Generating Blade Above Inlet Highlight

## APPENDIX B

### THRUST CALIBRATIONS

Thrust calibrations of the turbopowered simulators were conducted in the Boeing Flight Simulation Chamber (FSC), and with the simulators installed in the model during the static ground tests and during the wind tunnel test. The initial calibration conducted in the Flight Simulation Chamber provided the effects of nozzle back pressures above and below ambient pressure, thus simulating ground effects, nozzle back pressuring due to thrust vectoring in excess of 90° to the free stream, and ram conditions in forward flight. The trends obtained from this calibration were coupled with absolute levels obtained from in-place calibrations during the wind tunnel test. The FSC calibrations related the thrust, as measured by strain gauge balances, to: ideal thrust calculated from fan exit static and total pressure and total temperature; fan RPM; and fan tip-drive air supply pressure and temperature. During static tests the relationship of thrust versus RPM was used in determining thrust. Because of expected inlet total pressure distortion in the wind tunnel for certain combinations of inlet angles of attack, forward speed, and power setting, the thrust was determined from fan exhaust pressure and temperature measurements during wind tunnel tests. Thrust versus tip-drive supply pressure served as a back-up method of determining thrust.

#### Model Description

A schematic of the lift/cruise fan nacelle is shown in Figure B.1. The turbo-powered simulators were 14 cm (5.5 inches) Technology Development Inc. tip-turbine driven fans supplied by NASA for this test. The model scale was thus selected to fit the available fans. A fan map and a thrust calibration with ambient back pressure to the fan (zero convergence fan nozzle) were available from NASA CR-2051 (Reference 4). It was decided to operate the model fans at the pressure ratio of the "study" engine Allison PD370-16, a T701 derivative (Reference 8). Since thrust data were available only for zero fan back pressure, the nozzle area was set equal to fan flow area plus 2% allowance for boundary layer growth. The model scale was therefore defined by the square root of the ratio of model thrust produced at that exit area to full scale

THE **BOEING** COMPANY

thrust, with nozzle pressure ratios reproduced in the model.

External lines of lift-cruise nacelles were scaled from a drawing of the NASA V/STOL technology demonstrator (Reference 9) modified in a few areas as discussed below. The inlet was patterned after a 0.9 scale lift/cruise inlet model tested in support of the V/STOL program (Reference 10). The internal lines of the 0.9 scale model were non-axisymmetric, with the contraction ratio higher on the bottom of the inlet (with the nacelle in the forward thrust position). The 0.094 scale powered model, fabricated for the present test program, required about 20% less inlet area because of the tip turbine flow. The throat was therefore reduced to maintain the throat Mach number and thereby maintain the inlet's ability to operate at high angles of attack and low mass flows. The reduced throat area requirement of the model coupled with the scaled, large highlight allowed the selection of an axisymmetric inlet with a contraction ratio  $A_{HI}/A_{TH} = 2.0$  which exceeds that on the bottom of the non-axisymmetric full scale inlet (1.76). The coordinates of the powered lift/cruise model inlet are shown on Figure B.2. The outer wall of the fan nozzle of the lift/cruise nacelle was axisymmetric. The centerbody was designed with an elliptical cross-section assuming that the engine and airplane accessories would be distributed between the top and bottom of the core engine. This design reduces the internal nozzle curvatures and also provided a representative flow area in the vertical plane for thrust vectoring vanes. The fan duct was held at nearly constant area, increasing only 2% to the nozzle exit plane. The fan nozzle of the PD370-16 engine being simulated would be a variable area nozzle and actually divergent at low speeds. Thrust vectoring vanes were installed in the lift-cruise fan nozzle exits to provide yaw control when the nacelles are tilted  $90^{\circ}$  for lift production.

The primary nozzles of the lift/cruise engines had scaled exit areas and were slightly convergent, although the PD370-16 primary nozzle would be divergent. The model nozzle was supplied with high pressure air off the turbine air supply which was reduced to the required pressure through choke plates and screens.

The inlet of the nose fan was designed as a short non-axisymmetric bellmouth. The contraction ratio of the bellmouth varied from 1.76 on the forward part to 1.4 on the sides and aft portion. Figure B.3 shows several sections of the inlet. The nozzle of the nose fan was a cylindrical duct cut off at  $15^{\circ}$  to its axis. The fan hub was not faired out but left as a base in the nozzle exit plane. Like the lift/cruise fans, the nose fan was fitted with vanes for yaw control. A schematic of the model forebody is shown in Figure B.4. It should be noted that the upper half of the forebody was left on the fan simulator during calibrations in the flight simulation chamber.

The model nozzles were instrumented with total pressure rakes, static pressure taps and thermocouples to provide the required data to define their velocity and flow coefficients. The lift/cruise inlets were instrumented with static taps for flow calibration and one total pressure rake to detect inlet flow separation.

The schematics of the instrumentation are shown on Figure B.1 and depicted in Figure B.5. The outer probes in all fan nozzle rakes were placed in the tip turbine stream and manifolded together. The remaining probes were read individually on nacelle "B" and the nose fan "C", but manifolded by rake in nacelle "A". All statics were read individually.

#### Flight Simulation Chamber

A schematic of the Flight Simulation Chamber (FSC) is shown on Figure B.6. Air is drawn through the model into a stilling chamber, then through one or a set of critical flow venturis and finally exhausted to the atmosphere by an ejector. The model is mounted on a balance where thrust is measured. Airflow is measured by the Multiple Critical Flow Venturis (MCV). The chamber pressure may be maintained below ambient by proper selection of venturis and suction of the ejector, thus simulating the ram effect encountered in a wind tunnel or in flight. With powered models, the chamber may also be maintained at a pressure above ambient, simulating back pressurization due to ground proximity, jet interference, tailwind, etc.

A total pressure probe on an X-Y translating mechanism was mounted inside the FSC and used to survey the primary nozzle flow.

#### Test Procedure

Airflow through the FSC is a function of the selected venturi size and the total pressure within the chamber. The model was to be calibrated over a range of back pressures equivalent to speeds up to 77 meters/sec (150 knots), and over a range of power settings from near zero thrust to about 85% RPM. Data from Reference 4 indicated that the fan nozzle airflow at that RPM would be about 2.72 kg/sec (6 lb/sec). The test was therefore conducted by varying airflow from 2.72 kg/sec (6 lb/sec) to about 0.91 kg/sec (2 lb/sec) in 0.23 kg/sec (1/2 lb/sec) increments by installing appropriate multiple critical Venturi Combinations (MCV). At each MCV setting, fan RPM was varied over the required range to produce an FSC internal pressure from 5% below to 5% above ambient, corresponding to the ram effect at 82 meters/sec (160 knots). Generally, five back pressure levels were set:  $P_{FSC}/P_{ATMO} = .95, .975, 1.0, 1.025, 1.05$ . Occasionally, fan stall was encountered at higher back pressures and some test points were omitted. Generally, three scans of data were taken at each test point. A warmup run preceded data runs, because air at  $71^{\circ}\text{C}$  ( $160^{\circ}\text{F}$ ) was required to drive the tip-turbines and avoid icing of fan shroud, blade tips and stators.

#### Calibrations

Nacelle pressure instrumentation was routed out of the FSC to a bank of scannivalves and the output was recorded by the BTWT Astrodata System. FSC pressure measurements were routed directly to dedicated transducers. All pressure transducers and the entire electronic system were periodically calibrated by applying a pressure balanced by a deadweight tester to the transducer and comparing the output to the deadweight tester. Airflow measurements were made using calibrated Multiple Critical Flow Venturis (MCV's). The MCV's trace their calibration to the Colorado Engineering Experiment Station.

Thermocouples were compared to a standard thermometer prior to running, when the nacelle and chamber were at a steady temperature. The force measuring system included two balances, bellows to bridge the high pressure air supply to the metric side and pressure compensating bellows to reduce tare forces on the metric portion of the FSC. Balance calibrations were checked by hanging weights and bellows pressure tares were obtained by repeating balance calibrations with pressure applied to the bellows. Momentum tares as well as the proper operation of the pressure and flow measurement system were checked by running a known reference nozzle prior to installation of the model. The indicated flow coefficient of the known nozzle checks the FSC pressure, temperature and flow measuring system, while the indicated thrust coefficient provides the momentum tare, if any.

#### Velocity and Flow Coefficients

Equations for fan velocity coefficient, fan flow coefficient and inlet flow coefficient are given below, starting from averaged pressure measurements.

$$C_{VF} = \frac{F_{GTOT} - F_{PR}}{M_{TT}V_{ITT} + M_FV_{IF}} \quad B.1$$

where:

$F_{GTOT}$	= total thrust from balance
$F_{PR}$	= calculated primary thrust
$M_{TT}$	= tip turbine mass flow
$V_{ITT}$	= tip turbine ideal velocity = $f(P_{TTT}, P_0, T_{TTT})$
$M_F$	= fan mass flow
$V_{IF}$	= fan ideal velocity = $f(P_{TF}, P_0, T_{TF})$
$P_{TTT}, P_{T5}$	= average tip turbine exit total pressure (6 manifolded probes)
$T_{TTT}$	= tip turbine exit total temperature

- $T_{TF}$  = fan exit total temperature (average of 4)
- $P_{TF}, P_{T3}$  = average fan exit total pressure. For the nose fan and one L/C fan it is the area weighted average of 24 probes; for the other L/C fan it is the area weighted average of 6 rakes, each a manifold of 4 probes).
- $P_0, P_\infty$  = FSC chamber (freestream) static pressure

The primary thrust was obtained from a translating probe survey at the primary nozzle exit plane, from which the mass flow and thrust were calculated, and correlated with measured nozzle pressure ratio. The calculated mass flow of the primary was subtracted from the total measured supply flow to obtain the tip turbine flow. Subsequently, primary thrust was calculated by applying the above mass flow split to the measured supply flow and multiplying it by the ideal velocity based on measured primary total pressure and a velocity coefficient which relates the manifolded primary total pressure rake to the average pressure obtained by the survey.

$$F_{PR} = K_{PR} \times W_{MCV-2} \times V_{IPR} \times C_{VPR} \quad B.2$$

where:

- $K_{PR}$  = fraction of total supply flow to primary
- $W_{MCV-2}$  = total supply flow
- $V_{IPR}$  = ideal velocity =  $f(P_{TPR}, P_0, T_{TPR})$
- $C_{VPR}$  =  $\frac{V_{IPR}}{\text{ideal velocity based on probe survey of exit area}}$

The fan mass flow was measured as the difference of total mass flow drawn out of the FSC through its bank of critical flow Venturis and the total supply flow to the tip turbine and primary.

$$M_F = W_{MCV-4} - W_{MCV-2} \quad (\text{see Figure B.6}) \quad B.3$$

The fan flow coefficient was defined in an unusual manner due to the fact that the fan nozzle also passed the tip turbine flow, and because it was related to internal nozzle static pressure rather than ambient pressure. The tip turbine flow and the geometric area of the tip turbine including the fan shroud were excluded from the definition because the tip turbine flow could

be measured during the wind tunnel test. The average static pressure just inside the nozzle was used to extend the usefulness of the static flow coefficient to wind-on conditions where the nozzle exit plane is subjected to significant local pressure fields created by the airframe and ground proximity.

$$C_{DF} = M_F/M_{IF} \quad B.4$$

where:

$$M_{IF} = f(P_{TF}, P_{SF}, T_{TF}, A_F)$$

$P_{SF}$  = average fan nozzle exit static pressure  
(L/C fans: 4 taps, nose fan: 6 taps)

$A_F$  = flow area from rotor hub to fan shroud

The fan duct and nozzle were designed at a constant area equal to the fan exit area, plus 2% for boundary layer growth. Thus, using the fan rotor flow area was equivalent to using the fan nozzle exit area less the tip turbine and shroud area.

The third coefficient calculated was an inlet flow coefficient.

$$C_{D2} = M_F/M_{I2} \quad B.5$$

where:

$M_{I2}$  = ideal inlet flow =  $f(P_{T2}, P_{S2}, T_{T2}, A_2)$

$P_{T2}$  = inlet total pressure = atmospheric pressure

$P_{S2}$  = inlet static pressure (average of 4 taps)

$T_{T2}$  = inlet total temperature

$A_2$  = geometric flow area in the plane of the static pressure taps

### Results

Velocity coefficients and flow coefficients for lift/cruise fans "A" and "B" and lift fan "C" with yaw vanes set at  $0^\circ$  as determined in the flight simulation chamber are shown on Figures B.7-B.12. The data are plotted vs. fan total pressure ratio rather than the more common fan nozzle total to ambient

static pressure ratio. This was done because, in fan powered models, nozzle coefficients are strongly affected by fan power setting and back pressure ratio ( $P_{T2}/P_{S3}$ ) through their effect on total pressure distribution at the nozzle charging station. The data trends in Figures B.7-B.12 were subsequently used to calculate gross thrust and ram drag from pressure and temperature measurements in the wind tunnel. A correction to the velocity coefficients was applied based on results of in-place calibrations in the tunnel using the model internal balance.

Velocity and flow coefficient curves for back pressures above inlet pressure ( $P_{T2}/P_{S3} < 1.0$ ) often drop or rise steeply at low fan power settings, see Figures B.7 to B.12. This is due to fan stall and the ensuing increase in  $P_{T3}$  distortion. When distortion increases, the calculated average total pressure  $P_{T3}$  may be biased above or below the true effective total pressure.

Inlet distortion generated by a sharp blade across one inlet is shown on Figure B.13. The blade was positioned such that its upper edge was 2.34 cm (.92") above the inlet highlight. The inlet rake was completely in the wake of the blade, showing a recovery of .85. This inlet distortion produced a fan exit total pressure distortion as shown on the lower half of the Figure B.13, where data with and without the blade are compared. This distortion produces a variation in the calculated flow coefficient and velocity coefficient as shown on Figure B.14. The data show that if inlet separation occurs in the wind tunnel at high nacelle angles of attack, thrust and air-flow calculated from coefficients obtained without distortion may be in error by several percent.

Actual distortion measured during the wind tunnel test for fan "B" (lift/cruise fan) and fan "C" (lift fan) are shown on Figures B.15 to B.25. Nose fan data is shown on Figure B.15 to B.19 for forward speeds up to 62 m/sec at high fan power settings. In most cases, the distortion level is well below the level produced during the FSC calibration. At 62 m/sec, distortion is comparable. Thus, at high nose fan power settings as would occur in conjunction with lift/cruise nacelle tilt angles near 90°, the nose fan distortion is within acceptable limits for thrust calculation within a few percent.

Figure B.19 shows nose distortion at a low power setting, statically and at 62 m/sec. Although no inlet separation is indicated, distortion again is high in the exit, producing exit velocity variations of about 3:1. In addition, exit static pressure variation was seen at low power settings, causing large changes in computed mass flow relative to the static case. These effects probably produce significant errors in predicted thrust.

Lift/cruise fan total pressure distortion is shown on Figure B.20 to B.25. For a tilt angle of 90° at 62 m/sec (120 knots), distortion greatly exceeds levels tested during the FSC calibration at all airflows. Although this condition is not part of the flight profile, it is representative of lower flight speeds and power settings resulting in a similar value  $C_J$  and inlet velocity ratio. At lower flight speeds and nacelle tilt angles of 50° and 0°, the distortion is acceptable from the standpoint of thrust calculation accuracy.

Primary nozzle total pressure surveys using a translating probe were integrated to produce average total pressure from which flow and thrust were calculated. The survey results were related to a manifolded rake. Thrust and flow coefficients were then calculated for use with manifold pressure data. The results for primary nozzles "A" and "B" are tabulated below:

Nozzle	A	B	Remarks
$C_V$	.950	.968	
$C_D$	.950	.968	(based on ambient static)
$C_D$	1.40	1.43	(based on nozzle internal static pressure)

Fan nozzle total pressure profiles measured by six rakes with 4 probes each were fairly flat. An example for fan "B" at a fan total pressure ratio near 1.14 is shown as the "without blade" case in Figure B.13.

The inlets of fans "A" and "B" were calibrated for airflow. Figure B.26 presents an inlet flow coefficient defined as the ratio of actual airflow to theoretical airflow which is based on measured inlet static pressure, temperature and flow area. The coefficient was approximately 0.905 for both inlets.

For reduction of the static ground test data, thrust was related to fan RPM due to difficulties with pressure instrumentation. The relationship of thrust and fan RPM used is shown in Figure B.27. It was determined from an in-place calibration using the model internal balance to measure thrust. The fans were run individually with the model fan out of ground effects (ground height = 1.8 meters (72 inches) and the lift/cruise fans tilted to 90°. The calibration was not extended to low RPM in that the reliability of the indicated RPM deteriorates considerably at low RPM. The static tests were all conducted at or near 28,000 RPM.

During the wind tunnel testing the difficulties with the fan exit pressure instrumentation were rectified and an in-place calibration was conducted to relate thrust to fan exit instrumentation as had been done in the flight simulation chamber. The in-place calibration indicated that the thrust measured was lower than the calculated thrust based upon the flight simulation chamber coefficients. Fans "A" and "B" were consistently 2% low while fan "C" was 4% low. Thus the flight simulation chamber calibration results were adjusted accordingly for calculating thrust during the wind tunnel testing.

ORIGINAL PAGE IS  
OF POOR QUALITY

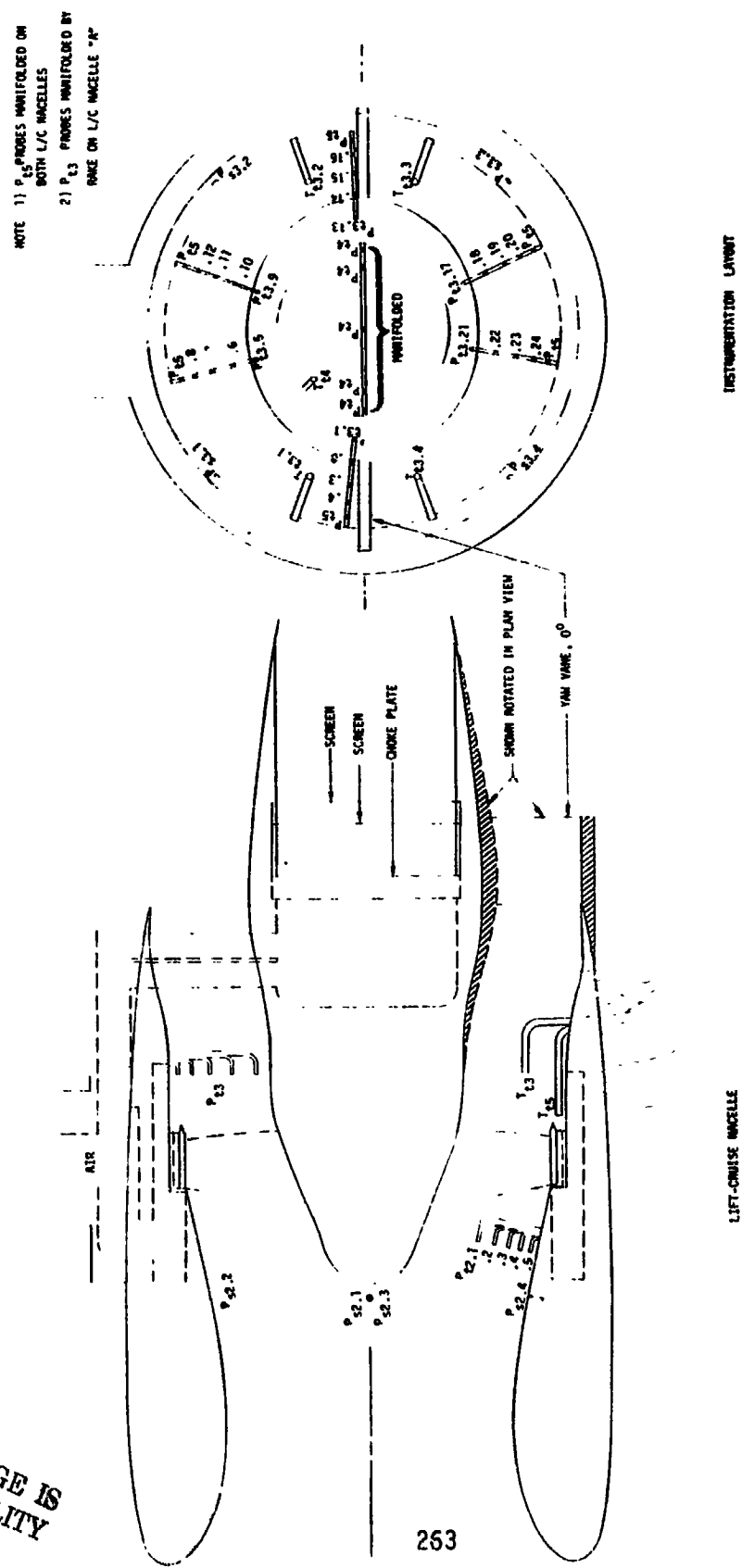


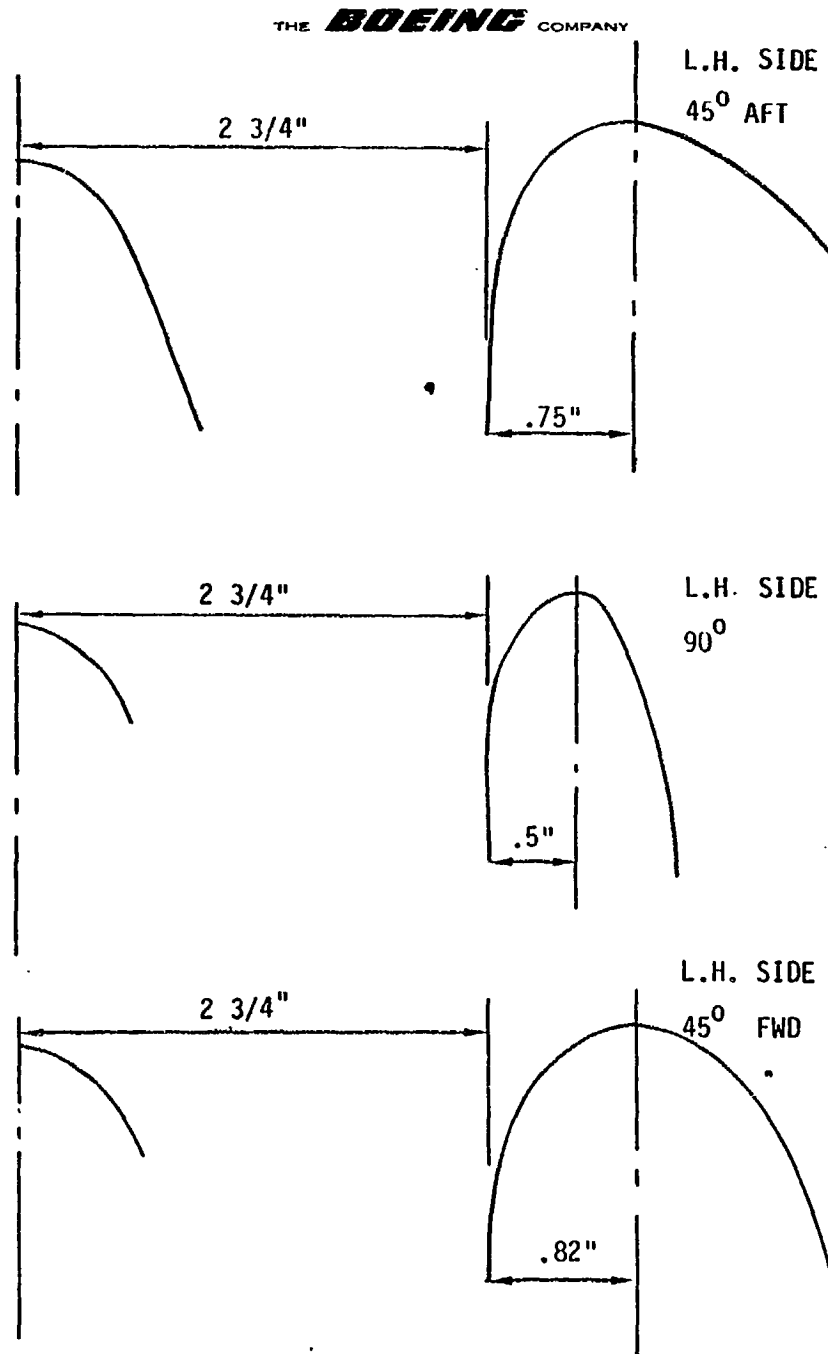
FIGURE B.1 LIFT-CRUISE FAN NACELLE MODEL

## LIFT/CRUISE INLET COORDINATES

(SEE FIG B.1 FOR INLET LINES)

	OUTSIDE		INSIDE	
	STATION INCHES	RADIUS INCHES	STATION INCHES	RADIUS INCHES
HILITc →	0	3.0818	0	3.818
	.0068	3.1465		
	.0223	3.1969	.0083	3.0022
	.0942	3.3038	.0271	2.9396
	.1457	3.3453	.0520	2.8837
	.2228	3.3897	.1145	2.7893
	.3000	3.4214	.1770	2.7173
	.3771	3.4461	.2707	2.6328
	.4542	3.4651	.3643	2.5643
	.6084	3.4951	.4581	2.5058
	.7627	3.5195	.5518	2.4592
	.9169	3.5407	.7391	2.3720
	1.0712	3.5594	.9266	2.3670
	1.2255	3.5760	1.1139	2.2563
	1.3797	3.5907	1.0314	2.2176
	1.5340	3.6030	1.4889	2.1894
	1.6882	3.6154	1.6762	2.1709
	1.8425	3.6256	1.8637	2.1613
	1.9967	3.6344	THROAT → 2.0510	2.1599
	2.1510	3.6419	2.2385	2.1606
	2.3052	3.6486	2.4258	2.1676
	2.6137	3.6576	2.6133	2.1815
	2.9222	3.6625	2.8006	2.2014
MAX	3.1239	3.6634	3.1754 3.5502 3.7954	2.2265 2.2887 2.3614

FIGURE B.2 LIFT/CRUISE NACELLE INLET COORDINATES



**CONTRACTION RATIOS (AHI/ATH)**

CENTER, FWD	AHI/ATH = 1.76 (AS DRAWN IN FIGURE B.4)
L.H. SIDE $45^{\circ}$ FWD	" " = 1.69
" $90^{\circ}$	" " = 1.40
" $45^{\circ}$ AFT	" " = 1.62

**FIGURE B.3 MODEL NOSE FAN INLET CONTOURS**

THE BOEING COMPANY

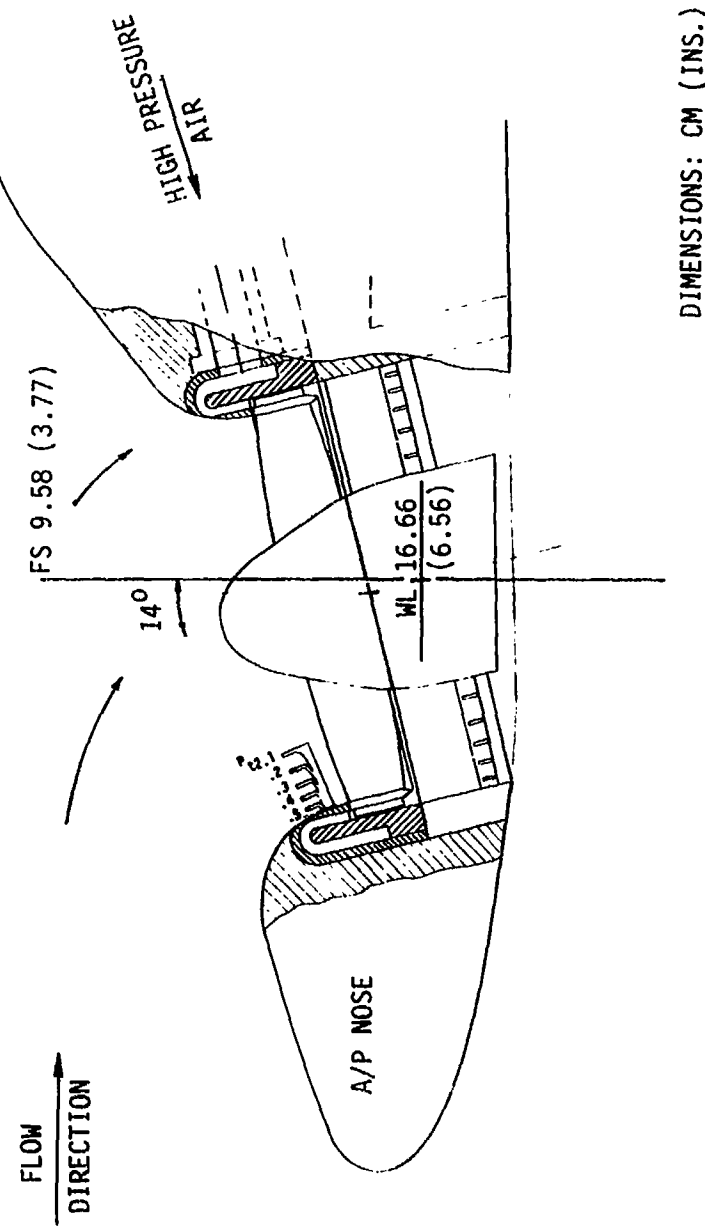


FIGURE B.4 NOSE FAN ASSEMBLY

ORIGINAL PAGE IS  
OF POOR QUALITY

FIGURE B.5 - INSTRUMENTATION OF LIFT CRUISE PAN NOZZLES



THE BOEING COMPANY

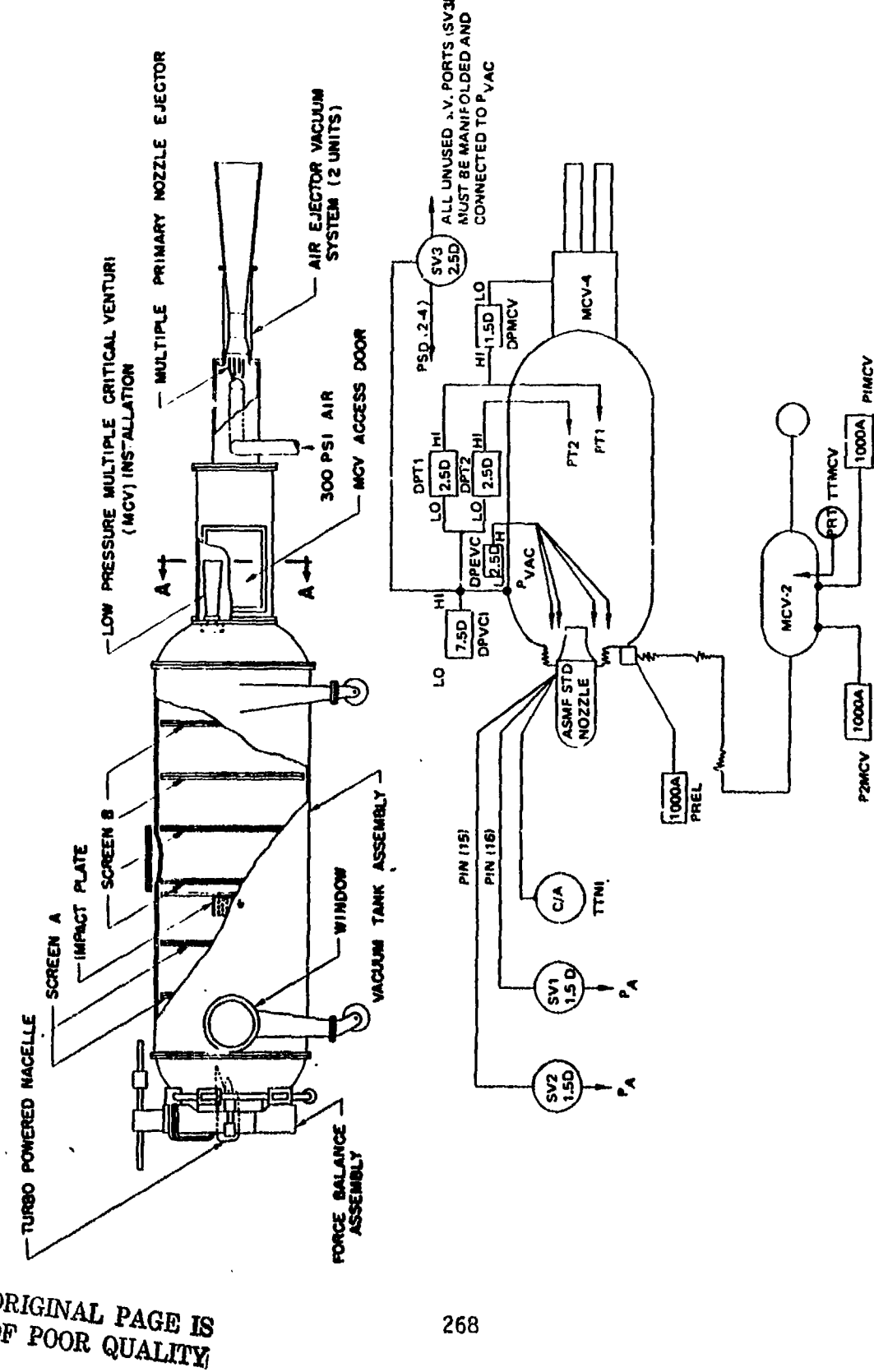


FIGURE B.6 FLIGHT SIMULATION CHAMBER

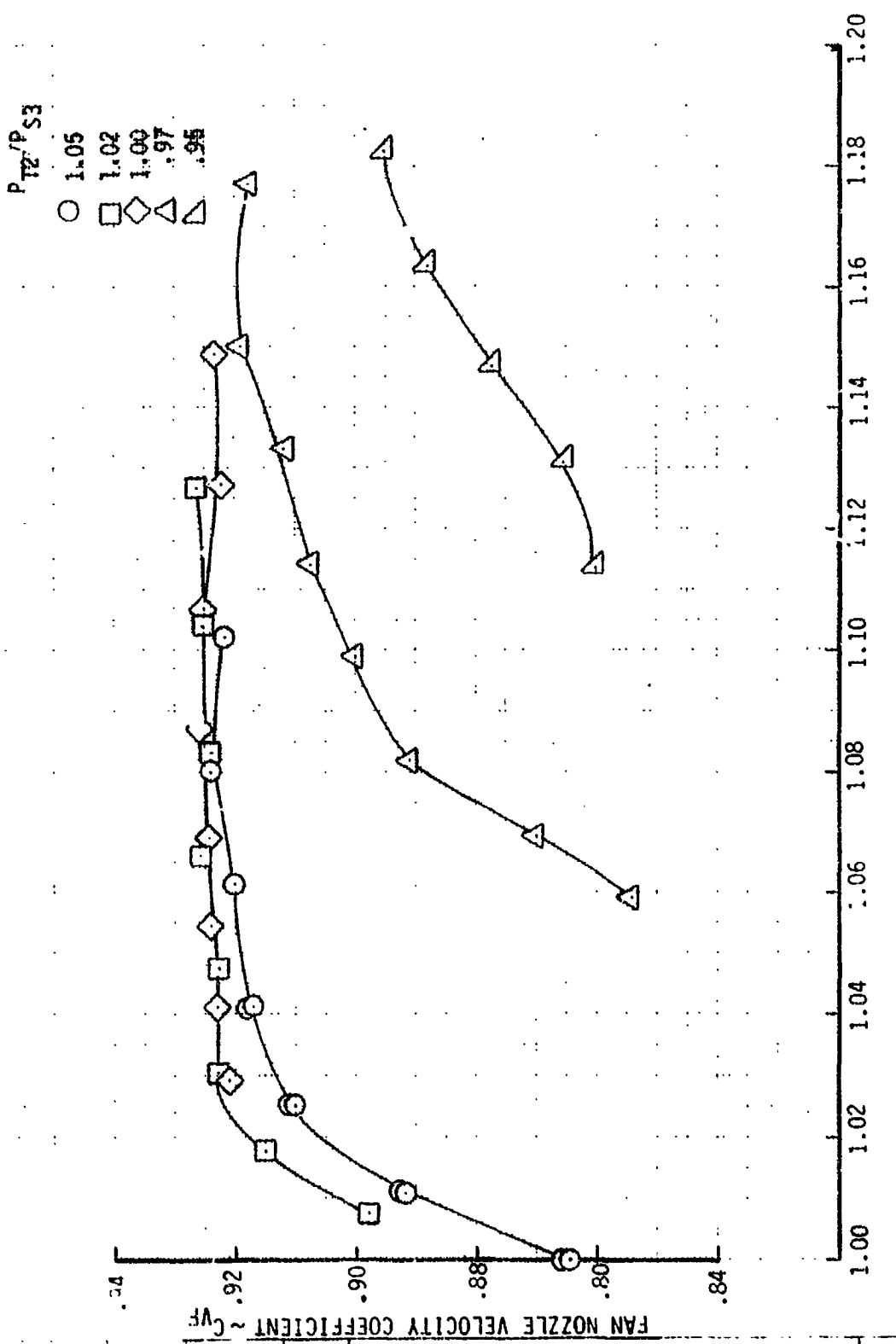
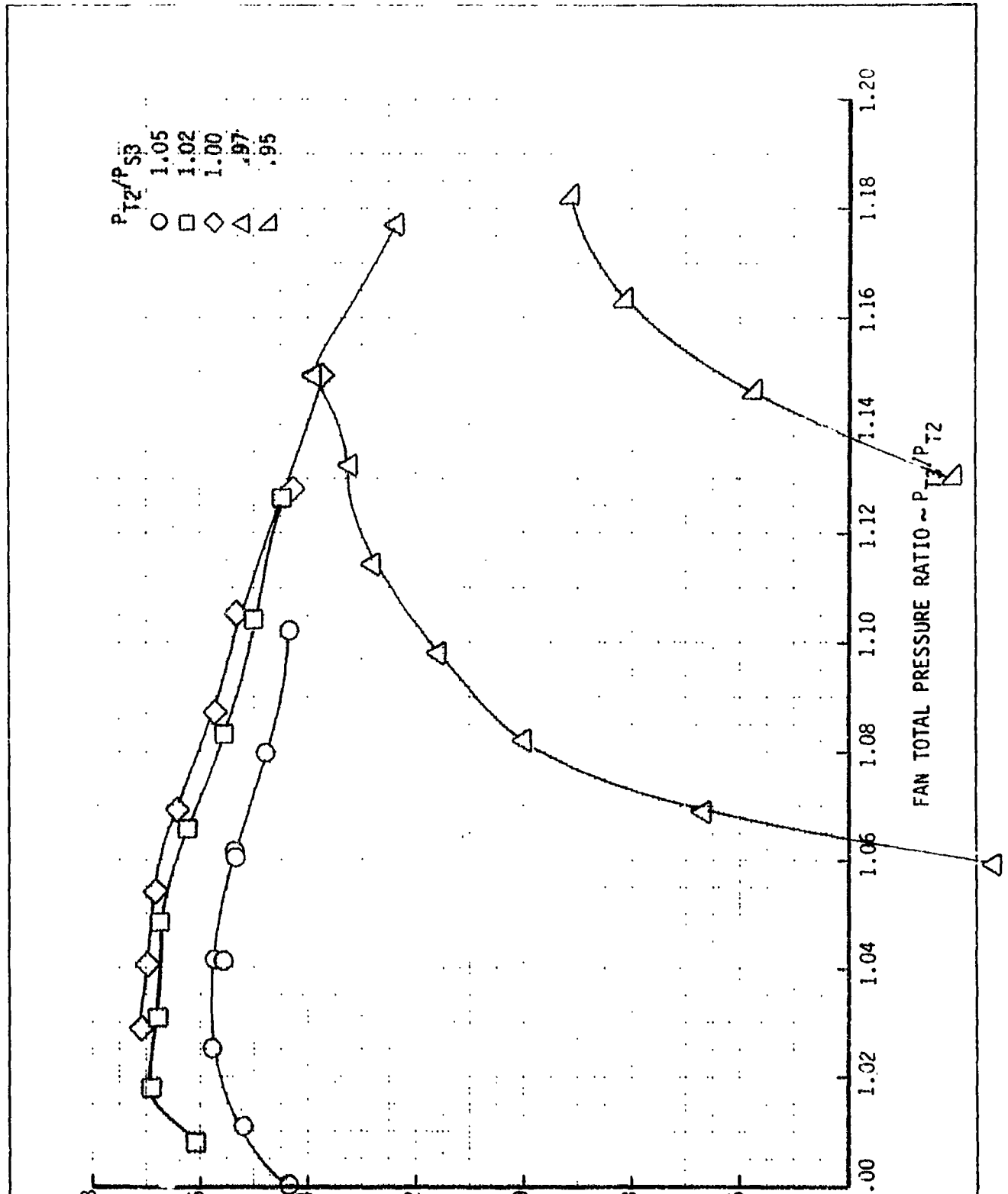
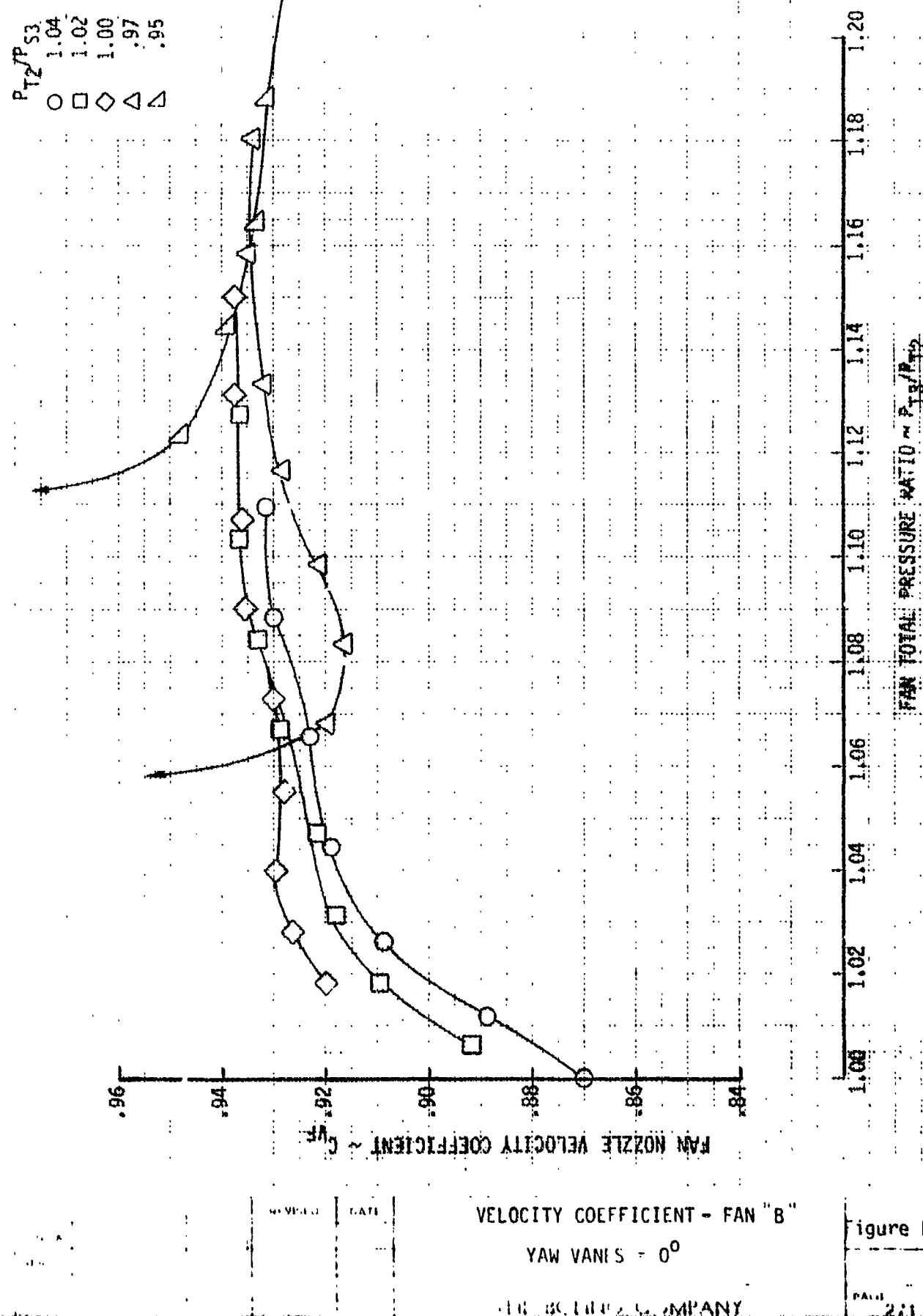
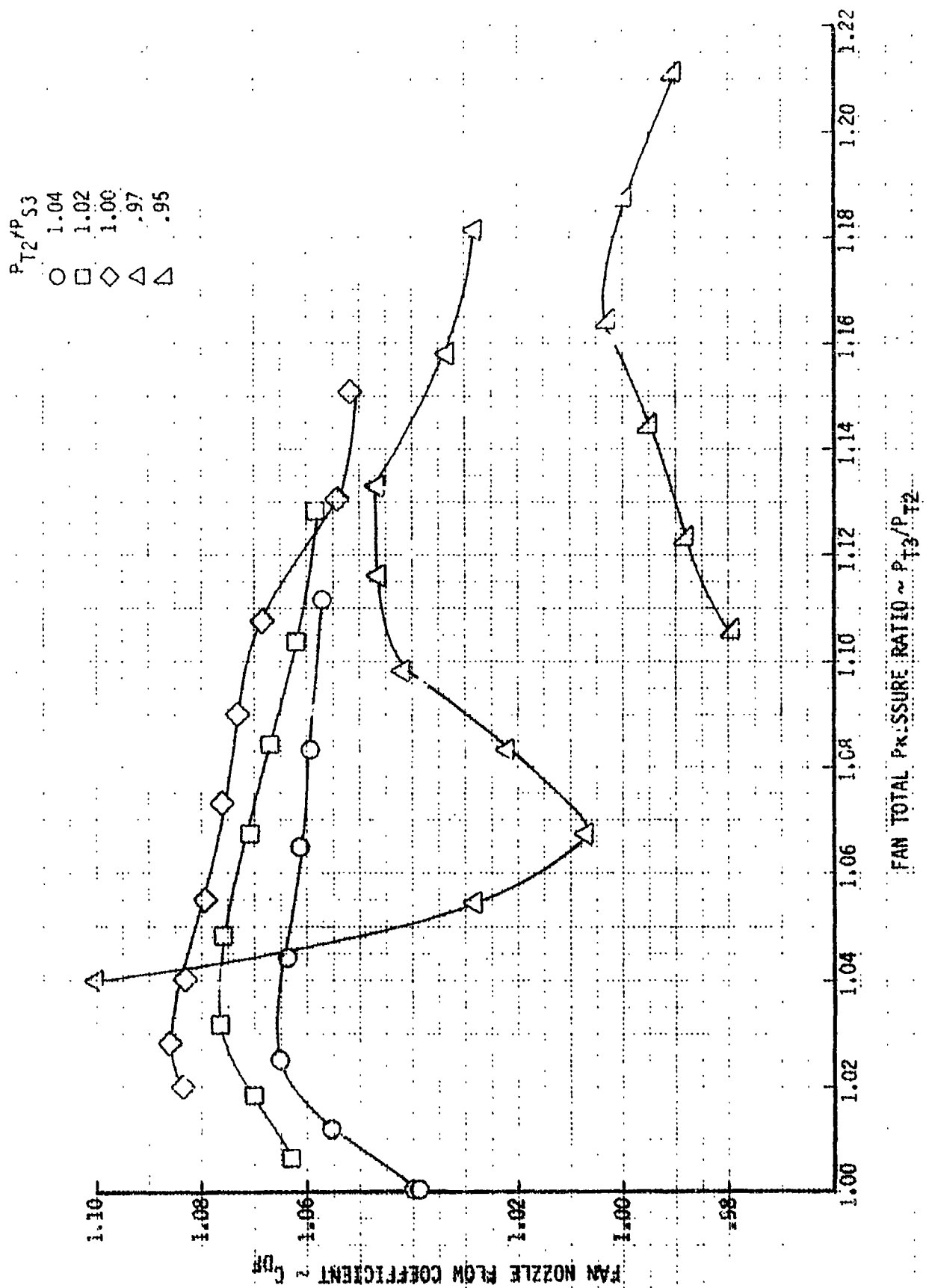


Figure B.7



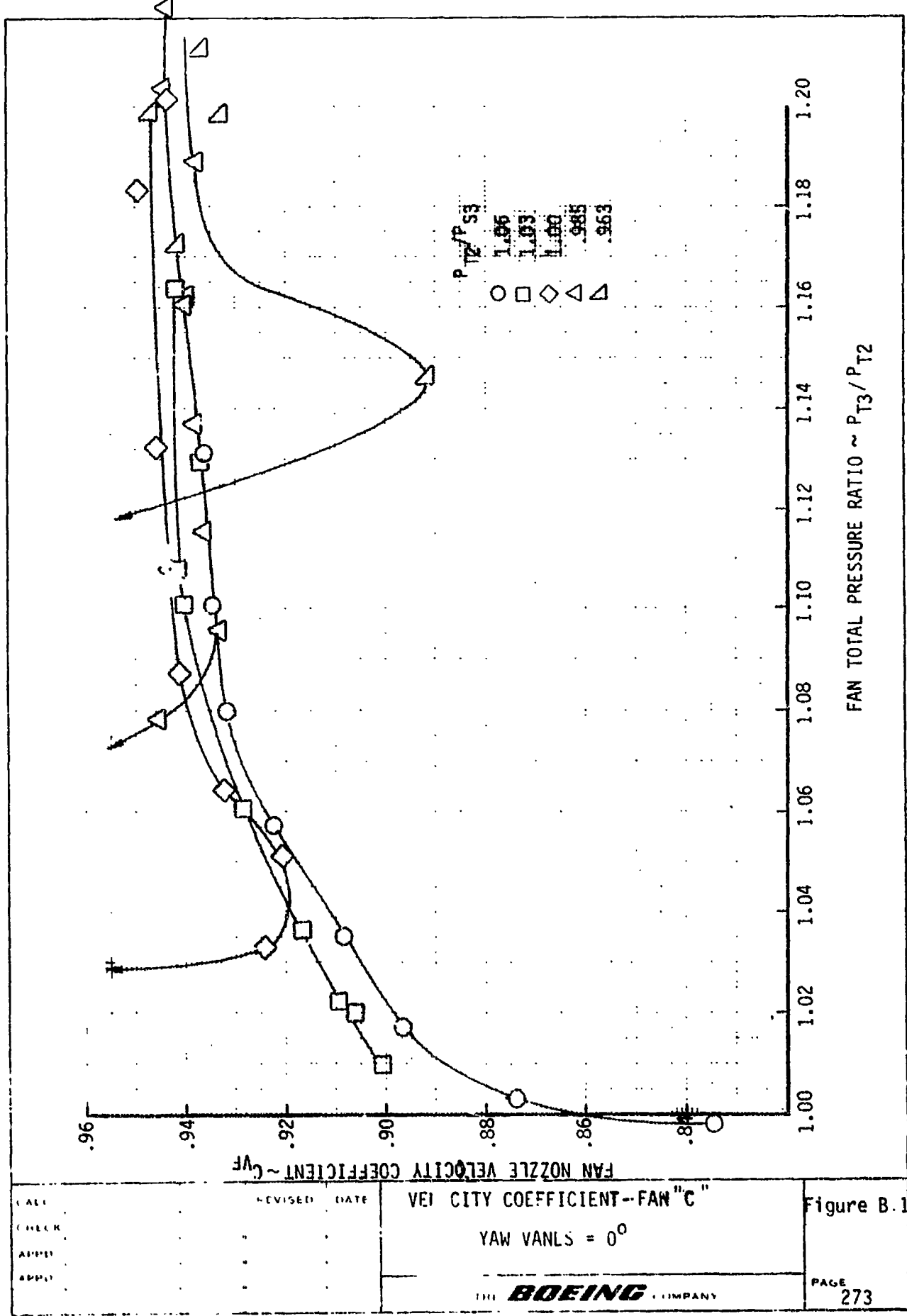
CALL	REvised	DATE	FLOW COEFFICIENT FAN "A"	Figure B.8
1000				
APRIL				
APRIL				
APRIL				
			YAW VANE = 0°	
			BOEING COMPANY	PAGE 270





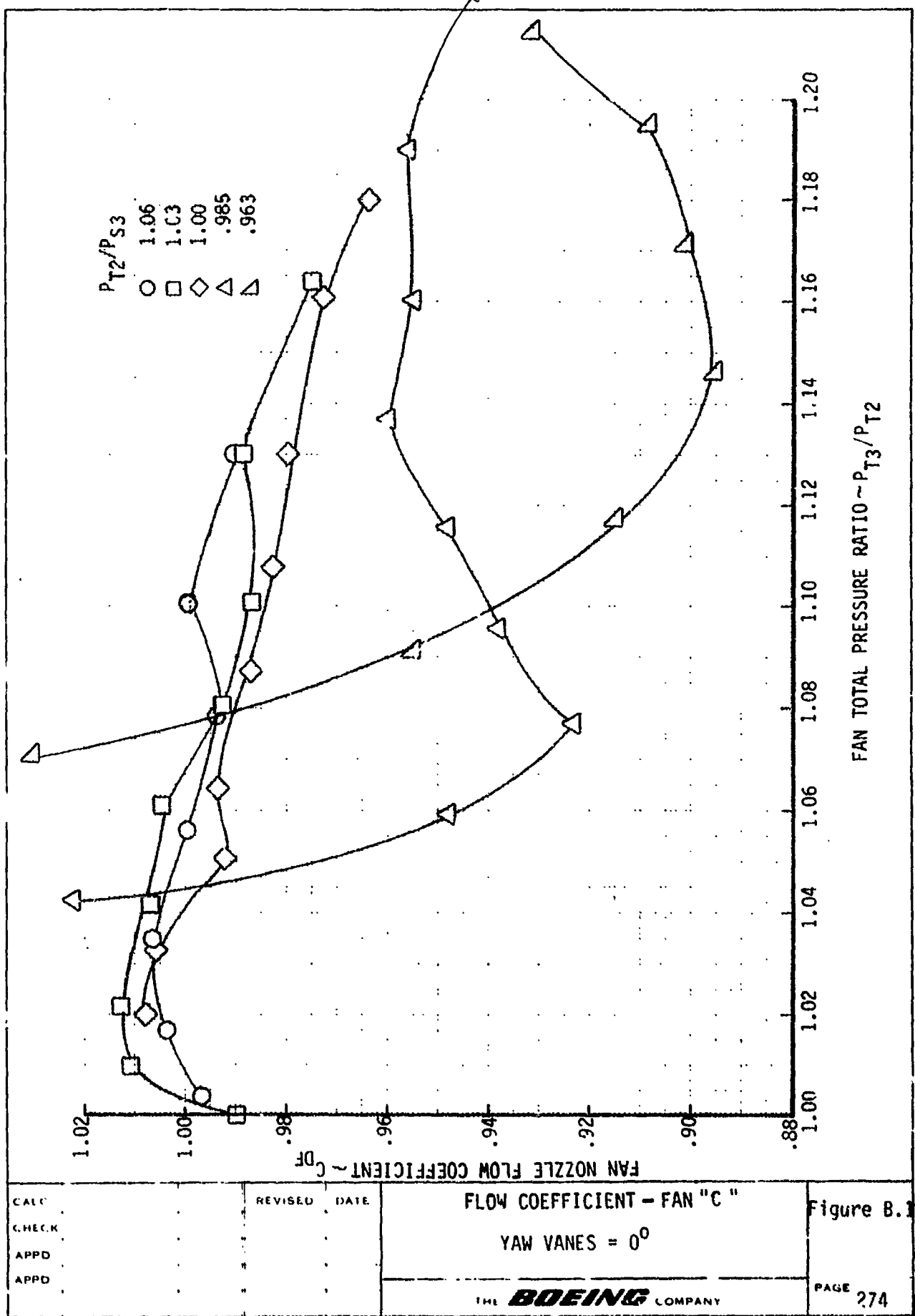
THE BUTLER COMPANY

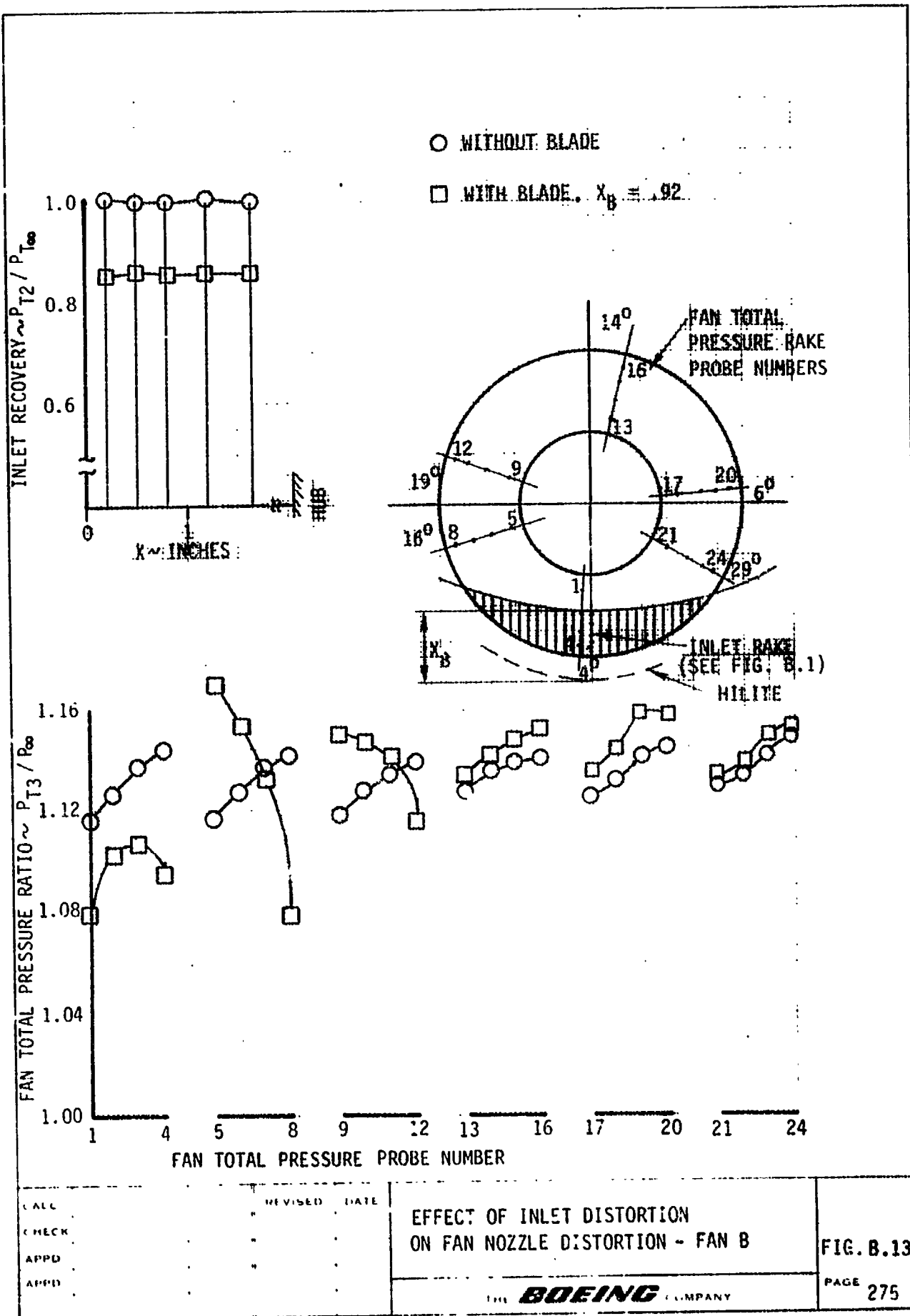
Figure B.10



FAN TOTAL PRESSURE RATIO ~  $P_{T2} / P_{T3}$

Figure B.11





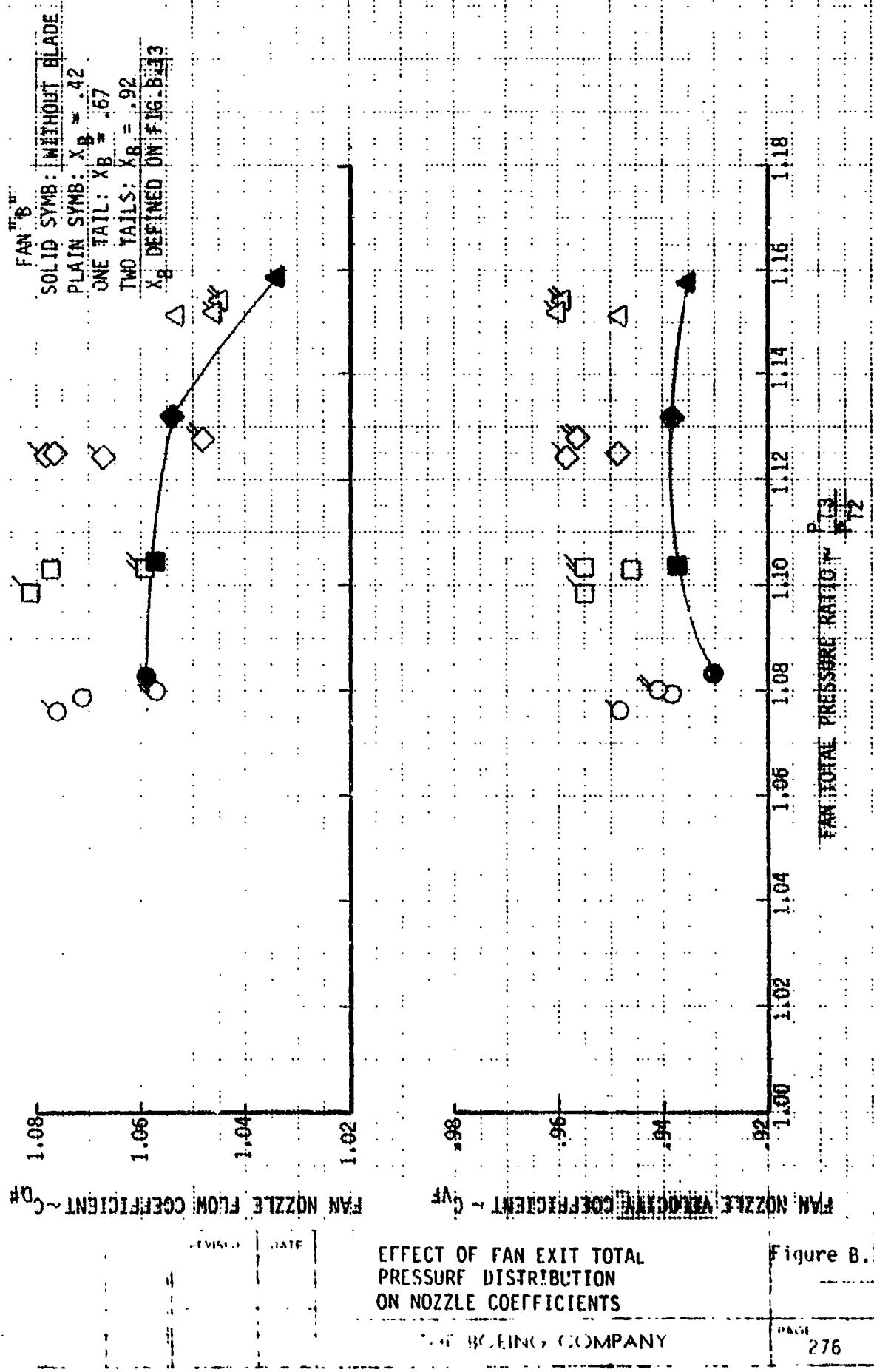
EFFECT OF INLET DISTORTION  
ON FAN NOZZLE DISTORTION - FAN B

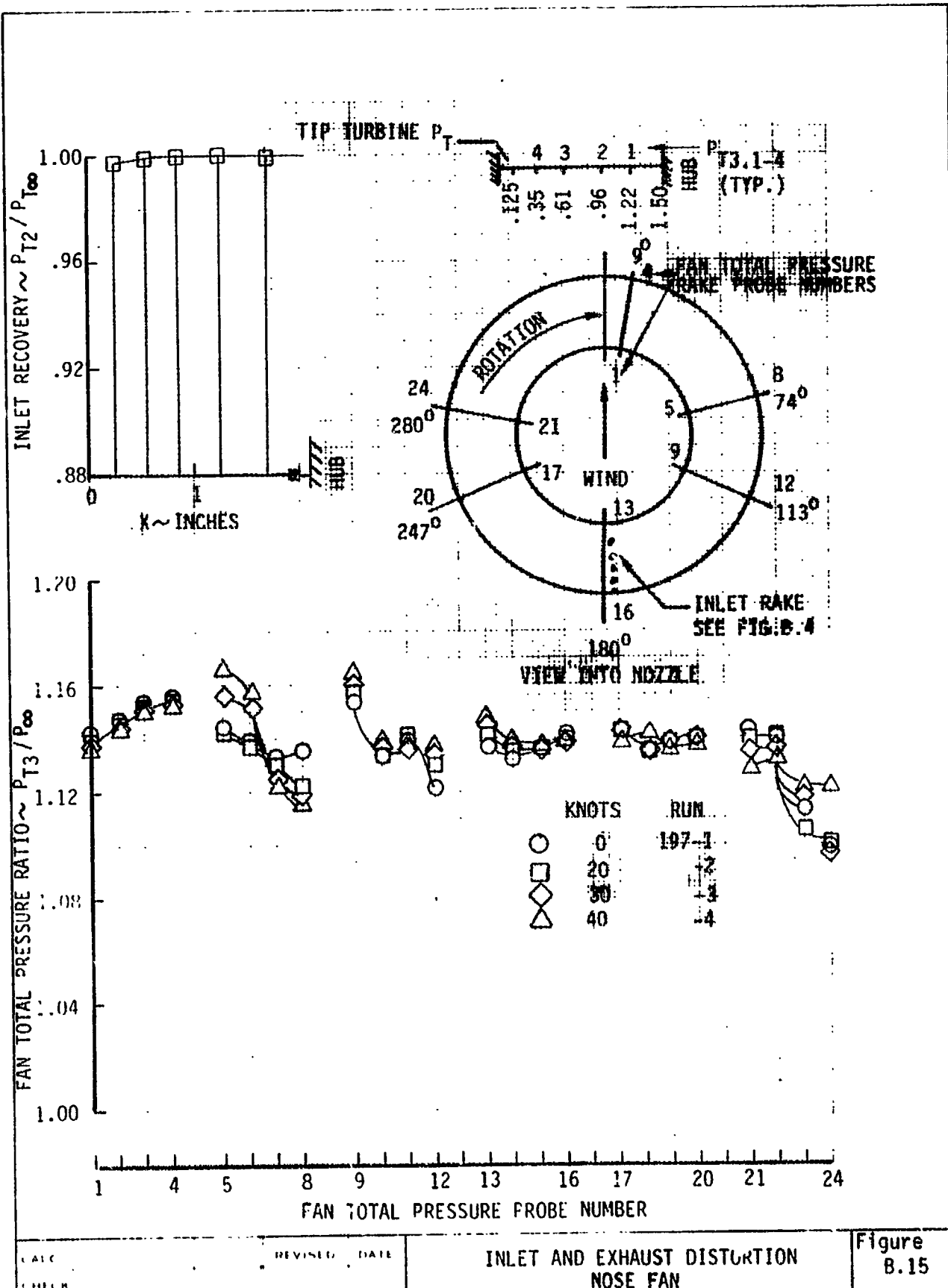
FIG. B.13

THE BOEING COMPANY

PAGE 275

6-6000

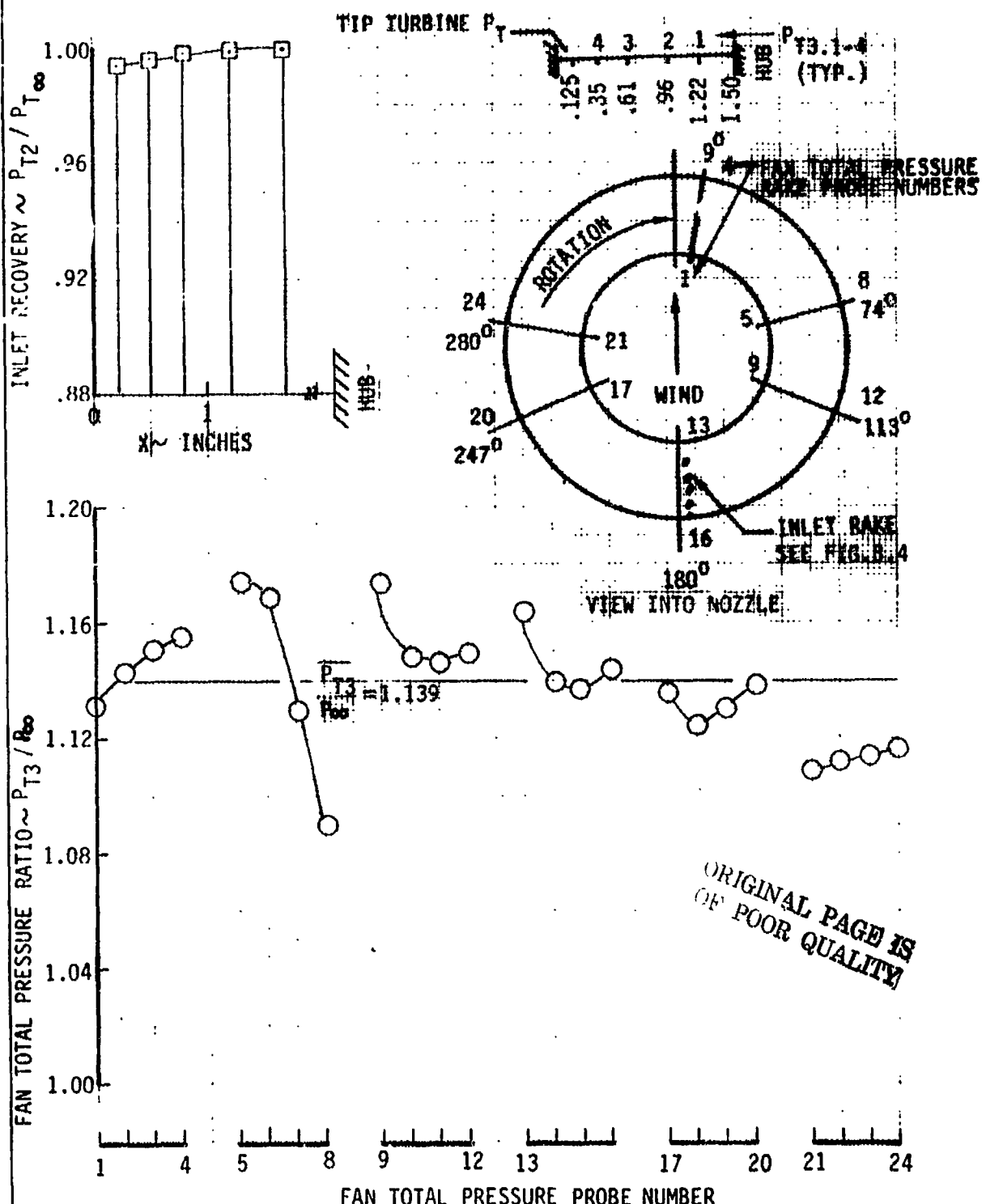




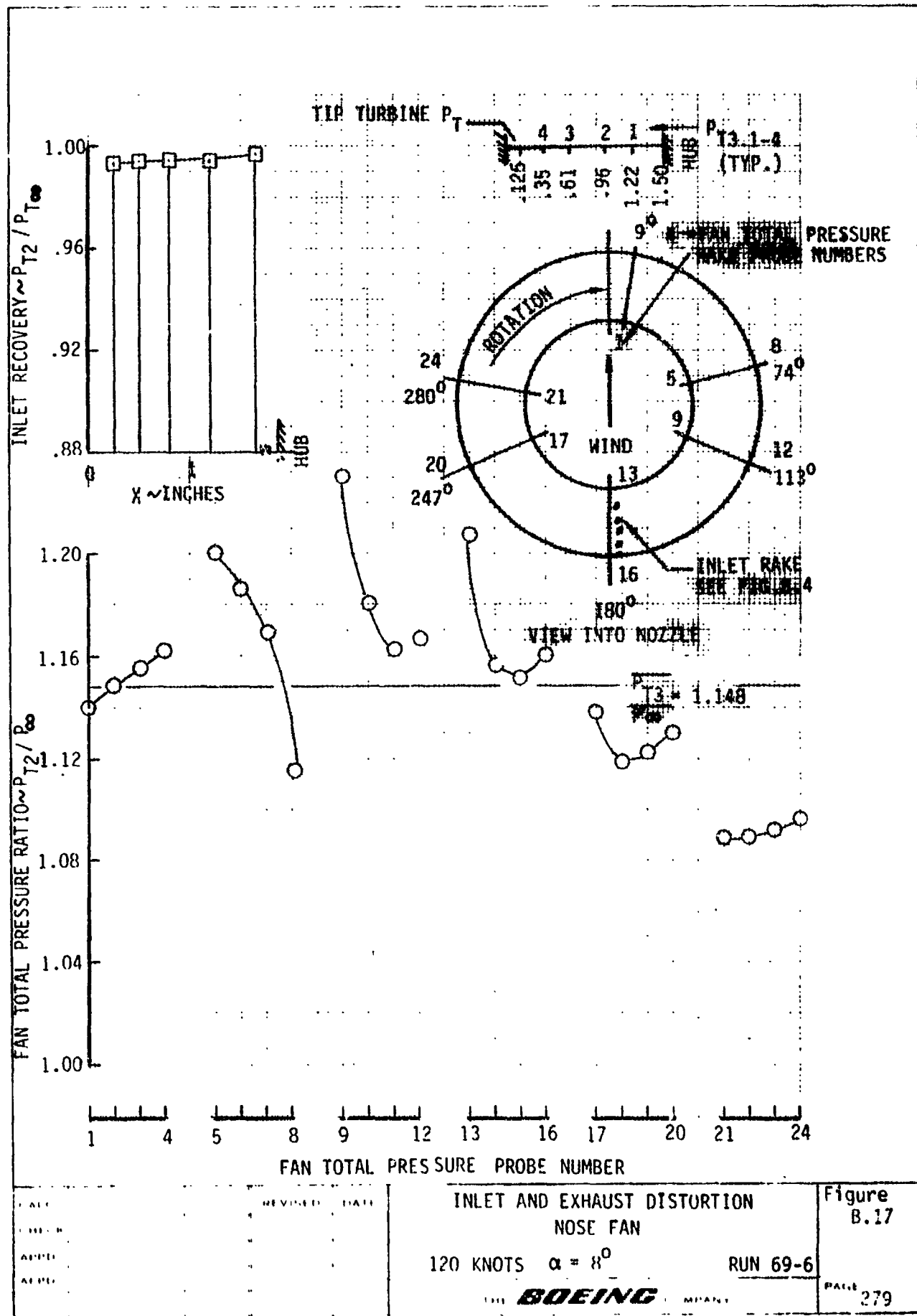
## INLET AND EXHAUST DISTORTION NOSE FAN

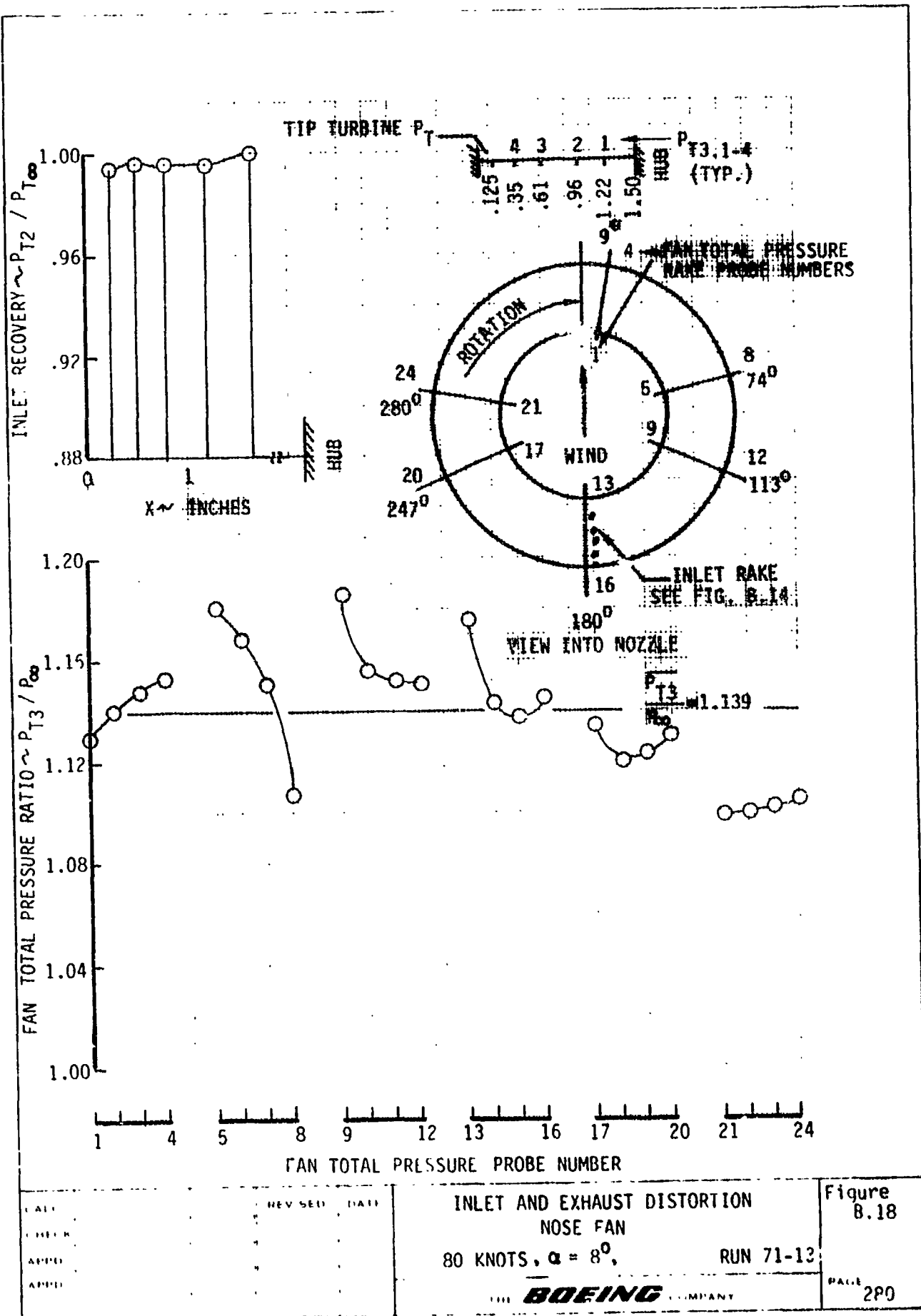
### EFFECT OF LOW FORWARD SPEEDS

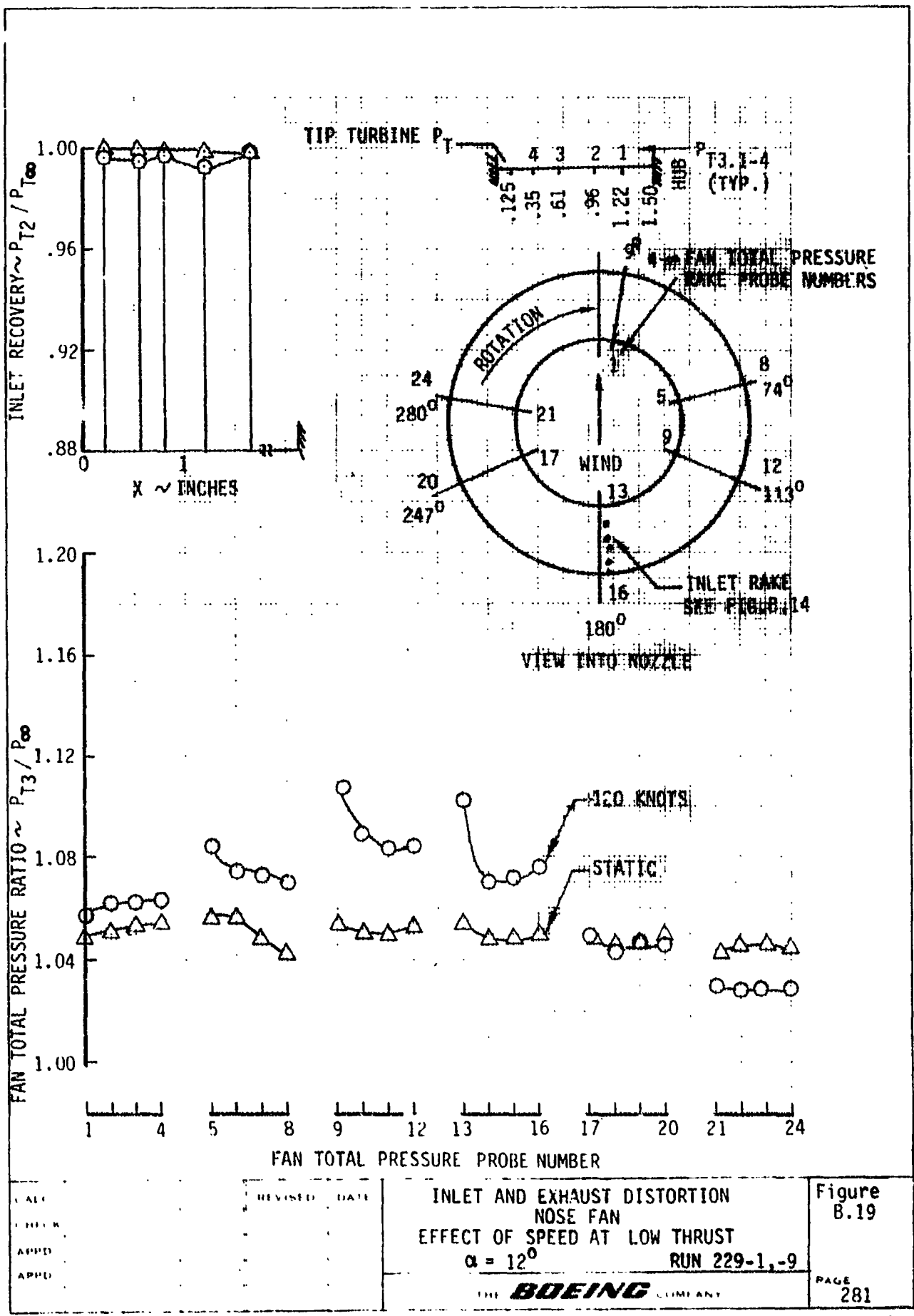
**Figure**  
**B.15**

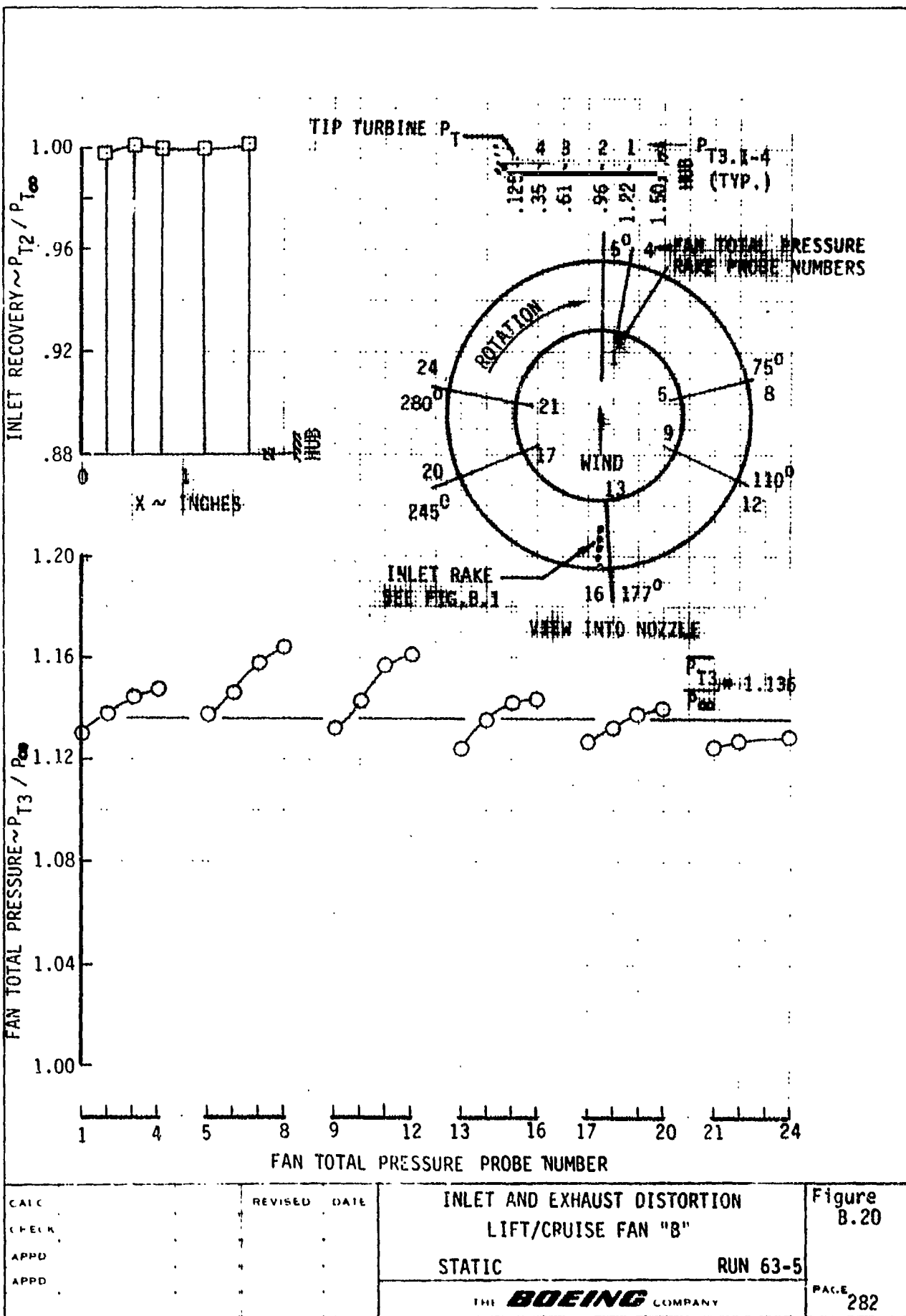


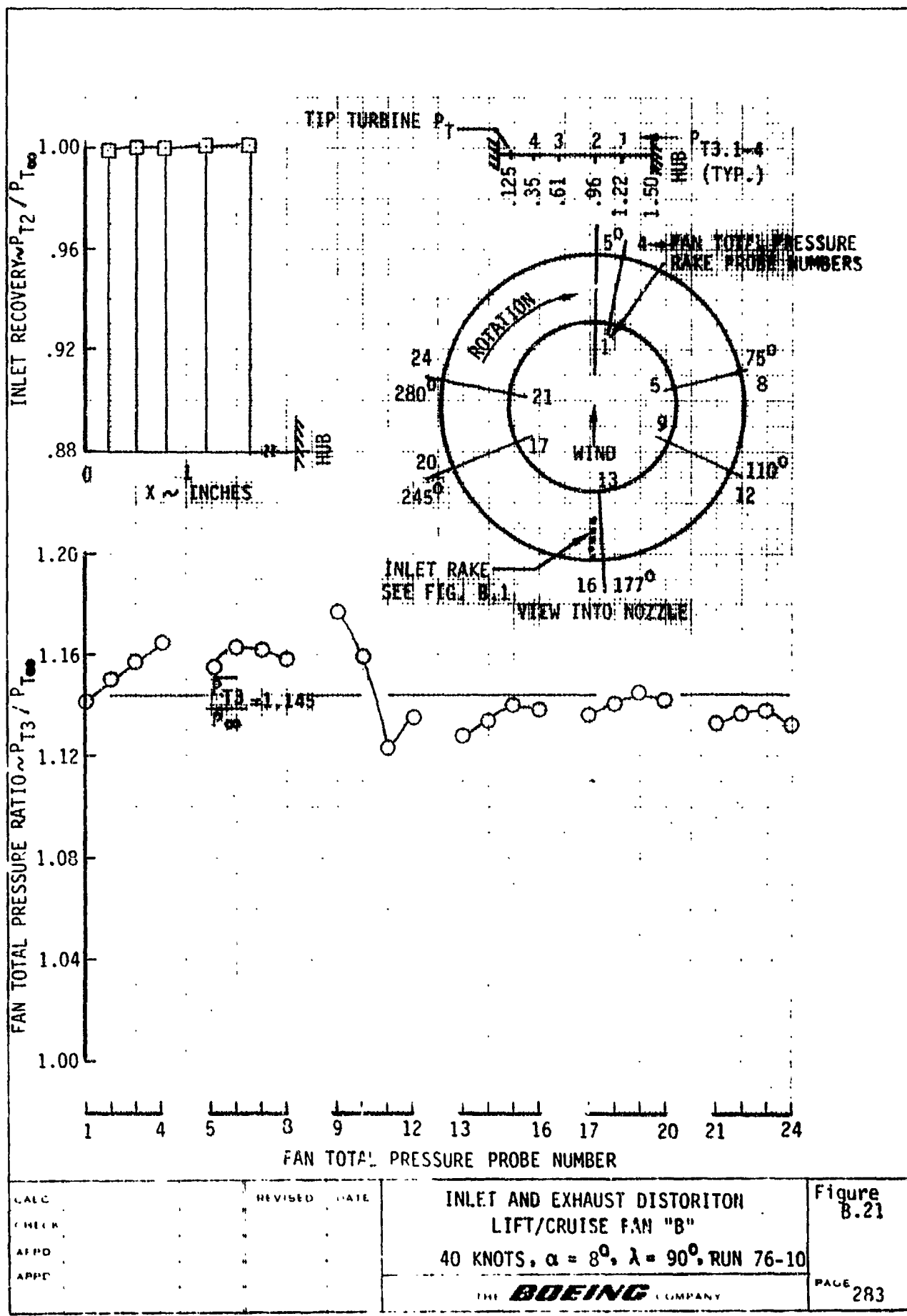
CALL	REVISED	DATE	INLET AND EXHAUST DISTORTION NOSE FAN	Figure B.16
CHECK				
APPD				
APPD				
			60 KNOTS, $\alpha = 8^\circ$ , RUN 76-6	
			THE BOEING COMPANY	PAGE 278

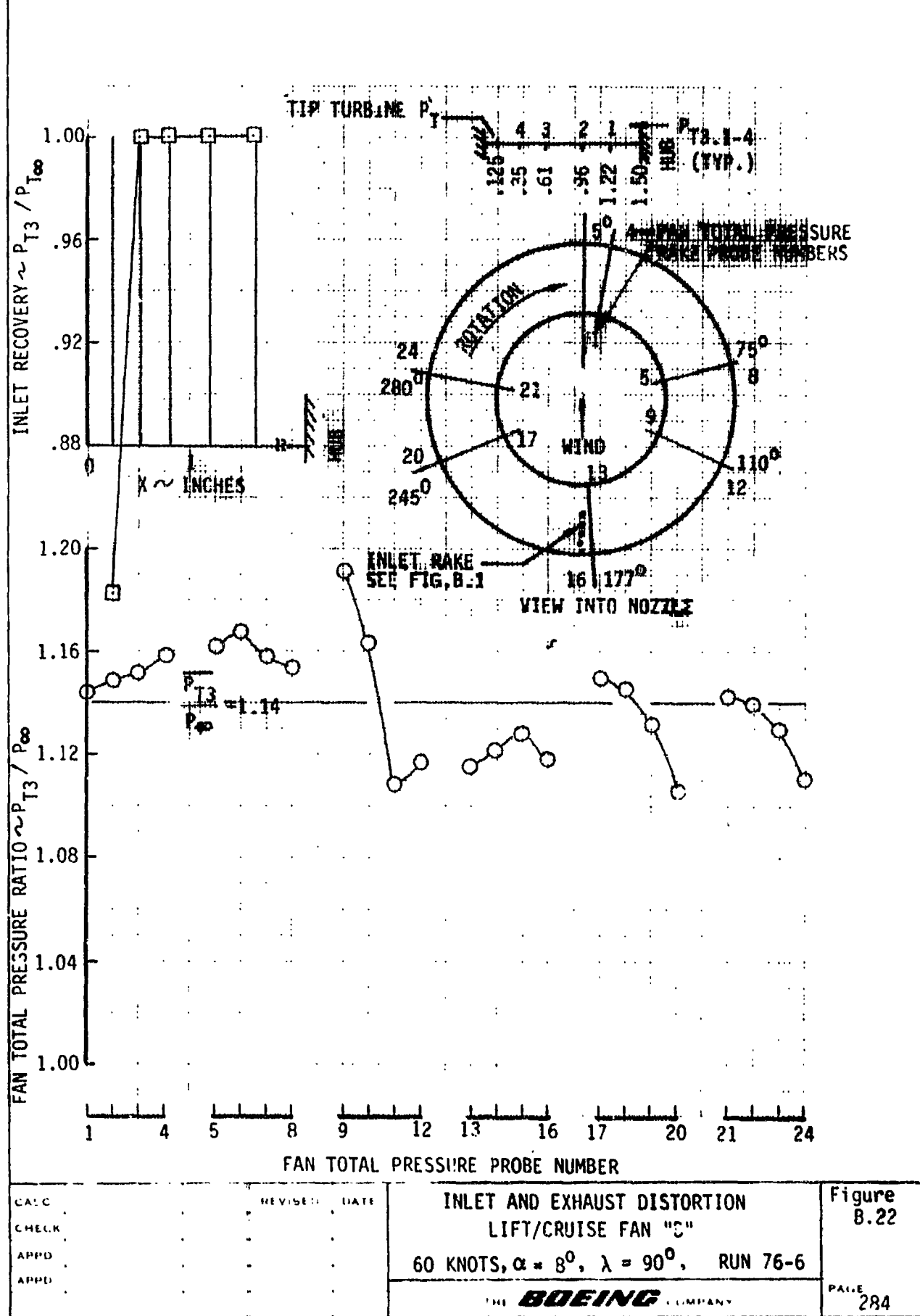


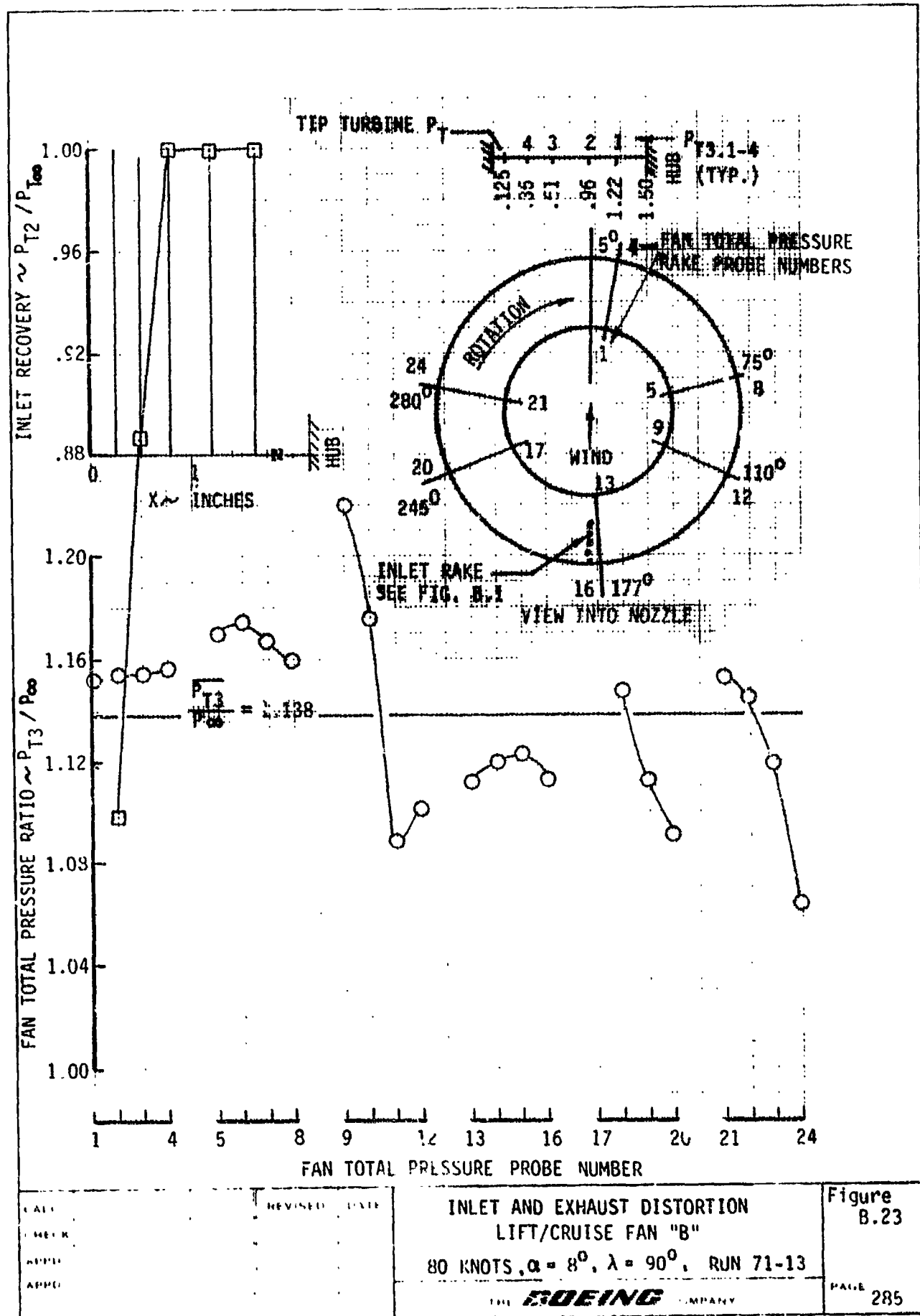












卷之三

REVISED DATE

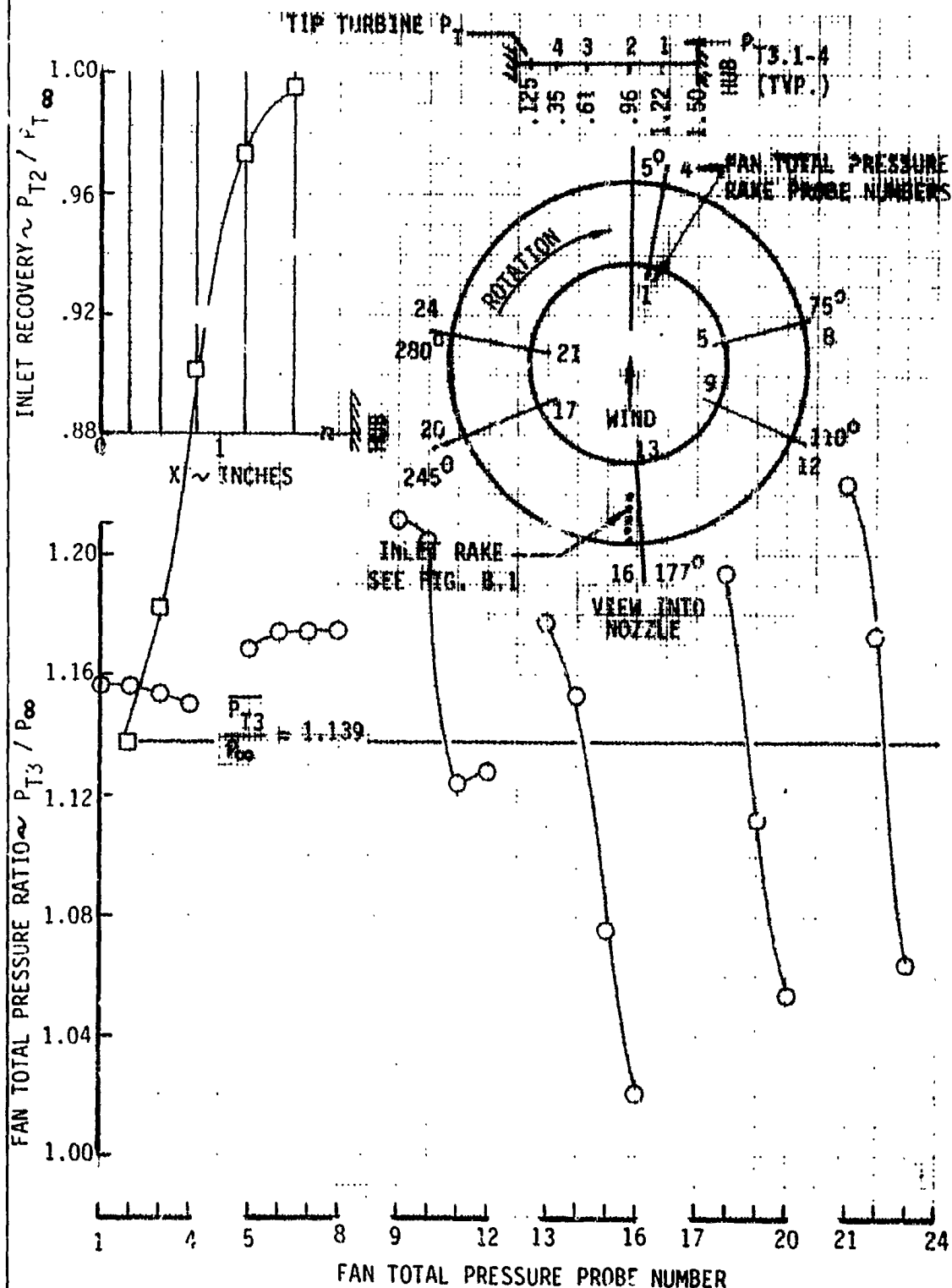
## **INLET AND EXHAUST DISTORTION LIFT/CRUISE FAN "B"**

80 KNOTS,  $\alpha = 8^\circ$ ,  $\lambda = 90^\circ$ , RUN 71-13

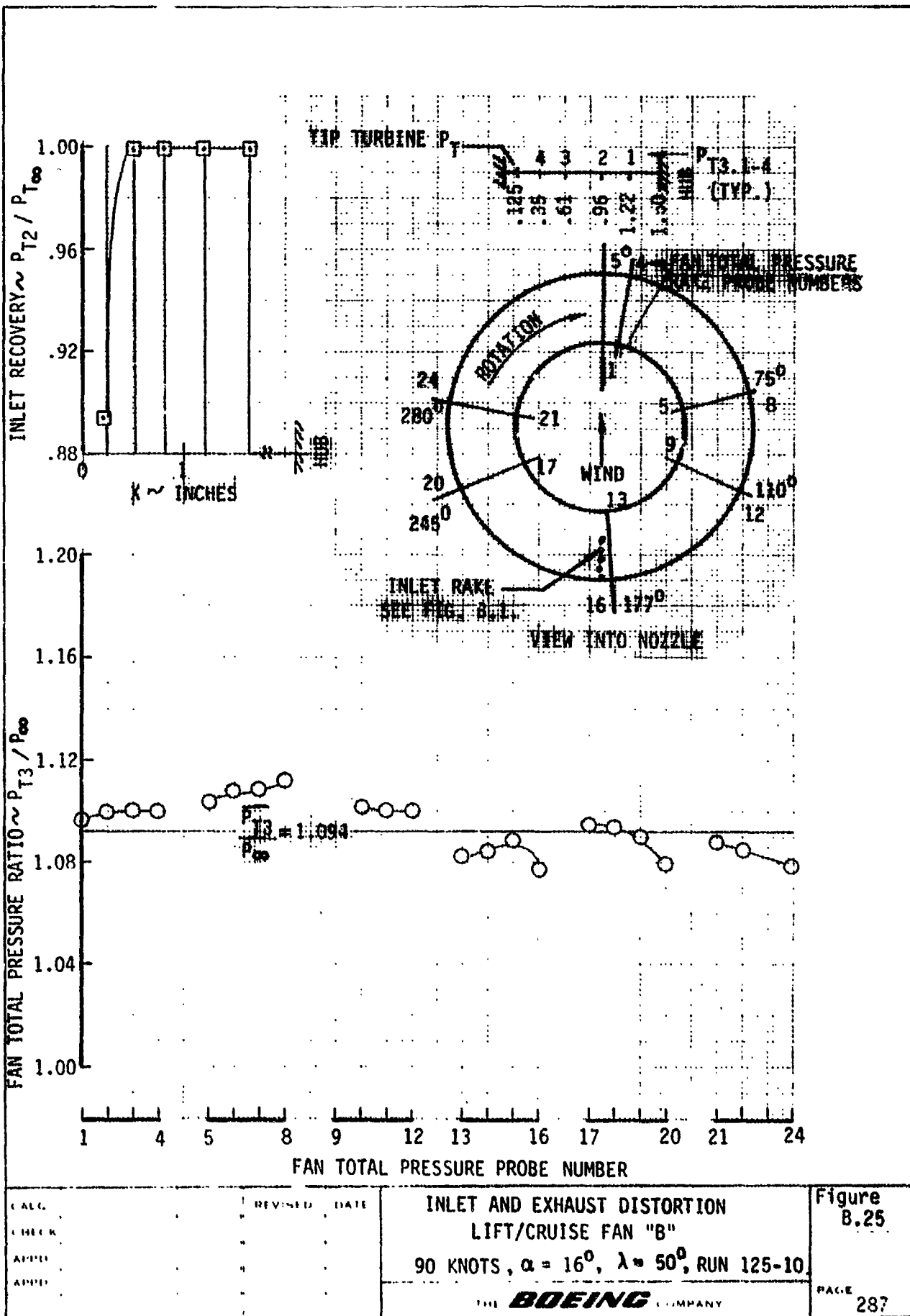
**Figure**  
**B.23**

PAGE 285

PAGE IS  
POOR QUALITY



CALC. CHECK	REVISED	DATE	INLET AND EXHAUST DISTORTION LIFT/CRUISE FAN "B" 120 KNOTS, $\alpha = 8^\circ$ , $\lambda = 90^\circ$ , RUN 69-6	Figure B.24
APPROD APPROD				Page 286

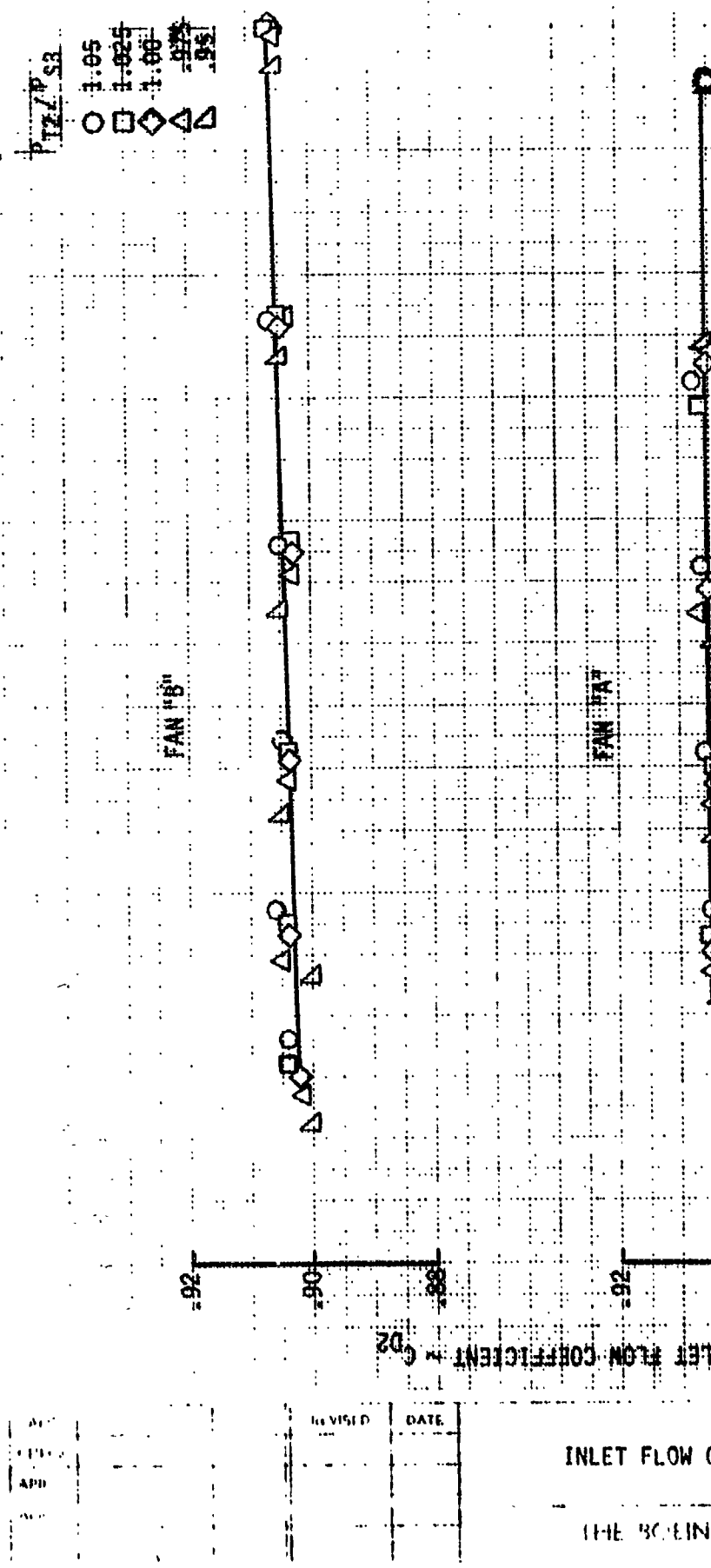


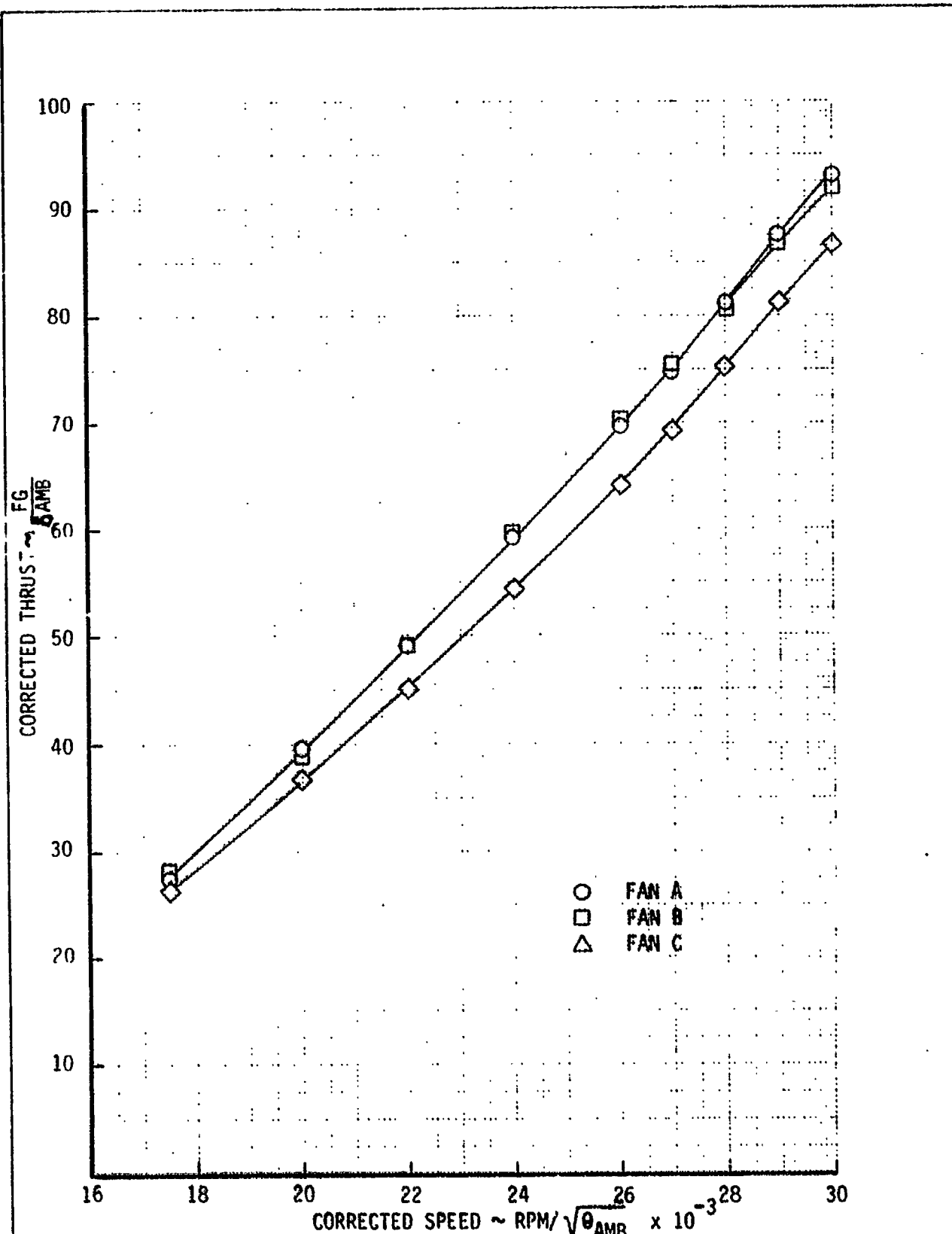
1.24	1.20	1.16	1.12	1.08	1.04
1.22	1.18	1.14	1.10	1.06	1.02
1.21	1.17	1.13	1.09	1.05	1.01
1.20	1.16	1.12	1.08	1.04	1.00
1.19	1.15	1.11	1.07	1.03	0.99

Figure B.26  
PAGE 288

### INLET FLOW COEFFICIENTS

THE BOEING COMPANY





CALC	REvised	DATE	CALIBRATION OF THRUST VS RPM	Figure 8.27
CHECK				
APPRO				
APPRO				

THE **BOEING** COMPANY

**APPENDIX C**  
**DATA REDUCTION**

## APPENDIX C

## DATA REDUCTION

In general, the force data presented in this report have had direct thrust and ram forces removed. Figure C.1 illustrates this procedure for a typical run. Direct thrust and ram forces were also removed from the three force components not illustrated. There are several reasons for removing these forces from the data as summarized below.

- It is not always possible to exactly balance the two lift/cruise fans. This can introduce rolling and yawing moments which are best removed to reveal the aerodynamic contributions.
- The nose fan thrust was not exactly constant with angle of attack. This introduces a variation of pitching moment with angle of attack which is best removed to reveal the aerodynamic forces.
- The ram force at a given  $C_J$  is not exactly representative of the airplane value. This occurs basically because of the mass flow added to drive the tip turbine and because of exhaust temperature differences between the model primary and the actual engine exhaust. Removing ram forces from the wind tunnel data facilitates correction to actual airplane ram conditions.

Removal of ram moments requires knowledge of the effective point of application of the ram forces on the model. For this purpose the results of a test of an isolated nacelle with 1.4 meter (55 inch) diameter Q-Fan installed were utilized. This test, reported in Reference 10, was run in the Ames 40'x 80' Wind Tunnel. As shown in Figure C.2, the results indicate an effective point of application which is well ahead of the inlet face plane. A constant value,  $L/D_{HI} = .75$ , was assumed for reducing the present data. The values of ram force for the model are summarized in Figure C.3. It is seen

that for a given fan pressure ratio (i.e., a given thrust setting) the value  $CFR/\sqrt{C_J}$  is relatively insensitive to  $C_J$  (forward speed variation) and  $\alpha$ . However, for the runs which were made at a lower thrust setting the value is somewhat different.

The gross thrust and ram force of each fan were calculated using equations C.1 and C.2. The definitions, coefficient values, and instrumentation locations associated with these equations are found in the description of the fan calibration, Appendix B.

$$F_G = C_{VF} (M_{TT} V_{ITT} + M_F V_{IF}) + C_{VPR} M_{PR} V_{IPR} \quad C.1$$

$$F_R = V_{FS} C_{DF} M_{IF} \quad C.2$$

For the purpose of removing direct thrust from the measured forces the following equations define the thrust contribution to each balance component. Note that these forces were removed from balance axis system data. The subscripts A, B, and C identify the individual simulators. Note that Fan A is the right L/C fan, Fan B is the left L/C fan, Fan C is the nose fan.

$$\text{Normal Force} = F_C \sin 76^\circ + F_B \sin \lambda_B + F_A \sin \lambda_A \quad C.3$$

$$\text{Axial Force} = -F_C \cos 76^\circ - F_B \cos \lambda_B - F_A \cos \lambda_A \quad C.4$$

$$\begin{aligned} \text{Pitching Moment} = & -\Delta x_C F_C \sin 76^\circ - \Delta z_C F_C \cos 76^\circ \\ & -\Delta x_B F_B \sin \lambda_B - \Delta z_B F_B \cos \lambda_B \\ & -\Delta x_A F_A \sin \lambda_A - \Delta z_A F_A \cos \lambda_A \end{aligned} \quad C.5$$

$$\text{Rolling Moment} = -\Delta y_B F_B \sin \lambda_B - \Delta y_A F_A \sin \lambda_A \quad C.6$$

$$\text{Yawing Moment} = -\Delta y_B F_B \cos \lambda_B - \Delta y_A F_A \cos \lambda_A \quad C.7$$

$$\text{Side Force} = 0 \quad C.8$$

The geometric constants used in the above equation were used to locate a point on the fan thrust axis relative to the moment reference center (MRC). (The reference system is shown in Figure C.5.)

$$\Delta x = \text{Fuselage Station} - (\text{Fuselage Station})_{\text{MRC}}$$

$$\Delta y = \text{Butt Line} - (\text{Butt Line})_{\text{MRC}}$$

$$\Delta z = \text{Water Line} - (\text{Water Line})_{\text{MRC}}$$

FAN	$\Delta x \sim \text{INCH}$	$\Delta y \sim \text{INCH}$	$\Delta z \sim \text{INCH}$
A	8.656	7.482	3.09
B	8.656	-7.482	3.09
C	-20.215	0	-2.369

The following equations were used to calculate the components of ram force to be removed from the measured force data. These increments were subtracted from the stability axis data before application of the wind tunnel wall effects corrections. The axis system is shown in Fig. C.5.

$$D_R = \text{Ram Drag} = F_R \cos \beta \quad \text{C.9}$$

$$SF_R = \text{Ram Side Force} = -F_R \sin \beta \quad \text{C.10}$$

$$\text{Ram Pitching Moment} = D_R (\Delta z \cos \alpha - \Delta x \sin \alpha) \quad \text{C.11}$$

$$\text{Ram Rolling Moment} = SF_R (\Delta z \cos \alpha - \Delta x \sin \alpha) \quad \text{C.12}$$

$$\text{Ram Yawing Moment} = -SF_R (\Delta x \cos \alpha + \Delta z \sin \alpha) + D_R \Delta y \quad \text{C.13}$$

The constants ( $\Delta x$ ,  $\Delta y$ , and  $\Delta z$ ) for this set of equations are as follows:

FAN	$\Delta x \sim$ INCH	$\Delta y \sim$ INCH	$\Delta z \sim$ INCH
A	$8.656 - 10.673 \cos\lambda$	7.482	$3.09 + 10.673 \sin\lambda$
B	$8.656 - 10.673 \cos\lambda$	-7.482	$3.09 + 10.673 \sin\lambda$
C	-22.02	0	5.078

The ratio of free stream to jet efflux velocity ( $V/V_J$ ) is defined as:

$$\frac{V}{V_J} = \sqrt{\frac{2 A_T}{C_J S}} = \frac{.561}{\sqrt{C_J}} \quad C.14$$

where

$S$  is the model reference area

$C_J$  is the thrust coefficient  $F_G/qS$

$F_G$  is the gross thrust as defined in equation C.1

$q$  is free stream dynamic pressure

$A_T$  is the propulsive exit area with appropriate adjustments such that  $V_J$  is representative of fan efflux velocity rather than a weighted average of the fan efflux and blown primary velocities.

Wall Corrections

Corrections for tunnel wall constraints were determined based on Heyson's Interference Theory (Reference 11. and 12.). In this theoretical approach, a lifting surface is represented by a number of lifting line elements oriented along the quarter chord line and trailing along the wake. Ten lifting elements were chosen for the T-39 model. The effective wake deflection angle was determined as discussed in Reference 13. Corrections were determined separately for the wing and the tail. The total model loads (lift and drag) as measured directly by the internal balance (i.e., including direct thrust and ram forces) were used in determining the interference velocities.

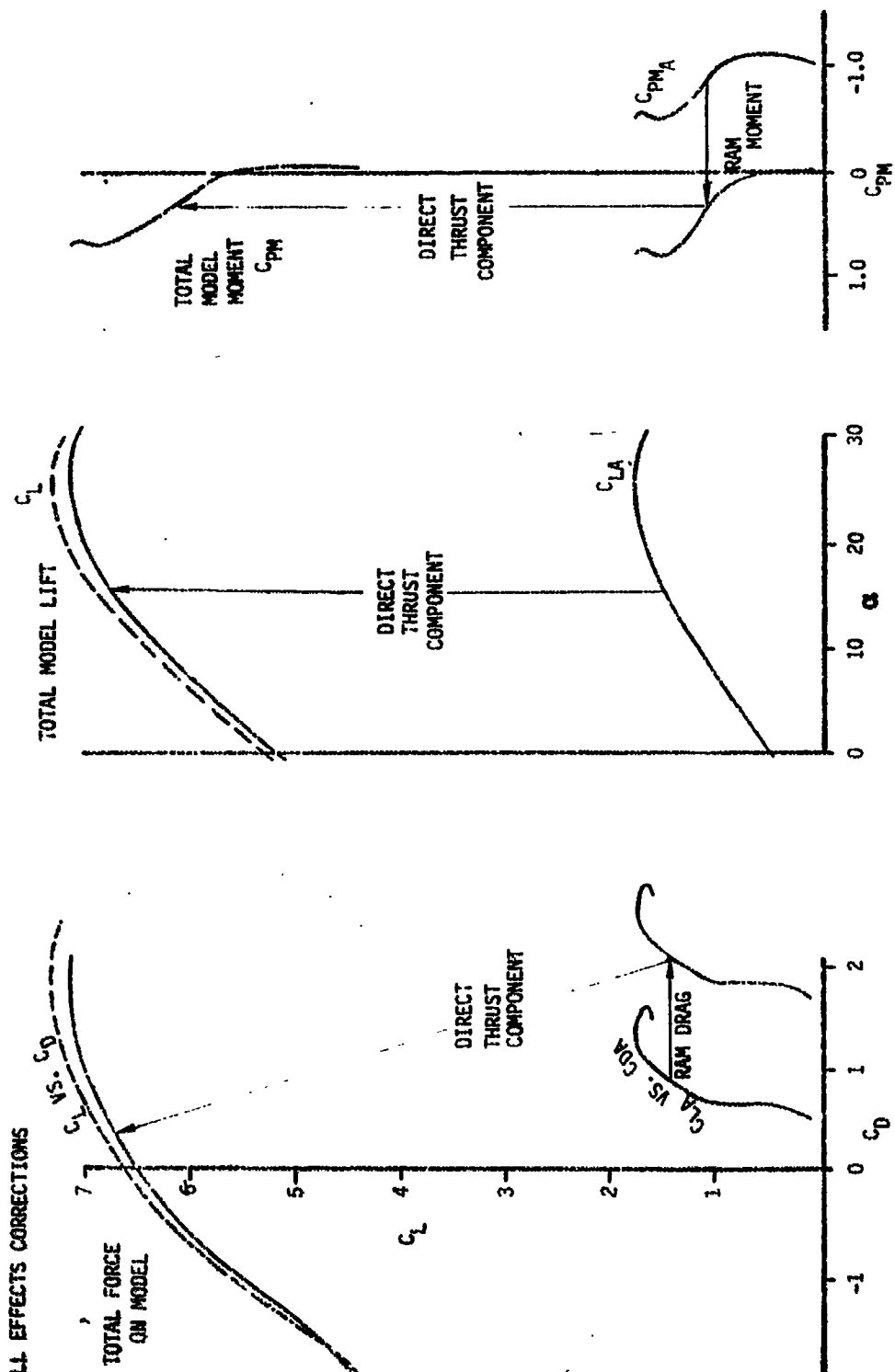
The corrections were computed in the form of a flow angle change, which changes the resolved lift and drag components, and a tunnel test section dynamic pressure change. In addition to the above corrections, a conventional solid blockage correction factor was applied to the dynamic pressure.

Figure C.4 presents a summary of typical wall correction factors computed at the wing where  $\Delta\alpha_w$  denotes the computed change in stream direction at the wing and  $Q/Q_U$  denotes the ratio of the final corrected stream dynamic pressure to the value before application of wall corrections.

The pitch center was not located at the model center with the result that the model changed height in the tunnel as angle of attack was varied. At  $\alpha = -8^\circ$  the model moment reference center (MRC) was 8.5 inches below tunnel center line while at  $\alpha = +30^\circ$  the MRC was 15.5 inches above tunnel center line. The height variation with alpha was linear. This variation was taken into account in the wall effects calculations.

Figures A.18 thru A.21 in Appendix A, present some data with the ground plane installed. These data were corrected for the wall effects of three walls only with the ground effect left in.

--> BEFORE WALL EFFECTS CORRECTIONS  
— AFTER WALL EFFECTS CORRECTIONS



ORIGINAL PAGE IS  
OF POOR QUALITY

FIGURE C.1 ILLUSTRATION OF REMOVAL OF DIRECT THRUST AND RAM FORCES

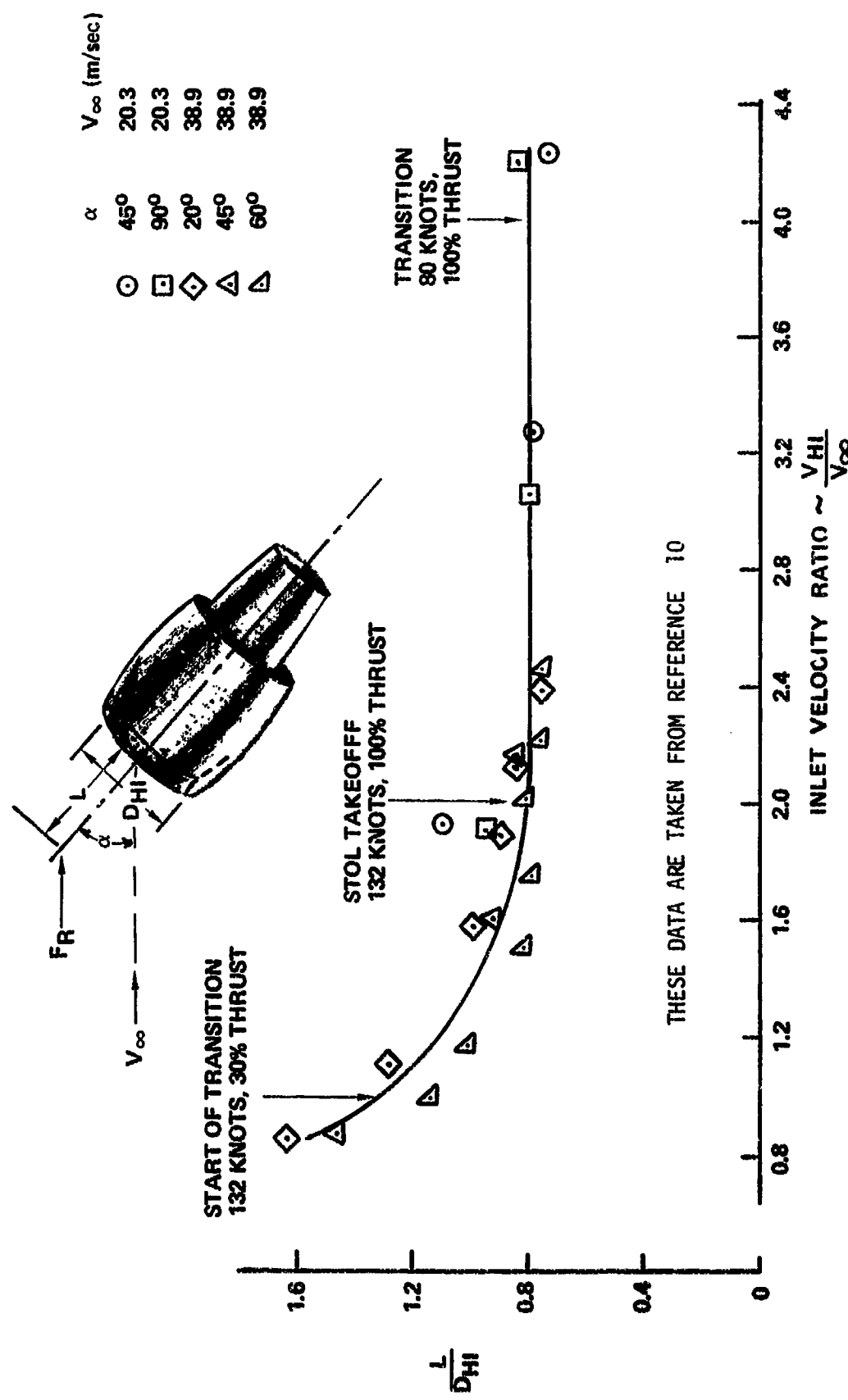


FIGURE C.2 LOCATION OF RAM DRAG RELATIVE TO INLET PLANE

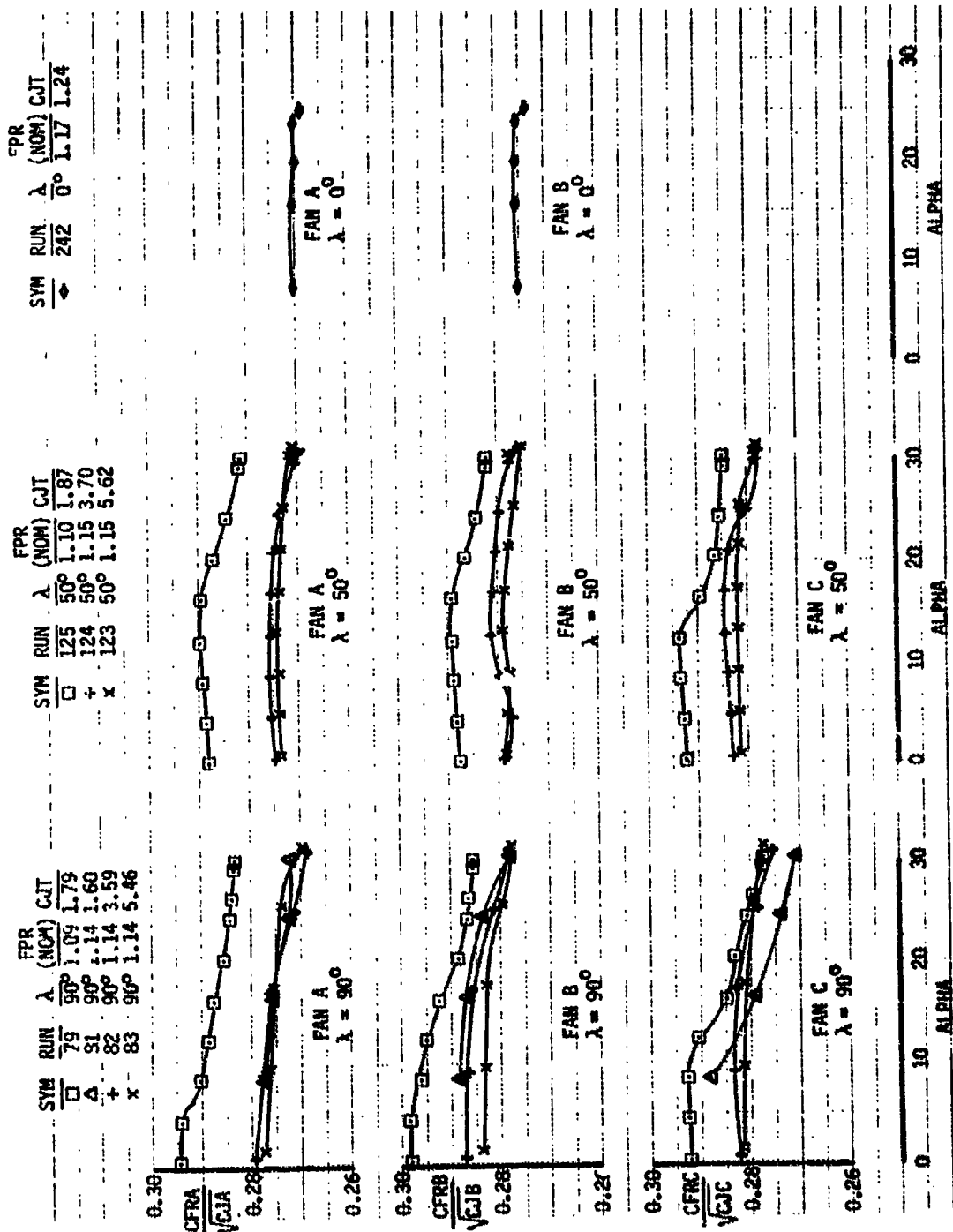
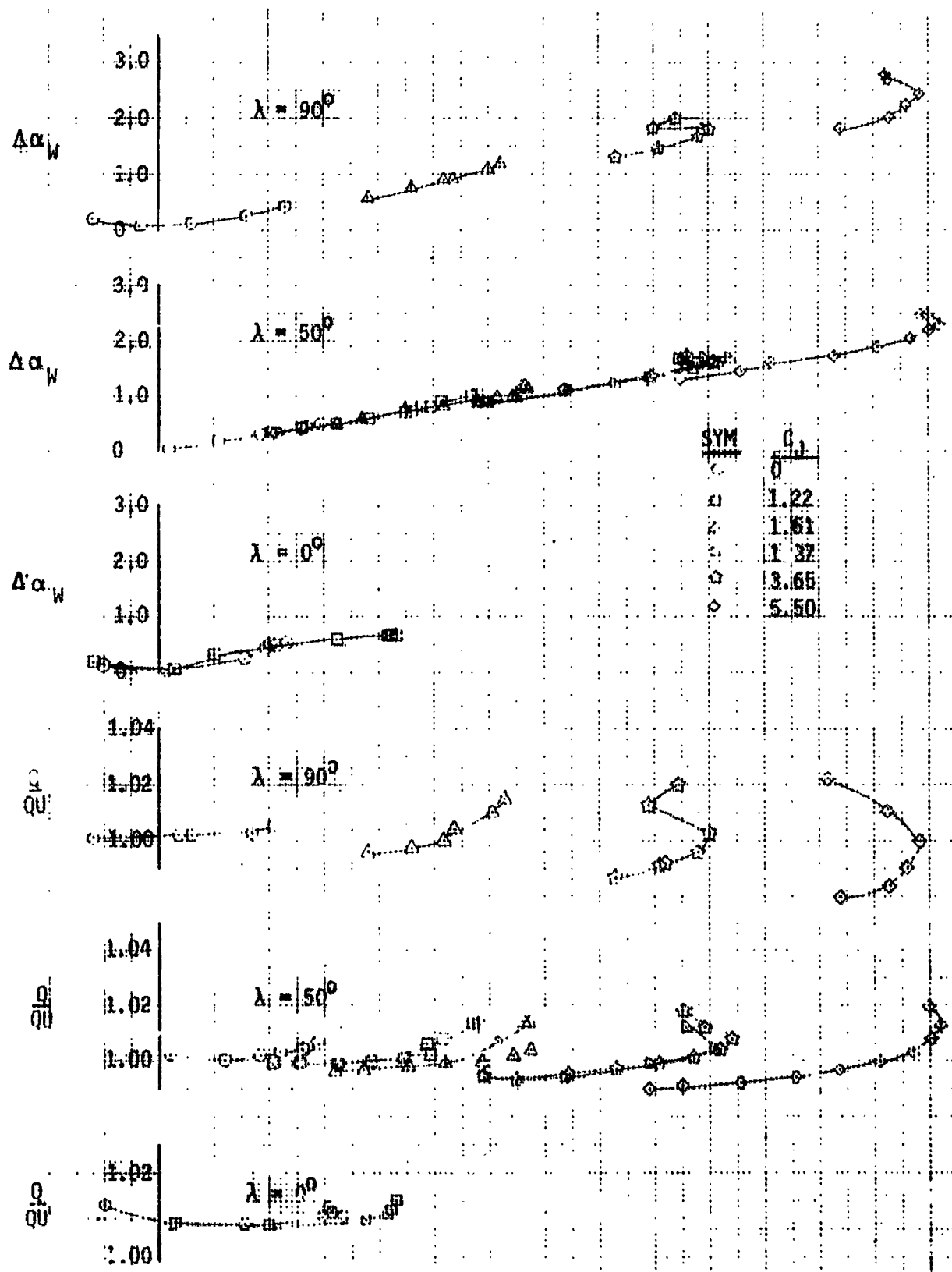


FIGURE C.3 SUMMARY OF TYPICAL RAM DRAG DATA



C<sub>l</sub> (NOTE C<sub>l</sub> INCLUDES DIRECT THRUST COMPONENT)

REV'D.	DATE
1-A	
1-B	
APR	
APR	

TYPICAL COMPUTED  
WALL CORRECTION FACTORS

THE BOEING COMPANY

FIG C.4

PAGE  
299

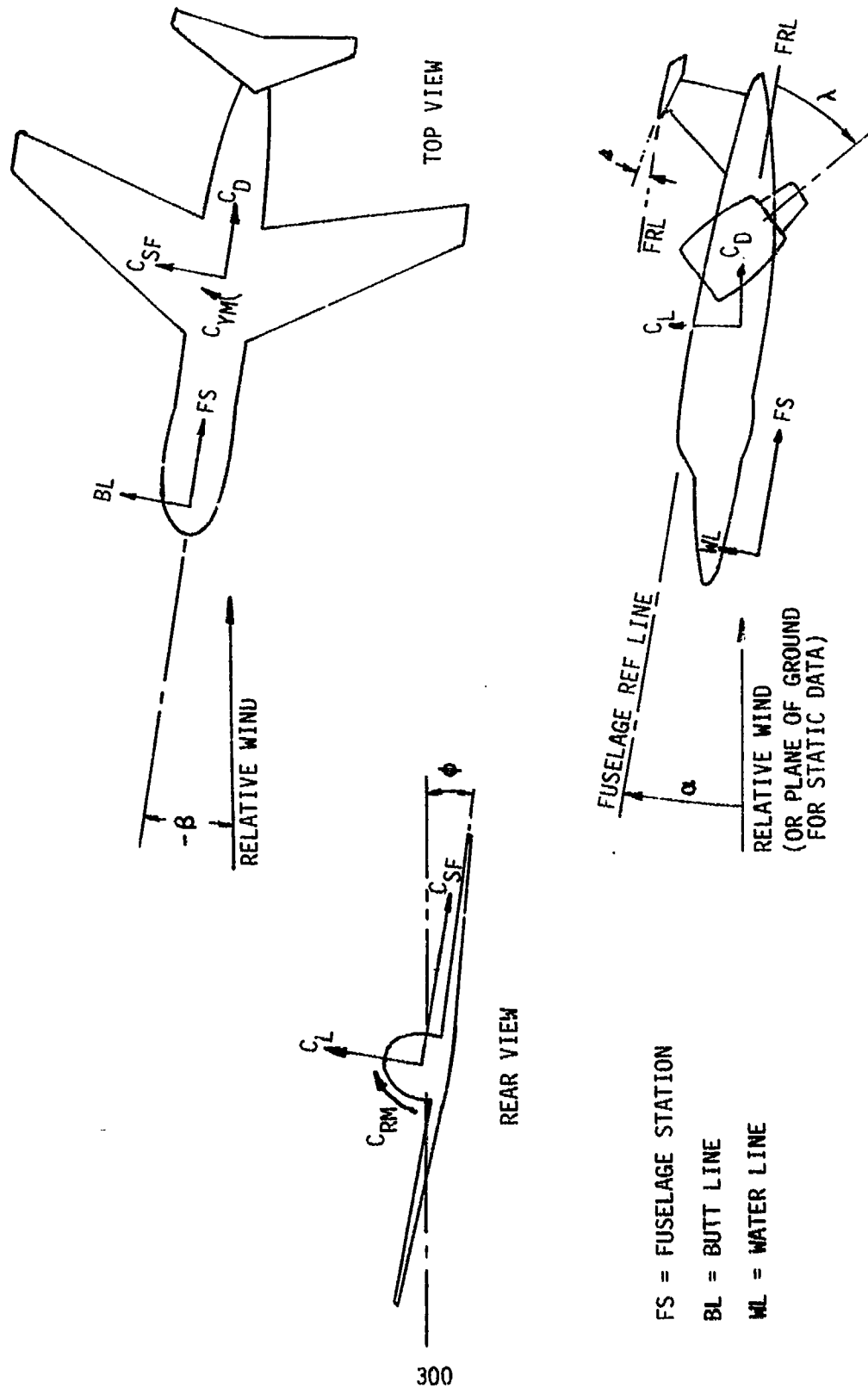


FIGURE C.5 SIGN CONVENTION